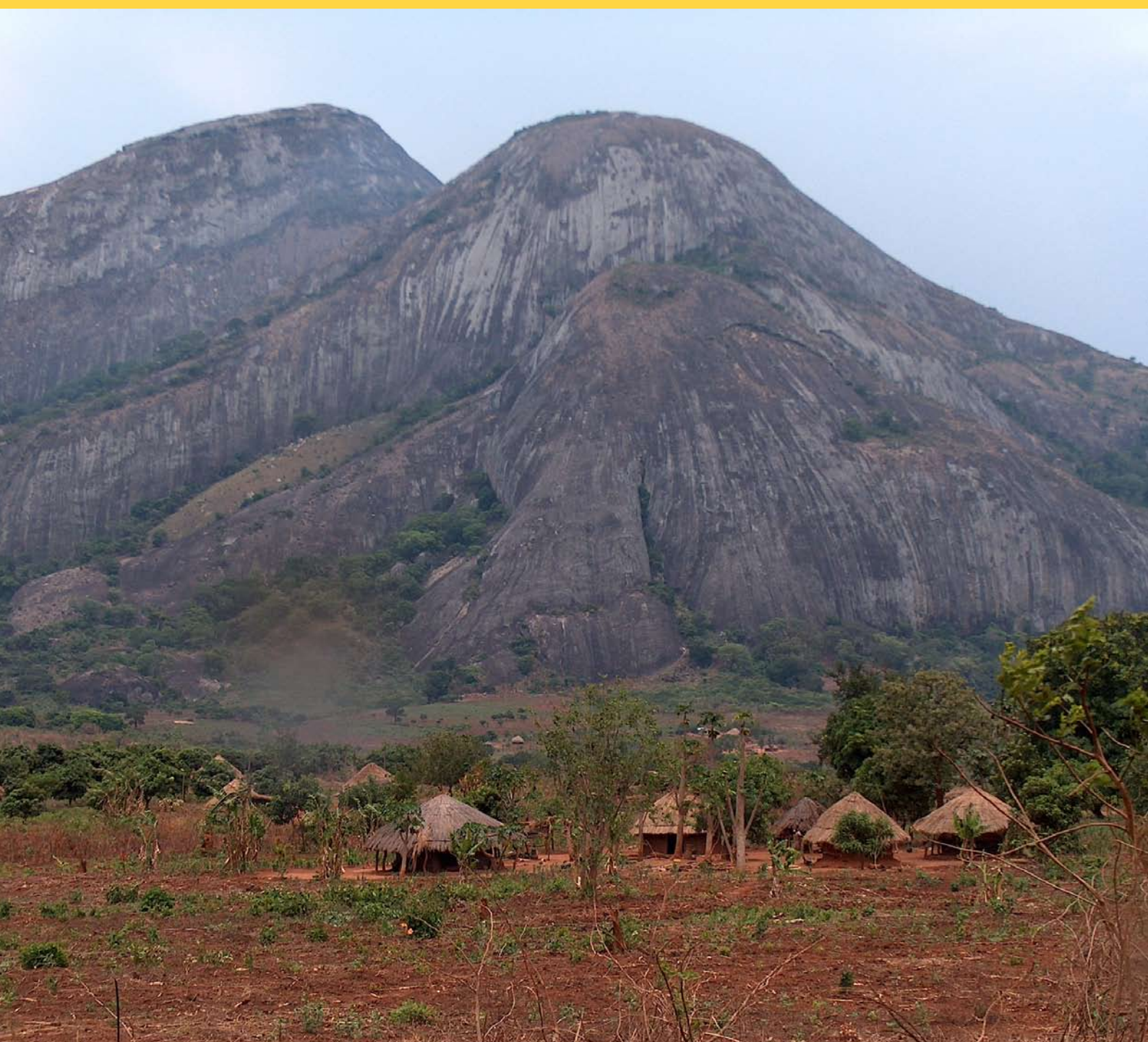


GEOLOGICAL SURVEY OF FINLAND

Special Paper 48

2008



GTK Consortium Geological Surveys in Mozambique 2002–2007



Edited by Yrjö Pekkala, Tapio Lehto and Hannu Mäkitie

Geological Survey of Finland, Special Paper 48

**GTK Consortium Geological Surveys in Mozambique
2002–2007**

Edited by
Yrjö Pekkala, Tapio Lehto and Hannu Mäkitie

Geological Survey of Finland
Espoo 2008

Pekkala, Yrjö, Lehto, Tapio & Mäkitie, Hannu (eds.) 2008. GTK Consortium Geological Surveys in Mozambique 2002–2007. *Geological Survey of Finland, Special Paper 48*. 321 pages, 196 figures, 14 tables and 6 appendices.

This publication presents 14 papers on various geological, map production and data management activities conducted by the GTK Consortium within the frame of the World Bank/Nordic Development Fund financed Mineral Resources Management Capacity Building Project in Mozambique, 2002 – 2007.

The first paper provides a general introduction to the work carried out by the GTK Consortium within separate project components. These are described in more detail in the following papers, starting with data management and map production, followed by an article on the interpretation of remote sensing data, and then an article on geophysical and petrophysical surveys.

Geological description begins with a paper on the radiometric ages of 35 rock samples from the mapping areas. The next two papers deal with structural aspects of the eastern margin of the Archaean Zimbabwe Craton in western Mozambique and with a new multiple terrane structure within the Tete-Chipata Belt in northwestern Mozambique. Granitoid rocks, the Tete Gabbro-Anorthosite Suite and Karoo volcanic rocks with associated intrusions are described in three papers. The Cretaceous – Quaternary stratigraphy is presented from the Massingir-Mapai area in southwest Mozambique.

The final three papers deal with the geochemical and industrial mineral surveys and with conclusions on the mineral resources potential in Mozambique.

Keywords (GeoRef Thesaurus AGI): areal geology, economic geology, granites, gneisses, sedimentary rocks, volcanic rocks, Pan-African Orogeny, Grenvillian Orogeny, geologic maps, airborne methods, geophysical surveys, absolute age, Archean, Proterozoic, Phanerozoic, Mozambique

Geological Survey of Finland, P.O. BOX 96, FIN-02151 Espoo, Finland

E-mail: yrjo.pekkala@gtk.fi, tapio.lehto@gtk.fi, hannu.makitie@gtk.fi

ISBN 978-952-217-046-0 (paperback)

ISBN 978-952-217-047-7 (PDF)

ISSN 0782-8535

Tampereen Yliopistopaino Oy – Juvenes Print 2008

CONTENTS

Editors' Preface by <i>Yrjö Pekkala, Tapio Lehto & Hannu Mäkitie</i>	5
Introduction to GTK projects in Mozambique 2002–2007 by <i>Yrjö Pekkala, Tapio Lehto & Matti I. Lehtonen</i>	7
Data management and map production in geological mapping projects in Mozambique by <i>Markku Tiainen, Antti Kahra, Eira Kuosmanen & Olli Rantala</i> ..	23
Integrated geological interpretation of remotely sensed data to support geological field mapping in Mozambique by <i>Ernst Schetselaar, Markku Tiainen & Tsehaie Woldai</i>	35
Geophysical maps and petrophysical data of Mozambique by <i>Tapio Ruotoistenmäki</i>	65
Mesoarchaeon to Lower Jurassic U-Pb and Sm-Nd ages from NW Mozambique by <i>Irmeli Mänttari</i>	81
Contribution to the structure at the eastern margin of the Archaean Zimbabwe craton, Mozambique by <i>Tapio Koistinen, Matti I. Lehtonen, Sérgio Fernando & Rogério Matola</i>	121
The Tete-Chipata Belt: a new multiple terrane element from western Mozambique and southern Zambia by <i>A.B. Phil Westerhof, Matti I. Lehtonen, Hannu Mäkitie, Tuomo Manninen, Yrjö Pekkala, Bosse Gustafsson & André Tahon</i>	145
Petrography and geochemistry of granitoid rocks in the northern part of Tete Province, Mozambique by <i>Hannu Mäkitie, Matti I. Lehtonen, Tuomo Manninen, João M. Marques, Grácio Cune & Hilário Mavie</i>	167
Igneous and tectonic setting of the allochthonous Tete Gabbro-Anorthosite Suite, Mozambique by <i>A.B. Phil Westerhof, André Tahon, Tapio Koistinen, Tapio Lehto & Christer Åkerman</i>	191
The Karoo volcanic rocks and related intrusions in southern and central Mozambique by <i>Tuomo Manninen, Toni Eerola, Hannu Mäkitie, Saku Vuori, Arto Luttinen, Adriano Senvano & Vladimiro Manhiça</i>	211
Sedimentary rocks of the Mapai Formation in the Massingir-Mapai region, Gaza Province, Mozambique by <i>Robbert Rutten, Hannu Mäkitie, Saku Vuori & João M. Marques</i>	251
Geochemical surveys in Mozambique; a data compilation project by <i>Esko Korkiakoski</i>	263
Review of industrial minerals in Mozambique by <i>Yrjö Pekkala, Tapio Kuivasaari, Reinaldo Gonçalves, Mário Deus, Fátima Chaique & Carlos Almeida</i>	289
Mineral resources potential in Mozambique by <i>Tapio Lehto & Reinaldo Gonçalves</i>	307

EDITORS' PREFACE

This Special Paper summarizes the work of the GTK Consortium in Mozambique 2002–2007, comprising geological mapping, mineral resources assessment, geochemical and industrial mineral surveys, GIS map production, data management and comprehensive reporting. The work was carried out within three project components: Geological Mapping LOT 2 and LOT 3, and Geochemical and Industrial Mineral (GIM) Surveys. Project LOT 2 was implemented by GTK with the partners ITC (The Netherlands), SGU (Sweden) and Gondwana Lda (Mozambique) and Project LOT 3 by GTK with the partners ITC, GEUS (Denmark) and Gondwana Lda. The GIM Project was implemented by GTK together with Gondwana Lda. Mapping areas LOT 2 and LOT 3 covered about 480 000 km² and resulted in production of 36 map sheets showing the geology and mineral resources at the 1:250 000 scale and 20 sheets at the 1:50 000 scale. Maps indicating high mineral potential were prepared at the 1:250 000 scale.

Much of the map preparation was based on integrated geological interpretation of remote sensing data, comprising previous geological maps, satellite images, and new regional and high resolution radiometric and magnetic airborne data. Field verification was performed at 20 000 observation sites, supported by nearly 30 000 digital photographs of outcrops and selected samples. Information on 650 mineral indications, occurrences and deposits was collected in a mineral occurrence database. Of these, about 140 more significant occurrences were checked in the field and the database updated accordingly. Laboratory work comprised 440 whole rock chemical analyses (XRF), 1600 mineral analyses (microprobe) and 1000 petrographical thin section studies. In addition, petrophysical properties of about 700 samples of major rock types were measured to support the interpretation of airborne geophysics. During the bedrock mapping of the LOT 2, 38 rock samples were collected for radiometric dating by GTK Consortium geologists. The zircon TIMS U-Pb and Nd-Sm mineral isochron ages were processed at GTK and the secondary ion microprobe (SHRIMP) zircon U-Pb isotopic data were measured at VSEGEI, St. Petersburg.

The geology and mineral occurrences are described in four volumes of Map Explanations totalling about 1400 pages, prepared in 2006. Map Explanation Volume 1 covers the whole of southern Mozambique. Only in the northwestern corner of this mapping area, south of Manica, are Proterozoic rocks exposed, while by far the majority of the area is covered by Phanerozoic units, from Karoo sediments and volcanics to extensive Cretaceous – Tertiary sedimentary rocks. Pliocene – Holocene formations essentially comprise reworked weathering products. Volume 2 covers the map sheets along the Zimbabwe border from the south

of Tete to the south of Manica. In this area the rocks of the Archaean Zimbabwe Craton were observed to extend clearly further east into Mozambique than previously assumed. Map Explanation Volume 3 covers the area to the east of Volume 2 up to the Indian Ocean, comprising Proterozoic lithologies in the west but mostly Phanerozoic units from the Karoo to the Quaternary towards the east. Map Explanation Volume 4 describes the geology of the northern part of Tete Province, bordering Zambia in the north and Zimbabwe in the west, which is characterized by Mesoproterozoic schists and granitoids, and Phanerozoic sedimentary rocks.

In the Geochemical component of GIM Surveys the available previous data were collected, reliable samples re-analyzed and digital, geochemical maps and databases were created, based on newly processed and evaluated data. Complementary analyses were made on 1 144 selected old samples and close to 2 000 new samples were collected and assayed.

Within the Industrial Minerals component the existing data were collected, evaluated and compiled into database. Field checking, sampling and laboratory testing (over 100 samples) was carried out on those deposits with the greatest potential.

A map of industrial minerals presenting over 350 deposits was prepared together with another map outlining the high priority areas for industrial mineral commodities. The final results and technical reports as well as the Annual Review of Industrial Minerals in Mozambique were compiled.

Espoo, June 2, 2008

Yrjö Pekkala, Tapio Lehto, Hannu Mäkitie

INTRODUCTION TO GTK PROJECTS IN MOZAMBIQUE 2002–2007

by
Yrjö Pekkala, Tapio Lehto & Matti. I. Lehtonen

Pekkala, Y., Lehto, T. & Lehtonen, M. I. 2008. Introduction to GTK projects in Mozambique 2002–2007. *Geological Survey of Finland, Special Paper 48*, 7–22, 3 figures.

During 2002–2007, Mozambique was the most important target country within GTK's international projects with a total value of €7.9 M. Geological mapping was part of Geological Infrastructure Development Program, a component in the World Bank and NDF financed Mineral Resources Management Capacity Building Project.

The mining policy of the Government of Mozambique focuses on the promotion of private investments to develop the mining sector, based on the favourable geological environment and mining potential of the country. As part of this policy, the Ministry of Mineral Resources (MIREM), through the National Directorate of Geology (DNG), intends to develop the geoscientific infrastructure of the country in support of mining investments promotion as well as sustainable social and economic development. The availability of basic geological information is an important parameter in promoting investments as well as an essential tool for planning the construction of infrastructure and for predicting natural disasters.

The GTK Consortium (GTK as the leading partner together with ITC the Netherlands, SGU Sweden, GEUS Denmark and Gondwana Lda Mozambique) was responsible for projects that produced geological and mineral resources maps covering an area of 480 000 sq km, which is about 60% of the total area of Mozambique (801 590 sq km). The "Geochemical and Industrial Mineral Surveys" project involved the compilation of all geochemical surveys carried out in the country and followed these up with new targeted surveys to identify areas with mineral potential for exploration. The evaluation of industrial minerals and construction materials in the whole of Mozambique will strengthen the basis for the improvement of infrastructure.

Key words (GeoRef Thesaurus AGI): areal geology, bedrock mapping, geochemical surveys, mineral resources, geologic maps, programs, Mozambique.

Geological Survey of Finland, P.O. Box 96, FIN-02151 Espoo, Finland

E-mail: yrjo.pekkala@gtk.fi, tapio.lehto@gtk.fi

PROJECT DESCRIPTION

The mining policy of the Government of Mozambique focuses on the promotion of private investments to develop the mining sector, based on

the favourable geological environment and mineral potential of the country. As part of this policy, the Ministry of Mineral Resources (Ministério dos Re-

curso Mineralis, MIREM), through the National Directorate of Geology (Direcção Nacional de Geologia, DNG), fosters the development of the national geo-scientific infrastructure in support of mining investment promotion and the sustainable social and economic development of the country. The availability of basic geological information is an important parameter to promote investments as well as an essential tool for planning the construction of infrastructure and for natural hazards mitigation.

Mozambique has made great efforts to develop the basic geo-scientific infrastructure of the country. Geological mapping and extensive geochemical and geophysical surveys have been carried out since independence. The archives of the DNG contain an impressive wealth of geo-scientific information. However, most of this information is now outdated in reference to the technology used and the geological concepts supporting mineral exploration. Moreover, the geological mapping carried out in the decade before independence (1975) and during the period of civil strife was limited by the

difficulties in carrying out fieldwork. Therefore, it is of utmost importance to complete and update the national geo-scientific infrastructure. The Government of Mozambique has therefore implemented the **Mineral Resources Management Capacity Building Project (MRMP)**, funded by the World Bank (IDA, AfDB, NDF). Within this major international project, the GTK Consortium was awarded three important components: Geological Mapping LOT 2 and LOT 3 and Geochemical and Industrial Mineral Surveys

The main objective of the country-wide mapping programme was to revise previous maps and unpublished mapping results in certain areas and to upgrade the quality of geological maps in others, to provide consistent coverage in terms of quality throughout the Mozambican territory. The geological mapping was based on a modern approach resolving stratigraphic and structural problems and providing good geochronological control data. The following papers present the activities and main results achieved in these studies.

LOT 2

The sub-component Geological Mapping – LOT 2 was a part of the Mineral Resource Management Capacity Building Project, Component 2: Geological Infrastructure Development Project in the Republic of Mozambique (GIDP), financed by the Nordic Development Fund. LOT 2 geological mapping was assigned to the GTK-ITC-Gondwana-SGU Consortium¹, hereafter referred to as the GTK Consortium. The Contract (No. 02/QCBS/B.2.2/MIREME-UCPM/2002) was signed in Maputo on 17.10.2002 by H.E. Castigo Langa, Minister of Mineral Resources and Energy, and Prof Gabriel Gaál, Research Director, Geological Survey of Finland (GTK). In December 2003, the LOT 2 Extension, covering approximately 50% of three 1:250 000 scale maps in the Province of Zambézia, was added to the original LOT 2 Contract. The LOT 2 Extension Contract was signed in Maputo on 9.1.2004 by Mr Elias Daudi, National Director of Direcção Nacional de Geologia (DNG), and Dr Yrjö Pekkala, Assistant Director (GTK). In this connection the reporting schedule was also revised and draft final products were to be submitted for review in the beginning of July 2006 and the final products by the end of November 2006.

The main task of the GIDP was to re-map, upgrade and improve existing geological maps in order to create a comprehensive and uniform coverage



Fig. 1. GTK mapping areas in Mozambique: LOT 2 and LOT 3 areas and their extensions.

of geological maps for Mozambique (Fig. 1). The objective of the LOT 2 Geological Mapping was to re-map and improve existing maps at the scale 1:250 000 of the Tete, Manica and Sofala provinces in NW Mozambique, as well as to map a number of selected areas with mineral potential within the same provinces at the scale 1:50 000. During the project the number of map sheets to be produced at the scale 1:250 000 was agreed to be 14 due to the combination of part sheets. The Extension Area was to be presented in three separate map sheets, also covering the Phanerozoic Formations, included in the LOT 3 Extension Contract. The agreed number of map sheets at the scale 1:50 000 was 20, distrib-

uted between three areas: Fíngoè, Changara and Manica.

The LOT 2 is bordered in west by Zimbabwe, in north by Zambia and in northeast by Malawi. The southern margin of the area is the 20° south latitude and the eastern margin the 35° east longitude. The Extension Area is located between the 35° east longitude and the Indian Ocean and latitudes 17° S and 18° S. The total LOT 2 mapping contract covered about 185 000 km².

¹ GTK: Geological Survey of Finland (leading partner) – ITC: International Institute for Geo-information and Earth Observation, the Netherlands – Gondwana: Mozambican geological consultancy partnership – SGU: Geological Survey of Sweden

Organization

The responsibilities in the project were divided between the Consortium partners as follows:

GTK: Management, financial follow-up, map production, interpretation of airborne geophysics;

ITC: Remote sensing with satellite images (Landsat and Aster), processing and interpretation, airborne geophysics to support field mapping and map interpretation, topographic baseline data;

GTK-Gondwana Lda-SGU-ITC: Geological mapping;

GTK-Gondwana Lda: Mineral occurrences, procurement and logistics.

Personnel involved in LOT 2, starting with the data collection, compilation and preliminary map interpretations followed by fieldwork and finally by the preparation of geological and mineral occurrence maps, map explanations and the various databases, were as follows:

- Management and reporting: Yrjö Pekkala, Tapio Lehto, Markku Tiainen (GTK), Elias Daudi, National Director of Direcção Nacional de Geologia (DNG)
- Geological Mapping: Matti Lehtonen (team leader), Tapio Koistinen, Hannu Mäkitie, Tuomo Manninen, Esko Korkiakoski, Saku Vuori, Toni Eerola (GTK), Christer Åkerman, Bosse Gustafsson (SGU), João Marques, Reinaldo Gonçalves, Maurizio Ferrara, Mário Deus, Amad Mamad (Gondwana), André Tahon, Phil Westerhof (ITC)

- Mineral deposits: Tapio Lehto, Esko Korkiakoski, Yrjö Pekkala, Tapio Kuivasaari (GTK) Reinaldo Gonçalves (Gondwana)
- Data management: Markku Tiainen, Antti Kahra (GTK)
- Databases: Olli Rantala, Antti Kahra, Tapio Lehto, Esko Korkiakoski, Jari Väättäinen, Marita Ranta-Pantti (GTK)
- Map production: Olli Rantala, Antti Kahra, Markku Tiainen, Eira Kuosmanen, Hilikka Saastamoinen, Merja Janhila, Anneli Lindh, Hanna Virkki, Riikka Koskinen, Mirjam Ajlani, Helena Saarinen (GTK)
- Processing and interpretation of remote sensing and geophysical data: Ernst Schetselaar, Tsehaie Woldai, Sally Barritt (ITC), Tapio Ruotoistenmäki, Hilikka Arkimaa (GTK)
- Topographic data: Markku Tiainen, Antti Kahra, Eira Kuosmanen, Tuomo Manninen (GTK)
- Geological explanations: Phil Westerhof (ITC), Matti Lehtonen, Tapio Koistinen, Hannu Mäkitie, Tuomo Manninen, Saku Vuori, Yrjö Pekkala, Tapio Lehto, Irmeli Mänttari (age determinations) (GTK), João Marques (Gondwana)
- DNG geologists and technicians involved in LOT 2 training and fieldwork: Grácio Cune, Olavo Deniasse, Sérgio Fernando, Rogério Matola, Hilário Mavie, Inácio Saranga, Celestino de Sousa, Gus-todio Cornélio, Ernesto Correia, Abdul Faquir, Vittorino Garife, Victorino Joaquim, Jose Nampulula, Viriato Nhampula, Luis Saunda, Ussene Vasco Ussene (DNG)

LOT 3

Within the framework of the Mineral Resource Management Capacity Building Project (Republic of Mozambique), Component 2 (Geological Infrastructure Development Project), financed by the Nordic Development Fund, the Sub-Component Geological Mapping – LOT 3 was assigned to the GTK-ITC-Gondwana-GEUS Consortium, hereafter referred to as the GTK Consortium². The contract for LOT 3 geological mapping was signed in Maputo on 12.9.2003 by H.E. Castigo Langa, Minister of Mineral Resources and Energy, and Prof Gabriel Gaál, Research Director, Geological Survey of Finland. The contract for the LOT 3 extension was signed in Maputo on 9.1.2004, by Mr Elias Xavier Félix Daudi, National Director of Geology (DNG), and Dr Yrjö Pekkala, Assistant Director of Geological Survey of Finland (GTK).

The objective of the project was to produce modern upgraded geological maps in digital format for

all 1:250 000 scale map sheets of southern and central Mozambique (Fig. 1). The existing mapping situation of the LOT 3 area before the project was that good quality geological maps at the scale 1:250 000 had been published from southern and south-eastern part of the area, whereas the western part was lacking geological maps of that scale. The Geological Map of Mozambique at the 1:1 M scale was the only published map from that part of Mozambique.

The geological mapping of LOT 3 was carried out by four organizations: GTK, ITC, GEUS and Gondwana Lda. The responsibilities for various tasks were shared between the partners according to the resources, expertise and personnel involved.

² GTK: Geological Survey of Finland (leading partner) – ITC: International Institute for Geo-Information and Earth Observation, the Netherlands – Gondwana Lda: Mozambican geological consultancy partnership – GEUS: Geological Survey of Denmark and Greenland.

Organization

GTK was in charge of the overall management, coordination, geological mapping, data management, map production, final products and reporting. ITC's main responsibility was remote sensing and the compilation of preliminary geological maps. GEUS took care of the preparation of simplified topographic maps, while Gondwana Lda participated in geological mapping, mineral resources assessment and logistics in Mozambique. The activities carried out within the project were subdivided into three major phases:

- 1) Data gathering and preparation;
- 2) Geological review and compilation of the map data;
- 3) Verification and final digital products.

This division into three phases was defined in the TOR document. However, many important activities, such as map production and data management, overlapped and continued throughout the project. The activities of the project were organised to be carried out by teams with different expertise, each team having clearly defined roles in the overall process:

- Management and reporting: Yrjö Pekkala, Markku Tiainen, Tapio Lehto (GTK), Elias Daudi, National Director of Direcção Nacional de Geologia (DNG)
- Geological Mapping: Hannu Mäkitie (team leader), Tuomo Manninen, Saku Vuori, Toni Eerola (GTK),

João Marques, Maurizio Ferrara, Amad Mamad (Gondwana), Robbert Rutten (ITC)

- Mineral deposits: Tapio Lehto, Yrjö Pekkala, Tapio Kuivasaari (GTK) Reinaldo Gonçalves (Gondwana)
- Data management: Markku Tiainen, Antti Kahra (GTK)
- Databases: Olli Rantala, Antti Kahra, Tapio Lehto, Esko Korkiakoski, Jari Väättäinen, Marita Ranta-Pantti (GTK)
- Map production: Olli Rantala, Antti Kahra, Markku Tiainen, Eira Kuosmanen, Hilikka Saastamoinen, Merja Janhila, Anneli Lindh, Hanna Virkki (GTK)
- Processing and interpretation of remote sensing and geophysical data: Ernst Schetselaar, Tsehaie Woldai, Sally Barritt (ITC), Tapio Ruotoistenmäki, Hilikka Arkimaa (GTK)
- Topographic data: Willy Weng, Björn Hermanssen (GEUS); Markku Tiainen, Antti Kahra, Eira Kuosmanen, Tuomo Manninen (GTK)
- Geological explanations: Phil Westerhof (ITC), Hannu Mäkitie, Tuomo Manninen, Saku Vuori, Yrjö Pekkala, Tapio Lehto, Irmeli Mänttari (age determinations) (GTK), João Marques, Maurizio Ferrara (Gondwana)
- DNG personnel involved in training and field-work were: Vladimiro Manhiça, Adriano Sérvano, Rogério Matola, Inácio Saranga, Hilário Mavie, Vittorino Garife and Carlos Pambo

GEOCHEMICAL AND INDUSTRIAL MINERAL SURVEYS (GIM)

The contract for the Geochemical and Industrial Mineral Surveys (GIM) project was signed on 12 October 2004 in Maputo by H.E. Mr Castigo Langa, Minister of Mineral Resources and Energy (MIREME) and Dr Yrjö Pekkala, Assistant Director of Geological Survey of Finland (GTK), the representative of GTK Consortium. The Project started officially after the advance payment was received from the African Development Bank (Credit no 3486/MOZ) on 14 March 2005.

The consultant received the Certificate of Compliance for the first GIM Action Plan on 28 April 2005. The updated Action Plan for 2006 was presented in the Annual Report. Concerning the general timeframe of the project, Mr Adeniji, AfDB Project Leader, confirmed in a meeting in Maputo on 7.12.2005 the extension of the project until the end of October 2007.

The main objective of the project was to train the staff of the National Directorate of Geology (DNG), the National Directorate of Mines (DNM), and of the Regional Offices in various geochemical and industrial mineral survey activities to increase their level of professional knowledge and experience.

To achieve the objectives, the GIM project was in close collaboration with other activities in the Geological Infrastructure Development Programme (GIDP), especially with the Geological Mapping projects and with the implementation of the Mineral Information System (MIS). In practice, the objectives were achieved through on-the-job training and close, continuous collaboration with the assigned counterparts in all activities of the project. The training of the DNG personnel was arranged as special courses and workshops in Mozambique and overseas and as continuous on-the-job practice defined by the training plan.

Organization

GTK Consortium personnel and staff of DNG (hereafter the Client) active in the GIM project were:

- Management and reporting: Yrjö Pekkala, Tapio Kuivasaari, Esko Korkiakoski, Tapio Lehto (GTK), Elias Daudi, National Director of Direcção Nacional de Geologia (DNG)
- Geochemistry: Esko Korkiakoski, Reijo Salminen (GTK)
- Industrial mineral deposits: Yrjö Pekkala, Tapio Kuivasaari, Tapio Lehto (GTK), João Marques, Reinaldo Gonçalves, Mário Deus (Gondwana),
- Databases: Olli Rantala, Antti Kahra, Esko Korkiakoski, Tapio Kuivasaari, Tapio Lehto, Jari Väättäinen, Marita Ranta-Pantti (GTK)
- Map production: Olli Rantala, Antti Kahra, Markku Tiainen, Eira Kuosmanen, Hilkka Saastamoinen, Merja Janhila, Anneli Lindh, Hanna Virkki, Mirjam Ajlani (GTK)
- DNG personnel involved in training and fieldwork: Vicente Manjate, Salomão Mujui, Celestino de Sousa, Viriato Nhampula, Mário Saveca, Horácio Mavie, Moisés Banze, Óscar Bato, Victorino Garife, Jeque Júnior, Arlindo Langa, Teotónio Cau (Geochemical surveys) and Carlos Dinis, Carlitos Almeida, Fátima Chaúque, Zaqir Issufo (Industrial Mineral Survey)

GENERAL GEOLOGY

History and synthesis of previous work

Holmes (1918) published the first description on the general geology of Mozambique. Other pioneer studies include those by Anthoine & Dubois (1925) and Andrade & de Freire (1929). Geological investigations continued during Portuguese colonial rule (Longyear Company 1955a,b; Freitas 1957, 1959), culminating with a monograph on the geology of Mozambique by Afonso (1976). Since independence in 1975 the DNG has launched various geo-scientific

programmes in collaboration with foreign and international organisations, including the BRGM (France), Bulgargeomin (Bulgaria), Aquater S.p.A. (Italy), Hunting Geology & Geophysics Ltd (UK) and UNDP. These programmes have mainly been in the fields of regional geochemistry and airborne geophysics.

Between 1981 and 1984, Hunting Geology and Geophysics Ltd initiated a new phase of geologi-

cal investigations (Hunting 1984). They carried out a comprehensive mineral exploration and reconnaissance geological mapping project in co-operation with DNG, covering Tete Province and parts of Manica, Sofala and Zambézia Provinces. The project was successful in setting the geological context for known mineral deposits in large areas of basement rocks, establishing an inventory of mineral occurrences and in defining priorities for future follow-up work.

At approximately the same time (1980–1984), the French BRGM surveyed the northern part of Mozambique, resulting in novel proposals concerning the existence of allochthonous units in the Mozambican Belt. The survey further resulted in the publication of a new geological map of Mozambique (scale 1:1 M) that also revealed new insights into the geology of the Tete area (Pinna *et al.* 1986, 1987, Pinna & Marteau 1987). An essential difference with former studies was the general acceptance of geologic-tectonic rejuvenation of almost all rock sequences. The main part of the crystalline basement, including the mafic to ultramafic intrusions, i.e., the Atchiza, Nhantreze and Tete Suites were shifted from the Neoarchaeo/ Palaeoproterozoic to the Mesoproterozoic/ Neoproterozoic in the stratigraphic column.

According to the BRGM map, the crystalline basement was subdivided into three major age groups:

- Archaean and Palaeoproterozoic units along the Zimbabwean border, composed of greenstone belts and a granite-gneiss terrains.
- Mesoproterozoic-Neoproterozoic (Irumide and Mozambican Tectonic Cycles) units that were subdivided into two parts:
 - Orogenic units that were formed at the end of the Precambrian B and the beginning of the Precambrian A (*sensu* BRGM map, 1987), corresponding to a projected elonga-

tion of the Irumide Belt of Zambia and Congo (1300 Ma) and subjected to Mozambican tectogenesis (1100 – 850 Ma). The Mozambique Belt was assigned to these units and indicated on account of ages of the magmatic sequences (charnockites, enderbites, anorthosites at 1070 – 900 Ma, and migmatites and granitoids at 1100 – 900 Ma).

- Metamorphic supracrustal sequences – granulites and (blasto-)mylonites at 1000 ± 150 Ma – that include allochthonous as well as autochthonous complexes.
- Late Neoproterozoic units (Pan-African Tectonic Cycle, 850 – 450 Ma, as well as the Katangan Tectonic Cycle, 850 – 600 Ma), marked by intensive tectonism, followed by Pan-African intrusions (500 ± 100 Ma).

The BRGM map provides the most important source for the stratigraphic sub-division of the rock units that underlie the territory of Mozambique. The ‘Provisional Stratigraphic Scheme of Mozambique’ (Lächelt *et al.* 1997) and the ‘Stratigraphic Correlation Scheme’ compiled on behalf of the SADC countries (Hartzer 1998) mainly follow the exposition of the 1987 BRGM map. A review of the mineral resources of Mozambique is contained in Afonso & Marques (1993) and Afonso *et al.* (1998). All existing information on the geology of Mozambique has recently been compiled and reviewed in an impressive monograph by Lächelt (2004).

Reliable radiometric age determinations are critical in understanding poly-metamorphic units and geodynamic development of the Mozambique basement. Prior to the Hunting (1984) and BRGM studies these were overwhelmingly K-Ar and Rb-Sr whole rock ages that gave mixed or, at best, cooling ages. Geochronological methods have since been developed (SHRIMP, U-Pb zircon, Sm-Nd and Ar-Ar) and produce far more reliable results.

The Project approach

The approach of the GTK Consortium to geological mapping was built on the older results, in particular the Hunting (1984) surveys (see also Barr *et al.* 1986, Barr & Brown 1988) and on information that has been drawn from the archives of DNG, from DSGM map data in 1974, from PNUD/DNG maps from 1981 and from ING photo-geological compilations from 1985. Correct litho-stratigraphic nomenclature and codes with formation names as

the principal litho-stratigraphic unit was generally adhered to. However, this requires the selection of a ‘type locality’ with an official topographic name for each formation. Since this task fell outside the mandate of the project, most formation names used here have to be considered as informal and provisional³.

³ In agreement with the Client, ‘Formation*’ will be used to indicate an informal use of the term.

The upgraded geological maps produced by the GTK Consortium have substantially benefited from new GIS-based image processing technology, new airborne data and new geochronological age deter-

minations. The methodology and processes used in the project are described in various articles of this volume.

Overall geological setting

The crystalline basement of Mozambique belongs to three major ‘building blocks’ or terranes, East, West and South Gondwana, that collided and amalgamated during the Pan-African orogeny to form the Gondwana Supercontinent. Prior to the Pan-African orogeny, each terrane had been affected by a geodynamic development of its own. In the mapping area, the boundary between East and West Gondwana (to form North Gondwana) is seen in the NE corner of the Tete area, where the crystalline rocks with a NNW-SSE trend in the Angónia district are in contact to a crystalline domain with a predominantly WSW-ENE ‘Irumide’ trend in the west. The Sânego Shear Zone represents the boundary between West and South Gondwana in the mapping area (Fig. 2a).

For readers interested in the geodynamic development of Gondwana, good reviews can be found in the following papers: Stern 1994, Hanson *et al.* 1994, Wilson *et al.* 1997, Kröner *et al.* 2001, Grantham *et al.* 2003, Jacobs and Thomas 2004, Johnson and Oliver 2004, Johnson *et al.* 2005 and Grantham *et al.* 2007.

The rocks of the mapping area can be divided in two groups: the crystalline basement of Archaean-Cambrian age and the Phanerozoic cover. The crystalline basement comprises a heterogeneous assemblage of paragneisses, granulites, migmatites, orthogneisses and often metamorphic igneous rocks. The Phanerozoic cover mainly comprises lithologies deposited during the Karoo (Permian-Jurassic), Cretaceous and East Africa Rift Events (Tertiary to Recent). The main stratigraphical divisions are illustrated in Figure 2a-c and are briefly described in the following.

The *Archaean* terrane occupies a zone a few tens of kilometres wide and c. 300 km long next to the state boundary between Zimbabwe, comprising the eastern and northeastern part of the Zimbabwe craton. In addition to dominant TTG gneiss lithology, the Archaean in Mozambique comprises the eastern extensions of the Odzi-Mutare-Manica Greenstone Belt around Manica and the Cronley-Munhinga Greenstone Belt c. 50 km south of Manica. A number of dominantly west vergent tectono- or

lithostratigraphic units have been thrust or deposited on top of the craton margin. These units mainly consist of *Palaeoproterozoic* supracrustal rocks of Rushinga and Gairezi Groups.

The *Mesoproterozoic* supracrustal rocks occupy large areas, especially in Tete Province, north of the Sânego Shear Zone, and are mainly composed of metasediments, quartz-feldspar gneisses and felsic to mafic metavolcanic rocks. All these are variously metamorphosed from low amphibolite to granulite facies and are intruded by felsic plutonic rocks during Grenvillian orogeny (900–1100 Ma). A separate unit of Mesoproterozoic supracrustal and plutonic rocks is the Barué Complex, which is tectonically bound to the Archaean craton in the west and Mesozoic rocks in the east (see Fig. 2a). The Nampula Complex on the eastern side of the Mesozoic rift is considered to correlate with the Barué Complex. A marked Mesoproterozoic gabbro-anorthosite body (Tete Suite) occupies an extensive area around and north of the city of Tete. A subhorizontal basal mylonite zone below the Tete Suite indicates an allochthonous nature and the observed structures demonstrate a northerly origin for the massive.

Neoproterozoic rocks are in a minority in the mapping area. An extensive ~860 Ma old Guro Suite comprises bimodal felsic and mafic intrusive rocks south of Tete, south of the Sânego Shear Zone. A coeval mafic-ultramafic Atchiza Suite is situated in the western part of Tete Province, on the northern side of the Sânego Shear Zone. Late Neoproterozoic to Cambrian Pan-African undeformed granites form isolated bodies in northern parts of the mapping area (Fig. 2a) and in the east, where they intrude the Nampula Complex (Fig. 2c).

The *Phanerozoic* cover is divided into the Karoo Supergroup, Cretaceous continental clastic and (sub-)volcanic formations and the younger East Africa Rift sequence. These rocks have not been affected by penetrative deformation. The Karoo rocks in the mapping area are deposited in graben-type rift structures. The Lower Karoo Group consists of a thick sequence of sandstones and argillites with coal seams close to the base. Bimodal lava flows principally comprise the Upper Karoo Group. The

Cretaceous volcano-sedimentary Lupata Group, terrestrial Sena Formation, carbonatites and associated alkaline rocks generally top the Karoo grabens. The East Africa Rift Sequence, initiating from Terti-

ary continental clastic formations and followed by Neogene volcanic vents, forms the youngest cover together with colluvial and alluvial deposits of the Quaternary.

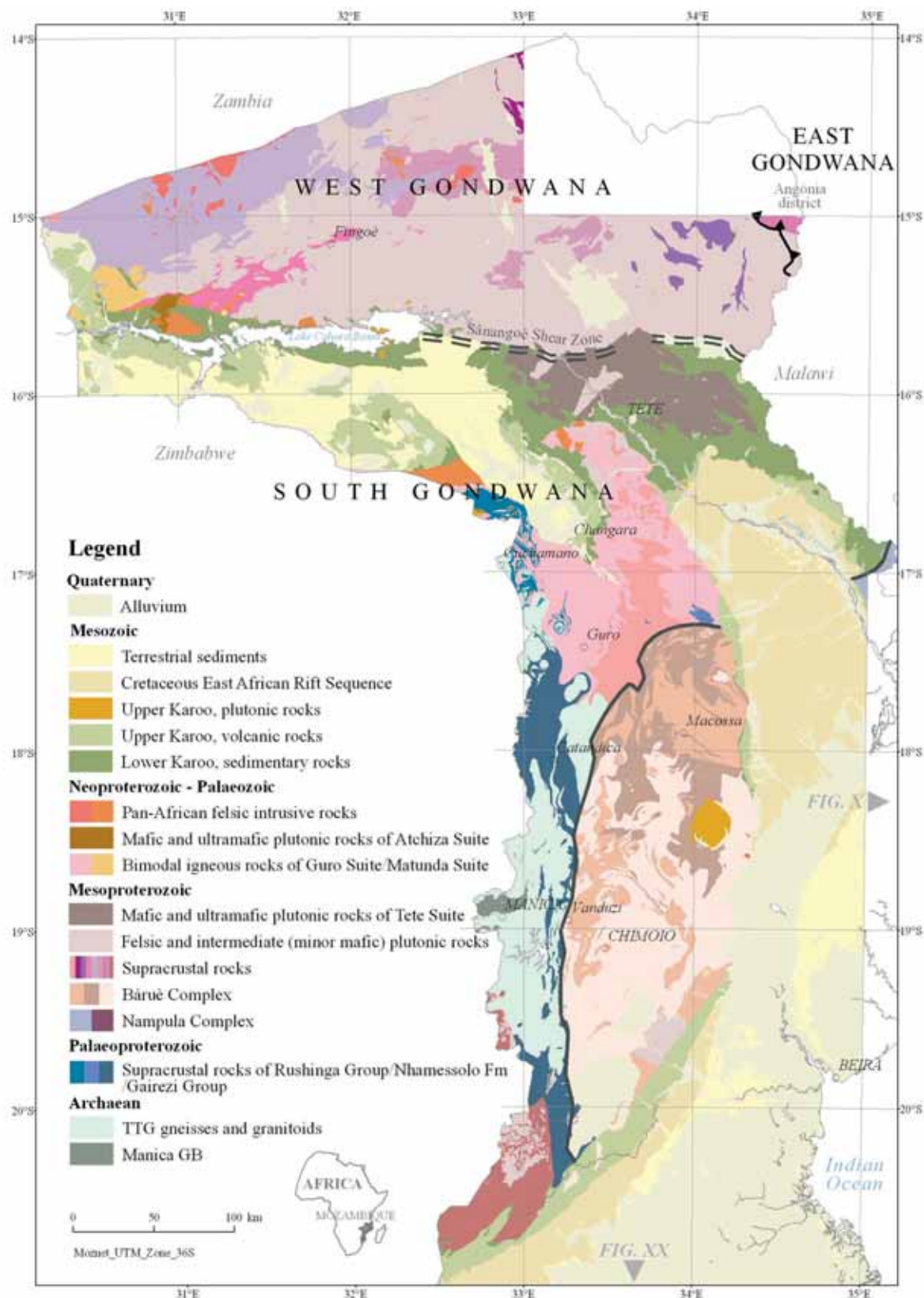


Fig. 2a. General geological map of western Mozambique based on the work of the GTK Consortium.

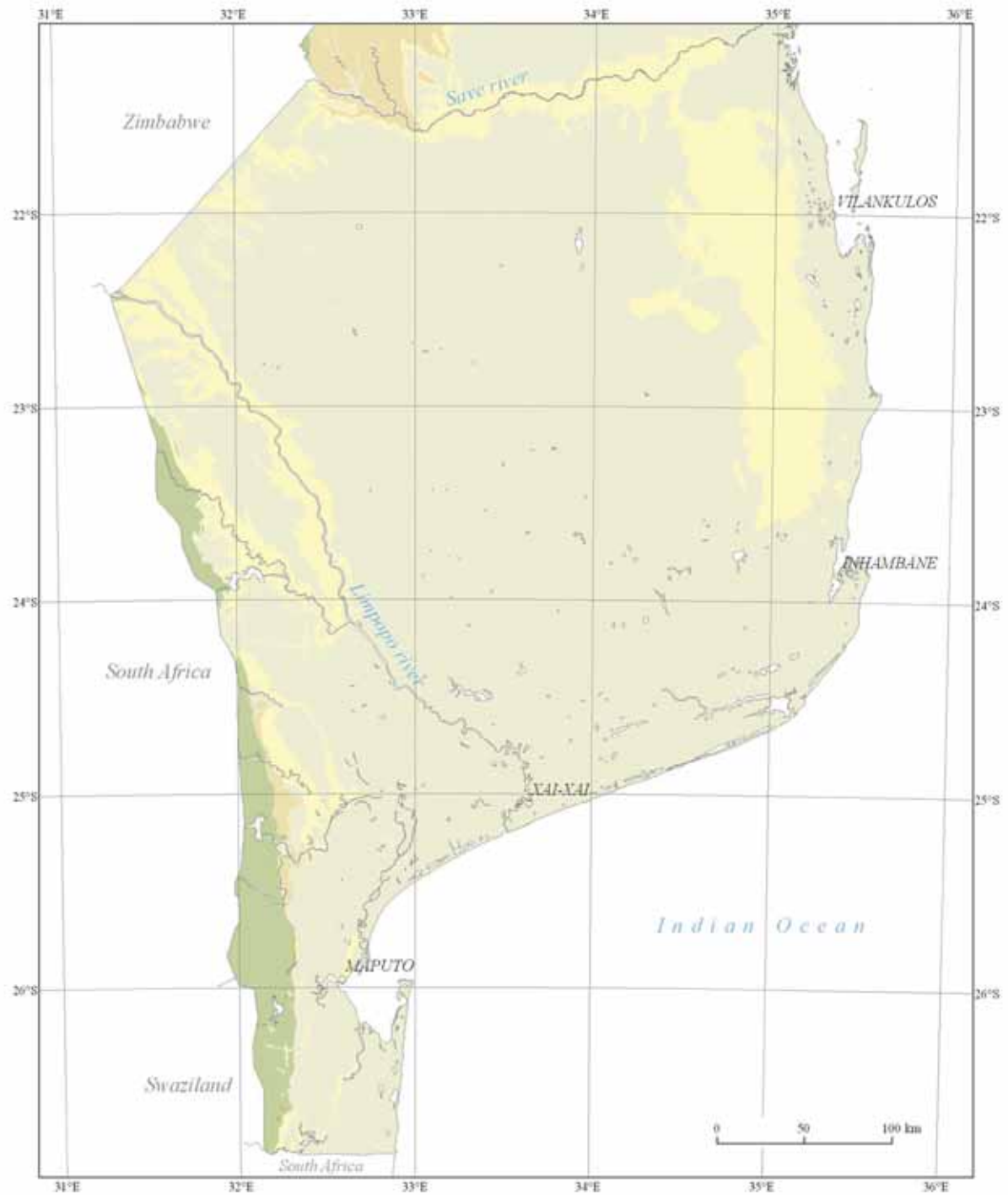


Fig. 2b. General geological map of southern Mozambique based on the work of the GTK Consortium.

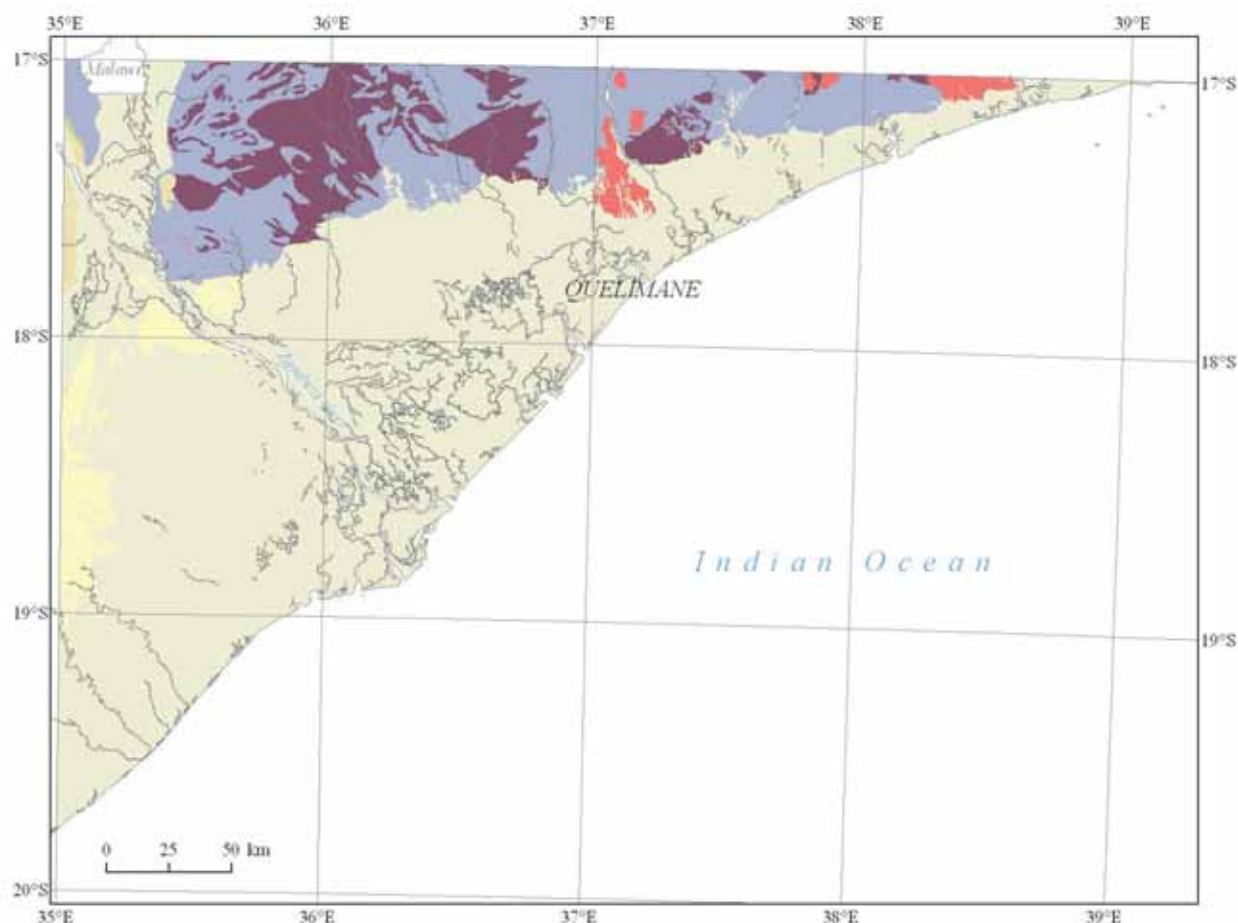


Fig. 2c. General geological map of the Quelimane area, based on the work of the GTK Consortium.

MAIN RESULTS

LOT 2

The geology, lithostratigraphy and mineral resources in LOT 2 are discussed in two separate volumes: Volume 2 and Volume 4, which are a part of a series of Map Explanations covering the GTK Consortium contract area as shown in Figure 3. Volume 2 is bounded by 16° S, 34° E and the international border with Zimbabwe and contains the following square degree sheets (SDS): 1631/1632, 1633, 1634, 1732/1733, 1734, 1832/1833, 1834, 1932/1933 and 1934⁴. Volume 4 deals with the geology of the northern part of Tete Province and covers the following SDS: 1430/1431, 1432, 1530/1531, 1532 and 1533/1534. Each Map Explanation emphasizes certain aspects of the geology of Mozambique. Volume 2 highlights the geodynamic development and mineral potential of the northern and eastern margins of the Zimbabwe Craton and surrounding Proterozoic Fold Belts and the coal potential of the Karoo Basins near Moatize. Volume 4 concentrates on the geodynamic development and mineral potential (coal, gold and base metals) of the northern part

of Tete Province as part of the Irumide Fold Belt.

All locations of observations are in UTM coordinates (WGS 84). Please note that in the area covered by LOT 2 the coordinates refer to the 36 K zone.

Geological mapping of the LOT 2 improved existing geological maps and created a seamless, digital coverage of geological maps at the scale 1:250 000. The geological base of these maps forms a new lithostratigraphic scheme, which is valid for the whole of Mozambique. Data on known mineral occurrences and indications, covering both metallic, industrial mineral and construction material resources have been compiled in a single database. The location, type and major mineral commodities have been plotted on the new geological maps. In addition, 1:250 000 scale maps delineating various mineral resource potential areas have been prepared.

⁴ A degree sheet (1° x 1° or ~ 110 x 110 km) is numbered after the coordinates of the upper right corner. For example, SDS 1834 is located south of 18° S and west of 34° E. SDS = Square Degree Sheet or DS = Degree Sheet.

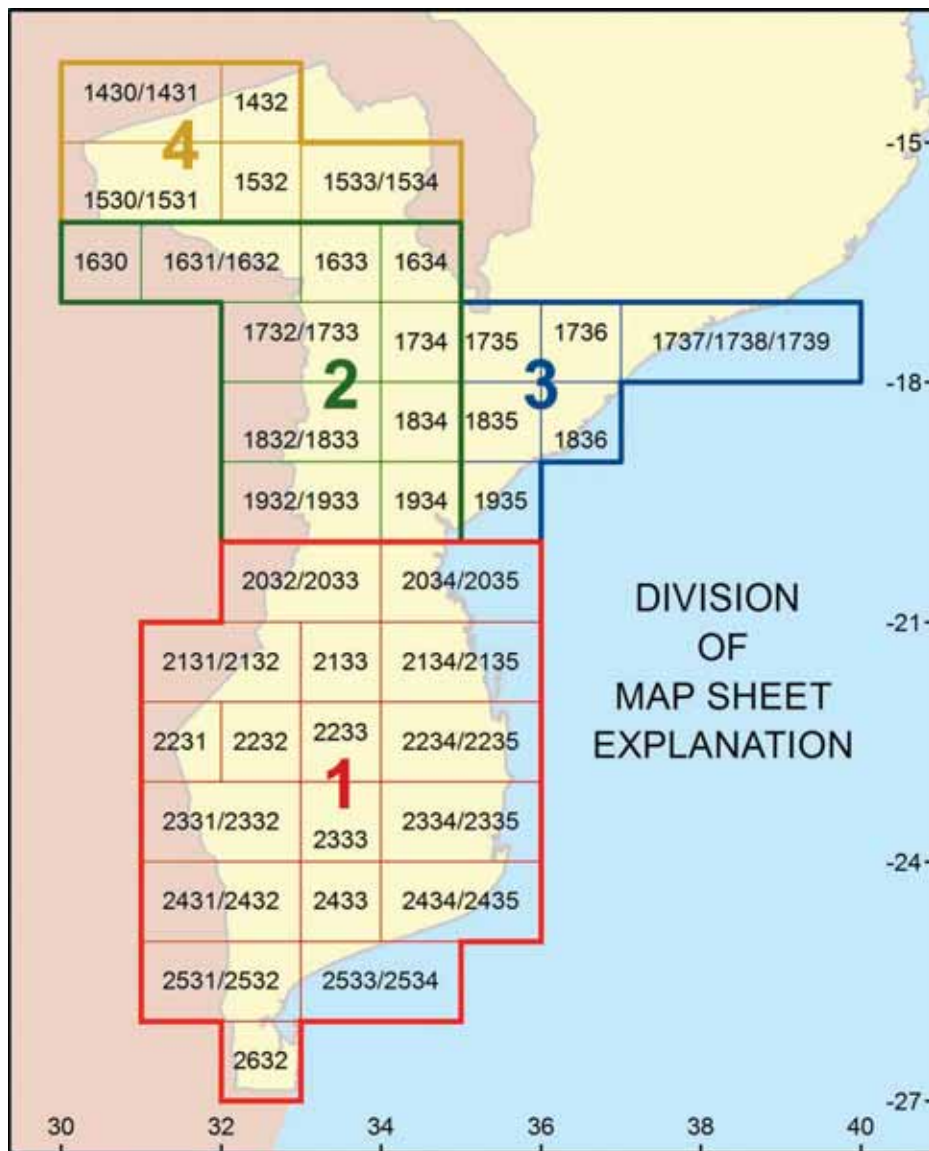


Fig. 3. Map Explanation Volume numbers in LOT 2 (+ Extension) and LOT 3 (+ Extension).

The geology and mineral occurrences in the LOT 2 are presented in 14 maps, at the 1:250 000 scale. Partial coverage with detailed 1:50 000 scale maps has been carried out in three areas with a high mineral resource potential, defined during the project. These areas were Fíngoè, Changara and Manica.

The geology and mineral resources of the Extension area, added to LOT 2 and LOT 3 contracts of the GTK Consortium in December 2003, are presented as three 1:250 000 scale maps and described in map explanation Volume 3.

The new lithostratigraphy, geology and mineral resources assessments are based on the compilation of existing geological maps, mainly from the 1980s, and summary maps from the 1990s assisted by the interpretation of recent satellite image and airborne geophysical survey data. The preliminary maps thus produced from LOT 2 area were verified by about 15 000 documented geological field observations,

matching with 25 000 digital photographs. A total of 36 age determinations as well as about 400 chemical, 800 petrographical and 1200 mineralogical analyses were performed. The data from the observation and sample points are registered in georeferenced databases in ArcGIS compatible format. Altogether, 385 mineral deposits and occurrences from the LOT 2 area were recorded and the data captured in the mineral resources database.

Geologically, the most significant results are the updated lithostratigraphy for Mozambique, more detailed and reliable geological units and especially the georeferenced and digital form of the data, including observations, photographs, analyses and age determinations. This makes data processing, map production and further geological modelling and interpretations much easier and more efficient, provided that there are sufficient human and software-hardware resources in the DNG.

Within the LOT 2 area the lithostratigraphic order of all previous and newly named rock units was established and based on the geological development of Mozambique. The exact location of many lithological boundaries was adjusted and confirmed by field verification. The Archaean terrain was considerably extended into the former Bárue Complex, which was respectively reduced. The allochthonous tectonic structure at the Archaean craton margin was demonstrated and the allochthonous nature of the Tete Suite was also established. The extensive Guro bimodal Suite was recognized as a new, re-interpreted rock unit. The old Luia Group was abandoned and a new subdivision made. The old concept of the existence of pre-Fíngoë granitoids was proved wrong. A part of the Chidue Group carbonate rocks was re-interpreted as carbonatite.

Radiometric age dating (Mänttari, this volume) generated a number of new results, including Archaean ages for granitoids, a Palaeoproterozoic age for the Rushinga and Gairezi Groups, a Mesoproterozoic age for most plutonic rocks of Tete Province, a Neoproterozoic age for the Atchiza Suite, extensive coverage of Pan-African metamorphism within the western part of Tete Province and a Jurassic age for the Gorongoso Suite, among others.

Economically the most important mineral occurrences in the LOT 2 area are the coal seams of the Cretaceous Karoo Formation located in the northern part of Tete Province. In addition, the complex Mucanha-Vúzi basin has several known coal occurrences at present under Lake Cahora Bassa. Current active exploration has commenced to verify the still available and exploitable coal resources.

In addition to coal deposits, two major Cretaceous carbonatite intrusions have been identified in the Tete area. Cone Negose has phosphate-rich rocks at its core bearing pyrochlore, monazite, barite and fluor-apatite. Another large carbonatite body

is formed by the Mt Muande - Mt Fema deposits containing carbonate, magnetite and apatite rich lenses and layers in the mylonitic contact zone between the Tete Suite and the Mussata porphyritic biotite granites.

Concentrations of gold, copper and iron can be found in the hydrothermally altered shear zones intersecting the supracrustals of the Fíngoë Supergroup. Banded iron formations with low grades of gold and sulphides are common in the mafic and pyroclastic volcanics in the lower part of the Fíngoë Supergroup. In the Fíngoë area some pegmatites, belonging to the Mesoproterozoic Marrupa Complex with even-grained granites and lenses of biotite garnet gneisses belonging to the Malowera group, are mined for blue beryls.

The Archaean Macequece and Vengo Formations of the Manica Greenstone Belt host a good potential for gold, copper, nickel, asbestos and iron ore resources. Lode and placer gold deposits have been mined for decades in this region. Small, good quality bauxite deposits are mined at Moriangané in Manica. Other bauxite occurrences are found in Mt Salambidua in Tete Province. The metasediments of the Gairezi Group and the Umkondo Supergroup along the border with Zimbabwe host deposits of iron, copper and limestone (marble). Fluorite occurs in Mesozoic fractures in association with the rift evolution and in carbonatite intrusions, e.g. Mt Muambe, SE of Tete. The Tertiary Cheringoma and Jofane Formations contain large resources of limestone, halite and gypsum.

Major zones of interest for mineral exploration within the LOT 2 area are the Manica greenstone belt (gold, copper, nickel), the Tete Gabbro-Anorthosite Suite (iron, titanium, apatite) and the Moatize sub-basins (coal). More details on the various geological and mineral resources within the LOT 2 area are presented by Lehto and Gonçalves in this volume.

LOT 3

Field verification and mapping of the LOT 3 area and its extension covered an overall area of 259 000 km² and extended over 36 map sheets at the 1:250 000 scale. Altogether, 3729 GPS-controlled field observations with digital photographs were entered into observation and image databases. Laboratory studies comprised petrophysical determinations of 700 samples, 37 chemical assays, petrographical studies of 95 thin sections, 200 microprobe analyses and two radiometric U-Pb age determinations. Petrophysical determinations, including magnetic

susceptibility and density, were carried out from most of the archived rock samples.

The previous 1:250 000 geological maps available from the LOT 3 area were mostly printed maps (Serviços de Geologia e Minas) from the 1950s and 1960s. Moreover, some Precambrian areas were mapped by Hunting (1984). These old maps covered the southern, eastern and northern part of the LOT 3 area. When considering the existing geological maps of the LOT 3, the GTK Consortium found the general outlines of the geology of Precambrian and

Jurassic crystalline rocks as well as most of the Cretaceous-Tertiary sediments to be sufficiently accurate and broadly in accordance with new geophysical and satellite image data. However, no maps were available from large areas known to be occupied by the Karoo volcanic rocks near South African border, in western Mozambique.

Furthermore, a significant majority of the LOT 3 is covered by Quaternary deposits that overlie the rocks of the Mozambique Basin. This, together with the limited time for fieldwork, did not allow many possibilities for major new discoveries. However, considerable work was performed in updating, digitizing and georeferencing the available data. The fieldwork was focused on the Precambrian and Jurassic rocks, which were moderately exposed in elevated areas. A comprehensive description of the geology is given in Map Explanations, Volume 1 and 3 (Fig. 3), covering the rocks/formations from the Precambrian, Jurassic, Cretaceous-Tertiary to the Quaternary.

Altogether, about 120 mineral resource occurrences were captured within the LOT 3 area. The deposits are shown in geological maps with the symbols applied in the “International Metallogenic Map of Africa, 2002”. In the LOT 3 area the most economically interesting mineral deposits are the gas occurrences in Pande and Temane fields in Inhambane as well as the heavy mineral sands in paleodunes in Gaza and Zambézia Provinces. The increasing demand for construction materials has directed attention to many rhyolite quarries and to gravel, sand and clay pits, especially in Maputo Province, where construction of all kinds is very active.

Detailed descriptions of all mineral occurrences, their potential and recommendations for further exploration in the LOT 3 are provided in the Map Ex-

planation Volume 1 and partly in Volume 3, as well as in the Mineral Resources Potential chapter of this volume.

The products of the LOT 3 Project comprise: digital databases, geological and mineral resources maps, geological explanations and a final technical report. Digital data were collected on an integrated DVD presenting the products of LOT 2 and LOT 3 projects. Digital databases comprise the observation and mineral databases in MS Access, an image database in Imatch, the results of laboratory studies in MS Excel tables and geological observations in an Esri Geodatabase and MS Access observation database.

The final geological maps have been submitted to the Client as paper prints, print-ready PDF files and as seamless GIS data. The GIS data have also been delivered to the MIS project to be arranged into the digital map database of DNG. The Geological Map Explanation, Volumes 1 and 3, and the Final Technical Report have been prepared as paper prints and in digital PDF format.

In addition to the final products specified in the contract, the original and processed geophysical images and satellite images, already submitted to the Client during Phase II, have also been delivered together with all final products on a removable hard disk. This external memory includes all relevant mapping and map production data, final products, map explanations and the final technical report of LOT 3 and LOT 2.

The final products, general information and information on all data used in the geological interpretation process have been collected onto an integrated DVD, which can be used to present the results of the project and to search for all the products and data prepared by the project.

Geochemical surveys

The results and various activities of the geochemical surveys are described in a separate article of this volume. The field procedures are described in detail in the Geochemistry Field Manual. The results and data interpretation are included in the separate Final Report: Results of the GIM Geochemical Survey. All existing geochemical data sets were collected and evaluated. The relevant/usable information (meta-data) of each sampling programme, including sampling density, sample media, field methodology and analytical methods, were compiled and transferred to the Survey Information Table (SIT). Selected (typically A0 size) geochemical maps were scanned

at DINACEGA/CENACARTA. The total number of scanned maps exceeded 300. The digital maps were then processed (unified and cropped) with Adobe Photoshop 5.0 (Limited edition). Georeferencing was carried out by the consultant with ArcMap 8.3 using the river systems of the TM satellite images as a basis for correlating the TM images with the geological mapping projects (LOT 1, 2 and 3).

Data capture was carried out by digitizing the sample locations from georeferenced geochemical maps into the ArcView shape files (point type), and calculating the coordinate values, and by capturing and tabulating the analytical data into the tables.

Due to the heterogeneity of the different data sets regarding element combinations, analytical methods, accuracy and other parameters, the data were collected into Analysis Data Tables (ADT).

The *Geochemical Data Base* (GDB) that was created comprised the Survey Information Table (SIT) with general survey specifications (i.e. metadata) and the Analysis Data Tables (ADT), including the actual analytical and coordinate data from different surveys. The GDB fulfils the requirements of MIS compatibility and is the most practical way to process, demonstrate and store the heterogeneous geochemical data.

Result of old surveys

The compiled spatial geochemical data of old regional sampling surveys were classified and plotted as various elementary maps correlated with different geological units verified by new mapping. The integrated geochemical data indicates several potential Au, Zn, Ni and Cu anomalies for future exploration, described in detail in a separate article of this volume.

Re-analysis of old samples

Two major sample sets were located, those of the Hunting team and BRGM. The Hunting team samples, collected in 1981–83, included 7610 un-sieved samples, representing about 5000 different locations. Since the samples were slightly heterogeneous, it was decided that only selected 1144 samples would be re-analysed for Au, Pd and Te by GFAAS at the GTK laboratory in Finland. More than 4000 samples of the BRGM project (1970–72) were also located, but unfortunately only a small proportion of them could be georeferenced on the BRGM field maps and it was therefore decided not to analyze these samples.

When comparing maximum values with medians from the original analytical results of the Hunting Team Survey, it can be noted that Cu (42 x median value) and particularly Ni (190 x median value) are locally distinctly anomalous. Several target areas have high anomalous copper contents, the highest value being 971 ppm related to the carbonatites occurring between the 1046 ± 20 Ma old Chogocoma granite and the Tete Suite.

High nickel contents (maximum 0.42%) are all associated with the Atchiza mafic-ultramafic Suite situated in the western part of Tete Province, north of Lake Cahora Bassa. The soil of the Atchiza area includes the highest Pd (132 ppb) and Co (390 ppm)

values of the whole Hunting Team Survey. However, at least some of the high Ni anomalies can be explained by nickel-bearing silicate minerals, like olivine, in the ultramafic rocks.

The new analysis for Au, Pd and Te of the Hunting Team samples, carried out by the GIM project, indicates that the Zumbo area close to the Zambian border has the most prominent and concentrated Au anomalies of the survey. The highest gold value of 434 ppb has been detected in Mucanhavuzi, east of Atchiza, highlighting this remote area as also being a potential gold target.

Results of new surveys

The Gondola-Nhamatanda area (Inchope), E-SE of Chimoio, was selected for the regional stream sediment survey. The area is known for its Nb-Ta-bearing Sn-pegmatites, and for the Monte Xiluve carbonatite complex as well as for alluvial gold deposits of the Muda River. The sampling area covered about 5 450 km², each cell representing 10 km², and altogether 473 stream sediment samples were collected.

All 473 samples were analyzed by ICP-AES (GTK method 511P) for 30 elements and by XRF (GTK method 175X) for 36 elements, including Nb and Ta, complemented by Au, Pd and Te values defined by GFAAS (GTK method 521U). Additionally, carbon was also defined by a carbon analyzer using GTK method 811L. More details are presented in the article “Geochemical surveys” of this volume.

The detailed follow-up soil survey carried out in 2006 was based on the results of an earlier regional stream sediment survey in 2005. The sampling included five separate areas, four of which were related to anomalous gold values, and one to a previous LKAB study with elevated Sn values. The sampling densities varied in grids from 50 m x 100 m to 500 m x 1000 m. Altogether, 1348 soil samples were collected for analysis.

Analytical procedures and methods were the same multielement-multimethod analysis (XRF/ICP-EAS/GFAAS/carbon analyzer) as for the stream sediment survey. However, XRF was used in Area 5 with earlier indications of tin anomalies.

The analytical data of *stream sediment* samples revealed the median Cu content to be 31 ppm, the maximum value being clearly anomalous at 190 ppm. The comparable values for Zn were 48 and 179 ppm. Sixty four percent of the Au values were below the detection limit of 0.5 ppb and only 5% of the samples were above 2 ppb. Interestingly, the maximum content was markedly high at 2.3 ppm. The major element data demonstrated median con-

tents of 62.6% for SiO_2 , 17.7% for Al_2O_3 , 5.9% for FeO and 2.5% for K_2O .

Economically, the most interesting results of the GIM stream sediment survey were related to gold contents, and several anomalous areas were detected for follow up *soil survey*. The highest gold value (2.3 ppm) was detected in a tributary of the Muda River. On the geological map this anomalous area is related to the Inchope orthogneisses occurring together with siliciclastic metasediments.

The results of the GIM soil survey generally indicated that the content of major ore elements was relatively low. The median values for Cu, Zn and Pb were 15 ppm, 20 ppm and 12 ppm, respectively. The maximum values were 286 ppm for Cu, 116 ppm for Zn and 72 ppm for Pb. As a whole, the gold content was low and only 161 samples out of 1262 had values over 1 ppb. Most of the anomalous values occurred close to Rio Arumua, including the highest content of 1040 ppb.

Industrial mineral survey

The implementation of the Industrial Mineral Survey started with the collection and evaluation of existing relevant data from the archives of the DNG, DNM and various other sources. The data were stored in the Industrial Mineral Database (IMD) in Microsoft Access format compatible with the Mineral Information System (MIS).

Basic information was captured from the explanation booklet of “Noticia Explicativa da Carta de Jazigos e Ocorrências Minerais de Moçambique 1:1 000 000” from 1995. In addition, an unpublished list of deposits and occurrences available at DNG was utilized. Information was collected on the deposit name, location, primary and subsidiary commodities, deposit status and type. A previous mineral data compilation for LOT 2 and LOT 3 was used as a basis for more detailed data compilation from respective reports. Most data originated from DNG reports prior to 1990s, while more recent exploration reports by mining companies are stored in the archives of DNM. From the data capture forms the data were transferred into MS Excel tables and then to the IMD. Data were compiled from a total of 355 deposits and occurrences, including numerous occurrences of construction materials that were visited and recorded during field trips to all provinces. Laboratory studies on 114 collected samples were carried out at GTK, consisting of petrological, chemical and microprobe analyses. XRD determinations were performed on all samples and particle size analysis, brightness measurements and laboratory scale processing tests on selected samples.

Results

The general impression is that Mozambique possesses a wide range of mineral commodities, but the infrastructure (transport, electricity, services) is generally poor. This seriously hampers exploration and especially possible exploitation. In most cases the

exploration carried out on the reported occurrences has been preliminary, without proper geophysics, drilling or testing, and even the location data are often inaccurate. Consequently, estimations on the volume and quality of reserves are often unreliable and the quality tests are mostly lacking. Random chemical analyses are occasionally available, but for most industrial minerals this is not enough to evaluate the economic potential of a deposit.

One practical outcome of the results of the GIM project was the presentation of the preliminary results of the project at the 21st Colloquium of African Geology (CAG21), Maputo in July 2006, with an overview of the status of the mineral resources sector in Mozambique. A compendium was prepared from the presentations of the GIM Workshop in Maputo, 19–21 April 2006 and delivered to the Client as CDs and hard copies. An Industrial Minerals Field Manual was prepared for fieldwork training. Its final version also included appendices detailing the basic facts concerning several major IM commodities.

The digital database with user-friendly input tables created by the project will also guide DNG geologists in storing and updating appropriate data in the DNG network environment after the completion of the project.

Thematic industrial mineral maps covering the whole country were prepared at a compilation scale of 1:500 000, with the topographic and geological base extracted from the databases of the various mapping projects. For selected high priority areas at total of 16 industrial mineral, construction material and dimension stone resource maps at the scale 1:250 000 have been prepared. Predictions for and the potential of 12 commodities are also indicated on these thematic maps.

The final reports of the GIM project are: 1) the Final Technical Report, which summarizes the activities in both components of the GIM project, i.e.

the geochemical survey and the industrial mineral survey, 2) Results of the Geochemical Survey and 3) Results of the Industrial Mineral Survey. Report 3 summarizes the results of the IM survey, provides recommendations for future surveys and defines some areas of potential for IM and construction ma-

terials where follow-up work is justified. Industrial mineral market trends and industrial mineral production and demand are discussed in the “Annual Review of Industrial Minerals in Mozambique”, which is the basis of the chapter “Review of Industrial Minerals” of this volume.

REFERENCES

- Afonso, R. S. 1976.** A Geologia de Moçambique. Notícia Explicativa da Carta Geológica de Moçambique na escala 1 : 2 000 000, 175 p., Serv. Geol. Min., Maputo, Mozambique.
- Afonso, R. S. & Marques, J. M. 1993.** Recursos Minerais da República de Moçambique. Contribuição para o seu conhecimento. Instituto de Investigação Científica Tropical de Portugal and Direcção Nacional de Geologia de Moçambique. 1st Edition, Lisbon, Portugal.
- Afonso, R. S., Marques, J. M. & Ferrara, M. 1998.** A Evolução Geológica de Moçambique. Instituto de Investigação Científica Tropical de Portugal and Direcção Nacional de Geologia de Moçambique. 1st Edition, Lisbon, Portugal.
- Andrade, C. F. De. 1929.** Esboço Geológico da Província de Moçambique. Ministério das Colónias, Imprensa Nacional, 232 p., Lisbon, Portugal.
- Anthoine, R. & Dubois, J. 1925.** Les grandes lignes de la géologie du Zambèze dans l'Est Africain Portugais. C. R. XIII Congr. Géol. Internat. Belgique, 1922, (2), 751–769, Belgium.
- Barr, M. W. C., Downing, K. N., Harding, A. E. & Loughline, W. P. 1986.** Regional correlation near the junction of the Zambezi and Mozambique Belts, East-Central Africa. Unpubl. Rept. 1345/Rel., Instituto Nacional de Geologia, Ministério dos Recursos Minerais, 53 p., Maputo, Mozambique.
- Barr, M. W. C. & Brown, M. A. 1988.** Gabbro-Anorthosite Complexes, Tete Province, Mozambique. Bol. Geol., 41, 7–39, Inst. Nac. Geol., Ministério dos Recursos Minerais, Maputo.
- Freitas, A. J. 1957.** Notícia Explicativa do Esboço Geológico de Moçambique (1 : 2 000 000). Bol. Serv. Industr. Geol., 23, 82 p., Lourenço Marques, Mozambique.
- Freitas, A. J. 1959.** A geologia e o desenvolvimento económico e social de Moçambique. Junta de Comércio Externo, 396 p., Lourenço Marques, Moçambique.
- Grantham, G. H., Maboko, M. & Eglinton, B. M. 2003.** A Review of the Evolution of the Mozambique Belt and Implications for the Amalgamation and Dispersal of Rodinia and Gondwana. – In: Yoshida, M., Windley, B. F. and Dasgupta, S. (eds.), Proterozoic of East Gondwana: Supercontinent Assembly and Breakup. Geological Society of London Special Publication, 206.
- Grantham, G. H., Macey, P., Ingram, B. A., Roberts, M.P., Armstrong, R. A., Hokada, T., Shiraishi, K., Bisnath, A. & Manhica, V. 2007.** Terrane correlation between Antarctica, Mozambique and Sri Lanka: Comparisons of geochronology, lithology, structure and metamorphism. USGS Open-File Report 2007–1047 Extended Abstract 004.
- Hanson, R. E., Wilson, T. J. & Munyanyiwa, H. 1994.** Geologic evolution of the Neoproterozoic Zambezi Orogenic Belt in Zambia. – Journal of African Earth Sciences, 18, No. 2, 135–150.
- Holmes, A. 1918.** The Precambrian and associated rocks of the district of Mozambique. Q. Journal of the Geological Society, London, LXXIV, (1).
- Hunting Geology and Geophysics Limited 1984.** Mineral Inventory Project. Final Report. Unpubl. Rept., Direcção Nacional de Geologia, Maputo, Mozambique, 329 p.
- Jacobs, J. & Thomas, R. J. 2004.** Himalayan-type indenter-escape tectonics model for the southern part of the late Neoproterozoic-early Paleozoic East African-Antarctic Orogen. Geology, 32, (8), 721–724.
- Johnson, S. P. & Oliver, G. J. H. 2004.** Tectonothermal history of the Kaourera Arc, northern Zimbabwe; implications for the tectonic evolution of the Irumide and Zambezi Belts of south central Africa. Precambrian Research, 130, no.1–4, 71–97.
- Johnson, S. P., De Waele, B., Tembo, F., Mapani, B. & Wingate, M. 2005.** Subduction of continental crust during Gondwana amalgamation: Very-high-pressure metamorphism and metasomatism in the Zambezi Belt. Frontier Research on Earth Evolution Report 2002–2004.
- Kröner, A. 2001.** The Mozambique belt of East Africa and Madagascar: significance of zircon and Nd model ages for Rodinia and Gondwana supercontinent formation and dispersal. South African Journal of Geology, Vol. 104, 151–166.
- Lächelt, S., Marques, J. M. & Senvano, A. S. 1997.** Provisional Stratigraphic Scheme of Moçambique. DNG, Maputo and SADC (Hartzer, 1998, Pretoria).
- Lächelt, S. 2004.** Geology and Mineral Resources of Mozambique. DGN, Maputo, 515 p. ISBN 1-919908-52-8.
- Longyear Company 1955a.** Report to the Government of Portugal on the Tete Area. Mozambique-Portuguese East Africa. Vol. 5. Unpubl. Rept., DNG, Maputo.
- Longyear Company 1955b.** Review of the Geology and Mineral Occurrences of Mozambique (Portuguese East Africa), by Alexander Luty-Lutenko. Unpubl. Rept., DNG, Maputo.
- Pinna, P., Marteau, P., Becq-Giraudon, J-F. & Manigault, B. 1986.** Notice Explicative de la Carte Géologique à 1 : 1 000 000 de la République Populaire du Mozambique. Unpubl. Rept., Instituto Nacional de Geologia de Moçambique/BRGM, Orléans, France.
- Pinna, P. & Marteau, P. 1987.** Synthèse géologique du Mozambique. 14th Colloquium of African Geology, Abst., 55.
- Pinna, P., Marteau, P., Becq-Giraudon, J-F. & Manigault, B. 1987.** Carta Geológica de Moçambique, na escala 1 : 1 000 000, Instituto Nacional de Geologia de Moçambique, Maputo, Mozambique.
- Stern, R. J. 1994.** Arc assembly and continental collision in the Neoproterozoic East African Orogen: Implications for the consolidation of Gondwanaland. Annual Revs. Earth and Planetary Science Letters, 22, 319–351.
- Wilson, T., Grunow, A. M. & Hanson, R. E. 1997.** Gondwana assembly: The view from southern Africa and East Gondwana: Journal of Geodynamics, 23, 263–286.

DATA MANAGEMENT AND MAP PRODUCTION IN THE GEOLOGICAL MAPPING PROJECTS IN MOZAMBIQUE

by

Markku Tiainen, Olli Rantala, Antti Kahra & Eira Kuosmanen

Tiainen, M., Rantala, O., Kahra, A. & Kuosmanen, E. 2008. Data management and map production in the geological mapping projects in Mozambique. *Geological Survey of Finland, Special Paper 48*, 23–33, 11 figures.

This paper briefly describes the data flow in the geological mapping projects LOT 2 and LOT 3 in Mozambique, including a short description of the data sets, data management and databases developed and map production in different phases of the project. Both the final digital and paper printed products are described. The products comprised geological and mineral deposit maps as print-ready files, paper prints and GIS map database, mineral deposit database, field observation databases and tables of the results of laboratory studies. All data (250 GB) have been delivered to the Client (Direcção Nacional de Geologia, Moçambique; DNG) on an external disk with an integrated DVD for presentation of the products.

Key words (GeoRef Thesaurus, AGI): geologic maps, bedrock, data management, cartography, data bases, Mozambique.

Geological Survey of Finland, P.O. Box 96, FIN-02151 Espoo, Finland

E-mail: markku.tiainen@gtk.fi

INTRODUCTION

Two geological mapping projects (LOT 2 and LOT 3) covered north-western, central and southern Mozambique (see Fig. 1). The projects comprised the re-interpretation of existing geological data, collection of new data and compilation of new geological maps of the project areas. The activities carried out during the project were subdivided into three main phases:

- 1) Data gathering and preparation of the data;
- 2) Geological review and compilation of the map data; and
- 3) Verification and final digital products.

Most of the project activities, such as map production and data management, were overlapping

and continued throughout the project. The main tasks and products of different phases are described in a data flow chart (Fig. 2). The core of the whole process has been the digital map library (DML) that was continuously updated by new data during the project. The final version of the DML was ready at the end of the project at the same time as the final products were completed and handed over to the Client (Direcção Nacional de Geologia, Moçambique; DNG).

Map production and data management of LOT 2 and LOT 3 projects were coordinated by GTK. Practical work was conducted in three organizations, GTK, ITC and GEUS. ITC was in charge of the processing of remote sensing data and the topo-

graphical base data of LOT 2. Topographical base data of LOT 3 area were prepared by GEUS. The data bases and final geological maps were prepared

by GTK. Details of the databases, maps and map production process are described in the Final Technical Reports of LOT 2 and LOT 3 projects.

MAP PRODUCTION PROCESS

Map production procedure included the design of databases, preparation, digitization, scanning and storage of data as well as processing and interpretation of data and finally map preparation and printing of geological maps. Several versions of preliminary maps have been prepared for fieldwork and evaluation purposes. The total number of final geological

and mineral deposits map products, including English and Portuguese versions, was 144 map sheets, and the total number of printed maps delivered to the client during the project was about 700 prints. The map production team has continually worked in close co-operation with the mapping geologists.

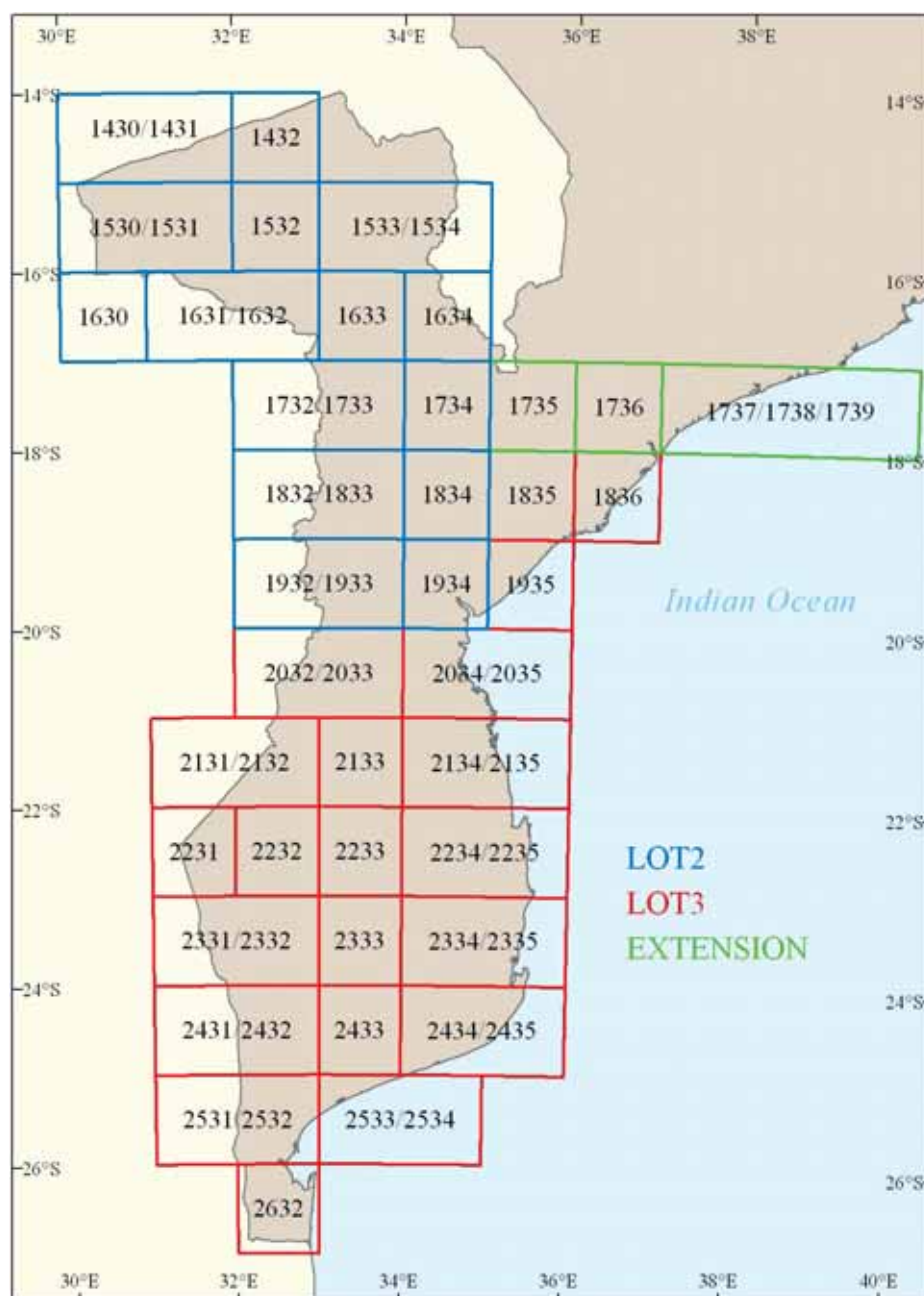


Fig. 1. The mapping area of the GTK Consortium (LOT 2, LOT 3 and LOT 2/3 extension), with an index of the geological map sheets published at the scale 1:250 000.

All digital geological data have been compiled as seamless GIS data from which the printed maps were prepared as square degree sheets, with the standard layout and legend. The final maps include

19 one square degree sheets, 19 double sheets at the scale 1:250 000 and 20 map sheets at the scale 1:50 000 (Figs 1 & 3).

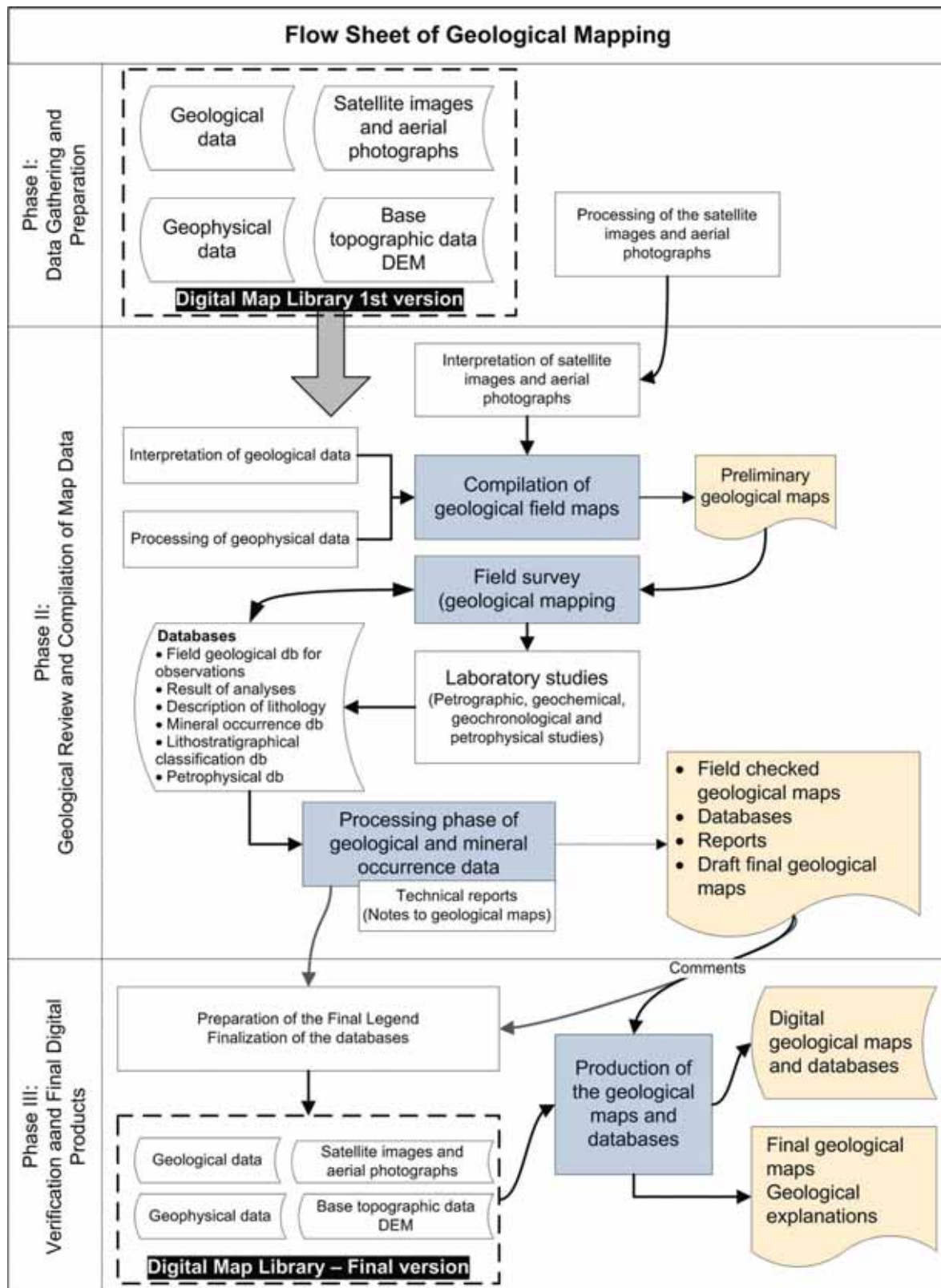


Fig. 2. Flow chart of the data. The preparation and compilation of new products are in grey boxes and the results of the compilation processes are in yellow boxes.

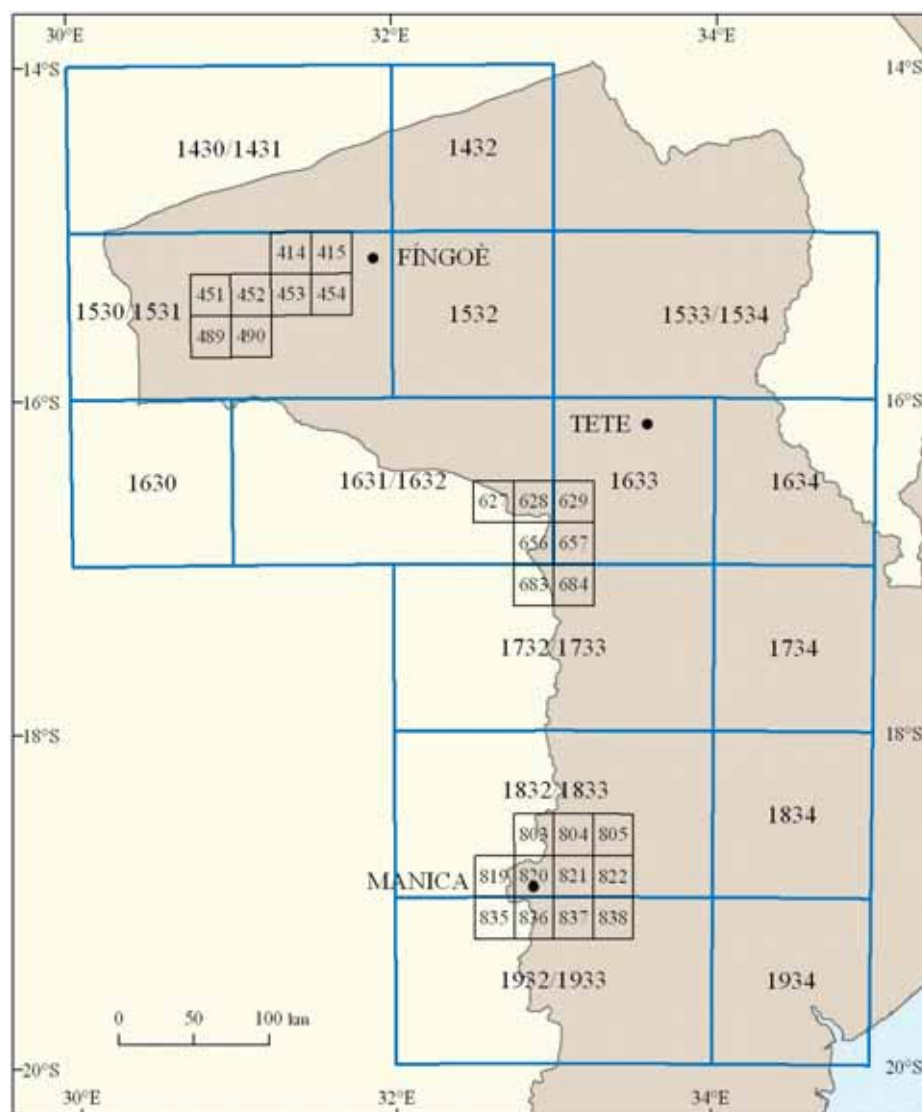


Fig. 3. Detailed geological maps, 20 map sheets in total, including 6 double sheets, were produced at the 1:50 000 scale from Fingoë, Cuchamano and Manica areas.

PRELIMINARY MAP PRODUCTS

Preliminary maps were based on the compilation of existing geological data, aerial photograph interpretation and on the new interpretation of satellite images as well as airborne magnetic and radiometric surveys. The most important source data comprised the following data sets:

1) Geological data:

- 1:1 million scale geological map of Mozambique (scanned);
- Hunting Team geological maps at the scale 1:250 000 (digitised);
- Geological maps of the map series ‘Carteologica de Mozambique na escala 1:250 000’ from the 1950s and 1960s (scanned);

2) Satellite images comprising Landsat ETM 7 imagery and ASTER VNIR scenes;

3) Shuttle Radar Topography Mission (STRM) elevation data;

3) Aerial photographs from selected areas;

4) Airborne geophysical data of Fugro;

5) Mineral resource data from reports; and

6) Topographic paper maps at the scale 1:250 000 (scanned).

Several combinations of different data sets have been prepared to visualise geological features and to support geological interpretation of the mapping areas. The preliminary geological maps were prepared for fieldwork before the field seasons. Details of the geological interpretation procedure are described in the paper by Schetselaar et al. of this volume.

GEOLOGICAL MAPPING, MAP PRODUCTION AND NEW GEOLOGICAL MAPS

The purpose of the geological field work, carried out in Mozambique during 2002–2006, was to check the preliminary geological interpretations and also to resolve the problems that arose during the compilation of preliminary geological maps and to collect samples for laboratory studies. A considerable amount of new geological information was produced, including over 17 000 geological field observations, 28 000 photographs, 350 XRF analyses, 200 microprobe analyses, 38 age determinations and 785 petrophysical determinations. New geological interpretations have also been made during the geological mapping process. All observation data have been stored in MS Access databases and MS Excel spreadsheet tables and delivered to the Client/DNG.

The first and most labour-intensive part of map production process was the preparation of all required data layers. Geological polygon data, based on remote sensing interpretations and new geological observations in the field, were compiled by mapping geologists in co-operation with the GIS geologist. Topographical data were compiled from several sources, partly digitized from topographical paper maps and satellite images. A significant part of the road data were collected by GPS during the field work. Hydro data, such as rivers and lakes, were partly taken from landuse data received through the DNG and partly digitized from topographical base maps and satellite images.

The ArcGIS compatible geological map database includes the following layers:

- Lithostratigraphical polygons with label points;
- Structural lines;
- Observation points;
- Tectonic measurements;
- Sampling points;

- Dating points; and
- Mineral deposits.

Topographical data layers comprised:

- A digital elevation model based on Shuttle Radar Topography Mission (SRTM);
- A simplified topographical base map, including lakes, rivers, roads, railroads, powerlines, contour lines, international boundary, towns, villages, highpoints and mountains.

Map layout and symbology was planned in co-operation with the Client and Consulting engineer (Fig. 4). The legend of the geological maps includes a short description of the geological units, arranged in stratigraphical and age order. Geological profiles were compiled onto four map sheets to explain the geological structure of the most important sections. A digital elevation model was used as one layer in the geological maps to visualize the topography of the map area. Index map and declination information were included on each map layout.

The final geological maps include five geological layers: lithological/lithostratigraphical polygons; dykes and structural lines as polylines; tectonic measurements, dating results and mineral deposit information as points. The final printed map products of LOT 2 and LOT 3 projects comprise five sets of maps: geological maps at the scale 1:250 000 with legend in English and Portuguese, geological maps at the scale 1:50 000 with legend in English and Portuguese; and mineral deposit and potential maps with the legend in English.

The new digital geological and mineral deposit data were prepared as a seamless ArcGIS map database from which the computer printed paper maps and print-ready PDF files were prepared at the end of the project. The geology of the project area was explained in four Map Explanation reports, each comprising an average of 450 pages.

DATABASES

During the project, databases were prepared for geological maps, mineral deposits, field observations and laboratory studies. The geological mapping data have also been stored in ESRI Geodatabase format and the results of laboratory studies in MS Excel tables. Mineral deposit data have been stored in an MS Access database. Digital photographs of the

field observation sites and rock samples are stored in an Imatch [photo/digital image] database.

The information collected on outcrops and in the analysis of samples has been arranged as MS Access databases and MS Excel tables:

- Observation forms, scanned as PDF files;
- Geological observation databases in MS Access format;

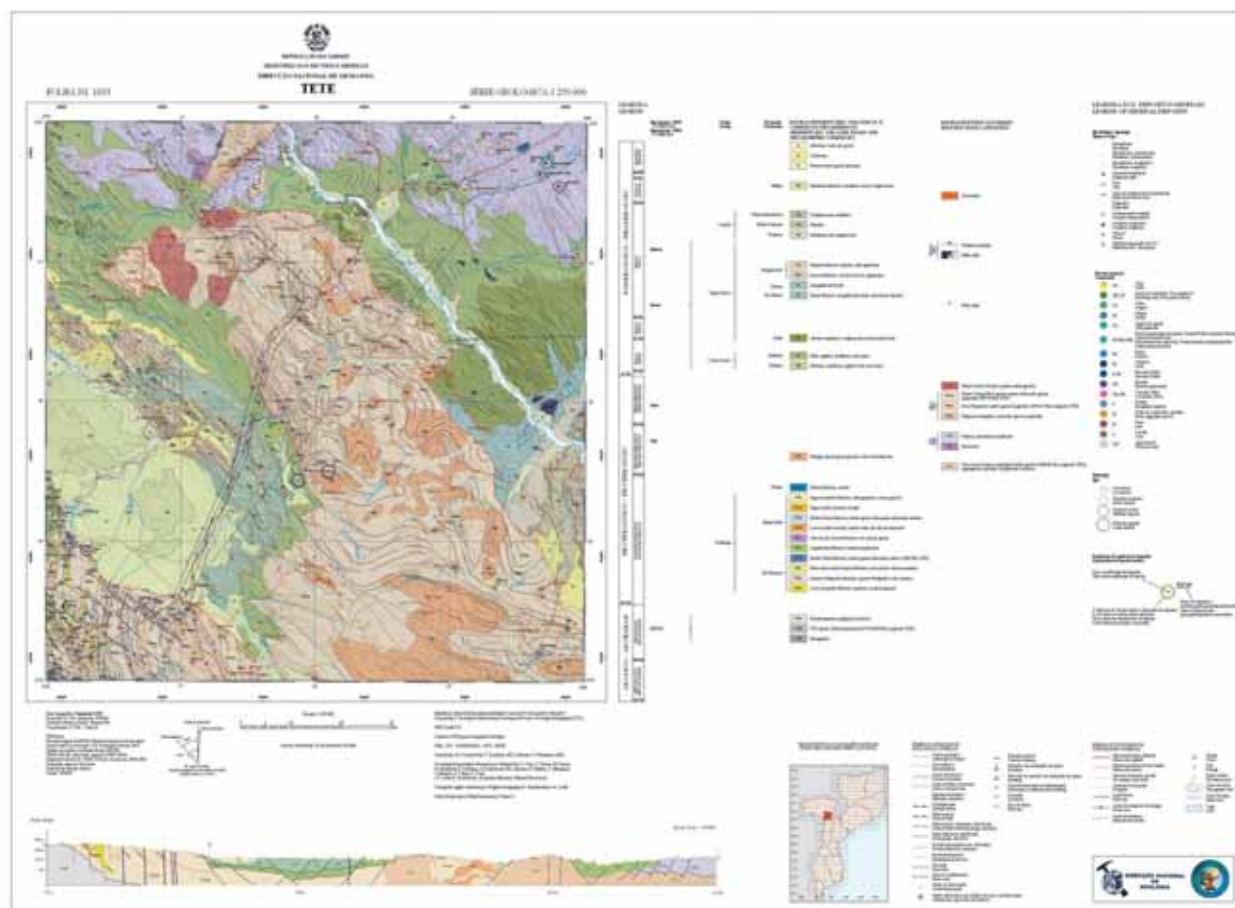


Fig. 4. An example of the layout of a geological map (Sheet 1633 Tete).

- Geological observation databases in ESRI Geodatabase format;
- Tectonic measurements and descriptions of the observed outcrops as MS Access databases;
- Digital photographs of outcrops and samples in an image database;
- Petrophysical measurements in MS Excel tables;
- Chemical analysis in MS Excel tables;
- Petrographical thin section studies in MS Excel tables; and
- Age determinations in MS Excel tables.

The MS Access databases and Geodatabase have been linked to geological maps through ESRI ArcGIS/ArcMap using the observation number as a key. Consequently, the field photographs and results of laboratory studies can be viewed together with the field observations shown on the geological map.

MINERAL DEPOSIT DATABASE

The inventory of known mineral deposits and occurrences uses ArcGIS and MS Access as the main programmes for the storage, retrieval, manipulation and display of geo-information. The MS Access structure of the mineral data base is illustrated in Figure 5. The compiled data are ready for incorporation into the Mineral Information System (MIS), which has been developed in conjunction with the Documentation Centre. The initial format (structure, mineral names with abbreviations) for the mineral deposit databank, obtained from the Council

for Geoscience (CGS), Pretoria, South Africa, was incorporated into the ArcGIS project format. The data, dealing with approximately 90 mineral deposits, was reformatted into ArcGIS shape files in order to facilitate matching with other georeferenced data when producing mineral deposit maps. The forms were designed for the collection of mineral resources data, and they were used both in the library and in the field. Data from the field forms were transferred into the database, often already in field (Fig. 6). Complementary data were extracted from both dig-

ital and analog DNG reports, published sources and from the Internet (such as company press releases and annual reports).

In addition, the GTK Consortium has compiled a new database of 520 mineral deposits and occur-

rences, including stone, aggregate, gravel and sand quarries. These data cover the entire LOT 2, LOT 3 and Extension Contract areas. During the compilation it was found that the old location of several mineral deposits and showings in different data-

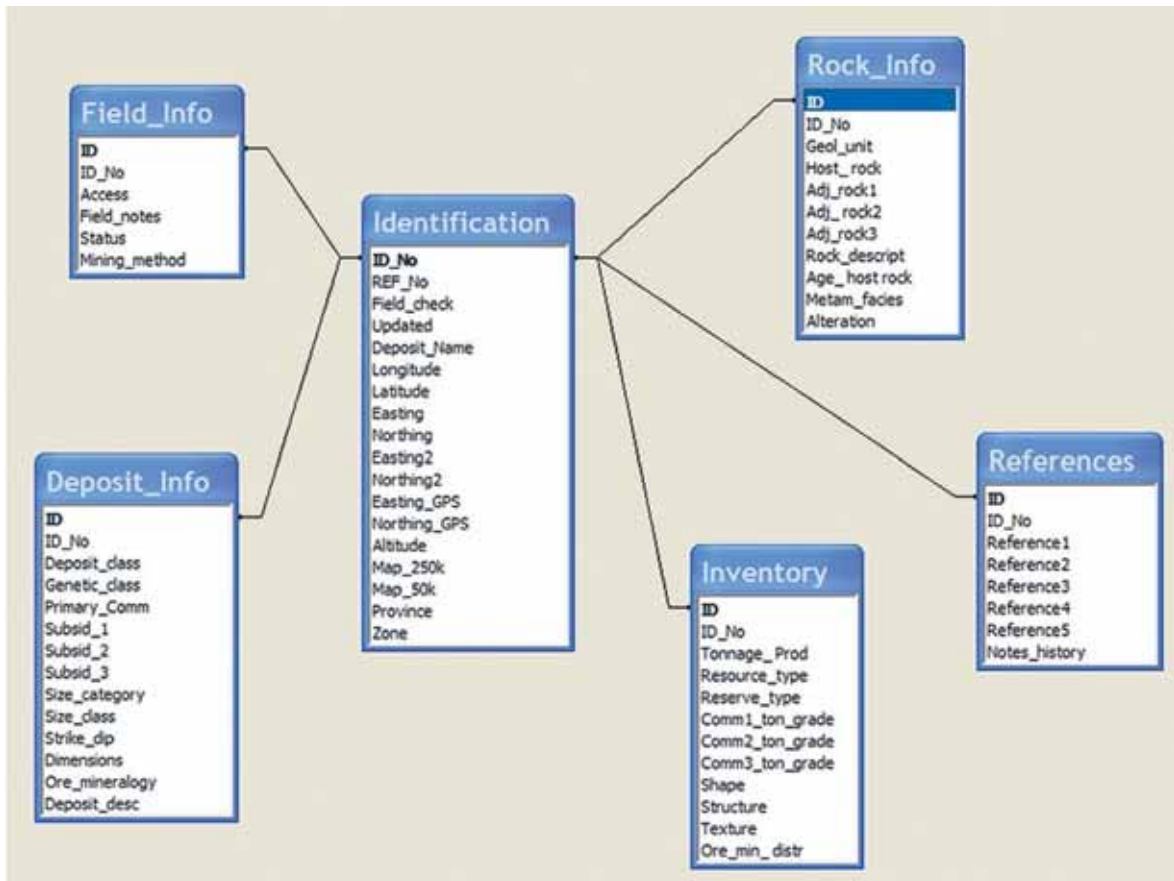


Fig. 5. Structure of the database used in the LOT 2 and LOT 3 mineral occurrence inventory.

MINERAL DEPOSIT DATA BASE

Code: 53

REF_No: 61

Field_check: ☒

Updated: 10.11.04

Compiled by: RG, TL

Deposit Name: Muende

Db id: 53

FIELD FORM 3- DEPOSIT INFO

Deposit class: Precious metal (Au, Ag, PGE) IM_subtype:

Genetic class: Shear zone-related Dimensions: 400 x 5-35 m

Primary Comm: Au

Subsid 1:

Subsid 2:

Subsid 3:

Ore mineralogy: Pyrite, quartz, arsenopyrite

Size category: small

Size class: 1

Strike: 90

Dip:

Deposit description: Disseminated lenses of massive pyrite in an extensively sheared zone of quartzitic rocks (acid volcanics) quartz veins and schists. Low grade mineralization of limited strike length hosted in E-W zone of tectonic quartzite and quartz seicite schist with pyrite, enriched in along NNE fractures.

Record: 48 of 652

Fig. 6. An example of data capture for the mineral database: attributes for deposit information.

bases was not coherently documented. Therefore, it was necessary to make GPS-controlled field checks on the deposits.

Inspection of mineral occurrences proved to be time consuming and often impossible. This was due to the inaccuracy of the reported coordinates (~ one

minute, meaning a maximum error of ~ one km) in existing documents and, having been abandoned for over 40 years, a general lack of surface features of most workings. Occasionally, even greater discrepancies of up to 2 to 3 km were found when comparing indicated locations with GPS-verified locations.

OBSERVATION DATABASES IN MS ACCESS FORMAT

Field observations from LOT 2 and LOT 3 areas have been saved from observation forms into two MS Access databases.

The database Final_moza_UTM36S_2006.mdb includes 17 927 observations from GTK Consortium mapping areas. All these observations have originally been made in the UTM36S coordinate system. Because a part of the GTK Consortium LOT 3 mapping area extends to the UTM37S coordinate system area, 177 observations have also been saved

to the database Final_Moza_UTM37S_2006.mdb. This arrangement will help users to export data to various GIS programmes.

Most data have been saved into following tables: description, lithology, metamorphic minerals, observation (main table), ore minerals, sample, structure and tectonics.

The structure of these two databases (36S and 37S) is identical. Tables, fields and relations are shown in Figure 7.

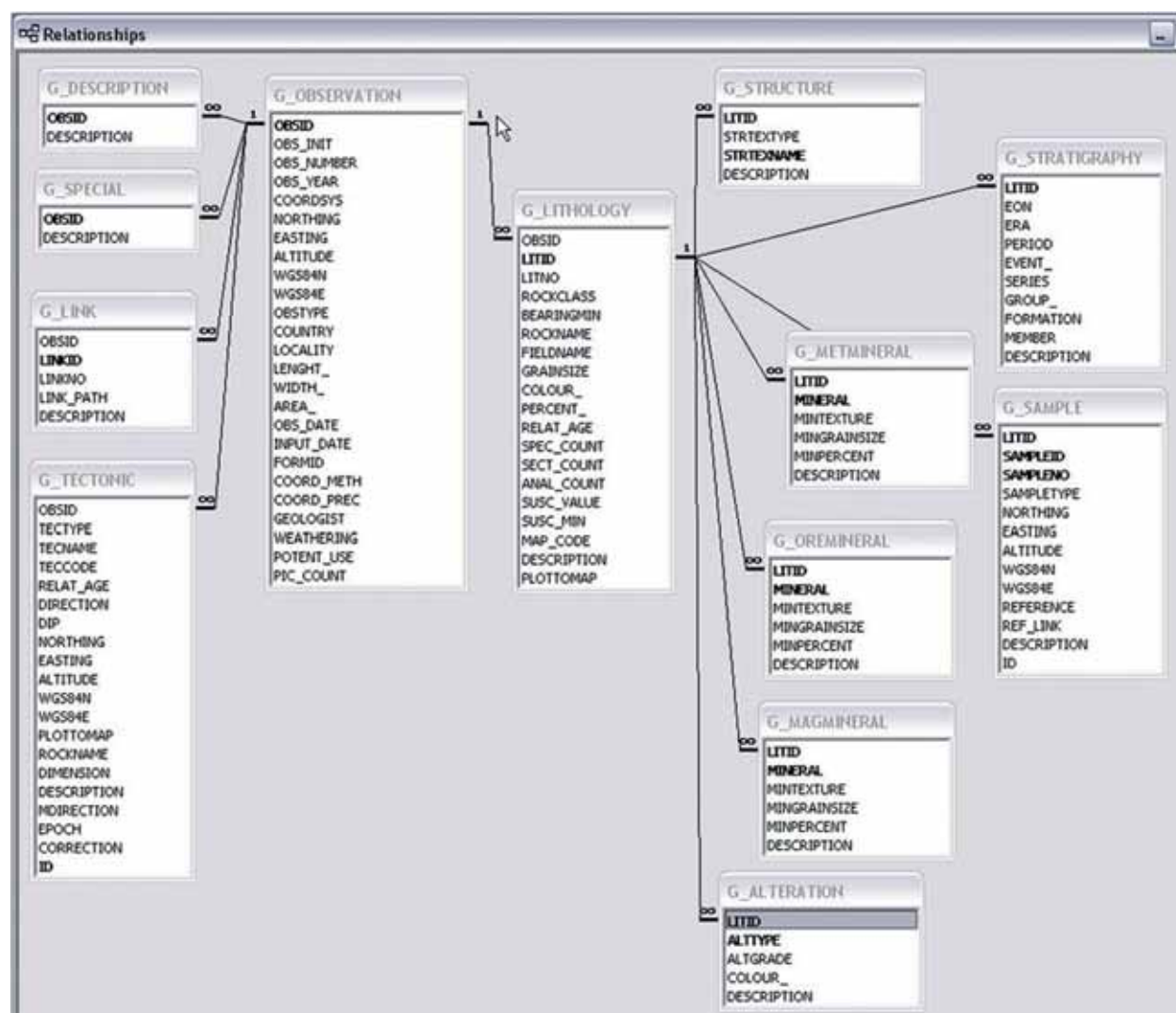


Fig. 7. Structure of the field observation database.

Observation database in ESRI Geodatabase format

The geodatabase Final_Moza_obs_geodatabase_2006.mdb includes basically the same information as the MS Access databases.

This database was developed to help users to utilize observation information in an ESRI ArcGIS environment. All information has been converted to one coordinate system (UTM36S). The data have been divided into such entities that are useful in map production (Fig. 8).



Fig. 8. Structure of the ESRI ArcGIS observation database.

Photographic/Digital image database

The GTK Consortium [photographic/digital image] database, including 28 000 digital photographs, has been constructed using the IMatch image database programme (www.photools.com). The software is designed to enable the viewing, editing and organization of a digital image collection.

The image files in the [photographic/digital image] database of the Mozambique include metadata in IPTC format and consist of the fields shown in Figure 9.

The metadata information includes information collected by the camera (date etc.) and geological information that has been transferred from observation databases. The user interface has been developed to help users to easily browse the digital photographs stored in the database (Fig. 10).

By using this application a user can locate images with the help of a keyword list based on rock names or by using the map sheet number or map name. It is also possible to download images. A downloaded image includes metadata information.

<input checked="" type="checkbox"/> OBSERVATION_OBSID
<input checked="" type="checkbox"/> OBS_INIT
<input checked="" type="checkbox"/> OBS_NUMBER
<input checked="" type="checkbox"/> OBS_YEAR
<input checked="" type="checkbox"/> COORDSYS
<input checked="" type="checkbox"/> NORTHING
<input checked="" type="checkbox"/> EASTING
<input checked="" type="checkbox"/> ALTITUDE
<input checked="" type="checkbox"/> COORD_METH
<input checked="" type="checkbox"/> COORD_PREC
<input checked="" type="checkbox"/> OBSTYPE
<input checked="" type="checkbox"/> COUNTRY
<input checked="" type="checkbox"/> MAP
<input checked="" type="checkbox"/> LENGTH
<input checked="" type="checkbox"/> WIDTH
<input checked="" type="checkbox"/> AREA
<input checked="" type="checkbox"/> GEOLOGIST
<input checked="" type="checkbox"/> ROCKNAME
<input checked="" type="checkbox"/> FIELDNAME
<input checked="" type="checkbox"/> LITHOLOGY2
<input checked="" type="checkbox"/> LITHOLOGY3
<input checked="" type="checkbox"/> LITHOLOGY4
<input checked="" type="checkbox"/> DESCRIPTION
<input checked="" type="checkbox"/> IPTC_date

Fig. 9. Structure of the [photographic/digital image] database.

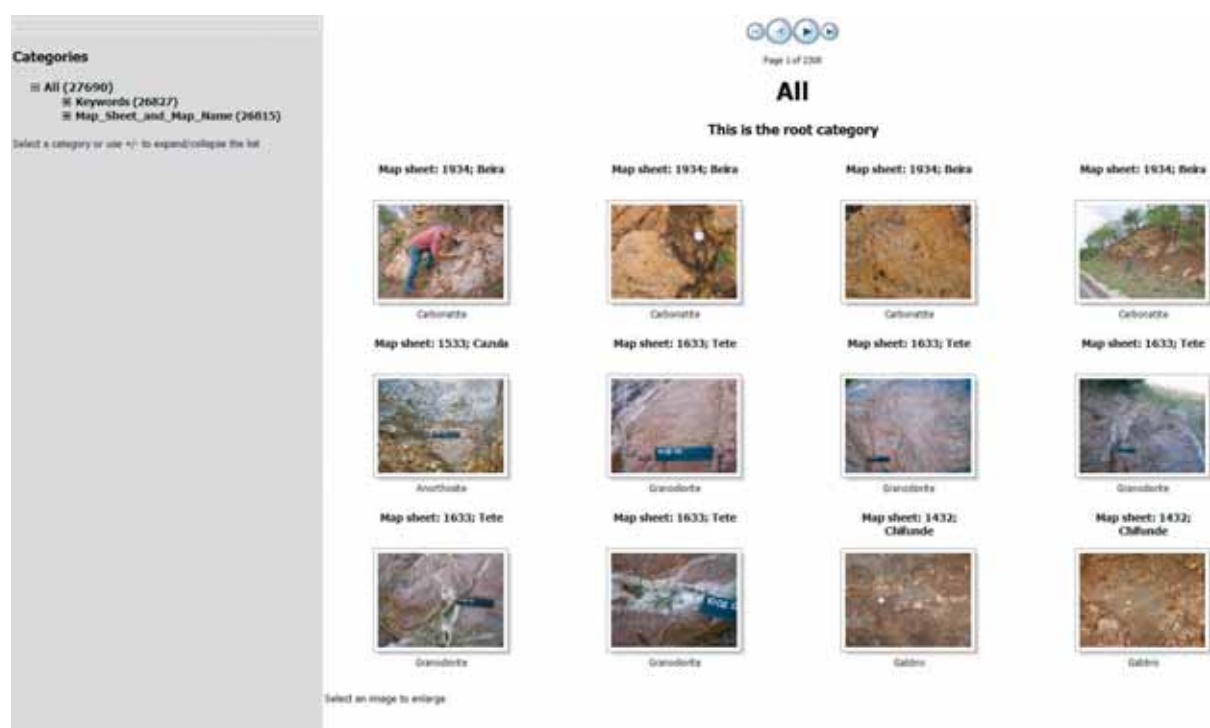


Fig. 10. Web-based user interface for image viewing.

FINAL PRODUCTS OF THE PROJECT

The products of the project in LOT 2 and LOT 3 area have comprised intermediate maps and reports during different phases and the final products at the end of the project.

The main intermediate products of the project, also used as milestones, were:

- A action plan for the project at the beginning of Phase I;
- Preliminary geological maps, satellite image maps at the beginning of Phase II and field work plans before the field seasons;
- Field-checked geological maps at the end of Phase II;
- Draft final geological maps at the beginning of Phase III.

The final phase of the projects included the preparation of final digital products, including print-ready files of geological maps and map sheet explanations, geological map data as a seamless map covering both LOT 2 and LOT 3 areas in ArcGIS compatible format and a final technical report of the project. Geological maps and map sheet explanations have also been printed as paper copies.

The final products of the projects comprise the following Geological and Mineral Resources maps:

- Geological maps at the scale 1:250 000, including mineral occurrences, paper prints and print-ready files;
- Mineral Resources Potential maps at the scale 1:250 000, paper prints and print-ready files;
- Geological maps at the scale 1:50 000, including mineral occurrences, paper prints and print-ready files.

The following databases:

- Digital geological maps and ArcInfo/ArcView compatible GIS database;
- Databases of field observation data and the results of laboratory studies.
- And the following documents:
- Geological map sheet explanations;
- Final technical report of the project;
- Integrated DVD of the products of LOT 2 and LOT 3 projects.

Digital databases comprise the observation and mineral databases in MS Access, the digital image database in IMatch, the results of laboratory studies in MS Excel tables and geological observations in Esri Geodatabases and MS Access observation databases.

The final geological maps have been submitted to the Client as paper prints, print-ready PDF files and as a seamless GIS data. The GIS data have also been delivered to the MIS project to be arranged into the digital map database of the DNG. Geological Map Explanations (Vol. 1–4) and the Final Technical Reports of LOT 2 and LOT 3 projects have been delivered to the Client as paper prints and as PDF files.

All the final products of the project have been collected in an integrated DVD that can be used to present and search the results, products and data prepared by LOT 2 and LOT 3 projects (Fig. 11).

All products and data of the projects were also delivered to the Client on a removable disk that includes 2500 separate files and 250 GB of data in total.

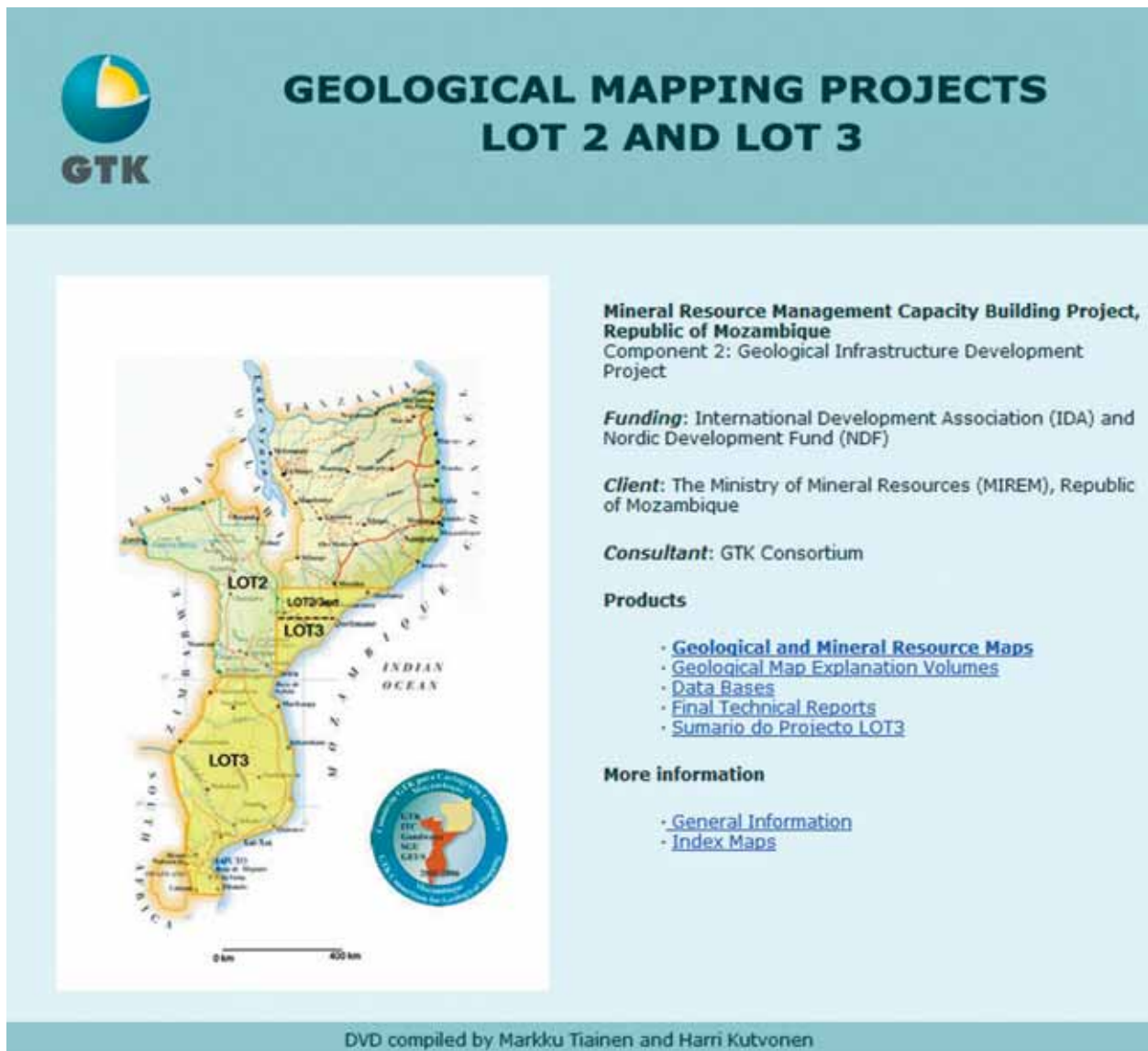


Fig.11. Front page of the searchable DVD that contains the products of the LOT 2 and LOT 3 geological mapping projects.

ACKNOWLEDGEMENTS

We wish to thank Dr. Jouni Vuollo, GTK, for comments that considerably improved the text.

INTEGRATED GEOLOGICAL INTERPRETATION OF REMOTELY SENSED DATA TO SUPPORT GEOLOGICAL MAPPING IN MOZAMBIQUE

by

Ernst M. Schetselaar^{1*}, Markku Tiainen² & Tsehaie Woldai³

Schetselaar, E. Tiainen, M. & Woldai, T. 2008. Integrated geological interpretation of remotely sensed data to support geological mapping in Mozambique. *Geological Survey of Finland Special Paper 48*, 35–63, 24 figures.

This paper presents the applied methodology and results of geological remote sensing interpretation in preparation of 1:250 000 and 1:50 000 scale geological field mapping of the LOT 2 / LOT 3 project areas and their extensions for the Mineral Resources Capacity Building Project (Republic of Mozambique) funded by the World Bank (IDA, AfDB, NDF). The data pre-processing, geometric registration, enhancement and integrated interpretation of remotely sensed and airborne geophysical data together with existing geological maps resulted in seamless provisional geological map coverage of the project areas that guided field mapping and complemented geological map compilation in areas where field data were sparse or lacking. The approach is knowledge-driven, since available geological map data from Mozambique and neighbouring countries were used, whenever possible, to establish relationships between image and geological map patterns that allowed calibration of the interpretation of contacts and units with respect to the previously known geological lithostratigraphy. Once these relationships were established, geologically significant discrepancies between map and image patterns highlighted features that provided follow-up targets to be tested in the subsequent field mapping campaigns.

Key words (GeoRef Thesaurus, AGI): interpretation, Landsat TM, ASTER, SRTM, airborne gamma-ray spectrometry, magnetic survey, geological mapping, Mozambique.

¹ *International Institute for Geo-Information Science and Earth Observation (ITC), Hengelosestraat 99, Enschede, the Netherlands.* *

² *Geological Survey of Finland (GTK), P.O. Box 96, FI-02151 Espoo, Finland*

³ *International Institute for Geo-Information Science and Earth Observation (ITC), Hengelosestraat 99, Enschede, the Netherlands.*

E-mail: ernst.schetselaar@nrcan.gc.ca

* *Present address: Geological Survey of Canada 245A-615 Booth Street, Ottawa, Ontario, Canada K1A-0E9, email: ernst.schetselaar@nrcan.gc.ca*

INTRODUCTION

Due to their underexploited mineral and energy potential, African countries like Mozambique need efficient methods for upgrading their geoscience knowledge base. An important part of this endeavour involves updating geological map coverage. Whereas in the past the coverage and publication of traditional geological maps of a limited region demanded multiple years of fieldwork, more time-efficient approaches of mapping larger regions within shorter time spans are required. An integrated geological mapping approach, in which existing geological map data are re-compiled on the basis of the interpretation of aerial photographs, satellite imagery and airborne geophysical data before and during progressing fieldwork provides solutions that meet this requirement, since it facilitates the time-efficient production of consistent up-to-date digital geological map databases covering large regions that can be easily upgraded in future mapping campaigns.

Integrated approaches to geological mapping are not entirely new. Geologists have long assembled diverse layers of geoscience data to study the relationships between the spatial patterns in each for resource exploration and mapping endeavours. In the past this has been accomplished using an 'analog' approach, forcing maps printed on mylar to be portrayed on a uniform map scale on a light table. However, with the increasing availability of digital datasets and the routine use of geographic information systems (GIS), the task of studying re-

lationships between data and producing provisional geological maps to assist field mapping has become easier and more versatile. Contrary to the "light table" approach, GIS allows maps and image data to be combined, overlaid and manipulated at any scale with any combination of layers and subject to any integrated enhancement. The compilation and interpretation of a variety of geoscience data produces predictive maps, containing structural, lithological, geophysical and surficial information for the geologist before he or she actually begins field work. These provisional geological maps may be iteratively revised and upgraded to publishable geological maps on the basis of evolving insight by repeatedly integrating newly acquired field and laboratory data in the interpretation process. They can also serve as first-order geological maps in areas where field mapping is not feasible. The fundamental difference with respect to traditional ground-based mapping is that in the latter the compilation of units away from field control (current and legacy field observations) is largely based on geological inference, while in the integrated approach this geological inference is repeatedly tested and calibrated against the interpretation of remote sensing imagery. In this paper we report on how we applied this methodology to the compilation of provisional geological map coverage of LOT 2 and LOT 3 in Mozambique in the preparation of 1:250 000 and 1:50 000 scale geological field mapping campaigns.

WORKING METHODOLOGY FOR THE PRODUCTION OF PROVISIONAL GEOLOGICAL MAPS

A seamless coverage of 1:250 000 scale provisional geological maps was prepared during the preliminary phase of the regional geological mapping of the LOT 2 and LOT 3 areas and their extensions in Mozambique with the objective to produce the most up-to-date geological map coverage over the project areas before fieldwork commenced. The preparatory compilation work comprised the recovery of old airborne geophysical surveys, digitizing of previously published maps, geometric co-registration

of the spatial data layers, various image processing and enhancement techniques and knowledge-driven geological image interpretation. In addition to describing the methodology, we present examples of image processing and interpretation results to illustrate how significant geological information was extracted from the multi-source image data sets. The data processing and interpretation tasks, described in more detail in the subsequent sections, were conducted in phase with fieldwork progress.

Digitizing and compilation of previously published geological maps

A digital compilation of geological map data was prepared from the raster-scanned and digitized (double degree) 1:250 000 scale geological

map sheets published by Hunting Ltd (1984) and 1:250 000 scale geological maps provided by the National Directorate of Geology (DNG). A feature

class list was prepared to encode the various lithological, structural and topographic features represented on the geological maps. Faults that also define lithological contacts were separately encoded and selectively copied to the coverage of geological structures. The arc-node topology for generating the coverage of geological units was generated by the selective extraction of those polyline codes that define the boundaries of lithological units. Dykes were digitized as polylines and were not included in the set of polylines that form the arc-node topology of the lithological units. Structural elements, such as foliation, and bedding elements were also extracted from the Hunting geological maps.

Merging and back calibration of airborne geophysical surveys

New airborne geophysical survey data were acquired by Fugro Airborne Surveys in 2003, to the south and west of the older airborne surveys acquired by Hunting Ltd in 1983. Inspection of grids from the airborne geophysical 1983 survey data revealed that its geological interpretation was seriously hampered by the effects of prominent flight-based level shifts and micro-levelling errors. Hence, the line data from the Hunting geophysical survey were recovered from the GEODESA archives at ITC to reduce levelling errors, since this allowed the production of grids that better suited the needs for geological interpretation. The recovery and processing of the line data proved to be effective in reducing significant level shifts in the eTh and K channels in the northern block of the survey and in reducing micro-levelling errors in the aeromagnetic data. The U channel, however, could not be improved, as the flight-based level shifts appeared to be 'smeared out' over adjacent flight lines. This was apparently induced by previous attempts to correct for level shifts in the U channel by filtering the data.

Merging of the magnetic grids was based on 20 metre downward continuation of the 1983 survey to the nominal flying height of the 2003 survey and levelling the data to the 2000 IRGF before computing the residual magnetic field. The K, eTh, eU and total count grid values (18 000) in the overlap area of the two surveys were used to generate regression equations for back-calibration of each channel of the 1983 gamma-ray spectrometry data. Areas with

extreme topography and hence excessive flying altitude were omitted from the regression analysis. The line data of K, eTh, eU, TC and the total magnetic field channels were registered on the MOZNET datum and gridded on 250-metre cells using a minimum curvature gridding algorithm. Reduction to the pole was carried out and 1st vertical derivative grids were derived from the IRGF subtracted magnetic field. This further facilitated the interpretation of regional geological units and structures.

Geometric transformation of LANDSAT 7 ETM and ASTER scenes

All LANDSAT ETM scenes provided to the project were georeferenced on UTM projection, zone 36S, Clarke 1866 Ellipsoid, Tete Datum. Overlays of GPS track logs collected during a reconnaissance mission in November 2002 revealed that the mis-registration between the GPS track logs collected by a handheld unit (Garmin 12XL) amounted to systematic shifts of 200–300 metres, predominantly in northings. Given that both the track log and ETM scenes were registered on the same projection and ellipsoid, it appeared that the systematic displacements were due to missing translation parameters between the older provincial datum and new national MOZNET datum (equivalent to WGS84). In December 2002 the required datum transformations (Bursa-Wolf transformation parameters) became available through a technical report on the adjustment of the old geodetic network of Mozambique, conducted for an urban-environmental management project by Norconsult International (1998).

Thirty-five LANDSAT ETM scenes covering the LOT 2 and LOT 3 areas and their extensions were re-sampled to fit the MOZNET datum using bicubic re-sampling (Fig. 1). The re-registration of the LANDSAT scenes to the MOZNET datum facilitated the registration of GPS stations collected during fieldwork without having to apply datum transformations to the GPS measurements afterwards.

The ASTER 1A and 1B scenes are by standard registered on UTM projection with WGS84 datum (equivalent to the MOZNET datum) to a nominal accuracy of 100 metres. They were interactively registered to 1 to 2 pixel accuracy by shifting the scenes until they fitted the GPS track logs within a tolerance of one to two pixels (15–30 metres).

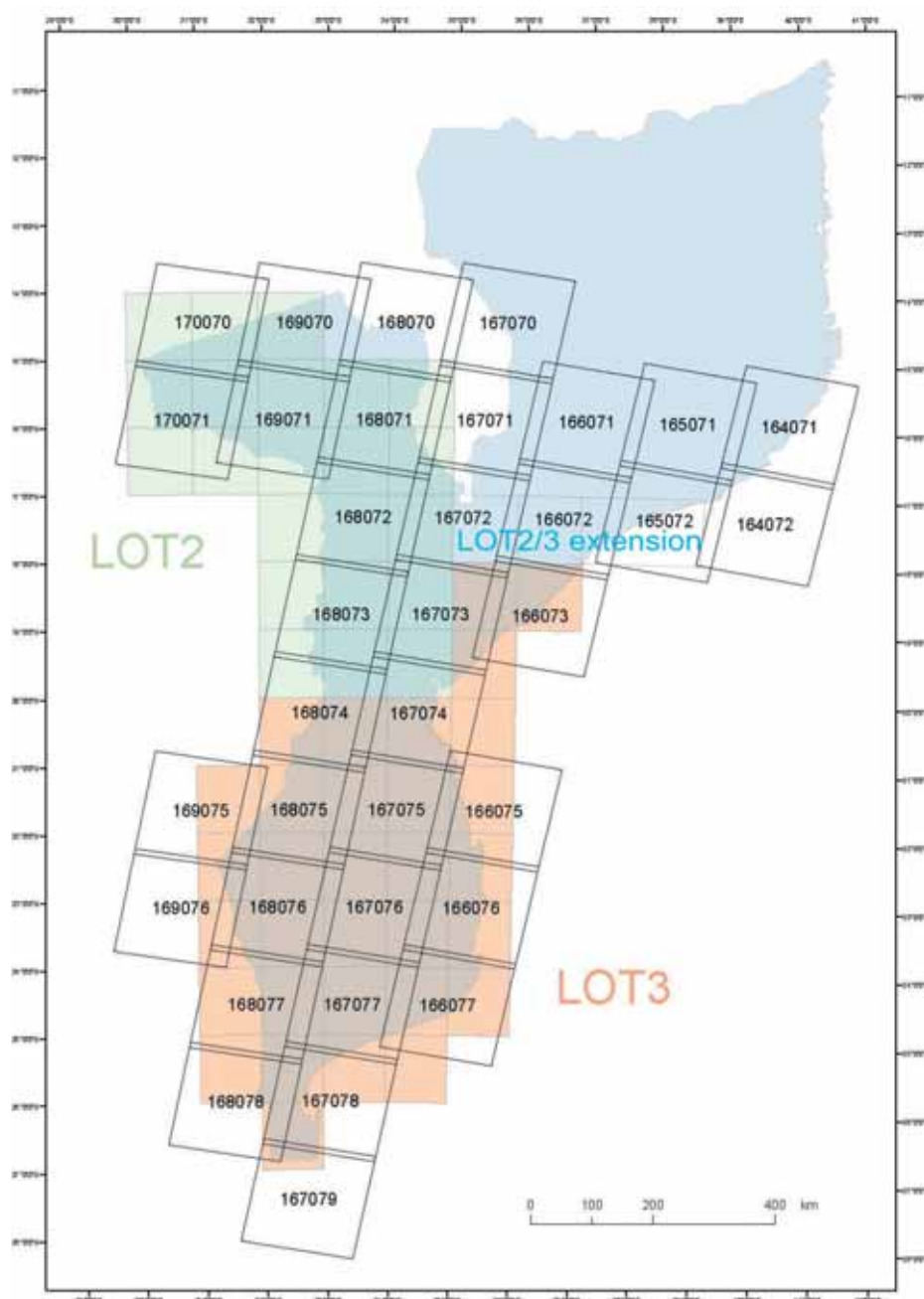


Fig. 1 Layout of the LANDSAT 7 ETM scenes over LOT 2, LOT 3 and LOT 2/3 extension areas.

Image enhancement

Several enhanced products were derived from the LANDSAT 7 ETM scenes to support geological image interpretation. The enhancement methods that were employed included: linear and interactive contrast stretching of single bands and colour composite images and principal component analysis.

In generating colour composite images from the twenty possible combinations of the six 30-metre bands, the discrimination of rocks (or related soil cover) was considered an important factor in selecting an optimal triplet for discrimination of

lithological units. Another less important factor for consideration was the possibility to detect lithological variations indirectly expressed as broad-scale geobotanic relationships in natural and semi-natural vegetation communities. The band combinations RGB (red, green, blue) 731 and RGB 732 provided attractive colour composites, particularly for LANDSAT scenes acquired over relatively dry areas or during dry periods. Both band triplets exploit the strong and broad absorption features of carbonate and hydroxyl-bearing minerals between about 2.2–2.4 microns, a range overlapping with the wavelength position of ETM band 7. The 731 and 732

band combinations also provide information on the spectral slope between 0.4 and 0.7 microns (the visible range comprising band 1, band 2 and band 3), which is diagnostic for the presence of iron-oxide minerals (Goetz *et al.* 1983). Good exposures of carbonate and mica rich rocks typically appear in shades of blue on such colour composites, whereas rocks with red alteration, due to high contents of iron-oxides, appear in yellow to reddish tones. The use of these diagnostic spectral properties of rocks and derived soil material is obviously hampered in areas with moderate to dense vegetation cover. In these areas, however, subtle geobotanic relationships between natural vegetation communities and their substrate may be exploited by using band combinations that include the prominent and steep slope between the visible red and near infra-red range of the green vegetation spectrum. Hence, RGB 473 was used as an additional combination to maximize spectral discrimination of lithological units in areas with higher green biomass densities. Examples of colour composite images generated from the above

mentioned band combinations are presented in Figure 2.

Principal component analysis was used to exploit the sun illumination of the LANDSAT scenes. PCA generates a new orthogonal set of bands along the lines of maximum variance among the original bands (Curran 1985). This effectively minimizes redundant information, particularly because the original bands tend to be highly correlated. The new bands, called principal components, are ordered according to the percentage of variance they explain. The first principal component contains the information that is common among the multispectral bands, which is usually strongly related to the scene illumination. As a result, PC1 provides optimal enhancement of relief features, which may be exploited for outlining lithological units on their variable geomorphologic expression. PC1 images, for example, appeared to enhance the differences between granites and intrusive rocks of mafic composition and the differences among different felsic suites themselves, as well as the more subtle small-scale linear patterns reflecting

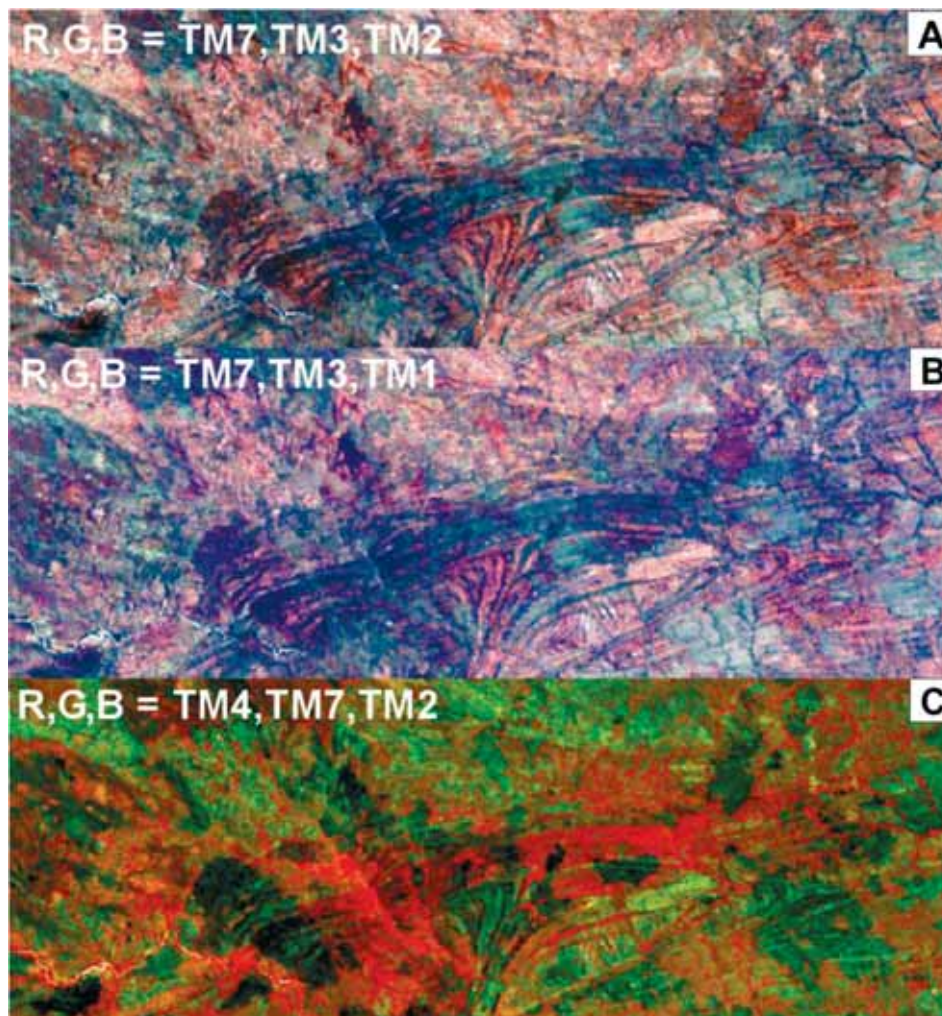


Fig. 2 Subscenes of LANDSAT ETM colour composite images for different band combinations. A) RGB 732; B) RGB 731; C) RGB 432.

differences in the degree of penetrative foliation/bedding fabric in various plutonic, metamorphic and sedimentary rock units.

The ASTER VNIR scenes were enhanced and displayed as false colour composite images (rgb 321). The stretching intervals of the three bands were interactively adapted to background brightness variations. Although the visible-near infrared (VNIR) spectral response of the ASTER scenes is highly sensitive to vegetation cover, their higher spatial resolution (15 metres in comparison to the 30-metre pixels for LANDSAT) provided advantages in the image interpretation of lithological units. The ASTER scenes appeared most useful for retracing the boundaries that were difficult to identify on the LANDSAT ETM scenes. This particularly applied to areas with vegetation burns and areas with complex contorted unit boundary geometries. Typical examples where the higher spatial resolution of the ASTER VNIR scenes provided a clear advantage in outlining geological units are illustrated in Figure 3.

The gamma-ray spectrometry channels were enhanced and displayed as ternary radioelement maps

in RGB colour space using linear contrast enhancement with cut-off percentages of 2%. In areas with a very high or low gamma-ray response, stretching intervals were interactively adjusted. The total field and first vertical magnetic derivative grids were enhanced in colour-shaded relief images, using an illumination inclination angle and azimuth of respectively 25 and 300 degrees for the relief shading and a rainbow hue spectrum. Figure 4 presents colour enhancements of the total magnetic intensity and ternary radioelement grids from the merged geophysical surveys.

In February 2004, during the course of the compilation phase of the LOT 3 project, digital elevation data with a spatial resolution of 90 metres from the Shuttle Radar Topographic Mission (SRTM) were released for the African continent. The tiles of SRTM data acquired over the project areas were downloaded from the USGS EROS website and merged in order to exploit their added value in geological image interpretation.

The SRTM data were relief-shaded from three different directions using an inclination angle of 30 degrees above the horizon and three declination



Fig. 3. Image interpretation of an ASTER VNIR scene at ca. 23°25' S and 31°50' E. The interpretation shows isolated outcrops of Umbelúzi rhyolite (Karoo Supergroup) east of its main boundary with the Cretaceous Grudja Formation. Note the isolated pockets of Quaternary cover (Qp1) covering the Grudja Formation (K/Ksm). Grid lines are north-oriented and spaced 2 km apart.

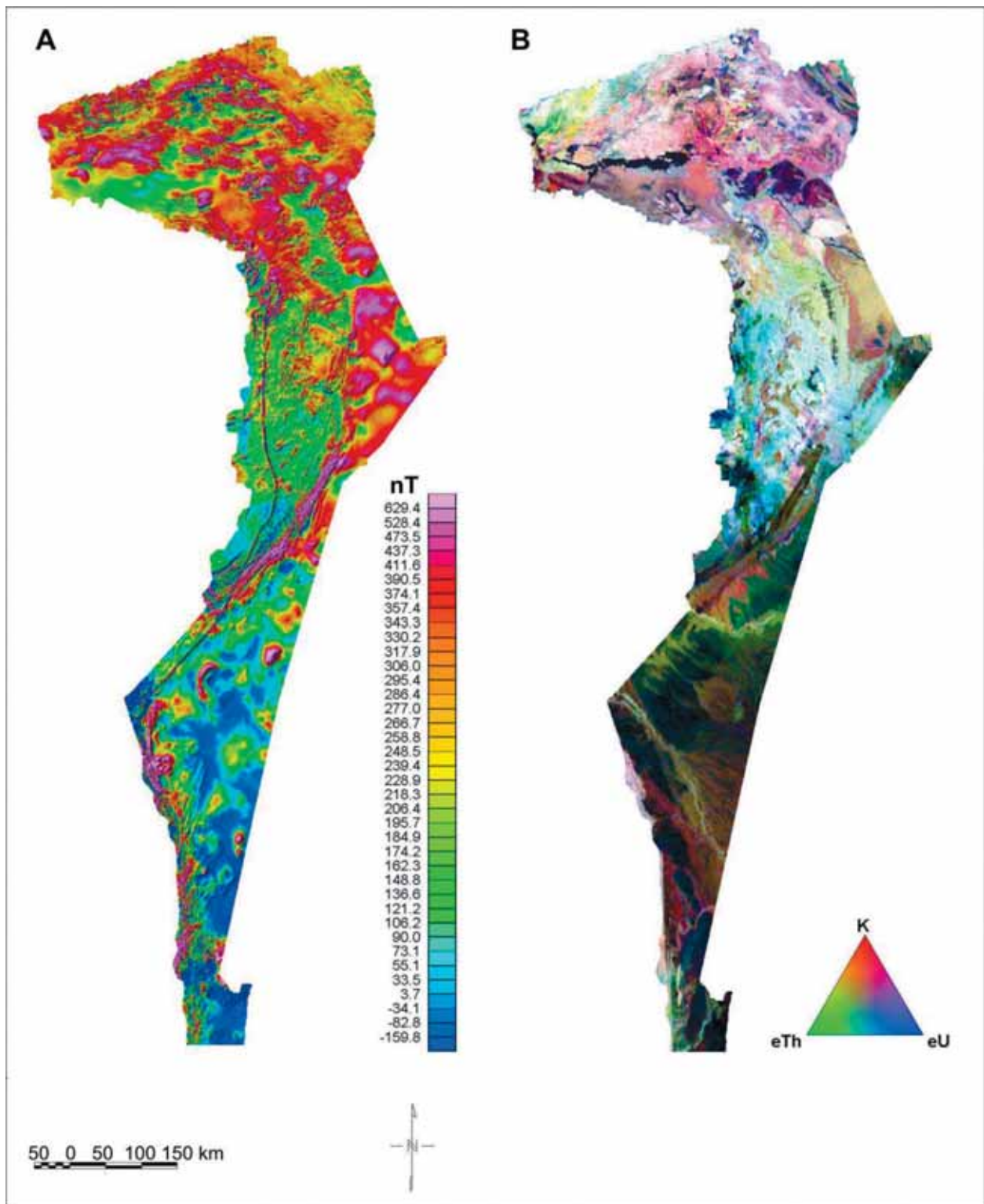


Fig. 4. Colour enhancements of airborne geophysical grids with a grid resolution of 250 metres. A) Colour-shaded relief image of the residual total magnetic field; B) Ternary radioelement grid, rgb KThU.

angles of 270, 315 and 360 degrees. The individual shaded-relief enhancements were combined in a colour composite image, such that topographic features were rendered in different colours. Figure 5 presents a subscene of the SRTM colour shaded-relief image that was enhanced interactively during

image interpretation through linear contrast stretching to adapt the enhancement to the local prevailing topographic relief characteristics. The resultant relief-shaded colour composite image appeared to be particularly useful in tracing the boundaries between Quaternary units.

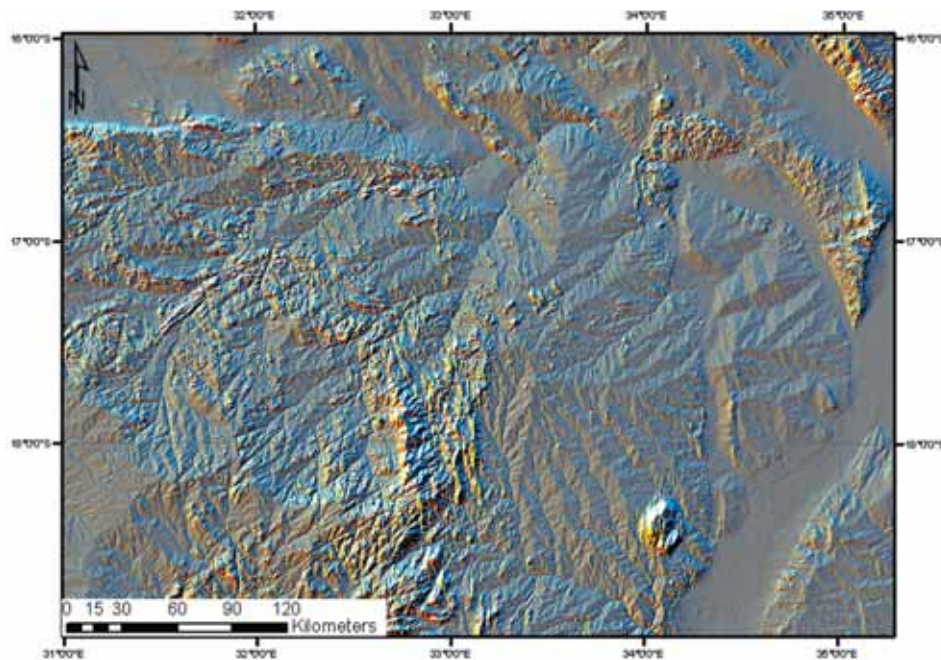


Fig. 5. Ternary shaded-relief image of shuttle radar topographic mission (SRTM) data (90 metre spatial resolution). The SRTM data are relief shaded using three illumination directions (inclination angle is 30° and declination angles are 270°, 315° and 360°) and combined in a colour composite image. Topographic features are displayed in different colours dependent on their orientation.

Twenty-eight LANDSAT TM scenes were combined in four image map mosaics that cover the LOT 2 and LOT 3 project areas. The band combination 7-3-1 in RGB was selected, as this provides optimal spectral information for geological interpretation. The mosaic was compiled in several steps, from small to large areas, to keep the colour balance in hand and to avoid boundary effects. Histogram matching and/or feathering in the overlap was sometimes needed. Finally, four blocks were combined into one image (Fig. 6). The mosaic has a spatial resolution of 30 metres and is 3 GB in size. The geometry has been compared with the GPS field measurements, where tracks were logged. The track logs fitted within one pixel to the corresponding roads on the mosaic.

Integrated image enhancement

Many geological remote sensing studies have demonstrated that the integrated enhancement of remotely sensed and airborne geophysical data sets may yield significant geological information that is not obvious in the enhanced products of the individual data sets (Harris *et al.* 1994). The integration of gamma-ray spectrometry grids and satellite imagery of higher spatial resolution, in particular, has proven useful to enhance geological information, because it allows the interpretation of geochemical information contained in the gamma-ray spectrometry

channels in the context of structural features, such as lithological contacts, faults and foliation trends. (Wilford *et al.* 1997, Schetselaar 2000).

The digital processing methods used to generate integrated enhancements are all based on the principle of mapping co-registered grids/images on distinct perceptual attributes of human colour vision using image algebraic operations. In practice, the geoscience data sets are first co-registered on a common pixel/grid cell size, after which they are 'fused' in colour composite images by the application of an algebraic algorithm to the pixels.

The HPF transform, a method proposed by Chavez *et al.* (1991), was used to merge K, eTh and eU grids with a mosaic of LANDSAT TM5 scenes, both registered on 30-metre pixels. The red, green and blue channels of the colour composite are computed as follows:

$$\begin{aligned} \text{red} &= \frac{1}{c}(a.K + b.TM\ 5) \\ \text{green} &= \frac{1}{c}(a.eTh + b.TM\ 5) \\ \text{blue} &= \frac{1}{c}(a.eU + b.TM\ 5) \\ c &= a + b \end{aligned}$$

The factors a, b and c were selected to weigh chromatic contrast (hue and saturation) with the intensity contrast from LANDSAT ETM5. For this

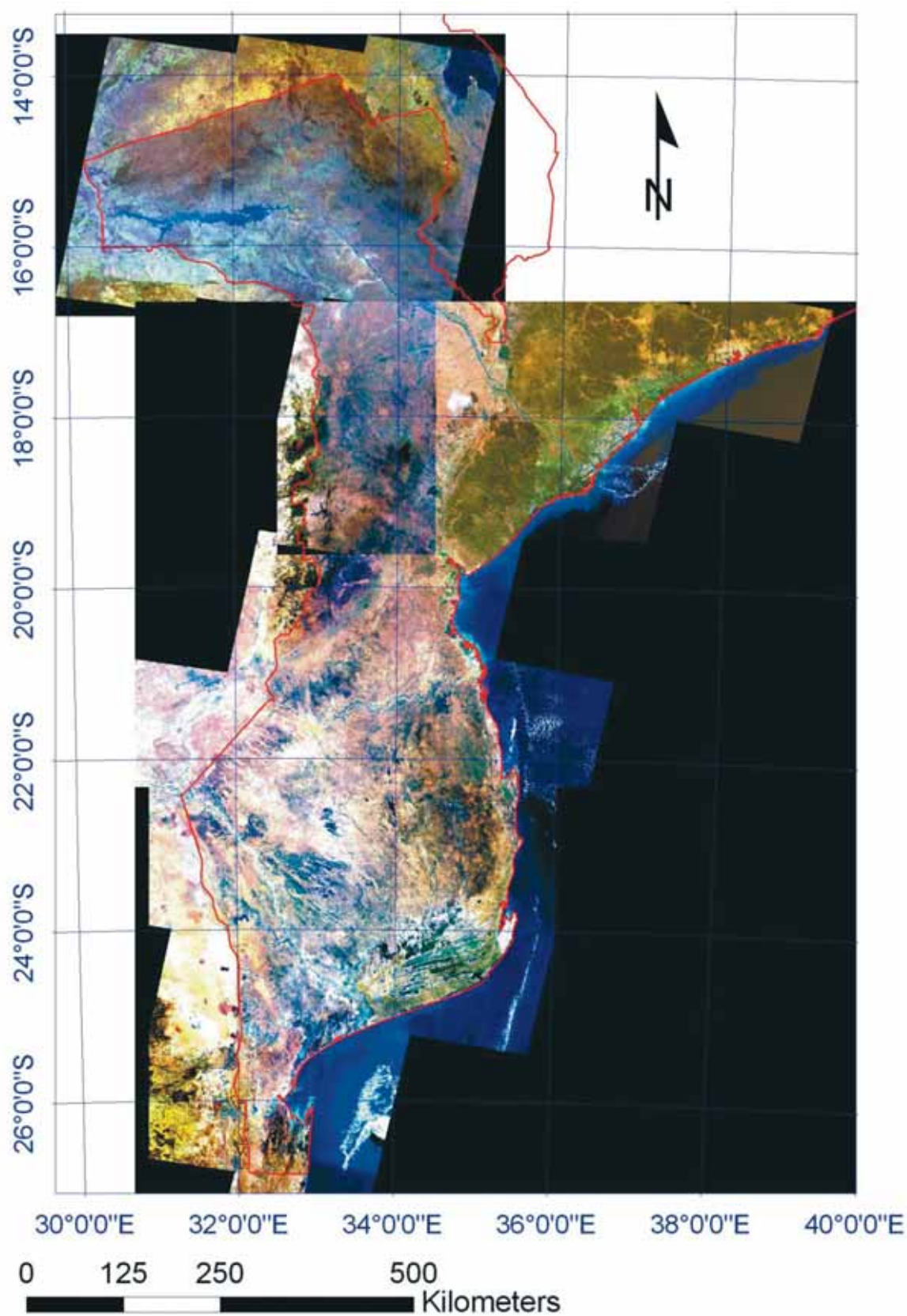


Fig. 6. The combined mosaic of the LANDSAT 7 ETM scenes covering the LOT 2, LOT 3 and their extensions.

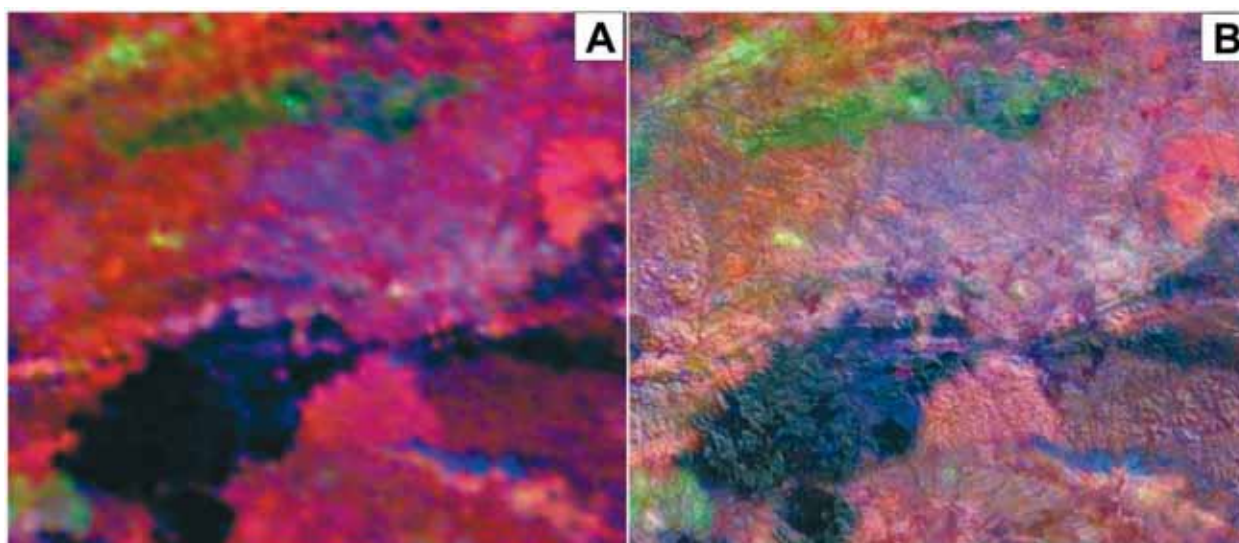


Fig. 7. Image clips to illustrate the effects on integrated enhancement of LANDSAT TM and gamma-ray spectrometry channels. A) Original ternary radioelement map; B) Ternary radioelement map 'sharpened' with LANDSAT ETM band 7.

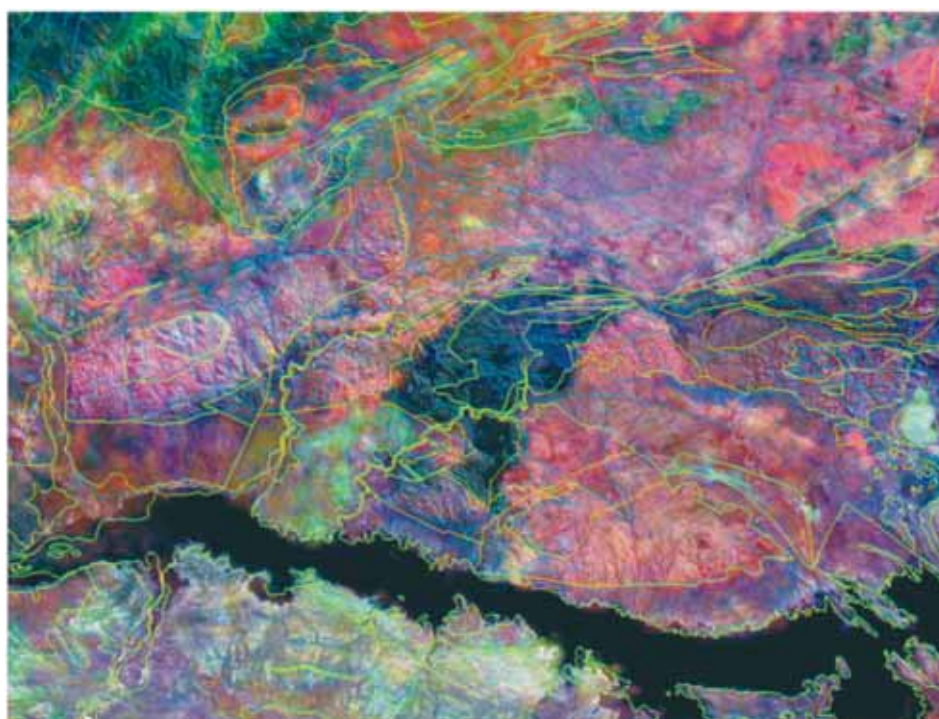


Fig. 8. IHS composite image of gamma-ray spectrometry data, rgb KThU. Intensity is modulated by LANDSAT TM5. Yellow lines show the Hunting compilation, blue lines the LANDSAT interpretation prepared by the GTK Consortium. Lake Cahora Bassa is shown as black.

study, $a = 1$ and $b = 3$ provided an optimal result for geological interpretation. This method is effective in enhancing structural details from the LANDSAT scenes while minimizing spectral distortions among the gamma-ray spectrometry channels. Image enhancement before and after processing and interpretation examples are illustrated in Figures 7 and 8, respectively.

In addition to employing LANDSAT ETM image data as an intensity substitute, relief-shaded SRTM

data were used for image fusion purposes. Figure 9 shows an example from the NW corner of LOT 3 (Upper Save river basin). Note that the relative stratigraphic positions of units, due to rendering topographic relief, have become obvious. Cretaceous units, such as the Sena Formation in red, pink and yellow-green hues, are clearly seen to underlie the Quaternary cover because they correspond to denudational slopes in areas of (badland) erosion.

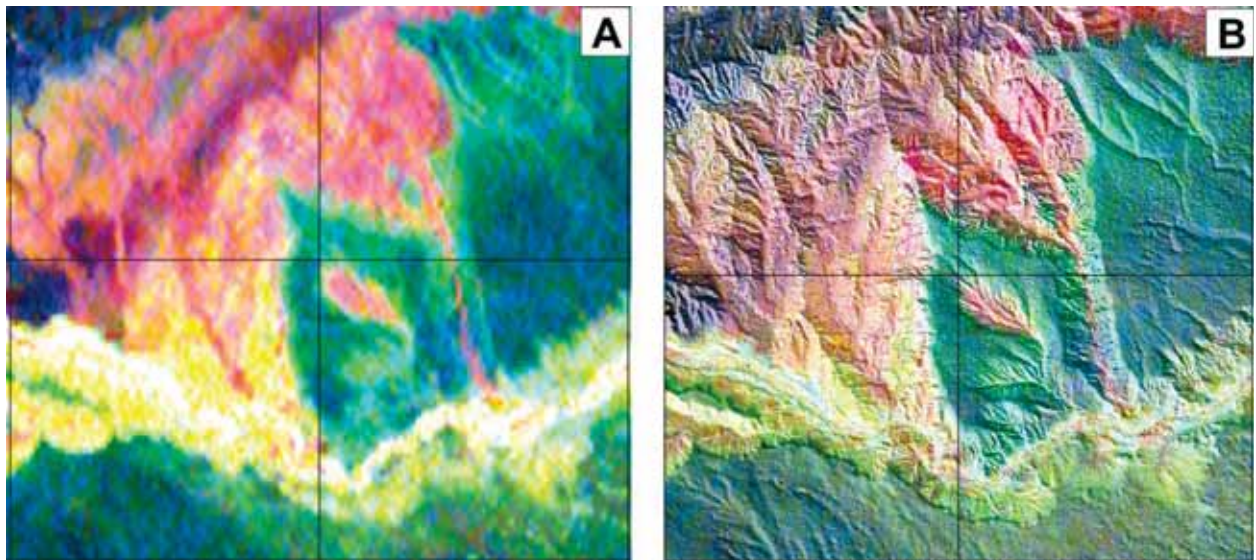


Fig. 9. Image fusion of relief-shaded SRTM and gamma-ray spectrometry grids (grid size is 50x50 km). A) A ternary radioelement map; B) The ternary radioelement map 'sharpened' with relief-shaded SRTM data.

The integrated rendering or image fusion methods that integrated ternary mapping of the radioelement concentrations with structural information from LANDSAT images and shaded-relief SRTM proved to be the most successful enhancement strategy to support geological image interpretation and mapping. Compositional geological information (mineralogy and K, eTh, eU geochemistry) appeared to

be less affected by weathering and vegetation cover when compared to the spectral information of the optical remote sensing data. Regionally consistent compositional patterns were readily apparent on these image enhancements and could be easily placed in the context of topographic and structural information rendered on shaded-relief SRTM and enhanced LANDSAT images.

Geological interpretation of compiled and processed data sets

At the end of February 2003 the digital compilation of the remotely sensed, airborne geophysical and geologic map data that cover the LOT 2 area was completed and properly registered on UTM projections and the MOZNET (WGS84) datum. Once this digital compilation was available, it became possible to implement interactive geological interpretation techniques in a digital (GIS) environment. The interpretation was conducted interactively in a GIS environment exploiting spatial query, overlay and image enhancement functions. This facilitated interactive enhancement of the various remotely sensed and airborne geophysical data and made it possible to compare the digital compilation of the geology maps published by Hunting.

The main objectives of the geological image interpretation were to:

- Resolve mismatches between adjacent sheets of the Hunting geological maps;
- Trace geological structures and lithological units from geological maps covering neigh-

bouring countries, particularly Zimbabwe, where the maps appear to be superior in showing lithological and structural details;

- Identify discrepancies between the Hunting geological maps and geological features inferred from the enhanced image products;
- Resolve intersecting boundary conflicts between image-inferred and map digitized geological features.

During the interpretation it appeared that in areas with no or a low density of field observations, many additional geological features could be identified from the remote sensing and airborne geophysical data sets. This was particularly true for the area south of the 16° S latitude, where virtually no fieldwork had been conducted. On the other hand, for some areas north of Lake Cahora Bassa the Hunting compilation contained geological details that could not be identified on any of the compiled data sets. Of the six lithological units of the Fíngoè Group

recognized in detailed field studies, for example, only four units (marble, quartzite, mica schist and metaconglomerate) could be extracted from the image data.

The interactive overlay of the digitized legacy geological maps on enhanced image data proved useful for matching the lithostratigraphic map units with subtle contrasts in tonal and textural image diagnostics, on which basis many more lithological units could be recognized. It should be noted, however, that the relationships between lithostratigraphic units and contrasting image diagnostic elements, such as tone, texture, shape and pattern, rarely yield straightforward one-to-one relationships. Several units on the map may match with only one identifiable unit on the enhanced imagery, or vice versa. As a result, in places with good field control and a lack of image diagnostic features, generalization of field-established lithological details into less differentiated units was unavoidable. The relationships between mapped lithological units, igneous, structural or stratigraphic patterns and image diagnostics were established by overlaying the digital geological maps on the image enhancements. Where gamma-ray spectrometry data complemented the geological information content of satellite imagery, it was helpful to first digitize boundaries on the basis of contrasting hues on the ternary radioelement image. Thereafter, boundaries could be further refined by interpreting ASTER and LANDSAT scenes.

All newly recognized units that were added to the compilation during the interpretation were assigned provisional numerical codes ranging from 0100 for Quaternary units to 2200 for Archaean units (Fig. 10). The last two digits of the numerical codes (i.e. 0107, 0106) have only been chrono-stratigraphically ordered where this was possible. The provi-

sional legend was used for the image interpretation of LOT 2 and LOT 3 in the preliminary map production phase and was replaced by new codes on the final map products.

The geological units and structures extracted by image interpretation were integrated with digitized information from the published geological maps. This was motivated by the need to provide the most up-to-date geological knowledge base for the project areas. For the LOT 3 area two interpretation products were provided. The first is a 'pure' image interpretation exclusively showing only those geological features that could be reliably recognized on the various image enhancements. The second is an integrated compilation, where features of geological maps that could not be identified via image interpretation are blended in with the image-interpreted features. Hence, the second product represented the most complete geological knowledge base, since our image interpretation significantly improved the geometry of previously mapped features while it also highlighted discrepancies with respect to existing geological maps, some of which evolved into new geological information after their significance had been established in the field.

A database was prepared that allows the transfer of codes from the Hunting geological map to the lithostratigraphic codes, respecting as much as possible the lithostratigraphic standards of Mozambique defined in the project documentation. Additional fields in the table allowed the generalization of lithological units and members into formations and groups. A 'comment' field contains remarks on lithostratigraphic interpretation problems and/or brief interpretation statements on which the allocation of the unit was based. A sample listing of a few records from this attribute table is provided in Table 1.

Table 1. Sample of attribute table used to transcribe lithostratigraphic codes of the Hunting geological map compilation (column HC) to the number codes used in this project (NEW-P).

HC	G_NAME	COMMENTS	SOURCE	NEW_P	Legend
PcR	Rushinga group, RH	Unit is inferred from Landsat TM and adjacent polygons Hunting compilation	TM interpretation	1701	[1701] Mica-hornblende gneiss
PcRt	Rushinga group, RH	<Null>	TM interpretation	1701	[1701] Mica-hornblende gneiss
PcRq	Rushinga group, RH	<Null>	Hunting compilation	1703	[1703] Quartzite
PcRq	Rushinga group, RH	Unit is inferred from Landsat TM and Zimbabwe geologic maps	TM interpretation	1703	[1703] Quartzite
PcRan	Rushinga group, RH	Unit is inferred from Landsat TM and Zimbabwe geologic maps	TM interpretation	1704	[1704] Anorthosite (?)
PcRm	Rushinga group, RH	Unit is inferred from Landsat TM and Zimbabwe geologic maps	TM interpretation	1705	[1705] Marble (?)
PcRcm	Rushinga group, RH	Unit is inferred from Landsat TM and Zimbabwe geologic maps	TM interpretation	1706	[1706] Calc-silicate gneiss (?)
PcRms	Rushinga group, RH	Unit is inferred from Landsat TM and Zimbabwe geologic maps	TM interpretation	1707	[1707] Mica schist w/ sillimanite and kyanite?
PcGq	Gairezi group, GZ	<Null>	Hunting compilation	1801	[1801] Saccharoidal quartzite with aluminous layers
PcGqs	Post - Umkondo dolerite	Post - Umkondo dolerites	Hunting compilation	1801	[1801] Saccharoidal quartzite with aluminous layers
PcG	Gairezi group, GZ	<Null>	Hunting compilation	1802	[1802] Mica schist with aluminous and quartzite layers
PcGx	Manica group, MN	?	Hunting compilation	1802	[1802] Mica schist with aluminous and quartzite layers
PcGd	Umkondo group	<Null>	Hunting compilation	1802	[1802] Mica schist with aluminous and quartzite layers
PcGxs	Umkondo group	<Null>	Hunting compilation	1802	[1802] Mica schist with aluminous and quartzite layers

PHANEROZOIC	SEDIMENTS, SEDIMENTARY AND VOLCANIC ROCKS 1 Quaternary Q 0101 Recent alluvial deposits 0101B Marine argillic alluvial deposits 0102 Interior dunes, consolidated 0103 Old terraces 0104 Coastal dunes and mobile dunes 0105 Flared dejection cones 2 Neogene N Paleogene E 0201 Mikindani Fm: Conglomeratic ferruginous sandstone and reddish sand 0202 Jafane/Murumbene Fm: Reef or sandy limestone, sand and silty mail 0203 Purple sandstone of Inhanga 0204 Cheongoma Fm: Humulitic limestone, glauconitic sandstone with basal limestone 0206 Tertiary undifferentiated 3 Cretaceous K 0301 Margas com Globotruncana Fm: Marl, sometimes with salt, limestone or gypsum 0302 Magoe Fm: Sandstone with pebbles from eruptive rocks of Karoo, with a clayish-carbonatic matrix 0303 Magoe Fm: Thin lacustrine limestone beds (basal and locally). Semiconsolidated sandstone (locally). 0304 Sena Fm: Conglomeratic sandstone, with pebbles from eruptive rocks of Karoo. 0304B is enriched in Th 0305 Maputo Fm: Marly argillic glauconitic sandstone, with conglomeratic at base 0307 Trachyte 0309 Upper Lupata Fm: Quartzofeldspathic conglomeratic sandstone 4 KAROO 0405 Upper basalt, amygdaloidal 0406 Intermediate rhyolite 0406B Umbekuzi (Intermediate) Rhyolite 0406C Dos pequenos Bombos (Upper) Rhyolite 0407 Lower basalt 0408 Undifferentiated tholeiitic basalt 0408B Moveni basalt (Lower and Upper) 0409 Rhyolite of Lupata 0410 Lower Lupata Fm: Sandstone, conglomerate 0401 Lower Karoo, undifferentiated 0402 Conglomeratic sandstone 0403 Basal conglomerate			5 PHANEROZOIC INTRUSIONS Intrusions and dykes of various ages, mainly Jurassic and Cretaceous 0502 Granite 0503 Syenite, monzonite 0505 Carbonatite 0508 Gabbro, diorite, basalt 0513 Contact silt with calc-silicates
	8 ZAMBUE Grp 0801 Quartzofeldspathic micagneiss 0802 Quartzofeldspathic migmatite 0804 Meta-arkose 0805 Marble, calc-silicate gneiss 12 LUIA grp 1201 Quartzofeldspathic mica gneiss 1202 Granulitic gneiss 1203 Quartzofeldspathic granulitic gneiss 1204 Roughly banded gneiss, orthogneiss 1205 Mafic gneiss 1206 Marble, calc-silicate rock 15 BARUE Cplx 1501 Quartzofeldspathic gneiss 1502 Quartzofeldspathic, local aluminous gneiss 1502B Felsic gneiss 1503 Mafic gneiss 1503B Mafic to ultramafic gneiss 1506 Quartzite 1507 Marble 1511 Hornblende gneiss, amphibolite 18 GAIREZI Grp 1801 Barchanitic quartzite with aluminous layers 1802 Mica schist with aluminous and quartzitic layers 1805 Quartzite 9 FINGOE Grp 0901 Mica schist, metagranulite 0902 Mica schist, metagranulite, metapelite 0903 Mica schist 0905 Quartzite 0906 Marble, calc-silicate gneiss 0912 Metaconglomerate 13 LURIO Supergrp 1301 Allochthonous mylonite 1302 Granulite gneiss 16 CHURE Supergrp 1601 High-grade gneiss and granulite 1602 Mica schist and gneiss 1603 Marble 10 ANGONIA Grp 1001 Quartzofeldspathic gneiss 1002 Mafic gneiss 1003 Leucocratic banded gneiss 1006 Limestone, calc-silicate gneiss 1009 Nephelinitic gneiss 14 NAMPULA Supergrp 1401 Migmatitic mesocratic gneiss 1402 Leucogneiss and granitic leptonite 17 RUSHINGA Grp 1701 Mica-hornblende gneiss 1703 Quartzite 1705 Marble 1706 Calc-silicate rock 1707 Mica schist 19 UMKONDO Grp 1903 Slate and silty slate 1904 Lower quartzite 1905 Silty slate 1906 Siliceous and calcic hornfels 1907 Dolomite, post-Umkondo			6 EARLY PHANEROZOIC OR/LATE NEOPROTEROZOIC PLUTONIC ROCKS 0602 Granite 0603 Granite, adamellite 7 PROTEROZOIC PLUTONIC ROCKS 0701 Granodiorite, adamellite Tete suite and equivalent coarse-grained rocks 0702 Gabbro, leucogabbro 0703 Anorthosite 0704 Pyroxenite 0706 Charnockitic granite 0707 Syenite, monzonite 0709 Gabbro 0710 Diabase, amphibolite ATCHIZA Cplx 0711 Serpentine, peridotite 0712 Gabbro, norite, diorite 0713 Metapyroxenite Other suites and rocks 0723 Charnockitic granite 0732 Metadolomite 0733 Gabbro 0741 Undifferentiated granites of Nampula Supergp.
ARCHEAN	21 GRANITE GNEISS Cplx 2101 Granitoid, isolated granitoid 2102 Charnockitic granitoid 2103 Banded TTG gneiss 22 MANIGA Grp M'Beza/Vengo Fm 2201 Mica schist, graphite schist, slate metagranulite 2202 Quartzite, meta-arkose, metasandstone 2204 Calc-silicate rock Macequece Fm 2221 Metabasalt 2222 Peridotite, serpentinite			

Fig. 10. Provisional legend distilled from previously published geological maps (Hunting Ltd. 1984) and unpublished DNG reports used for image interpretation.

Fieldwork planning

Areas of high outcrop density and secondary roads were interpreted from the 15-metre TM band 8 and colour composite images of bands 7, 3 and 1 for the entire project area. Most areas of good bedrock exposure can be recognized as positive features in the topographic relief with a rough and 'dotty' image texture. It was difficult to identify the primary and secondary roads, such that only segments of many could be identified. Some roads or paths do not appear to be connected to the paved road network and instead appear to originate from minor settlements in remote areas. Additional roads were identified from colour composites of geometrically corrected ASTER scenes, now available. A digital interpretation guide map was prepared to document areas considered of specific interest for follow-up work before the start of the first field season. The interpretation guide shows areas of specific interest as numbered polygons on the interpretation. The polygons are linked to an attribute table with a memo field for details on the reasoning followed during the interpretation, including preliminary geological ideas and hypothesis to be verified during fieldwork. The targets overlap with areas defined in the fieldwork activity plan, previously submitted. The interpretation guide also contains a number of traverse suggestions with concise description of follow-up targets along the traverse (Fig. 11).

Geological image interpretation results

This section provides a generalized summary of the geological image interpretation conducted for

LOT 2 and LOT 3. The geological interpretation of lithostratigraphic units and structures is based on qualitative descriptions of diagnostic interpretation elements derived from the LANDSAT 7 enhanced thematic mapper (ETM), magnetic, gamma-ray spectrometry, shuttle radar topographic mission (SRTM) data and the derived image fusion products. Table 2 lists the most frequently used image enhancements. Image sub-scenes with labelled overlays illustrate how the lithostratigraphic units and structures were outlined on the various enhancements generated from LANDSAT 7 ETM, airborne geophysical and shuttle radar terrain mapping (SRTM) data. The description of the image diagnostics for the lithostratigraphic units are grossly ordered from old to young into nine groups ranging in age from Archaean to Quaternary (Fig. 12). The internal order within each group, however, was highly provisional and accommodates, in addition to stratigraphic order, lateral variations in the lithostratigraphic encoding of rock units. This is because the stratigraphic and geochronology information was at this preliminary stage of geological mapping still based on a variety of older geological map publications. These were the most up-to-date sources of information before the fieldwork and associated U/Pb zircon dating sample campaigns were undertaken. The unit numbers on the interpretation examples correspond with those of the legends of the provisional geological maps of LOT 2 and LOT 3.

Table 2. Image enhancements commonly employed for the geological image interpretation of the LOT 2 and LOT 3 project areas.

Image enhancement	Spatial resolution	Enhancement procedure
Landsat 7 ETM731 colour composite	30 m	Colour composite image with standard deviation stretch 2 sigma for each band, red= band 7, green = band 3 and blue = band 1
Total field magnetic intensity grid	250 m	Histogram equalization combined with relief shading, declination 330°, inclination 25° in rainbow colour spectrum and in grey scale
1st. vertical derivative magnetic grid	250 m	Standard deviation stretch of 1st. vertical derivative magnetic grid in grey scale
Ternary relief-shaded SRTM	90 m	Colour composite image with standard deviation stretch for each band. Bands are relief shaded SRTM data with illumination azimuths at 120° angles with each other.
IHS [K-eTh-eU]-TMB7 composite image	30 m	Intensity-Hue-Saturation composite image where hue and saturation are modulated by radioelement grids (K = red, eTh = green, eU = blue) and intensity is modulated by high-pass filtered Landsat ETM band 7.
IHS [K-eTh-eU]-relief-shaded-SRTM composite image	90 m	Intensity-Hue-Saturation composite image where hue and saturation are modulated by radioelement grids (K = red, eTh = green, eU =blue) and intensity is modulated by relief-shaded SRTM data.

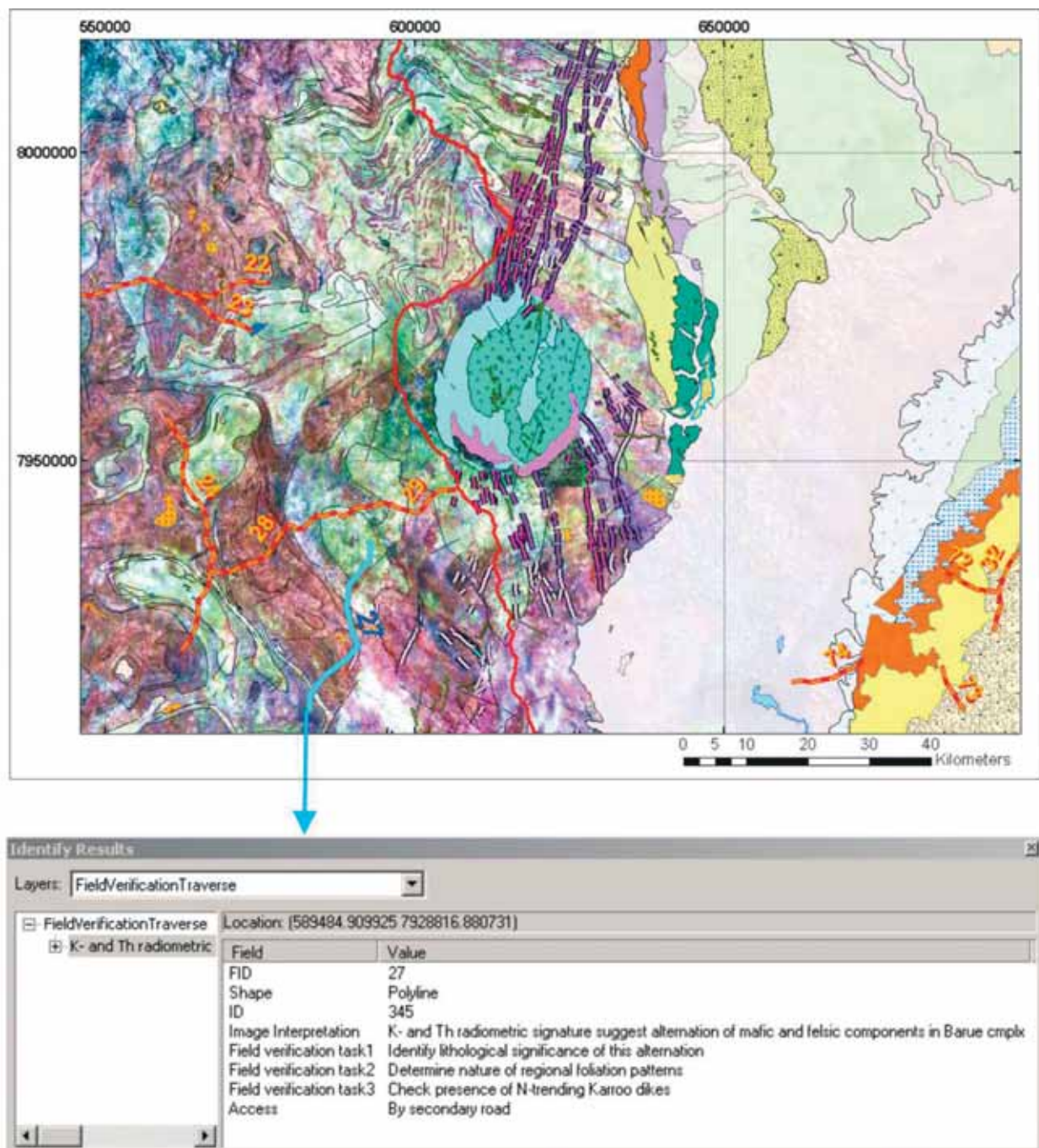


Fig. 11. Example of a digital fieldwork traverse plan (red-orange stippled lines) for the south of LOT 2 compiled on the basis of the interpretation of roads providing access to the target areas from ASTER VNIR scenes. Clicking on the traverse 27 (blue stippled line) opens the attributes associated to the traverse. The attributes include a concise description of the image interpretation together with a number of suggestions for verification in the field. The background shows an IHS [K-eTh-eU]-ETM7 composite image of the Barue Complex with an overlay of the provisional geological map compilation for the sedimentary cover and the Serra de Gorongosa intrusive ring complex with its satellite dykes.

Archaean granite-gneiss terrains and greenstone belts

Rocks that belong to the eastern margin of the Archaean Zimbabwe craton are exposed for ca. 300 km along the border between Mozambique and Zimbabwe (Fig. 12). These rocks are mainly composed of granitoid, banded TTG gneiss and include

the eastern portions of the E-W trending Udzi-Mutare-Manica and Cronley-Munhinga greenstone belts that extend from Zimbabwe. Both greenstone belts are characterized by prominent E-W trending linear magnetic anomalies (Fig. 13A), probably due to magnetic susceptibility contrasts between the metabasalt and metasedimentary units within them. The airborne radioelement concentrations of the Ar-

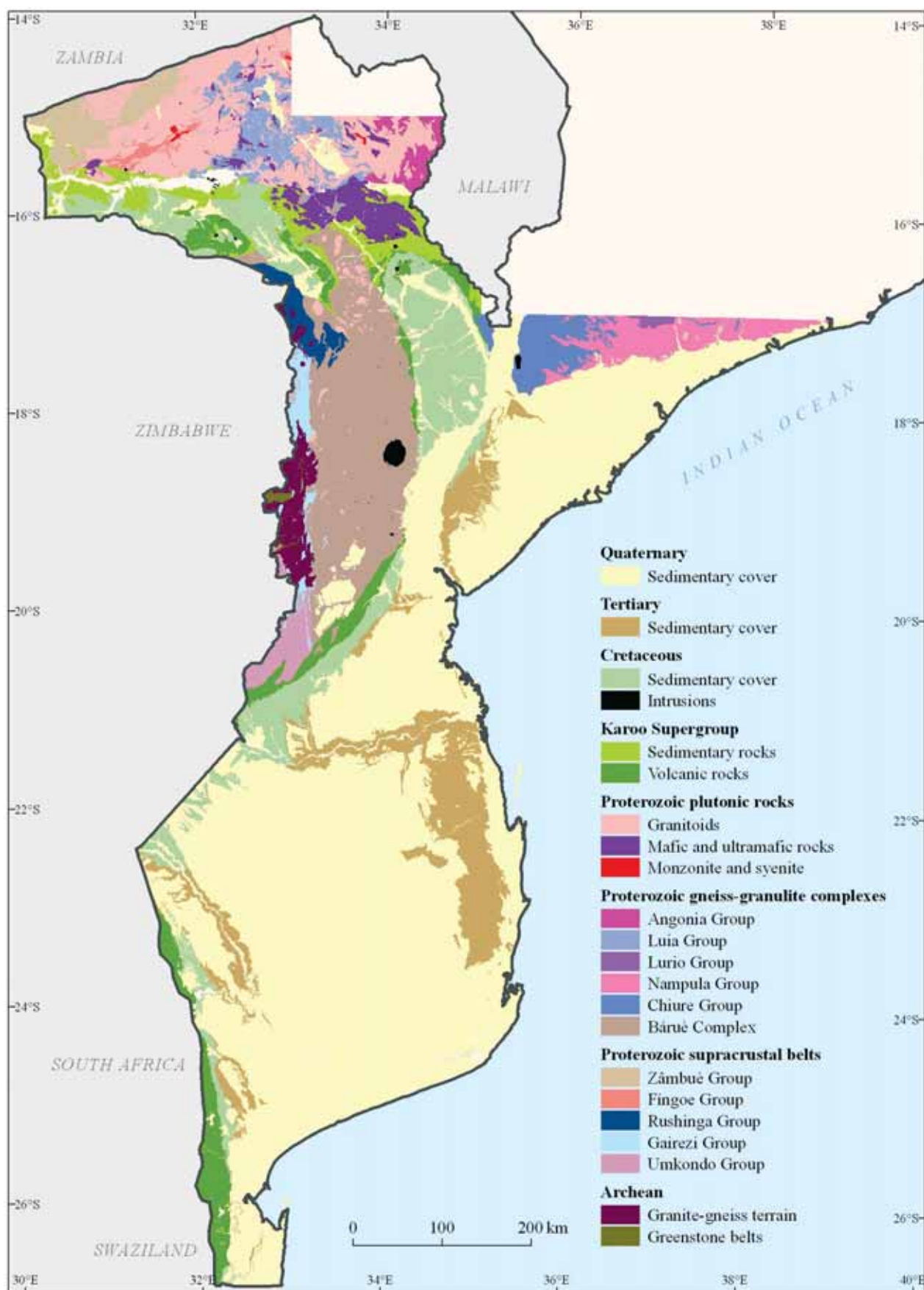


Fig. 12. Distribution of interpreted provisional lithological units (generalized in groups) from Archaean to Quaternary.

chaean units are generally low with the exception of some granitoid units. The greenstone belts generally display dark green hues and smooth image texture on the LANDSAT ETM colour composite images and form linear positive features that outline foliation form lines within the greenstone belts. Metabasalts have the darkest tone while schist and psammitite are slightly lighter in tone (Figs. 13B, D).

On a LANDSAT ETM731 colour composite image, the granitoids and gneisses exhibit light pink, white-yellow tones and display moderate to coarse image textures. Isolated Archaean granite-gneiss domes forming circular basement inliers beneath supracrustals of the Rushinga and Gairezi Groups have been outlined on the magnetic data (Fig. 13E) and LANDSAT ETM colour composite images

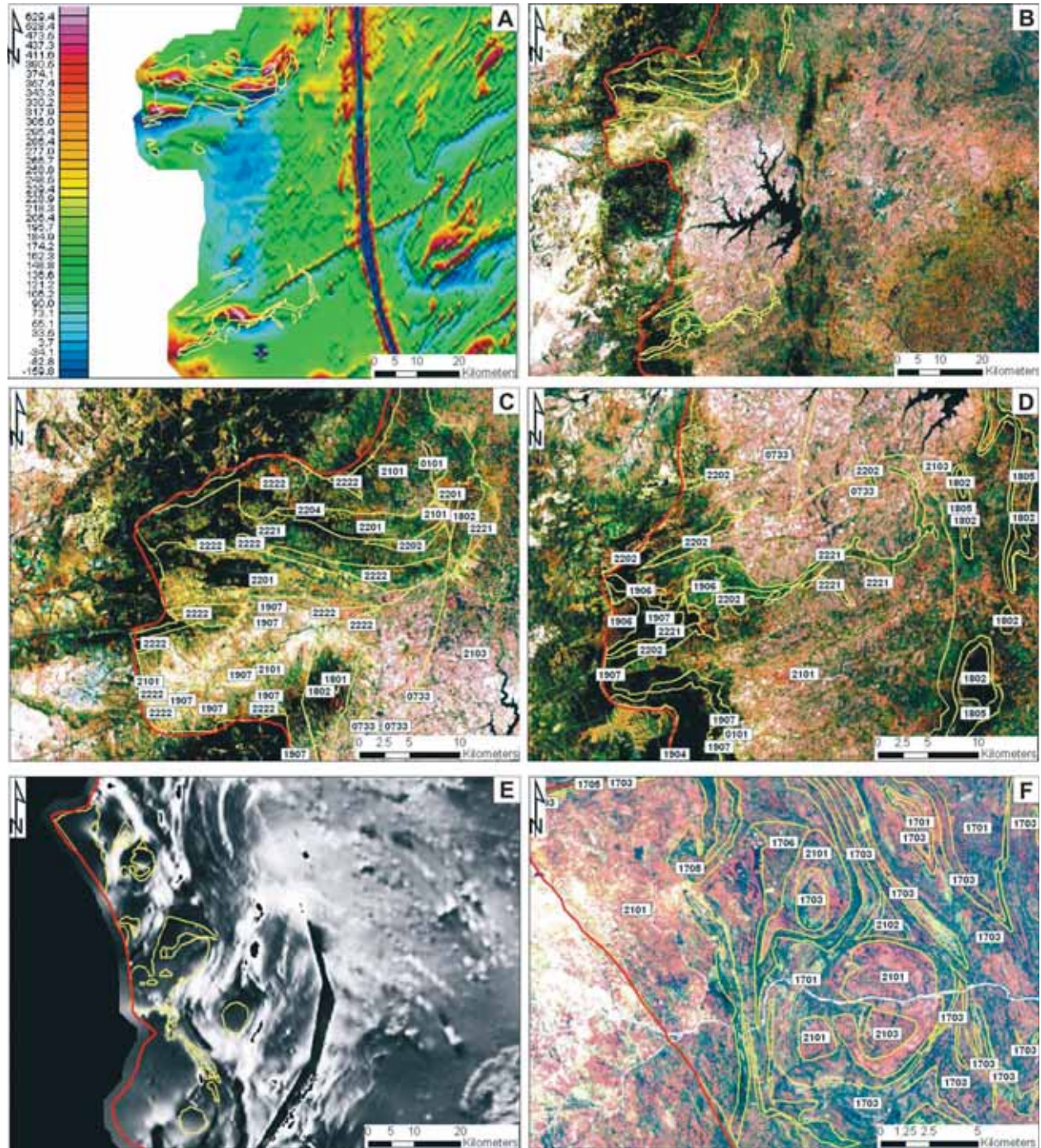


Fig. 13. Image interpretation examples of Archaean units. A) Total field magnetic intensity image displaying prominent E-W trending linear anomalies associated with the Manica and Cronley greenstone belts; B) LANDSAT ETM 731 colour composite image with outline of the Manica and Cronley greenstone belts (yellow lines); C) Detail of B showing interpreted units of the Manica greenstone belt 2201: Mica schist, graphite schist and metagraywacke, 2202: quartzite and metasandstone, 2204: calc-silicate rocks. 2221: metabasalt, 2222: peridotite, serpentinite; D) Detail of B showing interpreted units of the Cronley greenstone belt; E) Inliers and circular domes of Archaean granitoids to the North of Manica, corresponding to circular magnetic lows with smooth magnetic relief; F) Detail of image E interpreted Archaean domes.

(Fig. 13F). Their interpretation is supported by their inferred lower structural position and the similar hue and texture of the units on the LANDSAT colour composite images when compared with granitoid and gneiss units on 1:250 000 scale geological maps of the Zimbabwe craton towards the west.

Proterozoic supracrustals

The majority of Proterozoic supracrustal rock units occur in the Umkondo, Gairezi, Rushinga, Zambuè, and Fíngoè Groups (Fig. 12). In general, supracrustal units can be recognized on LANDSAT colour composites by their 'layered' appearance, since their outcrops correspond to linear topographic features. Alternations of linear valleys and ridges are common and suggest foliation and/or bedding-parallel competency contrasts between the various supracrustal units within a particular formation or group. Quartzite, quartzo-feldspathic gneiss, metaconglomerate and psammite form linear elevated ridges, whereas schist, phyllite and slate generally occur in areas of lower elevation. Curvilinear ridges and intervening linear valleys outline regional occasionally doubly-plunging fold structures, particu-

larly in the Zambuè, Fíngoè and Rushinga Groups (Figs. 14A, C). Occasionally, carbonate rocks (marbles) of the Zambuè and Rushinga Groups can be recognized on the basis of their spectral signature appearing in blue to cyan tones on the LANDSAT ETM 731 colour composite images. The quartzites of the Gairezi Group also show conspicuous spectral contrasts with the post-Umkondo basic dykes and sills on LANDSAT ETM 731 colour composite images (Fig. 14D). In addition to the above LANDSAT image diagnostics, supracrustal units can be recognized on gamma-ray spectrometry grids by their relatively low radioelement concentrations with the exception of the thorium-rich metasediments of the Zambuè Group. They also exhibit strong linear and curvilinear magnetic anomaly patterns on colour shaded-relief images of the 1st vertical derivative and the residual (IRGF subtracted) of the total magnetic field.

Proterozoic gneiss-granulite complexes

Quartzo-feldspathic, mafic and bimodal gneisses comprise a relatively large percentage of Proterozoic units in the LOT 2 project area and its exten-

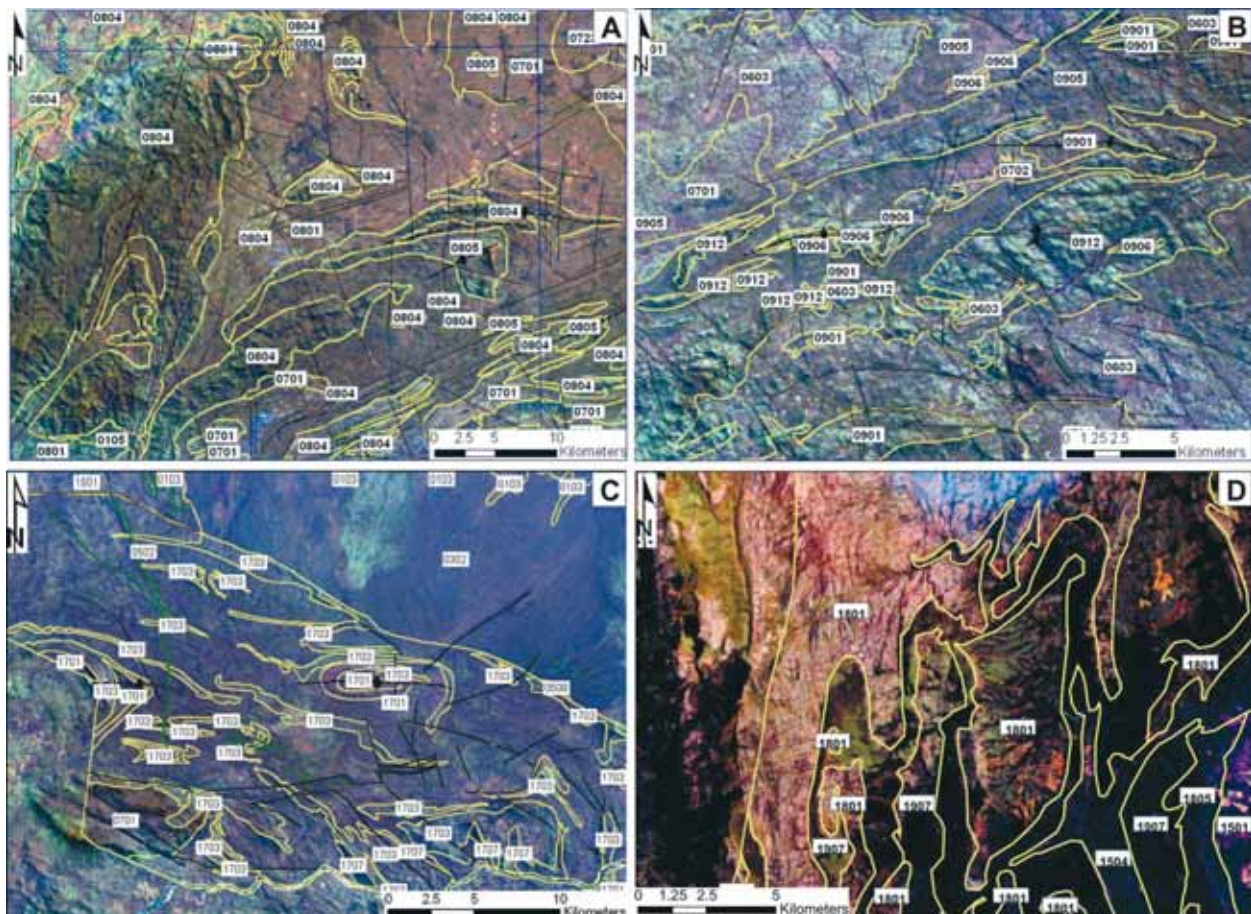


Fig. 14. LANDSAT ETM image interpretation examples of Proterozoic metasedimentary rock units. A) 0801: quartzo-feldspathic migmatitic gneiss, 0804: meta-arkose and 0805: marble and calc-silicate gneiss of the Zambuè Group; B) 0901: mica schist, metagraywacke, 0905: quartzite, 0906: marble, calc-silicate gneiss, 0912: metaconglomerate of the Fíngoè Group; C) 1701: mica-hornblende gneiss and 1703: quartzite of the Rushinga Group. Green lines outline Karoo dolerite dykes; D) 1801, 1805: quartzites of the Gairezi Group intruded by 1907: post-Umkondo dolerite sills.

sion east of it. They include the Luia, Chidue and Angonia Groups in the north, the Barue Complex in the south and the Nampula, Lurio and Chiure Supergroups in the east (Fig. 12). The gneisses of the Luia Group and the Chiure and Lurio Supergroups contain high-grade mafic and quartzo-feldspathic gneisses and granulite gneiss. Presumably, as a result of their mixed composition and interference with land-use patterns, the gneisses have variable tone and colour on LANDSAT ETM 731 colour

composite images ranging from white, light pink to dark green and grey tones. The Angonia and Luia Groups as well as the Chiure, Lurio and Nampula Supergroups are difficult to distinguish from each other and from the granitoids that intrude them. In general, subtle linear patterns within the gneiss belts in combination with a relatively smooth image texture provide the only diagnostic criteria that allow their differentiation from less foliated or unfoliated intrusive units (Figs. 15A, C). The gamma-ray spec-

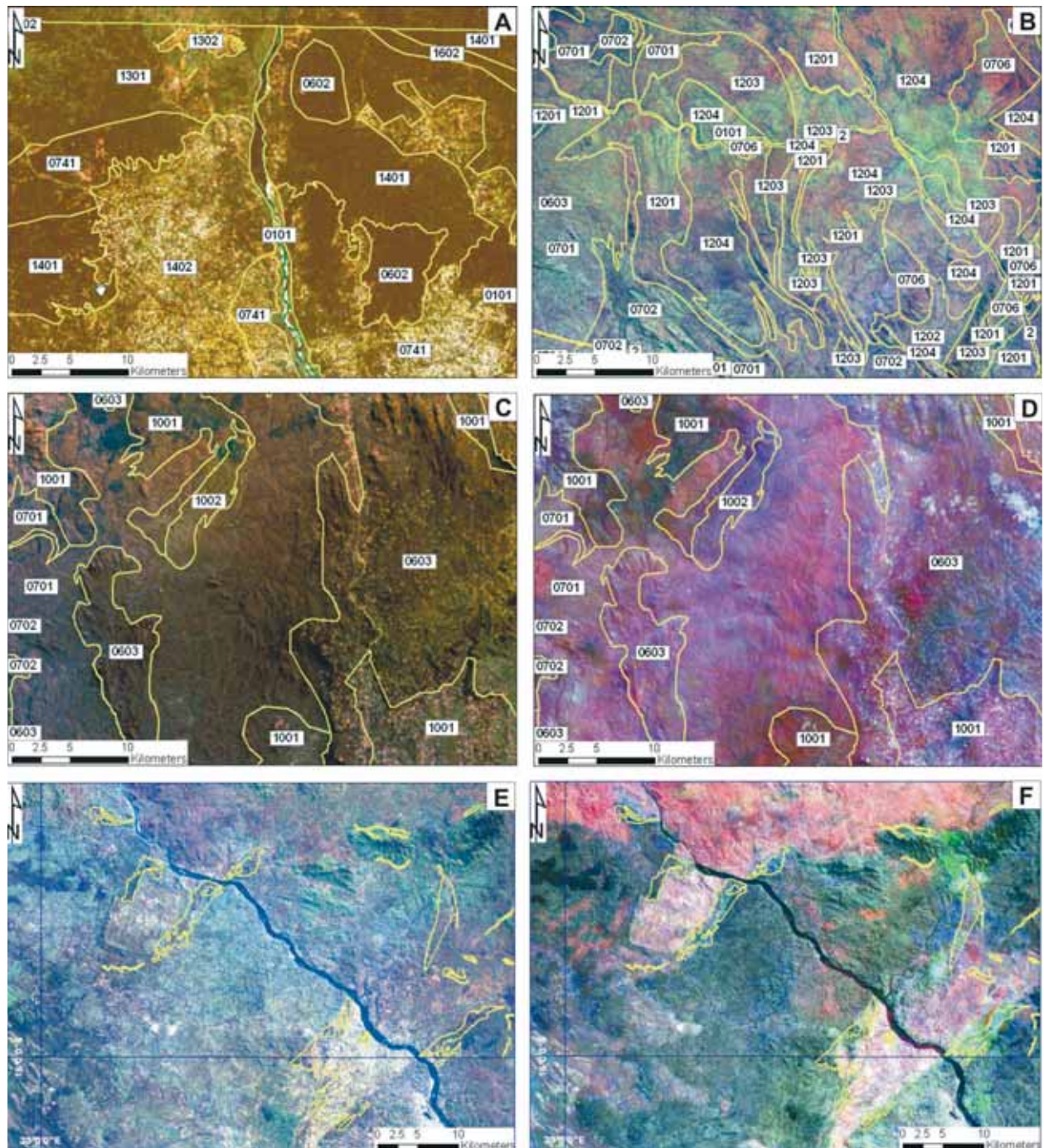


Fig. 15. Image interpretation examples of Proterozoic gneiss units. A) 1301: mylonite and 1302: granulite gneiss of the Lurio Supergroup; 1401: migmatitic gneiss and 1402: leucogneiss of the Nampula Group; 1601: high-grade gneiss and granulite of the Chiure Group; B) Gneiss units of the Luia Group; C) 1001: Quartzofeldspathic and mafic gneiss of the Angonia Group; D) Same as C but with IHS [K-eTh-eU]-TMB7 composite image in the background; E) LANDSAT ETM colour composite image northwest of Tete at ca. 16° S and 33° E with outlines of Chidue Group carbonates; F) IHS [K-eTh-eU]-TMB7 composite image of the area shown in Fig. E.

trometry grids provided slightly better diagnostics, since many of the gneiss units have low to moderate radioelement signatures that contrast with the higher radioelement concentrations of the surrounding granitoid units (Fig. 15D).

Internal differentiation of the Angonia, Luia Groups and Nampula Supergroups into units of different metamorphic grade and bulk mineralogical composition can only be locally established on basis of the linear topographic expression of granulite and calc-silicate gneiss of the Chidue Group (Fig. 15E), which also exhibit anomalously high thorium concentrations (Fig. 15F). This suggests that some of the Chidue Group carbonates were not of supracrustal origin but rather represent deformed and metamorphosed carbonatites. In general, however, diagnostic image characteristics needed to differentiate quartzo-feldspathic gneiss, mafic gneiss and granulite within any of these groups are lacking.

The Barue Complex displays conspicuous foliation trajectories involved in spectacular kilometric-scale basin and dome interference fold structures

that can be outlined on LANDSAT ETM, gamma-ray spectrometry, shaded-relief total magnetic field data and to some extent on shaded-relief SRTM data (Figs. 16A, D). Variation in bulk rock composition parallel to the gneissic banding is suggested by alternating bands of light-orange and dark-green hues on the LANDSAT ETM731 colour composite images (Fig. 16A), which correspond to zones with high total count values and thorium concentrations, respectively, low total count values and low thorium concentrations on the gamma-ray spectrometry grids (Fig. 16B). The most felsic units (1502B) correspond to negative magnetic anomalies (Fig. 16C).

Proterozoic to Early Palaeozoic plutonic rocks

Voluminous Mesoproterozoic and minor occurrences of early Palaeozoic plutonic rocks are exposed in the Tete province in the north of the LOT 2 area, whereas lesser amounts are exposed among the gneissic units of the Barue complex (Fig. 12).

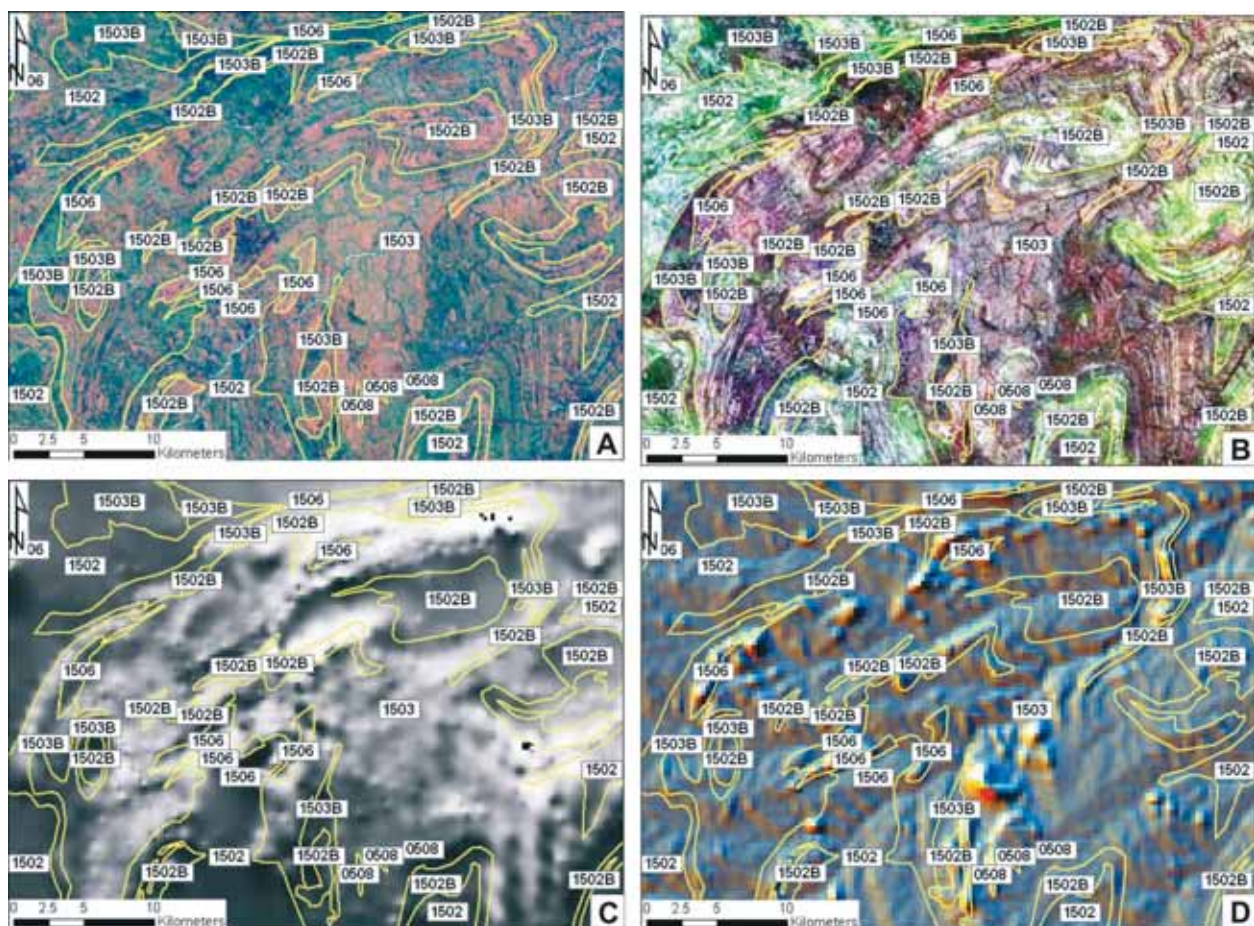


Fig. 16. Image interpretation examples of the gneissic units of the Barue Complex. A) LANDSAT ETM 731 colour composite with interpretation superimposed (in yellow); units: 1502: Intermediate to felsic gneiss 1502B: quartzo-feldspathic gneiss; 1503: mafic gneiss and 1503B: ultramafic to mafic gneiss; B) IHS composite image [K-eTh-eU]-TMB7 with interpretation superimposed; C) Total field magnetic data with interpretation superimposed. Note magnetic lows corresponding to unit 1502B; D) Relief-shaded SRTM data with interpretation superimposed.

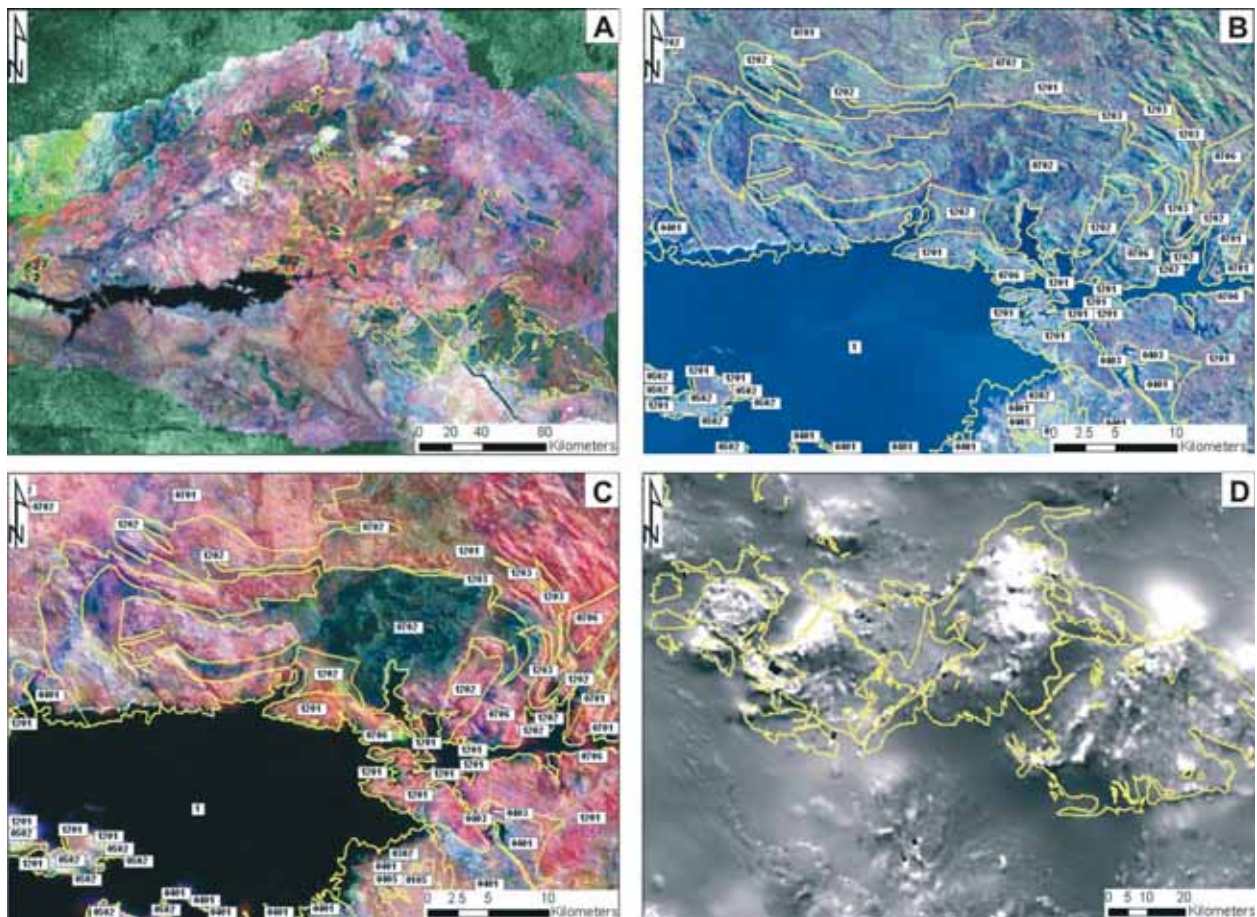


Fig. 17. Image interpretation examples of Proterozoic mafic and ultramafic plutonic units exposed in Tete Province. A) Regional view of mafic and ultramafic units of Tete Province (yellow outlines). The largest are 1: Atchiza Suite, 2: Chipera Suite and 3: Tete Suite; B) LANDSAT ETM colour composite of the Chipera mafic Suite (0702: gabbro); C) IHS [K-eTh-eU]-TMB7 composite image of Chipera mafic Suite. The low radioelement concentrations yield a dark grey tone on the IHS composite image that contrasts with the K-rich signature of adjacent gneissic and granitoid units; D) Total magnetic intensity image with outline of the Tete Suite.

They can be subdivided into two major suits: (1) ultramafic-mafic intrusions and (2) synkinematic to post-kinematic granitoids. The ultramafic-mafic rocks include three intrusive suites: the Atchiza Suite at the northwestern shore of Lake Cahorra Bassa, the Chipera Suite at the northeastern shore of Lake Cahorra Bassa and the Tete Suite to the north east of the town of Tete, which is by far the largest of the three (Fig. 17A). The mafic-ultramafic suits have a slightly darker image tone on the LANDSAT colour composite images and a relatively smooth texture in comparison to adjacent gneiss-granitoid terrains (Fig. 17B), low to very low radioelement concentrations (Fig. 17C) and a high total field magnetic background with rough magnetic textures (Fig. 17D). The granitoid suites have been classified based on local field relationships into three groups: pre-Fíngoè, post-Fíngoè and late tectonic granites. Although this classification has been maintained in our image interpretation, it was noted that the regional configuration of airborne radioelement sig-

natures provided scope for alternative classifications of the various granitoid plutonic suites. The classification of granitoids was amended after fieldwork and U/Pb zircon age dating, since granitoids previously believed to be older than the Fíngoè Group appeared to postdate it (Mänttari this volume).

Mesoproterozoic granitoids in the LOT 2 area have high total count signatures and elevated K or eTh airborne concentrations that stand out against those of supracrustal belts and mafic igneous rocks and gneiss belts (Fig. 18A). Relative bright image tones and coarse image textures on LANDSAT colour composite images, in addition, allow the differentiation of Mesoproterozoic granitoid units from gneiss and supracrustal belts, although this does not consistently apply throughout LOT 2. Charnokitic granites, such as the 'Castanho Granite', underlie rugged mountainous terrains displaying a highly dissected topographic relief. This allows their differentiation from the supracrustal belts and mafic igneous units with which they are in contact

(Figs. 18B, C). Pan-African Early Paleozoic granite plutons (unit 0602) stand out as conspicuous high total count anomalies with elevated airborne eU concentrations (Fig. 18D).

Karoo Supergroup **(Upper Carboniferous - Jurassic)**

Sedimentary and volcanic rocks of the Karoo Supergroup were deposited in E-W and NW-SE trending rift basins that formed during the predecessor and subsequent stages of Gondwana breakup (Maninen *et al.* this volume). Sedimentary rocks of the Karoo Supergroup are dominantly exposed along the Zambezi River and its tributaries and along the shores of Lake Cahorra Bassa, whereas volcanic rocks (mainly basalt and rhyolite) are exposed at the margins of the Precambrian basement throughout the LOT 2 and LOT 3 areas as far south as the

border of Mozambique with Swaziland. Figure 12 shows the distribution of Karoo and superimposed post-Karoo basins in the LOT 2 and LOT 3 areas.

Sedimentary and volcanic units of the Karoo Supergroup display characteristic linear image patterns related to sedimentary bedding, igneous jointing or internal drainage. This rendered differentiation with the underlying Precambrian units straightforward. Volcanic rocks of the Karoo Supergroup are dominated by basalt, with diagnostically low radioelement concentrations that contrast with the relatively high radioelement concentrations of the rhyolite flows.

Sedimentary units of the Karoo Supergroup exposed around Lake Cahora Bassa and the Zambezi River can be easily differentiated based on the contrasting image tone, topographic relief, drainage and fracture patterns on LANDSAT ETM colour composite images (Fig. 19A), whereas the basaltic units can be easily distinguished from the sedimen-

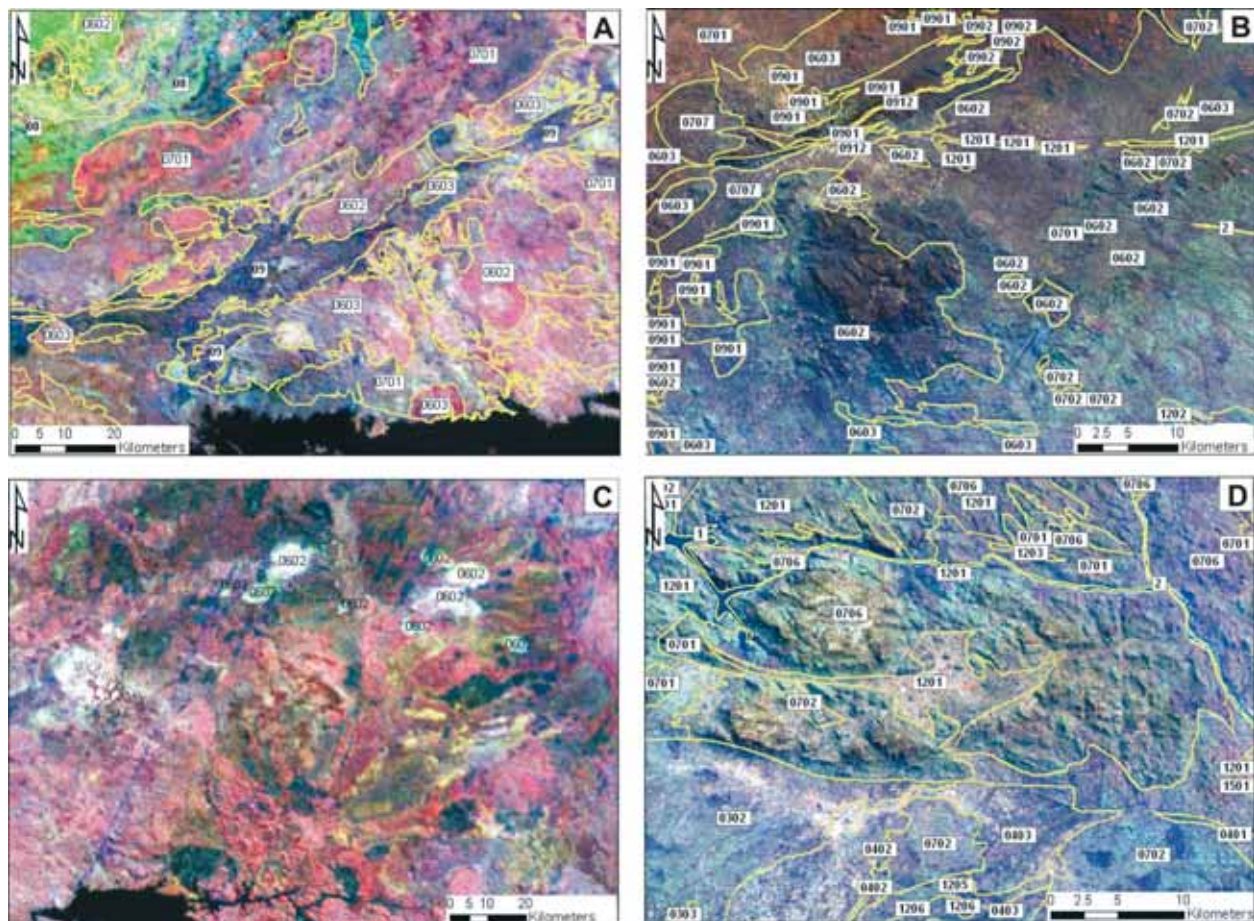


Fig. 18. Regional view and image interpretation examples of Meso- and Neoproterozoic granitoid intrusions in Tete Province. A) IHS [K-eTh-eU]-TMB7 composite image showing distinct radioelement signatures of granitoids (units 0701, 0602 and 0603) in the Fíngõe area; B) LANDSAT ETM 731 colour composite image showing contrasting image texture on the basis of which unit 0701 (pre-Fíngõe granite) can be differentiated from younger granites 0602 and 0603; C) Rugged terrain underlain by unit 0706: Charnokitic granite yields a distinct rough image texture in addition to a brown tone on the LANDSAT ETM 731 colour composite image; D) IHS [K-eTh-eU]-TMB7 composite image showing distinct high radioelement concentrations of a regional cluster of post-kinematic Neoproterozoic granite plutons in northern Tete Province.

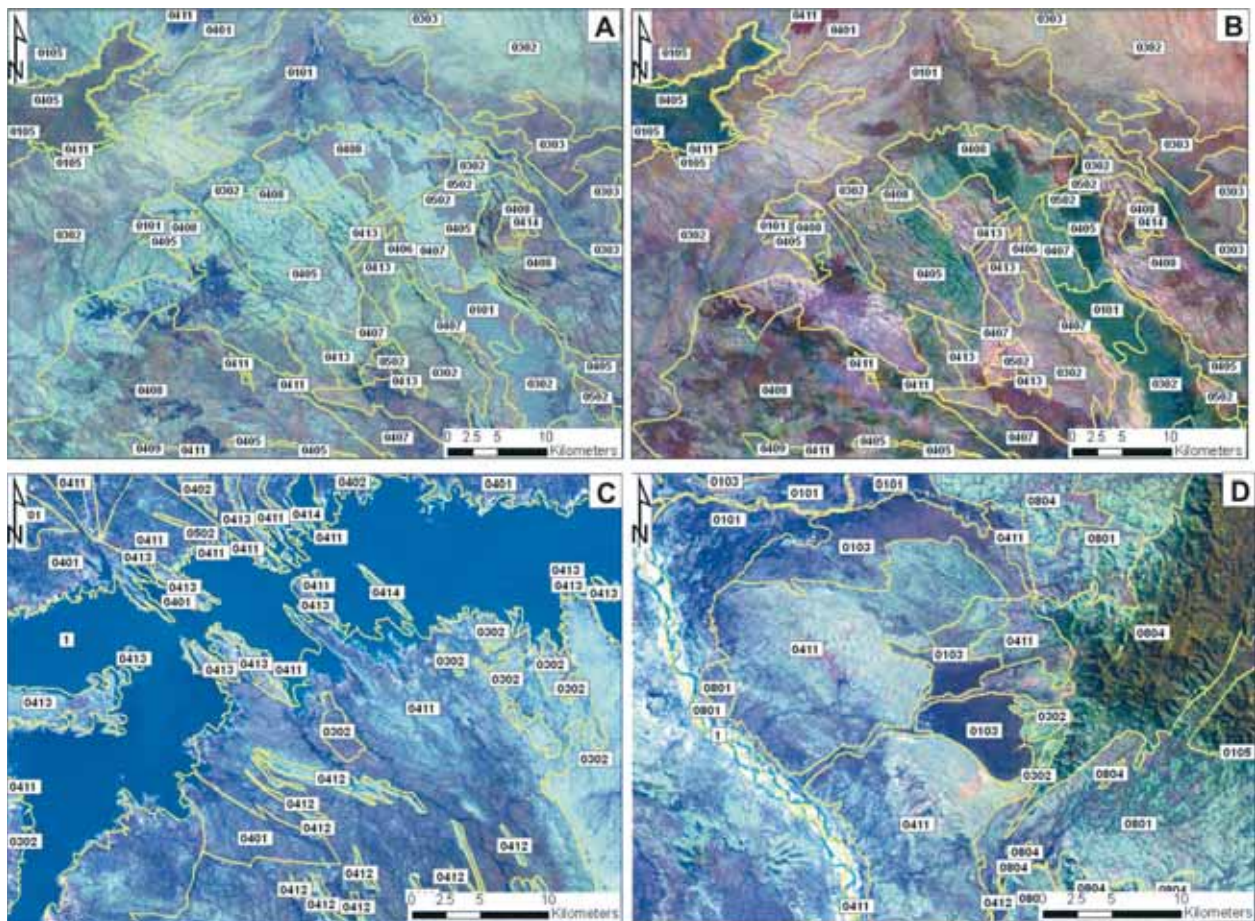


Fig. 19. Image interpretation examples of sedimentary and volcanic units of the Karoo Supergroup. A) LANDSAT ETM 731 colour composite west of Tete showing sedimentary and volcanic rock units: 0401: Lower Karoo, undifferentiated, 0405: Upper basalts, 0407: Lower basalts, 0408: tholeiitic basalts, 0411: Upper Karoo, undifferentiated, 0413: basalt, sandstone (Stormberg member), 0414: Dolerite; B) IHS [K-eTh-eU]-TMB7 composite image of the same area as shown in Fig. A; C) LANDSAT ETM 731 colour composite image of the shores of Lake Cahora Bassa showing sedimentary units of the Karoo Supergroup, 0401: Lower Karoo clastic sedimentary rocks (undifferentiated) 0411: Upper Karoo clastic sedimentary rocks (undifferentiated) 0412: conglomeratic sandstone, 0413 Stormberg member; D) LANDSAT ETM 731 colour composite image northwest of Lake Cahorra Bassa showing Upper Karoo sedimentary rocks (0411).

tary units based on their low gamma-ray spectrometry signatures (Fig. 19B). The coarser clastic units (sandstone and conglomerate) often stand out due to their bright image tone against the units consisting of finer grained clastics (Fig. 19C). The lower, slightly dissected relief renders their distinction from the strongly dissected Precambrian basement and peneplains underlain by Quaternary cover (Fig. 19D).

Further towards the south, exposures of volcanic units, mainly basalt and rhyolite of the Karoo Supergroup, exclusively exist. The basalts have a dark grey-blue image tone on LANDSAT ETM731 colour composite images with characteristic rectangular drainage patterns (Fig. 20A). The intensive dyke swarms that occur within the basalt units are readily apparent on grey-scale images of the 1st vertical derivative magnetic field (Fig. 20B). The rhyolites that are interlayered with the basalts in the southern

half of the LOT 3 area have a prominent positive topographic expression with highly dissected relief on shaded-relief SRTM data (Fig. 20C), and exhibit light cream to orange hues and internal linear fracture patterns on LANDSAT ETM 731 colour composite images (Fig. 20D).

Cretaceous intrusions

Younger intrusions include alkaline ring complexes, carbonatites and alkaligranite dikes and are all inferred to be Cretaceous in age (Hunting, 1984). The most prominent of these intrusions are Cone Negoso on the north shore of Lake Cahorra Bassa consisting of carbonatite with satellite trachyte cones to the south of it, the Salambidua complex on the border with Malawi and the large Serra de Gorongosa ring complex (now dated to 181 Ma,

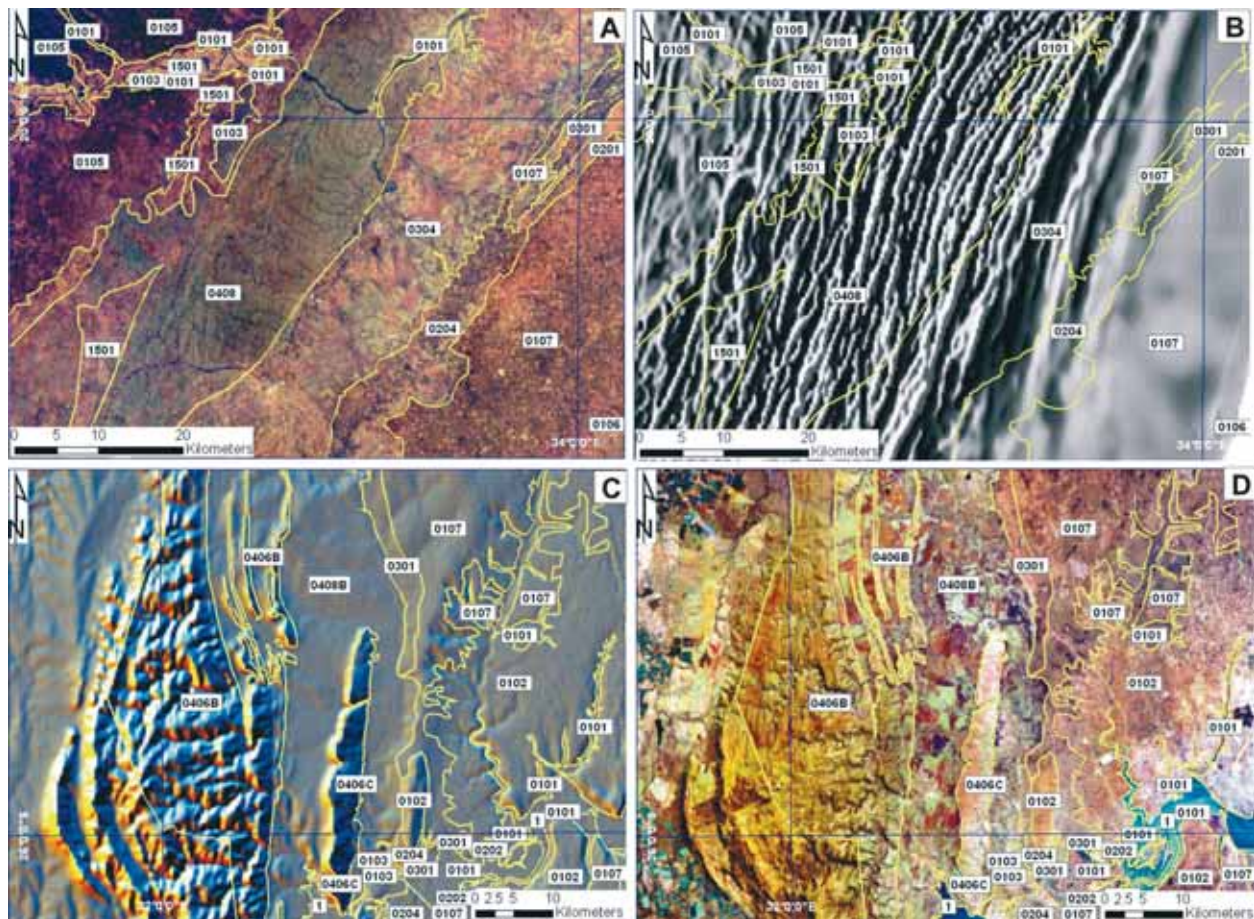


Fig. 20. Image interpretation examples of volcanic units of the Karoo Supergroup. A) LANDSAT ETM 731 colour composite at 20° S and 34° E showing tholeiitic basalt of the Karoo Supergroup; B) First vertical derivative magnetic field of the area shown in Fig. A illustrating straight linear anomaly patterns associated with a dyke swarm within unit 0408. The continuation of the linear anomaly pattern east of unit 0408 suggests the presence of unit 0408 in the subsurface beneath Cretaceous-Tertiary sedimentary cover; C) Relief-shaded SRTM data showing a strong contrast in topographic expressions between rhyolite (units 0406B/0406C) and tholeiitic basalt (unit 0408); D) LANDSAT ETM 731 colour composite of the areas shown in Fig. C.

Lower Jurassic, see Mänttari (this volume) consisting of alkali granite, gabbro, syenite, monzonite as well as a contact skarn consisting of calc-silicate rocks in the hosting gneisses of the Barue Complex (Fig. 12). All of these intrusions have a prominent topographic expression that can be easily recognized from relief-shaded SRTM data (Figs. 21A, B). The carbonatites, in addition, yield some of the highest total count, thorium and uranium anomalies on the gamma-ray spectrometry grids (Figs. 21C, D). The associated satellite cones and dykes are too small to yield anomalies in the geophysical data but can be easily identified from the LANDSAT ETM 731 colour composite images (Figs. 21E, F).

Cretaceous sedimentary units

Cretaceous sedimentary units are exposed within the NNW, NNE, and E-W trending rift basins where they unconformably overlie the older sedimentary

units or tholeiitic basalt of the Karoo Supergroup. Locally, however, Cretaceous sedimentary rocks overstep the Karoo and directly rest unconformably on the Precambrian basement (Fig. 12). The sedimentary rocks are predominantly composed of coarse-grained continental and marine clastics, mainly sandstone and conglomeratic sandstone. The oldest Cretaceous formations, however, consist of silty marl that exhibits a characteristic dark tone and dendritic drainage pattern on the LANDSAT ETM 731 colour composite images (Fig. 22A). The coarse-grained sedimentary rocks generally display light image tones and also exhibit spectacular dendritic drainage patterns in steeply dissected terrain (badland morphology), the Magoë Formation in particular (Fig. 22B). The sandstones of the Sena Formation have bimodal potassium and thorium-rich radioelement signatures which may suggest that the gneissic units of the Barue Complex, with a similar bimodal radioelement composition of its gneissic units, are its main provenance (Fig. 22C).

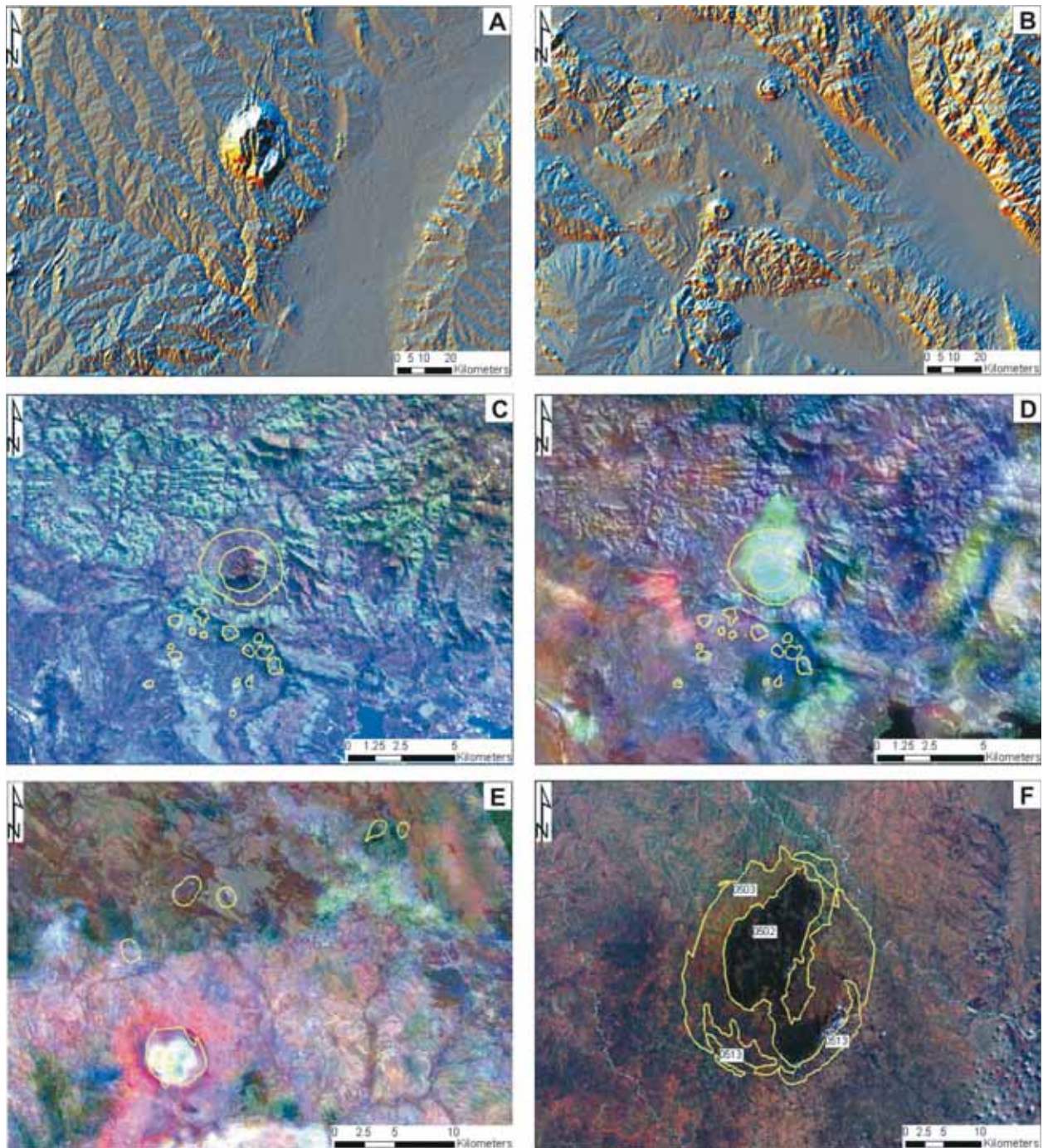


Fig. 21. Image interpretation examples of Cretaceous intrusions. A) SRTM ternary relief shaded image showing topographic expression of the Serra de Gorongosa ring complex; B) Topographic expression of carbonatite and alkaline ring complexes in Tete Province; C) Cone Negose carbonatite with satellite trachyte cones on a LANDSAT ETM 731 colour composite image; D) as C on an IHS [K-eTh-eU]-TMB7 composite image. Note the prominent thorium and uranium anomalies associated to the main intrusion; E) Serra Salambidue carbonatite and syenite-monzonite stocks (outlined in yellow lines) on an IHS [K-eTh-eU]-TMB7 composite image. Note the high total count and uranium anomalies corresponding to the carbonatite intrusion; F) Detailed image interpretation of the Serra de Gorongosa ring complex. 0502: Alkali granite, 0503: syenite, monzonite; 0513: skarn within hosting gneisses of the Barue Complex.

Towards the south in the LOT 3 area, several new inliers of the Sena Formation were discovered by our remote sensing interpretation. This was based on their contrasting K-rich gamma-ray spectrometry signature and dissected relief expression in erosional windows through Quaternary cover along the

deepest levels of dendritic drainage systems (Fig. 22D). Thin slivers of the Grudja and Maputo Formations are also found along river valleys in southern Mozambique, where their distinction from the overlying Tertiary Jofane and Cheringoma Formations is difficult.

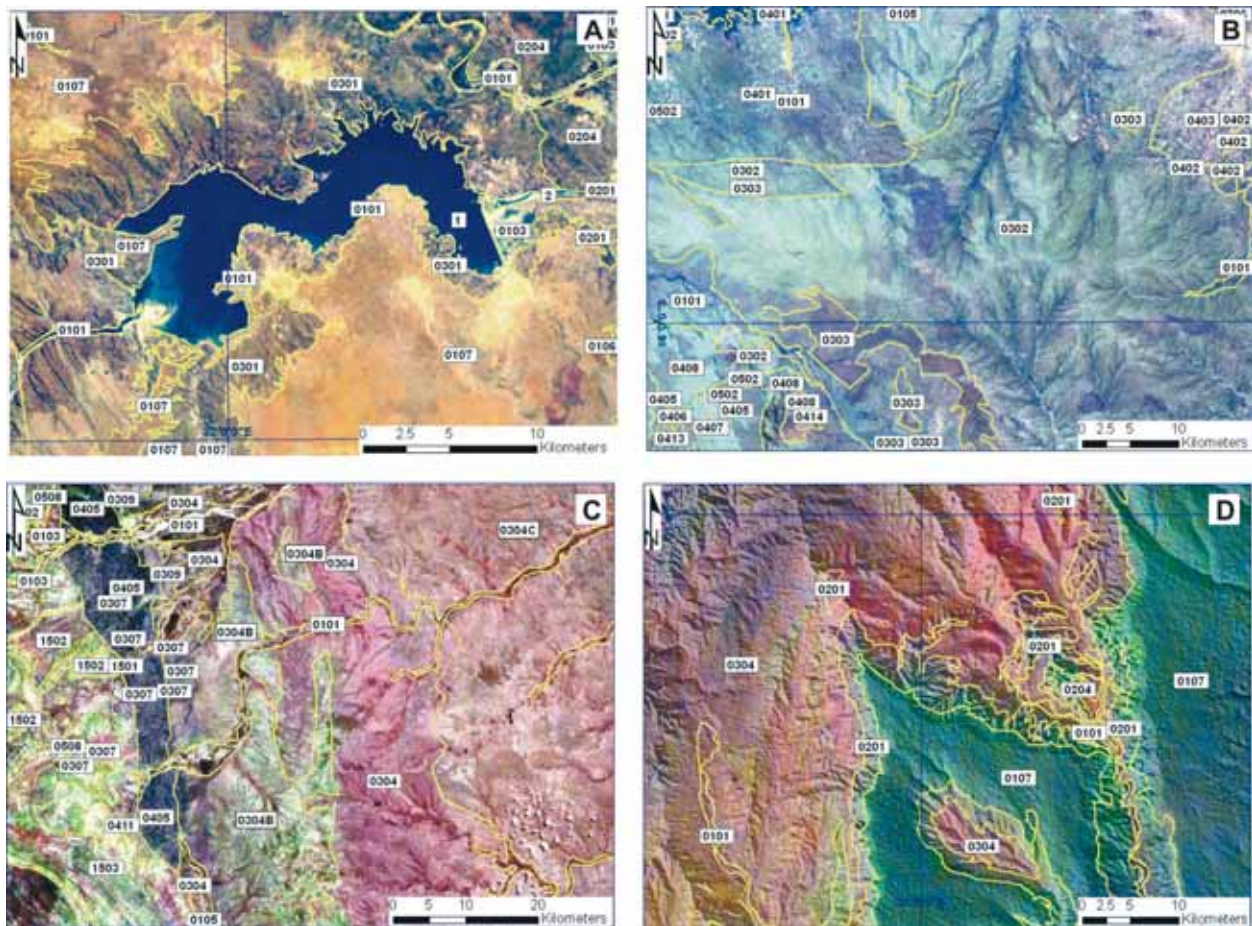


Fig. 22. Image interpretation examples of Cretaceous sedimentary rock units (Grudja, Mágoè and Maputo Formations). A) LANDSAT ETM 731 colour composite image of the Massingir area (ca. 24° S and 32° E). Unit 0301 corresponding to Cretaceous rocks of the Grudja Formation is outlined on the basis of the dark-grey image tone and dendritic drainage patterns; B) LANDSAT ETM 731 colour composite image west of Tete (16° S) showing spectacular dendritic drainage patterns associated to the Mágoè Formation (unit 0302); C) IHS [K-eTh-eU]-TMB7 composite image of Sena Formation. Note that units 0304, 0304B and 0304C can be differentiated on the basis of their distinct radioelement signatures, which may either represent a lateral facies or a stratigraphic differentiation; D) IHS [K-eTh-eU]-relief-shaded SRTM composite image of unit 0304 (Sena Formation) at ca. 21° S and 33° E. Note the potassium-rich signature of unit 0304 that strongly contrasts with the thorium-rich signatures of units 0201, 0204 and 0107. The isolated inlier of unit 0304 does not appear on the previously published geological map of this area.

Tertiary sedimentary rock units

Tertiary (Paleogene to Neogene) sedimentary rocks are predominantly exposed in the LOT 3 area along the Save and Limpopo river valleys, along the north-south trending coast and the Sabe basin east of the Barue Complex (Fig. 12). The Tertiary sequence is composed of sandstone, silty marl and carbonates including the numulitic limestone of the Jofane Formation (unit 0202) and reef limestone of the Cheringoma Formation (unit 0204). These units exhibit widely spaced dendritic drainage patterns in steeply sloping terrain along river valleys but generally lack internal drainage patterns on gently sloping and flat terrains. They display, dependent on land cover, variable generally light image tones (green, orange or yellow) and a smooth image texture on LANDSAT ETM 731 colour composite im-

ages (Figs. 23A, B). The Inhaminga sandstone (unit 0203) and Mikindani Formation (unit 0201) that is also dominantly composed of sandstone display darker image tones and moderately rough image textures (Figs. 23A, B). Along the Save river, within LOT 3, the Jofane Formation exhibits dark image tone when exposed by erosion along the Save River (Fig. 23C). In the extreme south of Mozambique, thin layers of Jofane Formation are recognized from their relatively bright tones (Fig. 23D).

Quaternary to recent units

Quaternary and recent sediments cover approximately 50 percent of the LOT 2 and LOT 3 areas. They form the extensive floodplains of the on-shore part of the Mozambique basin of Southern and Eastern Mozambique and the infill of the more localized

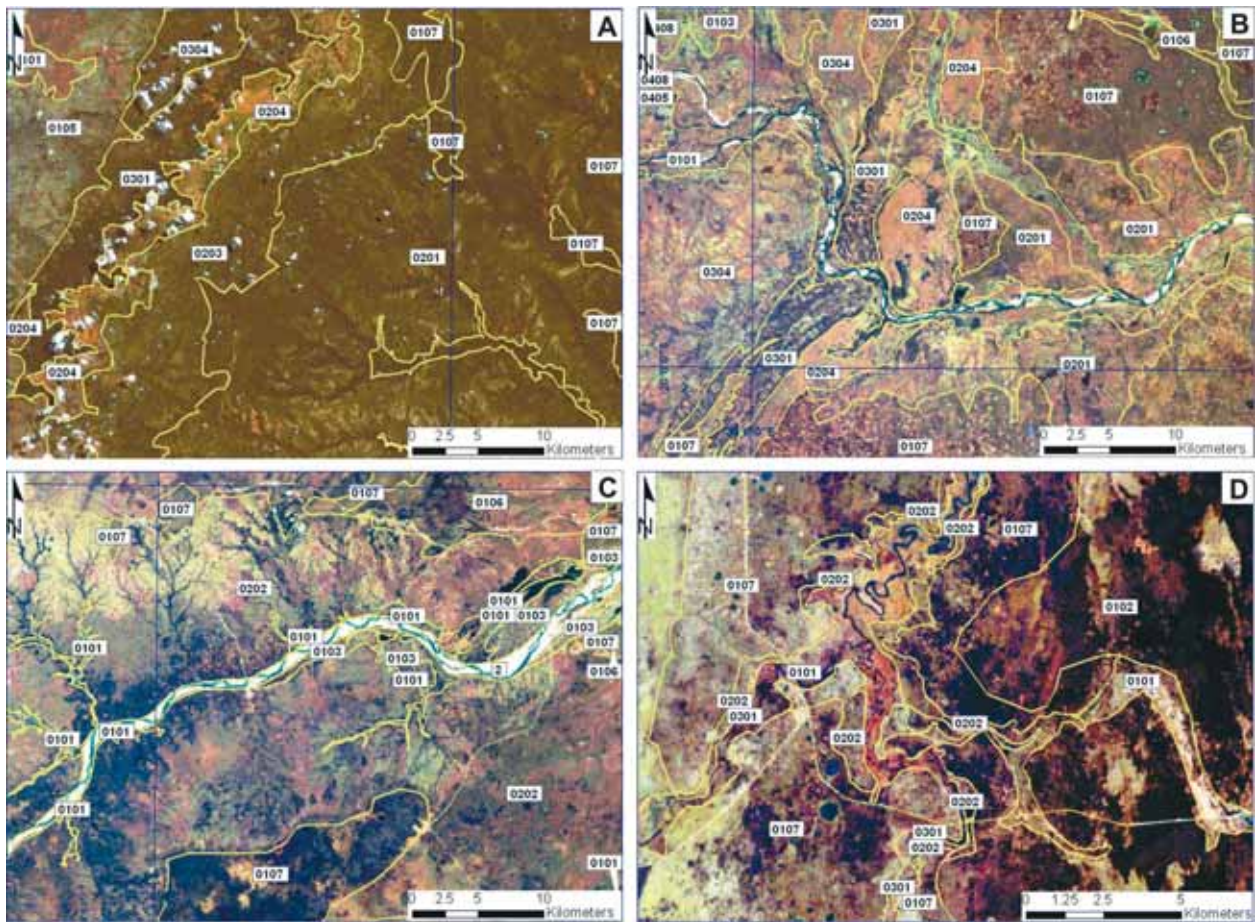


Fig. 23. Image interpretation examples of Tertiary sedimentary rock units (Mikindani, Jofane, Inhalinga and Cheringoma Formations). A) LANDSAT ETM 731 colour composite image at ca. 18°30' S and 35° E, displaying a stratigraphic sequence of Tertiary units. From top to bottom: Mikindani Formation (unit 0201), Inhalinga sandstone (unit 0203) and Cheringoma Formation (unit 0204); B) Characteristic pink-orange hue and smooth image texture of the Cheringoma Formation on a LANDSAT ETM 731 colour composite image at ca. 20° S and 34° E; C) Exposures of the Jofane Formation (unit 0202) in the River Save valley; D) Thin slivers of the Jofane Formation can be identified based on their light tone in southern Mozambique.

rift basins to the north of it (Fig. 12). The Quaternary cover is largely composed of unconsolidated or semi-consolidated argillic and sandy alluvial, fluvial, Aeolian and marine sediments. Their stratification is usually sub-horizontal in the east but towards the west along the border with South Africa, they have been tilted by neotectonic faulting. South of 22° S, large tracts of the flood plain are covered by sands that were formed by Aeolian reworking into inland dunes. In many areas the various Quaternary deposits can be elucidated by careful interpretation of the age relationships between inland and coastal land forms (Figs. 24A, B). Recent alluvial and marine sediments (unit 0101) can be recognized on the basis of their dark image tone and low topographic elevation in association to rivers, lakes and mangroves along the coast (Fig. 24B).

Interpretation of shaded-relief SRTM images is helpful in mapping the relative stratigraphic position of the Quaternary units and elucidating their con-

tacts in both denudational and aggradational landforms. Sandy deposits generally form positive relief features, namely ridges and plateaus that display a light orange or brown image tone and rough image texture, whereas the argillic sediments are confined to topographic depressions that display a dark image tone and smooth image texture on LANDSAT 7 ETM 731 colour composite images (Fig. 24C). The break of the slope between the floors and rims of circular depressions, known as 'dambos', can be recognized on the satellite imagery and relief-shaded SRTM data and coincides with the contacts between the argillic alluvial deposits and overlying cover sands (Fig. 24D). Furthermore, the argillic (unit 0106) and overlying cover sand deposits (unit 0107) have a subtle but consistent contrast in radiometric signature that can be used, in addition to the satellite imagery and relief-shaded SRTM data, in mapping their distribution (Figs. 24E, F).

Characteristic linear patterns (presumable linear dunes and blow-outs) indicate the wind transport direction and allow the differentiation of coastal and inland dune deposits from each other and the cover sands of the flood plains. The gamma-ray spectrometry grids are sometimes useful for determining the

provenance of the Quaternary sediments. Terraces along the Limpopo River, for example, are composed of thorium-rich sediments suggesting that thorium-rich Cretaceous sedimentary rocks of the Sena formation upstream of the river terraces provided the source of these sediments.

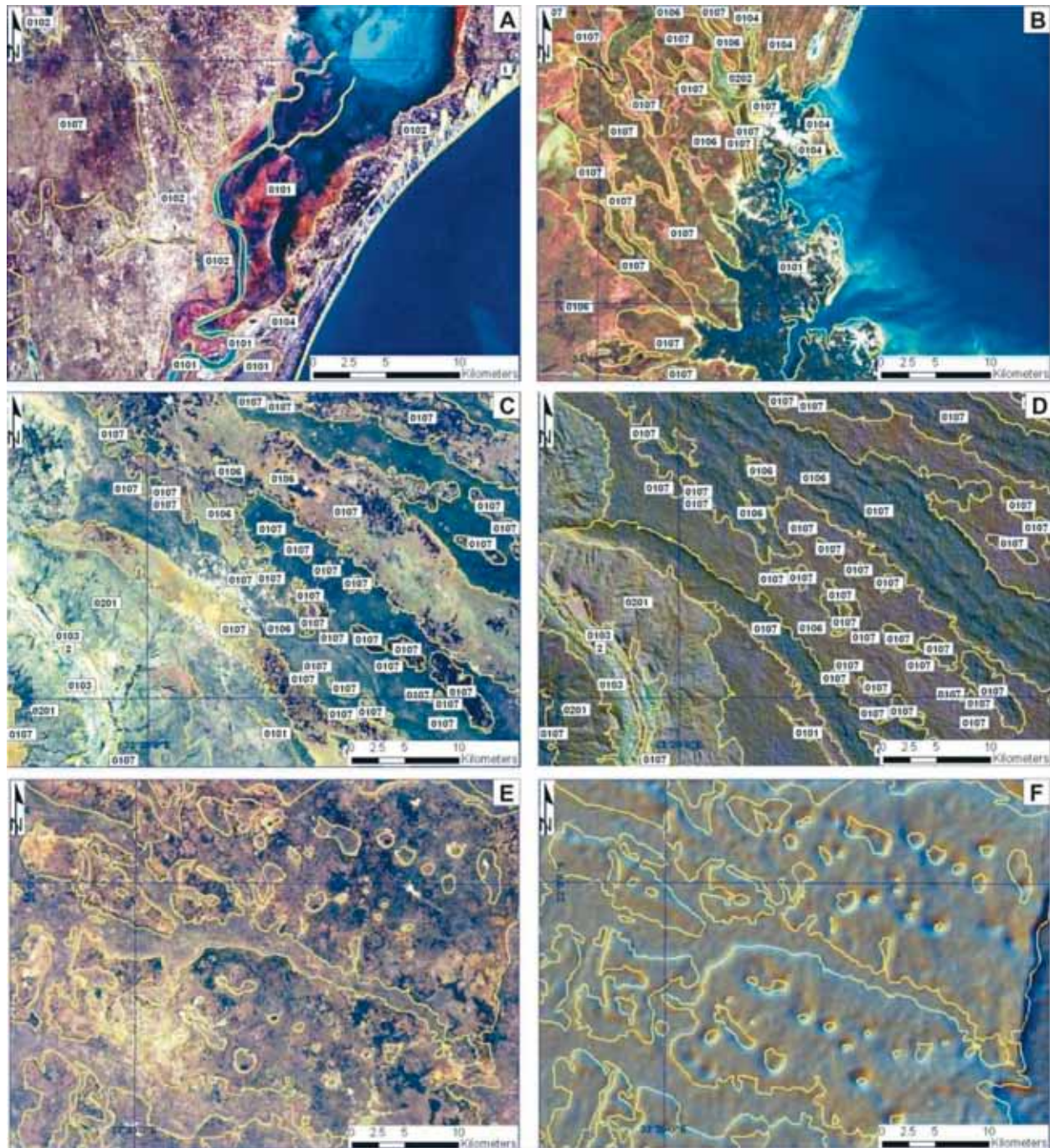


Fig. 24. Image interpreted units of Quaternary to recent cover. A) LANDSAT ETM 731 colour composite image at 25°30' S/35° E showing Quaternary units: 0101 recent alluvial deposits, 0102: interior dunes, 0104: coastal dunes and 0107: aeolian reworked fluvial sands; B) LANDSAT ETM 731 colour composite image at ca. 20° S/34° E showing Quaternary units: 0101 recent alluvial deposits (in mangroves), 0104: coastal dunes, 0106: argillic deposits and 0107: aeolian reworked fluvial sands; C) Units 0106 and 0107 on the LANDSAT ETM 731 colour composite image at ca. 23° S, 32°30' E; D) IHS [K-eTh-eU]-relief-shaded SRTM composite image of the area shown in Fig. C; E) Differentiation of units 0106 and 0107 on the LANDSAT ETM 731 colour composite image at ca. 22° S/33°30' E; F) Ternary relief-shaded SRTM image showing linear and circular topographic expressions of the subhorizontal contacts between units 0106 and 0107.

CONCLUSION

In this paper we have presented the data processing and integration methodology and a summary of geological image interpretation results that supported the regional geological field mapping component of LOT 2, LOT 3 and their extensions. We have shown that the integrated enhancement and digital interpretation of airborne geophysical, optical remote sensing and SRTM data lend themselves to extract a large number of lithological and structural patterns. These patterns appeared to be regionally consistent and supported geological map compilation in combination with insights obtained from geological field mapping. Integrated image enhancement, in which image data of higher spatial resolution (e.g. LANDSAT ETM and shaded-relief

SRTM data) substituted the intensity of the ternary radioelement colour composite, proved to be very effective for geological mapping. It was by far the most useful enhancement technique for outlining bedrock units in the Precambrian basement and helped in analyzing relationships between the Phanerozoic sedimentary cover, landscape morphology and topography. A systematic comparison of the newly published geological map coverage and the image database will highlight a number of geologically significant discrepancies that justify field follow-ups in a variety of terrains and for a variety of purposes (e.g. geological mapping, earth resource exploration as well as land use and hazard studies).

ACKNOWLEDGEMENTS

We thank Sally Barrit for airborne geophysical data processing that allowed us to merge the older Hunting survey with the more recent Fugro airborne geophysical surveys. Gerard Reinink is acknowledged for his contribution to the various image processing tasks, including geometric correction, preparing the LANDSAT ETM mosaic of the project areas and the enhancement and delivery of the individual LANDSAT and ASTER VNIR scenes. Many thanks to Ruben Vargas and Koert Si-

jmons for their contribution in compiling the legacy geological maps and map production of the provisional geological maps compiled from the geological image interpretation presented in this paper. Thanks to Eira Kuosmanen for preparing a generalized geological map of the project area. Finally we want to thank Hilikka Arkimaa for critical reading of the manuscript and for comments that improved this paper.

REFERENCES

- Chavez, P. S., Sides, S. C. & Anderson, J. A. 1991. Comparison of three different methods to merge multi-resolution and multi-spectral data: LANDSAT TM and SPOT Panchromatic. *Photogrammetric Engineering and Remote Sensing* 57, 295–303.
- Curran, P. J. 1985. *Principles of Remote Sensing*, Longman Group UK Limited, Essex, England, 282 p.
- Goetz, A. F. H., Barrett, N. R. & Rowan, L. C. 1983. Remote sensing for exploration an overview, *Economic Geology*, special issue on techniques and results of remote sensing, pp. 573–590.
- Harris, J. R., Bowie, C., Rencz A. N. & Graham, D. 1994. Computer enhancement techniques for the integration of remotely sensed, geophysical and thematic data for the geosciences. *Canadian Journal of Remote Sensing*, 20, 210–221.
- Hunting Geology & Geophysics 1984. Mineral inventory project, ministério dos recursos minerais, direcção nacional de geologia, Mozambique, final report 329 p.
- Norconsult International 1998. The Mozambique national geodetic network, local government reform and engineering project urban/environmental management, technical report on adjustment old network.
- Schetselaar, E. M. 2000. On preserving spectral balance in image fusion and its advantages for geological image interpretation. *Photogrammetric Engineering and Remote Sensing*, 67, 925–934.
- Wilford, J. R., Bierwith, P. N., & Craig, M. A. 1997. Application of airborne gamma-ray spectrometry in soil/regolith mapping and applied geomorphology. *AGSO Journal of Australian Geology & Geophysics*, 17, 201–216.

GEOPHYSICAL MAPS AND PETROPHYSICAL DATA OF MOZAMBIQUE

by
Tapio Ruotoistenmäki

Ruotoistenmäki, T. 2008. Geophysical maps and petrophysical data of Mozambique, *Geological Survey of Finland, Special Paper 48*, 65–80, 15 figures.

The airborne geophysics that covers the GTK Consortium Project area comprise of four data sets: 1) airborne geophysical data compiled by Hunting Geology & Geophysics and covering mainly the Tete Province, 2) aeromagnetic data of southern Mozambique, digitized by Getech, 3) airborne geophysical grids of Fugro and 4) gravity data compiled by Getech. The Hunting data were available as contour maps and as digital grids comprising total magnetic field, potassium, thorium, uranium channels and total count. The grids were useful for a quick assessment on how to exploit the data in map production and for geological field work. The new Fugro line data including K, eTh, eU, TC and total magnetic field channels, were received late in the Project (September 2003), but were quickly registered on the MOZNET datum and gridded on 200 meter cells using a minimum curvature gridding algorithm. Various geophysical maps were prepared of this data to support the lithostratigraphic mapping.

Key words (GeoRef Thesaurus AGI): geophysical surveys, airborne methods, petrophysics, geophysical maps, Mozambique.

Geological Survey of Finland (GTK), P.O. Box 96, FI-02151 Espoo, Finland
E-mail: tapio.ruotoistenmaki@gtk.fi

INTRODUCTION

In this report a short introduction is given to the geophysical and petrophysical data and maps that were collected and prepared during the Mozambique LOT 3 mapping project carried out by the Geological Survey of Finland in 2003–2007. The maps were prepared as reference and working maps to support geologists in lithological mapping and their format is therefore relatively informal. They were made in Geosoft and ArcView-tiff formats (‘geocoded’) and submitted to the National Directorate of Geology (DNG) on a separate CD.

The maps are presented as colour maps or as hill-

shaded versions that better show local variations and lineations by emphasizing the gradients of the anomalies. Moreover, some maps have been connected to lithological maps in order to illustrate the link between lithological characteristics and corresponding geophysical patterns (Fig. 1). Some visually observed features are also emphasized on the maps. Moreover, a magnetic profile interpretation crossing the Karoo group is presented. During the field work the geologists measured petrophysical parameters for ca. 300 samples whose susceptibility-density diagram will be discussed.

GRAVITY DATA AND MAPS

The available gravity grid covers only the southern part of Mozambique. The records on land area have mainly been collected along roads and thus the data are locally relatively sparse (white areas). In some sea areas the measurements are denser. The gravity map is given in Fig. 2, and combined with the lithology in Fig. 3.

From the maps it can be seen that the mafic Karoo group rocks in (A) and (B) are correlated with gravity highs. The gentle flanks of the anomalies also suggest that these rocks are dipping below the

lighter sedimentary cover (C), southeast in (A) and northeast in (B).

Moreover, the maps demonstrate that in off-shore areas (D) the gravity is high due to the mafic rocks of sea floor and shallow upper mantle. The gravity high at (E) indicates that there are high density rocks below the less dense sedimentary. These high density rocks can possibly be connected with ancient marine basalts underthrusting the western coast of Mozambique, thus being potential for oil or gas exploration.

MAGNETIC DATA AND MAPS

The magnetic grid used for this work mainly covers the western part of Mozambique. In general, the grid density of magnetic data is higher, than that of gravity data and they are more sensitive to shallow sources, thus being more useful for local-scale mapping compared to gravity data. The magnetic map of the western Mozambique is presented in Fig. 4 and combined with lithology in Fig. 5.

The mafic Karoo rocks in (A) and (B) are connected with long linear anomaly zones, possibly representing ancient (Gondwana?) rift zones; i.e. mafic sills intruded in extensional fractures. Again, it can be seen that these rocks are continuing below the lighter sedimentary cover (C), southeast in (A) and northeast in (B). The dark linear 'anomaly' close to the western border is apparently due to an electric power line or railroad. These maps clearly demonstrate that the anomaly (A) is a distinct block border

separating the low-anomaly sedimentary 'blocks' in (C) from the strongly folded, more magnetic area NW of anomaly (A).

The magnetic map in Fig. 4 indicates that there might be some circular and semicircular anomalies due to (intrusive?) sources below the sedimentary cover, such as the one south of (A). Some examples of these circular structures are shown in the more detailed magnetic map in Fig. 6.

In Fig. 7 a schematic magnetic interpretation is given across the linear anomaly group of Karoo rocks and the circular magnetic anomaly on the Phanerozoic sedimentary area. From the figure it can be seen that the interpretation supports the dipping of Karoo group rocks below the sedimentary cover. Moreover, the depth to the upper surface of the circular minimum source appears to be ca. 4 km.

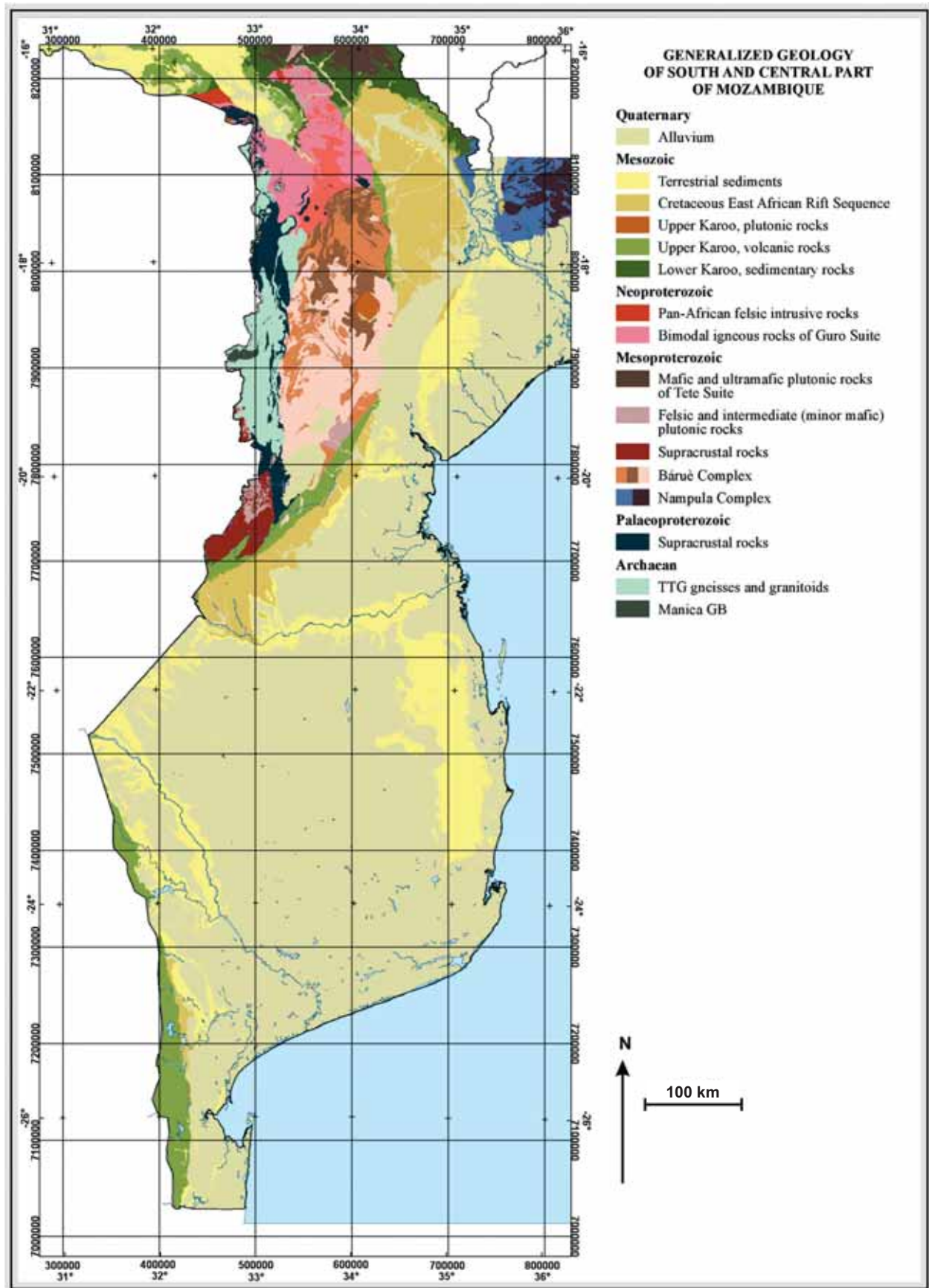


Fig. 1. Simplified geology of Mozambique compiled by GTK Consortium geologists. The rectangular coordinates are given in metres; i.e. one coordinate grid square is 100 x 100 kilometres.

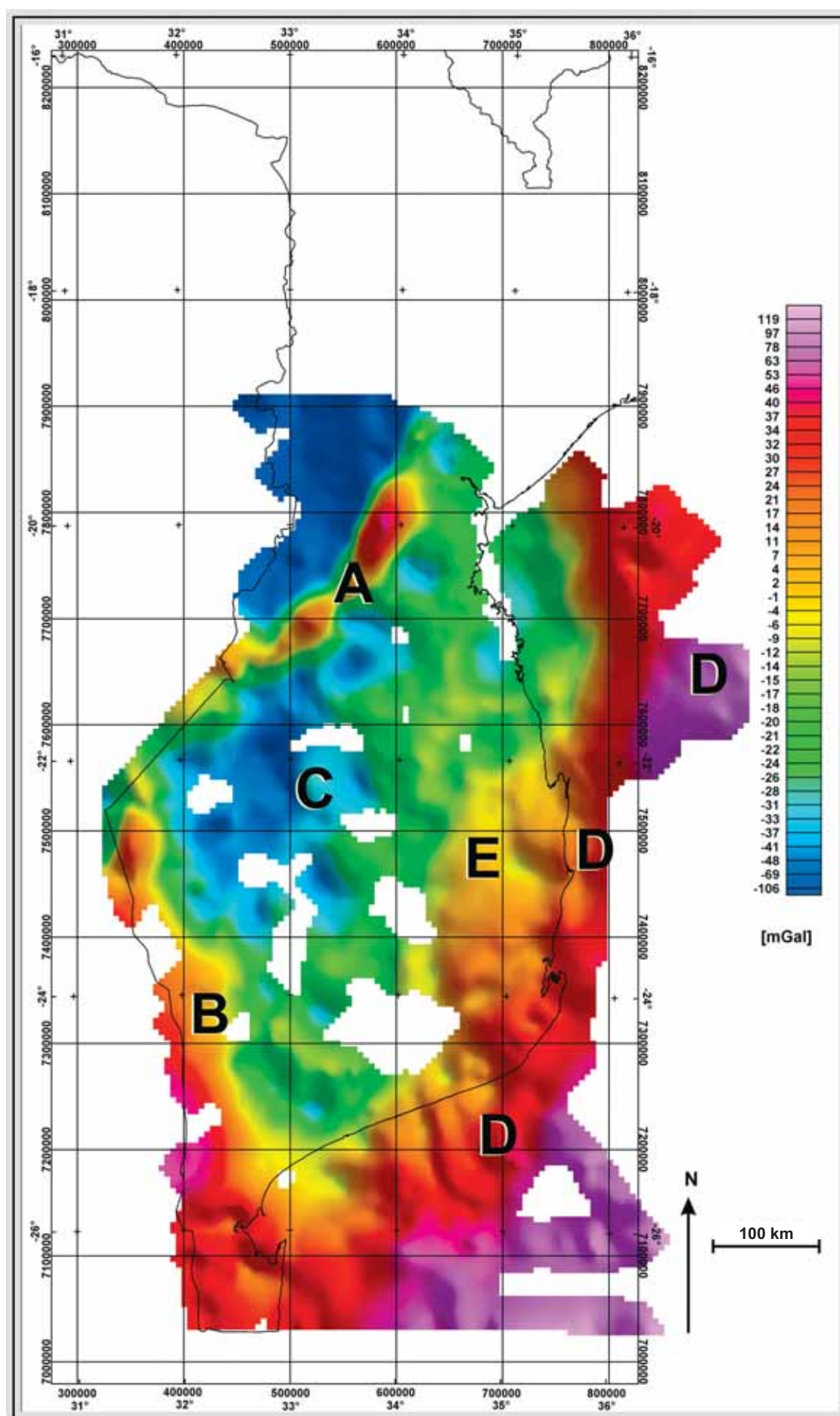


Fig. 2. Gravity map of the southern part of Mozambique. Anomalies (A) – (E) are discussed in more detail in the text.

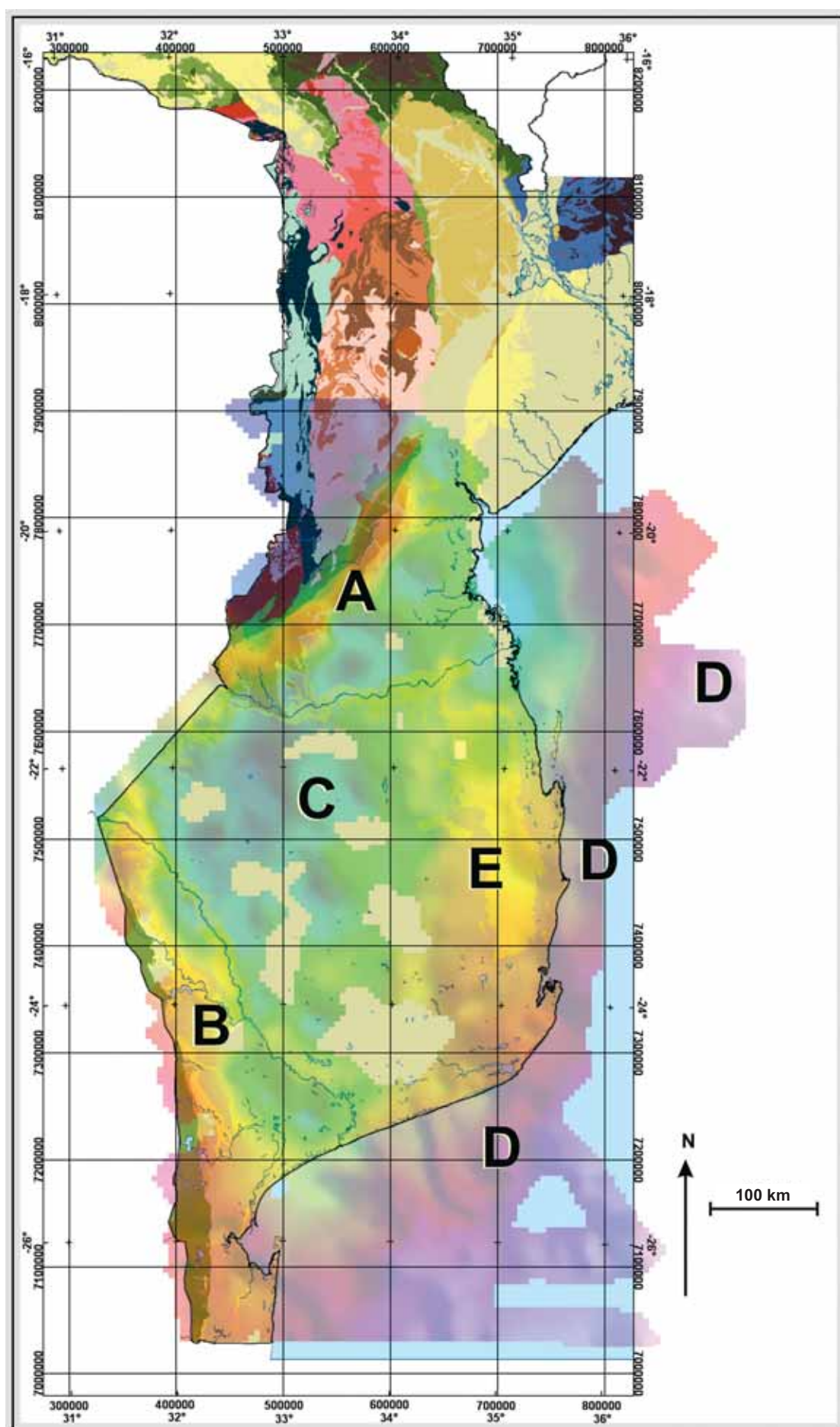


Fig. 3. Gravity map of the southern part of Mozambique combined with lithology. See text for details.

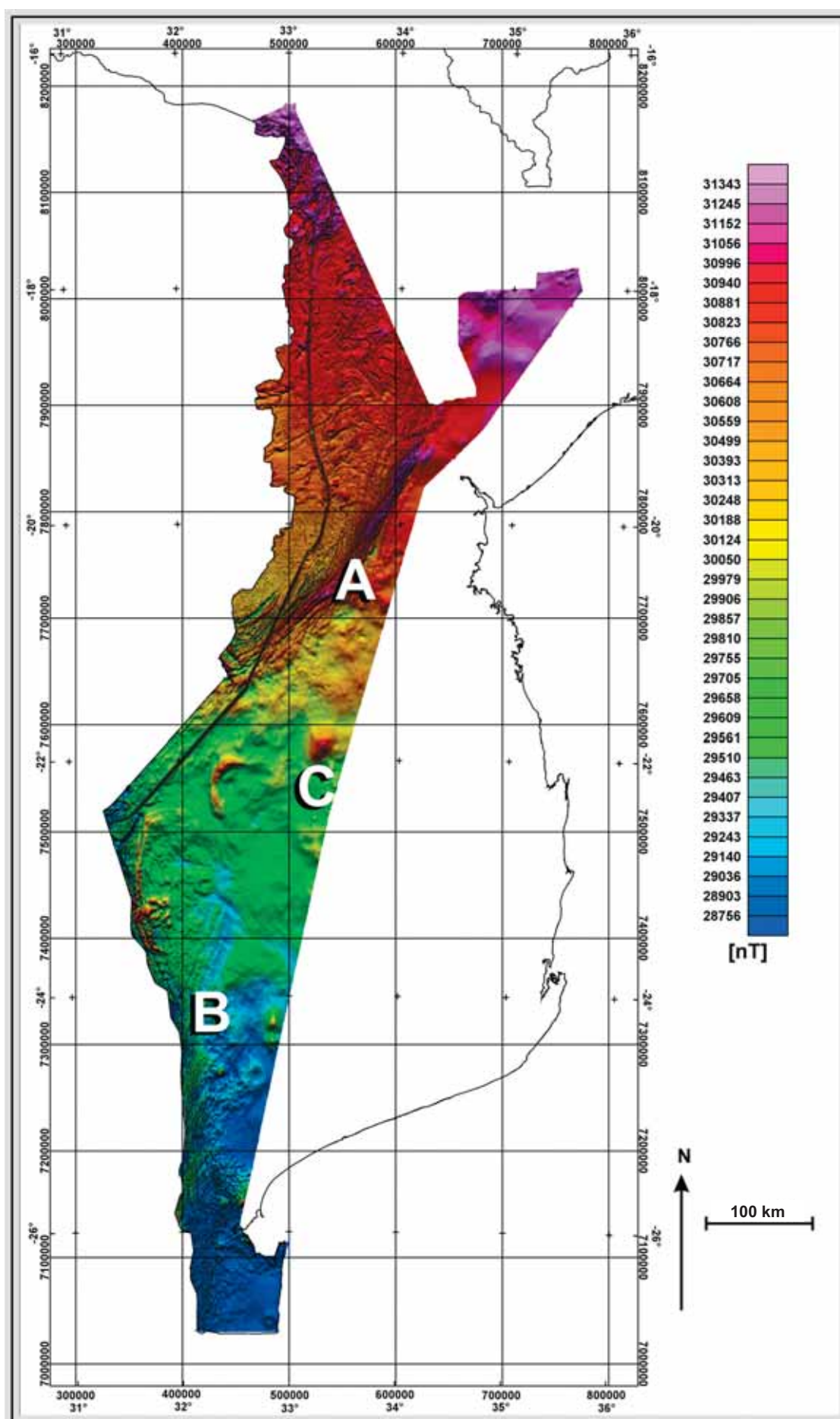


Fig. 4. Magnetic map of the western part of Mozambique illuminated from the NE and NW. See text for details.

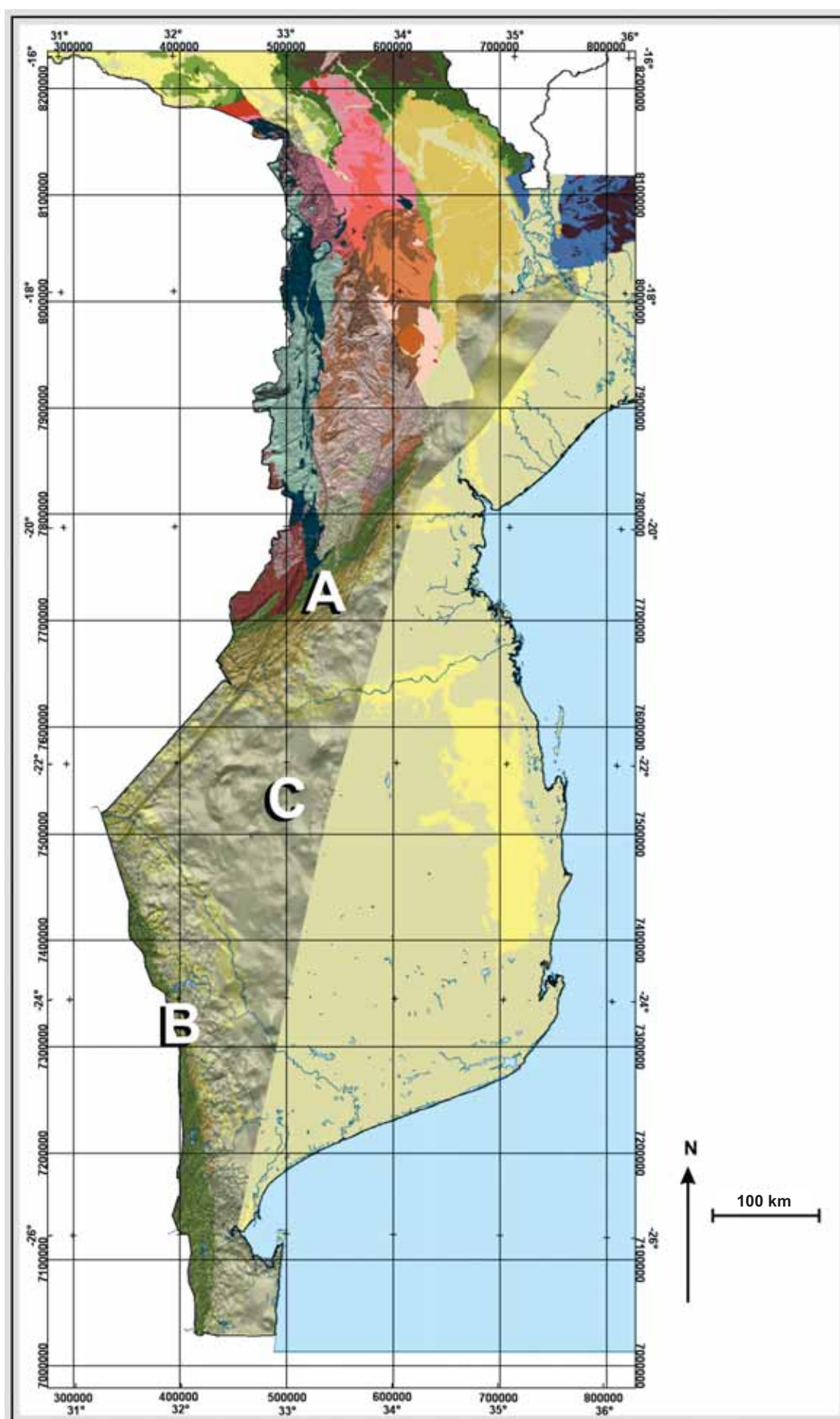


Fig. 5. Magnetic map of the western part of Mozambique in grey tones combined with lithology. See text for details.

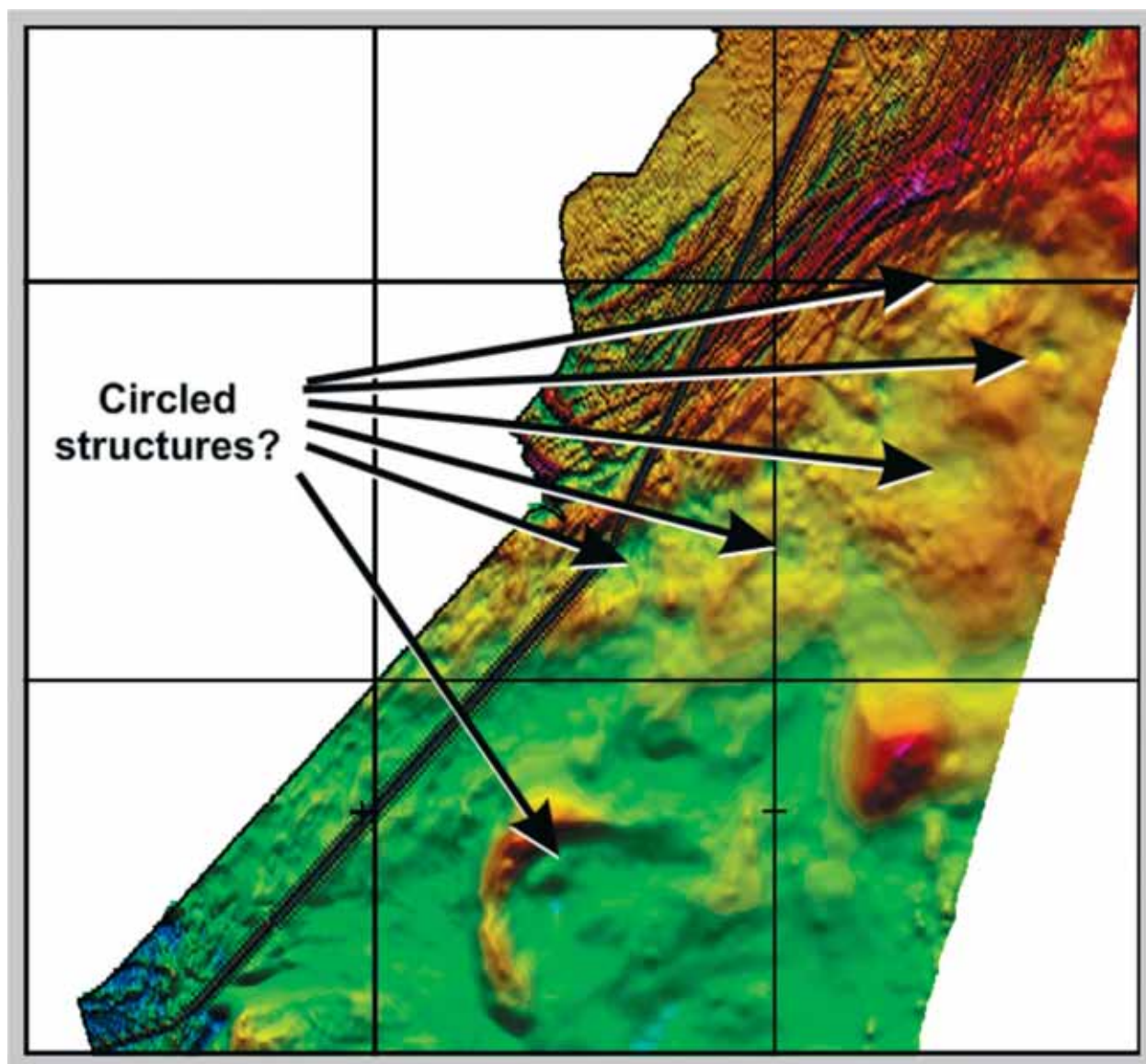


Fig. 6. Detail of the magnetic map showing some possible circular structures that may be due to intrusive sources. The coordinate grid square is 100x100 kilometres.

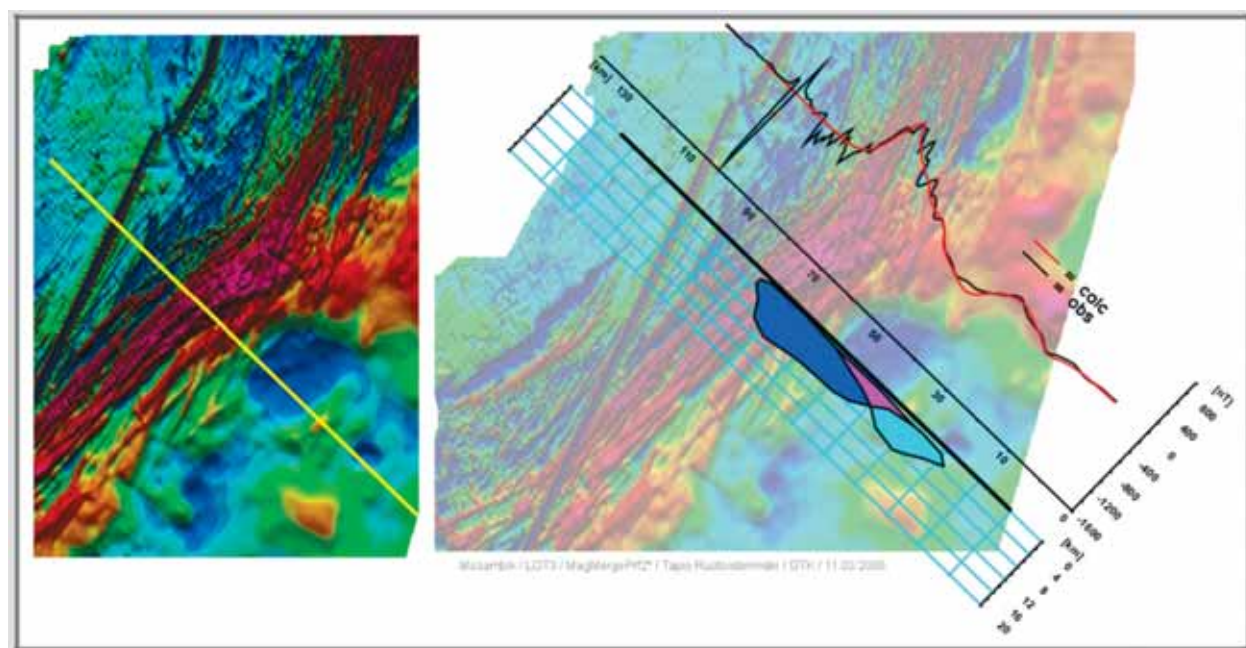


Fig. 7. Magnetic interpretation across the contact zone from Karoo to the Phanerozoic sedimentary area.

RADIOMETRIC DATA AND MAPS

In general, the radiometric data are noisy and strongly dampened by overburden, especially in wetland areas; over lakes, radiometric anomalies cannot be detected at all. However, apparently due to the relatively dry overburden in Mozambique, the data appear to be of high quality and useful for regional-scale interpretation and lithological classification.

The radiometric data measured in the area consist of 3+1 components: potassium, thorium, uranium and total radiation. In Fig. 8 the radiometric maps of potassium and thorium are presented and in Fig. 9 are maps for total radiation and uranium. It can be seen that particularly the Archaean – Proterozoic rocks in the NW corner of the maps are very anomalous. Moreover, the rocks of the Karoo group are connected with higher radiometric anomalies.

It is interesting to note that potassium radiation is especially highly increased in the riverbeds and del-

tas (due to mica containing clays?), as can be seen in the combination map of potassium radiation and the topographic map in Fig. 10. The high radiation ‘fingers’ in the map separated from the anomalies of the main riverbeds of Limpopo River in the Gaza area (indicated by “G” in the figure) apparently show the maximum extent of flooding of the river.

The radiometric ternary map, showing U-Th-K anomalies with a colour composition in Fig. 11 and its combination with lithology in Fig. 12, correlate very well with lithology, especially in the Archaean – Proterozoic block in the NW corner of the map area and with Karoo group rocks. Moreover, it gives indications of soil and rock variations in the Phanerozoic sedimentary block. It must be remembered, however, that the good correlation of radiometric maps with the bedrock map is at least partly due to their usage in drafting those maps.

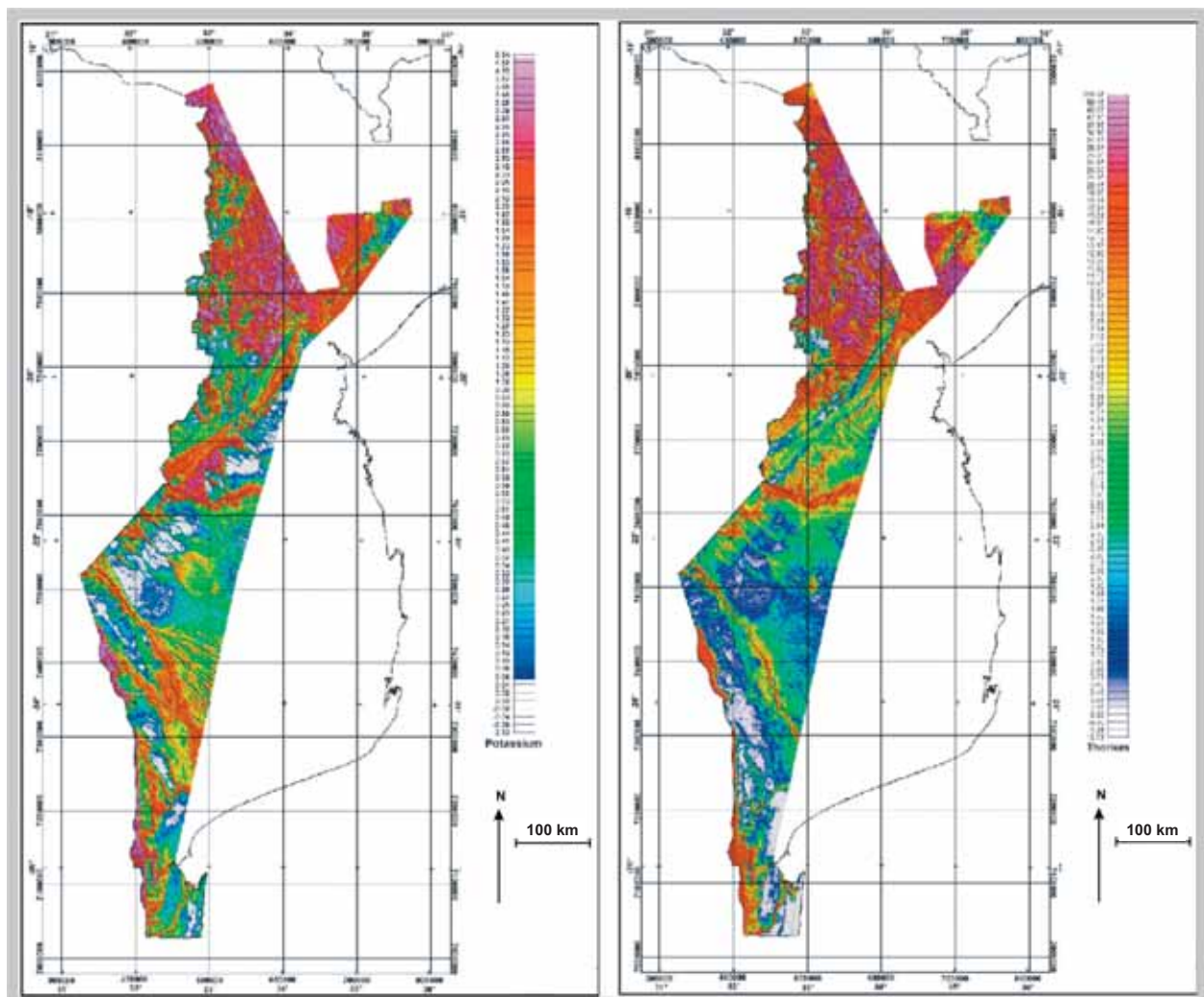


Fig. 8. Radiometric maps: Potassium and thorium. Red: high radiation level; blue-white: low radiation level.

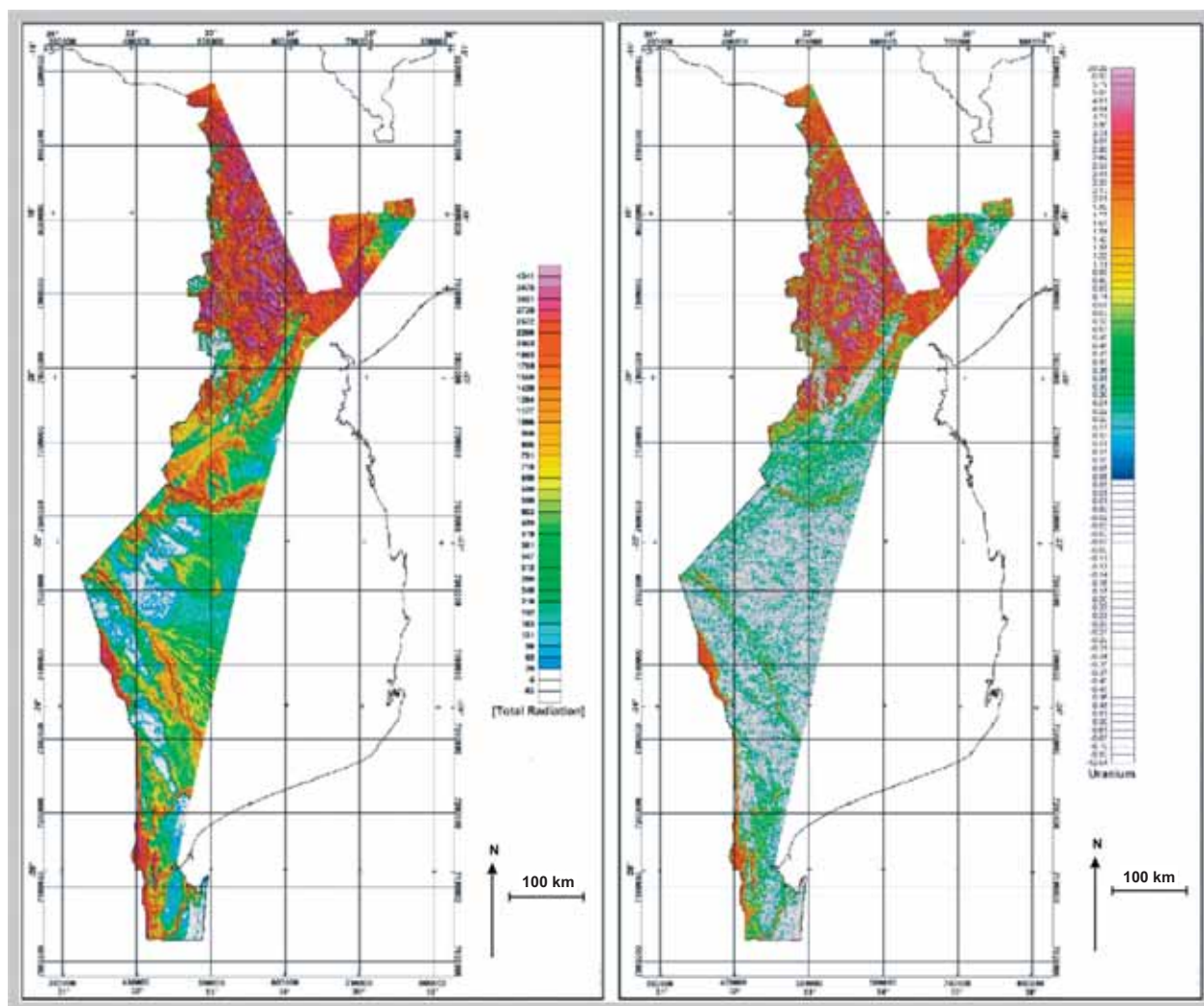


Fig. 9. Radiometric maps: Total radiation and uranium



Fig. 10. Topographic map of central Mozambique connected with the potassium radiation map.
 (G) = Limpopo River flood delta.

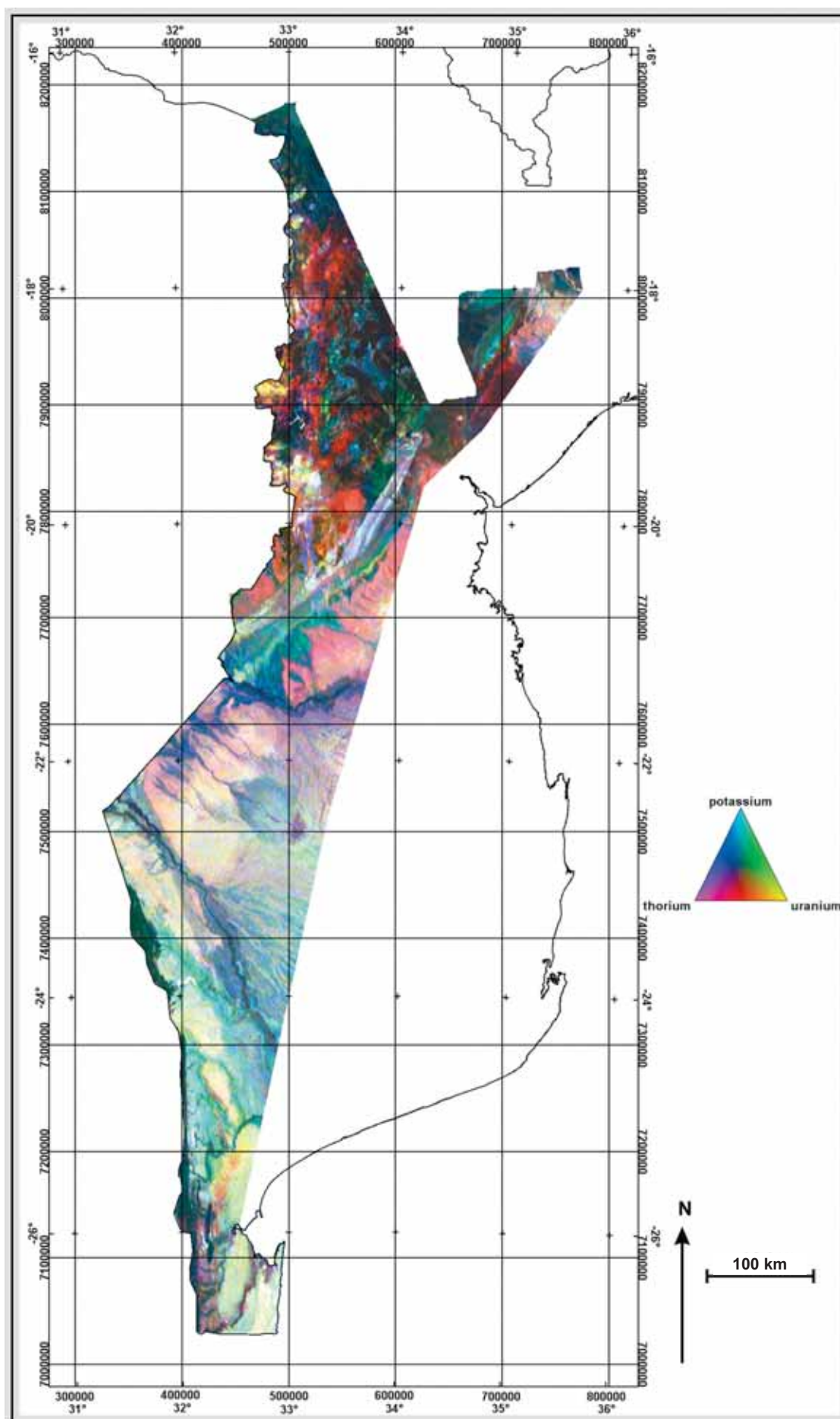


Fig. 11. Radiometric ternary map.

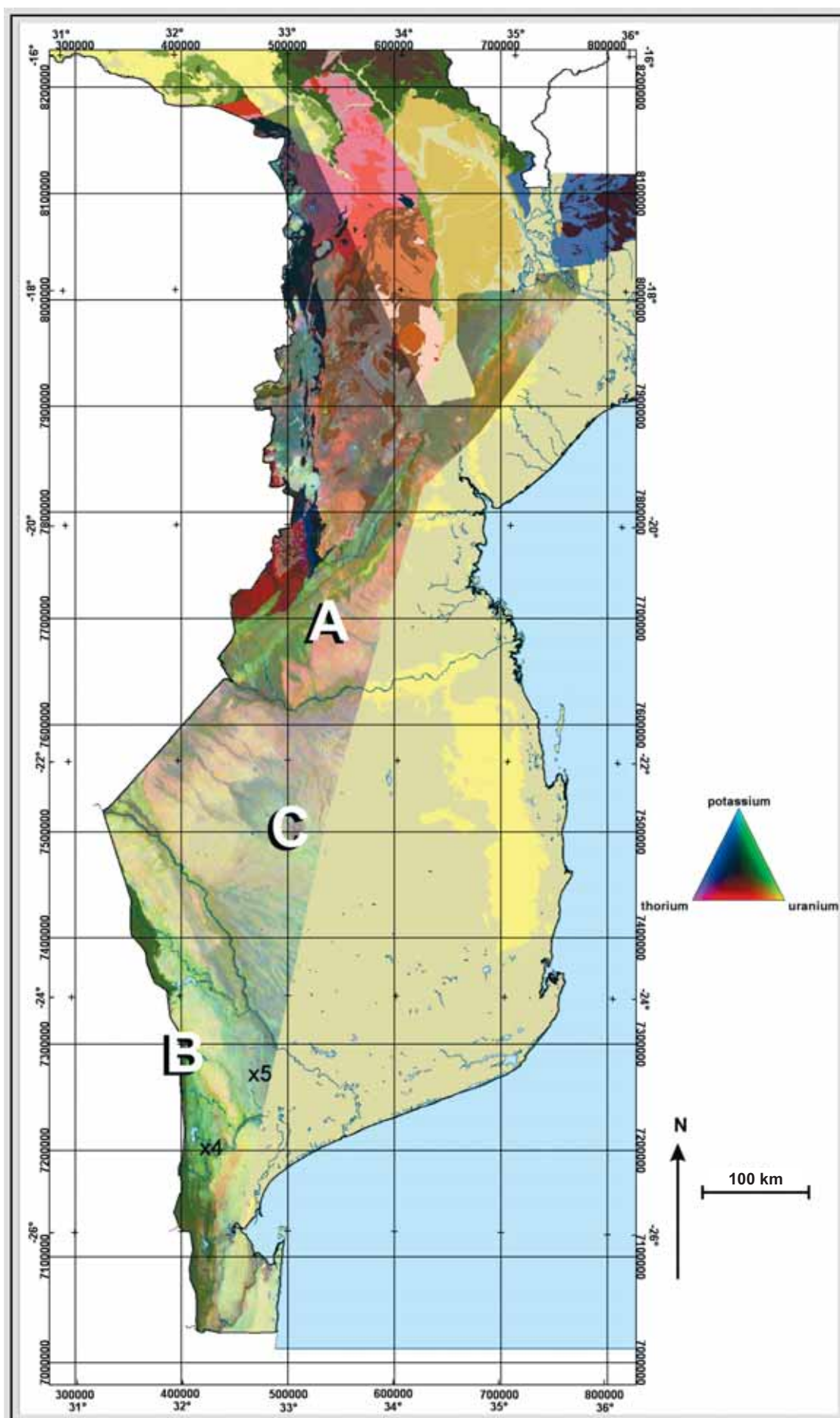


Fig. 12. Radiometric ternary map combined with lithology.

EXAMPLES OF LOCAL SCALE ANOMALIES

The aerogeophysical data are described in more detail in reports by Schetselaar *et al.* (2004) and Westerhof (2005). The gravity data are described in a short report by GETECH (2003). The details of the data are not discussed here.

In Fig. 13 more detailed versions of magnetic, radiometric ternary, gravity and lithological maps of the Archaean-Proterozoic – Phanerozoic block boundary are presented. The lithological variations along the rifted zone x1- x2 are clearly visible on all maps. The gravity anomaly, in particular, does not appear to exactly follow the surface geology, which indicates deeper density variations in the area. Again, in these maps, the applicability of ternary

radiometric data for delineating lithological variations is emphasized, such as the plutonite intrusions west and north from x2. These intrusions (Archaean plutonic rocks) are also connected with the gravity minimum, which indicates that they are relatively felsic or altered.

The circular magnetic minimum structure at x3 (interpreted in Fig. 7) is connected with a larger gravity minimum zone. However, the surface geology appears to give no indications of the source of this feature, which means that the source of this anomaly lies below the sedimentary rocks, as is also interpreted above.

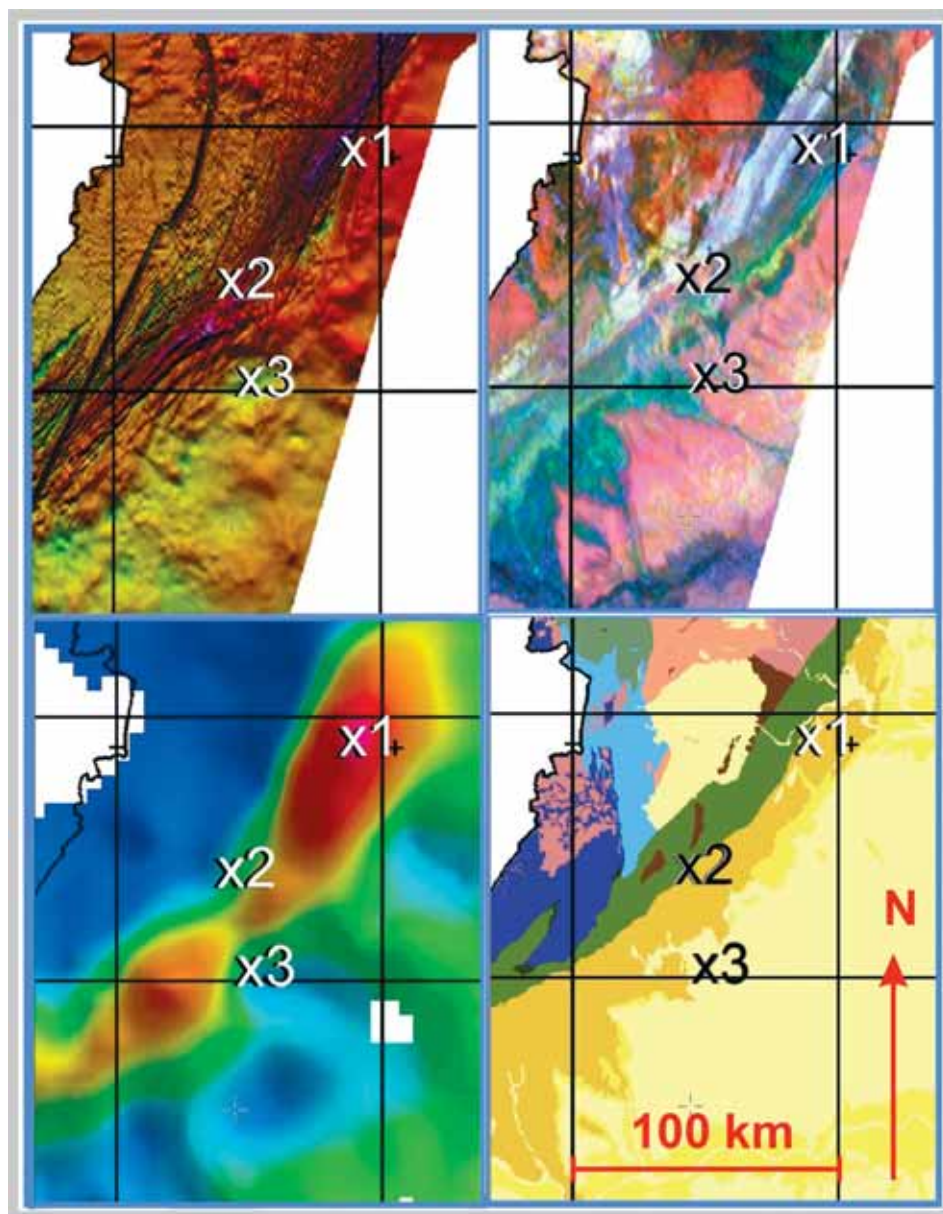


Fig. 13. Detailed versions of magnetic, radiometric ternary, gravity and lithological maps of the Archaean-Proterozoic – Phanerozoic block boundary.

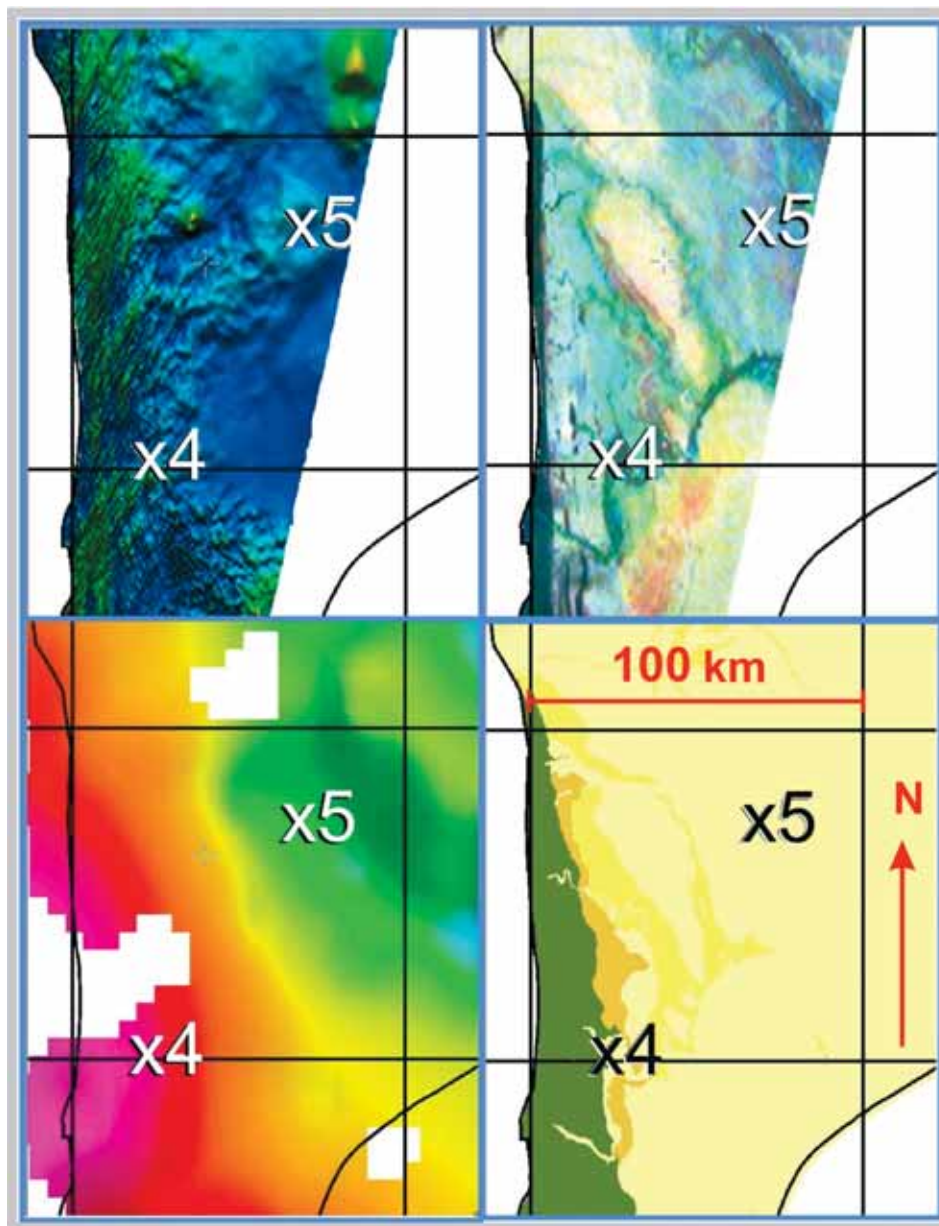


Fig. 14. Detailed versions of magnetic, radiometric ternary, gravity and lithological maps in the southern part of the study area.

In Fig. 14, corresponding map versions of the southern part of the study area are given. From the maps it is evident that the linear magnetic anomalies due to Karoo rocks at x4 continue below the sedimentary cover to the NE. This can be seen, for example, in the continuation of the corresponding gravity anomaly to the NE. Again, the circular mag-

netic anomaly at x5 correlates with a larger gravity minimum zone, but not with surface geology in the lithological and radiometric maps, which indicates that the anomaly source is below the sedimentary cover. Moreover, in this area the radiometric ternary map also clearly shows the variations in bedrock and sedimentary cover.

PETROPHYSICAL DATA

During the geological mapping, density and magnetic susceptibility were measured for ca. 300 samples collected in the northern part of the LOT 3 area.

Their susceptibility – density diagram is presented in Fig. 15. In the diagram the samples can be classified into three main groups:

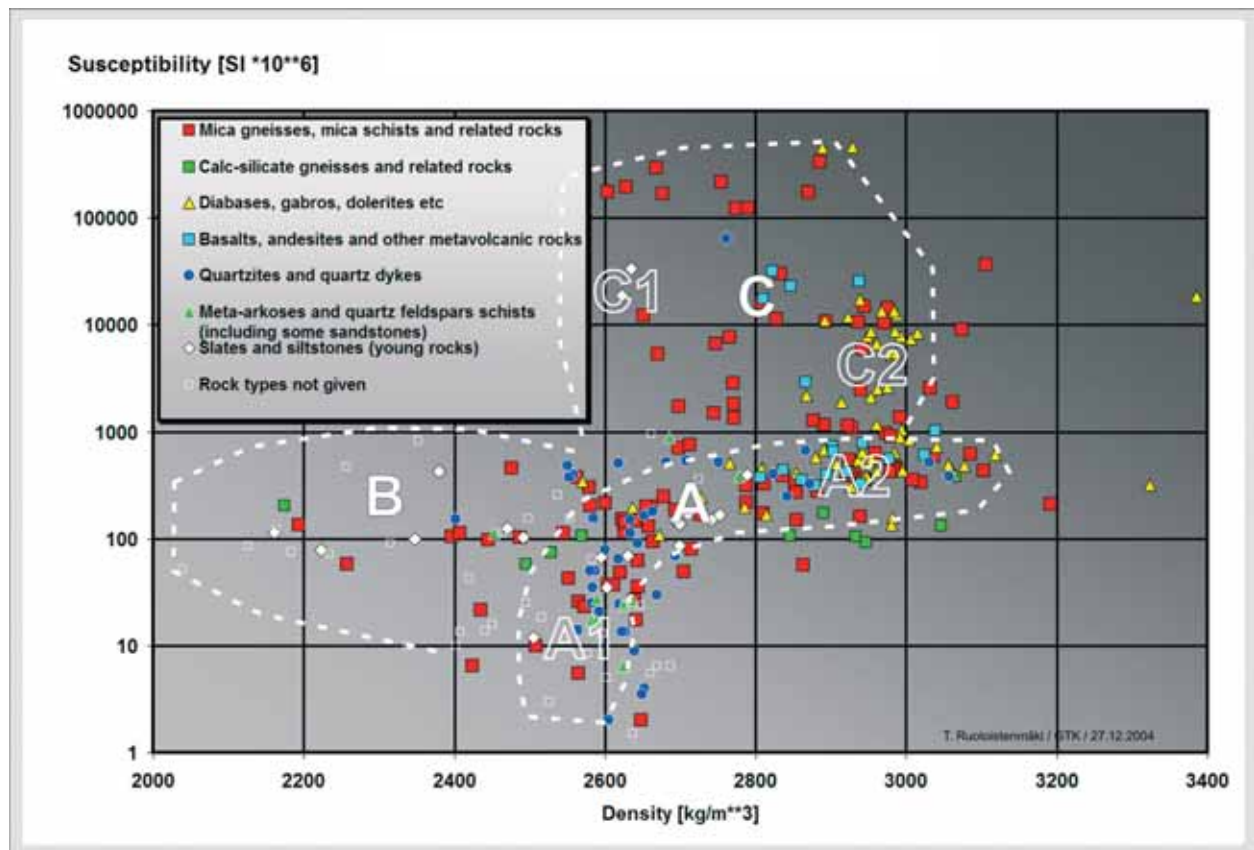


Fig. 15. Susceptibility – density diagram of samples collected in the northern part of LOT3 area.

- 1) Group A represents paramagnetic rocks where susceptibility is mainly due to mafic silicates. Sub-group A1 represents light-coloured felsic rocks (e.g. quartzites and mica schists) and A2 dark-coloured mafic rocks (e.g. basalts).
- 2) Group B mainly consists of altered low-density paramagnetic rocks, e.g. slates and siltstones.
- 3) Group C samples are ferrimagnetic rocks where group C1 represents magnetic light-coloured felsic rocks and group C2 magnetic dark-coloured mafic rocks (e.g. diabases and gabbros).

SUMMARY

The geophysical maps of Mozambique provide a valuable tool for mapping the bedrock and soil cover in areas where the coverage of roads is sparse and thus many locations are difficult to access. The radiometric maps particular appear to be exceptionally informative due to the relatively thin cover of vegetation and low number of bogs and lakes.

Moreover, the combination of gravimetric and magnetic maps is useful for detecting major lithological and structural variations, including those below the Phanerozoic sedimentary cover. In coastal areas, the continuation of the seafloor even below the Phanerozoic sedimentary cover can be followed. These areas could possibly have potential for oil and gas occurrences.

The petrophysical susceptibility – density classification gives indications of major geophysical rock groups in the area and they could in the future be used for preliminary interpretation of geophysical (i.e. lithological) variations, structures and blocks.

The need for more extensive petrophysical sampling covering the main lithological units in Mozambique is apparent. These data would provide the key for detailed analysis of the high quality aerogeophysical data that are already available from Mozambique. This work would not necessarily require high quality laboratories. For a good start, a geologist who can reliably define the rock types, equipped with GPS, a digital susceptibility meter and a good digital scale (and bucket of water) would be enough.

REFERENCES

- GETECH 2003.** Southern Mozambique gravity and magnetic data. Data and descriptions. CD in National Directorate of Geology, Maputo.
- Schetselaar, E., Barritt, S. & Reinink, G. 2004.** Mineral resources management capacity building project, Mozambique. Component 2: Geological Infrastructure Development Project, Geological mapping (LOT 2/3). Report on the geoscience data compilation, phase II.
- Westerhof, A. B. 2005.** Remote sensing techniques in map production. Report in: GTK Workshop in National Directorate of Geology, Maputo, September 8–12, 2005.

MESOARCHAEAN TO LOWER JURASSIC U-Pb AND Sm-Nd AGES FROM NW MOZAMBIQUE

by
Irmeli Mänttari

Mänttari, I. 2008. Mesoarchaeon to Lower Jurassic U-Pb and Sm-Nd ages from NW Mozambique. *Geological Survey of Finland, Special Paper 48*, 81–119, five figures, two tables and three appendices.

This paper exclusively presents isotopic ages for 35 rock samples from NW Mozambique sampled during the geological mapping of the LOT2 area. Dating methods include SHRIMP and TIMS zircon U-Pb dating and the mafic rocks were dated using Sm-Nd mineral isochrones. The age range of felsic to mafic magmatic rocks varies from 2.91 Ga to 0.18 Ga. Several samples have ~500 Ma low Th/U zircon phases evidencing Pan-African metamorphism. Additional thermal event at ~0.8 Ga is indicated by anomalously high lower intercept ages. An indication of the existence of a ~3.1 Ga protolith was found from two samples.

The oldest dated rock sampled from the eastern extension of the Archaean Zimbabwe craton to Mozambique is a tonalite with a zircon U-Pb age of 2907 ± 16 Ma. Four apparently Archaean ages of 2.71–2.50 Ga were dated from other TTG gneisses located in southern to northern parts of the Archaean domain. Additionally, these show Pan-African metamorphism at 520 ± 16 Ma. A ~1.8 Ga dolerite intrudes the Manica greenstones. Within the Archaean domain, Palaeoproterozoic Gairezi Group garnet gneiss cut by a ~1.0 Ga dolerite and Rushinga Group garnet-sillimanite gneiss indicate a maximum sedimentation age of ~2.0 Ga and supplementary Archaean provenances. These sedimentary units suffered metamorphism at 518 ± 6 Ma. The tectonically emplaced Mesoproterozoic Bárue Complex in the core of the southern LOT2 area encloses ~1.1 (–1.3) Ga felsic igneous rocks with ~520 Ma metamorphic monazite. Crystalline rocks in the northern part of the LOT2 area covering the northern part of the Tete Province mainly have Mesoproterozoic ages. A felsic/intermediate volcanic rock from Fingoè Supergroup yields a zircon U-Pb age of 1327 ± 16 Ma and all the dated granitic rocks are younger than this with ages between 1.2 Ga and 1.04 Ga. A gabbro from the Chipera Massif equivalent to the Tete Suite was dated at 1047 ± 29 Ma (ϵ_{Nd} of +1.4). The few dated detrital zircon cores from Zámbe Supergroup metasediments indicate a 1.3–1.2 Ga maximum sedimentation age and additional 2.7 Ga, 2.52 Ga, and 2.1 Ga sedimentary provinces. Late Mesoproterozoic Grenville ages were also dated from the Chacocoma granite (~1.05 Ga) located S of the coeval Tete Suite mafic plutonic rocks and from the Mashonaland dolerite (1.1 Ga; $\epsilon_{\text{Nd}} = -7.3$) intruding Umkondo metasediments further to the south from the LOT2 area. Neoproterozoic rocks comprise the ~0.86 Ga aplite granites belonging to Guro Bimodal Igneous Suite close to the northern part of the Archaean terrain. Moreover, Atchiza Suite gabbro, NW of the lake Cahora Bassa and the Matunda Suite gneiss located west of the Atchiza gabbro have ages of ~0.86–0.80 Ga. Pan-African metamorphism is evidenced by low Th/U metamorphic zircon domains. Palaeozoic Suites include the ~0.5 Ga Pan-African felsic rocks intruding the Mesoproterozoic rocks of the northern parts of the Tete province. Mesozoic Jurassic ~180 Ma Karoo event magmatism is evidenced by a syenite from the Gorongosa Intrusive Suite intruding the Mesoproterozoic Bárue Complex, Rukore Suite granite next to Zimbabwe border, and the Moeza dyke north of Tete.

Key words (GeoRef Thesaurus, AGI): igneous rocks, gneisses, absolute age, U/Pb, Sm/Nd, Archean, Proterozoic, Paleozoic, Mesozoic, Zimbabwe Craton, Mozambique.

GTK - Geological Survey of Finland, P.O.Box 96, FIN-02151 Espoo, Finland

E-mail: irmeli.manttari@gtk.fi

INTRODUCTION

The “*Mineral Resource Management Capacity Building Project, Republic of Mozambique, Component 2: Geological Infrastructure Development Programme, Geological Mapping LOT 2, 2002–2006*” produced updated geological maps at the scale 1: 250 000 with explanations, covering the Provinces of Tete, Manica, and Sofala in NW Mozambique. During the bedrock mapping of the LOT 2 area, 37 rock samples were collected for radiometric dating (Table 1) by geologists of a consortium lead by GTK (Geological Survey of Finland). The zircon TIMS U-Pb and Nd-Sm mineral isochron ages were processed at GTK and the secondary ion microprobe (SHRIMP) zircon U-Pb isotopic data were measured at VSEGEI, St. Petersburg.

For SHRIMP dating, only a limited number of analyses were performed. Therefore, especially in the case of sedimentary rocks, the age results may only be considered as preliminary. Therefore, further U-Pb analyses would be needed for comprehensive understanding of sedimentary provinces and the

maximum sedimentation ages. In general, the zircon in many Archaean rock samples was strongly altered and therefore TIMS dating yielded highly discordant U-Pb isotopic data. In addition, the very strong effect of the Pan-African metamorphism at ~0.5 Ga and sometimes the Early Pan-African processes at ~0.8 Ga either disturbed the zircon U-Pb system, preferably in metamict grains, or crystallized a new zircon phase.

This paper exclusively presents the radiometric age results for 35 rock samples from the LOT 2 area, NW Mozambique. Further geological connections and sample information must be obtained from the original map explanations (GTK Consortium, 2006a-d), from the other papers in this volume (e.g. Koistinen *et al.* 2008, Mäkitie *et al.* 2008, Westerhof *et al.* 2008), and from previous publications (Hunting team 1984, Koistinen *et al.* 2006, Mäkitie *et al.* 2006, Mänttari *et al.* 2006, Westerhof 2006, and references therein).

ANALYTICAL METHODS

TIMS U-Pb

For ID-TIMS U-Pb dating, heavy minerals were separated using heavy liquids (methylenediiodide and Clerici's solution) and a Frantz magnetic separator. The final selection of the minerals for U-Pb analysis was carried out by hand picking. The decomposition of selected zircon and monazite and extraction of U and Pb for multigrain ID-TIMS isotopic age determinations mainly followed the procedure described by Krogh (1973, 1982). ^{235}U - ^{208}Pb (zircon) and ^{235}U - ^{206}Pb (monazite) spiked and unspiked isotopic ratios were measured using a VG Sector 54 thermal ionization multicollector mass spectrometer (TIMS) in the static mode. According to repeated measurements of Pb standard SRM981,

the measured isotope ratios were corrected for $0.12\text{--}0.10 \pm 0.05\%$ / a.m.u. mass discrimination. Pb/U ratios were calculated using the PbDAT program (Ludwig, 1993). Plotting of the U-Pb isotopic data and age calculations were performed using the ISOPLOT/EX 3.00 program (Ludwig 2003). Common lead corrections were carried out using the age-related Stacey's and Kramers's (1975) lead isotope compositions ($^{206}\text{Pb}/^{204}\text{Pb} \pm 0.2$, $^{208}\text{Pb}/^{204}\text{Pb} \pm 0.2$, and $^{207}\text{Pb}/^{204}\text{Pb} \pm 0.1$). The total procedural blank level was 20–50 pg. All the ages were calculated with 2σ errors and without decay constant errors. In the figures, the data-point error ellipses are at the 2σ level.

SHRIMP U-Pb dating

Selected zircon grains were mounted in epoxy resin together with chips of the TEMORA (Middleale Gabbroic Diorite, New South Wales, Australia) and 91500 (Geostandard zircon; Wiedenbeck *et al.* 1995) reference zircons. The grains were sectioned approximately in half and polished. Back-scattered electron images (BSE) and cathodo luminescence (CL) images were prepared for all zircons. The zircon U-Pb analyses were performed using a SHRIMP-II ion microprobe at Center of Isotopic Research, VSEGEI, St.Petersburg, Russia. Each analysis consisted of 5 scans through the mass range. The spot diameter was ~20 μm , and primary beam current was ~4 nA. The raw data reduction using the SQUID Excel Macro of Ludwig (2000) was done in a similar manner to that described by Williams (1998, and references therein). The Pb/U ratios were normalized relative to a value of 0.0668 for the $^{206}\text{Pb}/^{238}\text{U}$ ratio of the TEMORA reference

zircon, equivalent to an age of 416.75 Ma (Black *et al.* 2003). The common lead correction was carried out using the measured ^{204}Pb and modern lead isotope composition (Stacey and Kramers 1975). Uncertainties given for individual analyses (App.1) are at the one σ level. The concordia plots and age calculations were performed using ISOPLOT/EX 3 (Ludwig 2003). In a few cases, the concordia ages were calculated using SQUID (Ludwig 2000). All the results are calculated at the 2σ level with the ignored decay constant errors. The uncertainties of the means of the Pb/U standard calibrations (see App. 1) are not included in table errors but are included in final concordia age errors: either added to the age calculated by Isoplot, or when calculated using SQUID, they are automatically taken into account in the final ages. In figures, the data-point error ellipses as well as the error bars are at the 2σ level.

Sm-Nd mineral dating

For Sm-Nd analyses, handpicked mineral concentrates were washed ultrasonically in warm 6 N HCl for 30 min, and rinsed several times in ultra clean water. The samples (150–200 mg) were dissolved in HF-HNO₃ using Savillex® screw cap teflon beakers for 48h. A mixed ^{149}Sm - ^{150}Nd spike was added to the sample prior to dissolution. After evaporation of fluorides the residue was dissolved in 6N HCl. Sm and Nd were separated in two stages using a conventional cation-exchange procedure (7 ml of AG50Wx8 ion exchange resin in a bed of 12 cm length) and a modified version of the Teflon-HDEHP (hydrogen diethylhexyl phosphate) method developed by Richard *et al.* (1976). The measurements were performed in a dynamic mode on a VG SECTOR 54 mass-spectrometer using Ta-Re triple filaments. The $^{143}\text{Nd}/^{144}\text{Nd}$ ratio is normalized to $^{146}\text{Nd}/^{144}\text{Nd} = 0.7219$. The aver-

age value for the La Jolla standard was $^{143}\text{Nd}/^{144}\text{Nd} = 0.511850 \pm 10$ (std, 50 measurements since 2002). The Sm/Nd ratio of the spike was calibrated against the Caltech-mixed Sm/Nd standard (Wasserburg *et al.* 1981). Based on duplicated analyses the error in $^{147}\text{Sm}/^{144}\text{Nd}$ was estimated to be 0.4%. Initial $^{143}\text{Nd}/^{144}\text{Nd}$ and ε were calculated with the following parameters: $\lambda^{147}\text{Sm} = 6.54 \times 10^{-12} \text{a}^{-1}$, $^{147}\text{Sm}/^{144}\text{Nd} = 0.1966$ and $^{143}\text{Nd}/^{144}\text{Nd} = 0.51264$ for present CHUR (Jacobsen and Wasserburg 1980). T-DM was calculated according to DePaolo (1981). Measurement on the rock standard BCR-1 provided the following values: Sm = 6.58 ppm, Nd = 28.8 ppm, $^{147}\text{Sm}/^{144}\text{Nd} = 0.1380$, $^{143}\text{Nd}/^{144}\text{Nd} = 0.51264 \pm 0.00002$. The blank measured during the analyses was 30–100 pg for Sm and 100–300 pg for Nd. Programs by Ludwig (2003) were used for age calculations.

AGE RESULTS

General information

The sample locations of the 35 dated rock samples are presented in Figure 1. The rock types, corresponding Suite and Group names, and related coordinates are collected in Table 1. The analytical data are presented in three appendices, namely Appendix 1, Appendix 2, and Appendix 3 for U-Pb SHRIMP, U-Pb TIMS, and Sm-Nd TIMS isotopic

data, respectively. Some selected zircon CL images as well as the U-Pb concordia diagrams and Sm-Nd plots are collected in Figures 2 and 3, 4, respectively. For further geological information, please refer to the original map explanations (GTK Consortium 2006a–d).

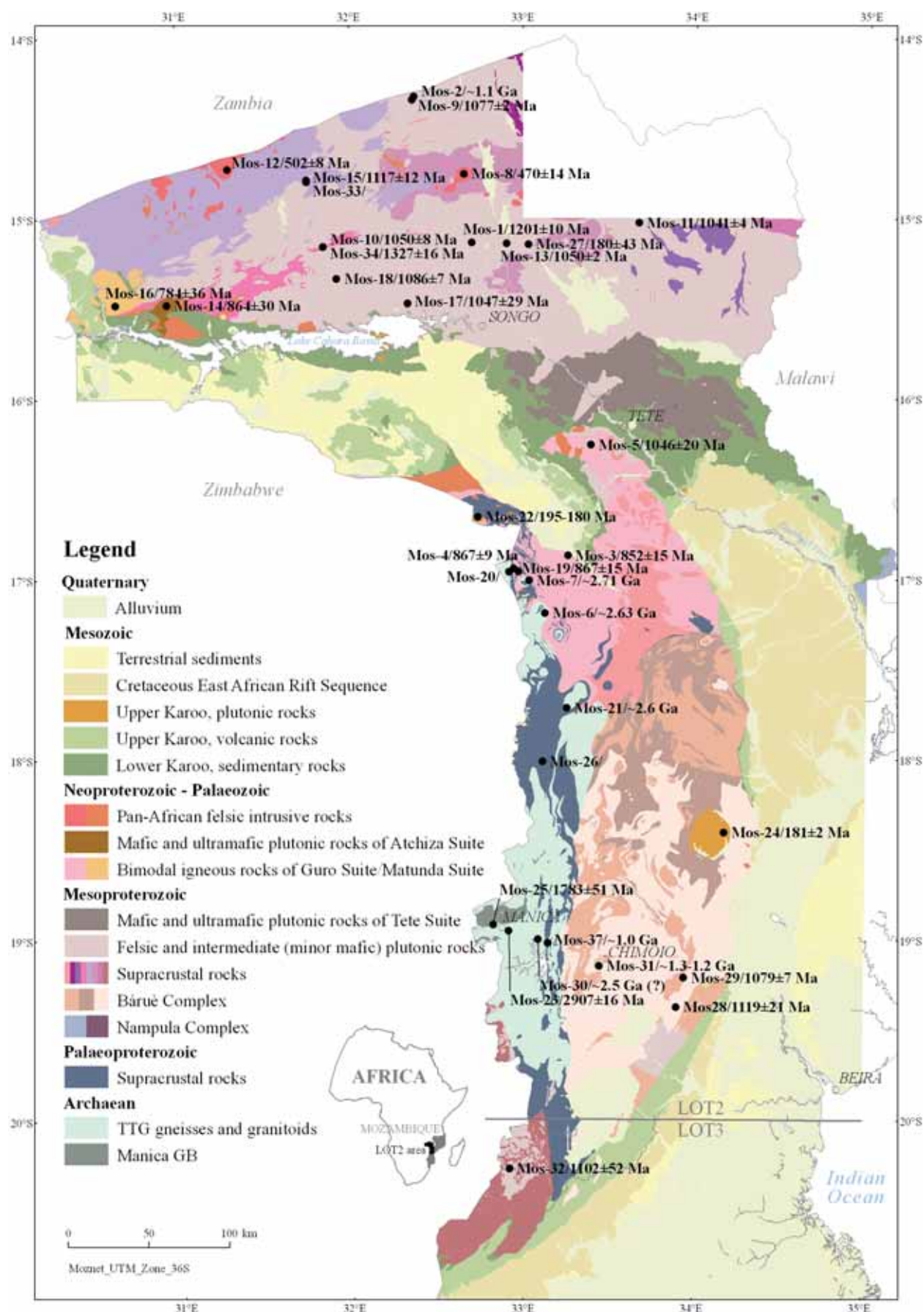


Fig. 1. Simplified geological map of the LOT 2 area, NW Mozambique (simplified and modified after the work by the GTK Consortium). Sample numbers and sites of the dated rock samples are marked on map. See Table 1 for further sample information.

Table 1. Sample information and dating methods.

LAB ID	FIELD NUMBER	EASTING	NORTHING	ROCK-TYPE	SUITE/GROUP	DATING METHOD
Mos-1	1055-02	468284	8326745	Granite gneiss	Rio Capoché granite	U/Pb on Zr, SHRIMP
Mos-2	2253-03	432370	8416395	Monte Dombe granite	Cassacatiza Suite	U/Pb on Zr, TIMS
Mos-3	1024-02	527931	8134434	Aplite granite	Guro Bimodal Suite	U/Pb on Zr, SHRIMP
Mos-4	1072-02	494386	8126625	Aplite granite	Guro Bimodal Suite	U/Pb on Zr, TIMS
Mos-5	1097-03	541966	8202648	Granite	Chacocoma granite	U/Pb on Zr, SHRIMP
Mos-6	1170-03	513559	8099375	Massanga gneiss	Mudzi Metamorphic Complex	U/Pb on Zr, TIMS
Mos-7	1284-03	5037824	8119250	Gneiss	Mudzi Metamorphic Complex	U/Pb on Zr, SHRIMP
Mos-8	2450-03	463512	8369001	Granite	Macanga Granite	U/Pb on Zr, SHRIMP
Mos-9	2007-03	431180	8414421	Granite	Cassacatiza Suite	U/Pb on Zr, TIMS
Mos-10	2001-02	376147	8323791	Granite	Monte Sanja Suite	U/Pb on Zr, TIMS
Mos-11	2297-03	571952	8338810	Desaranhama granite	Furancungo Suite	U/Pb on Zr, TIMS
Mos-12	4493-03	316890	8371137	Granite	Sinda Suite	U/Pb on Zr, SHRIMP
Mos-13	6034-03	489885	8326199	Granite	Castanho Granite	U/Pb on Zr, TIMS
Mos-14	2395-03	279324	8287732	Gabbro	Atchiza Suite	Sm/Nd mineral isochron
Mos-15	4241-03	365684	8364734	Granite	Cassacatiza Suite	U/Pb on Zr, SHRIMP
Mos-16	13016-03	247659	8287248	Granite gneiss	Matunda Suite	U/Pb on Zr, SHRIMP
Mos-17	13014-03	433666	8286298	Gabbro	Chipera Massif	Sm/Nd mineral isochron
Mos-18	13032-03	384685	8304453	Granite	Monte Capirimpica granite	U/Pb on Zr, TIMS
Mos-19	2638-04	497125	8124948	Aplite granite	Guro Bimodal Suite	U/Pb on Zr, SHRIMP
Mos-20	2943-04	491312	8124697	Garnet-sillimanite gneiss	Rushinga Group	U/Pb on Zr, SHRIMP
Mos-21	1519-04	527153	8040960	Fudeze orthogneiss	Mudzi Metamorphic Complex	U/Pb on Zr, SHRIMP
Mos-22	2893-04	472183	8158374	Granite	Rukore Suite	U/Pb on Zr, TIMS
Mos-23	13625-04	491095	7904308	Tonalite	Mavonde Complex	U/Pb on Zr, SHRIMP
Mos-24	15273-04	624078	7964477	Syenite	Gorongosa Intrusive Suite	U/Pb on Zr, TIMS
Mos-25	25416-04	481495	7908114	Dolerite	Archaean terrain	Sm/Nd mineral isochron
Mos-26	1011-02	512044	8008145	Garnet gneiss	Gairezi Group	U/Pb on Zr, SHRIMP
Mos-27	14410-03	503380	8325794	Moeza Dike	Rukore Suite	Sm/Nd mineral isochron
Mos-28	19313-04	594472	7857362	Granite	Báruè Complex	U/Pb on Zr, SHRIMP
Mos-29	19290-04	599246	7875441	Inchapa granodiorite	Báruè Complex	U/Pb on Mon and Zr, TIMS and SHRIMP
Mos-30	19140-04	509199	7898986	Messeca granodiorite	Mavonde Complex	U/Pb on Zr, TIMS
Mos-31	6845-04	547097	7882708	Monte Chissui tonalite	Báruè Complex	U/Pb on Zr, TIMS
Mos-32	13888-04	491576	7758265	Dolerite	Mashonaland dolerite (post-Umkondo)	Sm/Nd mineral isochron
Mos-33	4158-03	365692	8363637	Metasandstone	Zámbuè Supergroup	U/Pb on Zr, SHRIMP
Mos-34	3157-03	376146	8323802	Felsic/intermediate metavolcanic rock	Fíngoè Supergroup	U/Pb on Zr, SHRIMP
Mos-37	1714-05	515362	7896822	Dolerite	Post-Gairezi	Sm/Nd mineral isochron

Zr=zircon; Mon=monazite

Mos-1 / 1055-02 Rio Capoché Granite gneiss

Zircon separated from Rio Capoché granite is either short to long prismatic with clear crystal faces or the grains are ellipsoidal to quite tabular with smooth crystal faces. Within these transparent and reddish crystals, there are also translucent and more brownish grains. In all, although the shape of the crystals may vary, the population looks quite homogeneous. In CL images (Fig. 2), many grains show CL-paler zoned core domains surrounded by

CL-darker zones. However, as the magmatic zoning continues similarly through the whole crystal these do not show structurally separate core and rim domains. There are also longer zoned zircon grains without CL-pale centre domains and a few are completely CL-black.

A total of 18 zircon domains were dated using SHRIMP (App. 1). Seven of the analyses were rejected due to high common lead proportions.

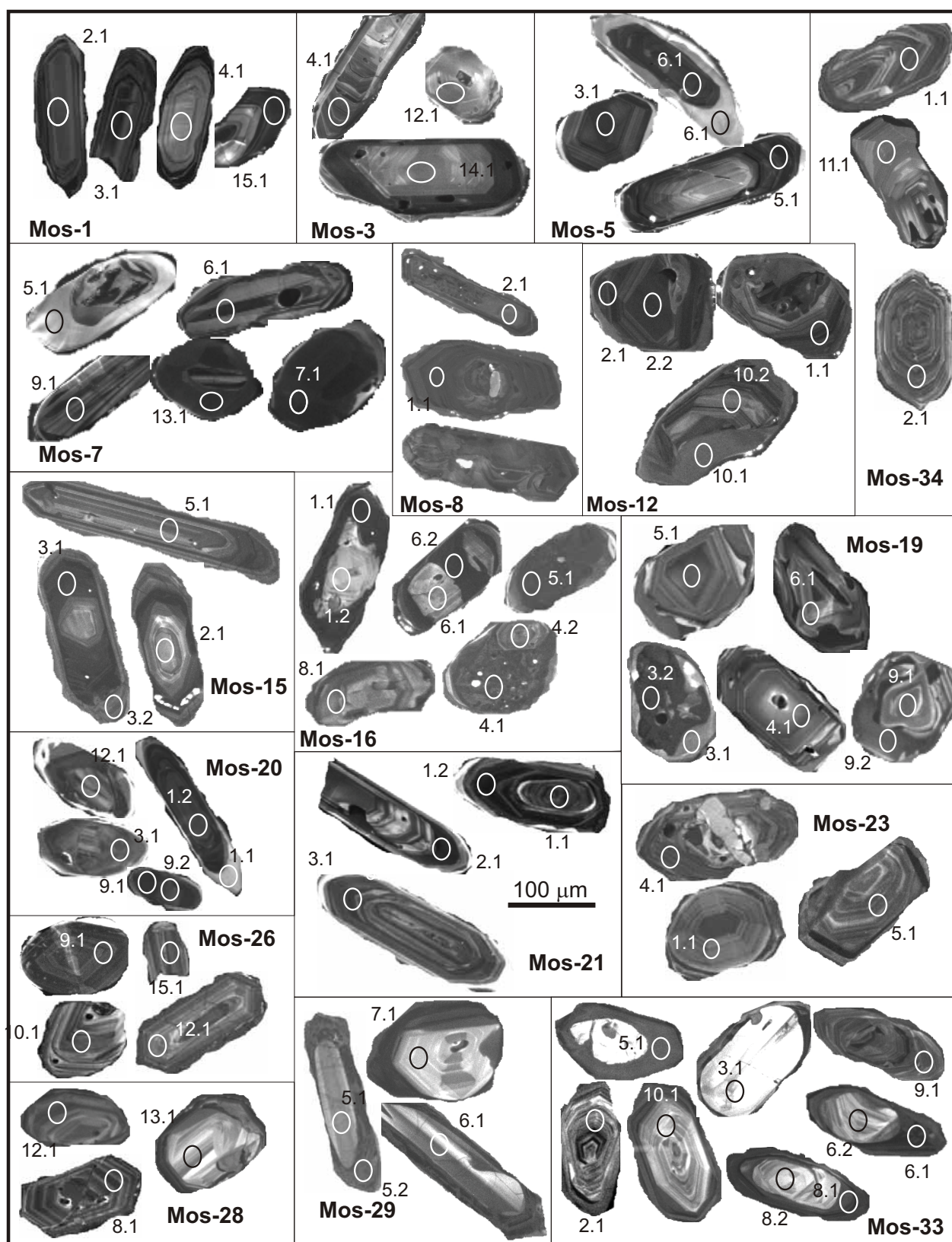


Fig. 2. Selected CL images for SHRIMP U-Pb dated samples. The analysis spot sites and corresponding analysis numbers are indicated (see Table 3). **Mos-1 granite gneiss:** 2.1 and 3.1 belong to the 1.20 Ga age group; 4.1 has a high common lead content, and 15.1 shows post-crystallization lead loss. **MOS-3 aplite granite:** Magmatic ~850 Ma zircon. **MOS-5 granite:** Magmatic ~1.05 Ga zircon (3.1 and 5.1) and a supposedly inherited zircon with a CL-dark, disturbed core and a CL-bright metamorphic rim with a metamorphic age of ~1.05 Ga. **Mos-7 gneiss:** 6.1 and 9.1 are ~2.7 Ga magmatic zircon; younger and possibly metamorphic CL-dark zircon domains (7.1 and 13.1); CL-pale, low Th/U metamorphic rim 5.1 is ~520 Ma. **Mos-8 granite:** CL-dark ~470 Ma zircon with visible zoning (1.1 and 2.1); zircon showing a blurry internal structure (no analysis). **Mos-12 granite:** Zoned and homogeneous ~500 Ma zircon domains. **Mos-15 granite:** All analysed zircon domains are ~1.1 Ga. **Mos-16 granite gneiss:** ~800 Ma ages from 8.1, 6.1, 1.2, and 4.2; ~500 Ma from low Th/U domains 5.1, 6.2, 4.1, and 1.1; rounded, completely metamict zircon 4 enclosing a ~750 Ma zoned zircon (recrystallized?). **Mos-19 aplite granite:** Magmatic 850 Ma zircons (4, 5, and 6); metamorphic 850 Ma ages from rounded metamict zircon (3.2), its CL-pale rim (3.1), and from the CL-dark rim domain of zircon 9, which has a ~500 Ma core. **Mos-20 garnet-sillimanite**

On the concordia diagram (Fig. 3A), five analyses from zoned zircon domains plot in a cluster yielding a concordia age of 1201 ± 10 Ma. The remaining six concordant analyses plot roughly between 1050 Ma

and 1150 Ma. The younger data analysed mostly on CL-dark zoned domains probably show minor lead loss and therefore 1201 ± 10 Ma is interpreted as the age for the Rio Capoché granite.

Mos-2 / 2253-03 Monte Dombe granite, Cassacatiza Suite

Monte Dombe granite has a rather heterogeneous zircon population. Zircon can be transparent to translucent, brownish to yellowish and short prismatic or colourless and tabular with pyramidal edges, and the turbid, brownish grains exhibit mostly larger grain sizes.

Four zircon fractions were analysed for their Pb/U ratios using TIMS (App. 2). In general, the $^{206}\text{Pb}/^{204}\text{Pb}$ ratios are low and the analyses show a

high degree of discordance. As is normal, the most abraded fraction shows the lowest U content and the highest $^{206}\text{Pb}/^{204}\text{Pb}$ ratio. The analysed fractions plot roughly on the same line intercepting the concordia curve at 1102 ± 24 Ma (Fig. 3B). However, as the zircon population of the Monte Dombe granite is fairly heterogeneous and the analyses very discordant, it is difficult to judge the factual meaning of the 1102 ± 24 Ma age.

Mos-3 / 1024-02 aplogranite gneiss, Guro Suite

Sample Mos-3 contains abundant zircon with quite a homogeneous outlook. Grains are principally long prismatic (l:w ~3–4), fairly colourless to yellowish-brownish, and transparent to translucent and contain occasional inclusions. Large, turbid, dark, and more formless grains are in the minority. In CL images (Fig. 3), the zircon shows clear magmatic zoning and only a few show a dark, spotty CL indicating metamictization. A few probable cores were identified and some grains show thin later zircon growth.

Fifteen zircon spots were dated using SHRIMP II (Appendix 1). As the supposed metamorphic rims were too thin for dating, all the age data come from magmatic domains only. On the concordia diagram (Fig. 4C), the concordant to nearly concordant data scatter between 760 and 920 Ma. The upper intercept age and the weighted average of the $^{207}\text{Pb}/^{206}\text{Pb}$ ages are equivalent. Thus, the age of the aplogranite gneiss is 852 ± 15 Ma. Later, most probably Pan-African metamorphism is evidenced by the thin zircon envelopes around the magmatic crystals.

Mos-4 / 1072-02 aplogranite gneiss, Guro Suite

Aplogranite gneiss Mos-4 yielded a large amount of zircon with varying grain-size. It is predominantly almost colourless, transparent, and euhedral to subhedral (l:w = 3–5), and frequently contains dark inclusions. In the $< 75 \mu\text{m}$ grain-size fraction, the grains have smooth surfaces. In the coarser grain-size fraction, dark brown and formless, most probably inherited zircon grains also occur. For U-Pb dating only the bright euhedral crystals were selected.

Four zircon fractions were analysed for their Pb/

U ratios using TIMS (App. 2). The zircon fractions have moderate U concentrations and the abraded fractions show the lowest U contents and the highest $^{206}\text{Pb}/^{204}\text{Pb}$ ratios within a grain-size group. In general, the $^{206}\text{Pb}/^{204}\text{Pb}$ ratios are high and especially the abraded analyses show only minor discordance. The four analysed zircon fractions plot well on the same discordia line with concordia intercept ages of 867 ± 9 Ma and 389 ± 61 Ma (MSWD = 1; $n = 4$) (Fig. 3D).

gneiss: 2.8 Ga zoned zircon (1.2) enveloped by a CL-bright, low Th/U ~500 Ma rim (1.1); zircon core 9.2 plotting on a 1.98 Ga reference line is surrounded by a ~500 Ma CL-dark, low Th/U zircon phase (9.1); zoned core 12.1 plots on the ~2.5 Ga reference line and 3.1 is a ~500 Ma phase. **Mos-21 orthogneiss:** A > 3 Ga core (1.1) and ~2.60 Ga magmatic zircon phases (1.2, 2.1, and 3.1). **Mos-23 tonalite:** ~2.9 Ga magmatic zircon grains (1.1, 4.1, and 5.1). **Mos-26 garnet gneiss:** ~3.1 Ga rounded zircon (9.1); 15.1 is ~2.7 Ga; 10.1 and 12.1 plot on a 2.04 Ga cluster. **Mos-28 granite:** Zircon 8 is magmatic zircon in the 1119 ± 21 Ma zircon group and 13 and 12 are examples of inherited grains. **MOS-29 granodiorite:** 5.1, 6.1, and 7.1 magmatic ~1.08 Ga zircon domains; analysis from the CL-dark, low Th/U rim is highly discordant, indicating metamorphism at ~500 Ma. **MOS-33 metasediment:** The youngest zoned zircon domain is ~0.83 Ga (2.1); detrital cores give ages of 2.7 Ga (6.2), 2.1 Ga (8.2), and 1.3–1.2 Ga (3.1, 10.1); CL-dark metamorphic rim zircon phases are 1.2 Ga (5.1) and 0.4 Ga (8.1) (analysis 6.1 was rejected due to a high common lead proportion). **MOS-34 felsic/intermediate metavolcanic rock:** Typical magmatic 1.3 Ga zircon (1.1 and 2.1); younger zircon domain 11.1 must have suffered lead loss.

Mos-5 / 1097-03 Chacocoma granite

The amount of zircon in Chacocoma granite is large, the population is morphologically homogeneous, and its grain-size varies. Zircon is euhedral, long (l:w ~4–5), transparent to translucent, and colourless to brownish. Among these, elongated and more tabular grains, as well as grains with poorly developed crystal faces were detected. In CL (Fig. 2), the zircon is commonly dark, shows magmatic zoning, and is occasionally enveloped by thin, or rarely wider, metamorphic CL-bright, structurally homogeneous rims. These, in turn, can be corroded and replaced or enveloped by a still later and thinner zircon phase. In a few grains, metamorphic or magmatic CL-medium dark rims occur between the CL-bright rims and core domains. Furthermore, some zircon grains or zircon domains show disturbed magmatic zoning to more blurry structures indicating the beginning of metamictization.

A total of 15 zircon domains were dated using SHRIMP II (App. 1). Nine of these represent mag-

matically zoned crystals with or without thin metamorphic rims. In addition, two CL-bright and one CL-medium dark rim domains were wide enough for dating. The CL-dark, mostly zoned core domains of the grains with wide rim domains were also dated.

On the concordia diagram (Fig. 3E), the rather concordant age data scatter primarily between 960 and 1080 Ma. One zoned zircon (Mos-5.8.1) gives an apparently higher $^{207}\text{Pb}/^{206}\text{Pb}$ age of ~1.2 Ga. However, the error is large and it partly overlaps with the other data. The U-Pb data from rim and core domains in single zircon grains are coeval. Because there is no way to divide the data into separate age/domain groups and the age data are scattered, the weighted average of $^{207}\text{Pb}/^{206}\text{Pb}$ ages would give an age estimate for the rock. The data with the apparently highest $^{207}\text{Pb}/^{206}\text{Pb}$ age are excluded from the 1046 ± 20 Ma mean age.

Mos-6 / 1170-03 Massanga gneiss, Mudzi Metamorphic Complex

The amount of zircon in supposed Archaean Massanga gneiss is extremely low. Zircon is either euhedral elongated (l:w ~2) or round to oval, very bright, and rather colourless. The grain-size varies from medium to extremely fine-grained.

Only three zircon fractions were analysed for their Pb/U ratios (App. 2) with TIMS as the zircon amount was extremely small. In general, the $^{206}\text{Pb}/^{204}\text{Pb}$ ratios are high. On the concordia diagram (Fig. 3F), the three fractions give an upper intercept age of

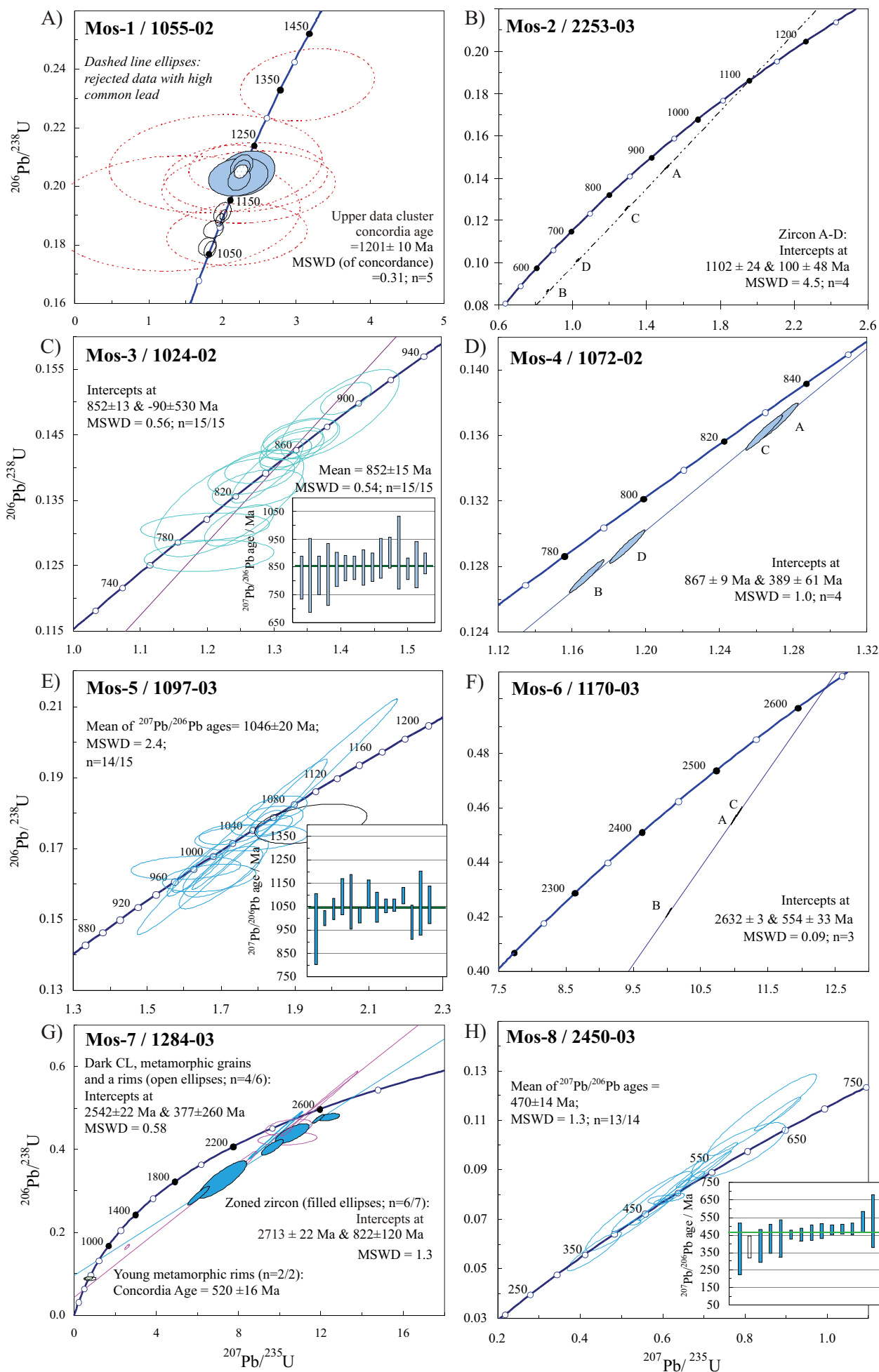
2.63 Ga for the gneiss. Although the discordia line is practically determined only by two data points, the Archaean age is evident. This is already seen in ~2.6 Ga $^{207}\text{Pb}/^{206}\text{Pb}$ ages for the analysed zircon fractions. However, as the age data from gneiss Mos-37 from the same metamorphic complex most probably indicate a ~2.71 Ga magmatic age and metamorphism at ~2.5 Ga, it may be that the 2.63 Ga age estimate from Massanga gneiss is an average age.

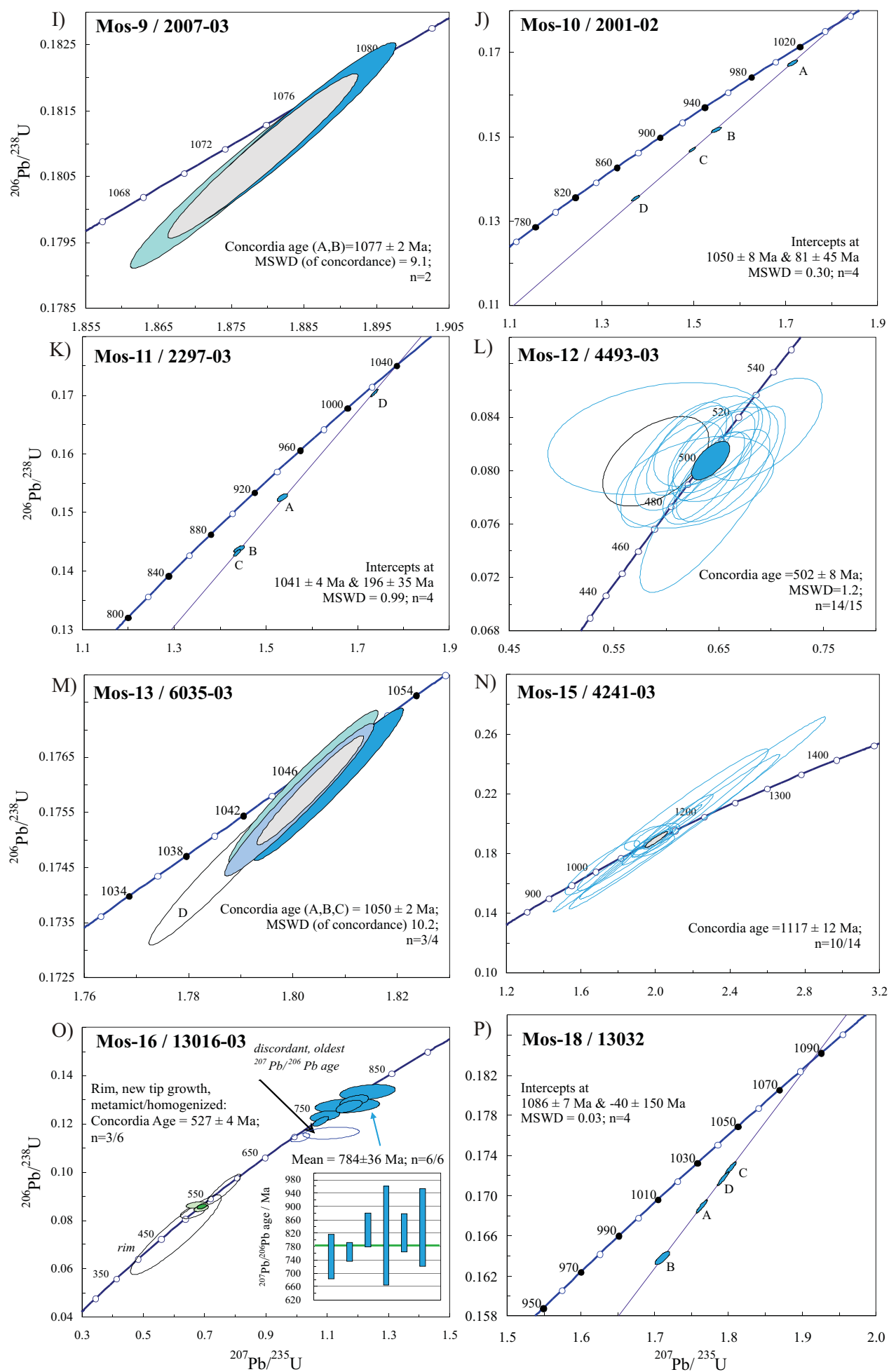
Mos-7 / 1284-03 gneiss, Mudzi Metamorphic Complex

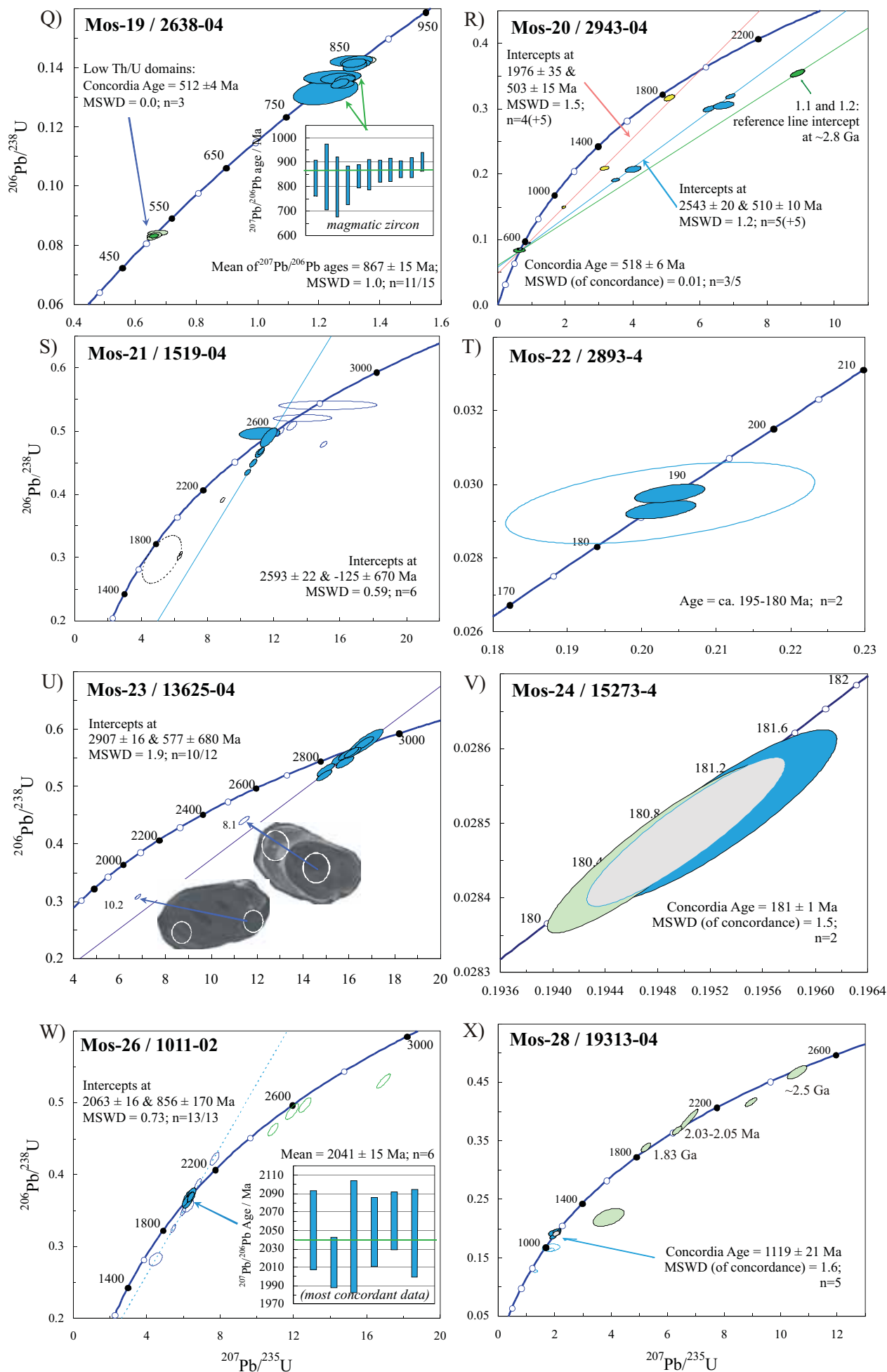
The zircon in Mos-7 gneiss splits into two main populations. One population consists of mainly long or elongated (l:w ~4–2), euhedral, partly corroded (?), pale brown, translucent to turbid grains and the other of very bright, colourless, elongated to oval or round grains. Among these, other intermediate phases with varying grain-sizes also occur. In CL images (Fig. 2), the majority of the zircon grains show magmatic zoning, which in a few cases is disturbed with a blurry structure. Only small, often disturbed/altered possible cores were found. In addition to zoned zircons, there are also rounded, internally relatively homogeneous, CL-dark, prob-

ably metamorphic grains. Many zircons are enveloped by metamorphic CL-bright and/or darker rim phases.

A total of 15 zircon domains were dated using SHRIMP (App. 1). As the zircon material was shown to be quite complex internally, the analyses were performed on zoned zircons, CL-bright rims, and CL-dark, supposedly metamorphic grains. On the concordia diagram (Fig. 3G), the U-Pb data plot partly in a cluster and most of the data are discordant. The age results are divided into three groups according to the dated zircon domains: 1) The zoned zircon domains form the oldest ~2.71 Ga







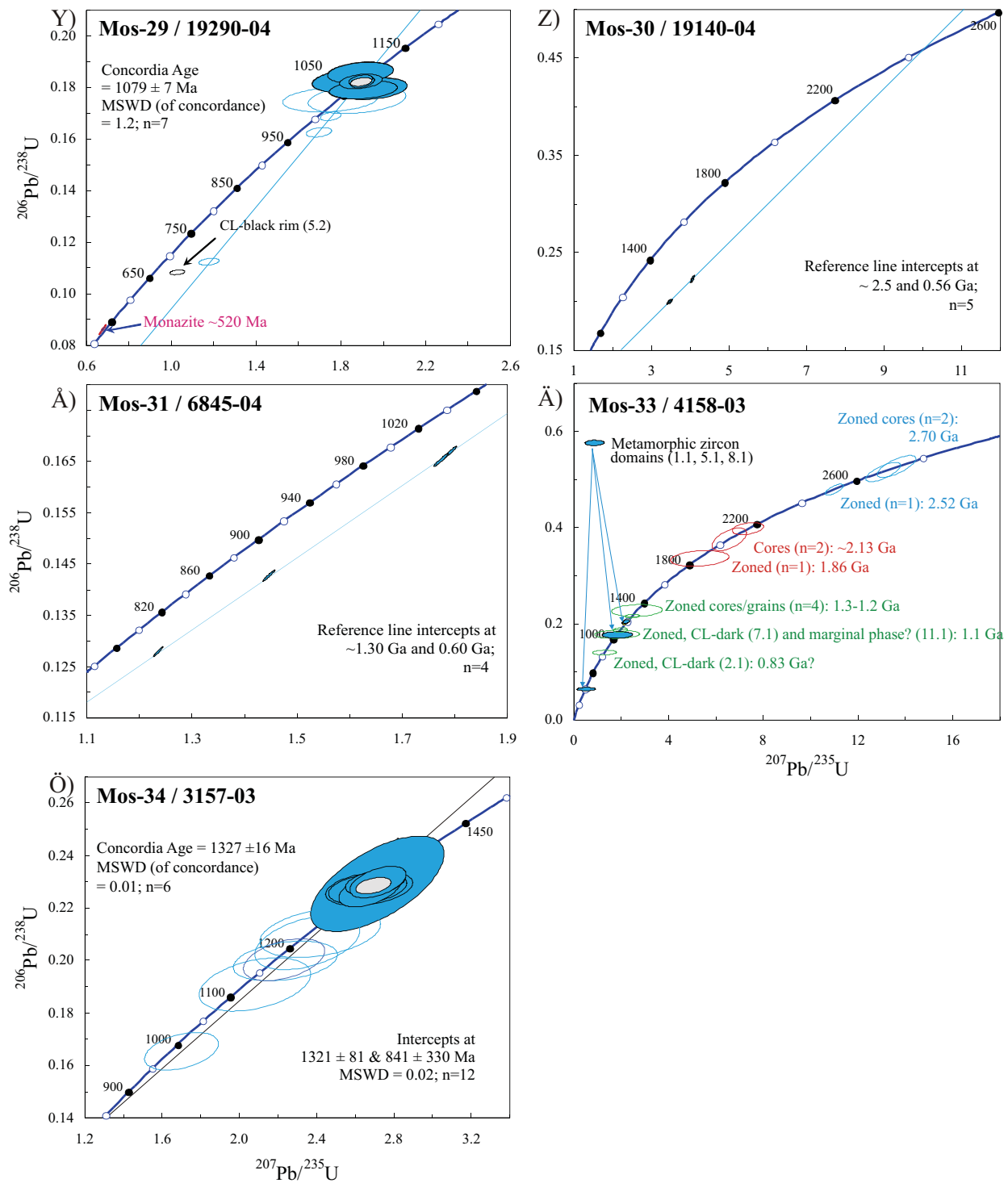


Fig. 3. Concordia plots showing SHRIMP and TIMS zircon U-Pb isotopic data, samples from NW Mozambique. A) Mos-1/1055-02 Rio Capoeche granite gneiss (SHRIMP); B) Mos-2/2253-03 Monte Dombe granite, Cassacatiza Suite (TIMS); C) Mos-3/1024-02 aplite granite, Guro Suite (SHRIMP). The inset shows the weighted average of the $^{207}\text{Pb}/^{206}\text{Pb}$ ages; D) Mos-4/1072-02 aplite granite, Guro Bimodal Suite (TIMS); E) Mos-5/1097-03 Chacocoma granite (SHRIMP). The inset shows the weighted average of the $^{207}\text{Pb}/^{206}\text{Pb}$ ages; F) Mos-6/1170-03 Maassanga gneiss, Mudzi Metamorphic Complex (TIMS); G) Mos-7/1284-03 gneiss, Mudzi Metamorphic Complex (SHRIMP); H) Mos-8/2450-03 Macanga granite (SHRIMP). The inset shows the weighted average of the $^{207}\text{Pb}/^{206}\text{Pb}$ ages; I) Mos-9/2007-03 granite, Cassacatiza Suite (TIMS); J) Mos-10/2001-02 granite, Monte Sanja Suite (TIMS); K) Mos-11/2297-03 Desaranhama granite, Furancungo Suite (TIMS); L) Mos-12/4493-03 granite, Sinda Suite (SHRIMP); M) Mos-13/6035-03 granite, Castanho Granite (TIMS); N) Mos-15/4241-03 granite, Cassacatiza Suite (SHRIMP); O) Mos-16/13016-03 granite gneiss, Matunda Suite (SHRIMP). The inset shows the weighted average of the $^{207}\text{Pb}/^{206}\text{Pb}$ ages for the older group data (zoned cores, healthy magmatic crystal, and an internally quite homogeneous grain); P) Mos-18/13032 Monte Capirimpica granite (TIMS); Q) Mos-19/2638-04 aplite granite, Guro Suite (SHRIMP). The inset shows the weighted average of the $^{207}\text{Pb}/^{206}\text{Pb}$ ages for the older group magmatic zircon grains; R) Mos-20/2943-04 garnet-sillimanite gneiss, Rushinga Group (SHRIMP); S) Mos-21/1519-04 Fudeze orthogneiss, Mudzi Metamorphic Complex (SHRIMP); T) Mos-22/2893-04 granite, Rukore Suite (TIMS); U) Mos-23/13625-04 tonalite, Mavonde Complex (SHRIMP). Discordant Pb/U data from rim domains; V) Mos-24/15273-04 syenite, Gorongosa intrusive Suite (TIMS); W) Mos-26/1011-02 garnet gneiss, Gairezi Group (SHRIMP). The inset shows the weighted average of the $^{207}\text{Pb}/^{206}\text{Pb}$ ages; X) Mos-28/19313-04 granite, Bárue Complex (SHRIMP); Y) Mos-29/19290-04 In-chapa granodiorite, Bárue Complex (zircon SHRIMP and monazite TIMS); Z) Mos-30/19140-04 Messeca granodiorite, Mavonde Complex (TIMS); Å) Mos-31/6845-04 Monte Chissui tonalite, Bárue Complex (TIMS); Ä) MOS-33/4158-03 metasandstone, Zâmbuê Group (SHRIMP); Ö) MOS-34/3157-03 felsic/intermediate metavolcanic rock, Fingoê Supergroup (SHRIMP).

age group. 2) The ~ 2.54 Ga upper intercept age for three rounded, internally homogeneous grains and a metamorphic rim (Mos7.7.1, 8.1, 13.1, 3.1) presumably reflects metamorphism at that time. This group also includes analyses from another internal-

ly homogeneous rim (Mos7.15.1) and from a zircon domain showing disturbed zoning (Mos7.10.1). 3) The Pan-African metamorphism at 520 ± 16 Ma is indicated by two CL-bright, low Th/U rim growths (Mos7.5.1 and 11.1).

Mos-8 / 2450-03 Macanga Granite

The Macanga granite yielded abundant zircon with a fairly heterogeneous population. In addition to long prismatic slim, principally translucent crystals, the large, mostly translucent to turbid, short/equidimensional, and brownish zircon grains are the most common ones. In CL images (Fig. 2), the zircon mainly shows dark CL and blurry or already nonexistent zoning due to the high degree of metamictization in most of the U-rich grains. The dated spots have been selected to represent as undisturbed zoning as possible.

A total of fifteen zircon domains were dated using SHRIMP (App. 1). One data point was rejected due to a high common lead content. On the concordia diagram (Fig. 3H), the U-Pb data are mostly concordant and scatter between 350 Ma and 650 Ma. A weighted average of the $^{207}\text{Pb}/^{206}\text{Pb}$ ages is considered to give the best age estimate for the rock. Thus, the age for the Macanga granite is 470 ± 14 Ma. However, although the dated domains represented as undisturbed zoned domains as possible, they may still show lead loss and the original age of the rock could be older.

Mos-9 / 2007-03 granite, Cassacatiza Suite

The Cassacatiza granite contains abundant zircon that is either transparent and colourless or transparent-translucent and yellowish. The crystals are chiefly long prismatic (l:w = 3–7), medium to coarse-grained (>200 μm), and inclusion rich.

Four zircon fractions were analysed for their Pb/U ratios using TIMS (App. 2). Zircon is quite poor in U and has uniform radiogenic $^{208}\text{Pb}/^{206}\text{Pb}$ ratios.

Two fractions (A and B) with the longest air-abrasion times show the highest $^{206}\text{Pb}/^{204}\text{Pb}$ ratios and the U-Pb results of these are concordant and equal. They give a concordia age of 1077 ± 2 Ma (Fig. 3I). The fraction C shows the most discordant age result with the lowest $^{206}\text{Pb}/^{204}\text{Pb}$ ratio. The fourth, non-abraded fraction D plots just below points A and B, but the result is not equal with these.

Mos-10 / 2001-02 granite, Monte Sanja Suite

Monte Sanja granite contains a large amount of medium- to fine-grained, transparent to translucent, colourless or yellowish zircon with short prismatic to almost needle-like morphologies. Some of the zircon grains contain dark inclusions.

Four zircon fractions were dated using TIMS

(App. 2). Zircon is quite low in U, has uniform radiogenic $^{208}\text{Pb}/^{206}\text{Pb}$ ratio, and an extremely low $^{206}\text{Pb}/^{204}\text{Pb}$ ratio. The dated zircon fractions spread well along the discordia line that intercepts the concordia curve at 1050 ± 8 Ma and 81 ± 45 Ma (Fig. 3J).

Mos-11 / 2297-03 Desaranhama granite, Furancungo Suite

Desaranhama granite yielded a large amount of mainly coarse- to medium-grained, reddish, translucent to turbid zircon with sharp edges and varying prism lengths (l:w = 3–8). Especially the larger crystals contain inclusions.

Using TIMS, four zircon fractions were dated (Appendix 2). The zircon is quite low in U, has

uniform radiogenic $^{208}\text{Pb}/^{206}\text{Pb}$, and low $^{206}\text{Pb}/^{204}\text{Pb}$ ratios. The longest abraded zircon fraction D with a $^{207}\text{Pb}/^{206}\text{Pb}$ age of 1037 Ma plots near to concordia curve and the other fractions are rather discordant (Fig. 3K). The upper intercept age 1041 ± 4 Ma determines the age for the Desaranhama granite.

Mos-12 / 4493-03 granite, Sinda Suite

Sinda granite contains abundant, short to long prismatic zircon that is either quite colourless or yellowish, has a moderately coarse grain-size, and is largely transparent. In addition to a prismatic morphology, flat, equidimensional, and subhedral types also occur. In CL images (Fig. 2), zircon frequently shows magmatic zoning. In a few grains, the zoning is quite blurry or homogenized and some show homogeneous zircon growth cutting the initial zoned phase. In addition, a few cores were detected. However, these are mostly disturbed and/or too small for reliable dating.

A total of 15 zircon domains were dated using SHRIMP (App. 1). Dated zircon domains include zoned crystals and rim growths. All the data are concordant and plot in a same cluster on a concordia diagram (Fig. 3L), despite the different type of the dated domains. The concordia age for most of the data is 502 ± 8 Ma ($n = 14/15$). Accordingly, the seemingly younger cutting zircon phase (see Fig. 2: Mos-12/10.1) must represent later phases of the same magmatic event.

Mos-13 / 6035-03 granite, Castanho Granite

The zircon content of the Castanho granite is very high. The coarser grain-size fraction ($>75 \mu\text{m}$) mainly consists of long prismatic (l:w $\sim 3\text{--}5$), pale brown and transparent zircon, while the fine-grained ($<75 \mu\text{m}$) zircon is relatively colourless, transparent, and the grains are generally shorter and more oval shaped. The zircon occasionally contains small inclusions.

Four zircon fractions were analysed for their Pb/U ratios using TIMS (App. 2). The zircon is quite poor in U, has an extremely high $^{206}\text{Pb}/^{204}\text{Pb}$ ratio, and uniform radiogenic $^{208}\text{Pb}/^{206}\text{Pb}$ ratios. On the concordia diagram (Fig. 3M), three dated zircon fractions are just concordant with 0.65% errors for the Pb/U ratios. The concordia age for the concordant data is 1050 ± 2 Ma ($n = 3$). The slightly discordant fraction D also plots together with the other data.

Mos-14 / 2395-03 gabbro, Atchiza Suite

The mineral separation of the Atchiza gabbro yielded abundant fresh plagioclase and pyroxene. The Sm-Nd data (App. 3 and Fig. 4D) reveal a low REE level and trend almost parallel with the chondritic trend. The whole rock, plagioclase, and py-

roxene analyses yield an isochron with an age of 864 ± 30 Ma (MSWD = 1) (Fig. 4A). This is the crystallization age of the main magmatic minerals. The initial epsilon value is -3.0 .

Mos-15 / 4241-03 granite, Cassacatiza Suite

The major part of the zircon in Cassacatiza granite is long (l:w $\sim 3.5\text{--}5$) prismatic, has a varying grain size, and is covered by yellowish to brownish pigment. The medium-sized grains are normally translucent, the largest are turbid, and the smaller ones quite bright. Among the long crystals, there are also a small amount of short (l:w ~ 2) ones. The population looks quite uniform and the zircon shows sharp crystal edges. In CL images (Fig. 2), the zircon generally shows well preserved oscillatory zoning. Only a few grains demonstrate blurry zoning and the start of homogenisation of the internal structures. Many have a thin, CL-brighter rim around the

zoned zircon domains.

A total of 14 zircon domains were dated using SHRIMP (Appendix 1). The age data mostly comes from the zoned, magmatic domains and only few supposed rim and core phases were suitable for dating. On the concordia diagram (Fig. 3N), the entire data plot in a cluster and 10 of the 14 spots define a concordia age of 1117 ± 12 Ma. Two of the rejected analyses have higher common lead contents, one is discordant, and the fourth one has an anomalously high U concentration. The quite homogeneous age data indicate zircon crystallization at 1117 ± 12 Ma.

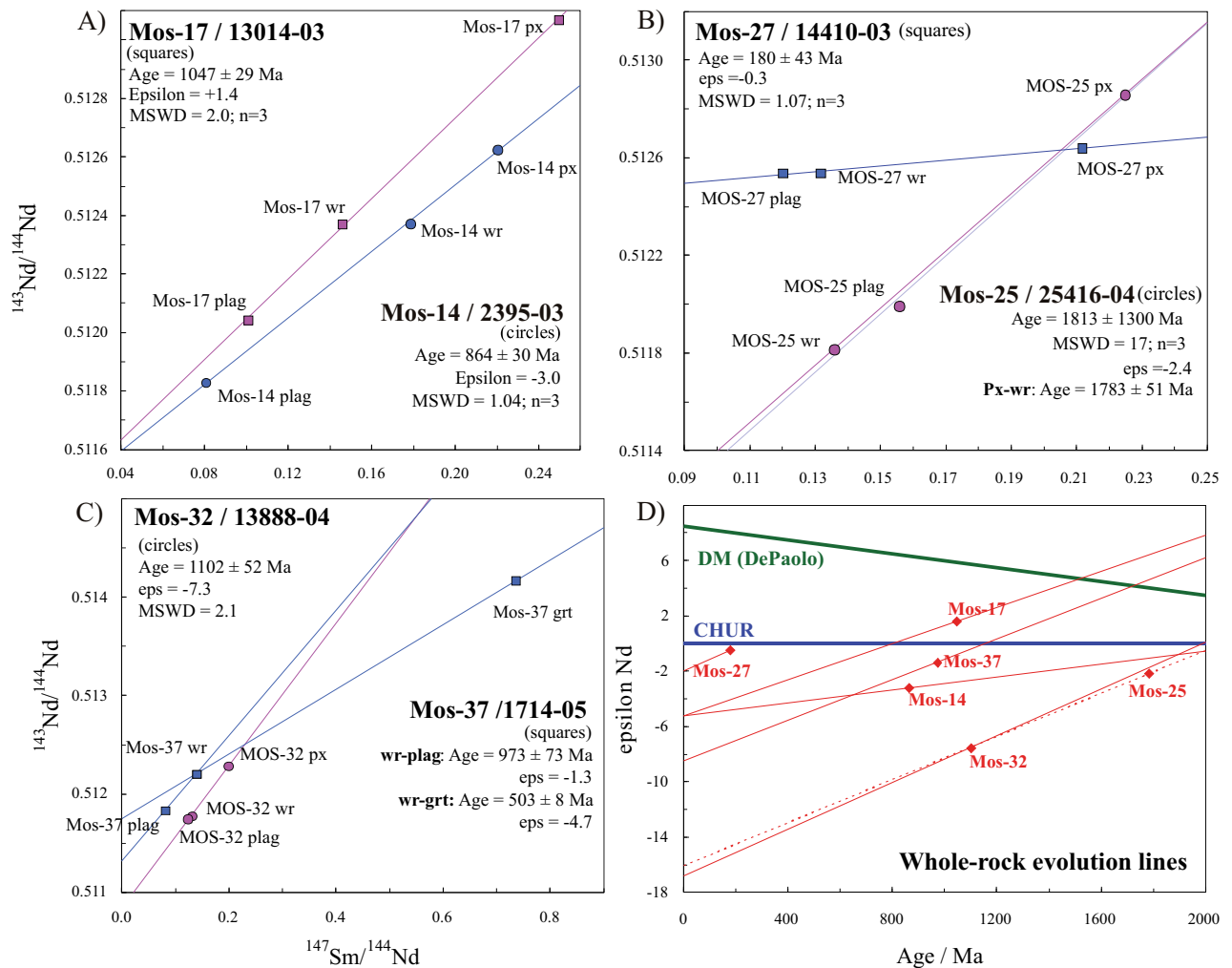


Fig. 4. Sm-Nd data. A) Mos-14/2395-03 gabbro, Atchiza Suite and Mos-17/13014-03 gabbro, Chipera Massif; B) Mos-25/25416-04 dolerite, Archaean domain and Mos-27/14410-03 Moeza Dike, Rukore Suite; C) Mos-32/13888-04 Post-Umkondo dolerite, Mashonaland dolerite and Mos-37/1714-05 Post-Gairezi dolerite; D) Whole rock evolution lines for Mos-14/2395-03, Mos-17/13014-03, Mos-25/25416-04, Mos-27/14410-03, Mos-32/13888-04, and Mos-37/1714-05.

Mos-16 / 13016-03 granite gneiss, Matunda Suite

Matunda gneiss yielded abundant, mostly relatively fine-grained zircon with an apparently heterogeneous population. The zircon is mostly prismatic (l:w ~4–2) and has clear crystal faces. Colourless, mostly transparent grains are either short prismatic or oval-shaped and turbid ones show anhedral forms. In CL images (Fig. 2), the zircon population looks quite heterogeneous, including at least the following types: 1) Totally altered/metamict, CL-dark zircon with occasional thin, CL-bright rims. These are the most common ones. 2) Zircon with preserved zoning in core domains. The corroded, CL-bright core domains are enveloped by a CL-dark zircon phase. 3) A few moderately healthy looking zoned crystals without rims or replacing/enveloping zircon material.

Only 15 zircon domains were dated using SHRIMP (App. 1). One data point was rejected due to a high common lead content. On the concordia diagram (Fig. 3O), the age data divides into two separate age groups: 1) The younger group consists of ages from low Th/U rim and/or replacing zircon phases, metamict and already quite homogenized grains, and from a new tip growth. A concordia age of 528 ± 4 Ma can be calculated for the late metamorphism. 2) The older data deviate between 700 Ma and 830 Ma and come from zoned core domains and healthy zoned crystals. The six apparently older analyses deviate on the concordia curve (Fig. 3O) and therefore no concordia age can be calculated. The weighted average of the $^{207}\text{Pb}/^{206}\text{Pb}$ ages for these zircon domains is 784 ± 36 Ma.

A ~700 Ma healthy, long, and zoned zircon crystal (Mos16.10.1) and the core (Mos16.12.1) with the highest $^{207}\text{Pb}/^{206}\text{Pb}$ age of over 900 Ma plot outside the two main age groups. However, as the error for the >900 Ma Pb-Pb age is very high and the ~700

Ma zircon has an anomalous appearance, these deviating analyses may be considered unimportant. The initial age of the abundant rounded, metamict grains remains unresolved as they now show similar ages to the clearly metamorphic zircon phases.

Mos-17 / 13014 gabbro, Chipera Massif

Chipera gabbro yielded a relatively small amount of brown pyroxene and abundant fresh plagioclase. The Sm-Nd data (App. 3 and Fig. 4A) yield an isochron, which gives an age of 1047 ± 29 Ma for the

gabbro. The initial ratio of +1.4 is still much lower than the coeval depleted mantle, which according to the model by DePaolo (1981), for example has an $\epsilon_{\text{Nd}}(1047 \text{ Ma})$ of +5.6.

Mos-18 / 13032 Monte Capirimpica granite

Monte Capirimpica granite has abundant brown, transparent to translucent, prismatic (l:w = 3–4) zircon. The population is quite homogeneous and the zircon mostly medium grained with a rather even size distribution.

Four zircon fractions were dated using TIMS

(App. 2). The zircon has a moderate U concentration and varying $^{206}\text{Pb}/^{204}\text{Pb}$ ratios, one being rather low. The radiogenic $^{208}\text{Pb}/^{206}\text{Pb}$ ratios are uniform. On the concordia diagram (Fig. 3P), the four fractions plot well on the same discordia line with an upper intercept age of 1086 ± 7 Ma.

Mos-19 / 2638-04 aplite granite, Guro Suite

In aplite granite Mos-19, the zircon content of the nonmagnetic fraction is extremely low and the population looks quite heterogeneous in terms of outlook and grain size. The fine-grained zircon is transparent, colourless to brownish and has either tabular or oval to prismatic morphology. The larger grains are either turbid and dark brown or transparent and quite colourless. The shapes vary from short prismatic to longer crystals. The number of flat, rounded grains is significantly high. The magnetic fraction contains abundant dark brown, turbid, paler coloured, and translucent zircon, principally with a euhedral shape. The zircon in CL (Fig. 2) shows a variety of internal structures. Most of the rounded and flat grains have a CL-dark and spotty internal structure with sporadic CL-paler rims and spots inside. In addition, there are clearly-zoned crystals with or without structurally homogeneous rim domains.

Using SHRIMP, a total of 21 zircon domains were dated (App. 1). One analysis was rejected due to a high common lead content. On the concordia

diagram (Fig. 3Q), the data divide into two main age groups. The older data, including both zoned ($n = 11$) zircon domains and metamorphic, homogeneous rims and their metamict core domains ($n = 4$), plot roughly between 850 Ma and 800 Ma. These data seemingly split further into two sub-clusters. However, because the Pb/Pb ages are overlapping, all the data are considered as a single age group. The weighted average of the $^{207}\text{Pb}/^{206}\text{Pb}$ ages for the zoned zircon only is 867 ± 15 Ma (Fig. 3Q). The younger group includes five analyses: three determine a concordia age of 512 ± 4 Ma and two show slightly older ages. All these show an exceptionally low Th/U ratio.

In summary, the zircon crystallized at 867 ± 15 Ma. Approximately coevally at 850–830 Ma, the flat, round, and metamict zircon suffered radiogenic lead loss (see Fig. 2; zircon 3). This zircon feasibly has a sedimentary origin and its initial age is unknown, as the U-Pb system of a metamict zircon is easily affected by hydrothermal events. Cambrian metamorphism at 512 ± 4 Ma is evident.

Mos-20 / 2943-04 Garnet-sillimanite gneiss, Rushinga Group

Rushinga Group garnet-sillimanite gneiss yielded a small amount of zircon with a fine and uniform grain-size. The general tone is quite pinkish but single crystals are almost colourless, transparent, and elongated. Zircon shows either clear crystal faces or the surfaces are quite smooth. The darker grains are translucent. It is supposed that the older grains are healed/metamorphosed to transparent, colourless grains. Almost every one of the mounted zircon grains is enveloped by a CL-bright rim (Fig. 2). The mostly CL-dark inner/core domains are either altered or show compositional zoning. A few zoned cores are surrounded first by a CL-dark phase and secondly by a thin CL-bright rim (Fig. 2).

Using SHRIMP, 17 zircon domains were dated (App. 1). Two analyses have high common lead contents and were therefore rejected. On the concordia diagram (Fig. 3R), the U-Pb data divide into four separate groups: 1) Five concordant or slightly discordant, low Th/U analyses determine a concordia age of 518 ± 6 Ma. These youngest ages were measured from either CL-bright rims or CL-dark, compositionally zoned or homogeneous zircon domains (Fig. 2). 2) Four discordant data points from

zircon cores and grains fall on the same discordia line. Calculating these data solely or combined with the ~ 500 Ma data, the upper intercept age will be ~ 2.0 Ga. 3) Five discordant analyses from cores enveloped by CL-bright rims determine an upper intercept age of ~ 2.54 Ga when calculated with or without the youngest ~ 500 Ma data. 4) The highly discordant analysis (1.2; see also Fig. 2) from a CL-dark zoned core has a $^{207}\text{Pb}/^{206}\text{Pb}$ age of ~ 2.7 Ga and the enveloping CL-bright rim plots in the ~ 500 Ma group. When plotted together, an age of ca. 2.8 Ga can be estimated for the zircon core.

From the limited available age data, it is clear that the provenance is composed at least from rocks with ages of ~ 2.8 Ga, ~ 2.5 Ga, and ~ 2.0 Ga. The maximum age for sedimentation would be ~ 2.0 Ga. On the other hand, as the U-Pb data are highly discordant and the metamorphism at ~ 500 Ma could have shifted the older data points slightly, the ages should only be considered as rough estimates. The concordia age of 518 ± 6 Ma (Fig. 3R) determined by analyses from the low Th/U and CL-bright zircon rims records Pan-African metamorphism. This age is also a minimum age for the sedimentation.

Mos-21 / 1519-04 Fudeze orthogneiss, Mudzi Metamorphic Complex

Fudeze orthogneiss contains abundant prismatic zircon with a varying grain size. The population looks homogeneous and only the degree of colour and brightness varies between the smallest and the largest zircons. The zircon shows compositional zoning in CL images (Fig. 2). A few inherited cores were detected. However, with the few exceptions they are too small or altered for reliable U-Pb dating.

Using SHRIMP, a total of 16 zircon domains were dated (App. 1). One analysis has a high common lead content and was therefore rejected. Unfortunately, this analysis was the only one from a thin CL-bright zircon rim. Furthermore, the four most

discordant data are ignored in this context. On the concordia diagram (Fig. 3S), the concordant and nearly concordant U-Pb data plot mostly between 2.6 and 2.8 Ga. Four discordant and two concordant analyses on zoned zircon define a discordia line that intercepts the concordia curve at ~ 2.59 Ga.

In addition to ~ 2.6 Ga zircon, five older ages between 3.05 Ga and 2.65 Ga were measured from zoned zircon and an inherited core. These commonly also show higher Th/U compared to those of the ~ 2.6 Ga zircon. The apparent core in zircon 1 has a $^{207}\text{Pb}/^{206}\text{Pb}$ age of 3.05 Ga, whereas the main zircon domain belongs to the ~ 2.6 Ga age group (see Fig. 2). Thus, the age for the Fudeze orthogneiss is ~ 2.59 Ga.

Mos-22 / 2893-04 granite, Rukore Suite

Rukore granite yielded abundant zircon with a homogeneous population. The long to short crystals are mainly transparent, almost colourless, have clear crystal faces, and occasionally contain dark inclusions.

Three zircon fractions were dated using TIMS (App. 2). Two of them give concordant Lower Jurassic ages (Fig. 3T). As the Pb-U data from the

two individual, young, and low-U fractions are not exactly equal, the results may indicate some uncertainty within Pb and U fractionation during the mass spectrometry. Therefore, it is suggested that an age approximation of 195–180 Ma is used for the granite. The third analysis (B) is discordant and suggests the involvement of some older lead.

Mos-23 / 13625-04 tonalite, Mavonde Complex

The zircon content of the Mavonde Complex tonalite is anomalously low. The very fine-grained zircon is largely brown, transparent, and prismatic. The large grains are either white to yellowish, totally turbid, and stubby or dark brown, translucent/transparent, prismatic (stubby to $l:w \leq 4$). In CL images (Fig. 2), most of the zircons show clear magmatic zoning. A few are totally altered (turbid whitish/yellowish) and altered inherited cores are thought to be quite common.

The SHRIMP U-Pb age results from the tonalite are quite unambiguous and therefore only 12 anal-

yses were carried out (App. 1). On the concordia diagram (Fig. 3U), the ten concordant or nearly concordant analyses from magmatic, zoned zircon plot in a cluster at 2.9 Ga. The upper intercept age of 2907 ± 16 Ma is the age for the tonalite. Thus, this deformed tonalite is Mesoarchaeal. The altered/metamict cores indicate even older zircon ages for inherited components. Two analyses give very discordant age results (Fig. 3U). These were measured from a structurally rather homogeneous core and from a low Th/U zircon rim phase.

Mos-24 / 15273-04 syenite, Gorongosa Intrusive Suite

The zircon in Gorongosa syenite is mostly transparent to translucent, almost colourless to yellowish, and elongated. The crystal faces are frequently striated and the grains are preferably quite platy. In addition to this type of zircon, a small quantity of darker brown, stubby grains were detected. These

are considered as inherited.

The two zircon fractions analysed using TIMS (App. 2) give concordant and equal Lower Jurassic ages. The concordia age of 181 ± 2 Ma (Fig. 3V) determines the age for the syenite.

Mos-25 / 25416-04 dolerite, Archaean terrain

The dolerite Mos-25 contains abundant pyroxene and plagioclase for Sm-Nd isochron. The pyroxene is fresh, transparent, and brown. Plagioclase ranges from clear colourless to turbid white.

The Sm-Nd data (App. 3; Figs. 4B and 4D) reveal a relatively high REE level and the trend shows significant enrichment in LREE (cf. chondritic $^{147}\text{Sm}/^{144}\text{Nd} = 0.1966$; Jacobsen and Wasserburg 1980). The whole rock, plagioclase, and pyroxene analy-

ses do not yield any decent isochron ($\text{MSWD} = 17$) (Fig. 4B). An anomalous feature is the relatively high Sm/Nd in the analyzed plagioclase fraction. The age of 1783 ± 51 Ma derived from the analyses on whole rock and pyroxene may be considered as the best estimate for the magmatic crystallization of the rock. The initial epsilon-value is -2.2 and suggests the involvement of older LREE-enriched material in the genesis of the rock.

Mos-26 / 1011-02 garnet gneiss, Gairezi Group

The garnet-kyanite gneiss contains several zircon types with quite a uniform grain-size. These include: 1) transparent, colourless, round to oval and elongated grains, which are at least partly metamorphic, 2) translucent to turbid, white prismatic crystals, and 3) thoroughly turbid, usually yellowish, most probably metamict zircon. In CL images (Fig. 2), the zircon frequently shows compositional zoning. The few roundish, structurally fairly homogeneous zircon grains are the clear exceptions. The CL-bright zircon rims are very few in this sample.

Using SHRIMP, 17 zircon domains were dated (App. 1). On the concordia diagram (Fig. 3W), the

majority of the U-Pb data plot on the same regression line, intercepting the concordia curve at 2.06 Ga. These are mostly magmatic zircons. The lower intercept age of 0.86 Ga is quite high and therefore may indicate some real thermal event. However, as it is determined only by a few discordant data points the age is absolutely not an exact age. If well determined, the lower intercept age may have an important role in estimating the minimum age for the sedimentation. The maximum age of 2041 ± 15 Ma for the sedimentation is determined by calculating the mean age for the $^{207}\text{Pb}/^{206}\text{Pb}$ ages of concordant data.

In addition to ~2.04 Ga zircons, the SHRIMP age data also indicate Archaean provenances for the sed-

iment. The four Archaean zircons have $^{207}\text{Pb}/^{206}\text{Pb}$ ages of ~3.1 Ga, 2.7 Ga, and ~2.6 Ga ($n = 2$).

Mos-27 / 14410-03 Moeza dike, Rukore Suite

The mafic Moeza dike contains abundant pyroxene and plagioclase for Sm-Nd isochron dating with whole-rock powder. The pyroxene is fresh and brown, and the plagioclase looks somewhat heterogeneous in transparency and colour.

The results of the Sm-Nd analyses are shown in

Appendix 3 and Figures 4B and 4D. The REE-level is high and the pattern clearly LREE enriched. The Sm-Nd analyses on minerals and whole rock yield an age of 180 ± 43 Ma, thus suggesting an age close to Jurassic Karoo basalts. The initial epsilon value of -0.3 is clearly low compared to coeval MORB.

Mos-28 / 19313-04 granite, Bárue Complex

The granite sample from Bárue Complex contains abundant rather homogeneous-looking zircon. The grain size of the usually stubby or short prismatic zircon is largely fine to medium. It is totally transparent and colourless or turbid to translucent and pale brown. The larger grains are usually deeper in colour and less transparent compared to finer-grained zircons. In CL images (Fig. 2), the mounted zircon shows generally compositional zoning. Moreover, evident core and rim domains are quite common.

A total of 14 zircon domains were SHRIMP dated (App. 1). Five concordant analyses from zoned zircon crystals determine an age of 1119 ± 21 Ma (Fig. 3X). The older zircon domains have ages of ~1.83 Ga, 2.03–2.05 Ga, and 2.50 Ga. For the most part these were dated from cores enveloped by thin, CL-dark zircon rims around them (Fig. 2). The magmatic age for the granite is 1119 ± 21 Ma and the older data from inherited zircon indicate either a sedimentary precursor or the inherited grains originate from neighbouring quartzite.

Mos-29 / 19290-04 Inchapa granodiorite, Bárue Complex

The Inchapa granodiorite yielded only a small amount of brownish, turbid to translucent, coarse- to fine-grained zircon and abundant monazite. The larger zircon grains are typically shorter prismatic and the smaller grains show long prismatic morphology. Among these, a few transparent and merely colourless grains were detected. In CL images (Fig. 2), the short grains show oscillatory zoning. CL-dark zircon rims frequently envelope the zoned centre domains. A few completely CL-dark grains were also detected.

Using SHRIMP, 17 zircon domains were dated (App. 1). Three analyses were rejected due to high

common lead contents. On the concordia diagram (Fig. 3Y), the U-Pb data from zoned zircon largely plot at around 1100 Ma. The seven concordant analyses define an age of 1079 ± 7 Ma for the granodiorite. The U-Pb data from the CL-dark rims are highly discordant, indicating lead loss from high U zircon domains.

TIMS analysis of monazite gives slightly reversely discordant age data (App. 2 and Fig. 3Y). This may be due to the excess of ^{206}Pb from ^{230}Th of a high Th-mineral (Schärer 1984). However, the result clearly indicates the Pan-African metamorphic effect at ~520 Ma.

Mos-30 / 19140-04 Messeca granodiorite, Mavonde Complex

The zircon population in Messeca granodiorite looks rather homogeneous. Larger grains are completely turbid, grey-brown, and mostly euhedral, although sub- to anhedral forms also exist. The fine-grained zircon is mostly translucent, gray-brown, and short prismatic ($l:w = 2-3$).

Five zircon fractions were analysed using TIMS U-Pb (App. 2). The U-Pb data are highly discordant and plot in two clusters (Fig. 3Z), in spite of the different analysed grain-size fractions and air-abrasion times used. The practically two-point reference line intercepts the concordia curve at ~2.5 Ga and 0.56

Ga. It may be argued that the seemingly Archaean, high-U zircon was affected by later metamorphism. Therefore, the upper intercept age of the extremely

discordant data could only be taken as a rough age estimate.

Mos-31 / 6845-04 Monte Chissui tonalite, Bárue Complex

The main part of the zircon in Monte Chissui tonalite is extremely bright, has a tint of pink colour, and is either euhedral or more oval in shaped. The length to width ratio of the crystals and grains is mostly 2 to 4. In addition to the bright ones, only a few translucent and turbid grains were detected.

The TIMS dating of four zircon fractions (App. 2 and Fig. 3Å) yielded discordant U-Pb data despite the very bright appearance of zircon. The analyses A and D plot close each other and therefore the

discordia line is practically determined by three points only. The apparent concordia intercept ages are ~1.30 Ga and 0.60 Ga. The fairly high lower intercept age most probably indicates the effect of metamorphism(s) and the discordia upper intercept may therefore have been shifted to an older age. Consequently, it is suggested that this age is considered merely as a maximum age for the tonalite. The highest $^{207}\text{Pb}/^{206}\text{Pb}$ ages of ~1150 Ma would then be the minimum age for the rock.

MOS-32 / 13888-04 Mashonaland dolerite

The Mashonaland dolerite contains abundant pyroxene and plagioclase for Sm-Nd isochron dating with whole-rock powder. Pyroxene in the sample Mos-32 is fresh, fairly transparent and greenish-grey. Plagioclase ranges from clear colourless to slightly turbid white. The Sm-Nd data (App.3;

Figs. 4C and 4D) reveal a relatively high level of REE in plagioclase. The data on minerals and whole rock give an age of 1102 ± 52 Ma. The initial ϵ_{Nd} of -7.3 suggests major involvement of older LREE-enriched material in the genesis of this rock.

MOS-33 / 4158-03 metasandstone, Zámbe Supergroup

The Zámbe Supergroup metasandstone yielded only a small amount of zircon with varying grain size. The zircon morphology varies from long prismatic (l:w = 3–5) to oval-shaped, it is transparent to translucent, and reddish-brownish to almost colourless. Many grains are pigmented. The zircon in CL (Fig. 2) shows a range of complex internal structures. Cores are often rounded and/or corroded and surrounded by CL-dark zircon rims. There are also mixed types, from totally metamict CL-dark zircon to zoned euhedral grains. Almost all the grains are enveloped by CL-dark rims.

Eighteen zircon domains were dated using SHRIMP (Appendix 1 and Fig. 3Å). The U-Pb data are concordant and show varying ages and Th/U ratios. The analyses from CL-dark rim phases show high common lead contents but only two analyses showing the highest common lead were rejected from data processing, as zircon rim data would otherwise be totally missing. Zoned, mostly rounded cores yield Archaean (~2.7 Ga and 2.5 Ga) and Palaeoproterozoic (2.1 Ga and 1.9 Ga) sources for the sandstone. Four analyses from zoned cores and

euhedral zircon grains plot around 1.3–1.2 Ga. Furthermore, a zircon rim around a rounded zoned core plots on the younger end of this group.

Three analyses plot around 1.07 Ga. Two of these analyses (1.1 and 11.1) have very high common lead contents: one comes from a younger, low Th/U zircon phase of zircon 1 and the other probably hit on marginal zone between the zoned core and rim domains. The third analysis (7.1) was performed from a zoned, CL-dark zircon.

The ~0.83 Ga age was measured from a magnetically zoned zircon (2.1). A CL-dark, low Th/U zircon rim (Appendix 1: analysis 8.1) with a Palaeoproterozoic rounded core indicates metamorphism at ~0.4 Ga. However, as this analysis shows an extremely high common lead content its age result is inaccurate.

The maximum sedimentation age determined from these limited data is certainly ~1.2 Ga. The two single younger magmatic ages of ~1.07 Ga and 0.83 Ga may indicate an even younger maximum sedimentation age. Nevertheless, single data points are not considered to provide reliable evidence.

MOS-34/ 3157-03 felsic/intermediate metavolcanic rock, Fíngoè Supergroup

The metavolcanic rock from Fíngoè Supergroup yielded abundant zircon. The crystals are mostly prismatic (l:w = 3–4), transparent, and either quite colourless or weakly brownish. The colourless grains contain inclusions. In CL (Fig. 2), the zircon shows oscillatory zoning. A few grains have homogeneous zircon growth around corroded and zoned centre domains and several apparent cores were detected. However, due to the limited number of analyses the cores were ignored during dating.

Using SHRIMP, a total of 12 zircon domains were dated (App. 1). All the data are concordant or nearly concordant and the analyses are all from zoned, euhedral zircons. On the concordia diagram (Fig. 3Ö), the data scatter between 950 and 1400 Ma. The six oldest analyses plot in a cluster determining the concordia age of 1327 ± 16 Ma for the zircon crystallization. The younger U-Pb data most probably indicate lead loss connected to metamorphism at ~ 0.8 Ga, which is the lower intercept age of the discordia line defined by all the data (See Fig. 3Ö).

MOS-37 / 1714-05 dolerite, Post-Gairezi Group

Post-Gairezi dolerite yielded garnet and transparent plagioclase for Sm-Nd analyses. The quality of pyroxene was too poor for analysis. For analysis, the garnet separate was ground and leached stepwise in HCl according to the method of DeWolf et al. (1996). The Sm-Nd data (App. 3; Figs. 4C and 4D) reveal a relatively high REE level and the trend shows significant enrichment in LREE (cf. chondritic $^{147}\text{Sm}/^{144}\text{Nd} = 0.1966$). Three analyses do not

plot on the same isochron. The age estimate for the garnet-whole rock pair is 503 ± 8 Ma, whereas analyses on plagioclase and whole rock define a slope that gives an age of 973 ± 73 Ma and an initial epsilon value of -1.3 . Provided that the plagioclase has remained as a closed system since its magmatic crystallization, the age estimate for the dike is 973 ± 73 Ma. The ~ 500 Ma is consistent with the Pan-African metamorphism.

SUMMARY OF THE AGE RESULTS

General summary

This report presents isotopic ages for 35 rock samples from NW Mozambique sampled during geological mapping of the LOT 2 area. The age range of felsic to mafic magmatic rocks varies from 2.91 Ga to 0.18 Ga. Several samples have ~ 500 Ma low Th/U zircon phases evidencing Pan-African

metamorphism. An indication for the existence of a ~ 3.1 Ga protolith was found from two samples. The age data and comments on these are summarized in Table 2 and the age distribution of 32 supposedly magmatic rock samples is illustrated in Figure 5.

Archaean domain – Zimbabwe craton

The Archaean Zimbabwe craton extends marginally into Mozambique. The oldest dated rock with a zircon U-Pb age of 2907 ± 16 Ma is a tonalite located near the town of Manica, south of the Manica greenstone belt. No inherited zircon was found from this tonalite. Four apparently Archaean ages of 2.71–2.50 Ga were dated from TTG gneisses located in southern to northern parts of the Archaean domain. 3.1 Ga and 2.7 Ga inherited zircon grains were found from the 2.60 Ga orthogneiss. Furthermore, the 2.71 Ga gneiss has metamorphic zircon

domains indicating either metamorphism or a prolonged thermal history at ca. 2.54 Ga and finally Pan-African metamorphism at 520 ± 16 Ma.

A Palaeoproterozoic Sm-Nd mineral age of ~ 1.8 Ga was measured for a dolerite intruding the Archaean Manica greenstones. An initial ϵ_{Nd} of -2.2 suggests the involvement of older LREE-enriched material in the genesis of the rock. Garnet in ~ 1.0 Ga dolerite crosscutting the Palaeoproterozoic Gairezi mica schist within the Archaean domain reflects Pan-African metamorphism at ~ 500 Ma. Palaeopro-

Table 2. Summary of the age results, samples from NW Mozambique.

LAB ID	FIELD NUMBER	ROCK TYPE	SUITE/ GROUP	DATING METHOD	AGE RESULT	AGE TYPE, NUMBER OF FRACTIONS, ETC.	AGE	REMARKS
Mos-1	1055-02	Granite gneiss	Rio Capoeche granite	SHRIMP U-Pb	1201 ± 10 Ma	Concordia age; n=5/11; zoned zircon	Magmatic age	6/11 analyses show lead loss at 1050–1150 Ma.
Mos-2	2253-03	Monte Dombe granite	Cassacatiza Suite	TIMS U-Pb	1102 ± 24 Ma	Upper intercept age; n=4/4	~Magmatic age	Heterogeneous zircon population. MSWD=4.4. Rather discordant Pb/U data. Maximum age?
Mos-3	1024-02	Aplite granite	Guro Bimodal Suite	SHRIMP U-Pb	852 ± 15 Ma	Mean of ²⁰⁷ Pb/ ²⁰⁶ Pb ages; n=15/15	Magmatic age	Age data scatter between 760 and 920 Ma. Rims too thin for reasonable dating
Mos-4	1072-02	Aplite granite	Guro Bimodal Suite	TIMS U-Pb	867 ± 9 Ma	Upper intercept age; n=4/4	Magmatic age	MSWD=1.0
Mos-5	1097-03	Granite	Chacocoma granite	SHRIMP U-Pb	1046 ± 20 Ma	Mean of ²⁰⁷ Pb/ ²⁰⁶ Pb ages; n=14/15; mostly zoned zircon	Magmatic age	Age data scatter between 960 and 1080 Ma. A few thin, low Th and U metamorphic zircon rims are coeval with the magmatic zircon grains. One zircon shows an apparently higher ²⁰⁷ Pb/ ²⁰⁶ Pb age of ca. 1.2 Ga.
Mos-6	1170-03	Massanga gneiss	Mudzi Metamorphic Complex	TIMS U-Pb	~2.63 Ga	Upper intercept age; n=3/3	Magmatic age (metamorphic?)	Actually, almost a two point line. No material for further analyses. Just a rough age estimate.
Mos-7	1284-03	Gneiss	Mudzi Metamorphic Complex	SHRIMP U-Pb	~2.71 Ga ~2.54 Ga 520 ± 16 Ma	Upper intercept age; n=6/6; zoned Upper intercept age; n=4/6; metamorphic grains, rim Concordia age; n=2/2; Cl-bright, low Th/U rims	Magmatic age Metamorphic age? Metamorphic age	~2.70–2.72 Ga zircons. Scattering and overlapping magmatic and metamorphic age data.
Mos-8	2450-03	Granite	Macanga Granite	SHRIMP U-Pb	470 ± 14 Ma	Mean of ²⁰⁷ Pb/ ²⁰⁶ Pb ages; n=13/14; zoned	Magmatic age? Metamorphic age?	The facts that the Pb/U data scatter between 350 Ma and 650 Ma and zircons show Cl-dark, sometimes blurry internal structure may signify disturbing of the original magmatic age
Mos-9	2007-03	Granite	Cassacatiza Suite	TIMS U-Pb	1077 ± 2 Ma	Concordia age; n=2/4	Magmatic age	Fraction D only slightly discordant but not equal with A and B fractions. C is clearly discordant.
Mos-10	2001-02	Granite	Monte Sanja Suite	TIMS U-Pb	1050 ± 8 Ma	Upper intercept age; n=4/4	Magmatic age	MSWD=0.3. Low ²⁰⁶ Pb/ ²⁰⁴ Pb ratios.
Mos-11	2297-03	Desaranhama granite	Furancungo Suite	TIMS U-Pb	1041 ± 4 Ma	Upper intercept age; n=4/4	Magmatic age	MSWD=1.0
Mos-12	4493-03	Granite	Sinda Suite	SHRIMP U-Pb	502 ± 8 Ma	Concordia age; n=14/15; mostly zoned	Magmatic age	Replacing structurally homogeneous zircon phase and zoned core domains are coeval.
Mos-13	6035-03	Granite	Castanho Granite	TIMS U-Pb	1050 ± 2 Ma	Concordia age; n=3/4	Magmatic age	One fraction slightly discordant but plots on a same cluster.
Mos-14	2395-03	Gabbro	Atchiza Suite	Sm-Nd	864 ± 30 Ma	Mineral isochron age; n=3; pyroxene+plagioclase+whole-rock	Magmatic age	Initial εNd = -3.0
Mos-15	4241-03	Granite	Cassacatiza Suite	SHRIMP U-Pb	1117 ± 12 Ma	Concordia age; n=10/14; mostly zoned zircon domains	Magmatic age	

Table 2. Continued.

LAB ID	FIELD NUMBER	ROCK TYPE	SUITE/ GROUP	DATING METHOD	AGE RESULT	AGE TYPE, NUMBER OF FRACTIONS, ETC.	AGE	REMARKS
Mos-16	13016-03	Granite gneiss	Matunda Suite	SHRIMP U-Pb	784 ± 36 Ma 528 ± 4 Ma	Mean of ²⁰⁷ Pb/ ²⁰⁶ Pb ages; n=6; mostly zoned zircon domains Concordia age; n=3/6 (rim, tip, metamict grain - all low Th/U)	Ages for zoned zircon domains Metamorphic age	The older data scatter roughly between 700 and 850 Ma. The metamict grains most probably even older! One zircon has a ²⁰⁷ Pb/ ²⁰⁶ Pb age of ca. 0.9 Ga (older?).
Mos-17	13014-03	Gabbro	Chipera Massif	Sm-Nd	1047 ± 29 Ma	Mineral isochron age; n=3; pyroxene+plagioclase+whole-rock	Magmatic age	Initial eNd = +1.4
Mos-18	13032-03	Granite	Monte Capirimpica granite	TIMS U-Pb	1086 ± 7 Ma	Upper intercept age; n=4/4	Magmatic age	MSWD=0.03
Mos-19	2638-04	Aplite granite	Guro Bimodal Suite	SHRIMP U-Pb	867 ± 15 Ma	Mean of ²⁰⁷ Pb/ ²⁰⁶ Pb ages; n=11; all zoned	Magmatic age?	Contains also flat, rounded detrital-type metamict zircon grains showing now either 850-800 Ma or ~500 Ma ages.
Mos-20	2943-04	Garnet-sillimanite gneiss	Rushinga Group	SHRIMP U-Pb	512 ± 4 Ma 2.0 Ga	Concordia age; n=3/5; low Th/U Upper intercept age of youngest detrital zircon grains	Metamorphic age Maximum sedimentation age	Provenances: ca. 2.8 Ga, 2.5 Ga, and 2.0 Ga
Mos-21	1519-04	Fudeze orthogneiss	Mudzi Metamorphic Complex	SHRIMP U-Pb	518 ± 6 Ma ~2.59 Ga	Concordia age; n=3/5; low Th/U Upper intercept age; n=6; all zoned zircons	Metamorphic age Magmatic age	~500 Ma minimum age for sedimentation Inherited zircons ~2.7 and ~3.1 Ga
Mos-22	2893-04	Granite	Rukore Suite	TIMS U-Pb	195–180 Ma	Concordia age; n=2	Magmatic age	The two data points are not exactly equal
Mos-23	13625-04	Tonalite	Mavonde Complex	SHRIMP U-Pb	2907 ± 16 Ma	Upper intercept age; n=10/12; all zoned zircons	Magmatic age	No inherited ages for zircons.
Mos-24	15273-04	Syenite	Gorongosa Intrusive Suite	TIMS U-Pb	181 ± 2 Ma	Concordia age; n=2	Magmatic age	
Mos-25	25416-04	Dolerite	Archaean terrain	Sm-Nd	1783 ± 51 Ma	Mineral isochron age; n=2; pyroxene+whole-rock	Magmatic age	Initial eNd = -2.2. Plagioclase anomalous (high Sm/Nd).
Mos-26	1011-02	Garnet gneiss	Gairezi Group	SHRIMP U-Pb	2041 ± 15 Ma ~0.85 Ga	Mean of ²⁰⁷ Pb/ ²⁰⁶ Pb ages; n=6; mostly zoned Lower intercept age	Maximum sedimentation age Lead loss	Provenances: 3.1 Ga, 2.7-2.6 Ga, and 2.0 Ga Minimum sedimentation age?
Mos-27	14410-03	Dolerite	Moeza Dike, Rukore Suite	Sm-Nd	180 ± 43 Ma	Mineral isochron age; n=3; plagioclase+pyroxene+whole-rock	Magmatic age	Initial eNd = -0.2.
Mos-28	19313-04	Granite	Bárue Complex	SHRIMP U-Pb	1119 ± 21 Ma	Concordia age; n=5; all zoned	Magmatic age	Inherited zircons ~2.5 Ga, ~2.03 Ga, and ~1.83 Ga
Mos-29	19290-04	Inchapa granodiorite	Bárue Complex	SHRIMP TIMS U-Pb	1079 ± 7 Ma ~520 Ma	Concordia age; n=7; all zoned zircons Monazite; n=1	Magmatic age Metamorphic age	No inherited zircon. Slightly reversely discordant data point.

Table 2. Continued.

LAB ID	FIELD NUMBER	ROCK TYPE	SUITE/ GROUP	DATING METHOD	AGE RESULT	AGE TYPE, NUMBER OF FRACTIONS, ETC.	AGE	REMARKS
Mos-30	19140-04	Messec granodiorite	Mavonde Complex	TIMS U-Pb	~2.5 Ga (?)	Reference line intercept age; n=5 Lower intercept at ~0.5 Ga	Magmatic age with effect of ~0.5 Ga metamorphism?	Inaccurate age: highly discordant data, practically a two point line, affected by ~0.5 Ga metamorphism. SIMS dating is needed to solve the problem.
Mos-31	6845-04	Monte Chissui tonalite	Bárúé Complex	TIMS U-Pb	~1.3 Ga (~1.15 Ga)	Upper intercept age; n=4 (Highest ²⁰⁷ Pb/ ²⁰⁶ Pb age)	~Magmatic age	Discordant data with anomalously high lower intercept age. Therefore, the upper intercept age may be too high.
Mos-32	13888-04	Dolerite	Mashonaland dolerite (Post-Umkondo)	Sm-Nd	1102±52 Ma	Mineral isochron age; plagioclase+pyroxene+whole-rock	Magmatic age	Initial eNd = -7.3.
Mos-33	4158-03	Meta-sandstone	Zámbuè Supergroup	SHRIMP U-Pb	1.2 (-1.3) Ga	n=4 (zoned domains)	Maximum sedimentation age	Single analyses on zoned zircons at 1.07 Ga and 0.83 Ga? Detrital cores 2.7 Ga, 2.52 Ga, 2.1 Ga, and 1.3-1.2 Ga. Metamorphic zircon domains at ~1.2, ~1.07, and ~0.4 Ga
Mos-34	3157-03	Felsic/intermediate metavolcanic rock	Fingoè Supregroup	SHRIMP U-Pb	1327±16 Ma	Concordia age; n=6; zoned zircon	Magmatic age	Anomalously high lower intercept age of ~0.8 Ga may indicate lead loss at that time.
Mos-37	1714-05	Dolerite	Post-Gairezi dolerite	Sm-Nd	~1.0 Ga ~500 Ma	Mineral isochron age: plagioclase + whole-rock Mineral isochron age: garnet + whole-rock	Magmatic age Metamorphic age	

terozoic Gairezi Group garnet gneiss and Rushinga Group garnet-sillimanite gneiss indicate a maximum sedimentation age of ~ 2.0 Ga and additionally

Archaean provenances. These sedimentary rocks suffered metamorphism at ~ 0.85 Ga and at 518 ± 6 Ma.

Mesoproterozoic domains – Grenvillian orogeny

Báruè Complex

This Mesoproterozoic unit is tectonically emplaced to its present position in the central and southern part of the LOT2 area. A 1.12 Ga granite (Mos-28) intruding quartzite contains 2.50 Ga, 2.03 Ga, and 1.8 Ga inherited zircon grains. Further, a granodiorite east of Inchapa has a zircon age of 1079 ± 7 Ma and Pan-African metamorphism is indicated by ~ 520 Ma monazite. The age for the Monte Chisui tonalite is poorly constrained and estimated to be 1.15–1.30 Ga.

Area north of the E–W trending Zambezi rift covering the northern part of Tete Province

A felsic/intermediate volcanic rock from the Fíngo Supergroup yields a zircon U-Pb age of 1327 ± 16 Ma with an anomalous lower intercept age of ~ 0.8 Ga, possibly reflecting a thermal event at

that time. The few dated detrital zircon cores from Zámbe Supergroup metasandstone definitely indicate a 1.3–1.2 Ga maximum sedimentation age and additional 2.7 Ga, 2.52 Ga, and 2.1 Ga sedimentation provinces. The two single younger magmatic ages of ~ 1.07 Ga and 0.83 Ga may indicate an even younger maximum sedimentation age.

The following lists of granite ages show that all the dated granitic rocks are younger than the Fíngo Supergroup. A Rio Capoeche granite has a zircon U-Pb age of 1201 ± 10 Ma. Zircon from granite belonging to the Cassacatiza Suite has an age of 1117 ± 12 Ma. Six other granites show ages clustering between 1.10 Ga and 1.04 Ga. These are ~ 1.10 Ga Ma Monte Dombe granite, 1086 ± 7 Ma Monte Capirimpica granite, 1077 ± 2 Ma Cassacatiza granite, 1050 ± 2 Ma Castanho granite, 1050 ± 8 Ma granite from the Monte Sanja Suite, and 1041 ± 4 Ma Desaranhama granite from the Furancungo Suite. A gabbro sample from Chipera Massif equivalent to

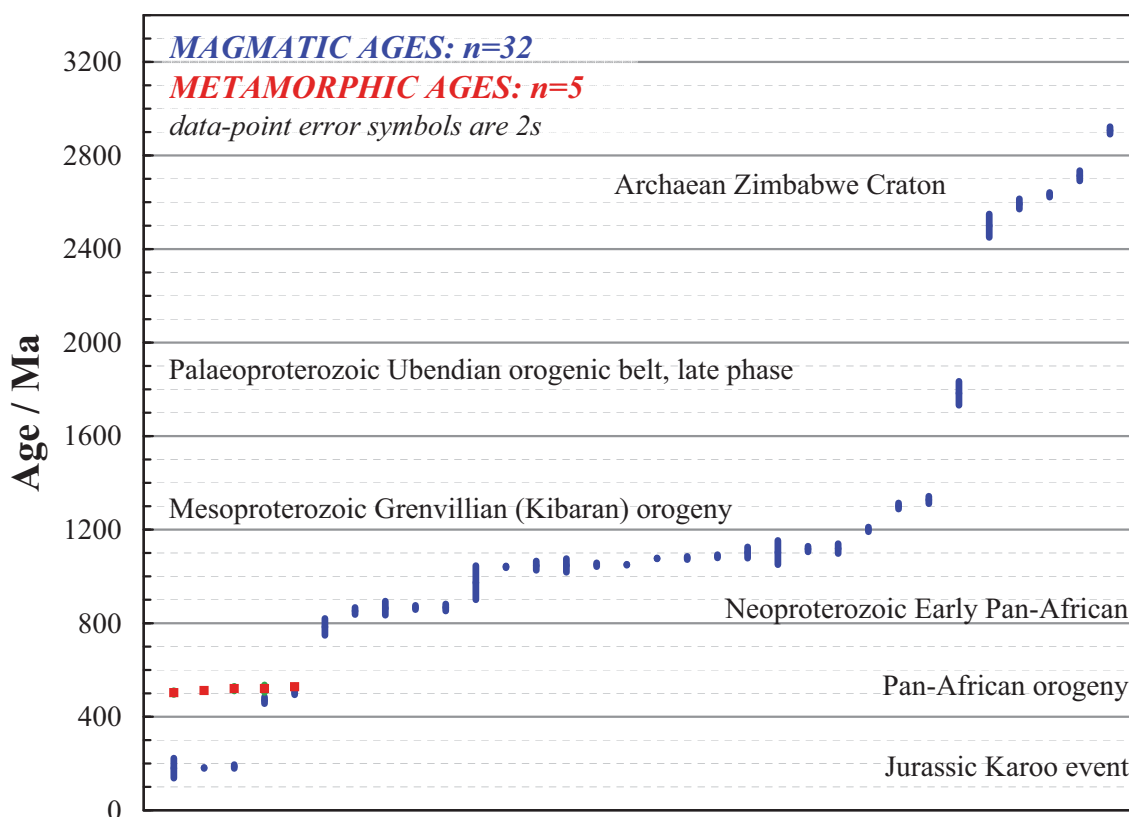


Fig. 5. Age distribution of magmatic ($n = 32$) and metamorphic ($n = 5$) ages, samples from NW Mozambique. Corresponding major tectonic events are also indicated.

the Tete Suite has a Sm-Nd mineral age of 1047 ± 29 Ma and an ϵ_{Nd} of +1.4.

Others

South of the Tete Suite mafic and ultramafic plutonic rocks, a Chacocoma granite yielded a Pb-Pb

mean age of 1046 ± 20 Ma. Further to the south of the LOT2 area, a sill-like Mashonaland dolerite intruding Umkondo metasediments yields an age of 1.1 Ga with an ϵ_{Nd} value of -7.3, indicating major involvement of LREE-enriched material in the genesis of this rock.

Neoproterozoic Suites – Early phases of Pan African orogeny

Guro Bimodal Suite

Three aplite granites in Guro Bimodal Igneous Suite, close to the northern part of the Archaean terrain, yield zircon ages of 867 ± 9 Ma, 852 ± 15 Ma, and 867 ± 15 Ma. Pan-African metamorphism at 512 ± 4 Ma is evidenced by low Th/U metamorphic zircon domains.

Atchiza and Matunda Suites

Atchiza Suite gabbro, NW of the lake Cahora Bassa in the northern part of the LOT 2 area, has an age of ~ 860 Ma and an ϵ_{Nd} of -3.0. The mean Pb-Pb age for the Matunda Suite gneiss located west of the Atchiza gabbro is ~ 0.8 Ga, but the oldest magmatic zircon is 0.85 Ga. 528 ± 4 Ma metamorphic zircon domains indicate the strong effect of Pan-African metamorphism.

Palaeozoic and Mesozoic Suites

Pan-African felsic intrusive rocks

Two Palaeozoic granites intruding the Mesoproterozoic northern part of the LOT2 area, N of Tete Province have ages of 470 ± 14 Ma and 502 ± 8 Ma.

Karoo event

Three samples show Jurassic Karoo igneous ages.

A syenite from the Gorongosa Intrusive Suite intruding the Mesoproterozoic Báruè Complex has an age of 181 ± 2 Ma. Granite of the Rukore Suite intruding the Palaeoproterozoic Rushinga Group supracrustals next to the Zimbabwe border yields an age of 195–180 Ma. A N–S trending Moeza dyke in Mesoproterozoic bedrock north of Tete has a Sm-Nd age of 180 ± 43 Ma with an initial ϵ_{Nd} of -0.3.

ACKNOWLEDGEMENTS

The personnel, namely A. Larionov, D. Matukov, S. Presniakov, and N. Rodionov of CIR/VSEGEI in St. Petersburg, are thanked for the SHRIMP analyses. H. Huhma was responsible for the Sm-Nd analyses, A. Pulkkinen helped with the mass spectrometry, and E. Kuosmanen produced the geological map. They are all thanked. M. Karhunen, M. Niemelä, and T. Hokkanen all from GTK are warmly

thanked for rock crushing and milling, heavy mineral separation, and laboratory work, respectively. Last but definitely not least, I am grateful to the project geologists who did the sampling and helped with the geological aspects, to R. Lahtinen for the manuscript review, to P. Hölttä and A. B. Westerhof for comments on manuscript, and to R. Siddall for revising the English.

REFERENCES

- Black, L. P., Kamo, S. L., Allen, C. M., Aleinikoff, J. N., Davis, D. W., Korsch, R. J., & Foudoulis, C. 2003. TEMORA 1: A quality zircon standard for Phanerozoic geochronology. *Chemical Geology* 200, 155–170.
- DePaolo, D. J. 1981. Neodymium isotopes in the Colorado Front Range and crust-mantle evolution in the Proterozoic. *Nature* 291, 684–687.
- De Wolf, C. P., Zeissler, C. J., Halliday, A. N., Mezger, K., & Essene, E. J. 1996. The role of inclusions in U-Pb and Sm-Nd garnet geochronology: Stepwise dissolution experiments and trace uranium mapping by fission track analysis. *Geochimica Cosmochimica Acta* 60, 121–134.
- GTK Consortium 2006a. Map Explanation; Volume 1: Sheets 2032–2632. Geology of Degree Sheets, Espungabera/Chibabava, Nova/Mambone, Massangena, Chidoco, Save/Bazaruto, Chicualacuala, Machaila, Chigubo, Mabote/Vilanculos, Rio Singuédzi/Massingir, Rio Changana, Funhalouro/Inhambane, Chilembene, Chókwè, Zavala/Inharrime, Maputo,

- Xai-Xai/Zavala and Bela-Vista, Mozambique. (DNG), Direcção Nacional de Geologia, Maputo.
- GTK Consortium 2006b.** Map Explanation; Volume 2: Sheets 1630–1934. Geology of Degree Sheets Mecumbura, Chiooco, Tete, Tambara, Guro, Chemba, Manica, Catandica, Gorongosa, Rotanda, Chimoio and Beira, Mozambique. Direcção Nacional de Geologia (DNG), Maputo.
- GTK Consortium 2006c.** Map Explanation; Volume 3: Sheets 1735–1739, 1835–1836 and 1935. Geology of Degree Sheets Mutarara, Quelimane, Namacurra/Maganja, Pebane, Marromeu/Inhaminga, Chinde and Savane, Mozambique. Direcção Nacional de Geologia (DNG), Maputo.
- GTK Consortium 2006d.** Map Explanation; Volume 4: Sheets 1430–1432 and 1530–1534. Geology of Degree Sheets Inhamambo, Maluwera, Chifunde, Zumbo, Fingoè-Mágoè, Songo, Cazula and Zóbuè, Mozambique. Direcção Nacional de Geologia (DNG), Maputo.
- Hunting Geology and Geophysics Limited 1984.** Mineral Inventory Project. Final Report. Unpublished Report, Direcção Nacional de Geologia, Maputo, Mozambique, 329 p.
- Jacobsen, S. B. & Wasserburg, G. J. 1980.** Sm-Nd isotopic evolution of chondrites. *Earth Planetary Science Letters* 50, 139–155.
- Koistinen, T. J., Lehtonen, M. I., Cune, G., Ferrara, M., Manninen, T., Marques, J., Mäkitie, H., & Vuori, S. 2006.** Geological mapping east and north of the Archaean Zimbabwe craton, NW Mozambique. 21st Colloquium of African Geology. Maputo, Mozambique, 03.–05.07.2006. Extended abstract. Abstract Book, 92–93.
- Koistinen, T., Lehtonen, M., Fernando, S. & Matola, R. 2008.** Contribution to the structure at the eastern margin of the Archaean Zimbabwe craton, Mozambique. *Geological Survey of Finland, Special Paper* 48, 121–144.
- Krogh, T. E. 1973.** A low-contamination method for hydrothermal decomposition of U and Pb for isotopic age determinations. *Geochimica and Cosmochimica Acta* 37, 485–494.
- Krogh, T. E. 1982.** Improved accuracy of U-Pb zircon ages by the creation of more concordant systems using an air abrasion technique. *Geochimica and Cosmochimica Acta* 46, 637–649.
- Ludwig, K. R. 1993.** PbDat 1.24 for MS-dos: A computer program for IBM-PC Compatibles for processing raw Pb-U-Th isotope data. Version 1.07.
- Ludwig, K. R. 2000.** SQUID 1.00, A User's Manual; Berkeley Geochronology Center Special Publication. No.2, 2455 Ridge Road, Berkeley, CA 94709, USA.
- Ludwig, K. R. 2003.** Isoplot/Ex 3.00. A geochronological toolkit for Microsoft Excel. Berkeley Geochronology Center. Special publication No. 4.
- Mäkitie, H., Lehtonen, M. I., Manninen, T., Koistinen, T., Eerola, T., & Mänttari, I. 2006.** New data of granitoids from northern Tete province, Mozambique. 21st Colloquium of African Geology. Maputo, Mozambique, 03.–05.07.2006. Extended abstract. Abstract Book, 109–110.
- Mäkitie, H., Lehtonen, M. I., Manninen, T., Marques, J. M., Cune, G. & Mavie, H. 2008.** Petrography and geochemistry of granitoid rocks in the northern part of Tete Province, Mozambique. *Geological Survey of Finland, Special Paper* 48, 167–189.
- Mänttari, I., Koistinen, T., Lehtonen, M. I., Manninen, T., Mäkitie, H., Huhma, H., & Kuosmanen, E. 2006.** U-Pb and Sm-Nd ages for 27 magmatic rocks, NW Mozambique. 21st Colloquium of African Geology. Maputo, Mozambique, 03.–05.07.2006. Extended abstract. Abstract Book, 203–205.
- Richard, P., Shimizu, N., & Allègre, C. J. 1976.** $^{143}\text{Nd}/^{146}\text{Nd}$, a natural tracer: an application to oceanic basalts. *Earth and Planetary Science Letters* 31, 269–278.
- Schärer, U. 1984.** The effect of initial ^{230}Th disequilibrium on young U-Pb ages: the Makalu case, Himalaya. *Earth and Planetary Science Letters* 67, 191–204.
- Stacey, J. S. & Kramers, J. D. 1975.** Approximation of terrestrial lead isotope evolution by a two-stage model. *Earth and Planetary Science Letters* 26, 207–221.
- Wasserburg, G. J., Jacobsen, S. B., DePaolo, D. J., McCulloch, M. T., & Wen, T. 1981.** Precise determination of Sm/Nd ratios, Sm and Nd isotopic abundances in standard solutions. *Geochimica and Cosmochimica Acta* 45, 2311–2323.
- Westerhof, A.B. 2006.** Tectonic framework of central and southern Mozambique in relation to Africa's major building blocks. 21st Colloquium of African Geology. Maputo, Mozambique, 03.–05.07.2006. Extended abstract. Abstract Book, 174–177.
- Westerhof, A. B., Lehtonen, M. I., Mäkitie, H., Manninen, T., Pekkala, Y., Gustafsson, B. & Tahon, A. 2008.** The Tete-Chipata Belt: a new multiple terrane element from western Mozambique and southern Zambia. *Geological Survey of Finland, Special Paper* 48, 145–166.
- Wiedenbeck, M., Allé, P., Corfu, F., Griffin, W. L., Meier, M., Oberli, F., von Quadt, A., Roddick, J. C., & Spiegel, W. 1995.** Three natural zircon standards for U-Th-Pb, Lu-Hf, trace element and REE analysis. *Geostandards Newsletter* 19, 1–23.
- Williams, I. S. 1998.** U-Th-Pb Geochronology by Ion Microprobe. In: McKibben, M.A., Shanks III, W.C. & Ridley, W.I. (eds), *Applications of microanalytical techniques to understanding mineralizing processes*, *Reviews in Economic Geology* 7, 1–35.

Appendix 1. Zircon SHRIMP U-Pb isotopic data, samples from NW Mozambique.

Spot	Dated zircon domain	% 206Pb _c	ppm U	ppm Th	232Th/ 238U	ppm 206Pb*	(1) 206Pb/ 238U Age	(1) 207Pb/ 238U Age	% Dis- cor- dancy	(1) 207Pb* /206Pb*	±%	(1) 207Pb* /238U	±%	(1) 206Pb* /238U	±%	err corr
Mos-1 / 1055-02 Rio Capoeche granite gneiss																
<i>MOS-1.1.1</i>	<i>quite homogeneous, CL-bright core domain</i>	3.80	29	13	0.48	5	1087 ±24	1355 ±340	25	0.0870	18.0	2.200	18.0	0.1836	2.4	0.13
MOS-1.1.2	zoned, CL-dark tip domain	0.17	754	52	0.07	123	1121 ±4	1117 ±19	0	0.0769	0.9	2.012	1.0	0.1898	0.4	0.38
MOS-1.2.1	zoned, CL-medium	0.92	49	27	0.56	9	1198 ±17	1251 ±130	4	0.0822	6.8	2.320	6.9	0.2042	1.5	0.22
MOS-1.3.1	zoned, CL-medium	0.49	153	92	0.62	27	1210 ±9	1179 ±52	-3	0.0793	2.6	2.258	2.8	0.2065	0.8	0.29
<i>MOS-1.4.1</i>	<i>zoned, CL-bright centre domain</i>	7.23	14	6	0.48	3	1216 ±37	825 ±640	-32	0.0670	31.0	1.910	31.0	0.2077	3.3	0.11
<i>MOS-1.5.1</i>	<i>zoned, CL-bright centre domain</i>	5.27	21	9	0.47	4	1192 ±26	1261 ±380	6	0.0830	19.0	2.310	19.0	0.2032	2.4	0.12
MOS-1.6.1	zoned, CL-pale centre domain	1.70	51	21	0.43	9	1191 ±14	1171 ±150	-2	0.0789	7.4	2.210	7.5	0.2030	1.3	0.18
<i>MOS-1.7.1</i>	<i>zoned, CL-pale centre domain</i>	3.23	15	7	0.47	3	1359 ±26	1573 ±220	16	0.0970	12.0	3.150	12.0	0.2347	2.2	0.18
<i>MOS-1.8.1</i>	<i>zoned, CL-pale centre domain</i>	3.20	34	22	0.65	6	1209 ±17	1032 ±210	-15	0.0736	11.0	2.090	11.0	0.2062	1.6	0.15
<i>MOS-1.9.1</i>	<i>zoned, CL-bright centre domain</i>	4.29	19	10	0.56	3	1174 ±27	1326 ±390	13	0.0850	20.0	2.350	20.0	0.1997	2.5	0.12
MOS-1.10.1	zoned, CL-dark, tip domain	0.55	316	96	0.31	56	1207 ±6	1136 ±38	-6	0.0776	1.9	2.260	2.0	0.2060	0.6	0.28
MOS-1.11.1	zoned, CL-dark, tip domain	0.81	169	17	0.10	27	1094 ±7	1028 ±58	-6	0.0735	2.9	1.874	3.0	0.1849	0.7	0.23
MOS-1.12.1	zoned CL-dark	0.67	182	79	0.45	32	1187 ±9	1190 ±53	0	0.0797	2.7	2.222	2.8	0.2022	0.8	0.28
<i>MOS-1.13.1</i>	<i>zoned, CL-pale centre domain</i>	5.54	12	5	0.41	2	1125 ±44	250 ±1200	-77	0.0510	51.0	1.350	52.0	0.1908	4.2	0.08
MOS-1.14.1	zoned CL-dark	0.34	353	40	0.12	54	1056 ±6	1056 ±35	0	0.0745	1.7	1.829	1.9	0.1779	0.7	0.35
MOS-1.15.1	zoned CL-dark	0.89	237	75	0.33	37	1061 ±7	1003 ±54	-6	0.0726	2.7	1.791	2.8	0.1790	0.7	0.25
MOS-1.16.1	zoned CL-dark	0.58	249	41	0.17	41	1125 ±8	1095 ±46	-3	0.0760	2.3	1.997	2.4	0.1906	0.8	0.32
MOS-1.17.1	zoned CL-dark	0.18	505	113	0.23	82	1111 ±5	1089 ±23	-2	0.0758	1.1	1.966	1.2	0.1882	0.5	0.38
MOS-3 / 1024-02 aplite granite, Guro Suite																
MOS3.1.1	zoned	--	369	207	0.58	48	904 ±6	863 ±19	-5	0.0678	0.9	1.408	1.1	0.1506	0.7	0.60
MOS3.2.1	zoned	--	763	254	0.34	97	891 ±16	882 ±36	-1	0.0684	1.7	1.399	2.6	0.1482	1.9	0.74
MOS3.3.1	zoned	--	199	106	0.55	24	861 ±7	850 ±26	-1	0.0674	1.3	1.327	1.5	0.1428	0.8	0.54
MOS3.4.1	zoned	0.03	586	208	0.37	72	865 ±6	846 ±23	-2	0.0673	1.1	1.331	1.3	0.1436	0.7	0.55
MOS3.5.1	zoned	0.03	427	245	0.59	52	856 ±6	848 ±21	-1	0.0673	10.0	1.318	1.2	0.14193	0.7	0.57
MOS3.6.1	zoned	0.17	1036	485	0.48	113	767 ±6	902 ±66	15	0.0691	3.2	1.203	3.3	0.1263	0.8	0.24
MOS3.7.1	zoned (dark CL)	0.16	466	233	0.52	54	813 ±19	824 ±56	1	0.0665	2.7	1.233	3.7	0.1344	2.5	0.68
MOS3.8.1	zoned (dark CL)	0.03	1181	343	0.30	133	792 ±5	819 ±67	3	0.0664	3.2	1.197	3.3	0.1308	0.7	0.20
MOS3.9.1	zoned	--	242	113	0.48	27	794 ±8	902 ±28	12	0.0691	1.3	1.248	1.7	0.1310	1.0	0.61
MOS3.10.1	zoned	0.04	280	149	0.55	33	837 ±7	813 ±39	-3	0.0662	1.9	1.266	2.1	0.1386	0.8	0.41
MOS3.11.1	zoned	0.06	573	269	0.48	69	840 ±11	844 ±19	0	0.0672	0.9	1.290	1.7	0.1392	1.4	0.84
MOS3.12.1	zoned	0.09	311	199	0.66	38	845 ±6	820 ±35	-3	0.0664	1.7	1.283	1.8	0.1401	0.8	0.41
MOS3.13.1	zoned	0.10	261	131	0.52	32	869 ±7	849 ±32	-2	0.0674	1.5	1.340	1.8	0.1443	0.9	0.50
MOS3.14.1	zoned	0.03	323	200	0.64	38	826 ±7	859 ±42	4	0.0677	2.0	1.276	2.2	0.1367	0.9	0.40
MOS3.15.1	zoned	--	187	72	0.40	23	872 ±6	841 ±31	-4	0.0671	1.5	1.340	1.7	0.1448	0.8	0.45

Appendix 1. Continued.

Spot	Dated zircon domain	% ²⁰⁶ Pb _c	ppm U	ppm Th	²³² Th/ ²³⁸ U	ppm ²⁰⁶ Pb*	(1) ²⁰⁶ Pb/ ²³⁸ U Age	(1) ²⁰⁷ Pb/ ²⁰⁶ Pb Age	% Dis- cor- dancy	(1) ²⁰⁷ Pb* / ²⁰⁶ Pb*	±% ±%	(1) ²⁰⁷ Pb* / ²³⁵ U	±% ±%	(1) ²⁰⁶ Pb* / ²³⁸ U	±% ±%	err corr
MOS-5 / 1097-03 Chacocoma granite																
MOS5.1.1	rim (pale CL)	0.09	105	23	0.23	15	973 ±16	1092 ±38	11	0.0759	1.9	1.704	2.6	0.1629	1.8	0.69
MOS5.1.2	core (zoned,dark CL)	0.04	457	164	0.37	64	979 ±18	1002 ±16	2	0.0726	0.8	1.641	2.2	0.1640	2.0	0.93
MOS5.2.1	core (dark CL)	0.07	451	86	0.20	66	1011 ±56	1041 ±22	3	0.0740	1.1	1.73	6.1	0.1700	6.0	0.98
MOS5.2.2	rim (medium CL enveloped by thin CL-pale rim)	0.11	127	20	0.16	19	1052 ±10	1058 ±40	1	0.0746	2.0	1.824	2.2	0.1773	1.0	0.45
MOS5.3.1	zoned(unaltered)	--	494	225	0.47	75	1045 ±7	1097 ±17	5	0.0761	0.9	1.845	1.1	0.1759	0.7	0.61
MOS5.4.1	zoned(unaltered)	0.02	600	201	0.35	91	1052 ±7	1055 ±13	0	0.0745	0.6	1.821	1.0	0.1773	0.7	0.75
MOS5.5.1	zoned(unaltered)	0.03	965	283	0.30	135	969 ±23	1104 ±30	12	0.0763	1.5	1.707	2.9	0.1622	2.5	0.86
MOS5.6.1	rim (CL-pale)	0.85	96	24	0.26	13	963 ±9	1071 ±58	10	0.0751	2.9	1.668	3.1	0.1611	1.0	0.33
MOS5.6.2	core(disturbed zoning,dark CL)	0.17	1212	533	0.45	171	979 ±8	955 ±75	-3	0.0709	3.7	1.604	3.8	0.1640	0.8	0.22
MOS5.7.1	zoned (dark CL)	--	995	351	0.36	148	1031 ±6	983 ±36	-5	0.0719	1.8	1.720	1.9	0.1735	0.7	0.36
MOS5.8.1	zoned (dark CL+thin rim)	0.01	547	175	0.33	83	1048 ±12	1193 ±59	12	0.0798	3.0	1.943	3.2	0.1765	1.3	0.40
MOS5.9.1	zoned (dark CL+thin rim)	0.00	417	126	0.31	62	1027 ±8	1064 ±68	4	0.0748	3.4	1.781	3.5	0.1726	0.9	0.25
MOS5.10.1	zoned(dark CL)	0.06	446	164	0.38	62	971 ±13	1013 ±16	4	0.0730	0.8	1.635	1.7	0.1626	1.4	0.87
MOS5.11.1	zoned(dark CL)	0.27	174	54	0.32	27	1072 ±8	1048 ±32	-2	0.0743	1.6	1.852	1.8	0.1809	0.8	0.46
MOS5.12.1	zoned(dark CL)	0.05	492	154	0.32	78	1096 ±60	1053 ±14	-4	0.0744	0.7	1.900	6.0	0.1850	6.0	0.99
MOS-7 / 1284-03 gneiss, Mudzi Metamorphic Complex																
MOS7.1.1	zoned(osc)	0.01	284	122	0.44	116	2497 ±19	2670 ±7	6	0.1819	0.4	11.86	1.0	0.4730	0.9	0.91
MOS7.2.1	zoned(striped)	0.06	318	204	0.66	110	2184 ±35	2585 ±22	16	0.1728	1.3	9.610	2.3	0.4033	1.9	0.82
MOS7.3.1	rim (homog,CL-pale+dark core)	0.04	284	97	0.35	84	1897 ±110	2469 ±25	23	0.1612	1.5	7.610	6.6	0.3420	6.4	0.97
MOS7.4.1	zoned(osc)	0.01	518	63	0.13	127	1621 ±48	2373 ±21	32	0.1524	1.3	6.010	3.6	0.2858	3.3	0.94
MOS7.5.1	rim (light CL+dark, altered core)	0.92	27	0	0.00	2	516 ±12	680 ±360	24	0.062	17.0	0.710	17.0	0.0834	2.4	0.14
MOS7.6.1	zoned(striped)	--	476	341	0.74	195	2513 ±16	2728 ±25	8	0.1884	1.5	12.380	1.7	0.4767	0.8	0.45
MOS7.7.1	homog CL-dark inner domain/rounded (+thin rim)	0.01	361	102	0.29	141	2411 ±37	2523 ±70	4	0.1665	4.2	10.410	4.5	0.4536	1.8	0.40
MOS7.8.1	homog CL-dark inner domain/rounded (+thin rim)	--	361	98	0.28	132	2284 ±28	2620 ±92	13	0.1765	5.5	10.350	5.7	0.4252	1.5	0.26
MOS7.9.1	zoned(striped)	0.05	265	44	0.17	74	1814 ±90	2461 ±59	26	0.1605	3.5	7.190	6.7	0.3250	5.7	0.85
MOS7.10.1	zoned(disturbed,dark CL)	0.02	554	230	0.43	206	2321 ±110	2495 ±7	7	0.1638	0.4	9.790	5.5	0.4330	5.5	1.00
MOS7.11.1	rim(CL-pale/metam)	1.57	50	1	0.01	4	522 ±9	475 ±270	-10	0.0566	12.0	0.658	12.0	0.0843	1.7	0.14
MOS7.12.1	zoned(osc,CL-dark)	0.10	614	98	0.17	85	966 ±15	1860 ±17	48	0.1137	0.9	2.535	1.9	0.1617	1.6	0.87
MOS7.13.1	homog,CL dark/metam?/rounded	0.00	343	114	0.34	152	2681 ±130	2553 ±7	-5	0.1696	0.4	12.050	5.9	0.5160	5.9	1.00
MOS7.14.1	zoned(striped)	0.08	136	47	0.36	51	2339 ±46	2610 ±37	10	0.1754	2.2	10.580	3.2	0.4370	2.3	0.73
MOS7.15.1	tip/rim?,homog(dark CL)	0.02	346	114	0.34	131	2356 ±19	2555 ±7	8	0.1697	0.4	10.320	1.1	0.4411	1.0	0.92
Mos-8 / 2450-03 Macanga granite																
MOS-8.1.1	zoned(dark CL)	0.07	2098	931	0.46	157	540 ±5	484 ±14	-11	0.0568	0.6	0.684	1.1	0.0873	0.88	0.81
MOS-8.2.1	zoned(dark CL)	0.22	690	161	0.24	47	488 ±4	525 ±31	7	0.0579	1.4	0.628	1.6	0.0787	0.8	0.50
MOS-8.3.1	zoned(dark CL)	1.25	4456	2196	0.51	283	454 ±40	369 ±75	-23	0.0540	3.3	0.542	9.7	0.0729	9.1	0.94
MOS-8.4.1	zoned(dark CL)	0.14	8518	8975	1.09	824	687 ±16	480 ±14	-43	0.0567	0.6	0.879	2.6	0.1125	2.5	0.97
<i>MOS-8.5.1</i>	<i>zoned</i>	<i>9.67</i>	<i>545</i>	<i>297</i>	<i>0.56</i>	<i>38</i>	<i>455</i>	<i>586</i>	<i>22</i>	<i>0.0600</i>	<i>18.0</i>	<i>0.600</i>	<i>18.0</i>	<i>0.0731</i>	<i>3.0</i>	<i>0.17</i>
MOS-8.6.1	zoned(dark CL)	0.17	1677	623	0.38	120	516 ±34	488 ±17	-6	0.0569	0.8	0.654	7.0	0.0833	6.9	0.99

Appendix 1. Continued.

Spot	Dated zircon domain	% 206Pb _e	ppm U	ppm Th	232Th /238U	ppm 206Pb*	(1) 206Pb/238U Age	(1) 207Pb/206Pb Age	% Dis- cor- dancy	(1) 207Pb* /206Pb*	±%	(1) 207Pb* /235U	±%	(1) 206Pb* /238U	±%	err corr
MOS-8.7.1	zoned(dark CL)	2.23	1472	2107	1.48	126	601 ±27	531 ±77	-13	0.0580	3.5	0.782	5.9	0.0977	4.7	0.80
MOS-8.8.1	zoned(dark CL)	0.98	2480	2741	1.14	169	488 ±35	381 ±32	-28	0.0542	1.4	0.588	7.7	0.0786	7.5	0.98
MOS-8.9.1	zoned(dark CL)	0.24	7157	5892	0.85	479	482 ±4	429 ±42	-12	0.0554	1.9	0.594	2.1	0.0777	0.9	0.41
MOS-8.10.1	zoned(dark CL)	0.36	1800	2058	1.18	119	477 ±3	464 ±23	-3	0.0563	1.0	0.596	1.2	0.0768	0.7	0.56
MOS-8.11.1	zoned(dark CL)	1.51	2290	3419	1.54	113	356 ±20	432 ±54	18	0.0555	2.4	0.434	6.2	0.0567	5.7	0.92
MOS-8.12.1	zoned(dark CL)	1.27	3798	1714	0.47	371	685 ±39	388 ±47	-76	0.0544	2.1	0.842	6.4	0.1122	6.0	0.94
MOS-8.13.1	zoned(dark CL)	0.68	3937	1960	0.51	303	549 ±29	453 ±19	-21	0.0560	0.9	0.686	5.7	0.0889	5.6	0.99
MOS-8.14.1	zoned(dark CL)	0.18	3999	2882	0.74	290	521 ±4	452 ±13	-15	0.0560	0.6	0.650	1.0	0.0841	0.8	0.82
MOS-8.15.1	zoned(dark CL)	0.86	5167	3666	0.73	306	426 ±3	473 ±21	10	0.0565	0.9	0.532	1.1	0.0683	0.7	0.58
MOS-12 / 4493-03 granite, Sinda Suite																
MOS-12.1.1	zoned(dark CL)	0.05	694	597	0.89	48	498 ±11	403 ±54	-24	0.0548	2.4	0.607	3.4	0.0804	2.4	0.70
MOS-12.2.1	zoned(dark CL)	0.34	346	367	1.10	24	498 ±8	425 ±50	-17	0.0553	2.3	0.612	2.8	0.0803	1.7	0.60
MOS-12.2.2	core/inner domain?(homog)	0.26	376	749	2.06	26	505 ±8	425 ±47	-19	0.0553	2.1	0.622	2.7	0.0815	1.7	0.64
MOS-12.3.1	rim/homog domain cutting the zoning	0.27	270	113	0.43	19	509 ±9	463 ±58	-10	0.0563	2.6	0.638	3.2	0.0822	1.7	0.55
MOS-12.3.2	zoned	0.04	486	416	0.88	33	494 ±8	542 ±30	9	0.0583	1.4	0.640	2.2	0.0796	1.7	0.78
MOS-12.4.1	zoned(+small core)	0.22	414	321	0.80	29	502 ±8	517 ±40	3	0.0577	1.8	0.645	2.5	0.0811	1.7	0.69
MOS-12.5.1	rim/homog domain cutting the zoning	0.09	232	147	0.65	16	494 ±9	589 ±44	16	0.0596	2.0	0.654	2.8	0.0796	1.8	0.67
MOS-12.5.2	zoned	1.23	117	181	1.60	8	510 ±10	295 ±160	-73	0.0522	7.0	0.593	7.3	0.0824	2.1	0.28
MOS-12.6.1	zoned	0.07	159	201	1.31	11	515 ±10	623 ±56	17	0.0606	2.6	0.694	3.2	0.0831	1.9	0.60
MOS-12.7.1	zoned	0.41	329	293	0.92	23	504 ±9	544 ±62	7	0.0584	2.8	0.654	3.3	0.0812	1.8	0.53
MOS-12.8.1	zoned	0.26	344	181	0.55	24	492 ±9	545 ±44	10	0.0584	2.0	0.639	2.7	0.0794	1.8	0.67
MOS-12.9.1	new tip?, weakly zoned, CL-pale	0.04	296	177	0.62	20	483 ±17	604 ±53	20	0.0600	2.4	0.644	4.4	0.0778	3.7	0.83
MOS-12.9.2	zoned inner domain	0.17	345	567	1.70	24	506 ±8	517 ±44	2	0.0577	2.0	0.649	2.7	0.0817	1.7	0.65
MOS-12.10.1	rim, homog	0.59	182	122	0.69	13	491 ±9	513 ±99	4	0.0576	4.5	0.627	4.9	0.0791	1.8	0.38
MOS-12.10.2	zoned, inner domain	0.68	352	397	1.16	25	500 ±8	331 ±69	-51	0.0530	3.1	0.590	3.5	0.0807	1.7	0.49
MOS-15 / 4241-03 granite, Cassacatiza Suite																
MOS-15.1.1	zoned	0.11	638	779	1.26	98	1060 ±16	1126 ±14	6	0.0772	0.7	1.903	1.8	0.1788	1.7	0.92
MOS-15.2.1	zoned	0.11	226	116	0.53	36	1102 ±18	1127 ±24	2	0.0772	1.2	1.985	2.2	0.1864	1.8	0.83
MOS-15.3.1	zoned(dark CL)	0.02	4951	638	0.13	867	1196 ±19	1117 ±6	-7	0.0768	0.3	2.159	1.7	0.2038	1.7	0.98
MOS-15.3.2	rim/tip, CL-pale	0.00	559	45	0.08	89	1091 ±17	1148 ±32	5	0.0780	1.6	1.984	2.4	0.1845	1.7	0.73
MOS-15.4.1	zoned	0.07	590	329	0.58	96	1120 ±17	1130 ±15	1	0.0774	0.7	2.024	1.8	0.1898	1.7	0.91
MOS-15.5.1	zoned	0.25	449	433	1.00	78	1186 ±38	1099 ±19	-8	0.0762	1.0	2.121	3.6	0.2019	3.5	0.96
MOS-15.6.1	zoned	0.42	1371	494	0.37	188	952 ±44	1080 ±15	12	0.0754	0.7	1.654	5.0	0.1591	5.0	0.99
MOS-15.6.2	zoned(CL-pale)	0.10	1254	495	0.41	209	1143 ±120	1162 ±28	2	0.0786	1.4	2.100	11.0	0.1940	11.0	0.99
MOS-15.7.1	zoned	0.15	589	557	0.98	102	1187 ±110	1066 ±43	-11	0.0749	2.1	2.090	10.0	0.2020	9.7	0.98
MOS-15.8.1	zoned	0.34	196	81	0.43	32	1128 ±18	1097 ±34	-3	0.0761	1.7	2.005	2.5	0.1912	1.8	0.71
MOS-15.9.1	core/inner domain? (CL-pale, homog)	0.26	200	236	1.22	33	1120 ±18	1060 ±37	-6	0.0747	1.8	1.954	2.6	0.1898	1.8	0.70
MOS-15.9.2	rim, dark CL	0.11	1237	137	0.11	198	1100 ±21	1125 ±14	2	0.0772	0.7	1.980	2.2	0.1861	2.1	0.95
MOS-15.10.1	zoned	0.51	1418	270	0.20	208	1010 ±41	1022 ±43	1	0.0733	2.1	1.713	4.8	0.1695	4.4	0.90
MOS-15.11.1	zoned	0.16	1117	378	0.35	202	1231 ±130	1140 ±29	-8	0.0777	1.5	2.250	12.0	0.2100	12.0	0.99

Appendix 1. Continued.

Spot	Dated zircon domain	% ²⁰⁶ Pb _c	ppm U	ppm Th	²³² Th / ²³⁸ U	ppm ²⁰⁶ Pb*	(1) ²⁰⁶ Pb/ ²³⁸ U Age	(1) ²⁰⁷ Pb/ ²⁰⁶ Pb Age	% Dis- cor- dancy	(1) ²⁰⁷ Pb* / ²⁰⁶ Pb*	± %	(1) ²⁰⁷ Pb* / ²³⁵ U	± %	(1) ²⁰⁶ Pb* / ²³⁸ U	± %	err corr
MOS-16 / 13016-03 granite gneiss, Matunda Suite																
MOS-16.1.1	rim, dark CL, homog	1.70	1679	23	0.01	108	457 ±41	594 ±84	23	0.0597	3.9	0.605	10.0	0.0734	9.3	0.92
MOS-16.1.2	core, pale CL, zoned	0.12	99	86	0.90	11	806 ±8	838 ±59	4	0.0670	2.8	1.230	3.0	0.1331	1.0	0.34
MOS-16.2.1	homog, medium CL/metam? /rounded(+thin dark CL rim)	--	336	196	0.60	37	784 ±6	822 ±29	5	0.0665	1.4	1.186	1.6	0.1294	0.8	0.49
MOS-16.3.1	rim, dark CL(+metamict core?)	0.78	574	7	0.01	41	512 ±7	528 ±46	3	0.0580	2.1	0.660	2.5	0.0826	1.3	0.54
MOS-16.4.1	metamict main domain (+thin CL-pale rim)	0.43	998	29	0.03	80	570 ±15	591 ±27	4	0.0597	1.2	0.760	3.0	0.0924	2.8	0.91
MOS-16.4.2	zoned, small grain inside a metamict grain	0.35	364	295	0.84	39	749 ±5	749 ±34	0	0.0642	1.6	1.090	1.8	0.1231	0.7	0.42
MOS-16.5.1	homog, dark CL, rounded (+thin CL-pale rim)	0.02	1770	12	0.01	130	531 ±3	482 ±43	-10	0.0568	2.0	0.671	2.1	0.0858	0.7	0.32
MOS-16.6.1	core, zoned, pale CL	0.59	117	103	0.91	13	773 ±7	813 ±75	5	0.0662	3.6	1.163	3.7	0.1274	1.0	0.26
MOS-16.6.2	rim, homog, dark CL	0.39	1884	14	0.01	139	528 ±3	555 ±19	5	0.0587	0.9	0.691	1.0	0.0854	0.6	0.57
MOS-16.7.1	zoned/disturbed(+thin rim)	2.27	506	386	0.79	51	703 ±5	733 ±71	4	0.0637	3.4	1.013	3.4	0.1153	0.7	0.21
MOS-16.8.1	zoned, pale CL, fresh crystal	0.00	261	219	0.87	29	771 ±6	830 ±26	7	0.0668	1.2	1.169	1.5	0.1271	0.9	0.57
MOS-16.9.1	zoned, dark CL	0.13	1408	631	0.46	146	736 ±5	763 ±14	4	0.0646	0.7	1.077	1.0	0.1209	0.7	0.72
MOS-16.10.1	zoned, fresh grain	0.50	825	866	1.08	81	696 ±4	747 ±25	7	0.0642	1.2	1.009	1.3	0.1141	0.7	0.49
MOS-16.11.1	zoned tip domain (zoned, replaced inner domain)	0.13	696	4	0.01	51	522 ±3	564 ±26	7	0.0589	1.2	0.685	1.4	0.0844	0.7	0.48
MOS-16.12.1	core?/zoned domain	--	481	504	1.08	48	707 ±6	912 ±67	22	0.0694	3.3	1.110	3.4	0.1160	0.9	0.26
MOS-19 / 2638-04 aplite granite, Guro Suite																
MOS-19.1.1	zoned, CL-pale inner domain	0.11	486	311	0.66	60	858 ±4	804 ±40	-6	0.0659	1.9	1.294	2.0	0.1424	0.5	0.26
MOS-19.1.2	quite homogeneous, CL-dark rim	0.11	2071	313	0.16	245	832 ±2	834 ±13	0	0.0669	0.6	1.270	0.7	0.1377	0.3	0.39
MOS-19.2.1	quite homogeneous, CL-pale rim	1.18	581	162	0.29	69	824 ±4	810 ±54	-2	0.0661	2.6	1.243	2.7	0.1363	0.6	0.21
MOS-19.3.1	quite homogeneous, CL-pale rim	0.38	645	135	0.22	79	857 ±4	863 ±35	1	0.0678	1.7	1.330	1.7	0.1422	0.5	0.27
MOS-19.3.2	CL-dark and spotty inner domain	0.04	2475	625	0.26	290	825 ±2	836 ±12	1	0.0669	0.6	1.259	0.6	0.1364	0.3	0.46
MOS-19.4.1	zoned, CL-dark	0.44	522	354	0.70	61	825 ±4	834 ±37	1	0.0669	1.8	1.258	1.8	0.1364	0.5	0.28
MOS-19.5.1	zoned, CL-dark	0.20	675	482	0.74	82	852 ±4	869 ±24	2	0.0680	1.2	1.325	1.3	0.1412	0.4	0.35
MOS-19.6.1	zoned, CL-bright	0.70	281	167	0.61	33	827 ±5	798 ±63	-4	0.0657	3.0	1.241	3.1	0.1369	0.7	0.22
<i>MOS-19.7.1</i>	<i>CL-pale replacing phase</i>	<i>2.68</i>	<i>480</i>	<i>122</i>	<i>0.26</i>	<i>56</i>	<i>796 ±5</i>	<i>750 ±96</i>	<i>-6</i>	<i>0.0643</i>	<i>4.5</i>	<i>1.164</i>	<i>4.6</i>	<i>0.1314</i>	<i>0.7</i>	<i>0.15</i>
MOS-19.8.1	quite homogeneous, CL-medium inner domain	0.52	991	6	0.01	72	518 ±2	528 ±42	2	0.058	1.9	0.669	2.0	0.0837	0.5	0.24
MOS-19.9.1	quite homogeneous, CL-dark core domain	0.07	651	30	0.05	46	513 ±3	515 ±30	1	0.0576	1.4	0.658	1.5	0.0828	0.6	0.38
MOS-19.9.2	quite homogeneous, CL-dark rim	0.08	662	419	0.65	81	854 ±4	843 ±24	-1	0.0672	1.1	1.312	1.2	0.1416	0.4	0.36
MOS-19.10.1	zoned, CL-dark	0.13	646	496	0.79	78	848 ±4	863 ±23	2	0.0678	1.1	1.314	1.2	0.1406	0.5	0.41
MOS-19.11.1	weakly zoned, CL-dark	0.16	1079	14	0.01	80	530 ±2	485 ±30	-8	0.0568	1.4	0.671	1.4	0.0857	0.4	0.27
MOS-19.12.1	zoned, CL-dark	0.01	782	363	0.48	91	814 ±4	872 ±17	7	0.0681	0.8	1.265	0.9	0.1347	0.5	0.49
MOS-19.13.1	zoned, CL-medium	0.16	503	384	0.79	62	857 ±5	849 ±32	-1	0.0674	1.5	1.320	1.6	0.1421	0.6	0.35
MOS-19.14.1	zoned, CL-medium	0.18	915	345	0.39	107	822 ±3	879 ±21	7	0.0684	1.0	1.281	1.1	0.1360	0.4	0.40
MOS-19.15.1	zoned/spotty, CL-dark	0.03	1315	30	0.02	93	509 ±2	507 ±21	0	0.0574	1.0	0.650	1.0	0.0821	0.4	0.39
MOS-19.16.1	zoned, CL-dark	0.51	1377	110	0.08	108	561 ±2	618 ±49	10	0.0604	2.3	0.757	2.3	0.0909	0.4	0.18
MOS-19.17.1	zoned, CL-dark	0.13	979	529	0.56	113	813 ±3	903 ±19	11	0.0692	0.9	1.281	1.0	0.1343	0.4	0.37
MOS-19.18.1	zoned (hit partly on CL-dark center domain?)	2.13	699	276	0.41	81	798 ±10	840 ±68	5	0.0671	3.3	1.219	3.5	0.1318	1.4	0.39

Appendix 1. Continued.

Spot	Dated zircon domain	% 206Pb _c	ppm U	ppm Th	232Th /238U	ppm 206Pb*	(1) 206Pb/238U Age	(1) 207Pb/206Pb Age	% Dis- cor- dancy	(1) 207Pb* /206Pb*	±% 207Pb* /235U	(1) 206Pb* /238U	±% 206Pb*	err corr
Mos-20 / 2943-04 garnet-sillimanite gneiss, Rushinga Group														
MOS-20.1.1	CL-bright rim	2.09	120	6	0.05	9	506 ± 8	490 ± 247	-3	0.0570	11.2	0.641	11.3	0.0816
MOS-20.1.2	zoned main domain (+CL-bright rim)	0.13	274	46	0.18	84	1959 ± 11	2673 ± 12	36	0.1822	0.7	8.922	1.0	0.3552
MOS-20.2.1	CL-dark, smoothly zoned (+thin CL-bright rim)	1.65	845	23	0.03	69	576 ± 3	951 ± 65	65	0.0708	3.2	0.911	3.2	0.0934
MOS-20.3.1	CL-dark, smoothly zoned (thin CL-bright rim)	0.33	485	14	0.03	35	521 ± 3	528 ± 83	1	0.0579	3.8	0.673	3.8	0.0843
MOS-20.4.1	CL-bright rim on zircon 8	6.71	56	7	0.12	4	475 ± 16	619 ± 795	30	0.0604	36.8	0.638	37.0	0.0765
MOS-20.4.2	core (CL-dark and bright rims around it)	0.47	293	61	0.22	76	1691 ± 9	2367 ± 16	40	0.1519	0.9	6.281	1.1	0.3000
MOS-20.5.1	CL-bright rim on zircon 8	1.17	127	7	0.05	9	497 ± 7	631 ± 246	27	0.0608	11.4	0.671	11.5	0.0801
MOS-20.6.1	zoned, CL-dark	0.36	656	82	0.13	84	891 ± 4	1553 ± 23	74	0.0962	1.2	1.967	1.3	0.1482
MOS-20.7.1	CL-bright rim on zircon 8	21.00	32	5	0.16	3	500 ± 28	-2636 ± 0	-628					
MOS-20.8.1	center/core?, CL-dark	1.87	225	49	0.23	41	1211 ± 11	2244 ± 38	85	0.1414	2.2	4.029	2.4	0.2067
MOS-20.9.1	CL-dark domain (+core+CL-bright rim)	1.92	1218	30	0.03	84	491 ± 2	351 ± 87	-29	0.0535	3.9	0.584	3.9	0.0792
MOS-20.9.2	core, CL-medium	0.48	379	81	0.22	68	1220 ± 7	1810 ± 30	48	0.1106	1.6	3.179	1.7	0.2084
MOS-20.10.1	smoothly zoned, CL-dark (+metamict core)	0.91	501	9	0.02	36	515 ± 4	520 ± 110	1	0.0577	5.0	0.661	5.1	0.0831
MOS-20.11.1	center, zoned CL-pale domain	0.29	308	137	0.46	84	1776 ± 10	1908 ± 19	7	0.1168	1.0	5.106	1.2	0.3171
MOS-20.12.1	zoned core (+CL-bright rim)	0.03	467	92	0.20	128	1787 ± 7	2426 ± 12	36	0.1572	0.7	6.926	0.8	0.3195
MOS-20.13.1	zoned core (+CL-bright rim)	0.28	376	62	0.17	62	1122 ± 6	2149 ± 21	91	0.1338	1.2	3.508	1.3	0.1901
MOS-20.14.1	core, CL-medium	1.64	258	105	0.42	69	1720 ± 11	2449 ± 30	42	0.1593	1.8	6.719	1.9	0.3058
Mos-21 / 1519-04 Fudeze orthogneiss, Mudzi Metamorphic Complex														
MOS-21.1.1	zoned core	0.26	607	186	0.32	249	2511 ± 8	3048 ± 6	21	0.2294	0.4	15.061	0.5	0.4762
MOS-21.1.2	zoned, CL-dark	0.19	747	115	0.16	251	2128 ± 8	2509 ± 8	18	0.1652	0.5	8.905	0.6	0.3910
MOS-21.2.1	zoned, CL-dark	0.14	467	43	0.10	188	2474 ± 10	2599 ± 8	5	0.1743	0.5	11.239	0.7	0.4678
MOS-21.3.1	zoned, CL-dark	0.71	672	115	0.18	252	2324 ± 9	2598 ± 9	12	0.1742	0.6	10.424	0.7	0.4340
MOS-21.4.1	zoned, CL-dark	0.26	968	77	0.08	255	1721 ± 6	2361 ± 8	37	0.1513	0.5	6.384	0.6	0.3060
MOS-21.5.1	zoned, CL-medium, tip	0.14	314	102	0.34	121	2389 ± 11	2595 ± 10	9	0.1739	0.6	10.754	0.8	0.4486
MOS-21.5.2	zoned, CL-dark, middle	0.21	699	69	0.10	179	1677 ± 7	2073 ± 133	24	0.1282	7.6	5.251	9.2	0.2972
MOS-21.5.3	zoned, CL-medium, center	0.01	459	373	0.84	214	2788 ± 12	2866 ± 129	3	0.2050	7.9	15.291	7.9	0.5410
MOS-21.6.1	zoned, CL-medium	-0.01	211	72	0.35	90	2596 ± 16	2489 ± 75	-4	0.1632	4.4	11.159	4.5	0.4958
MOS-21.7.1	CL-bright rim	31.01	30	3	0.12	5	760 ± 62	2022 ± 1606	166	0.1245	90.6	2.148	91.0	0.1251
MOS-21.8.1	zoned, CL-medium	--	550	337	0.63	246	2702 ± 9	2756 ± 86	2	0.1916	5.3	13.750	5.3	0.5205
MOS-21.9.1	zoned, CL-medium	0.16	208	60	0.30	88	2569 ± 27	2589 ± 21	1	0.1732	1.2	11.693	1.8	0.4896
MOS-21.10.1	zoned, CL-medium	0.32	180	84	0.49	72	2463 ± 14	2597 ± 13	5	0.1740	0.8	11.164	1.0	0.4653
MOS-21.11.1	zoned, CL-medium	0.36	491	92	0.19	128	1698 ± 8	2365 ± 12	39	0.1517	0.7	6.306	0.9	0.3014
MOS-21.12.1	zoned, CL-medium	0.09	328	195	0.61	143	2650 ± 13	2714 ± 12	2	0.1867	0.7	13.091	0.9	0.5084
MOS-21.13.1	zoned, CL-medium	0.05	250	218	0.90	107	2609 ± 12	2654 ± 9	2	0.1801	0.6	12.386	0.8	0.4988

Appendix 1. Continued.

Spot	Dated zircon domain	% ²⁰⁶ Pb _e	ppm U	ppm Th	²³² Th / ²³⁸ U	ppm ²⁰⁶ Pb*	(1) ²⁰⁶ Pb/ ²³⁸ U Age	(1) ²⁰⁷ Pb/ ²⁰⁶ Pb Age	% Dis- cor- dancy	(1) ²⁰⁷ Pb* / ²⁰⁶ Pb*	±0%	(1) ²⁰⁷ Pb* / ²³⁵ U	±0%	(1) ²⁰⁶ Pb* / ²³⁸ U	err ±%	corr
Mos-23 / 13625-04 tonalite, Mavonde Complex																
MOS-23.1.1	zoned, CL-dark	0.11	425	292	0.71	204	2861 ±16	2909 ±9	2	0.2104	0.5	16206	0.9	0.5586	0.7	0.79
MOS-23.2.1	CL-medium dark, weakly zoned core/centre domain	0.16	136	64	0.49	68	2934 ±39	2911 ±15	-1	0.2108	0.9	16747	1.9	0.5763	1.6	0.87
MOS-23.3.1	zoned, CL-dark	0.05	223	86	0.40	110	2930 ±19	2909 ±9	-1	0.2105	0.6	16702	1.0	0.5754	0.8	0.81
MOS-23.4.1	zoned, CL-dark	0.08	384	203	0.55	184	2862 ±16	2900 ±7	1	0.2093	0.4	16130	0.8	0.5589	0.7	0.84
MOS-23.5.1	zoned, CL-dark	0.56	426	187	0.45	199	2793 ±18	2921 ±11	5	0.2121	0.7	15855	1.0	0.5423	0.8	0.77
MOS-23.6.1	zoned, CL-dark	0.23	293	145	0.51	131	2694 ±16	2898 ±9	8	0.2090	0.6	14949	0.9	0.5188	0.7	0.80
MOS-23.7.1	zoned, CL-dark	0.25	259	137	0.55	118	2736 ±19	2873 ±10	5	0.2058	0.6	15008	1.0	0.5288	0.9	0.81
MOS-23.8.1	CL-dark, quite homogeneous core	0.26	565	305	0.56	214	2351 ±13	2729 ±8	16	0.1884	0.5	11436	0.8	0.4402	0.7	0.82
MOS-23.8.2	CL-medium dark, weakly zoned tip	0.23	206	79	0.40	97	2821 ±19	2883 ±11	2	0.2071	0.7	15671	1.0	0.5489	0.8	0.78
MOS-23.9.1	zoned, CL-dark	0.19	254	147	0.60	121	2838 ±19	2901 ±9	2	0.2094	0.6	15969	1.0	0.5532	0.8	0.82
MOS-23.10.1	zoned, CL-dark	0.10	352	142	0.42	168	2847 ±16	2888 ±8	1	0.2077	0.5	15902	0.9	0.5552	0.7	0.83
MOS-23.10.2	CL-dark replacing homogeneous phase	0.15	896	34	0.04	236	1724 ±9	2463 ±8	43	0.1607	0.5	6794	0.8	0.3066	0.6	0.79
Mos-26 / 1011-02 garnet gneiss, Gairezi Group																
MOS-26.1.1	homogeneous, CL-dark	0.12	270	207	0.79	108	2460 ±16	2574 ±11	5	0.1717	0.7	10998	1.0	0.4646	0.8	0.75
MOS-26.2.1	zoned, dark and pale stripes	0.15	195	94	0.50	71	2270 ±16	2131 ±16	-6	0.1325	0.9	7708	1.3	0.4221	0.9	0.67
MOS-26.3.1	zoned, CL-medium dark	--	279	58	0.21	93	2109 ±14	2063 ±12	-2	0.1275	0.8	6800	1.1	0.3869	0.8	0.71
MOS-26.4.1	zoned, CL-dark	0.11	509	56	0.11	153	1930 ±12	2035 ±12	5	0.1254	0.7	6037	1.0	0.3490	0.7	0.74
MOS-26.5.1	zoned, dark and pale stripes	0.34	112	41	0.38	35	1994 ±18	2048 ±24	3	0.1263	1.4	6313	1.7	0.3624	1.0	0.60
MOS-26.6.1	zoned, CL-medium dark	0.11	293	116	0.41	93	2027 ±13	2061 ±16	2	0.1273	0.9	6485	1.2	0.3694	0.8	0.64
MOS-26.7.1	quite homogeneous, CL-pale, round	0.18	77	50	0.67	24	2021 ±21	2044 ±31	1	0.1261	1.7	6400	2.1	0.3682	1.2	0.57
MOS-26.7.2	homogeneous, CL-dark, round	0.11	328	302	0.95	102	1994 ±13	2015 ±14	1	0.1240	0.8	6201	1.1	0.3625	0.8	0.71
MOS-26.8.1	weakly zoned, CL-bright, round (metamorphic?)	0.61	94	229	2.51	23	1602 ±18	1885 ±54	18	0.1153	3.0	4486	3.3	0.2821	1.3	0.40
MOS-26.9.1	zoned, CL-dark, round	0.04	335	198	0.61	153	2755 ±17	3063 ±7	11	0.2316	0.4	17031	0.9	0.5333	0.8	0.86
MOS-26.10.1	zoned, CL-medium	0.11	216	109	0.52	69	2024 ±14	2049 ±19	1	0.1264	1.1	6429	1.4	0.3688	0.8	0.61
MOS-26.11.1	zoned, CL-medium dark	0.12	500	197	0.41	140	1815 ±11	1981 ±12	9	0.1217	0.7	5453	1.0	0.3251	0.7	0.73
MOS-26.12.1	zoned, CL-dark	0.15	448	244	0.56	134	1929 ±11	2024 ±12	5	0.1246	0.7	5995	1.0	0.3489	0.7	0.70
MOS-26.13.1	weakly zoned, CL-pale	0.37	133	52	0.40	41	1966 ±17	2065 ±29	5	0.1276	1.7	6270	1.9	0.3565	1.0	0.51
MOS-26.14.1	quite homogeneous, CL-pale (?zoned rim)	0.12	210	79	0.39	88	2571 ±19	2636 ±12	3	0.1781	0.7	12036	1.2	0.4901	0.9	0.79
MOS-26.15.1	zoned, dark and pale stripes	0.12	194	157	0.84	83	2611 ±18	2698 ±13	3	0.1849	0.8	12732	1.1	0.4993	0.9	0.75
MOS-26.16.1	zoned, CL-medium dark	0.21	169	98	0.60	54	2047 ±16	2051 ±22	0	0.1266	1.2	6521	1.5	0.3737	0.9	0.60
Mos-28 / 19313-04 granite, Bárue Complex																
MOS-28.1.1	zoned, CL-dark	0.13	390	280	0.74	140	2245 ±14	2410 ±10	7	0.1558	0.6	8945	1.0	0.4165	0.7	0.78
MOS-28.2.1	zoned, CL-dark	0.27	348	327	0.97	57	1120 ±8	1162 ±34	4	0.0786	1.7	2057	1.9	0.1898	0.8	0.42
MOS-28.3.1	zoned center domain, CL-dark	0.06	386	256	0.69	128	2101 ±36	2049 ±12	-2	0.1264	0.7	6714	2.1	0.3852	2.0	0.95
MOS-28.4.1	quite homogeneous, CL-brigh	0.43	14	35	2.58	3	1269 ±34	2090 ±89	65	0.1294	5.0	3884	5.8	0.2176	2.9	0.50
MOS-28.5.1	zoned, CL-medium	0.45	360	383	1.10	57	1088 ±8	1090 ±40	0	0.0758	2.0	1921	2.2	0.1839	0.8	0.38
MOS-28.6.1	zoned, CL-dark	1.14	687	479	0.72	76	770 ±5	1073 ±48	39	0.0752	2.4	1314	2.5	0.1268	0.7	0.29
MOS-28.7.1	quite homogeneous centre domain	0.17	185	121	0.68	74	2475 ±20	2495 ±15	1	0.1638	0.9	10571	1.3	0.4681	1.0	0.75

Appendix I. Continued.

Spot	Dated zircon domain	% 206Pb _c	ppm U	ppm Th	232Th /238U	ppm 206Pb*	(1) 206Pb/238U Age	(1) 207Pb/206Pb Age	% Dis- cor- dancy	(1) 207Pb* /206Pb*	±%	(1) 207Pb* /235U	±%	(1) 206Pb* /238U	err ±%	corr
MOS-28.8.1	zoned, CL-medium	0.05	344	445	1.34	57	1130 ±8	1180 ±33	4	0.0793	1.7	2.095	1.9	0.1916	0.8	0.42
MOS-28.9.1	zoned, CL-bright	1.68	95	124	1.34	14	997 ±14	1221 ±133	22	0.0810	6.8	1.867	6.9	0.1672	1.5	0.22
MOS-28.10.1	zoned, CL-dark	1.47	634	192	0.31	90	976 ±6	1276 ±42	31	0.0833	2.2	1.877	2.3	0.1635	0.7	0.30
MOS-28.11.1	zoned, CL-dark	0.92	183	197	1.11	30	1123 ±13	1080 ±82	-4	0.0754	4.1	1.979	4.3	0.1903	1.2	0.29
MOS-28.12.1	zoned, CL-dark	0.09	246	152	0.64	71	1879 ±15	1830 ±17	-3	0.1119	1.0	5.219	1.3	0.3384	0.9	0.68
MOS-28.13.1	weakly zoned, CL-bright	0.01	269	188	0.72	85	2017 ±14	2027 ±14	0	0.1249	0.8	6.324	1.1	0.3673	0.8	0.71
MOS-28.14.1	zoned, CL-dark	0.57	220	231	1.09	37	1139 ±11	1133 ±57	0	0.0775	2.9	2.064	3.0	0.1932	1.0	0.34
Mos-29 / 19290-04 Inchapa granodiorite, Bárue Complex																
MOS-29.1.1	zoned, CL-medium, long (+CL-dark rim)	0.26	630	741	1.22	88	971 ±4	1087 ±28	12	0.0757	1.4	1.697	1.4	0.1626	0.5	0.32
<i>MOS-29.1.2</i>	<i>homogeneous CL-dark rim</i>	<i>4.38</i>	<i>2220</i>	<i>164</i>	<i>0.08</i>	<i>252</i>	<i>768 ±3</i>	<i>902 ±83</i>	<i>17</i>	<i>0.0691</i>	<i>4.0</i>	<i>1.205</i>	<i>4.0</i>	<i>0.1265</i>	<i>0.4</i>	<i>0.11</i>
<i>MOS-29.2.1</i>	<i>zoned, CL-pale, long (+CL-dark rim)</i>	<i>6.15</i>	<i>270</i>	<i>97</i>	<i>0.37</i>	<i>17</i>	<i>418 ±5</i>	<i>762 ±230</i>	<i>82</i>	<i>0.0646</i>	<i>11.0</i>	<i>0.597</i>	<i>11.0</i>	<i>0.0670</i>	<i>1.2</i>	<i>0.11</i>
MOS-29.3.1	zoned, CL-pale, long (+CL-dark rim)	0.66	124	99	0.82	19	1065 ±9	1166 ±65	9	0.0787	3.3	1.950	3.4	0.1796	1.0	0.28
MOS-29.4.1	zoned, CL-pale, long (+CL-dark rim)	0.34	174	70	0.42	27	1063 ±8	1123 ±67	6	0.0771	3.4	1.905	3.5	0.1792	0.8	0.24
MOS-29.5.1	zoned, CL-medium, long (+CL-dark rim)	0.24	746	928	1.29	108	1006 ±4	1076 ±22	7	0.07528	1.1	1.752	1.2	0.1688	0.4	0.35
MOS-29.5.2	homogeneous CL-dark rim	0.65	1792	71	0.04	167	659 ±2	902 ±28	37	0.06912	1.4	1.026	1.4	0.1076	0.4	0.26
MOS-29.6.1	zoned, CL-medium, long (+CL-dark rim)	0.15	567	475	0.86	89	1083 ±5	1070 ±22	-1	0.07504	1.1	1.892	1.2	0.1829	0.5	0.39
MOS-29.7.1	zoned, CL-pale, short (+CL-dark rim)	2.38	160	165	1.07	26	1109 ±10	1104 ±110	0	0.0763	5.6	1.980	5.6	0.1877	1.0	0.17
MOS-29.8.1	zoned, CL-pale, short (+CL-dark rim)	1.05	111	115	1.07	18	1081 ±10	1017 ±77	-6	0.0731	3.8	1.840	3.9	0.1826	1.0	0.26
MOS-29.9.1	zoned, CL-medium dark, short	0.08	498	124	0.26	78	1079 ±5	1088 ±22	1	0.07573	1.1	1.902	1.2	0.1822	0.5	0.41
MOS-29.10.1	zoned, CL-pale, short (+CL-dark rim)	0.66	155	158	1.05	25	1099 ±9	1037 ±65	-6	0.0738	3.2	1.892	3.4	0.1858	0.9	0.27
MOS-29.11.1	zoned, CL-medium, short (+CL-dark rim)	0.39	292	182	0.65	46	1081 ±7	1076 ±41	0	0.0753	2.1	1.894	2.2	0.1825	0.7	0.30
MOS-29.12.1	zoned, CL-pale, short (+CL-dark rim)	0.96	79	110	1.44	12	1042 ±12	1137 ±97	9	0.0776	4.9	1.877	5	0.1754	1.3	0.25
MOS-29.13.1	zoned, CL-pale, short (+CL-dark rim)	1.58	91	127	1.45	14	1041 ±11	999 ±100	-4	0.0725	5.1	1.751	5.2	0.1752	1.1	0.21
<i>MOS-29.13.2</i>	<i>homogeneous CL-dark rim</i>	<i>3.86</i>	<i>3664</i>	<i>64</i>	<i>0.02</i>	<i>193</i>	<i>370 ±2</i>	<i>992 ±69</i>	<i>168</i>	<i>0.0722</i>	<i>3.4</i>	<i>0.588</i>	<i>3.4</i>	<i>0.0591</i>	<i>0.4</i>	<i>0.11</i>
MOS-29.14.1	zoned, CL-medium, long (+CL-dark rim)	0.41	725	445	0.63	70	684 ±3	1101 ±32	61	0.0762	1.6	1.177	1.7	0.1120	0.5	0.30
MOS-33 / 4158-03 metasandstone, Zámbe Supergroup																
MOS-33.1.1	hazy zoning, younger, CL-dark domain	9.66	695	18	0.03	117.0	1051 ±14	1066 ±283	1	0.0749	14.1	1.829	14.2	0.1771	1.5	0.11
MOS-33.1.2	zoned, CL-bright domain	5.43	199	119	0.62	60	1861 ±33	1880 ±168	1	0.1150	9.3	5.305	9.6	0.3346	2.0	0.21
MOS-33.2.1	zoned, CL-dark (+dark thin rim)	9.88	969	528	0.56	126	827 ±12	861 ±333	4	0.0678	16.0	1.279	16.1	0.1369	1.5	0.09
MOS-33.3.1	zoned, CL-bright, rounded core (+thin CL-dark rim)	6.80	167	182	1.13	35	1310 ±27	1324 ±318	1	0.0854	16.4	2.652	16.6	0.2254	2.3	0.14
MOS-33.4.1	CL-bright, rounded core	1.45	265	85	0.33	92	2155 ±23	2154 ±61	0	0.1342	3.5	7.348	3.7	0.3970	1.3	0.35
MOS-33.5.1	homogeneous, CL-dark rim (+rounded core)	0.45	902	116	0.13	157	1185 ±8	1166 ±49	-2	0.0788	2.4	2.191	2.6	0.2017	0.8	0.30
<i>MOS-33.6.1</i>	<i>quite homogeneous, CL-dark rim</i>	<i>41.59</i>	<i>1708</i>	<i>405</i>	<i>0.24</i>	<i>250</i>	<i>611 ±28</i>	<i>635 ±1446</i>	<i>4</i>	<i>0.0609</i>	<i>67.2</i>	<i>0.835</i>	<i>67.3</i>	<i>0.0995</i>	<i>4.8</i>	<i>0.07</i>
MOS-33.6.2	zoned, CL-medium rounded core	0.13	182	213	1.21	81	2683 ±36	2689 ±27	0	0.1839	1.6	13.090	2.3	0.5161	1.6	0.71
MOS-33.7.1	zoned, CL-dark, euhedral	3.53	1017	86	0.09	167	1089 ±10	1110 ±128	2	0.0766	6.4	1.943	6.5	0.1841	1.0	0.16
MOS-33.8.1	CL-dark rim	21.91	2688	103	0.04	176	373 ±9	385 ±817	3	0.0543	36.4	0.446	36.4	0.0595	2.4	0.06
MOS-33.8.2	zoned, CL-bright core	0.00	59	67	1.16	19	2051 ±45	2058 ±67	0	0.1271	3.8	6.567	4.6	0.3747	2.6	0.56
MOS-33.9.1	zoned, CL-dark euhedral grain	0.33	870	127	0.15	150	1177 ±9	1147 ±47	-3	0.0780	2.3	2.154	2.5	0.2003	0.8	0.33
MOS-33.10.1	zoned, CL-medium	0.00	185	66	0.37	33	1216 ±18	1251 ±69	3	0.0822	3.5	2.353	3.9	0.2076	1.7	0.43

Appendix 1. Continued.

Spot	Dated zircon domain	% ²⁰⁶ Pb _c	ppm U	ppm Th	²³² Th/ ²³⁸ U	ppm ²⁰⁶ Pb*	(1) ²⁰⁶ Pb/ ²³⁸ U Age	(1) ²⁰⁷ Pb/ ²⁰⁶ Pb Age	% Dis- cor- dancy	(1) ²⁰⁷ Pb* / ²⁰⁶ Pb*	±%	(1) ²⁰⁷ Pb* / ²³⁵ U	±%	(1) ²⁰⁶ Pb* / ²³⁸ U	±%	err corr
MOS-33.11.1	zoned, CL-medium (+dark rim; marginal phase?)	13.79	571	126	0.23	100	1041 ±20	1071 ±426	3	0.0751	21.2	1.814	21.3	0.1752	2.1	0.10
<i>MOS-33.12.1</i>	<i>homogeneous, CL-dark rim (+rounded core)</i>	<i>69.01</i>	<i>8067</i>	<i>3233</i>	<i>0.41</i>	<i>1015</i>	<i>286 ±36</i>	<i>1678 ±1802</i>	<i>487</i>	<i>0.1030</i>	<i>97.6</i>	<i>0.644</i>	<i>98.4</i>	<i>0.0454</i>	<i>12.8</i>	<i>0.13</i>
MOS-33.12.2	zoned, CL-medium rounded core	0.00	151	215	1.47	68	2733 ±39	2720 ±28	0	0.1875	1.7	13.651	2.5	0.5281	1.8	0.72
MOS-33.13.1	hazily zoned domain in blurry CL-dark grain	0.00	539	163	0.31	222	2525 ±21	2524 ±17	0	0.1666	1.0	11.014	1.4	0.4794	1.0	0.70
MOS-33.14.1	zoned, CL-dark center domain (+thin rim)	4.05	1990	1752	0.91	380	1247 ±9	1286 ±95	3	0.0837	4.9	2.464	4.9	0.2135	0.8	0.16
MOS-34 / 3157-03 felsic/intermediate metavolcanic rock, Fingõe Supergroup																
MOS-34.1.1	zoned, quite dark in CL	0.00	715	328	0.47	141	1334 ±13	1331 ±37	0	0.0857	1.9	2.717	2.2	0.2299	1.1	0.49
MOS-34.2.1	zoned, quite dark in CL	---	908	1038	1.18	179	1333 ±10	1324 ±42	-1	0.0854	2.2	2.704	2.3	0.2297	0.9	0.37
MOS-34.3.1	zoned, quite dark in CL	0.00	567	383	0.70	111	1319 ±14	1325 ±42	0	0.0854	2.1	2.674	2.5	0.2271	1.2	0.49
MOS-34.4.1	zoned, quite dark in CL	0.00	728	1366	1.94	142	1321 ±13	1314 ±57	-1	0.0849	2.9	2.664	3.1	0.2275	1.1	0.35
MOS-34.5.1	zoned, quite dark in CL	-0.28	461	236	0.53	90	1321 ±14	1319 ±63	0	0.0852	3.2	2.671	3.4	0.2275	1.2	0.34
MOS-34.6.1	zoned, quite dark in CL	-0.40	374	258	0.71	64	1178 ±17	1218 ±93	3	0.0809	4.7	2.236	5.0	0.2005	1.6	0.31
MOS-34.7.1	zoned, CL-medium	0.00	160	68	0.44	32	1331 ±39	1334 ±78	0	0.0858	4.0	2.714	5.2	0.2293	3.3	0.63
MOS-34.8.1	zoned, CL-medium	---	187	78	0.43	33	1212 ±23	1260 ±83	4	0.0826	4.3	2.356	4.7	0.2068	2.1	0.43
MOS-34.9.1	zoned, CL-dark center domain	0.29	265	166	0.65	46	1176 ±18	1219 ±69	4	0.0809	3.5	2.231	3.9	0.2001	1.7	0.43
MOS-34.10.1	zoned, CL-medium	0.37	233	167	0.74	33	983 ±16	1061 ±85	8	0.0747	4.2	1.697	4.6	0.1647	1.8	0.39
MOS-34.11.1	zoned, CL-medium	0.52	155	65	0.43	25	1124 ±23	1176 ±104	5	0.0791	5.3	2.078	5.7	0.1905	2.2	0.38
MOS-34.12.1	zoned, CL-medium	0.50	169	71	0.43	31	1232 ±21	1275 ±97	4	0.0832	5.0	2.416	5.3	0.2105	1.8	0.35

Errors are 1-sigma; Pb and Pb* indicate the common and radiogenic lead portions, respectively. (1) Common Pb corrected using measured ²⁰⁴Pb. The rejected data are in *italics*.

2σ errors in standard calibration (not included in above errors): 0.28% for MOS-1(1-11) and 0.37% for MOS-1(12-17); 0.34% for MOS-3, MOS-5, and MOS-7; 0.77% for Mos-8; 1.25% for MOS-12 and MOS-15; 0.38% for MOS-16; 0.37% for MOS-19 (9-18), 0.40% for MOS-19 (1-8), MOS-20 and MOS-21; 1.15% for MOS-23, MOS-26 and MOS-28; 0.28% MOS-29; 0.70% for Mos-33-Mos35.

Appendix 2. TIMS-ID U-Pb isotopic data on zircon and monazite, samples from NW Mozambique.

Sample information	Sample weight	U ppm	Pb ppm	$^{206}\text{Pb}/^{204}\text{Pb}$ measured	$^{208}\text{Pb}/^{206}\text{Pb}$ radiogenic	$^{206}\text{Pb}/^{238}\text{U} \pm 2\sigma$ %	$^{207}\text{Pb}/^{235}\text{U} \pm 2\sigma$ %	ISOTOPIC RATIOS ¹⁾	Rho^2	APPARENT AGES / $\text{Ma} \pm 2\sigma$
Analysed mineral and fraction	mg							$^{206}\text{Pb}/^{206}\text{Pb} \pm 2\sigma$ %	$^{206}\text{Pb}/^{238}\text{U}$	$^{207}\text{Pb}/^{235}\text{U}$
Mos-2 / 2253-03 Monte Dombe granite, Cassacatiza Suite										
A) zircon >4.2 g cm ⁻³ , >75µm, colourless, ± Fe pigmented, transparent, prismatic, abraded 10 h	0.42	505	82	842	0.14	0.1449	0.65	0.07562	0.18	935
B) zircon >4.2 g cm ⁻³ , <75µm, brownish-yellowish, ± Fe pigmented, short to medium prismatic, translucent, abraded 1 h	0.35	1871	196	330	0.12	0.0860	0.65	0.07323	0.40	635
C) zircon >4.2 g cm ⁻³ , <75µm, colourless, ± Fe pigmented, transparent, prismatic, abraded 4 h	0.28	1053	149	622	0.12	0.1255	0.65	0.07480	0.22	843
D) zircon >4.2 g cm ⁻³ , >75µm, brownish-yellowish, ± Fe pigmented, long prismatic, translucent, abraded 10 h	0.44	1307	152	469	0.12	0.1006	0.65	0.07418	0.28	718
Mos-4 / 1072-02 aplite granite, Guro Suite										
A) zircon >4.2 g cm ⁻³ , >75µm, transparent, quite colourless prismatic, inclusions, abraded 22 h	0.50	220	31	7499	0.14	0.1369	0.65	0.06741	0.15	833
B) zircon >4.2 g cm ⁻³ , >75µm, transparent, quite colourless prismatic, inclusions	0.55	331	43	5240	0.11	0.1273	0.65	0.06654	0.15	786
C) zircon >4.2 g cm ⁻³ , <75µm, transparent, quite colourless prismatic, inclusions, abraded 17 h	0.31	377	54	14457	0.16	0.1362	0.65	0.06733	0.15	830
D) zircon >4.2 g cm ⁻³ , <75µm, transparent, quite colourless prismatic, inclusions	0.48	390	52	10674	0.14	0.1291	0.65	0.06684	0.15	796
Mos-6 / 1170-03 Massanga gneiss, Mudzi Metamorphic Complex										
A) zircon >4.2 g cm ⁻³ , >75µm, transparent, elongated, abraded 20 h	0.46	211	106	27622	0.11	0.4554	0.33	0.17497	0.05	2522
B) zircon >4.2 g cm ⁻³ , <75µm, transparent, elongated, abraded 10 h	0.45	258	119	24154	0.09	0.4209	0.35	0.17260	0.06	2436
C) zircon >4.2 g cm ⁻³ , transparent, elongated, abraded 30 h	0.51	190	96	43666	0.11	0.4583	0.32	0.17510	0.05	2529
Mos-9 / 2007-03, granite, Cassacatiza Suite										
A) zircon >4.2 g cm ⁻³ , >150µm, prismatic, almost colourless, transparent, inclusions, abraded 10 h	0.54	139	28	4094	0.20	0.1805	0.65	0.07539	0.15	1073
B) zircon >4.2 g cm ⁻³ , 150-75 µm, prismatic, almost colourless, transparent, inclusions, abraded 20 h	0.53	163	32	6211	0.19	0.1811	0.65	0.07542	0.15	1075
C) zircon >4.2 g cm ⁻³ , <75 µm, prismatic, almost colourless, transparent, inclusions, abraded 2 h	0.57	239	46	1839	0.19	0.1741	0.65	0.07571	0.15	1052
D) zircon >4.2 g cm ⁻³ , 150-75 µm, prismatic, almost colourless, transparent, inclusions	0.56	179	35	2553	0.18	0.1793	0.65	0.07511	0.15	1066

Appendix 2. Continued.

Sample information		Sample weight mg	U ppm	Pb ppm	²⁰⁶ Pb/ ²⁰⁴ Pb measured	²⁰⁸ Pb/ ²⁰⁶ Pb radiogenic	²⁰⁶ Pb/ ²³⁸ U ±2σ %	ISOTOPIC RATIOS ¹⁾		Rho ²		APPARENT AGES / Ma±2σ	
Analysed mineral and fraction								²⁰⁷ Pb/ ²³⁵ U ±2σ %	²⁰⁷ Pb/ ²⁰⁶ Pb ±2σ %	²⁰⁶ Pb/ ²³⁸ U	²⁰⁷ Pb/ ²³⁵ U	²⁰⁷ Pb/ ²⁰⁶ Pb	
Mos-10 / 2001-02 granite, Monte Sanja Suite													
A) zircon >4.2 g cm ⁻³ , >75µm, prismatic, almost colourless, transparent, abraded 20 h		0.27	108	24	414	0.31	0.1676	0.36	1.713	0.52	0.07416	0.33	1014
B#2) zircon >4.2 g cm ⁻³ , >75µm, prismatic, almost colourless, transparent, abraded 2 h		0.47	139	29	348	0.29	0.1516	0.37	1.547	0.56	0.07405	0.37	949
C#2) zircon >4.2 g cm ⁻³ , <75µm, prismatic, almost colourless, transparent, abraded 17 h		0.46	213	40	733	0.31	0.1468	0.33	1.495	0.40	0.07384	0.19	928
D) zircon >4.2 g cm ⁻³ , >75µm, prismatic, almost colourless, transparent		0.36	306	54	479	0.30	0.1351	0.42	1.372	0.52	0.07365	0.27	877
Mos-11 / 2297-03 Desaruhanama granite, Furancungo Suite													
A) zircon >4.2 g cm ⁻³ , 150-75µm, prismatic, reddish, translucent, inclusions, abraded 17 h		0.49	324	61	328	0.13	0.1525	0.35	1.535	0.62	0.07302	0.46	945
B) zircon >4.2 g cm ⁻³ , 150-75µm, prismatic, reddish, translucent, inclusions		0.54	282	51	272	0.12	0.1436	0.34	1.440	0.65	0.07274	0.49	906
C) zircon >4.2 g cm ⁻³ , <75µm, prismatic, reddish, translucent, inclusions, abraded 17 h		0.37	423	70	466	0.13	0.1429	0.34	1.436	0.46	0.07288	0.28	904
D) zircon >4.2 g cm ⁻³ , 150-75µm, prismatic, reddish, translucent, inclusions, abraded 30 h		0.50	140	26	1117	0.13	0.1705	0.33	1.736	0.37	0.07384	0.14	1022
Mos-13 / 6034-03 granite, Castanho Granite													
A) zircon >4.2 g cm ⁻³ , >75µm, long prismatic, transparent, abraded 17 h		0.54	253	46	10876	0.11	0.1760	0.65	1.807	0.65	0.07447	0.15	1048
B) zircon >4.2 g cm ⁻³ , >75µm, long prismatic, transparent, abraded 2h		0.56	211	38	14189	0.11	0.1760	0.65	1.802	0.65	0.07428	0.15	1046
C) zircon >4.2 g cm ⁻³ , <75µm, long prismatic, transparent, abraded 30 h		0.53	282	50	25921	0.11	0.1757	0.65	1.801	0.65	0.07435	0.15	1044
D) zircon >4.2 g cm ⁻³ , <75µm, long prismatic, transparent		0.29	332	59	8217	0.11	0.1744	0.65	1.787	0.65	0.07428	0.15	1037
Mos-18 / 13032-03 granite, Monte Capirimpica Granite													
A) zircon >4.2 g cm ⁻³ , >75µm, prismatic, brownish, translucent to transparent, abraded 10 h		0.53	554	105	1127	0.16	0.1689	0.33	1.763	0.35	0.07573	0.13	1032
B) zircon >4.2 g cm ⁻³ , >75µm, prismatic, brownish, translucent to transparent		0.55	461	91	421	0.16	0.1637	0.33	1.710	0.47	0.07578	0.30	1012
C) zircon >4.2 g cm ⁻³ , <75µm, prismatic, brownish, translucent to transparent, abraded 20 h		0.44	567	111	945	0.17	0.1727	0.33	1.802	0.36	0.07570	0.14	1027
D) zircon >4.2 g cm ⁻³ , <75µm, prismatic, brownish, translucent to transparent		0.47	616	117	1265	0.16	0.1717	0.33	1.792	0.35	0.07572	0.12	1021

Appendix 2. Continued.

Sample information		Sample weight mg	U ppm	Pb ppm	$^{206}\text{Pb}/^{204}\text{Pb}$ measured	$^{208}\text{Pb}/^{206}\text{Pb}$ radiogenic	$^{206}\text{Pb}/^{238}\text{U}$ $\pm 2\sigma$ %	$^{207}\text{Pb}/^{235}\text{U}$ $\pm 2\sigma$ %	ISOTOPIC RATIOS ⁽¹⁾		Rho^2 ($^{206}\text{Pb}/^{238}\text{U}$ / $^{207}\text{Pb}/^{235}\text{U}$)	APPARENT AGES / $\text{Ma} \pm 2\sigma$	
Analysed mineral and fraction													
Mos-22 / 2893-04 granite, Rukore Suite													
A) zircon >4.2 g cm-3, 150-75µm, prismatic, transparent, abraded 17 h													
B) zircon >4.2 g cm-3, <75µm, prismatic, transparent, abraded 9 h													
C) zircon >4.2 g cm-3, 150-75µm, prismatic, transparent, abraded 26 h													
Mos-24 / 15273-04 syenite, Gorongosa Intrusive Suite													
A) zircon >4.2 g cm-3, 150-75µm, elongated, transparent, quite colorless, abraded 17 h													
B) zircon >4.2 g cm-3, <75µm, elongated, transparent, quite colorless, abraded 9 h													
Mos-29 / 19290-04 Inchapa granodiorite, Barue Complex													
A) monazite: transparent, abraded 20 minutes													
Mos-30 / 19140-04 Messeca granodiorite, Mavonde Complex													
A) zircon >4.0 g cm-3, >75µm, translucent, prismatic, abraded 17 h													
B) zircon >4.0 g cm-3, <75µm, translucent, prismatic, abraded 9 h													
C) zircon >4.0 g cm-3, <75µm, translucent, prismatic, abraded 20 h													
D) zircon >4.0 g cm-3, >75µm, translucent, prismatic, abraded 30 h													
E) zircon >4.0 g cm-3, >75µm, translucent, prismatic, abraded 5 h													
Mos-31 / 6845-04 Monte Chissui tonalite, Bárue Complex													
A) zircon >4.0 g cm-3, >75µm, transparent, euhedral to subhedral, abraded 17 h													
B) zircon >4.0 g cm-3, <75µm, transparent, euhedral to subhedral, abraded 9 h													
C) zircon >4.0 g cm-3, <75µm, transparent, euhedral to subhedral, abraded 20 h													
D) zircon >4.0 g cm-3, >75µm, transparent, euhedral to subhedral, abraded 30 h													

¹⁾ Isotopic ratios corrected for fractionation, blank (30-50 pg), and age related common lead (Stacey and Kramers, 1975; $^{206}\text{Pb}/^{204}\text{Pb} \pm 0.2$; $^{207}\text{Pb}/^{204}\text{Pb} \pm 0.1$; $^{208}\text{Pb}/^{204}\text{Pb} \pm 0.2$;

²⁾ Errors for common lead composition of low-U, young zircons in sample MOS-22 are $^{206}\text{Pb}/^{204}\text{Pb} \pm 0.5$; $^{207}\text{Pb}/^{204}\text{Pb} \pm 0.3$; $^{208}\text{Pb}/^{204}\text{Pb} \pm 0.5$).

³⁾ Rho=Error correlation between $^{207}\text{Pb}/^{235}\text{U}$ and $^{206}\text{Pb}/^{238}\text{U}$ ratios. Abbreviations: zircon=zircon

Appendix 3. Sm-Nd isotopic data, samples from NW Mozambique.

Analysed fraction	Sm ppm	Nd ppm	$^{147}\text{Sm}/^{144}\text{Nd}$	$^{143}\text{Nd}/^{144}\text{Nd}$	± 2	T (Ma)	eps(T)
Mos-14 / 2395-03 gabbro, Atchiza Suite							
whole-rock	1.06	3.60	0.1784	0.512373	0.00002	864	-3.20
pyroxene	0.54	1.48	0.2202	0.512624	0.00002	864	-2.93
plagioclase	0.20	1.48	0.0805	0.511829	0.00002	864	-2.99
Mos-17 / 13014-03 gabbro, Chipera Massif							
whole-rock	0.94	3.90	0.1458	0.512371	0.00002	1047	1.57
pyroxene	2.08	5.04	0.2496	0.513069	0.00002	1047	1.27
plagioclase	0.54	3.27	0.1007	0.512042	0.00002	1047	1.19
MOS-25 / 25416-04 dolerite, Archaean terrain							
whole-rock	5.69	25.32	0.1359	0.511816	0.00002	1783	-2.2
pyroxene	2.63	7.08	0.2248	0.512859	0.00002	1783	-2.2
plagioclase	1.99	7.70	0.1558	0.511993	0.00002	1783	-3.3
MOS-27 / 14410-03 dolerite, Moeza Dike, Rukore Suite							
whole-rock	11.61	53.34	0.1316	0.512537	0.00002	180	-0.5
pyroxene	5.58	15.94	0.2116	0.512640	0.00002	180	-0.3
plagioclase	2.06	10.37	0.1201	0.512538	0.00002	180	-0.2
MOS-32 / 13888-04 Post-Umkondo dolerite, Mashonaland dolerite							
whole-rock	3.57	16.50	0.1307	0.511777	0.00002	1102	-7.6
pyroxene	1.52	4.61	0.1993	0.512285	0.00002	1102	-7.3
plagioclase	1.82	8.92	0.1233	0.511744	0.00002	1102	-7.2
MOS-37 / 1714-05 dolerite, Post-Gairezi							
whole-rock	6.27	27.21	0.1394	0.512204	0.00002	973	-1.4
plagioclase	1.26	9.39	0.0811	0.511832	0.00002	973	-1.4
garnet	3.03	2.49	0.7357	0.514169	0.00002	973	-37.4

2 σ error in $^{147}\text{Sm}/^{144}\text{Nd}$ is 0.4%.

CONTRIBUTION TO THE STRUCTURE AT THE EASTERN MARGIN OF THE ARCHAEOAN ZIMBABWE CRATON, MOZAMBIQUE

by
Tapio Koistinen¹, Matti I. Lehtonen¹,
Sérgio Fernando² & Rogério Matola²

Koistinen, T., Lehtonen, M. I., Fernando, S. & Matola, R. 2008. Contribution to the structure at the eastern margin of the Archaean Zimbabwe craton, Mozambique. *Geological Survey of Finland Special Paper 48*, 121–144, 15 figures.

The eastern margin of the Archaean Zimbabwe craton is situated in Mozambique close to the border with Zimbabwe. In the east the craton terminates against the Mozambique belt and in the north against the Zambezi belt. The exposed Archaean rock distribution in western Mozambique was mapped and correlated to that in Zimbabwe, and the lithological picture of the eastern margin of the Zimbabwe craton was thereby updated. Archaean exposures were found to occur more to the east than hitherto known. The previously incompletely mapped tectonic structure in the craton margin zone was updated.

The original disruption of a former Archaean domain took place at ~2 Ga ago, demonstrated by the appearance of Palaeoproterozoic quartzose, pelitic and carbonatic sediments, with volcanic intercalates. These characterize the craton margin along its length in various proportions. The subsequent history divides into several events involving repetitions of tectonic activity and periods of magmatism.

Generally, the attitude of the cover rocks is flat or gently east-dipping. Thereby, close to the basement-cover junction, several domes with an Archaean core are found. In addition, a previously unreported extensive thrust regime also involving the Archaean basement is introduced here. The thrust sheets represent evolution related to the closure of the newly formed basin by the collision of an unknown partner in the east. The timing of the collision has not so far been exactly constrained, but it supposedly occurred not much after ~2 Ga ago. A subsequent thrusting event at ~1100 Ma has been postulated by another study further to the south; what remains in between is unresolved. The latter thrusting period ended with the transition to a subvertical major sinistral shear zone along the craton edge in the southern part of the study area, obscuring or even eliminating the early thrust structure. The present crustal block east of the shear zone is composed of late Mesoproterozoic intrusive associations containing undated supracrustal intercalates. The shear zone was still activated during the late Pan-African period.

A particular bimodal Neoproterozoic intrusive suite was identified and its distribution mapped, and it was named the Guro Suite. It is approximately distributed in the northeastern corner of the Zimbabwe craton, with its analogies reported in the west, in Zimbabwe. In the presently exposed area they intrude the cover rocks and, owing to continuous injection, also themselves, while their intrusive relation to the buried margin of the Archaean gneisses remains open. They are emplaced strikingly parallel to the planar structure of the wall rock, and they are spectacularly layer-parallel deformed in a continuous manner. They record a ~800+ Ma crustal extension period next to the Zambezi belt in the north. The extension subsequently reversed into modest

to moderate convergence, demonstrated by flattening of the intermediately emplaced discordant pegmatites and formation of north-trending narrow synclines of the cover rocks, probably at ~500 Ma.

Karoo and Cretaceous basins, modified by erosion and superposed rift faults, characterize the landscape in the east of the craton margin, as well as many prominent inselbergs. The landscape-shaping faults include an earlier phase characterized by silicified fault gouge, and a later phase regarded as a component of the East Africa Rift Event.

Key words (GeoRef Thesaurus AGI): cratons, tectonics, thrust sheets, shear zones, domes, granites, gneisses, schists, greenstone belts, Archaean, Palaeoproterozoic, Mesoproterozoic, Neoproterozoic, Mozambique.

¹ Geological Survey of Finland, P.O. Box 96, 02151 Espoo, Finland

² National Directorate of Geology, Praça 25 de Junho 380, Maputo, Mozambique

E-mail: tapkoist@welho.com

INTRODUCTION

The “Mineral Resource Management Capacity Building Project, Republic of Mozambique, Component 2: Geological Infrastructure Development Programme, Geological Mapping LOT 2, 2002–2006” produced updated geological maps at the scale 1 : 250 000 with explanations, covering the Provinces of Tete, Manica and Sofala in NW Mozambique. This report deals with the eastern margin of the Zimbabwe craton, which is essentially on the Mozambican side of the national border (Fig. 1).

There is a long tradition of geological mapping and gold exploration in the Manica greenstone belt, as shown by small mines in the past and gold panning at present. Therefore, the geology of the Manica area is traditionally well known. The area belongs to the intact Zimbabwe craton, not affected by post-Archaean overprinting tectonic or thermal effects, characteristic of the wide marginal zone of the Archaean crust to the east of Manica (Manhiça *et al.* 2001; Mänttari this volume). The structure and metamorphism in the section from Manica as far east as to Chimoio (Fig. 1) has been extensively reported (Manhiça *et al.* 2001), while much of the eastern margin elsewhere had remained almost unknown. The current study makes a contribution to reducing this gap in knowledge.

The eastern margin of the Zimbabwe craton in Mozambique is mainly bound by the north-south running Mozambique belt in the east. In the north the craton margin abruptly swings to the west around the northeastern corner of the craton and in doing so immediately enters Zimbabwe, where it forms the northern margin of the craton, paral-

lel to the Zambezi belt. Observations of the turning point in Zimbabwe are, however, very limited because of the interruption of critical formational and tectonic continuities by wide Karoo to Recent troughs from Changara to the northwest (Fig. 1). In Zimbabwe the widely exposed northern margin has been extensively studied and reported (e.g. Stockl-mayer 1980, Barton *et al.* 1991, Dirks *et al.* 1998, 2006), which provided data for comparison over the border. On the Mozambican side the discovery of a bimodal intrusive suite, dated as Neoproterozoic, immediately seemed to tie the evolution at the northeastern corner of the craton in Mozambique to that in the northern margin of the craton in Zimbabwe, where comparable Neoproterozoic activity had been reported (Barton *et al.* 1991). Therefore much attention was paid to determining the regional distribution of the bimodal suite, its mode of emplacement and internal structures. Together with the still younger pegmatites it proved to be a useful tool for finding details on the late tectonism.

Taking into account the common occurrence of tectonic thrust structures at many craton margins in general, it is not surprising that such structures have also been anticipated in some papers at the eastern margin of the Zimbabwe craton in Mozambique, although they have not actually been discovered. The evidence for these began to accumulate north of Manica during the current project. Even though such major tectonism probably also operated east of Manica, later transcurrent shear tectonism along the Archaean/Proterozoic junction there has obscured the earlier features.

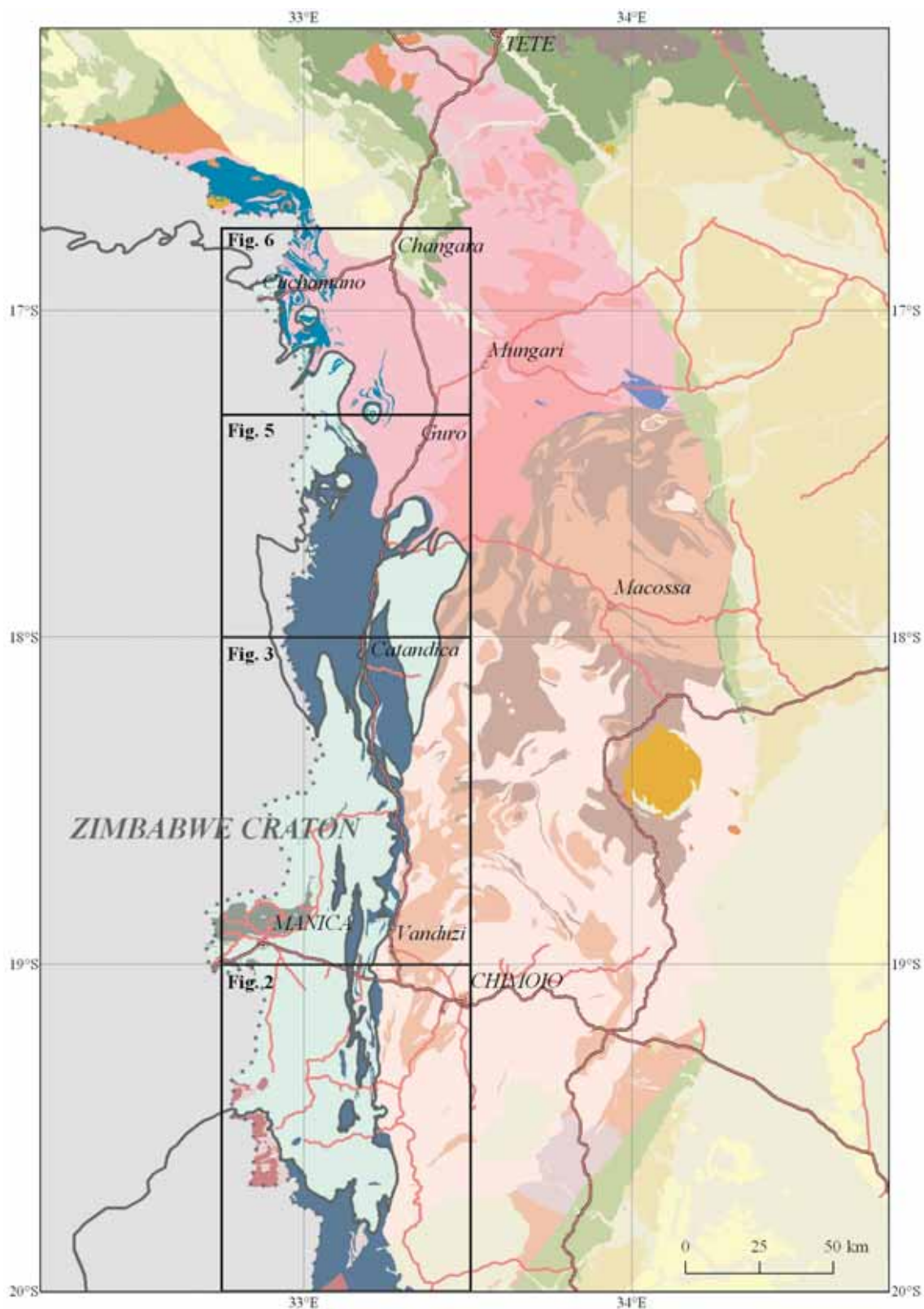


Fig. 1. The eastern margin of the Archaean Zimbabwe craton. The heavy line, partly in Zimbabwe (Geological Map of Zimbabwe 1:1 000 000, 1985; Stocklmayer 1980) marks the boundary of the exposed Archaean. Details are given in Figs 2, 3, 5 and 6; see also Pekkala *et al.*, Fig. 2a, this volume.

PREVIOUS WORK

Earlier geological investigation and mapping of the Archaean craton and its marginal areas in Mozambique has been sparse. Holmes (1918) published the first contribution on the general geology of Mozambique. In the 1950s and 1960s, during the colonial period, geological mapping at the scale of 1:250 000 was carried out in Mozambique and parts of the craton areas were also covered. The investigations of that time culminated in a monograph on the geology of Mozambique by Afonso (1976). After independence, in the late 1970s and at the beginning of the 1980s, the Swedish iron ore producer LKAB investigated the mineral resources of the country, also covering the Archaean iron ores in the area north of Manica (LKAB 1978). Between 1981 and 1984, Hunting Geology and Geophysics Ltd carried out a comprehensive mineral exploration and reconnaissance geological mapping project, covering Tete Province and parts of Manica, Sofala and Zambézia Provinces (Hunting 1984). Due to security risks at the time because of a civil war, the mapping of Archaean areas by the Hunting team was very limited. The publication of a new geological map of Mozambique (Pinna *et al.* 1987) at the scale 1:1 000 000 provided new insights into the geology of the

country (Pinna *et al.* 1986). Since this period, only a few papers have been published on the Archaean in Mozambique. For example, Manhiça *et al.* (2001) studied the deformation and metamorphism of the Archaean and Proterozoic boundary.

In Zimbabwe, close to the Mozambican border, mapping and several investigations on the craton and its northern margin have been carried out during recent decades (e.g. Stockmayer 1980, Barton *et al.* 1991, Dirks *et al.* 2003, 2006). According to Barton *et al.* (1991), the northern margin of the craton contains a mixture of thrust masses or 'nappes' that include Archaean, Mesoproterozoic/Kibaran (~1.0–1.4 Ga) and Neoproterozoic/Pan-African (0.8–0.5 Ga) components. This northern allochthonous terrane is known as the Migmatic Gneiss Terrane and extends into Mozambique.

The Archaean Odzi-Mutare-Manica and Cronley-Munhinga greenstone belts that extend from Zimbabwe to Mozambique have been extensively studied in Zimbabwe (e.g. Coward *et al.* 1976, Vearncombe *et al.* 1988, Chenjerai *et al.* 1993, Wilson *et al.* 1995), but maps and papers from the Mozambican side are rather limited (e.g. Manuel 1992 and unpublished maps related to gold exploration).

REGIONAL GEOLOGY

Most of the Archaean rocks on the Mozambican side are TTG granitoids and gneisses, corresponding to those described in neighbouring areas in Zimbabwe. Archaean greenstones are met only in the Manica area and south of it. Two greenstone belts extend to Mozambique from Zimbabwe, the Odzi-Mutare-Manica and Cronley-Munhinga Greenstone Belts, which continue in Mozambique for some 25 km in an E-W direction (Figs 2–3, 4A).

The present data do not allow the granitoids of the granite-greenstone terrain to be subdivided into age groups, but a few kilometres wide tonalite terrain (Fig. 4B) east of Manica yielded the oldest known age in the area (2.9 Ga, Mänttari this volume). The main lithologies comprise TTG gneisses, granitoids and minor gabbroic rocks. In the southern, autochthonous part of the craton margin the Archaean rocks are attributed to the Mavonde Complex, the term applied in Mozambique, while the reworked Archaean granitoids and gneisses of the northern part (Figs 4F, 7B, 7F, 11C–D) are attributed to the Mudzi Complex, the term quoted from the adjacent part in northeastern Zimbabwe (Barton *et al.* 1991).

These two have been combined in the map drawings below (Figs 2–3, 5–6).

The Manica Greenstone Belt represents the eastern extension of the Odzi-Mutare Greenstone Belt of Zimbabwe. These are collectively called the Odzi-Mutare-Manica Greenstone Belt. The Manica Greenstone Belt is subdivided into (from bottom to top) Macequece and Vengo Formations. The Macequece Formation is principally composed of ultramafic and mafic metavolcanic rocks (Fig. 4C–D) with intercalations of banded ironstone and meta-chert. Serpentinites are common and are accompanied by talc ± chlorite ± tremolite schists. The contact between these two rock types is often vague and transitional. Spinifex textures are not uncommon in these ultramafic metavolcanic rocks. Andesitic, dacitic and rhyodacitic metavolcanic rocks, mostly pyroclastic in origin, overlie the mafic-ultramafic metavolcanics. Some elongated, narrow zones of lithic breccias and diamictite (Fig. 4E) occur stratigraphically between the mafic-ultramafic and the felsic-intermediate metavolcanic rocks.

Major lithologies of the Vengo Formation in the north eastern part of the belt comprise graphitic phyllites and thin interbeds of quartzite with grey marble, BIF and ferruginous lithic quartzite. The only known metagreywackes are located in the southwest as an extension from Zimbabwe.

The Cronley-Munhinga Greenstone Belt crosses the Zimbabwe - Mozambique border some 50 km south of the Odzi-Mutare-Manica Greenstone Belt. The narrow Cronley-Munhinga sequence (5 km to less than 1 km wide) is only composed of mafic and ultramafic metavolcanics and their metasomatic derivatives, with some quartzite.

Proterozoic lithologies dating back to Palaeo-, Meso- and Neoproterozoic Eras rim the Archaean craton margin and its outskirts. The oldest cover rocks on the basement belong to the metasedimentary-metavolcanic sequence of the Rushinga Group in the northernmost part (Figs 5–6) and its equivalent, the metasedimentary Gairezi Group in the central and southern parts of the craton margin (Figs 2–3). The Nhamessola Formation, including voluminous very coarse marbles, occurs at some distance from the known craton margin, south east of Mungari (blue spots in Fig. 1). Based on new radiometric age determinations of detrital zircons (Mänttari this volume) of the Rushinga and Gairezi Groups as well as on isotopic analyses revealing elevated $\delta^{13}\text{C}$ values (Karhu 2006) in the carbonate rocks from the Rushinga Group and the Nhamessola Formation, a Palaeoproterozoic age of sedimentation for all these units is concluded.

The Rushinga Group is subdivided into an older Rio Embuka Formation, principally composed of quartzite and pelitic metasediment and overlying the Monte Pitão Formation consisting of marble, metapelite and quartzite (Fig. 14). The Nhamessola Formation consists of the marble equivalent to the Monte Pitão Formation. The Gairezi Group is composed of quartzite and mica schist with minor marble and resembles the lithology of the Rio Embuka Formation. Occurrences of conglomerate are found below the Gairezi quartzite southeast of Manica. The quartzite of the Rushinga and Gairezi Groups is composed of very coarse sugary quartz, with little muscovite. Minor sillimanite in the quartzite occurs in the north, in the area of highest regional metamorphic grades. The bedding of the quartzite

is rather vaguely expressed or not identified. Furthermore, it is usually obscured by overprinting features such as weakly developed foliation or modest pressure solution bands. Cross bedding is occasionally found in the Gairezi quartzite. In contrast, the schistosity is strongly developed in the Gairezi mica schist, and is composed of at least two generations. The early fabric is a continuous fine schistosity, while the overprinting feature is coarse crenulation or spaced schistosity (Fig. 12H). The mica schist of the Rushinga Group is frequently dotted by fibrolitic sillimanite nodules in the north, while further south in the equivalent Gairezi Group the mica schist is characterised in places by abundant large prisms of kyanite and staurolite plus abundant garnet. The area west of Guro-Catandica (Fig. 12G), in particular, is illustrative in this respect. Sillimanite also occurs in the Gairezi mica schist close to the edge of the craton margin east of Manica, demonstrating the growth of metamorphic grade to the east in the southern part of the craton margin.

The Mesoproterozoic Báruè Complex in juxtaposition with the Archaean craton margin east of Manica is a part of the Mozambique belt. It is composed of a variety of medium- to high-grade gneisses, migmatites and granitoids, with subordinate intercalations of mafic rocks, quartzites, marbles and associated calc-silicate rocks. The sedimentary protoliths of these lithologies most likely correspond to monotonous turbiditic sequences originally deposited at the passive continental margin of the Kalahari craton.

Abundant masses of Neoproterozoic intrusions characterize the east-dipping outer rim of the craton margin in the north, where eastwards they gradually take all space from the Palaeoproterozoic metasediments overlying the basement. This felsic-mafic intrusive association was identified and dated by the current project and named the bimodal Guro Suite. The felsic component consists of fine-grained, foliated aplitic granites, occasionally injected by pegmatite veins to make a migmatitic aspect. The mafic component is represented by metagabbro, locally deformed into mafic gneiss or schist with intruding pegmatite. The generally strict parallelism of the two layer-like components has produced a visually spectacular alternation of pale and dark bands when viewed in cross section (Fig. 13C).

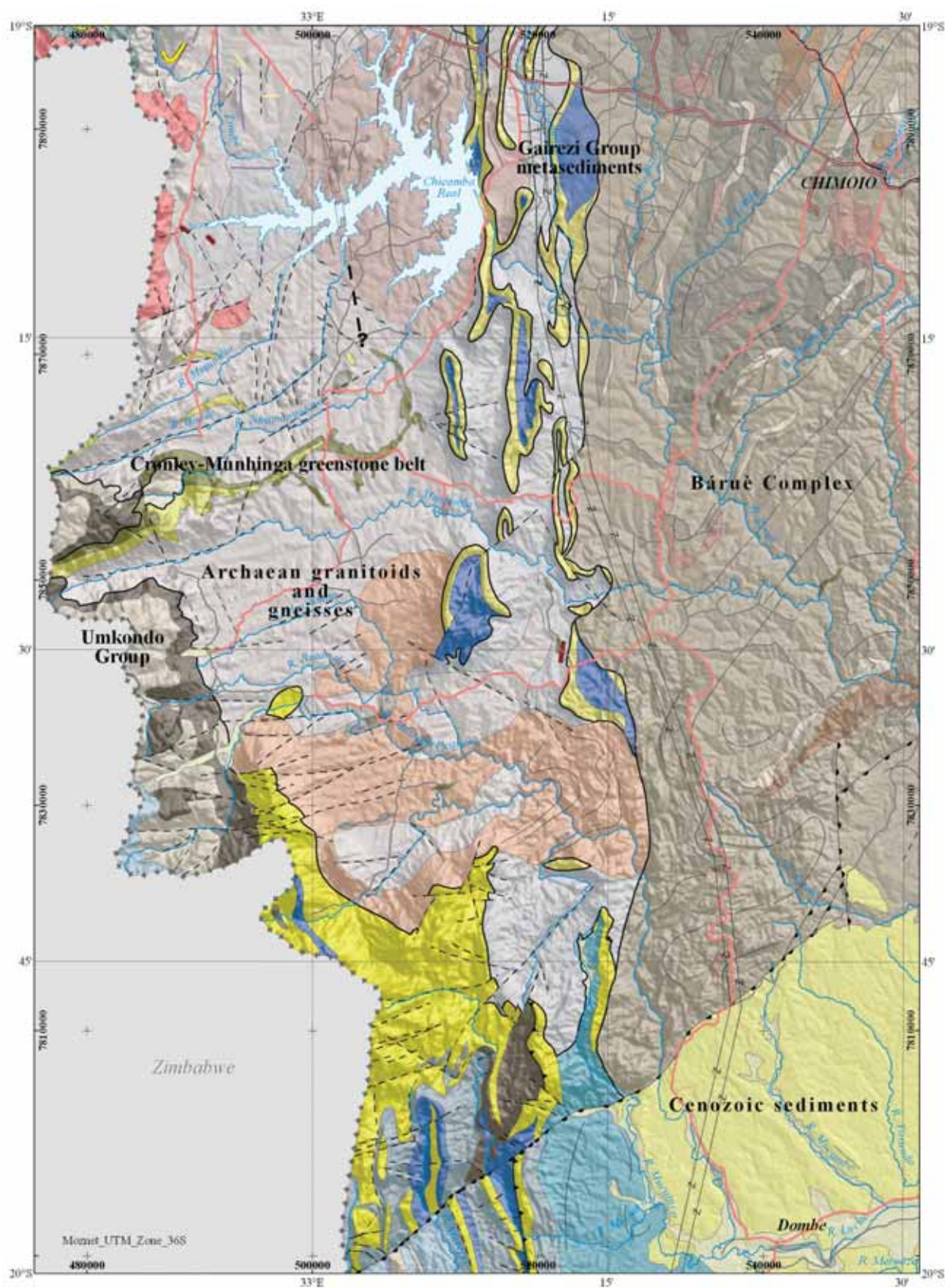


Fig. 2. Southern part of the craton margin. See text for details.

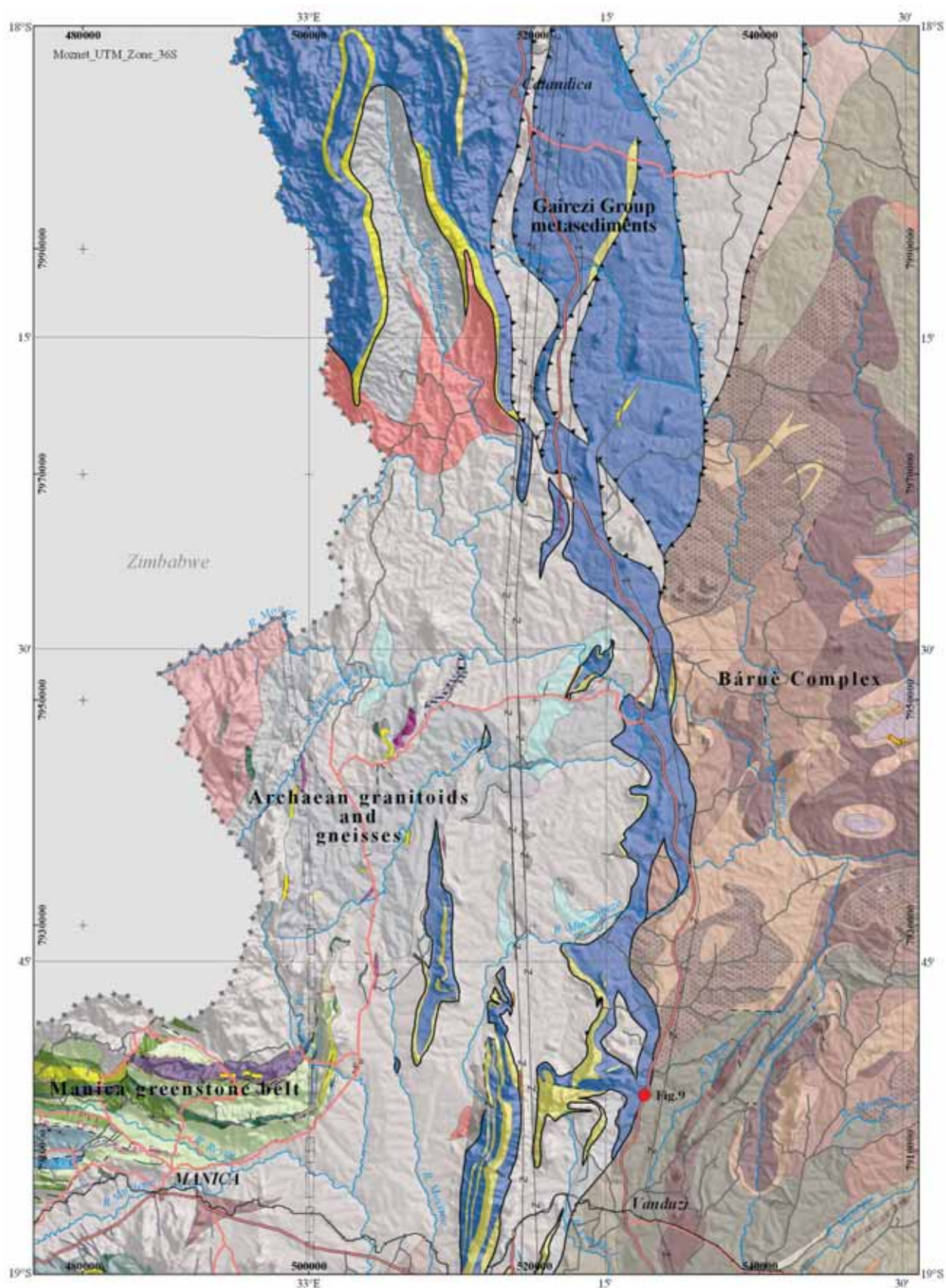


Fig. 3. Craton margin east of Manica. Note the symbol line at ~ 33°E: the approximate western extent of post-Archaean tectonic/metamorphic overprinting.

OBSERVATIONS OF VARIABLE STRUCTURAL STYLES ACROSS AND ALONG THE CRATON MARGIN ZONE

It is clear that there is east-west lithological zoning across the craton margin zone. The uniformly exposed craton margin in the west is characterized by an Archaean gneissic-migmatitic basement, rimmed by visually quite contrasting Palaeoproterozoic Rushinga-Gairezi metasedimentary, nonmigmatized sequences. More to the east, the generally east-dipping cover metasedimentary sequences become replaced by various types of intrusions, dating from Mesoproterozoic and Neoproterozoic times.

It is also clear that the structure style varies in the area, and various tectonic levels are exposed. The setting is promising for studying the variable products of structural evolution, both laterally and vertically, at the eastern margin of the Zimbabwe craton. For convenience, the description below is therefore divided into sections according to the dominant characteristics of each subdomain.

Intact Archaean, Manica

The city of Manica lies slightly south of the east-west running Manica greenstone belt, which is the eastern part of the Odzi-Mutare-Manica greenstone belt. The TTG granitoids on each side of the belt meet the greenstone lithologies along shear zones. The granitoids are solid, variably orientated-foliated or frequently gneissic, even migmatitic. Porphyritic varieties occur.

The common regional structural grain of the Manica area in Mozambique and the Odzi-Mutare area in Zimbabwe tie both areas to the unmodified Archaean craton itself, while the reoriented struc-

tures only in the east represent the modified part of the craton, closer to its true margin (Manhiça *et al.* 2001). The structural trend in Mutare and Manica is east-west, thus at right angles to the craton margin, which is 60 km east of Manica. No overprint on the Archaean at Manica region is reported in the isotopic data from the 2.9 Ga tonalite (Fig 4B) in the eastern vicinity of Manica (Mos-23, Mänttäre this volume). The ~1.8 Ga mafic dyke (Mos-25, Mänttäre this volume) cutting the greenstone belt north of Manica is undeformed.

Overprinted Archaean: the craton margin east of Manica

About 20 km east of Manica the eastern tip of the Manica greenstone belt rather abruptly swings towards the north. The northerly trend dominates everywhere in the tens of kilometres wide marginal part of the craton, and it is clearly parallel to the well-defined boundary against the Mozambique belt in the east (Figs 2 and 3). The Palaeoproterozoic Gairezi quartzite and mica schist outliers in the area form highly compressed, upright, narrow subcontinuous and interlocking synclines with horizontal north-south axes. The sense of curving from an east-west to a north-south trend east of Manica demonstrates a sinistral component in the overprinting deformation, most recently active at ~470–500 Ma ago (Manhiça *et al.* 2001). The Archaean Messeca granodiorite (dated sample Mos-30) in the reorientated terrain east of Manica has obviously recorded the effects of a ~500 Ma thermal overprint (Mänttäre this volume). While the 2.9 Ga old tonalite at Manica did not record such effects, the boundary of the western extent of the overprint is also well constrained

on this basis. The estimated NNW-running boundary between the intact Archaean in the west and the overprinted Archaean in the east is marked on Figs 2 and 3, also quoting information from nearby areas in Zimbabwe (Stocklmayer 1980).

During the formation of narrow, highly compressed synclines of the overlying Gairezi schists, the underlying Archaean basement must have suffered some tectonic shortening in an E-W direction. Although much of the Archaean fabric of the granitoids has been preserved in hand specimens and on an outcrop scale, similar to those in the intact Manica domain, sets of narrow penetrative shears frequently occur. The variable sets of shears probably represent accommodation of the previous trend into the new dominant orientation.

Keeping in mind that further north there are extensive thrust sheets, the question arises of whether the Gairezi metasediments represent direct deposition on the basement in this area, or whether they were tectonically transported before the forma-



Fig. 4. Photographs of various aspects of Archaean exposures.

A) A view towards the NE from Serra Isitaca. The Penhalonga valley is in the foreground, the forested ridge of Serra Penhalonga beyond and the hazy range of Serra Vengo in the background.

B) The oldest dated rock in Mozambique, the tonalite east of Manica (0491095/7904308, Mos-23, Mänttari this volume).

C) Spinifex-textured ultramafic komatiite of the Macequece Formation. The scale bar is 8 cm (0477781/7914693).

D) Basaltic pillow lava of the Macequece Formation. The scale bar is 8 cm (0486694/7914559).

E) Diamictite with angular to subrounded blocks of banded ironstone, metachert and a minor amount of metavolcanic rocks. Macequece Formation, Serra Penhalonga. The scale bar is 8 cm (0477114/7912164).

F) The surfaces of the Archaean gneiss exposures are readily stained dark, as seen below the third author in the figure (0526500/8024322).

tion of the synclines. Unfortunately, however, the basal contact of the Gairezi quartzite or schist on the basement is not usually exposed owing to talus debris at the roots of the ridges. The few observed

conglomerates close to the base are in rather poor condition. The mica schist is commonly present in the cores of these synclines, but this contact is also seldom exposed.

Taking into account the prominent expression of thrust tectonics north of Manica, and in reference to a similar history at the Kalahari craton margin in the south (Manhiça *et al.* 2001), it is likely that thrust tectonics even effectively operated here. If so, this was mostly in upper levels that now been removed. There is some evidence of recumbent deformation within the schist packs of the quartzite-schist synclinal outliers. For example, there are isoclinal folds within the Gairezi mica schist in a limb of an open, upright syncline east of Manica, close to the underlying Archaean bedrock surface (Fig. 10C). A mafic dike dated at ~1 Ga (Mos-37, Mänttari this volume) crosscuts at high angles the foliation of the schist in this outcrop, therefore positioning the isoclinal folds and potential related thrusts to be older than 1 Ga. For reasons discussed later on, even two periods of thrusting are postulated with unknown evolution in between.

The Mudze River profile as far as 220 km to the north (Fig. 7, for location see Fig. 6) shows compa-

table tectonic features. The canyon formed by the Mudze River allows observation of the structure in a continuous outcrop. The Palaeoproterozoic (Mos-20, Mänttari this volume) contrasting sedimentary strata, the quartzite and schist, are here separated by a subhorizontal shear zone (Fig. 8D). In the middle of the profile the shear zone was folded into an upright syncline. Even here the syncline and the minor folds elsewhere in the river channel trend north-south with horizontal axes, analogously to those east of Manica. Notably, the several decimetres thick product of shearing has been recrystallised into a solid metamorphic rock, implying an overprinting thermal pulse. The Pan-African thermal pulse is detected in the nearby dated Archaean sample Mos-7 (Mänttari this volume).

The Mudze River profile in the north represents a structural analogy to the overprinted Archaean crust with cover outliers east of Manica. Unequivocal evidence of major thrusting in the area between these two regions is demonstrated later on.

Termination of the Archaean crust against a major shear zone, east of Manica

Archaean rocks are not found east of a major sinistral strike-slip shear zone running north-south, 60 km east of Manica. Nor do the Palaeoproterozoic Gairezi quartzites and schists extend beyond the shear zone. Likewise, the rocks of the Mozambique belt, locally the Mesoproterozoic Bárue Complex, do not cross the shear boundary from the east. The total width of the shear zone presumably varies owing to transpressional-transtensional relations, with mixing of fragments from each side.

No natural outcrop just within the shear zone was found. Incidentally, by the side of a paved highway north of Vanduzi there happens to be an exposure where a narrow contact zone between the above-described major crustal blocks is exposed in a man-made ditch, which is washed by seasonal rainwater. In the ditch the western boundary of the Bárue block is in contact with Gairezi quartzite, which rims the Archaean crust (see details in Figures 9–10, for location see Fig. 3). The Gairezi schist/quartzite association in the next road cut to the north is also affected by shearing, although the eastern block is not exposed there.

The Archaean-Mesoproterozoic block boundary was traced northwards and southwards from the above-described observation point. Due to the scarcity of outcrops, observations were made on the colour of soils *in situ*. The task was made easier by

a practically diagnostic red-brown darkish soil resulting from weathering of the Gairezi mica schist, mostly rimming the craton edge and also scattered into separate domains, while on the 'Bárue side' of the shear zone the local soil is pale and yellowish. Soil on the Archaean granitoid is pale, usually rather grey, even whitish. Brown soil on mafic dykes or sills mixes these hues. Owing to such readily available information on the soil colour for each rock type, the shear zone and the mentioned major lithological domains were probably outlined with great accuracy, even in areas with few outcrops.

On the eastern side of the shear zone, the Bárue Complex extends a hundred kilometres eastwards, where it meets the fault-bounded troughs of Karoo and Cretaceous sediments. The Bárue Complex is mostly composed of granitoids and felsic gneisses, largely of intrusive origin, while some other units carry preserved supracrustal elements shown by obscure bedding and concretions related to bedding within sometimes highly fused material. Datings of some intrusions yielded late Mesoproterozoic ages (Manhiça *et al.* 2001, Mänttari this volume), while the migmatitic supracrustal units and enclaves have not been dated.

On the map, large smooth curves of planar structures characterize the area of the Bárue Complex. They illustrate the generally flat attitudes of rock

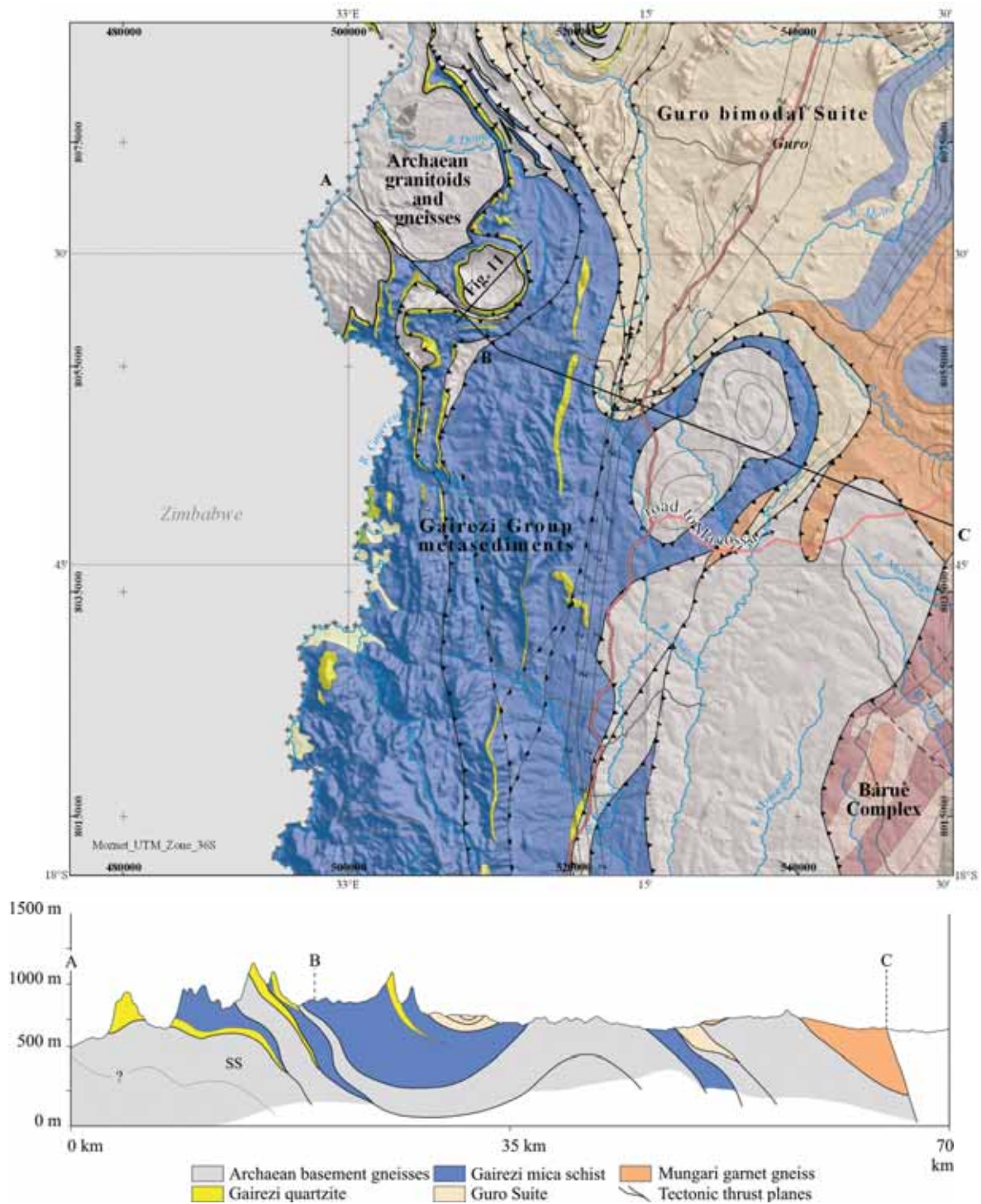


Fig. 5. Middle part of the craton margin. The long profile A-B-C (lower part of the figure) illustrates an interpretation of the extensive imbrication structure, mixing stratigraphy. Note the slight upwarp marked by a pair of letters (SS) written in the profile A-B-C. Just behind the profile the upwarp has grown to form the Senga Senga dome: cf. Fig. 11. East of C (white in the profile) the bedrock belongs to the Bárue Complex.

units, which have been bent to form open warps, domes and basins. This is particularly clear in the northern part of the domain, where the alternation of tabular units is most clearly seen on satellite maps

(Schetselaar this volume) and confirmed in the field as well. The overall structural pattern of the Bárue Complex is in contrast to that of the adjacent Archaean-Palaeoproterozoic domain in the west.

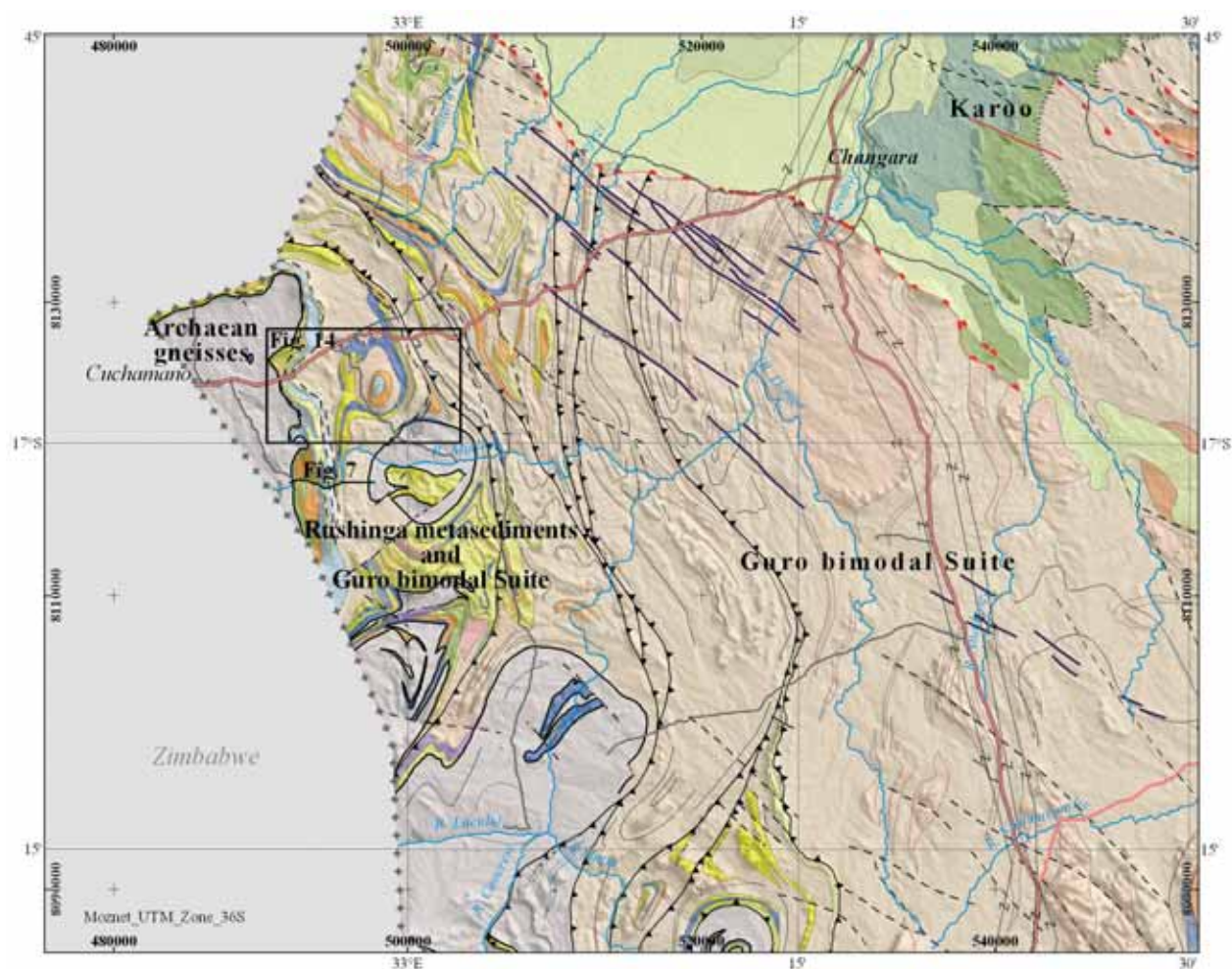


Fig. 6. Northern part of the craton margin, showing the Archaean crust dominating in the west, the Palaeoproterozoic Rushinga beds together with the Neoproterozoic bimodal intrusive Guro Suite in the middle, and ultimately only rocks of the Guro Suite in the outer margin. A northwest-southeast running silicified normal fault separating the Precambrian and Phanerozoic exposure is shown red south of Changara. See Fig. 15 A-B for its expression in the field.

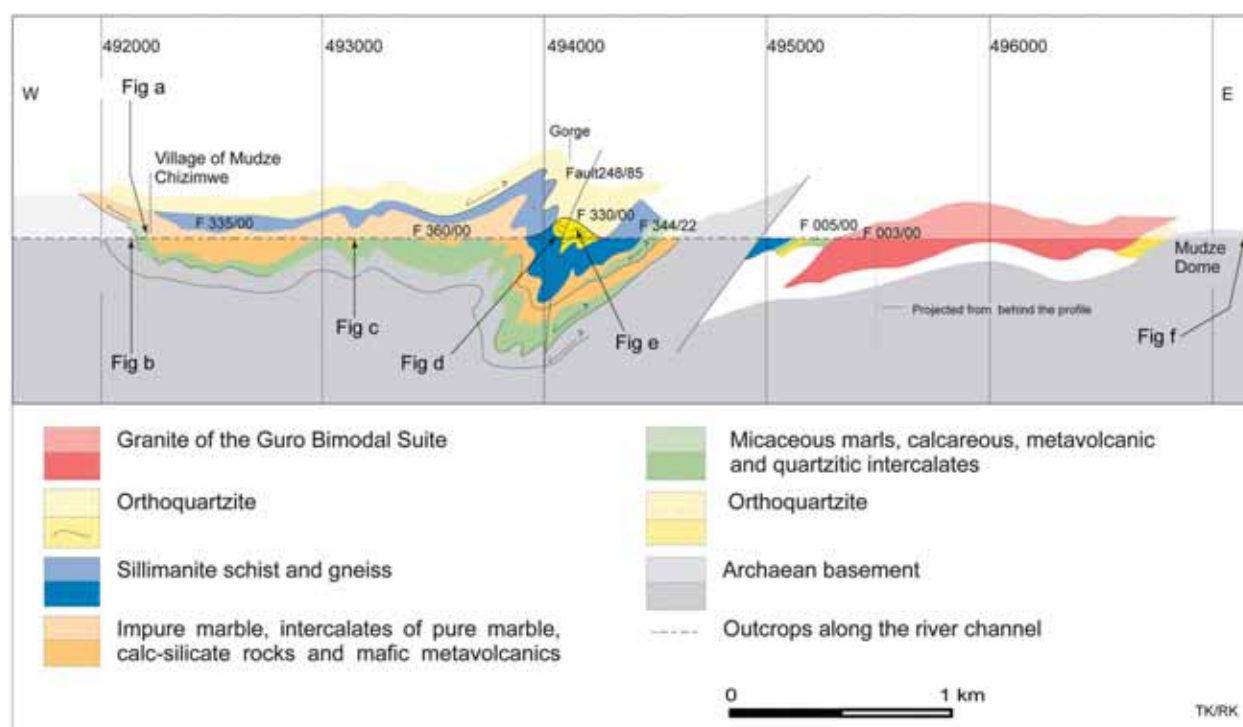


Fig. 7. An east-west profile along the Mudze River; for location, see Fig. 6. Markings 'Fig. a--f' refer to Fig. 8.

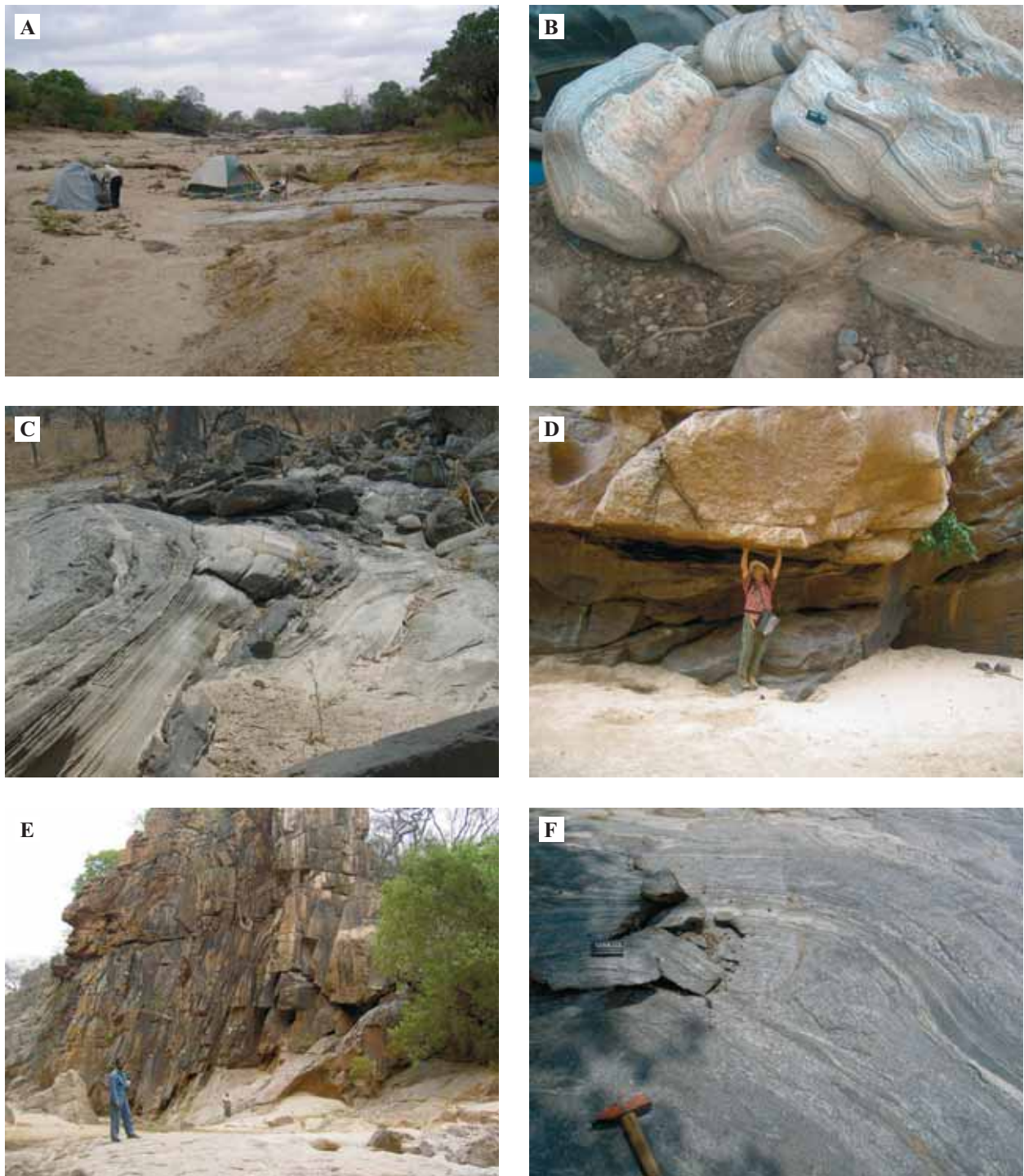


Fig. 8. Photographs of rocks and structures in the Mudze River profile (of Fig. 7).

A) Mudze River channel. The tents are on sand over white limestone; the outcrop in far background is Archaean TTG gneiss.

B) Archaean banded TTG gneiss.

C) Impure banded limestone.

D) Basal contact of massive white quartzite (touched by the first author in the figure), underlain by sillimanite schist with quartz-rich layers. The product of shearing along the basal contact of the quartzite, 10–100 cm thick, has been recrystallised into a secondary micaceous metamorphic rock.

E) An upright anticlinal fold of white quartzite, part of the polyhinge syncline with a north-south running horizontal fold axis, formed after the recumbent shears referred to above. Note the two field assistants for the scale. The surface of the white quartzite is decorated by brown vertical bands, precipitated from rainwater.

F) Archaean TTG gneiss from the Mudze dome, sample for dating in the tag site (05037824/8119250, Mos-7, Mänttäre this volume).

Extensive thrust sheets north of Manica

Towards north the shear zone at the eastern craton margin is subvertical east of Manica and continues northwards, but when turning towards the east it also transits into a south-dipping thrust surface. This is the northern boundary of the Bárue Complex southeast of Mungari (Fig. 5).

North of Manica, the Gairezi metasediments increase while exposures of the Archaean basement decrease (Figs 3–5). This means that the Archaean crust plunges down towards the north, where the stratigraphic-tectonic level consequently becomes higher. Close to the uniform Archaean area in the west the basement occurs in domes, and to the east both in domes and as long narrow bands. Some of the domes with dated Archaean cores have also previously been described (Hunting 1984, Dirks pers. comm. 2004). Domes in the area with relatively flat attitudes of the cover strata on the basement demonstrate the rather horizontal general attitude of the basement-cover junction.

Previously unknown occurrences of Archaean rocks were mapped even tens of kilometres east of the ‘traditional’ Archaean exposures (e.g. Mos-21, Mänttari this volume). The domal shape of the Archaean gneiss occurrences at the Macossa road junction is interpreted here as a domed tectonic slab (Fig. 5, profile A-B-C). Originally, an indication of the probably Archaean origin of rocks in this particular location was interpreted from processed radia-

tion images (Schetselaar *et al.* this volume), where the composite colour signature corresponded well to that in the uniform Archaean area known in the west, and was then confirmed by dating.

Figs 3, 5 and 6 show rather continuous tabular-shaped occurrences of Archaean gneisses, bound by thrust planes. Two profiles illustrate the structure in vertical section, their sites marked in Fig. 5. The 70 km long profile A-B-C across the area (Fig. 5, lower part) represents a section with an interpretation of several thrust sheets stacking in the region. The short profile across the Senga Senga ring structure (Figs 11–12) unambiguously explains the ring structure in the cross section as a dome overlain by a repetition of contrasting stratigraphic units. Thus, the Senga Senga proved to be a key place, supporting analogous interpretations in other parts of the area. The contacts between each contrasting unit at Senga Senga are mylonites, highly sheared, hidden in narrow ditches or gullies at its lowest levels, but well exposed on slopes. The separate Archaean sheet above the core and well exposed on the mountainside in the SW (Fig. 11; Fig. 12C, D) is relatively thin, but consistently continuous. On the map, elsewhere in the region and in the vicinity of this dome there are other bands of Archaean basement or quartzite of the Gairezi Formation. They may prove to be more continuous - and possibly more numerous - if the area is mapped in greater detail.

Termination of the craton margin against the Zambezi belt in the north and latest ductile structures

The northern margin of the Archaean Zimbabwe craton runs east-west, adjacent and parallel to the Zambezi belt, in Zimbabwe. Only marginally it extends to the Mozambican side before trending to the south (Fig. 1). Nevertheless, this particular minor part of the craton margin in the study area is illustrative.

The Palaeoproterozoic metasediments-metavolcanic rocks at the northeastern corner of the craton are incorporated in the Rushinga Group, a stratigraphic equivalent of the Gairezi Group in the south. In this respect there is no essential difference between the southern and northern parts of the craton margin. The real difference comes from the occurrence of Neoproterozoic to Palaeozoic magmatism only in the north. This is represented by the Neoproterozoic bimodal Guro Suite and subsequent pegmatites. The former are most abundant in an extensive area east of Cuchamano, around Changara (Figs 1 and 6), the latter south and west of Tete. The southernmost known exposure of the Guro Suite (0533953/8038289), east of the Macossa road junc-

tion (Fig. 5), is adjacent to a local exposure of the Archaean basement gneiss (0533988/8038382). On the whole, the distribution of the Neoproterozoic intrusive activity extending from northern Zimbabwe (the Basal Rushinga Intrusive Complex – BRIC, Barton *et al.* 1991) to Mozambique (the Guro Suite) seems to form an east-west zone, parallel to the Zambezi belt. The distribution of the pegmatites, rapidly becoming rare and not occurring to the south of Changara, also seems to form an east-west zone, possibly representing the ‘pegmatite province’.

The rocks of the Guro Suite have not been found to intrude the exposed Archaean basement, although the undefined eastern tip of the basement, buried amongst the Guro Suite, remains a question mark in this respect. The granite-gabbro association of the Guro Suite comes close to the basement in the area east and southeast of Cuchamano (see Figs 6 and 14), much like the Neoproterozoic rocks of BRIC in Zimbabwe.

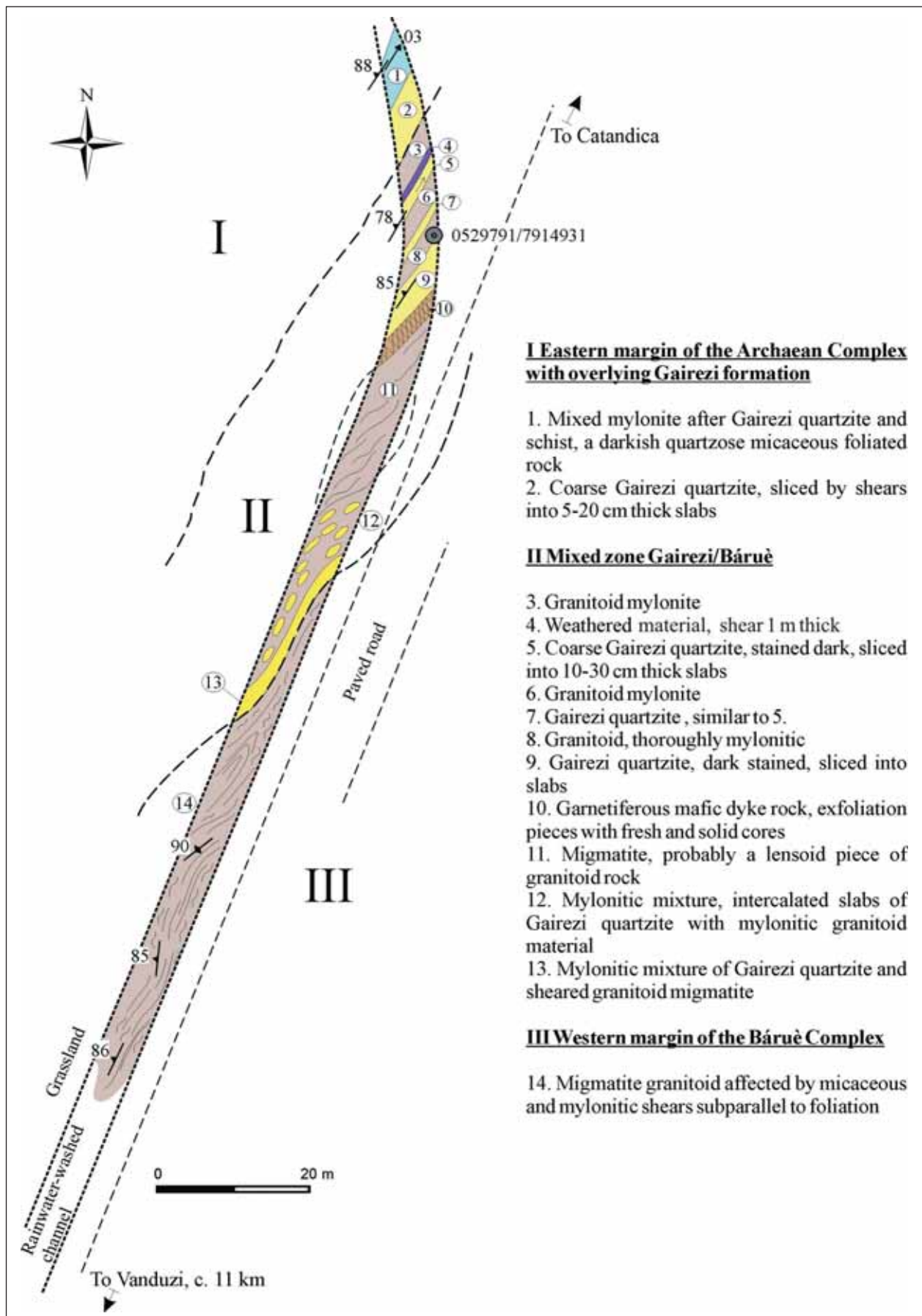


Fig. 9. A roadside ditch bottom outcrop, which represents the core region of the shear zone between the Archaean craton margin and the Báruè Complex of the Mozambique belt. For location (0529791/7914931), see Fig. 3; see also Fig. 10A.

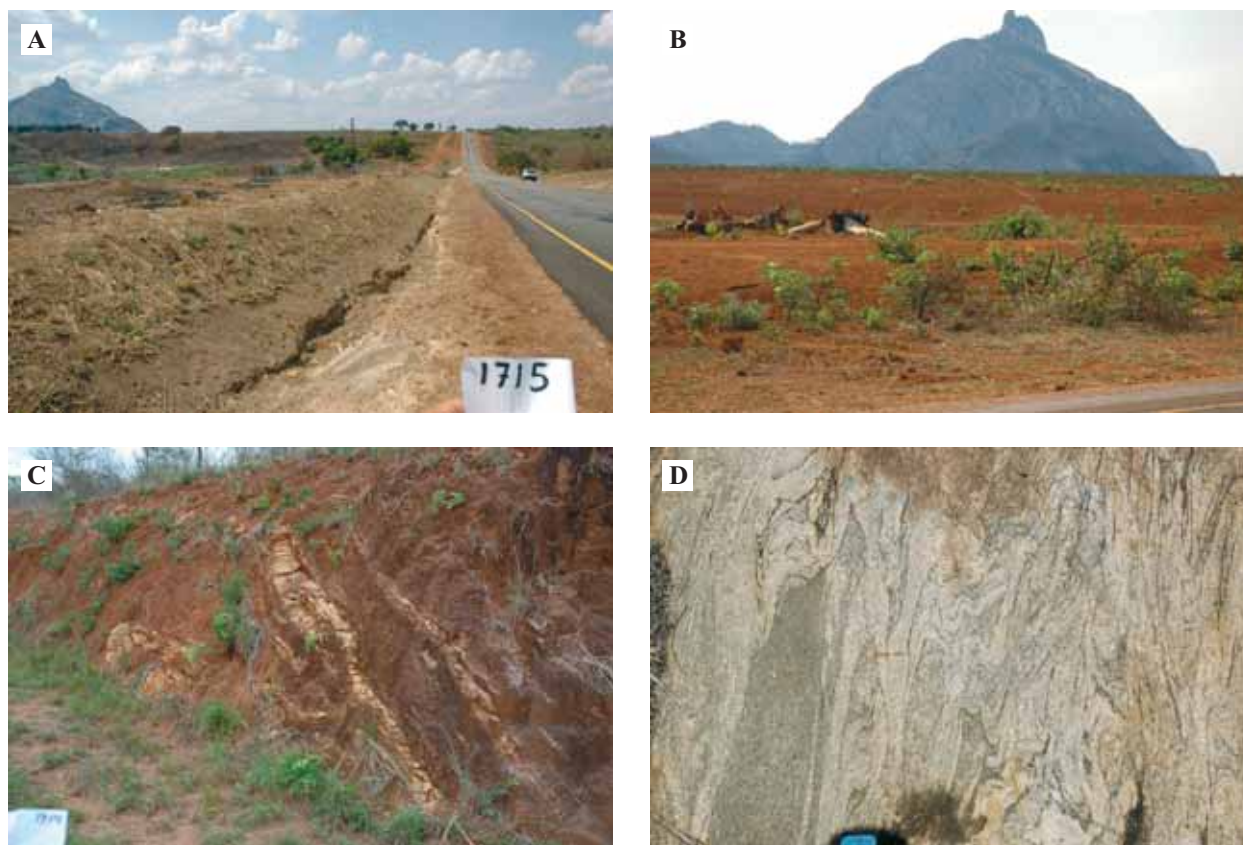


Fig. 10. Photographs of various aspects related to the exposure and surroundings in Fig. 9.

A) The roadside ditch outcrop of Fig. 9, looking north. The foreground rock, migmatite, belongs to the Bárue Complex in the east. Note the pale soil after the Bárue rock in the foreground, and compare it to the red soil after the Gairezi mica schist in the background, which belongs to the western side of the shear.

B) A granitoid inselberg, the same as seen in Fig. A, surrounded by red soil after Gairezi mica schist.

C) Thoroughly weathered Gairezi schist, with quartz veins marking a fossil isoclinal structure, tilted in the limb of a subsequently formed syncline. A dated mafic dike cuts across the foliation of the schist outside the photo area (0515362/7896822, Mos-37, Mänttari this volume).

D) Complexly folded migmatite of the Bárue Complex, a little south of the roadside outcrop of Fig. A (0524566/7895154).

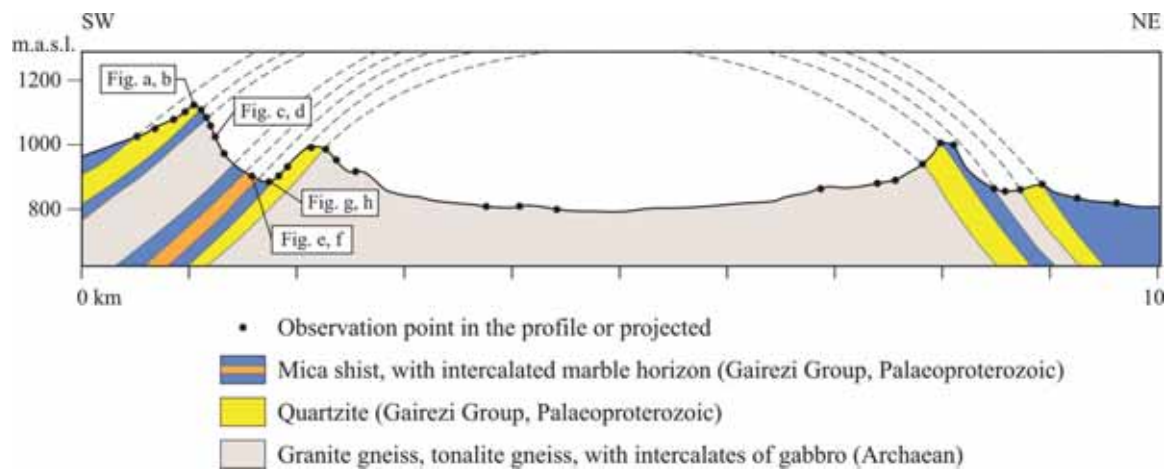


Fig. 11. A section across the Senga Senga ring structure; for location, see Fig. 5. Markings 'Fig. a,b—g,h' refer to Fig. 12.

► Fig. 12 (opposite page). Photographs of various units shown in the cross section, Fig. 11.

A) The highest point of a quartzite ridge at Senga Senga. The second author with a field assistant are standing on the south dipping layers of the white Gairezi quartzite (0510290/8059716).

B) A view towards the northwest. In the far horizon the Archaean flatland extends to the Zimbabwe border and beyond. The small inselbergs visible through the background haze are sizeable bodies of gabbro.

C) A rocky wall, 200 m high, exposing the tectonic sheet of Archaean banded gneiss, with (undated) mafic bands.

D) Close-up of the banded, migmatitic gneiss of Fig. 12C (0510304/8059871).

E) An outcrop of Gairezi marble with quartzitic intercalates (058901/8062183).

F) Close-up of marble.

G) Gairezi mica schist containing abundant kyanite, garnet and staurolite (0510745/8060168).

H) Gairezi mica schist, showing the silky shine of an early, fine and continuous schistosity, crenulated in the axial surface of subsequent folds (0507904/8064042).



The felsic and mafic intrusive components of the Guro Suite usually occur together as extensive intercalating sheets (Figs 13B-C). The felsic sheets, which dominate over the gabbro, also occur alone in many outcrops, and obviously owing to their better weathering resistance they tend to form narrow ridges if the sheets are tilted (Fig. 13 A). In extensive parts of the area the attitude of the sheets is shallow (Fig. 13C) to subhorizontal, which implies that the thickness of the whole Guro Suite mass may be rather small, perhaps 1-1.5 km at the most, excluding the alien intercalates. In the outermost areas, at some distance from the craton margin, the regional structural pattern becomes more complex due to crossfolding (cf. Figs 13F, an example at the outcrop scale).

The strikingly 'banded' aspect of the mafic-felsic association everywhere within the Guro Suite results from its early history. On close inspection it is observed that not only are the components strictly parallel to each other, but they also contain an internal layer-parallel foliation, which in the felsic component is a mesoscopic streaky fabric, and in the gabbroic component rather a fine grained schistosity. The individual gabbroic layers are usually thinner than a couple of metres, including abundant black bands one or two centimetres thick. While tracing the black bands laterally, boudins of well-preserved and coarser-grained gabbro are met even tens of metres apart, with the streaky felsic component curving around. The uniform black bands, so often very thin, are here all interpreted as thinned, laterally extensive boudin tails. It is interpreted that the felsic-mafic association has been extensively, perhaps massively layer-parallel deformed. This early process seems to have been continuous, since the already extremely thinned black bands are frequently seen to be folded by isoclinal, extremely flattened folds (Figs 13D, E, F).

The common parallelism of the felsic-mafic intrusive sheets of the Guro Suite and the Palaeoproterozoic metasediments is a striking feature, which was further emphasized by continued recumbent tectonic deformation parallel to the intrusive sheets. Ever more injections were added and joined the layer-parallel deformation. Closer to the Tete area, where there are no Palaeoproterozoic metasediments, the Guro Suite magmas intruded porphyritic Mesoproterozoic wall rocks. They had probably already started to flatten, providing a guiding planar structure for the Guro Suite emplacement, and under the common conditions they became variably flattened to augen gneisses and flaser gneisses, and ultimately

ly also to strongly schistose derivatives. The whole process seems to have included multiple emplacement of the magma pulses in an active recumbent tectonic regime, magmatic flow, and its transition to recumbent tectonic deformation, all without interruption: an extensional tectonic regime. An extensional Neoproterozoic tectonic regime has been reported in the neighbouring northern margin of the Zimbabwe craton (Barton *et al.* 1991, Dirks *et al.* 1998, Dirks & Jelsma 2006).

Pegmatites provide an extra tool for tracing latest tectonic movements and metamorphic temperatures in the area. They cut straight across the internal fabric within the Guro sheets. Hence the recumbent fabric-forming deformation of the Guro Suite came to an end before the intrusion of the pegmatites. In places the pegmatites have later been deformed and material is squeezed fabric-parallel into the wall rock, where the pegmatitic mobile material is sheared into rows and pinch-and-swell accumulations of size-reduced grains, which results in thin layers of migmatitic banded rock. Although they are minor features on the outcrop scale, they may be the equivalents of much greater strain localised somewhere in the same region. On the map of the area (Figs 5 and 6) tectonic thrust surfaces have been drawn separating different intrusive sheets of the Guro Suite on each side, or with narrow layers of Rushinga meta-sediments in between. They may be understood as early thrust boundaries reactivated into backthrusts of the extensional phase, thereby serving as active channels for the emplacement of the Guro intrusive sheets, or they can also be read as thrust shears once more reactivating the fossil tectonic surfaces during the convergent Pan-African episode.

The late pegmatites are abundant south and west of the city of Tete, but their amount rapidly decreases southwards. In this area the Mesoproterozoic foliated and folded intrusions make up the majority of the bedrock. The abundant pegmatites often contain large enclaves of wall-rock-forming mega-agmatites. The rounded shapes of the originally sharply angular pegmatite dike corners demonstrate flattening of the agmatites by E-W compression.

Finally, the Pan-African convergence ended up with the formation of upright small to moderate folds (Fig. 7; Figs 8C, E), and many large folds, such as the hundreds of metres wide north-south synclines of the Gairezi outliers east of Manica (Figs 2-3). The likely timing of these events is ~500+ Ma, the timing of late thermal overprint shown in Archaean, Palaeoproterozoic and Neoproterozoic samples from the area (Mänttari this volume).

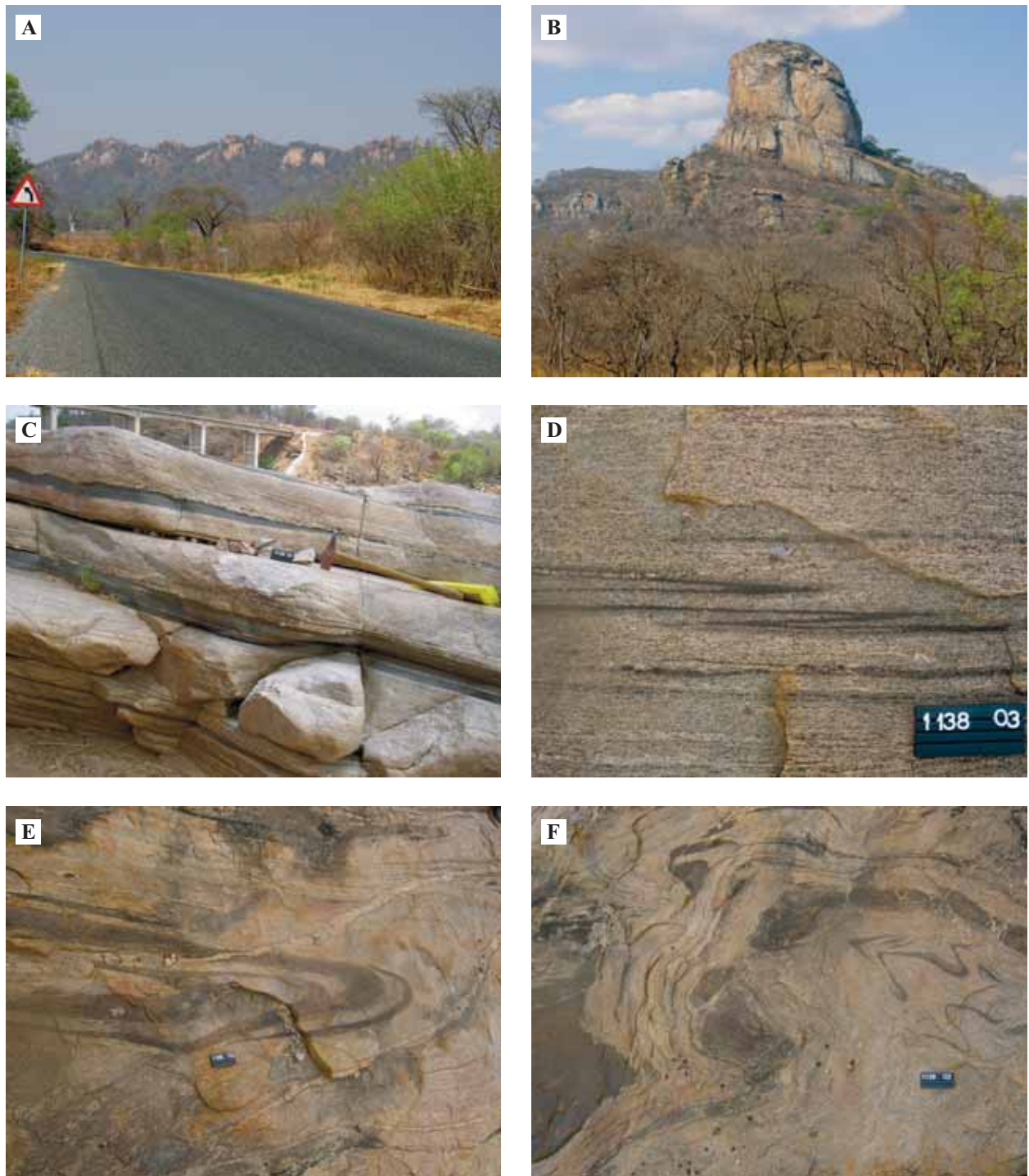


Fig. 13. Characteristics of the bimodal intrusive Guro Suite rocks.

A) Thick tilted bands of the felsic component form narrow, long ridges, as in this example west of Changara (0511131/8131226,).

B) Mt. Calinga Muci at the Mungari road junction is a spectacular landmark composed of gently dipping, thick felsic and thin mafic components of the Guro Suite (0543378/8089369).

C) Alternating felsic and mafic components of the Guro Suite with gentle dip, south of Changara. The sample for dating was taken from the hammer site layer (0527931/8134434, Mos-3, Mänttari this volume).

D) Tight folds of early fabric in the felsic component of the Guro Suite, with repetitive fabric in the new axial plane. An outcrop S of Tete (0551345/8192806).

E) Banded assemblage of the Guro Suite, with isoclinal, early fold hinges refolded at high angles by subsequent tight folds.

F) Banded assemblage of the Guro Suite, boudins of gabbro, deformed by a late generation of overprinting folds.

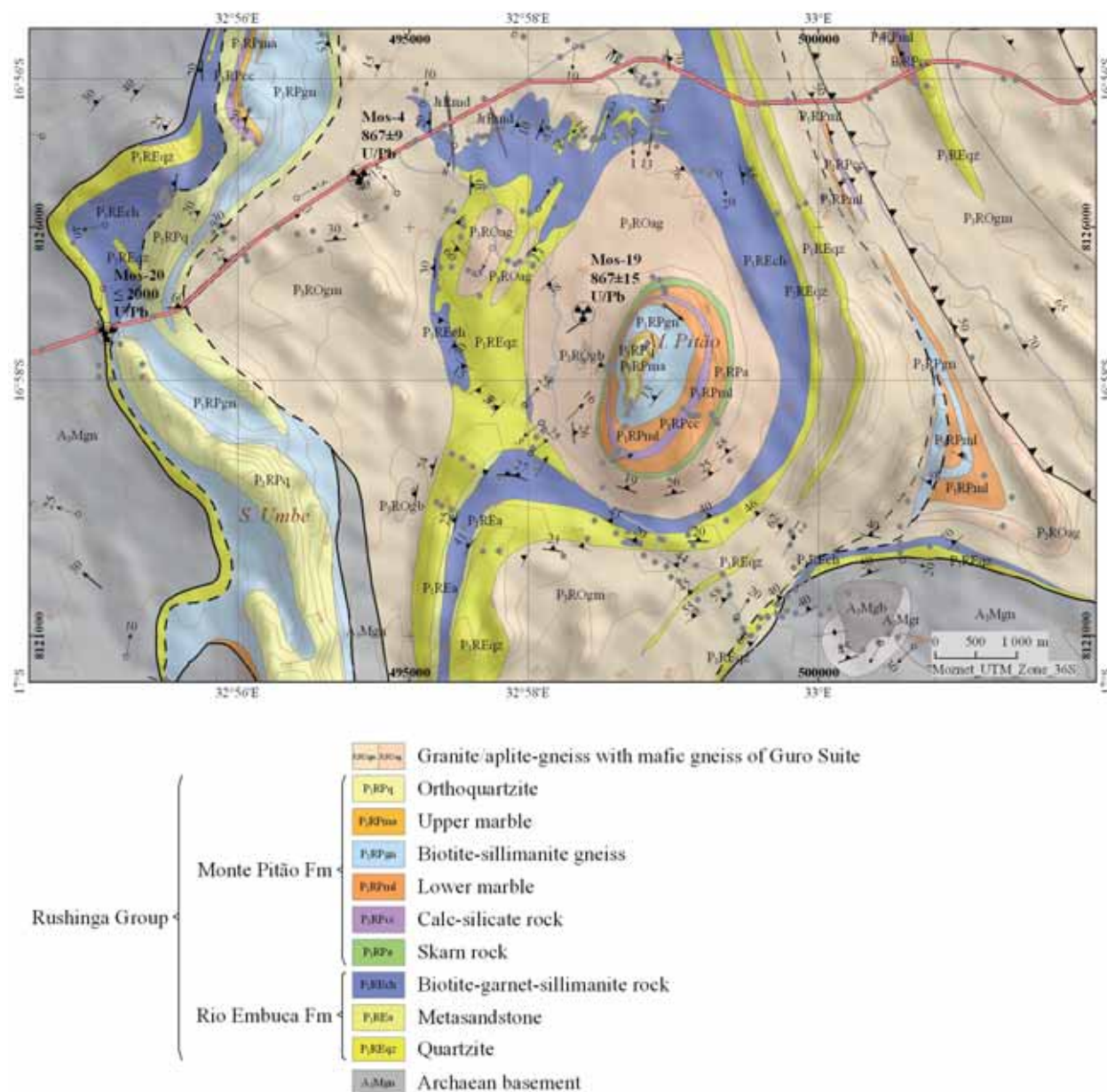


Fig. 14. The figure shows the abundance of the Neoproterozoic bimodal Guro Suite rocks conformably intruding the Palaeoproterozoic Rushinga stratigraphic pile in the vicinity of the basement-cover junction, east of Cuchamano. The Archaean basement gneiss (grey tone) extends from here to Zimbabwe, and also occurs as domes, one of which (the Mudze dome) is partly seen in the right hand lower corner of the figure. In the central part of the map the 200 m high hill is composed of upper Rushinga lithology, the Monte Pitão Formation. The underlying Rio Embuca Formation is exposed around the hill with gentle dips. For the location of the area in the map, see Fig. 6. For details concerning the three dated samples, Mos-4, Mos-19 and Mos-20 marked on the figure, see Mänttari in this volume. The sample (Mos-7, in Fig. 8F) for dating the Archaean gneiss of the Mudze dome came from slightly outside the figure boundary.

Late brittle structures: major faults

Latest major structures are characteristically rift faults, which control the deposition in the down-thrown side from Karoo to recent times. The continuing activity, related to the East Africa Rift Event, is manifested by earthquakes.

The Precambrian basement/Phanerozoic cover junction in the study area (Figs 2–3, 5–6) is almost invariably a steeply dipping normal fault, usually also separating an elevated terrain from the slightly lower ground of the downthrown side, the topography difference caused by more effective erosion of

softer rocks on the lowland side. On the present erosion level the material within the fault is composed of brownish fault gouge, a 10–30 metres thick tabular body produced by near-surface shearing. This has been brecciated with quartz precipitated into fractures. Frequently there are empty cavities with quartz crystals. Owing to the resistivity of the silicified fault zone, the basement-cover boundary is usually a linear ridge or a linear row of elongate hills. As to the timing of these faults, an observation close to the Changara bridge shows that a Karoo mafic

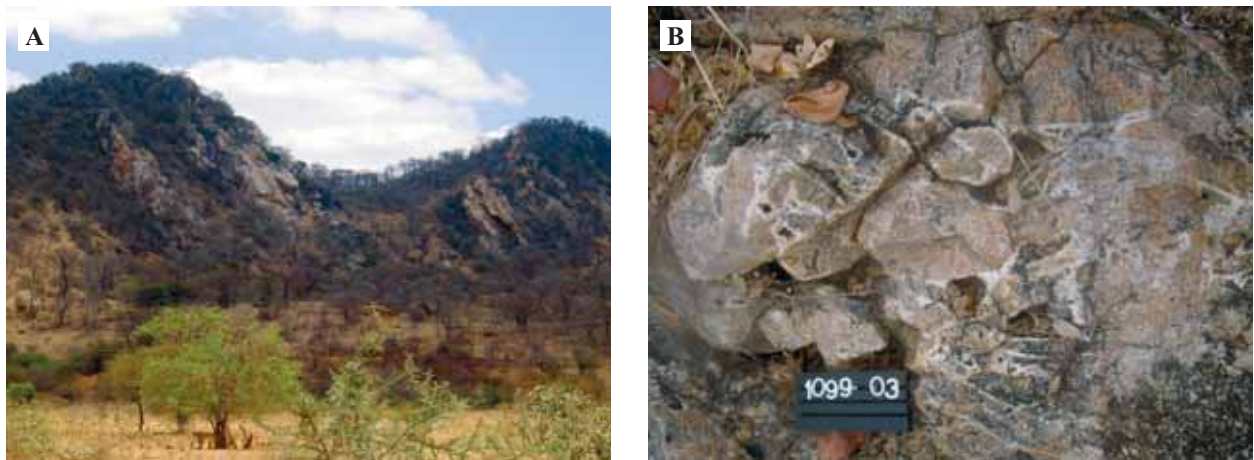


Fig. 15. Field expressions of late faulting.

A) A linear resistant ridge south of Changara, a steeply dipping silicified fault scarp, in the boundary between the Precambrian and Phanerozoic. See Fig. 6 for location.

B) Fault gouge, brecciated and silicified, from the ridge of Fig. A (0526099/8137092).

dyke has been affected. The roots of the fault scarps are covered by talus. Depending on the level of erosion, some of these faults cut across with the same lithology on each side.

In the study area an example of this class of faults is excellently seen on the southern side of the city of Changara, by the main road (red line with red spots in Fig. 6, expressions in the field shown by Fig. 15). Northwest of Tete (outside the present study area), where some of these faults also crosscut carbonates, the fault gouge breccia contains an association of platy 'porcelain' quartz plus carbonate.

Another class of faults distinctly separates elevated terrains from lowlands, without silicification along the fault. Examples in the study area are the

one running NNE on the western side of the city of Catandica (Fig. 5), and another one runs NE north of Dombe (Fig. 2) and crosses the border with Zimbabwe. The former is a hundreds of metres high fault scarp, through which a minor serpentine road leads to the Gairezi highlands close to the Zimbabwe border, a thousand metres higher than the city of Catandica. The mica schists of the Gairezi Group in the highlands with undulating topography are rather fresh and solid, while in the seasonally wet Catandica lowlands they have been thoroughly weathered into red soil, in part covered by laterite.

These latest topography-shaping faults are regarded as rift faults related to the East Africa Rift Event.

DISCUSSION AND CONCLUSIONS

Early in the fieldwork it became clear that the area from Tete to Guro, including the Cuchamano-Changara area (Fig. 1), has a unique feature compared to the craton margin zone further south. The presence of a voluminous bimodal intrusive suite, subsequently dated and named the Guro Suite, most clearly signalled this uniqueness. Its dating to the Neoproterozoic closely relates this part of the eastern craton margin to the neighbouring northern margin of the craton in Zimbabwe, where analogous Neoproterozoic magmatism has been reported and interpreted to record a Neoproterozoic phase of crustal extension. The abundant masses of subsequent pegmatites are also restricted to the north, mainly to the south and west of Tete. The metasedimentary-metavolcanic rocks rimming the Archaean basement are, however, the same all along the craton

margin, their detrital zircon dated to the Palaeoproterozoic. The outermost zone in the east is composed of Mesoproterozoic intrusions of the Mozambique belt, with supracrustal intercalates of unknown age.

Extensive thrust sheets were mapped on the eastern margin, resulting in tectonic mixing of the Archaean basement and Palaeoproterozoic cover. The long profile in the lower part of Fig. 5 schematically represents the likely structure. The northwestern part of the profile is well established (Figs 5 and 11), supporting the overall interpretation. Such an extensive thin-skinned structure is fundamental enough to justify a suggestion that it concerns the eastern craton margin in general. However, in the south, east of Manica, the uniform Archaean crust abruptly ends at the boundary with the Mozambique belt, without obvious thrusts in between. An explanation

for the local lack of obvious thrusts is visible on the geological map produced by the current project (Figs 3 and 5): the eastern boundary of the craton in this area is a transcurrent shear zone eliminating the southward continuations of the thrust sheets. The southern extensions of the thrust sheets would have been displaced out of sight in the present erosion level at the time when the Bárue Complex, a part of the Mozambique belt, moved sinistrally along the craton margin as a coherent block. Following the explanation of Manhiça *et al.* (2001), the present subvertical shear zone is understood as a steepened derivative of a thrust zone developed further south over the Kalahari craton. These authors dated this phase of thrusting at ~1100 Ma ago, in amphibolite facies conditions, and still found evidence of repeated shearing along the craton edge at ~500 Ma.

The northward movement of the Bárue Complex as a coherent block would explain the odd situation of the very coarse marbles of the Nhamessola Formation southeast of Mungari (blue spots on the map, Fig. 1). Their carbon isotopic composition (Karhu 2006) seems to relate them to the Palaeoproterozoic marbles common in the vicinity of the Archaean crust in the west. The very coarse Nhamessola marbles, the greatest concentration of which stretches over at least 20 km, are distributed along the northern margin of the Bárue block, along the eastwards-swinging continuation of the shear zone between the Archaean crust and the Mozambique belt east of Manica. A scenario in which the carbonates were tectonically transported away from their near-cratonic roots and relocated along the northern thrust boundary of the Bárue Complex would explain their present uncommonly eastern location.

The above consideration that the extensive thrust sheets are truncated by the major transcurrent shear zone east of Manica necessarily leads to the conclusion that these thrust sheets developed prior to the ~1100 Ma event demonstrated by Manhiça *et al.* (2001). Furthermore, the Palaeoproterozoic metasediments, including voluminous marbles of the Rushinga and Gairezi Groups at the craton margin, record the disruption of the Archaean crust and resulting marine basin at ~2 Ga ago. It has to be supposed that the closure of the basin took place within a reasonable time after 2 Ga ago, by the collision of the Archaean Zimbabwe craton with an unknown crustal segment in the east. What is now found in the east are 1000–1100 Ma old Mesoproterozoic intrusions with undated supracrustal intercalates. The

~1100 Ma thrusting event repeats the convergent evolution, while the potential intermediate evolution (collapse?) between the two remains open.

Tectonic boundaries and contrasting lithological boundaries are sites of potential inherited weakness and frequently they are zones of repeated tectonic movements. It seems that they have also served as channelways for the emplacement of the bimodal Guro Suite polyinjection magmas. The magmatic sheets of the Neoproterozoic (~860 Ma) Guro Suite are strikingly parallel to the metasedimentary beds of the Palaeoproterozoic Gairezi and Rushinga Groups, and further east-northeast parallel to the flattened structure of the Mesoproterozoic porphyritic intrusions. The flattening of the latter had possibly started under the early phase of the extensional development and continued together with the layer-parallel deformation of the Guro sheets.

The Guro Suite intruded the Palaeoproterozoic metasediments, which had not yet been folded by an upright style, but later both were folded by that style only while already being together. The unevenly distributed upright folding with a generally horizontal northerly fold axis of the Palaeoproterozoic-Neoproterozoic association in the north and the Palaeoproterozoic outliers east of Manica (e.g. Figs 3 and 7) took place probably not earlier than ~500 Ma ago. This suggestion is supported by a ~500 Ma thermal pulse all along the craton margin found in the dated samples, and is consistent with the fact that pegmatites crosscutting the completed planar fabric of the Guro Suite lithology are slightly to moderately flattened by E-W compression. As mentioned earlier, there is some evidence for one more phase of thrusting, or at least for reverse faults associated with the pegmatite emplacement, although probably limited to just a few wedges.

The late ductile deformation is hence divided into an extensional phase recorded by the Neoproterozoic Guro Suite and into the subsequent Pan-African Palaeozoic E-W compressional phase of the Mozambique belt deformation, in part complicated by crossfoldings in other directions.

Finally, postmetamorphic rift faults and selective erosion play an important role in shaping the landscape. The Phanerozoic rocks have generally eroded away, but some hard interbeds within the Karoo sediments or the mafic lavas of the Karoo here and there form table mountains. The lowland Precambrian area east of the craton margin is also characterized by many outstanding granitoid inselbergs.

ACKNOWLEDGEMENTS

Thanks are due T. Eerola, H. Mäkitie, T. Manninen and S. Vuori (GTK), C. Åkerman and B. Gustafsson (SGU), H. Mavie and G. Cune (DNG), who were participants in the fieldwork. Y. Pekkala, the Project Manager (GTK), Ph. Westerhof, the Project Advisor (ITC), J. Marques and M. Ferrara (Gond-

wana Ltd) joined us for fieldwork on several occasions. E. Kuosmanen, R. Koskinen and M. Ajlani (GTK) prepared the map data and drawings for publication. R. Lahtinen (GTK) is thanked for critical reading of the manuscript.

REFERENCES

- Afonso, R. S. 1976.** A Geologia de Moçambique. Notícia Explicativa da Carta Geológica de Moçambique na escala 1 : 2000 000, 175 p., Serviços de Geologia e Minas, Maputo, Mozambique.
- Barton, C. M., Carney, L., Crow, M. J., Duncley, P. N. & Simango, S. 1991.** The geology of the country around Rushinga and Nyamapanda. Bulletin of the Zimbabwe geological Survey, 92, 220 p.
- Chenjerai, K. G., Schmidt Mumm, A., Blenkinsop, T. G. & Chatora, D. R. 1993.** The Redwing Gold Deposit, Mutare Greenstone Belt, Zimbabwe: tectonic setting and regional exploration significance. Sub-Sahara Economic Geological Conference, Harare, Abstracts, 2–3.
- Coward M. P., James P. R. & Wright, L. 1976.** Northern margin of the Limpopo mobile belt, southern Africa. Bulletin of the Geological Society of America, 87, 601–611.
- Dirks, P. H. G. M., Jelsma, H. A., Vinyu, M. & Munyanyiwa, H. 1998.** The structural history of the Zambezi Belt in the northeast Zimbabwe: Evidence for crustal extension during the early Pan-African. South African Journal of Geology, 101 (1), 1–16.
- Dirks, P. H. G. M., Blenkinsop, T. G. & Jelsma, H. A. 2003.** Geology of Africa. Encyclopedia of Life Support Systems, EOLSS Publishers Co. Ltd.
- Dirks, P. H. G. M. & Jelsma, H. A. 2006.** The structural-metamorphic evolution of the northern margin of the Zimbabwe craton and adjacent Zambezi belt in northeastern Zimbabwe. Geological Society of America Special Paper 405, 291–313.
- Geological Map of Zimbabwe 1:1 000 000.** Seventh edition, reprinted, 1985. Geological Survey of Zimbabwe.
- Grantham, G. H., Maboko, M. & Eglington, B. M. 2003.** A review of the evolution of the Mozambique belt and implications for the amalgamation of Rodinia and Gondwana. Geological Society of London Special Publication 206, p. 401–426. In: Yoshida, M., Windley, B.F. & Dasgupta, S. (eds): Proterozoic East Gondwana: Supercontinent Assembly and Breakup.
- GTK Consortium 2006b.** Map Explanation, Volume 2: Sheets 1630–1634. Geology of Degree Sheets Mecumbura, Chitoco, Tete, Tambara, Guro, Chemba, Manica, Catandica, Gorongosa, Rotanda, Chimoio and Beira, Mozambique. Ministerio dos Recursos Minerais, Direcção Nacional de Geologia, Maputo.
- Holmes, A. 1918.** The Precambrian and associated rocks of the district of Mozambique. Q. Journal of the Geological Society, London, LXXIV, (1).
- Hunting Geology & Geophysics Limited 1984.** Mineral Inventory Project. Unpublished Report., 329 p., DNG, Maputo.
- Karhu, J. 2006.** Isotopic analyses of carbonates from Mozambique. Unpublished Report, University of Helsinki.
- Kröner, A. 2001.** The Mozambique belt of East Africa and Madagascar: significance of zircon and Nd model ages for Rodinia and Gondwana supercontinent formation and dispersal. South African Journal of Geology, Vol. 104, 151–166.
- Kröner, A., Hegner, E., Collins, A. S., Windley, B. F., Brewer, T. S., Razakamanana, T. & Pidgeon, R. T. 2000.** Age and magmatic history of the Antananarivo block, central Madagascar, as derived from zircon geochronology and Nd isotopic systematics. American Journal of Science, 300, 251–288.
- Kröner, A., Sacchi, R., Jaeckel, P. & Costa, M. 1997.** Kibaran magmatism and Pan-African granulite metamorphism in northern Mozambique: single zircon ages and regional implications. Journal of African Earth Sciences, 25, No. 3, 467–484.
- Kröner, A., Willner, H. P., Collins, A. S., Hegner, E. & Muhongo, S. 2000.** The Mozambique Belt of East Africa and Madagascar: New zircon and Nd ages – implication for Rodinia and Gondwana Supercontinent formation and dispersal. Journal of African Earth Sciences, 30, (4A), 49–50 (abstract).
- Kröner, A., Willner, H. P., Hegner, E., Jaeckel, P. & Nemchin, A. 2001.** Single zircon ages, PT evolution and Nd isotope systematics of high-grade gneisses in southern Malawi and their bearing on the evolution of the Mozambique Belt in southeastern Africa. Precambrian Research, 109, No. 3–4, 257–291.
- Manhiça, A. D. S. T., Grantham, G. H., Armstrong, R. A., Guise, P. G. & Kruger, F. J. 2001.** Polyphase deformation and metamorphism at the Kalahari craton – Mozambique belt boundary. In: Miller, J.A., Holdsworth, R.E., Buick, I.S. & Hand, M. (eds.): Continental Reactivation and Reworking, Geological Society, London, Special Publications, 184, 303–322.
- Mänttari, I. 2008.** Mesoarchean to Lower Jurassic U-Pb and Sm-Nd ages from NW Mozambique. Geological Survey of Finland Special Paper 48, 81–119.
- Manuel, I. R. V. 1992.** Geologie, Petrographie, Geochemie und Lagerstätten der Manica-Greenstone-Belt (Mozambique). Unpublished Ph.D. Thesis, Rheinisch-Westfälischen Hochschule, Aachen.

- Pekkala, Y., Lehto, T. & Lehtonen, M. I. 2008.** Introduction to GTK projects in Mozambique 2002–2007. Geological Survey of Finland Special Paper 48, 7–22.
- Pinna, P., Marteau, P., Becq-Giraudon, J-F. & Manigault, B. 1986.** Notice Explicative de la Carte Géologique à 1 : 1 000 000 de la République Populaire du Mozambique. Unpublished Report, Instituto Nacional de Geologia de Moçambique/BRGM, Orléans, France.
- Pinna, P., Marteau, P., Becq-Giraudon, J-F. & Manigault, B. 1987.** Carta Geológica de Moçambique, na escala 1 : 1 000 000. Instituto Nacional de Geologia de Moçambique, Maputo.
- Schetselaar, E. Tiainen, M. & Woldai, T. 2008.** Integrated geological interpretation of remotely sensed data to support geological mapping in Mozambique. Geological Survey of Finland Special Paper 48, 35–63.
- Stockmayer, V. R. 1980.** The geology of the Inyanga-north – Makaha area. Zimbabwe geological Survey, Bulletin No. 89, Salisbury.
- Vearncombe, J. R., Cheshire, P. E., De Beer, J. H., Kallick, A. M., Mallinson, W. S., McCourt, S. & Stettler, E. H. 1988.** Structures related to the Antimony Line, Murchison schist belt, Kaapvaal Craton, South Africa. *Tectonophysics*, 154, 285–308.
- Wilson, J. F., Nesbitt, R. W. & Fanning, C. M. 1995.** Zircon geochronology of Archaean felsic sequences in the Zimbabwe craton: a revision of greenstone stratigraphy and a model for crustal growth. In: Coward, M. P & Ries, A. C. (eds.): *Early Precambrian Processes*. Geological Society Special Publication, 95, 109–126.

THE TETE-CHIPATA BELT: A NEW MULTIPLE TERRANE ELEMENT FROM WESTERN MOZAMBIQUE AND SOUTHERN ZAMBIA

by

A.B. Phil Westerhof^{1,5}, Matti I. Lehtonen², Hannu Mäkitie²,
Tuomo Manninen³, Yrjö Pekkala², Bosse Gustafsson⁴ & André Tahon⁵

Westerhof, A. B. Phil, Lehtonen, M. I., Mäkitie, H., Manninen, T., Pekkala, Y., Gustafsson, B. & Tahon, A. 2008. The Tete-Chipata Belt: a new multiple terrane element from western Mozambique and southern Zambia. *Geological Survey of Finland, Special Paper 48*, 145–166, 9 figures.

Based on analysis of new data, the crystalline basement of Tete Province, western Mozambique, can be attributed to three major lithospheric plates – provisionally called East, West and South Gondwana – that collided and amalgamated during the Pan-African orogenic cycle. The collision and amalgamation of West Gondwana and East Gondwana (~640 to ~530 Ma) gave rise to the development of the East Africa Orogen (EAO). Next, South Gondwana collided and amalgamated (~560–520 Ma) with the already united plates above. Consequently, the N-S directed suture of the EAO impinges on the E-W directed Kuunga Orogen suture, comprising (from west to east) the Damara-Lufilian-Zambezi Belt, the Lúrio Thrust Belt and, further eastwards, thrust belts of Sri Lanka. Late Pan-African remobilization, manifesting final docking of the three plates and emplacement of granitoids and pegmatites, lasted from ~500 to 430 Ma.

The E-W to WSW-ENE trending structural domain, constituting the bulk of the crystalline basement of northern Tete Province, is attributed to a new structural element for which we propose the name “Tete-Chipata Belt (TCB)”. This belt continues into southern Zambia as the “Southern Irumide Belt”, a term that we discourage, for reasons that will be discussed below. The TCB has a triangular shape and is bound by the low-angle, west-verging Angónia (East Gondwana) thrust front in the east, the Mwembeshi Dislocation in the north and the Sanango Shear Zone in the south.

In northern Tete Province the TCB is mainly composed of Mesoproterozoic supracrustal and plutonic rocks. Supracrustal rock sequences have been grouped into the ~1.3 Ga volcano-sedimentary Fingoè Supergroup, the ~1.2–1.3 Ga sedimentary Zámbugue Supergroup and undated (>1.08 Ga) granulites and gneisses of the Chidzolomondo, Cazula and Mualadzi Groups. Plutonic rocks comprise a large number of granitoid clans and a bimodal suite with ages ranging from > 1.2 to ~1.05 Ga. Although geochemical discrimination diagrams generally suggest a setting intermediate between “volcanic-arc” and “within-plate”, we consider the older granitoids (> 1.2 to 1.08 Ga) to have been emplaced in a magmatic arc setting.

These litho-stratigraphic units show little cohesion, as manifested by differences in metamorphic grade, structural development, geodynamic setting and age. They form a collage of stacked “suspect terranes” together with adjacent analogue areas in southern Zambia. Litho-structural units in the Mozambican part of the TCB are tentatively correlated with a number of terranes, provisionally named Chewore-Rufunsu, Luangwa, Nyimba and Petauke-Sinda Terranes, previously identified in the Zambian part of the TCB. The Fingoè Terrane, located entirely in Tete Province, is interpreted as an ~1.3 Ga volcanic arc. It has approximately the same age as the Chewore ophiolite and is 300 Ma older than the Kaourera Arc, both identified in the Chewore-Rufunsu Terrane. The

Luia Terrane comprises undated (>1.08 Ga), partly retrograded granulites and gneisses and is intruded by a 1.05 Ga bimodal igneous suite composed of charnockites of the Castanho Granite and gabbro-anorthosite intrusives (including the allochthonous Tete Gabbro-Anorthosite Suite).

These terranes assembled and collided with the southern margin of the Central Africa craton (West Gondwana) in a continental-margin-arc setting during the Grenvillian orogenic cycle at ~ 1.06 Ga. During and subsequent to amalgamation, crustal thickening or orogenic collapse triggered a phase of younger (1.05 and 1.04 Ga) granitoids and bimodal magmatism. Some granitoids supposedly played the role of "stitching pluton".

Subsequently, during the Pan-African orogenic cycle, the TCB together with juvenile crust formed during a post-Grenville, early Pan-African Neoproterozoic extensional phase (~ 880 to 765 Ma) became involved in the collisional event between the Kalahari and Central Africa cratons (South and West Gondwana, respectively), resulting in the double-verging Damara-Lufilian-Zambezi Belt. This was not a simple collision between two large lithospheric plates, but rather a series of collisional events among several cratonic fragments, taking place between ~ 615 Ma and 520 Ma. The Pan-African orogenic cycle gave rise to widespread (prograde and retrograde) metamorphism and deformation with the bulk of the strain in the TCB absorbed by former sutures between individual terranes. A number of Pan-African terranes have also formed during this event. Finally, late to post-Pan-African granitic stocks have been emplaced into this collage of terranes.

Key words (GeoRef Thesaurus AGI): tectonics, terranes, Gondwana, Pan-African Orogeny, Grenvillian Orogeny, Irumide Belt, Mesoproterozoic, Neoproterozoic, Phanerozoic, Tete, Mozambique.

¹ Westcourt GeoConsult, Kon. Wilhelminalaan 11, Leidenschendam, the Netherlands

² Geological Survey of Finland, P.O. Box 96, FIN-02151 Espoo, Finland

³ Geological Survey of Finland, P.O. Box 77, FIN-96101 Rovaniemi, Finland

⁴ Geological Survey of Sweden, Box 670, 75128 Uppsala, Sweden

⁵ Formerly: International Institute for Geo-Information Science and Earth Observation (ITC), the Netherlands

E-mail: ap.westerhof@hetnet.nl

INTRODUCTION

Recently, the geology of Tete Province has been reviewed by a GTK-led consortium as part of a regional resource mapping program (2002–2006) sponsored by the Nordic Development Fund. The mapping program covered southern and central Mozambique (GTK Consortium 2006a–d), using modern geochronological techniques and mapping tools such as satellite imagery, airborne geophysical data and GPS-controlled field verification. The program has resulted in the definition of different litho-stratigraphic units and igneous suites and the re-definition and/or abolishment of older terms (cf. Hunting 1984a, b and earlier publications).

From the new data it can be concluded that the crystalline basement of northern Tete Province is composed of an assembly of relatively loosely bound lithospheric fragments of widely varying settings and ages – "suspect terranes" – that, together with adjacent analogue areas in southern Zambia, constitutes a new structural element for which the

name "Tete-Chipata Belt (TCB)" has been proposed (GTK Consortium 2006d). For reasons that will be discussed later, we discourage the term "Southern Irumide Belt", used for the same structural element in Zambia (Johnson *et al.* 2005, 2007).

The TCB is a triangular structural domain located between the Central Africa craton (Congo-Tanzania-Bangweulu craton) and Kalahari craton (Figs 1 and 2). The litho-tectonic units and sub-units – terranes and micro-terranes – in the Mozambican part of the TCB are described and tentatively correlated with terranes identified in southern Zambia. These terranes collided and amalgamated with the southern margin of the Central Africa craton during the ~ 1.0 Ga Grenville orogenic cycle. Subsequently, during the Pan-African orogenic cycle, the TCB became involved in the Damara-Lufilian-Zambezi (DLZ) collisional orogen between the Kalahari and the Central Africa cratons.

PAN-AFRICAN GEOLOGY OF MOZAMBIQUE

There are essentially two geodynamic scenarios to explain the formation of the Gondwana Supercontinent in southern and eastern Africa during the Pan-African orogenic cycle.

The first scenario involved consumption of the Mozambique Ocean between 841 and 632 Ma (Cutten & Johnson 2006) and collision and amalgamation (~640 to ~530 Ma) of two crustal plates, provisionally named West Gondwana and East Gondwana (Shackleton 1994, Wilson *et al.* 1997, Kröner *et al.* 2001, Jacobs *et al.* 2006). In this model West Gondwana comprised most of Africa and South America. East Gondwana was composed of juvenile crust, now attributed to the Arabian-Nubian Shield, and older crystalline basement in Madagascar, India, Antarctica and Australia. Collision and amalgamation of these two lithospheric plates created a N-S directed fold belt, 6000 km in length, named the East Africa Orogen (EAO) (Stern 1994) or, stressing its southernmost continuity, East Africa-Antarctica Orogen (EAAO) (Jacobs *et al.* 2006).

This orogenic cycle, shown by typical Pan-African K-Ar or Rb-Sr cooling ages of ~650 to 490 Ma, has been known for a long time (Cahen & Snelling 1966). Biotite cooling ages attributed to the East Gondwana Terrane in Tanzania show a pronounced age gradient and manifest diachronous cooling across the collision zone, with the western parts cooling below ~300 °C up to ~150 Ma earlier than the eastern parts. The oldest biotite ages of 618 ± 14 Ma from the western margin provide the best minimum estimate for the age of the pervasive amphibolite grade metamorphism. It is assumed that this regional metamorphic and deformational event occurred prior to ~650 Ma (Maboko 2000). In a recent review, Kröner (2006) reported peak granulite facies metamorphism in East Africa and Madagascar between 640 and 550 Ma. A clockwise P-T-t path for eastern Tanzania supports a continental collision model. Elsewhere, for instance in southern Tanzania and Malawi, a counter-clockwise P-T-t path can be observed, suggesting that other processes, such as magmatic underplating, in addition to continental collision, played a role.

The second scenario assumes collision and amalgamation of three Pan-African lithospheric plates (Grantham *et al.* 2003, GTK Consortium 2006b, d), provisionally named East, West and South Gondwana. East Gondwana is centered at the Arabian-Nubian Shield and older crystalline basement of the Dharwar Craton of southern India, Madagascar and the eastern granulites of Kenya and Tanzania (Fig. 1).

West Gondwana comprises most of the Central Africa craton. South Gondwana is mainly composed of Antarctica and the Kalahari craton, amalgamated since the ~1.0 Ga Grenvillian orogenic cycle. In this scenario the N-S directed suture of the EAO impinges on the E-W directed Kuunga Orogen suture, comprising (from west to east) the Damara-Lufilian-Zambezi (DLZ) Belt, the Lúrio Thrust Belt (LTB) and, further eastwards, thrust belts of Sri Lanka. In this scenario, Pan-African remobilization of Mesoproterozoic and older crust south of the Kuunga suture is restricted to metamorphic overprinting in linear N-S directed shear zones (Manica Shear Zone, Fig. 1) along the eastern margin of the Zimbabwe Craton (Manhiça *et al.* 2001, GTK Consortium 2006b).

In northern Mozambique, north of the LTB, the age of Pan-African metamorphic overprinting of Mesoproterozoic rocks, associated with amphibolite- to granulite-facies metamorphism, is estimated at about 560 to 520 Ma (Bingen *et al.* 2006, Viola *et al.* 2006). Macey *et al.* (2006) attribute the younger ages of ~550 Ma in the Nampula sub-Province, south of the LTB (Fig. 2), to the maximum age of the termination of the principal Pan-African D_2/M_2 collisional tectono-metamorphic event (D_1/M_1 is attributed to the older Mesoproterozoic, ~1.0 Ga, Grenville orogenic cycle) as manifested by five granitoid orthogneiss samples that provided metamorphic rim ages of 513 ± 10 Ma, 525 ± 20 Ma, 538 ± 8 Ma and 505 ± 10 Ma (Macey & Armstrong 2005, Grantham, unpublished data). Supracrustal rocks equally located in the Nampula sub-Province south of the LTB yielded metamorphic rim ages of 555 ± 12 , 502 ± 80 and 527 ± 18 Ma, and a weakly deformed porphyritic quartz monzonite with aligned twinned K-feldspar phenocrysts yielded a precise U-Pb concordia crystallization age of 532 ± 5 Ma (Macey & Armstrong 2005), which provides another constraint on a waning Pan-African D_2 deformation phase.

Closure of the Zambezi-Adamastor oceanic basin (Johnson *et al.* 2005) and collision and amalgamation of the Kalahari craton (South Gondwana) and Central Africa craton (West Gondwana) resulted in the Damara-Lufilian-Zambezi Belt, a major Neoproterozoic suture (Burke *et al.* 1977, Oliver *et al.* 1998, Porada & Berhorst 2000, John *et al.* 2003, Johnson & Oliver 2000, 2004). Mafic and ultramafic rock fragments in Neoproterozoic metasediments (Roan Group, Katanga Supergroup) of the Lufilian and Zambezi segments of the DLZ Belt supposedly

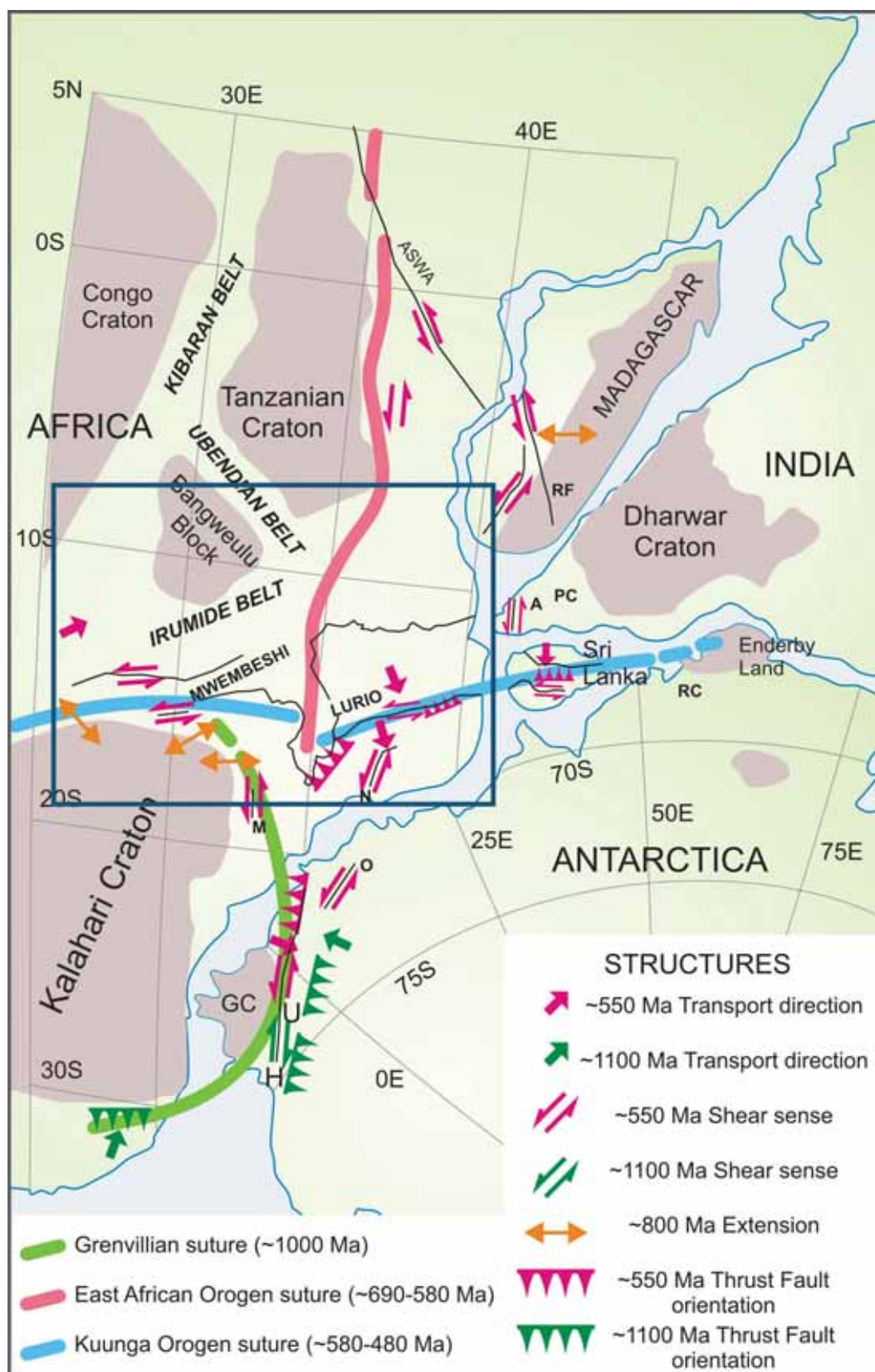


Fig. 1. Gondwana reconstruction (after Lawver et al. 1998). The model assumes the collision and amalgamation of three major lithospheric plates: East, West and South Gondwana. East and West Gondwana collide first and create the East African Orogen (thrust front marked by a red line). Both collide with South Gondwana, giving rise to the E-W-directed Kuunga Orogen, which comprises (from west to east) the Damara-Lufilian-Zambezi belt, the Lurio thrust belt and thrust belts in Sri Lanka (in blue). Ages and locations of various major structural/tectonic features (e.g., major thrust belts, shear zones) showing the direction of tectonic transport and shear sense. Key: PC = Palgat-Cauvery Shear Zone; RC = Rayner Complex; A = Achankovil Shear Zone; GC = Grunehogna cratonic fragment; H = Heimefrontfjella; RF = Ranotsara Shear Zone; U = Urfjell; N = Namama Shear Belt; O = Orvinfjella Shear Zone; M = Manica Shear Zone (adapted from Grantham et al. 2003). The study area shown in Figure 2 is here marked as a rectangular box.

represent relics of obducted ocean floor rocks, forming a tectonic *mélange*. The Chewore Ophiolite in the Chewore Inliers (Fig. 2) represents a larger fragment of oceanic crust. Amphibolites in the Damara segment of the DLZ Belt show MORB tholeiitic affinities (Breitkopf & Maiden 1988) and are supposedly also derived from ocean floor protoliths.

Pan-African, subduction-related HP-LT metamorphism is reflected by eclogites and whiteschists (kyanite+talc+yoderite) in ophiolite and by kyanite in metapelite (Vrána & Barr 1972, Vrána *et al.* 1975), and manifest peak metamorphic conditions with T estimated at 630–690 °C and P ranging from > 13 to 26–28 kb (John & Schenk 2003, John *et al.* 2004). Sm-Nd whole rock-garnet and Lu-Hf whole rock-garnet dating yield ages ranging from 659 ± 14 Ma to 595 ± 10 Ma, interpreted as indicating the age of Pan-African eclogite-facies metamorphism (John & Schenk 2003, John *et al.* 2004).

The Lufilian and Zambezi segments of the DLZ Belt can be described as a thin- and thick-skinned, double-verging orogen with thrust transport to the NNE-NE (Wilson *et al.* 1993, Hanson *et al.*

1994, Johnson & Oliver 2004) and SSE (Barton *et al.* 1991, Dirks *et al.* 1999, Vinyu *et al.* 1999, Müller *et al.* 2001). Transport directions and sinistral shear along the Mwembeshi Dislocation (see below) suggest oblique convergence between West and South Gondwana. The spatial arrangement of metamorphic ages and range in timing of peak metamorphic conditions indicate that the closure of the Zambezi-Adamastor Ocean and amalgamation of South and West Gondwana was not a simple collision between two large lithospheric plates, but rather a series of collisional events among several cratonic fragments, taking place between ~615 Ma and 520 Ma, a period of almost 100 Ma. This was followed by a period of uplift, denudation and cooling passing the ~350 °C isotherm in the DLZ Belt at ~480 Ma (Goscombe *et al.* 2000).

One of the cratonic fragments in the DLZ Belt was the rigid Choma-Kalomo block (Fig. 2), which supposedly acted as an indenter when it became caught between West and South Gondwana. Its presence within the collision zone changed the geometry of compression and thrusting, resulting in the arcu-

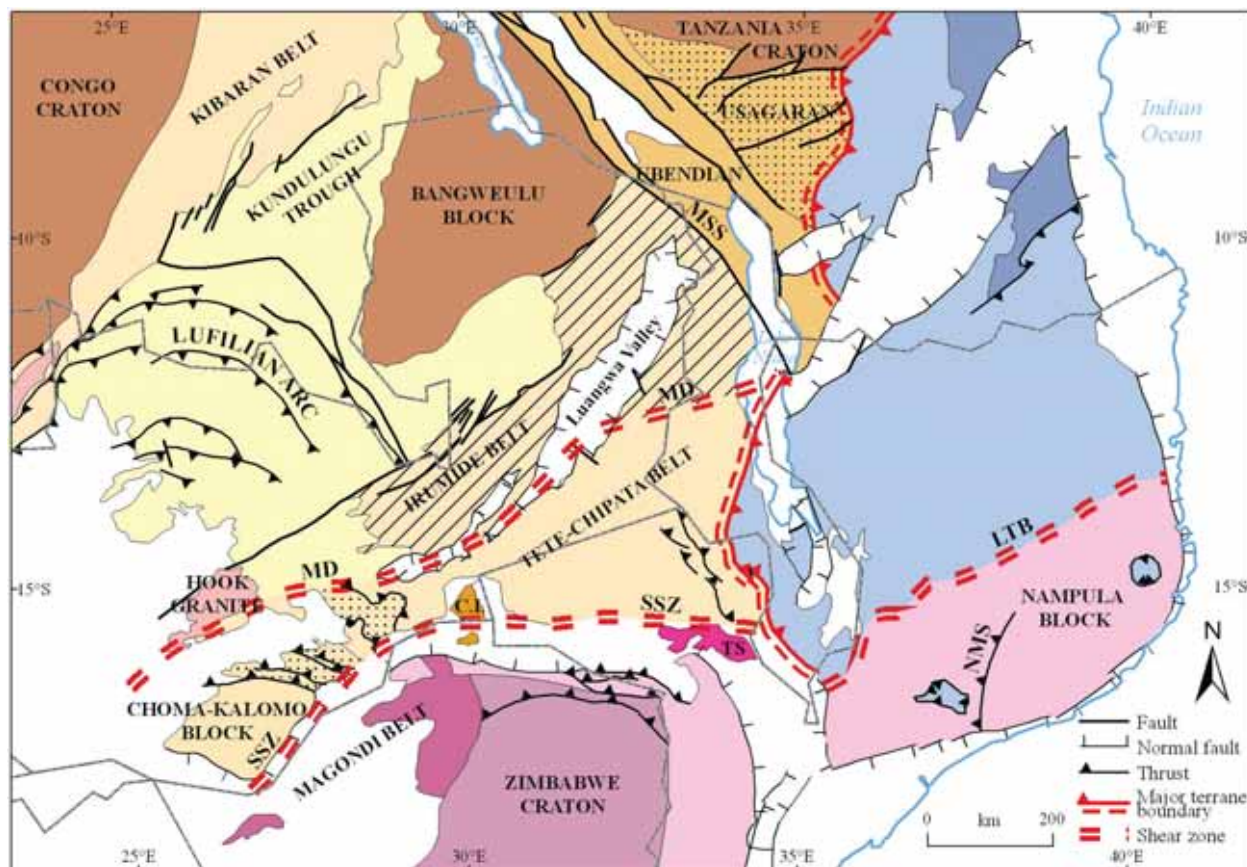


Fig. 2. Simplified geological map of the Tete-Chipata Belt (TCB) and the Zambezi-Lufilian segment of the Damara-Lufilian-Zambezi Belt (adapted from Vrána *et al.* 2004). Key: MSS = Mugesse Shear Zone, MD = Mwembeshi Dislocation, SSZ = Sanango Shear Zone, C.I. = Chewore Inliers, TS = Tete Suite, NMS = Namama Megashear, LTB = Lúrio Thrust Belt. The dotted section in the southwestern part of the TCB corresponds to Neoproterozoic (post-Rodinia, early Pan-African) metasediments (mainly pelites and carbonates) with minor metavolcanics, tectonically overlying Mesoproterozoic Mpande Gneiss. For Neoproterozoic juvenile rocks in Tete Province, see Fig. 7.

ate shape of the Lufilian segment – the Lufilian Arc (Fig. 2) – of the DLZ Belt (Bulambo *et al.* 2006), comprising Neoproterozoic folded and north-thrust-ed metasediments of the Katanga Supergroup.

Although the DLZ collisional event is well documented by Neoproterozoic metamorphic U-Pb data of older rocks, the scarcity of juvenile TTG suites having ages between ~616 and 520 Ma is notable. In Zambia, the few known examples of syn-kinematic felsic igneous rocks include the Hook Granite (~533 to ~566 Ma; Fig. 2) and nearby Mwembeshi Rhyolite (~551 Ma). They precede the clearly late to post-kinematic 0.47–0.50 Ga ages of the Sinda Suite granites (502 ± 8 Ma) and Macanga granite (470 ± 14 Ma) in the Tete area (Mänttari 2008). In northern Mozambique, late Pan-African geodynamic

development, reflecting transtensional tectonics coeval with final docking of all three major terranes, is manifested by a moderately deformed pegmatite that was refolded together with S_2 during the last co-axial D_2 deformation phase dated at 501 ± 5 Ma (Roberts *et al.* unpublished data, in Macey *et al.* 2006) and by a 490 ± 8 Ma leucosome taken from a shear band in the Namama megashear (Fig. 2), Nampula sub-Province (Macey & Armstrong 2005). Late to post-Pan-African collapse is reflected by a granite sample dated at 492 ± 2 Ma (Grantham *et al.* unpublished data, in Macey *et al.* 2006) and pegmatites at 430–480 Ma (Cronwright & Roberts, unpublished CHIME data, in Macey *et al.* 2006), indicating that the Pan-African thermal episode continued well into the Phanerozoic.

CRYSTALLINE BASEMENT OF TETE PROVINCE

Crystalline basement belonging to each of the major lithospheric plates described above – East, West and South Gondwana – is present in the Tete Province of western Mozambique. Based on structural, petrological and geochronological criteria a northern crystalline domain can be separated from a southern crystalline basement. The latter, exposed south of the Sanangoè Shear Zone (SSZ), south of the mid-Zambezi Karoo rift and along the eastern margin of the Zimbabwe Craton (Fig. 2), is attributed to South Gondwana (GTK Consortium 2006b, d). The northern crystalline basement can be divided into two domains with contrasting structural grains. The bulk part of the northern crystalline basement, characterized by a SW-NE to WSW-ENE structural grain, has been a part of West Gondwana since the Grenvillian orogenic cycle. A smaller, eastern part with NW-SE trending structures, belongs to East Gondwana. The Tete Suite, a major layered gabbro-anorthosite intrusive, overlies mylonitized crystalline basement belonging to two Pan-African lithospheric plates, West and South Gondwana, and is supposedly derived from the West Gondwana plate. Its igneous emplacement and subsequent allochthonous tectonic setting is described in GTK Consortium (2006b, d) and Westerhof *et al.* (2008).

The West Gondwana terrane in the northern Tete Province continues into Zambia, where it is known as the “Southern Irumide Belt” (Johnson *et al.* 2005, 2007). It is separated from the NE-SW trending Irumide Belt and the rest of the Central African craton by the Mwembeshi Dislocation (MD) (Fig. 2). The Irumide Belt manifests Grenvillian convergent tectonism along the southeastern margin of the

Central Africa craton (De Waele *et al.* 2006) and is composed of Palaeoproterozoic metamorphosed platform sediments of the ~1.88 Ga Muva Supergroup (De Waele & Fitzsimons 2004), which are most prominently exposed along the NW-verging Irumide front, in the northwestern part of the belt. Subsequently, two generations of granitoids have invaded the Muva metasediments. These comprise a minor suite of anorogenic plutons dated between 1.66 and 1.55 Ga (De Waele *et al.* 2003a,b) and voluminous K-feldspar porphyritic granitoids dated between 1.05 and 0.95 Ga (De Waele *et al.* 2006). Both generations of granitoids have bulk-rock geochemical signatures and highly negative $\epsilon_{Nd}(t)$ values manifesting their formation by the recycling of older continental crust (De Waele *et al.* 2003a). Using metamorphic monazite and zircon overgrowths, polyphase MP-HT metamorphism in the Irumide Belt has been dated at 1046 ± 3 Ma (Schenk & Appel 2001) and between 1020 ± 7 Ma and 1004 ± 20 Ma (De Waele *et al.* 2003b).

North of the Irumide Belt, the West Gondwana terrane is centered on the Central Africa craton, comprising the Congo craton (west) and the Tanzania craton plus the Bangweulu block (east), with the intracratonic Mesoproterozoic Kibaran belt in between (Fig. 2). Within the Ubendian and Usagaran fold belts (2.0 to 1.8 Ga) and along its southeastern margin, the Central Africa craton is overlain by Paleoproterozoic crust, comprising undeformed platform sediments (e.g. Mporokoso Group) and volcanics overlying the Bangweulu block and igneous and folded and metamorphic rocks exposed in a number of windows within the Lufilian Arc (Fig. 2).

Crystalline basement belonging to East Gondwana in northern Tete Province, east of the Pan-African thrust front, has a NW-SE structural grain and includes lithologies of the Angónia Group. The latter are continuous with rock units in Malawi (Bloomfield & Garson, 1965, Thatcher 1968) and northern Mozambique (Pinna *et al.* 1986, 1987). In Tete Province the Pan-African thrust front is clearly visible in satellite imagery (Fig. 3). The gneisses of the Angónia Group show complex, km-scale, Ramsay type-2 deformation, interpreted to reflect orthogonal shortening, with (north)east over (south)west transport, followed by N-directed sinistral strike-slip deformation (Grantham *et al.* 2006). ENE-plunging lineations are concentrated along the contact with the footwall Desaranhama Granite (Furancungo Suite; Fig. 6). Strongly altered and deformed talc-serpentine bodies, together with substantial amounts of mafic and ultramafic rock, may represent relicts of the Mozambique Ocean that existed between West and East Gondwana prior to Pan-African collision and amalgamation.

The 1041 ± 4 Ma Desaranhama Granite and orthogneisses of the Furancungo Suite (GTK Consortium 2006d, Mänttari 2008) also have a NW-SE trend but belong to the West Gondwana terrane. They show progressive deformation from W to E, towards the thrust front with the Angónia Group, with the rock fabric changing from rather massive to augen gneiss to blastomylonite (GTK Consortium 2006d).

The Furancungo Suite apparently served as a footwall for the Angónia thrust mass, thereby assuming a Pan-African, NW-SE striking fabric. The black dented line in Fig. 3 portrays the postulated original thrust front. Due to uplift and erosion subsequent to the Pan-African thrusting event, this front retreated some 60 km to the present tectonic contact, represented by the red dented line in Fig. 3.

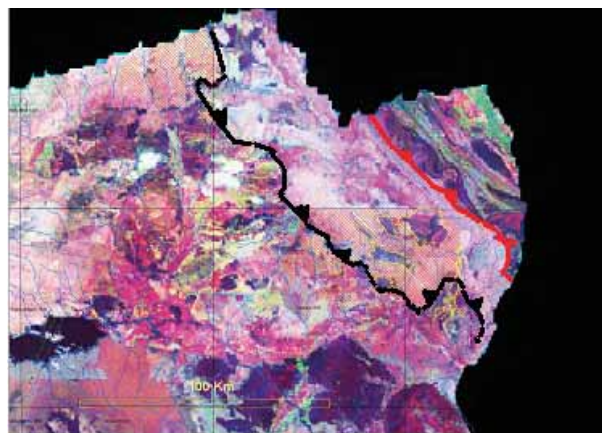


Fig. 3. Ternary radiometric image of the northeastern part of Tete Province. In red: Actual location of the SW-verging thrust front of the Angónia Group (East Gondwana) over Desaranhama Granite (Tete-Chipata Belt, West Gondwana). Note Ramsay type-2 interference structures close to the thrust plane in Angónia lithologies. The Desaranhama Granite, although belonging to the generally SW-NE to WSW-ENE trending Tete-Chipata Belt, also has a NW-SE grain because it served as a footwall for Angónia thrusting. Due to post-Pan-African uplift and erosion, the thrust front supposedly retreated from the position of the black to the red dented line. The width of Figure is 230 km.

THE TETE-CHIPATA BELT

As mentioned, the West Gondwana basement in northern Tete Province continues into Zambia as the Southern Irumide Belt (SIB). This term, coined by Johnson *et al.* (2005), implies a genetic relationship, suggesting that the SIB is part of the Irumide Belt *sensu lato*. There exists, however, general agreement that the Mwembeshi Dislocation (MD) constitutes a fundamental break (or suture; Johnson *et al.* 2007) in the geology of southern-central Africa and that there is no intrinsic relationship with the Irumide Belt *sensu stricto* as, for instance, between the Alpine fold belt and Alpine foreland, with both domains grading into one another. In the absence of such a geodynamic relationship we prefer a more neutral term for this newly defined structural element and have proposed the term “Tete-Chipata Belt” (TCB) (GTK Consortium 2006d). This triangular structural domain belonged to West Gondwana (Central Africa craton) since the Grenvillian orogenic cycle and is bounded by a Pan-African

shallowly E-dipping, W-verging thrust zone in the east and two major Pan-African strike-slip fault zones, i.e., the steep Sanangoè Shear Zone (SSZ) in the south and by the equally steep MD in the NW.

The Mwembeshi Dislocation (MD) is a curvilinear W-E to WSW-ENE to SW-NE trending ductile/brittle shear zone that runs along the southern margin of the Hook Massif, central Zambia (Fig. 2). Foliation in the syntectonic parts of the granitoid massif is continuous with the regionally developed S_1 fabric in adjacent Neoproterozoic country rocks. Two different phases of syntectonic granite magmatism yield U-Pb zircon upper intercept ages of 559 ± 18 Ma and 566 ± 5 Ma. A syntectonic rhyolite, with a U-Pb zircon upper intercept age of 551 ± 5 Ma, has been emplaced into the shear zone, demonstrating that local transtensional shearing took place in the same time frame as batholith emplacement, probably within an overall transpressive regime. Deformation along the MD ceased before ~ 535 Ma,

as manifested by post-tectonic, undeformed rhyolite and granite that yielded U-Pb zircon ages of 538 ± 2 Ma and 533 ± 3 Ma, respectively (Hanson *et al.* 1993). In places, reactivation of the MD has played a role in the development of the younger Karoo rift of Luangwa Valley (Fig. 2).

The Sanangòè Shear Zone (SSZ), the southern boundary of the TCB, was mapped as the Sanangòè Thrust Zone by Hunting (1984a, b) and Barr & Brown (1987, 1988). The shear zone can be followed westwards towards Estima and Lake Cahora Bassa but is largely concealed below Karoo and younger rocks of the mid-Zambezi rift (Fig. 2). In the absence of "terrane concepts" the SSZ was

traditionally considered as marking the boundary between two litho-structural domains, the Nyassa and Mid-Zambezi Structural Provinces (Hunting 1984a, b and earlier publications). We postulate that the SSZ is a Pan-African transpressional fault zone, generally similar in structural aspects and timing to the Mwembeshi Dislocation, formed within a structural weakness zone of the Zambezi segment of the DLZ belt and now forming the map boundary between West and South Gondwana (GTK Consortium 2006b, d). Mylonites associated with the steep SSZ should not be confused with the sub-horizontal mylonites underlying the Tete Suite (Westerhof *et al.* 2008).

LITHOLOGIC UNITS OF THE TETE-CHIPATA BELT

The crystalline basement of the Tete-Chipata Belt in northern Tete Province is composed of metamorphosed supracrustal and plutonic rocks. Recent resource mapping has resulted in the identification of new litho-stratigraphic units and re-definition of older ones (GTK Consortium 2006d). Supracrustal rock sequences have been grouped into the Fingoè and Zâmbuè Supergroups and Chidzolómondo, Cazula and Mualadzi Groups (Figs 4 and 5). These litho-stratigraphic units show little cohesion, as

manifested by different metamorphic grades, structural development, geodynamic setting and age (GTK Consortium 2006d). Mesoproterozoic plutonic rocks comprise a large number of granitoid clans and a bimodal suite with ages ranging from 1.2 to 1.04 Ga (Fig. 6) (Mänttari 2008). A small fraction of the crystalline basement in northern Tete Province is composed of juvenile rocks emplaced during the Pan-African orogenic cycle (Fig. 7).

Mesoproterozoic Supracrustal Units

Volcano-sedimentary strata of the ~1.3 Ga *Fingoè Supergroup* are exposed in a WSW-ENE trending fold belt and comprise upper greenschist to lower amphibolite facies felsic and mafic volcanics, including pyroclastic rocks, volcanic breccias and agglomerates, and metasediments such as calc-silicate schist and gneiss, quartzite, metachert and banded ironstone.

As a whole, the Supergroup is geochemically characterised by the abundance of calcium and sodium compared to alumina, as shown by the abundance of minerals such as plagioclase and epidote and by the scarcity or absence of minerals such as muscovite, Al-silicates and other aluminous phases in the parageneses of these rocks. The Zr/TiO₂ ratio vs. SiO₂ diagram classifies the analysed Fingoè metavolcanic rocks as basalts, andesites/rhyodacites and rhyolites (Fig. 5a). In the Na₂O+K₂O vs. SiO₂ diagram they mainly plot in the subalkaline field (Fig. 5b) with affinities intermediate between tholeiitic and calc-alkaline (Figs 5c, d). Relatively high Fe/Mg ratios plot in the tholeiitic high-Fe field (Fig. 5d).

Their geodynamic setting remains ambiguous: in the TiO₂-MnO-P₂O₅ triangle they plot within or near the "Oceanic Island Arc" field (Fig. 5e). In the V vs. Ti diagram, however, they occupy the "Ophiolite" field (Fig. 5f).

In contrast to the above lithologies, the ~1.2 to 1.3 Ga *Zâmbuè Supergroup* is predominantly composed of (upper) amphibolite facies metasediments assigned to (from old to young) the Malowera and Muze Groups (GTK Consortium 2006d). The first comprises basal garnetiferous ortho- and paragneisses and migmatites of the Rio Mese Formation (with garnets containing up to 6.7 wt.% MgO; GTK Consortium 2006d). The bulk of the Malowera Group is composed, however, of variously migmatized meta-arkoses and infolded orthoquartzites with subordinate, narrow, local horizons of mafic metavolcanic rocks, arkosic quartzites and similar narrow horizons of biotite-garnet(±sillimanite) gneiss. The overlying metasediments of the Muze Group comprise, apart from arkosic quartzite, and unlike the underlying Malowera rocks, thick horizons of mar-

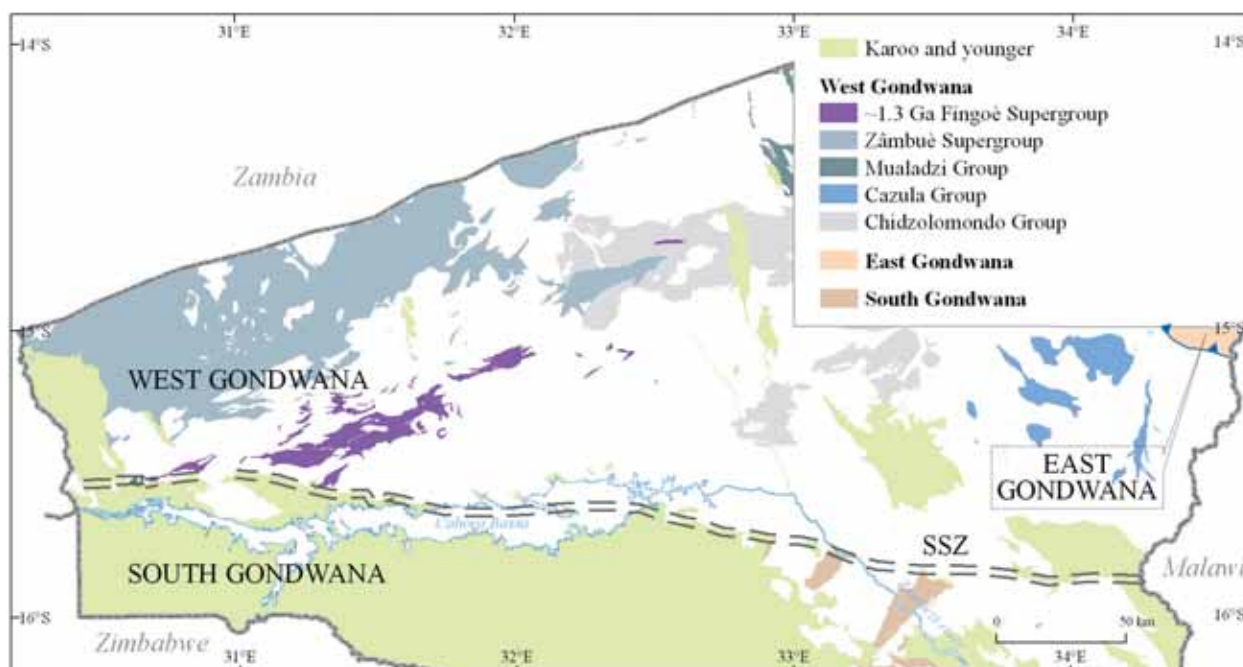


Fig. 4. Distribution of Mesoproterozoic supracrustal litho-stratigraphic units of the Tete-Chipata Belt in northern Tete Province. SSZ = Sanangòè Shear Zone

ble with interbeds of calc-silicate gneiss, skarnoid and metachert. Zircon U-Pb geochronology shows a wide range of ages. Zoned, mostly rounded cores yield Archean (~2.7 and 2.5 Ga) and Paleoproterozoic (~2.1 and 1.9 Ga) ages. So far, a maximum age of 1.2 to 1.3 Ga has been accepted for basal Malower meta-arkoses (GTK Consortium 2006d, Mänttari 2008).

The undated *Chidzolomondo Group* is mainly composed of mafic and intermediate granulites and retrograde gneisses (GTK Consortium 2006d). They include a mixture of locally strongly deformed (folded and/or sheared) metasediments and subordinate metavolcanics. The metasediments are dominated by light-coloured quartzo-feldspathic rocks (meta-arkose?), with subordinate bedded quartzites and occasional calc-silicate rocks. Garnet, cordierite and orthopyroxene (the latter with elevated Al_2O_3 contents up to 3.4 wt.%) are commonly present as minor minerals. Clinopyroxene is less common. Biotite (with elevated Ti-contents up to 5.6 wt.% TiO_2) is found in places. The high Al_2O_3 and TiO_2 contents in these minerals, the presence of antiperthitic plagioclase and granoblastic texture with straight grain boundaries meeting at triple points, are indicators of high-grade metamorphism and massive recrystallization. Using the geothermobarometers of Powell and Holland (1985, 1988, 1994) and Holland and Powell (1985, 1998) (see also <http://www.earthsci.unimelb.edu.au/tpg/thermocalc/>), the chemical compositions of the afore-mentioned minerals

indicate granulite-grade metamorphism having P-T conditions of 3.9–4.7 kbar and 740–790 °C.

Lithological classification diagrams show a wide range in compositions, but most analyses plot as basalt and andesite, while the rest are dacite and rhyodacite or, occasionally, rhyolite with a subalkaline tholeiitic to slightly calc-alkaline affinity (GTK Consortium 2006d). Charnockitic Castanho Granites and layered gabbro-anorthosite bodies (including the Tete Suite; see GTK Consortium 2006d, Westerhof *et al.* 2008) are restricted to the domain underlain by Chidzolomondo granulites. The bi-modal igneous association is thought to have formed by melting of the (dehydrated) lower crust. This means that the Chidzolomondo granulites were already "dry" when the Castanho Granite and layered gabbro-anorthosite magmas formed, thus prior to 1.05 Ga.

Supracrustal rocks of the undated *Mualadzi Group*, exposed north of the Chidzolomondo granulites, comprise granulite-grade mafic and ultramafic metavolcanics (komatiites?), a local and discontinuous banded ironstone horizon and minor quartzite and sheared and retrograde mica schist. In the past (e.g., Hunting 1984a, b), Mualadzi metavolcanics have been correlated in the past with Fingoè volcanics. Based on chemical diagrams such a correlation appears unlikely (Fig. 5, particularly the V vs. Ti plot). Since the unit is entirely surrounded by granites of the 1041 ± 4 Ma Furancungu Suite (GTK Consortium 2006d), its relation to adjacent units in the Tete Province remains enigmatic.

The analysed Mualadzi samples form a bimodal population with prevailing ultramafic and mafic compositions (Figs 5a, b). Felsic compositions are supported only by two analyses. From the remaining analytical data the Mualadzi volcanic rocks classify as subalkaline tholeiitic basalts and rhyolites (Figs 5a–c). Most mafic varieties plot in the fields of ultramafic and basaltic komatiites (Fig. 5d). On the

Jensen diagram most analyses plot both in high-Fe and high-Mg fields (Fig. 5d).

The bimodal character of the Mualadzi Group is not evidenced in the analytical results of the Fingoë volcanics, which have a wide compositional range from basalt to andesite to rhyolite. The chemistry of these two units also differs in diagrams indicating the geotectonic setting (Figs 5e, f).

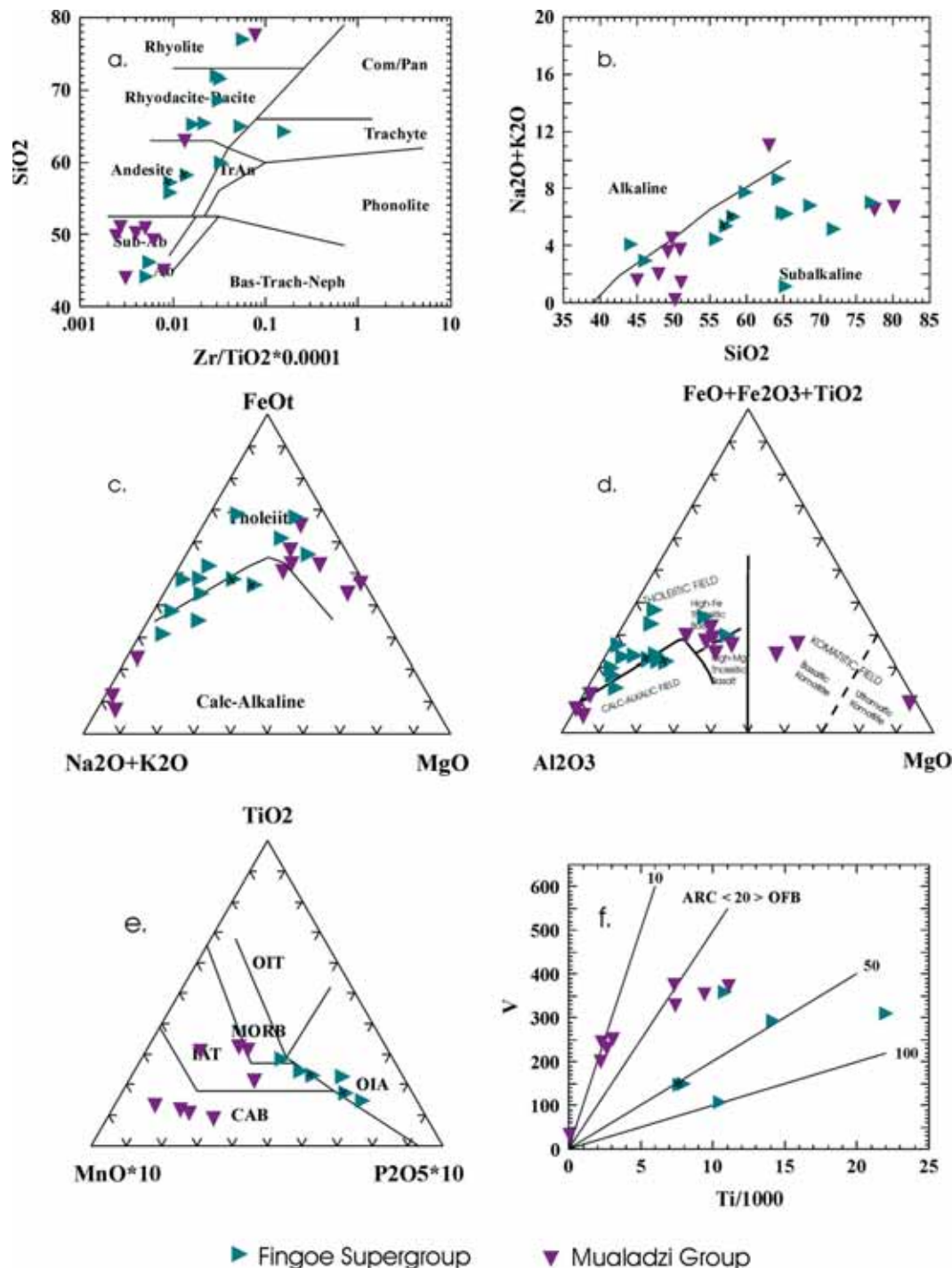


Fig. 5. Chemical classification diagrams for the rocks of the Fingoë Supergroup and Mualadzi Group. Abbreviations: OIT = Ocean Island Tholeiites, OIA = Ocean Island Andesites, MORB = Mid-Ocean Ridge Basalts, IAT = Island Arc Tholeiites, CAB = Calc-Alkaline Basalts, OFB = Ocean Floor Basalts.

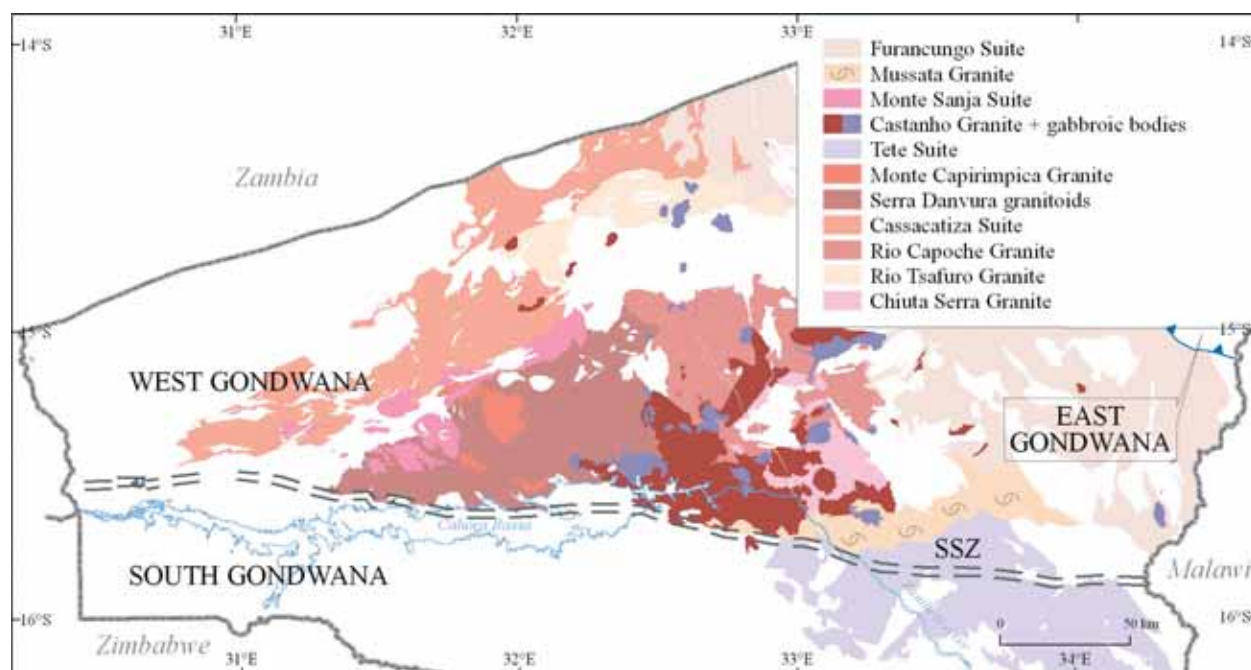


Fig. 6. Distribution of Mesoproterozoic granitoid and bi-modal suites and clans of the Tete-Chipata Belt in northern Tete Province. Note the intimate spatial relationship between Castanho Granite intrusions and small gabbro-anorthosite bodies.

The volcanics of the Mualadzi Group ($\text{SiO}_2 < 60\%$) have characteristics approaching volcanic arc lavas, while the chemical composition of the Fingoè volcanics ($\text{SiO}_2 < 60\%$) rather refers to ocean floor or ocean island arc environments. However, the interpretation of a volcanic arc tectonic setting is not supported by the bimodality of the Mualadzi Group volcanics. In the MORB normalised spidergram, low values of TiO_2 , Zr and Y and a drop of Zr between TiO_2 and Y in the Mualadzi Group are features that differ from the Fingoè volcanics (GTK

Consortium 2006d). The above dissimilarities in chemical characteristics and our field observations support our thesis that the Mualadzi volcanics do not belong to the Fingoè Supergroup and constitute a separate unit.

Schistose metasedimentary rocks of the undated *Cazula Group* comprise quartzite, quartz-feldspar gneiss, amphibolite and calc-silicate gneiss that form a series of enclaves in the 1041 ± 4 Ma Desaranhama granite of the Furancungo Suite.

Grenvillian Mesoproterozoic Intrusives

Based on structural features, fabric, composition (analytical results and aero-geophysical signatures) and age, Mesoproterozoic granitoids of the TCB can be grouped into several granitoid clans and a bi-modal suite emplaced during the Grenvillian orogenic cycle (GTK Consortium 2006d, Mänttari 2008). These are (from old to young): (1) Chiuta Serra (undated, but > 1.2 Ga), (2) Rio Capoeche (~ 1.20 Ga), (3) Rio Tsafuro (~ 1.12 Ga), (4) Serra Danvura (undated, but > 1.08 Ga), (5) Monte Capirimpica (~ 1.09 Ga), (6) Cassacatiza (~ 1.08 Ga), (7) Monte Sanja (1.05 Ga), (8) Mussata (undated, strongly mylonitized, occasionally phyllonitic; can be completely retrograded Chidzolomondo granulite) and (9) Fur-

ancungo granitoid clans or suites (Fig. 6). The latter comprises the 1.04 Ga Desaranhama Granite.

Finally, the 1050 ± 2 Ma Castanho Granite should be mentioned because of its particular geological position. Castanho Granite granitoids are restricted to the Chidzolomondo granulites and spatially intimately associated with gabbro-anorthosite bodies (Fig. 6). They belong to the charnockite series of amphibole- and pyroxene-bearing granitoids and form the felsic member of the bimodal Tete Province Anorthosite-Mangerite-Charnockite-Granite (AMCG) Suite, together with the coeval gabbro-anorthosite intrusives, including the Chipera Massif with a Sm-Nd age of 1047 ± 29 Ma (GTK Consor-

tium 2006d, Mänttari 2008) and the Tete Suite with a poorly constrained Sm-Nd age of 1025 ± 79 Ma (Evans *et al.* 1999).

The division, composition and litho-geochemical characteristics of these Mesoproterozoic plutonic rocks are reported in Mäkitie *et al.* (2008).

Pan-African Neoproterozoic-Phanerozoic Intrusives

Amphibolite-grade Neoproterozoic supracrustal rocks are widespread in the Zambian part of the TCB, tectonically overlying the Mesoproterozoic (1106 ± 19 Ma) Mpande Gneiss (Fig. 2). Dominantly pelitic units with minor psammite horizons generally constitute the inferior part of the sequence, overlain by extensive marbles and calc-silicate rocks. The sequence includes a local bimodal sequence of meta-basalt and meta-rhyolite that has yielded a U-Pb zircon upper-intercept age of 879 ± 19 Ma (M. Wardlaw, *unpublished data* in: Hanson *et al.* 1994) and approximately coeval but poorly constrained "bedded amphibolite" (Sm-Nd isochron age of 908 ± 48 Ma at Nampundwe mine near Lusaka; Burnard *et al.* 1993). A younger age limit is provided by the zircon age of a pre-kinematic, strongly mylonitized granitoid (the 820 ± 7 Ma Ngoma Gneiss). Supracrustal deposition and basin development supposedly took place between 880 and 829 Ma (Hanson *et al.* 1994).

In Tete Province, Neoproterozoic supracrustal rocks are absent in the TCB and only a small fraction of the plutonic rocks have been emplaced during the Pan-African orogenic cycle (Fig. 7). Early Pan-Af-

rican intrusive rocks in the TCB include the felsic to intermediate Matunda Suite and the (ultra-)mafic Atchiza and Ualáze Suites in the westernmost part of Tete Province. Late Pan-African Phanerozoic granitoid stocks, previously collectively termed the "late granite suite" (Hunting 1984a, b), are now attributed to the Sinda Suite (502 ± 8 Ma), Macanga (470 ± 14 Ma), Monte Tarai and Monte Inchinga granites (GTK Consortium 2006d, Mänttari 2008). They form small stocks, 3 to 30 km in diameter that intruded the older TCB basement (Fig. 7).

Matunda Suite is a fault-bounded unit, forming a domal structure of granitic gneisses, interlayered felsic and mafic gneisses and isolated metagabbro and diabase bodies, locally invaded by a swarm of thick pegmatite bodies. SHRIMP zircon dating of Matunda granitic gneiss yielded two clear age groups (GTK Consortium 2006d, Mänttari 2008). The youngest group gave an age of 528 ± 4 Ma, which can be correlated with late Pan-African metamorphism in the DLZ Belt. The data of the older group indicates zircon ages ranging from 700 Ma to 830 Ma, with one zircon age > 900 Ma. A direct magmatic age of this rock cannot be evidenced from

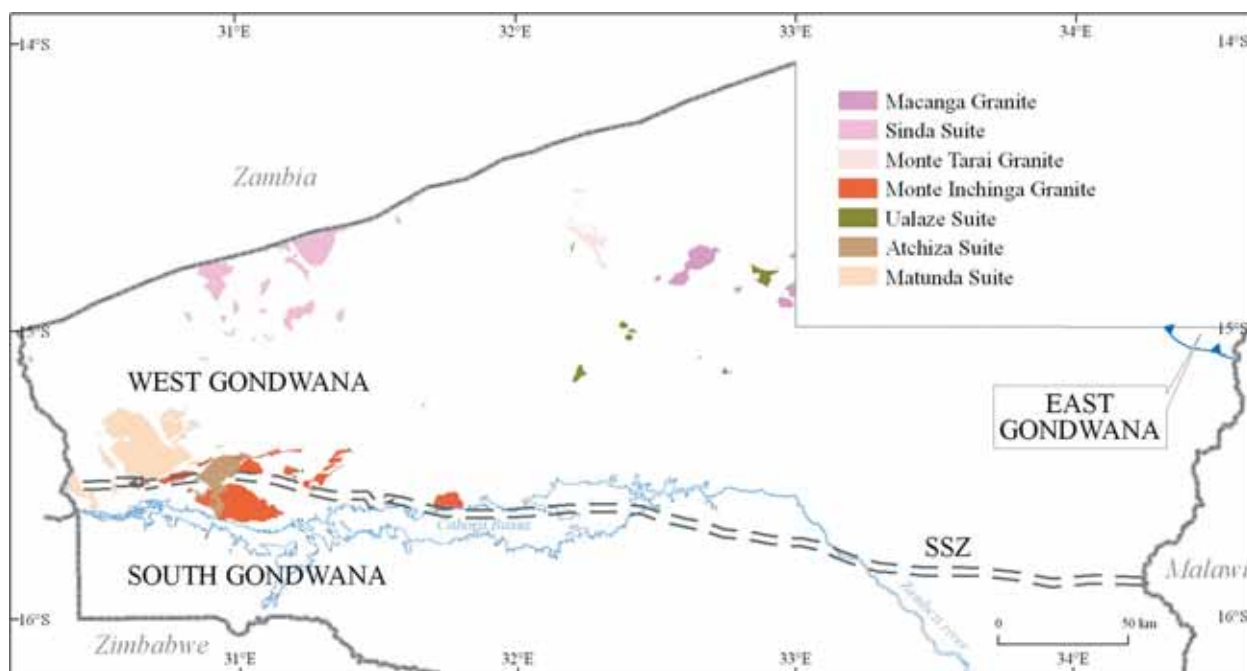


Fig. 7. Distribution of Pan-African Neoproterozoic-Phanerozoic granitoid and bi-modal suites and clans of the Tete-Chipata Belt in northern Tete Province.

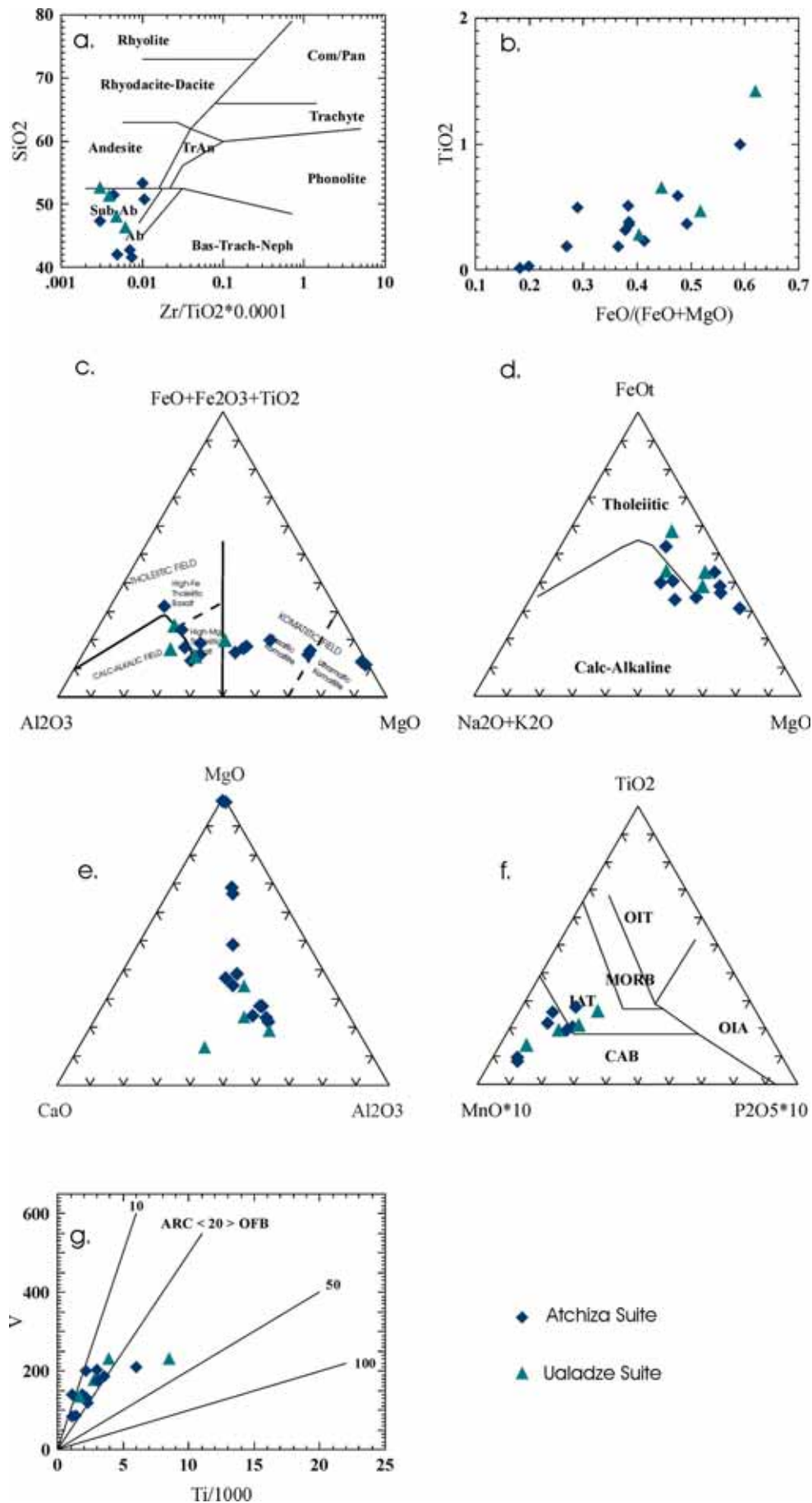


Fig. 8. Chemical classification for the rocks of the Atchiza and Ualadze Suites. Abbreviations: OIT = ocean island tholeiites, OIA = ocean island andesites, MORB = mid-ocean ridge basalts, CAB = calc-alkaline basalts, OFB = ocean floor basalts.

the data, but the best estimate yields an average age of 784 ± 36 Ma.

Atchiza Suite, formerly called the Monte Atchiza Complex (Hunting 1984a, b), is composed of a basal ultramafic succession (dunite/serpentine, pyroxenite and melagabbro), covered by a mafic upper sequence (gabbro, norite and diorite). An initial epsilon-value of -3.0 indicates contamination of the magma with older LREE-enriched material. Sm-Nd dating of pyroxene gabbro has yielded an isochron age of 864 ± 30 Ma (GTK Consortium 2006d, Mänttari 2008). The age fits with the phase of post-Grenvillian extension (rift/drift/dispersal of Rodinia) and the start of accumulation of supracrustals in the western part of the TCB. It is also coeval with bimodal magmatic rocks thrust on the northern and northeastern margins of the Zimbabwe craton (Dirks *et al.* 2003, GTK Consortium 2006b), which yield ages ranging from 850 to 870 Ma (Mariga *et al.* 1998, Vinyu *et al.* 1999, Dirks *et al.* 2003, GTK Consortium 2006b, Koistinen *et al.* 2008).

The analysed samples of the Atchiza Suite include dunite, pyroxenite and gabbro and the results are plotted in discrimination and classification diagrams (Fig. 8). Some of these diagrams are meant primarily for volcanic rocks, and are being used here to test a possible volcanic (ophiolitic) origin, as has been proposed for the Atchiza Suite. The Zr/TiO₂ vs. SiO₂ plot falls in the basaltic field (Fig. 8a) and AFM ratios classify the rocks as tholeiitic

(Fig. 8d). The low Fe/Mg ratio is confirmed in the TiO₂ vs. FeO/(FeO+MgO) diagram (Fig. 8b). On a Jensen diagram the analyses form a trend within the komatiitic and high-Mg fields, far from the Fe apex of the triangle, referring to the low Fe/Mg ratio of the magma (Fig. 8c). A magma evolution is seen in the CaO-MgO-Al₂O₃ diagram of Figure 8e, where the plotted analyses constitute an arching trend from the MgO apex towards the Al₂O₃ apex. An ophiolite origin of the Atchiza Suite cannot be verified from their major element chemistry. The Mn-Ti-P ratios of the analyses plot well outside a MORB composition (Fig. 8f) and the V vs. Ti plot classifies the rock as volcanic arc lavas rather than ocean floor basalts (Fig. 8g).

The Ualádze Suite, formerly the Ualádze mafic suite (Hunting 1984a, b), is represented by a roughly E-W-trending swarm of dolerite dykes (up to hundreds of metres in width) and small- to medium-sized gabbro bodies (max. 5 km in diameter) traversing the western half of the TCB. In places, dykes have preferentially NE-SW directions and, occasionally, components of ultramafic composition.

Analytical data (4 samples) have been plotted on chemical classification diagrams, together with analytical data of the Atchiza Suite (Fig. 8) (see GTK Consortium 2006d). The litho-chemical classification diagrams confirm, at least do not contradict, a common origin for these two suites as already proposed by Hunting (1984a, b).

THE STACKED MICRO-TERRANE MODEL

On the Zambian side of the border the crystalline basement of the TCB (or South Irumide Belt *sensu* Johnson *et al.* 2005) has been divided into a number of distinct terranes and smaller structural elements (micro-terrane) of various ages and tectonic settings, stacked on top of one another (Mapani *et al.* 2004). The Rufunsu Terrane, recently re-named the Chewore-Rufunsu Terrane (Johnson *et al.* 2007), which is lowermost in the structural stack, is according to Johnson *et al.* (2006b) composed of a wide variety of 1105–1040 Ma, supracrustal to mid-crustal rocks. The Chewore Inliers, comprising an uplifted block of Mesoproterozoic basement, emerging as a window from below the surrounding Karoo and younger cover in the Zambezi segment of the DLZ Belt (Fig. 2), may serve as a type-location to illustrate the "stacked micro-terrane model". They consist of a thin-skin, thrust collage of micro-terrane and even smaller structural elements. Stacked structural elements include (from NW to SE):

- *Granulite micro-terrane* – Composed of para- and quartzo-feldspathic orthogneisses and interbedded mafic granulites that suffered high-grade metamorphism (< 4.4 kb; 800 °C; Goscombe *et al.* 1994, 1998), dated at 1071 ± 8 Ma with metamorphic overprinting at 524 ± 16 Ma.
- *Quartzite micro-terrane* – Composed of quartzites and paragneisses that suffered high-grade metamorphism (7.9–8.6 kb, 720 °C). Not dated.
- *North Zambezi micro-terrane* – Banded paragneisses and calc-silicate rocks and minor concordant 1083 ± 8 Ma (Goscombe *et al.* 2000) quartzo-feldspathic orthogneisses that suffered high-grade metamorphism (7.9–8.6 kb, 630 °C; Goscombe *et al.* 1994, 1998).
- *South Zambezi micro-terrane* – Very coarse-grained porphyroblastic (Augen up to 7 cm)

quartzo-feldspathic biotite and/or muscovite K-feldspar gneisses and minor aluminous schists that suffered high-grade metamorphism (7.9–8.6 kb, 590 °C; Johnson & Oliver 2002).

- *Ophiolite micro-terrane* – Also called Chewore Ophiolite, composed of (1) altered peridotite, (2) massive and layered hornblende gabbro, (3) sheeted dolerite dykes and (4) whiteschist (talc-kyanite-yoderite paragenesis; Johnson & Oliver 1998, 2002) with imbricated metamorphosed pelites, greywackes and calc-silicate distal turbidites, pillow basalt and chert. Metalava and sheeted dykes reveal two groups of basalt, one with a MORB signature and the other with an island-arc affinity. SHRIMP zircon dating of plagiogranite yields an ocean floor age of 1393 ± 22 Ma (Oliver *et al.* 1998). The micro-terrane is interpreted as a marginal back-arc basin ophiolite (Chewore Ophiolite) together with island-arc rocks (Kaourera Arc). The latter yield ages ranging from 1082 ± 7 Ma (Johnson & Oliver 2004) to 1066 ± 21 Ma (Johnson, unpublished data) with reworking at

< 580 Ma (Johnson & Oliver 2000) to 517 ± 5 Ma (Johnson & Oliver 2004). The whiteschist assemblage manifests a Pan-African HP-LT, subduction-related metamorphic event with 13–15 kb and 550–600 °C (Johnson & Oliver 1998, 2000).

As in the Zambian part of the TCB, cohesion between major units (supergroup, group, suite, granitoid clan) mapped in the Mozambican part of the TCB (GTK Consortium 2006d) is poor in terms of age, lithology and tectono-metamorphic development. In analogy with equivalent rocks on the Zambian side of the border (Mapani *et al.* 2004), a “suspect terrane model” has been proposed (GTK 2006d). The boundaries between these terranes are poorly defined at the present state of structural mapping and, consequently, so far not portrayed in the new set of 1:250 000-scale maps prepared by the GTK Consortium (see also GTK Consortium 2006d). Provisionally, we distinguish and correlate the following terranes in the TCB of northern Tete Province (Fig. 9):

Chewore-Rufunsu Terrane

Elements of this terrane in the Chewore Inliers are described above. Johnson *et al.* (2005, 2006b) claim that this structural unit is located in Zambia, just west of and outside Mozambique. We cannot exclude, however, that garnetiferous para- and orthogneisses of the Rio Mese and Rio Mepembe for-

mations, hitherto attributed to the basal part of the Zâmbuè Supergroup, belong to the Rufunsu Terrane. Dating of equivalent lithologies in Zambia suggests Palaeoproterozoic and Archean ages (~2.6 Ga; Cox *et al.* 2002) for these rocks.

Luangwa and Nyimba Terranes

The Nyimba Terrane in Zambia is dominated by supracrustal rocks, including marble and calc-silicate rocks (Johnson *et al.* 2005) and pelitic migmatites and quartzites (Johnson *et al.* 2006b). The hanging and footwall contacts are interpreted as ductile thrust zones. Detrital zircons indicate late Archean and mid Paleoproterozoic sedimentary sources and low Th/U metamorphic overgrowth of these detrital zircons indicate HT metamorphism at ~1060 Ma (Johnson *et al.* 2006b).

Supracrustals of the Zâmbuè Supergroup in Mozambique, interpreted as a passive margin sequence, can be divided into a western tectono-stratigraphic domain predominantly composed of 1.2–1.3 Ga

meta-arkoses, quartzites (also with detrital zircons of Archean and Paleoproterozoic age) and subordinate metapelites and a domain with a basal zone composed of marble and calc-silicate gneisses, appearing as a crescent-shaped polygon in the geological map compiled by GTK Consortium. The two domains show clear structural and stratigraphic differences. The western structural-stratigraphic domain is provisionally called the Luangwa Terrane, the eastern one is correlated with the Nyimba Terrane identified in Zambia. The latter may actually represent a duplex structure with the Pan-African Sinda granite as “stitching pluton” in between.

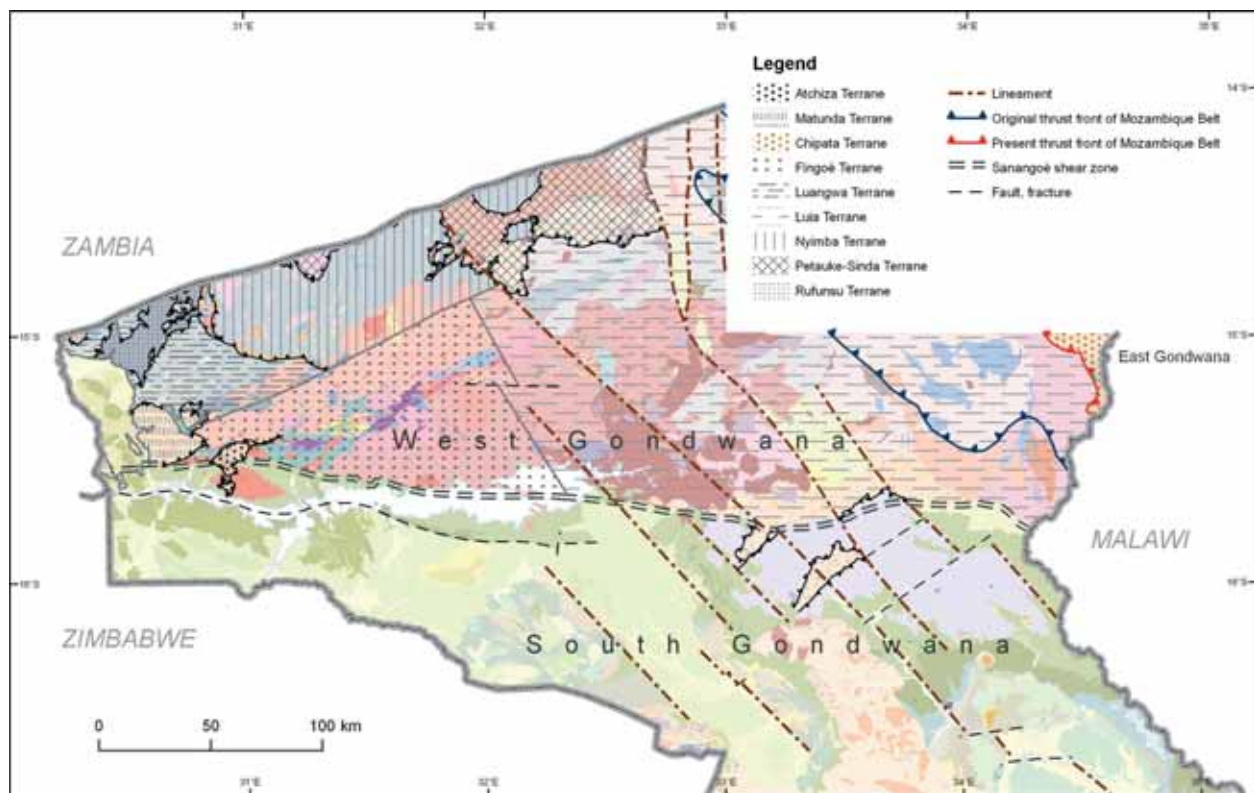


Fig. 9. Provisionally distinguished terranes in the Tete-Chipata Belt of northern Tete Province, Mozambique. For lithologies of geological map in background, see Figures 4, 6 and 7.

Petauke-Sinda Terrane

Continuing eastwards along the Zambia-Mozambique border, and structurally on top of the Nyimba Terrane, Mapani *et al.* (2004) have identified the Petauke-Sinda Terrane. This terrane consists of a suite of calc-alkaline basement gneisses (i.e., the Nyanji Gneiss), interpreted as an accreted island arc (Mapani *et al.* 2004) and dated at ~1130–1120 Ma (Rivers; in Johnson *et al.* 2005) and 1125 ± 15 Ma (Cox, pers. comm., in Johnson *et al.* 2005). The suite is overlain by amphibolite facies paragneisses and granitic orthogneisses with a crystallization age of ~740 Ma and metamorphic overprinting at ~530 Ma. Pan-African volcanics are exposed in the northern part of this terrane and are supposedly coeval with porphyritic granite that yields an age of ~720 Ma (Johnson *et al.* 2006b).

The Sinda-Petauke Terrane on the Zambian side of the border continues in Mozambique into the northeastern polygon of the 1077 ± 2 Ma Cassatiza Suite (Fig. 6), an I-type granite, plotting on

the boundary between volcanic-arc and within-plate granites. Texturally, the rather massive central parts of the Suite grade towards its contacts with the Zâmbuè and Fíngoè Supergroups into foliated, blastomylonitic gneisses. Older granitoid suites in the TCB on the Mozambican side of the border include the Chiúta Serra (>1.2 Ga), Rio Capoeche (~1.2 Ga), Rio Tsafuro, Serra Danvura (>1.09 Ga) and Monte Capirimpica (~1.09 Ga) (Fig. 6). On geochemical discrimination diagrams all suites plot as metaluminous to peraluminous granitoids with a calc-alkaline affinity, while the rocks with lower SiO_2 contents straddle the boundary between calc-alkaline and tholeiitic affinities and between “volcanic-arc” and “within-plate” granitoids (Mäkitie *et al.* 2008). Age-wise, they can be compared to the Mpande Gneiss (Fig. 2), a deformed, K-feldspar-rich granite in the central part of the Zambezi segment of the DLZ Belt, with a U-Pb zircon upper intercept igneous age of 1106 ± 19 Ma (Hanson *et al.* 1988).

Fíngoè Terrane

Further southwards we have identified the triangular Fíngoè Terrane (Fig. 9), comprising the 1327

± 16 Ma (Mänttari 2008) SW-NE trending volcano-sedimentary Fíngoè Supergroup and vast grani-

toid domains to the NW and SE. The southeastern domain is largely composed of the Serra Danvura granitoids. They have been invaded by younger granitoids including the 1086 ± 7 Ma Monte Capirimpica granite, granitoids of the 1050 ± 8 Ma Monte Sanja Suite and Pan-African Monte Ichinga granites. Small windows of Fíngoè supracrustals manifest a far wider extension of these supracrustals than exposed in the relatively narrow Fíngoè belt (Fig. 4).

The northwestern granitoid domain largely comprises the southwestern granitoid polygon assigned to the 1077 ± 2 Ma Cassacatiza Suite, with Fíngoè windows and intrusions of younger granitoids including the 1050 Ma Monte Sanja Suite and undated Marirongoe granitoids. The Fíngoè Terrane is provisionally interpreted as a 1.33 Ga active margin or island arc volcano-sedimentary belt overlain by a 1.20 Ga magmatic arc.

Luia Terrane

The rectangular “granulite/charnockite terrane” (Fig. 9), east of the Fíngoè Terrane, largely coincides with the area underlain by the Luia Group *sensu* Hunting (1984a, b) and the term “Luia Terrane” is consequently proposed. It is composed of supracrustal rocks attributed to the Chidzolomondo and Mualadzi Groups, which have been invaded by a variety of granitoid rocks, including 1050 ± 2 Ma charnockites of the Castanho Granites, in close association with 1047 ± 29 Ma gabbro-anorthosite bodies, Rio Capoche granitoids and small Pan-African intrusions of Macanga granites dated at 470 ± 14 Ma (GTK Consortium 2006d, Westerhof *et al.* 2008).

The eastern part of the Luia Terrane has been intruded by the granitoids of the Furancungo Suite, including the 1041 ± 4 Ma Desaranhama granite.

Occasional relicts of pyroxene in strongly mylonitized “granitoids” suggest that at least part of these rocks may have a granulitic or charnockitic protolith. Enclaves of supracrustal rocks, such as the ones attributed to the Cazula Group, may, in fact, represent erosional relicts of *Klippe*, belonging to the Angónia Group.

The Luia Terrane may continue into Zambia as Chipata Terrane identified by Mapani *et al.* (2004) and Johnson *et al.* (2006b, 2007). It is composed of a variety of retrogressed mafic, felsic and pelitic granulites with subordinate hornblende-biotite gneisses and granitoids. The granulites have crystallization ages of between 1160 and 1080 Ma and low Th/U metamorphic zircon overgrowths that yield the age of the high-grade granulite metamorphic event at ~ 1050 Ma.

Matunda and Atchiza Terranes

Finally, in the westernmost part of Tete Province two juvenile Pan-African “suspect terranes” are exposed, i.e., the Matunda Suite and the (ultra-)mafic Atchiza Suite.

Matunda granitic gneisses can be compared with the strongly deformed Ngoma Gneiss (Zambia), for which a U-Pb zircon upper-intercept age of 820 ± 7 Ma has been obtained, and with quartzo-feldspathic gneisses of the “North and South Zambezi micro-terranes” in the Chewore Inliers (Zimbabwe). The metamorphic conditions in these micro-terranes (Johnson & Oliver 2004, and references therein) also comply with the mineral assemblages observed in the Matunda Suite.

The 864 ± 30 Ma (Mänttari 2008) Atchiza dunite/serpentine-gabbro-norite-diorite body is local-

ly strongly deformed with E-W striking, shallowly dipping shear planes, supposedly related to subhorizontal thrusting or detachment faulting. The question is: “Are these bodies *in situ* or have they been transported tectonically to their present position?” Pan-African amphibolite-grade metamorphic overprinting dated at ~ 0.53 Ga of the Matunda Suite, intense deformation in both and the absence of high-grade Pan-African metamorphism in nearby Fíngoè supracrustals points to an allochthonous position and, consequently, the Matunda Suite and Atchiza Suite represent micro-terranes.

As mentioned, both an ophiolite and a layered igneous origin have been attributed to the Atchiza Suite (e.g., Real 1962, Afonso *et al.* 1998).

GEODYNAMIC DEVELOPMENT OF THE TETE-CHIPATA BELT

Analogous with recent research on the Zambian side of the border (Mapani *et al.* 2004, Johnson *et al.* 2005, 2006a,b, 2007), we postulate that the TCB is composed of a wide variety of supra- and midcrustal rocks of pre-Grenvillian Mesoproterozoic age, contained in a collage of terranes that assembled, collided and amalgamated with the southern margin of the Central Africa craton (West Gondwana) during the Grenvillian orogenic cycle (Johnson *et al.* 2006a).

Individual terranes within the TCB include an island arc in the Chewore Inliers – called the Kaourera Arc – dated at ~1080 Ma. Lithological and geochemical characteristics suggest that this arc may not be directly related to the back-arc-related Chewore Ophiolite, dated at ~1393 Ma, some 300 Ma older. Considering the structural complexity, older portions of the arc, approximately equivalent in age to the ophiolite, are expected in the collage of stacked terranes. The volcano-sedimentary succession of the Fíngoè Supergroup, assigned to the Fíngoè Terrane, dated at ~1327 Ma, and “older granitoids” such as the Chiúta Serra, the 1201 Ma Rio Capoché and Rio Tsafuro granitoids may qualify as relicts of magmatic arcs. The age difference between the Chewore Ophiolite and Kaourera Arc suggests the development of island arcs and back-arc basins over a time span of at least 300 Ma within an oceanic basin S of the Central Africa craton (Johnson & Oliver 2004, Johnson *et al.* 2006a).

The meta-arkose-quartzite±metapelite and marble-meta-arkose±quartzite successions of the Zâmbuè Supergroup were most likely deposited in a passive margin setting along the southern margin of the Central Africa craton at ~1.2–1.3 Ga. Note that the age range of zircons in Zâmbuè supracrustals is very similar to the age spectra reported by Rainaud *et al.* (2003) for detrital zircons extracted from metasediments within the Lufilian Arc and Irumide belt. Reversal from a passive to active margin is heralded by the formation of a continental “Andean-type” magmatic arc. We suggest that granitoids with ages between ~1200 and 1070 Ma in the northern Tete Province were emplaced either into this “Andean-type” magmatic arc or are comparable to the granitoids in the ~1080 Ga Kaourera Arc. Granulites may have been derived from the craton’s margin basement.

The above scenario is confirmed by detailed geochemical, isotopic and geochronological data from a wide variety of supracrustal to mid-crustal rocks of the Chewore-Rufunsu Terrane, which shows major

and trace-element compositions similar to magmas formed in present-day subduction zones (Johnson *et al.* 2007). Chondrite-normalized rare earth element (REE) profiles and whole-rock Sm–Nd isotope compositions indicate that the parental supra-subduction melts interacted with, and were contaminated by sialic continental crust, implying a continental-margin-arc setting. Secondary ionization mass spectrometry dating of magmatic zircon has yielded crystallization ages between ~1095 and 1040 Ma, similar to elsewhere in the TCB. U–Pb dating and *in situ* Lu–Hf isotopic analyses of abundant xenocrystic zircon extracted from the late Mesoproterozoic granitoids indicate that the contaminant continental basement was principally Paleoproterozoic in age and had a juvenile isotopic signature at the time of its formation.

Johnson *et al.* (2007) emphasize that these data are in contrast to those for the Irumide Belt, which is characterized by younger, ~1020 Ma, calc-alkaline gneisses that were formed by the direct recycling of Archaean crust without any significant addition of juvenile material. This underlines the fundamental significance of the Mwembeshi Dislocation and the independent structural position of the TCB *vis-à-vis* the Irumide Belt. Johnson *et al.* (2007) further suggest that the Southern Irumide Belt (TCB) developed by the subduction of oceanic crust under the margin of an unnamed continental mass until ocean closure at ~1040 Ma. Subsequent collision between the TCB and the Central Africa craton margin led to the cessation of magmatism in the TCB and the initiation of compression and crustal melting in the Irumide Belt.

Collision, obduction and amalgamation of island arc, “passive-reversed-to-active” continental margin and mid-crustal fragments in the Tete Province resulted in the juxtaposition of continental Zâmbuè and island arc Fíngoè supracrustals and Luia granulites. The boundary between the first two terranes is still visible as a lineament in satellite imagery. Slivers of continental crust, including the supposedly Paleoproterozoic and Archaean Rio Mese and Rio Mepembe garnetiferous para- and orthogneisses (GTK Consortium 2006d), provisionally attributed to the Chewore-Rufunsu Terrane, may have been derived from deeper fault blocks underlying the erstwhile passive margin. Alternatively, they may represent continental slivers of unknown derivation, formed during an older, post-Eburnean phase of continental rift/drift/dispersal and squeezed between the island arc and continental margin.

Subsequent to amalgamation of the collage of “suspect terranes” and the Congo continental margin, crustal thickening or orogenic collapse triggered the emplacement of younger (1.05 and 1.04 Ga) granitoids and massive bimodal magmatism. Some of these granitoids supposedly played the role of “stitching pluton” (e.g., the 1050 ± 8 Ma Monte Sanja granite). A bimodal suite is composed of charnockites of the Castanho Granites and gabbro-anorthosite intrusives of the Tete Suite and smaller stocks, forming the Tete Province AMCG Suite (GTK Consortium 2006d). The magmas of the charnockite intrusions, associated with the anorthosites, are thought to form by melting of the (dehydrated) lower crust as a result of the crystallisation heat and elevated isotherms of “underplated magmas”. This would explain the occurrence of Castanho Granite charnockites confined to the Chidzolomondo granulites of the Luia Terrane. Depending on the composition of the lower crust (itself possibly derived from earlier underplated magmas), the charnockitic melts may acquire a range of compositions, further complicated by potential crustal contamination on their ascent. One can thus conclude that anorthosites and associated charnockite intrusions are not co-magmatic, but are derived from coexisting melts, and that slight differences in emplacement age may exist.

Juvenile crust in the Tete-Chipata Belt was formed during a post-Grenvillian Neoproterozoic extensional phase (~880 to 765 Ma). Closure of the Zambezi-Adamastor oceanic basin (Johnson *et al.* 2005) and collision and amalgamation of the Kalahari craton (South Gondwana) and Central Africa craton (West Gondwana) resulted in the double-verging Damara-Lufilian-Zambezi Belt. This was not a simple collision between two large lithospheric plates, but rather a series of collisional events among several cratonic fragments, taking place between ~615 Ma and 520 Ma, over a period of ~100 Ma. We suggest that the creation and displacement of Pan-African tectonic fragments, such as the Matunda and Atchiza Terranes, took place during this event, most likely together with remobilization of existing sutures, whereby deformation and retrograde metamorphism, as manifested by zircon overgrowths, was focused along existing terrane boundaries. Finally, late to post-Pan-African granitic stocks have been emplaced into this collage of terranes, in cases as “stitching pluton”, employing sutures in between terranes (e.g., Sinda Suite). Post-Pan-African intracratonic remobilization of weakness zones during the late Paleozoic Gondwanide orogen (Trouw & De Wit 1999) remains a matter of speculation.

ACKNOWLEDGEMENTS

The authors wish to thank Dr. Kerstin Saalman and Dr. Pentti Hölttä for constructive comments and Mrs. Eira Kuosmanen for preparing the Figures.

REFERENCES

- Afonso, R. S., Marques, J. M. & Ferrara, M. 1998. A Evolução Geológica de Moçambique. Instituto de Investigação Científica Tropical de Portugal and Direcção Nacional de Geologia de Moçambique. 1st Edition, Lisbon, Portugal.
- Barr, M. W. C. & Brown, M. A. 1987. Precambrian gabbro-anorthosite complexes, Tete province, Mozambique. *Geological Journal* 22, 139–159.
- Barr, M. W. C. & Brown, M. A. 1988. Gabbro-Anorthosite Complexes, Tete Province, Mozambique. *Boletim Geológico*, 41, 7–39, Instituto Nacional de Geologia, Ministério dos Recursos Minerais, Maputo.
- Barton, C. M., Carney, J. N., Crow, M. J., Dunkley, P. N. & Simango, S. 1991. The geology of the country around Rushinga and Nyamapanda. Zimbabwe Geological Survey, Harare, Bulletin 92, 220 p.
- Bingen, B. J., Viola, G., Henderson, I. H. C., Smethurst, M., Boyd, R., Thomas, R. J., Bjerkgård, T., Feito, P., Hollick, L. M., Jacobs, J., Key, R. M., Rossi, D., Sandstad, J. S., Skår, Ø., Smith, R., Solli, A. & Tveten, E. 2006. Geochronology of Pan-African terrain assembly in NE Mozambique. XXI Colloquium of African Geology (CAG21), 2006, Maputo, Mozambique, Abstract Volume, 12–14.
- Bloomfield, K. & Garson, M. S. 1965. The geology of the Kirk Range – Lisungwe Valley area. *Bulletin of the Geological Survey of Malawi*, 17.
- Breitkopf, J. H. & Maiden, K. J. 1988. Tectonic setting of the Matchless belt pyritic copper deposits, Namibia. *Economic Geology* 83, 710–723.
- Bulambo, M., De Waele, B., Kokonyangi, J., Johnson, S. P., Kampunzu, A. B. & Tembo, F. 2006. SHRIMP zircon U-Pb geochronology and geochemistry of the Choma-Kalomo Block granitoids (Zambia): Geological implications. XXI Colloq. Afr. Geol. (CAG21), 2006, Maputo, Abstract Volume, 26–27.
- Burke, K., Dewey, J. F. & Kidd, W. S. F. 1977. World distribution of sutures; the sites of former oceans. *Tectonophysics*, 40, 69–99.
- Burnard, P. G., Sweeney, M. A., Vaughan, D. J., Spiro, B. & Thirlwall, M. F. 1993. Sulfur and lead isotope constraints on the genesis of a southern Zambian massive sulfide deposit. *Economic Geology* 88, 418–436.
- Cahen, L. & Snelling, N. J. 1966. The Geochronology of Equatorial Africa. North-Holland Publishing Cy., Amsterdam, 195 p.

- Cox, R. A., Rivers, T., Mapani, B., Tembo, D. & De Waele, B. 2002.** 11th IAGOD Quadrennial Symposium and Geology of Degree Sheets Mecumbura, Chioco, Tete, Tambara, Guro, Chemba, Manica, Catandica, Gorongosa, Rotanda, Chimoio and Beira, Mozambique. Direcção Nacional de Geologia (DNG), Maputo, 411 p. + Ann.
- Cutten, H. N. C. & Johnson, S. P. 2006.** Tectonic evolution of the Mozambique Belt, eastern Africa. Colloquium of African Geology (CAG21), 2006, Maputo, Mozambique. Abstract Volume, 33–34.
- De Waele, B., Nemchin, A. A. & Kampunzu, A. B. 2003a.** The Bangweulu Block of northern Zambia: where is the pre-Ubendian crust? Abstracts, Assembly and Breakup of Rodinia, South China Field Symposium, Hangzhou, 19–21.
- De Waele, B., Wingate, M. T. D., Mapani, B. & Fitzsimons, I. C. W. 2003b.** Untying the Kibaran knot: A reassessment of Mesoproterozoic correlations in southern Africa based on SHRIMP U-Pb data from the Irumide belt. *Geology* 31, 509–512.
- De Waele, B. & Fitzsimons, I. C. W. 2004.** The age and detrital fingerprint of the Muva Supergroup of Zambia: molasse deposition to the southwest of the Ubendian belt. Abstracts, Geoscience Africa, Johannesburg, 162–163.
- De Waele, B., Liégeois, J.-P., Johnson, S. P., Nemchin, A. A. & Tembo, F. 2006.** Recurrent reworking of the Irumide Belt of Zambia. Colloquium of African Geology (CAG21), 2006, Maputo, Abstract Volume, 38–39.
- Dirks, P. H. G. M., Kröner, A., Jelsma, H. A., Sithole, T. A. & Vinyu, M. L. 1999.** Structural relations and Pb-Pb zircon ages for a crustal-scale Pan African shear zone in the Zambezi Belt, northwest Zimbabwe. *Journal of African Earth Sciences* 28, 427–442.
- Dirks, P. H. G. M., Blenkinsop, T. G. & Jelsma, H. A. 2003.** Geology of Africa. Encyclopedia of Life Support Systems, EOLSS Publishers Co. Ltd.
- Evans, R. J., Ashwal, L. D. & Hamilton, M. A. 1999.** Mafic, ultramafic, and anorthositic rocks of the Tete Complex, Mozambique: petrology, age, and significance. *South African Journal of Geology* 102, 153–166.
- Goscombe, B., Fey, P. & Both, F. 1994.** Structural evolution of the Chewore Inliers, Zambezi Mobile Belt, Zimbabwe. *Journal of African Earth Sciences* 19, 199–224.
- Goscombe, B., Armstrong, R. & Barton, J. M. 1998.** Tectonometamorphic Evolution of the Chewore Inliers: Partial Re-equilibration of High-grade Basement during the Pan-African Orogeny. *Journal of Petrology* 39, 1347–1384.
- Goscombe, B., Armstrong, R. & Barton, J. M. 2000.** Geology of the Chewore Inliers, Zimbabwe: constraining the Mesoproterozoic to Paleozoic evolution of the Zambezi Belt. *Journal of African Earth Sciences* 30, 599–627.
- Grantham, G. H., Maboko, M. & Eglinton, B. M. 2003.** A Review of the Evolution of the Mozambique Belt and Implications for the Amalgamation and Dispersal of Rodinia and Gondwana. – In: Yoshida, M., Windley, B. F. and Dasgupta, S. (eds.), *Proterozoic of East Gondwana: Supercontinent Assembly and Breakup*. Geological Society of London Special Publication, 206.
- Grantham, G. H., Ingram, B. A., Roberts, M. P., Matola, R. & Manhica, V. 2006.** The geology of the Ulongue-Furancungo area, NW Mozambique. XXI Colloq. Afr. Geol. (CAG21), 2006, Maputo, Abstract Volume, 55.
- GTK Consortium 2006a.** Map Explanation; Volume 1: Sheets 2032–2632. Geology of Degree Sheets, Espungabera/Chibabava, Nova/Mambone, Massangena, Chidoco, Save/Bazaruto, Chicualacuala, Machaila, Chigubo, Mabote/Vilanculos, Rio Singuédzi/ Massingir, Rio Changana, Funhalouro/Inhambane, Chilembene, Chókwe, Zavala/ Inharrime, Maputo, Xai-Xai/Zavala and Bela-Vista, Mozambique. Direcção Nacional de Geologia (DNG), Maputo, 341 p. + Ann.
- GTK Consortium 2006b.** Map Explanation; Volume 2: Sheets 1630–1634, 1732–1734, 1832– 1834 and 1932–1934. Geology of Degree Sheets Mecumbura, Chioco, Tete, Tambara, Guro, Chemba, Manica, Catandica, Gorongosa, Rotanda, Chimoio and Beira, Mozambique. Direcção Nacional de Geologia (DNG), Maputo, 411 p. + Ann.
- GTK Consortium 2006c.** Map Explanation; Volume 3: Sheets 1735–1739, 1835–1836 and 1935. Geology of Degree Sheets Mutarara, Quelimane, Namacurra/Maganja, Pebane, Marromeu/ Inhaminga, Chinde and Savane, Mozambique. Direcção Nacional de Geologia (DNG), Maputo, 240 p. + Ann.
- GTK Consortium 2006d.** Map Explanation; Volume 4: Sheets 1430–1432 and 1530–1534. Geology of Degree Sheets Inhambambo, Maluwera, Chifunde, Zumbo, Fingoè-Mâgoè, Songo, Cazula and Zóbuè, Mozambique. Direcção Nacional de Geologia (DNG), Maputo, 382 p. + Ann.
- Hanson, R. E., Wilson, T. J. & Wardlaw, M. S. 1988.** Deformed batholiths in the Pan-African Zambezi belt, Zambia: Age and implications for regional Proterozoic tectonics. *Geology* 16, 1134–1136.
- Hanson, R. E., Wardlaw, M. S., Wilson, T. J. & Mwale, G. 1993.** U-Pb zircon ages from the Hook granite massif and Mwembeshi dislocation: constraints on Pan-African deformation, plutonism, and transcurrent shearing in central Zambia. *Precambrian Research* 63, 189–209.
- Hanson, R. E., Wilson, T. J. & Munyanyiwa, H. 1994.** Geologic evolution of the Neoproterozoic Zambezi Orogenic Belt in Zambia. *Journal of African Earth Sciences* 18, (2), 135–150.
- Holland, T. J. B. & Powell, R. 1985.** An internally consistent thermodynamic dataset with uncertainties and correlations, 2, Data and results *Journal of Metamorphic Geology* 3, 343–370.
- Holland, T. J. B. & Powell, R. 1998.** An internally consistent thermodynamic dataset for phases of petrological interest *Journal of Metamorphic Geology* 16, 309–343.
- Hunting Geology & Geophysics 1984a.** Ground Geophysics. Mineral Inventory Project in Tete Province and Parts of Manica, Sofala and Zambezia Provinces. Report on ground geophysical investigations for the 1982 and 1983 field season. Unpubl. Rept., DNG, Maputo.
- Hunting Geology & Geophysics 1984b.** Landsat Interpretation - Stage 2. Mineral Inventory Project. Revised landsat interpretation, description of mapped units, Tete area. Unpubl. Rept. to DNG, Maputo.
- Jacobs, J., Bauer, W. & Thomas, R. T. 2006.** A Himalayan-type indenter-escape tectonic model for the southern part of the Late Neoproterozoic/Early Paleozoic East African- Antarctic Orogen. Colloquium of African Geology (CAG21), 2006, Maputo, Mozambique. Abstract Volume, 71–72.
- John, T. & Schenk, V. 2003.** Partial eclogitisation of gabbroic rocks in a late Precambrian subduction zone (Zambia): prograde metamorphism triggered by fluid infiltration. *Contributions to Mineralogy and Petrology* 146, 174–191.
- John, T., Schenk, V., Haase, K., Scherer, E. & Tembo, F. 2003.** Evidence for a Neo-proterozoic ocean in south-central Africa from mid-oceanic ridge-type geochemical signatures and pressure-temperature estimates of Zambian eclogites. *Geology* 31, 243–246.
- John, T., Scherer, E., Haase, K. & Schenk, V. 2004.** Trace element fractionation during fluid-induced eclogitization in a subduction slab: trace element and Lu-Hf/Sm-Nd isotope systematics. *Earth and Planetary Science Letters* 227, 441–456.

- Johnson, S. P. & Oliver, G. J. H. 1998.** A second natural occurrence of yoderite. *Journal of Metamorphic Geology* 16, 809–818.
- Johnson, S. P. & Oliver, G. J. H. 2000.** Mesoproterozoic oceanic subduction, island arc formation and the initiation of back-arc spreading in the Kibaran Belt of central southern Africa: evidence from the ophiolite terrane, Chewore Inliers, northern Zimbabwe. *Precambrian Research* 103, 125–146.
- Johnson, S. P. & Oliver, G. J. H. 2002.** High fO_2 metasomatism during whiteschist metamorphism. *Journal of Petrology* 43, 271–290.
- Johnson, S. P. & Oliver, G. J. H. 2004.** Tectonothermal history of the Kaourera Arc, northern Zimbabwe; implications for the tectonic evolution of the Irumide and Zambezi Belts of south central Africa. *Precambrian Research* 130, 71–97.
- Johnson, S. P., Rivers, T. & De Waele, B. 2005.** A review of the Mesoproterozoic to early Palaeozoic magmatic and tectonothermal history of south-central Africa: implications for Rodinia and Gondwana. *Journal of the Geological Society of London* 162, 433–450.
- Johnson, S. P., De Waele, B., Evans, D., Tembo, F. & Banda, W. 2006a.** A record of Neoproterozoic divergent processes along the southern Congo Craton margin. In: XXI Colloquium of African Geology, 2006, Maputo, Mozambique, Abstract Volume, 73–74.
- Johnson, S. P., De Waele, B. & Tembo, F. 2006b.** The southern Irumide belt of Zambia. In: XXI Colloquium of African Geology, 2006, Maputo, Mozambique, Abstract Volume, 75–77.
- Johnson, S. P., De Waele, B., Tembo, F., Katongo, C., Tani, K., Qing, C., Iizuka, T. & Dunkley, D. 2007.** Geochemistry, Geochronology and Isotopic Evolution of the Chewore-Rufunsa Terrane, Southern Irumide Belt: a Mesoproterozoic Continental Margin Arc. *Journal of Petrology* 48, 1411–1441.
- Koistinen, T., Lehtonen, M. I., Fernando, S. & Matola, R. 2008.** Contribution to the structure at the eastern margin of the Archaean Zimbabwe craton, Mozambique. *Geological Survey of Finland, Special Paper* 48, 121–144.
- Kröner, A., Willner, H. P., Hegner, E., Jaeckel, P. & Nemchin, A. 2001.** Single zircon ages, PT evolution and Nd isotope systematics of high-grade gneisses in southern Malawi and their bearing on the evolution of the Mozambique Belt in southeastern Africa. *Precambrian Research* 109, 257–291.
- Kröner, A. 2006.** The Mozambique Belt of East Africa and Madagascar: A Review. *Colloquium of African Geology (CAG21)*, 2006, Maputo, Mozambique. Abstract Volume, 96.
- Lawver, L. A., Gahagen, L. M. & Dalziel, I. W. D. 1998.** A tight fit early Mesozoic Gondwana, a plate reconstruction perspective. Special Issue, *Memoirs of National Institute of Polar Research* 53, 214–229.
- Maboko, M. A. H. 2000.** Nd and Sr isotopic investigation of the Archean-Proterozoic boundary in northeastern Tanzania: constraints on the nature of Neoproterozoic tectonism in the Mozambique Belt. *Precambrian Research* 102, 87–98.
- Macey, P. H. & Armstrong, R. A. 2005.** U-Pb SHRIMP Geochronology of Gneisses and Granites of the Mozambique Metamorphic Belt in the Nampula-Zambezia Provinces, Northern Mozambique. CGS, Unpublished Report.
- Macey, P. H., Ingram, B. A., Cronwright, M. S., Botha, G. A., Roberts, M. R., Grantham, G. H., Maree, I., Botha, P. M., Kota, M., Opperman, R., Haddon, I. G., Nolte, J. C. & Rowher, M. 2006.** Geological Explanation of the 1 : 250 000 Map Sheets: 1537 Alto Molócuè, 1538 Murrupula, 1539 Nampula, 1540 Mocingual, 1637 Errego, 1638 Gilé, and 1639 Angoche in Northeastern Mozambique. Council for Geoscience, South Africa, September 2006, 211 p.
- Mäkitie, H., Lehtonen, M. I., Manninen, T., Marques, J. M., Cune, G. & Mavie, H. 2008.** Petrography and geochemistry of granitoid rocks in the northern part of Tete Province, Mozambique. *Geological Survey of Finland, Special Paper* 48, 167–189.
- Manhiça, A. D. S. T., Grantham, G. H., Armstrong, R. A., Guise, P. G. & Kruger, F. J. 2001.** Polyphase deformation and metamorphism at the Kalahari Craton – Mozambique Belt Boundary. In: Miller, J.A., Holdsworth, R.E., Buick, I.S. & Hand, M. (eds.): *Continental Reactivation and Reworking*, Geological Society of London, Special Publication 184, 303–322.
- Mänttärä, I. 2008.** Mesoarchaean to Lower Jurassic U-Pb and Sm-Nd ages from NW Mozambique. *Geological Survey of Finland, Special paper* 48, 81–119.
- Mapani, B., Rivers, T., Tembo, F., De Waele, B. & Katongo, C. 2004.** Growth of the Irumide terranes and slices of Archaean age in eastern Zambia. Abstracts, *Geoscience Africa 2004*, Johannesburg, 414–415.
- Mariga, J., Hanson, R. E., Martin, M. W., Singletary, S.J. & Bowring, S. A. 1998.** Timing of polyphase ductile deformation at deep to mid-crustal levels in the Neoproterozoic Zambezi belt, NE Zimbabwe. *Geological Society of America, Abstracts with Programs*, 30, A292.
- Müller, M. A., Jung, S., Kröner, A., Baumgartner, L. P., Poller, U. & Todt, W. 2001.** Pan-African emplacement and granulite-facies metamorphism in the Mavuradonha Mountains, Zambezi Belt. Abstracts, *EUG XI, Strasbourg*, 564.
- Oliver, G. J. H., Johnson, S. P., Williams, I. S. & Herd, D. A. 1998.** Relict 1.4 Ga oceanic crust in the Zambezi Valley, northern Zimbabwe: Evidence for Mesoproterozoic supercontinent fragmentation. *Geology* 26, 571–573.
- Pinna, P., Marteau, P., Becq-Giraudon, J-F. & Manigault, B. 1986.** Notice Explicative de la Carte Géologique à 1 : 1 000 000 de la République Populaire du Mozambique. Unpubl. Rept., Instituto Nacional de Geologia de Moçambique/BRGM, Orléans, France.
- Pinna, P., Marteau, P., Becq-Giraudon, J-F. & Manigault, B. 1987.** Carta Geológica de Moçambique, na escala 1: 1 000 000, Instituto Nacional de Geologia de Moçambique, Maputo, Moçambique.
- Pinna, P. & Marteau, P. 1987.** Synthèse géologique du Mozambique. 14th Colloquium of African Geology, Abstract volume, p. 55.
- Porada, H. & Berhorst, V. 2000.** Towards a new understanding of the Neoproterozoic early Palaeozoic Lufilian and northern Zambezi belts in Zambia and the Democratic Republic of Congo. *Journal of African Earth Sciences* 30, 727–771.
- Powell, R. & Holland, T. J. B. 1985.** An internally consistent thermodynamic dataset with uncertainties and correlations, 1, Methods and a worked example *Journal of Metamorphic Geology* 3, 327–342.
- Powell, R. & Holland, T. J. B. 1988.** An internally consistent thermodynamic dataset with uncertainties and correlations: 3 Application, methods, worked examples and a computer program *Journal of Metamorphic Geology* 6, 173–204.
- Powell, R. & Holland, T. J. B. 1994.** Optimal geothermometry and geobarometry *American Mineralogist* 79, 120–133.
- Rainaud, C., Master, S., Armstrong, R. A. & Robb, L. J. 2003.** A cryptic Mesoproterozoic terrane in the basement to the central African Copperbelt. *Journal of the Geological Society of London* 160, 11–14.
- Real, F. 1962.** O Maciço Ultrabásico do Monte Atchiza (Moçambique). Reconhecimento Geológico-Mineiro. Junta de Investigação do Ultramar, DNG Library No. 1023.

- Schenk, V. & Appel, P. 2001.** Anti-clockwise P-T path during ultrahigh-temperature (UHT) metamorphism at ca. 1050 Ma in the Irumide Belt of Eastern Zambia. *Berichte der Deutschen Mineralogischen Gesellschaft, Beiheft zum European Journal of Mineralogy* 13, 161.
- Shackleton, R. M. 1994.** The final collision zone between East and West Gondwana; where is it? *Journal of African Earth Sciences* 23, 271–287.
- Stern, R. J. 1994.** Arc assembly and continental collision in the Neoproterozoic East African Orogen: Implications for the consolidation of Gondwanaland. *Annual Reviews. Earth and Planetary Science Letters* 22, 319–351.
- Thatcher, E. C. 1968.** The geology of the Dedza area. *Bulletin of the Geological Survey of Malawi* 29, 71 p.
- Trouw, R. A. J. & De Wit, M. J. 1999.** Relation between Gondwanide Orogen and contemporaneous intracratonic deformation. *Journal of African Earth Sciences* 28, 203–213.
- Vinyu, M. L., Hanson, R. E., Martin, M. W., Bowring, S. A., Jelsma, H. A., Krol, M. A. & Dirks P. H. G. M. 1999.** U-Pb and ⁴⁰Ar/³⁹Ar geochronological constraints on the tectonic evolution of the easternmost part of the Zambezi orogenic belt, northeast Zimbabwe. *Precambrian Research* 98, p. 67–82.
- Viola, G., Henderson, I., Bingen, B., Feito, P., Thomas, R. J., Hollick, L. & Jacobs, J. 2006.** A new tectonic framework for northern Mozambique. *Colloquium of African Geology (CAG21), 2006, Maputo, Mozambique. Abstract Volume*, 168.
- Vrána, S. & Barr, M. W. C. 1972.** Talc-kyanite-quartz schists and other high-pressure assemblages from Zambia. *Mineralogical Magazine and Journal of the Mineralogical Society* 38, 837–846.
- Vrána, S., Prasad, R. & Fediukova, E. 1975.** Metamorphic kyanite eclogites in the Lufilian arc of Zambia. *Contributions to Mineralogy and Petrology* 51, 139–1.
- Vrána, S., Kachlík, V., Kröner, A., Marheine, D., Seifert, A. V., Žáček, V. & Baburek, J. 2004.** Ubendian basement and its late Mesoproterozoic and early Neoproterozoic structural and metamorphic overprint in northeastern Zambia. *Journal of African Earth Sciences* 38, 1–21.
- Westerhof, A. B. Phil, Tahon, A., Koistinen, T., Lehto, T., & Åkerman, C. 2008.** Igneous and Tectonic Setting of the Allochthonous Tete Gabbro-Anorthosite Suite, Mozambique. *Geological Survey of Finland, Special Paper* 48, 191–210.
- Wilson T. J., Hanson R. E. & Wardlaw M. S. 1993.** Late Proterozoic evolution of the Zambezi belt, Zambia: implications for regional Pan-African tectonics and shear displacements in Gondwana. – In: Unrug, Banks and Veevers (eds.), *Gondwana 8 – Assembly, evolution, and dispersal (Gondwana 8 Symposium Volume)*, Balkema, Rotterdam, 69–82.
- Wilson, T., Grunow, A. M., & Hanson, R. E. 1997.** Gondwana assembly: The view from southern Africa and East Gondwana. *Journal of Geodynamics* 23, 263–286.

PETROGRAPHY AND GEOCHEMISTRY OF GRANITOID ROCKS IN THE NORTHERN PART OF TETE PROVINCE, MOZAMBIQUE

by

Hannu Mäkitie¹, Matti I. Lehtonen¹, Tuomo Manninen²,
João M. Marques³, Grácio Cune⁴ & Hilário Mavie⁵

Mäkitie, H., Lehtonen, M. I., Manninen, T., Marques, J. M., Cune, G. & Mavie, H. 2008. Petrography and geochemistry of granitoid rocks in the northern part of Tete Province, Mozambique. *Geological Survey of Finland, Special Paper 48*, 167–189, 16 figures, one table and two appendices.

The crystalline basement in the northern part of Tete Province, NW Mozambique, is largely composed of various Mesoproterozoic granitoids, with Neoproterozoic to Ordovician granitoids occurring to a smaller areal extent. These granitic rocks are divided into several types on the basis of petrography, texture, geophysical signature, chemical composition, and age. Most granitoids belong to the 1.2–1.0 Ga age group and are related to the Grenvillian Orogeny. The largest massives belong to the Furancungo Suite (~8300 km²), Cassacatiza Suite (~5700 km²), Serra Danvura granitoids (~4700 km²), Castanho Granite (~3400 km²) and Rio Capoeche Granite (~2600 km²), which all are composed of different magmatic phases. The Ordovician 0.50–0.47 Ga intrusions belong to post-Pan-African magmatism. Some intrusions have undergone Pan-African (c. 0.53 Ga) metamorphism.

Certain massives have specific textural characteristics. The extensive Cassacatiza Suite shares a parallel, ENE structural grain with the neighbouring supracrustal rocks of the Fingoé Supergroup and is cut by the NW trending Furancungo Suite in the north-east. The charnockitic c. 1.05 Ga Castanho Granite has spatial and mutual relationships with the contiguous Tete Gabbro-Anorthosite Suite. The Mussata granitoids near the Tete Suite are mylonitized due to the allochthonous nature of the latter.

Most of the Mesoproterozoic as well as the post-Pan-African granitoids in the northern part of Tete Province are ferroan, and alkalic to calc-alkalic in composition. They classify from quartz syenites and quartz monzonites to granites; tonalites are rare and lacking amongst the post-Pan-African granitoids. The aluminium saturation index varies from metaluminous to slightly peraluminous. The ferroan intrusions suggest an extensional tectonic regime. The absence of S-type granitoids indicates that sedimentary rocks did not dominate in the source regions. The post-Pan-African granites usually have higher La and Ce contents than the older granitoids.

Key words (GeoRef Thesaurus AGI): granites, granodiorites, quartz monzonite, quartz syenite, chemical composition, classification, Proterozoic, Mesoproterozoic, Phanerozoic, Tete, Mozambique.

¹ Geological Survey of Finland, P.O. Box 96, FIN-02151 Espoo, Finland² Geological Survey of Finland, P.O. Box 77, FIN-96101 Rovaniemi, Finland³ Gondwana Empreendimentos e Consultorias, Limitada, Caixa Postal 832, Maputo, Mozambique⁴ National Directorate of Geology, Praça 25 de Junho, 380, Maputo, Mozambique⁵ Ministry of Mineral Resources, Avenida Fernão de Magalhães, 34, Maputo, Mozambique

E-mail: hannu.makitie@gtk.fi

INTRODUCTION

Tete Province in northwestern Mozambique may be geologically divided into three main areas: (1) the Mesoproterozoic “West Gondwana” basement, which has undergone the Kibaran orogeny in the north with minor “East Gondwana” assemblages in the northeastern corner; (2) the Archaean Zimbabwe craton with Proterozoic cover sequences in south; and (3) the Phanerozoic graben-type sediments of the Zambezi rift (parallel to Cahora Bassa Lake) between these basement areas (e.g. Shackleton 1994, Rogers *et al.* 1995, Grantham *et al.* 2003, GTK Consortium 2006). Two-thirds of the first-mentioned area – the subject and thesis of this article – is composed of Mesoproterozoic (-Ordovician) granitoids (Fig. 1). Thus, knowledge of plutonic rocks is crucial in understanding the crustal evolution in the northern part of Tete Province.

Between 1980 and 1984, Hunting Geology and Geophysics Limited initiated a new phase of geological investigations (Hunting 1984) in Tete Province, carrying out a comprehensive mineral exploration and reconnaissance geological mapping project under the aegis of the Mozambican government. Approximately at the same time, the French BRGM

(Bureau de Recherches Géologiques et Minières) surveyed the northern part of Mozambique, resulting in the publishing of a geological map at the scale 1:1 000 000 that provided new insights in the geology of the Tete area (Pinna *et al.* 1986, 1987). However, the most updated mapping of the region was made during 2002–2006 within an extensive geological mapping project, *Mineral Resource Management Capacity Building Project, Republic of Mozambique, Component 2: Geological Infrastructure Development Programme, Geological Mapping LOT 2*, executed by Geological Survey of Finland (GTK) and financed by WB/NDF. The project produced new 1:250 000 scale geological maps with explanations (GTK Consortium 2006) from Tete Province.

The present paper summarizes petrographic and geochemical observations of the granitic rocks situated north of Cahora Bassa Lake and the Zambezi River, in the northern part of Tete Province (Fig. 1). All locations presented in figures and appendices are in UTM coordinates (WGS 84). Please note that in the study area reference is made to the 36S.

REGIONAL GEOLOGICAL SETTING

From a geodynamic point of view it is generally accepted that the crystalline basement of Mozambique is composed of three major lithospheric plates or terranes¹ that have collided and amalgamated during the Pan-African Orogenic Cycle. Prior to amalgamation, each terrane was characterised by an individual and specific geodynamic development. These terranes are called East Gondwana, West Gondwana and South Gondwana (e.g. Shackleton 1994, Grantham *et al.* 2003, Rogers *et al.* 1995, and references therein).

The crystalline basement of northern Tete Province belongs (in addition to West Gondwana) main-

ly to a smaller structural element called the Tete-Chipata Belt, which formed during the Grenvillian orogenic cycle (~1.1–1.0 Ga) (see Westerhof 2006, Westerhof *et al.* 2008a). The belt is bounded by the W-E trending Sanângoè Shear Zone (SSZ), which roughly follows Cahora Bassa Lake in the south, by a thrust front or pseudo-suture between the East and West Gondwana terranes in the east, and by the Mwembeshi Dislocation in the northwest, in Zam-

¹ The term “terrane” is used to indicate a tectonic unit of variable size, i.e., a lithospheric plate, a plate fragment or sliver or a tectonic mass such as a “nappe”. “Terrain”, on the other hand, is a generic term, broadly similar to “area”.

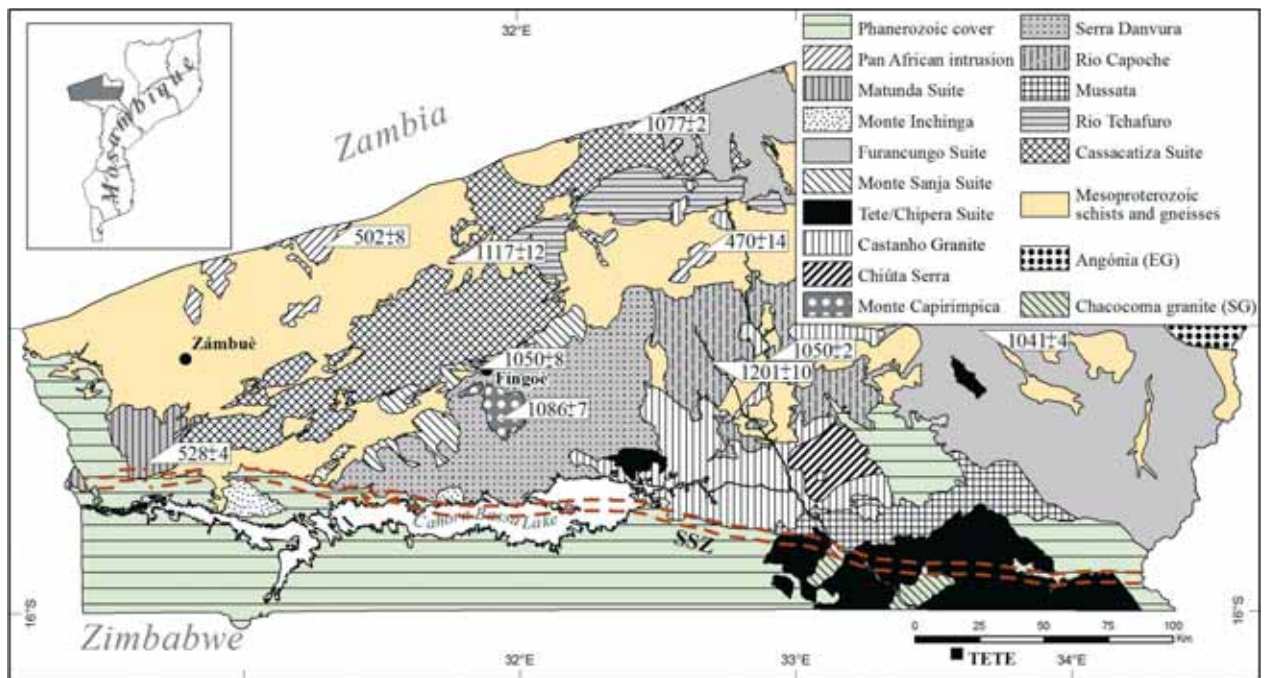


Fig. 1. Simplified geological map of the northern part of Tete Province showing the locations of the most voluminous granitoids with corresponding U–Pb ages in Ma. The U–Pb age obtained in Matunda Suite refers to Pan-African metamorphism. The Sanângo Shear Zone (SSZ) is marked as a red broken double line. Note that the town of Tete is situated in the SE corner of the figure and that a small portion (behind the legend) in the NE corner was not included in the present study. The map is drawn after the GTK Consortium (2006).

bia. Being located close to a triple junction between the Irumide belt, the Zambezi segment of the Zambezi-Lufilian-Damara belt and the Mozambique belt, the basement geology of the northern Tete Province is very complex (Westerhof *et al.* 2008a, and references therein).

New geochronological data by the GTK Consortium show that all granitoids in the northern part of Tete Province are younger than the ~1.3 Ga Fíngo Supergroup and other supracrustal rocks of the region (Mänttari *et al.* 2006, Mänttari 2008). Most granitoids of the region are 1.2–1.0 Ga old and related to the Grenvillian orogenic cycle, culminating in the formation of the Rodinia Supercontinent. The youngest granite intrusions belong to post-Pan-African magmatism, 0.50–0.47 Ga in age (Fig. 1). Mafic dykes several kilometres long, Neoproterozoic and Karoo in age, locally cut the granitoids.

Many of the granitoids form impressive and well-exposed, 100–300 m high *kopjes* (Fig. 2). Between the granitoid batholiths there occur either various Mesoproterozoic supracrustal rock units or granitoids. The central part of the study area is characterised by WSW-ENE trending metavolcanic and sedimentary rocks of the Fíngo Supergroup. Arkosic

metasediments of the Zâmbue Supergroup dominate the northwestern corner of the area, while granulitic gneisses of the Chidzolomondo, and Cazula and Mualadzi Groups prevail in the northeastern part of Tete Province (GTK Consortium 2006).

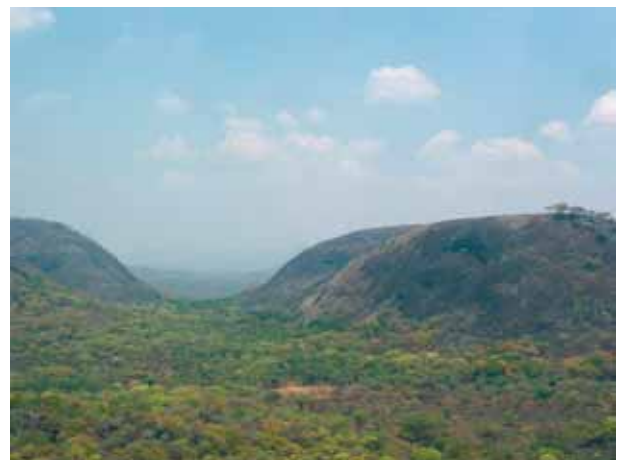


Fig. 2. Granitic kopjes in Tete Province near the Zambian border, 40 km NE of the Fíngo village.

GROUPING OF GRANITOIDS

Principles

Structural and fabric features, chemical and mineralogical composition, geophysical signature, and U–Pb age determinations of granitic rocks allow the distinction of several granitoid groups in the northern Tete Province (Table 1). Compared to the “old” unit names defined by Hunting (1984), the new names defined for various granitic units are also shown in Table 1.

One of the main problems with the newly defined granitoid (and metamorphic) units is to find names that meet the rules of stratigraphic (and lithodemic) nomenclature. The previous criteria “pre-/post-Fingoè” (Hunting 1984) to define major granitoid groups in Tete Province were based on observed/interpreted field relationships with supracrustal rocks of the Fingoè Supergroup. However, granites

should be interpreted and grouped on the basis of age and the role they played during the geodynamic evolution of the region. For instance, the “pre-Fingoè Granites” sensu Hunting (1984), between the Zâmbuè and Fingoè sequences, now defined as the Cassacatiza Suite, could represent a syn- to late-orogenic Grenvillian “*stitching pluton*”. They may have been emplaced at the site of an accretionary suture between the terrestrial “Zâmbuè terrane” in the north and the volcano-sedimentary Fingoè belt in the south, and were probably derived by anatexis from a deeper crustal level.

These examples underscore the need to understand the role and time of emplacement of granitoids in the geodynamic evolution of the region. Furthermore, there is no justification for naming the

Table 1. The proposed names for granitoids in the northern part of Tete Province. The U–Pb ages are after Mänttari (2008).

Eon/Era	U–Pb age in Ma	Granitoids (supracrustal rocks in <i>italic</i>)	Old name (e.g. Hunting 1984)
Phanerozoic	470±14 502±8	Macanga granite Sinda Suite	Sinda Granite
Neo-proterozoic	528±4, metamorphic/ (~0.8 Ga magmatic?)	Cassenga Leucogranite Monte Tarai granite Monte Inchinga granite Matunda Suite	SW part of pre-Fingoè Granites SW part of Zâmbuè Group
Meso-proterozoic	1041±4 1050±8 1050±2 1086±7 1077±2, 1117±12 1201±10 ~1.3 Ga	Boesi granite Marirongoe granite Furancungo Suite Messambe quartz monzonite Mussata Granite, mylonitic Monte Sanja Suite Castanho Granite Monte Capirimpica Granite Serra Danvura granitoids* Cassacatiza Suite Rio Capoche Granite* Rio Tchafuro Granite Chiúta Serra Granite <i>Supracrustal rocks:</i> <i>Mualadzi Group</i> <i>Fingoè Supergroup</i> <i>Zâmbuè Supergroup</i> <i>Cazula Group</i> <i>Chidzolómondo Group</i> <i>Rio Messeze Suite (ortho- and paragneisses)</i>	Desaranhama Granite Southernmost part of Luia Group Bulk of post-Fingoè Granites Granito Castanho Small part of post-Fingoè Granites Southern part of Pre-Fingoè Granites Northern part of pre-Fingoè Granites NE part of pre-Fingoè Granites <i>ENE extension of Fingoè Group</i> <i>Fingoè Group</i> <i>Zâmbuè Group</i> <i>Parts of Angónia Group and Luia Group</i> <i>NE part of Luia Group</i>

*) Note that “Monte Capingo granite” reported by Mäkitie et al. (2006) is here divided into Serra Danvura granitoids and Rio Capoche Granite.

different groups with numbered map codes, which automatically imply some chronological order – as was done in the maps of Hunting (1984) and the BRGM 1:1 000 000 scale geological map (Pinna *et al.* 1987).

Borges (1937) introduced the term “granito castanho” (brown granite) to describe certain granitic rocks with distinctive field characteristics, widespread in the central Tete Province. Later work by Assunção *et al.* (1956a, 1956b) showed that some, but not all, of these rocks belong to the charnockite series (Le Maitre 1989). In this study, the name “Castanho Granite” is proposed for this specific granitoid type. As a matter of fact, a significant proportion of observed rock types have syenitic, monzonitic and monzodioritic compositions and not

all are characterised by the presence of pyroxene, as assumed by Assunção *et al.* (1956a, 1956b).

The extensive Cassacatiza Suite (~5700 km²), Furuncungo Suite (~8300 km²), Serra Danvura granitoids (~4700 km²) and Rio Capoeche Granite (~2600 km²) each comprise different mappable granitic phases. Some granitoids with a smaller areal extent (<500 km²) may also locally display notable differences in modal composition. There are also a few small granitoid areas (occurrence <20 km²) not shown in Fig. 1. These include the Rio Messeze orthogneisses, Messambe quartz monzonite, Monte Tarai Granite, Cassanga Leucogranite and Monte Macanga Granite. In the following chapter, the granitoids of the northern Tete Province are described from the oldest to the youngest.

PETROGRAPHY

Rio Messeze orthogneisses

The Rio Messeze gneisses occur about 40 km east of the village of Fíngoè, where tonalitic orthogneisses have undergone polyphase deformation and are cut by granite dykes of different age (Fig. 3). The rock is moderately to weakly banded, with polyphase fold structures and variable structural trends. Elongated mafic inclusions as well as porphyroblastic K-feldspar grains occur in places.

The tonalitic composition of the gneiss is interesting because the granitoids in the northern part of Tete Province are mostly granitic in composition. The tonalitic rocks resemble “TTG assemblages” more than any other granitoids in the area. Dominant minerals of the orthogneiss are plagioclase and quartz, with subordinate biotite, hornblende, K-feldspar and epidote.



Fig. 3. Polyphase deformation in the Rio Messeze tonalitic gneiss east of the Chipungo village (0421927/ 8327571). The scale bar is 14 cm.

Chiúta Serra Granite

The Chiúta Serra (meta)Granite occurring about 75 km north of the town of Tete is characterized by, and partly delineated on the basis of a strongly dominant relief, expressed by mountain ridges and chains of major *kopjes* or *inselbergs*. Another mapping criterion for the Chiúta Serra Granite is its distinctive, high Th-K signature, which contrasts sharply with neighbouring lithological units.

The average rock type is a grey to brownish grey (colour depending on biotite and garnet content), coarse-grained, inequigranular, occasionally very coarsely porphyritic biotite granite, typically

with variable garnet content. This granite may contain small mafic xenoliths or larger (dm to metre scale), dark grey, retrograde amphibolite enclaves. Migmatitic metasediments, possibly belonging to the Chidzolomondo Group, occur in the inner parts of the main Chiúta Serra Granite body.

The contact relations seem to favour an older age than Rio Capoeche granitoids dated at ~1201 Ma. As a consequence, the Chiúta Serra granitoids are regarded as the oldest plutonic rocks in the northern part of Tete Province, possibly equal in age to the Rio Messeze orthogneisses.

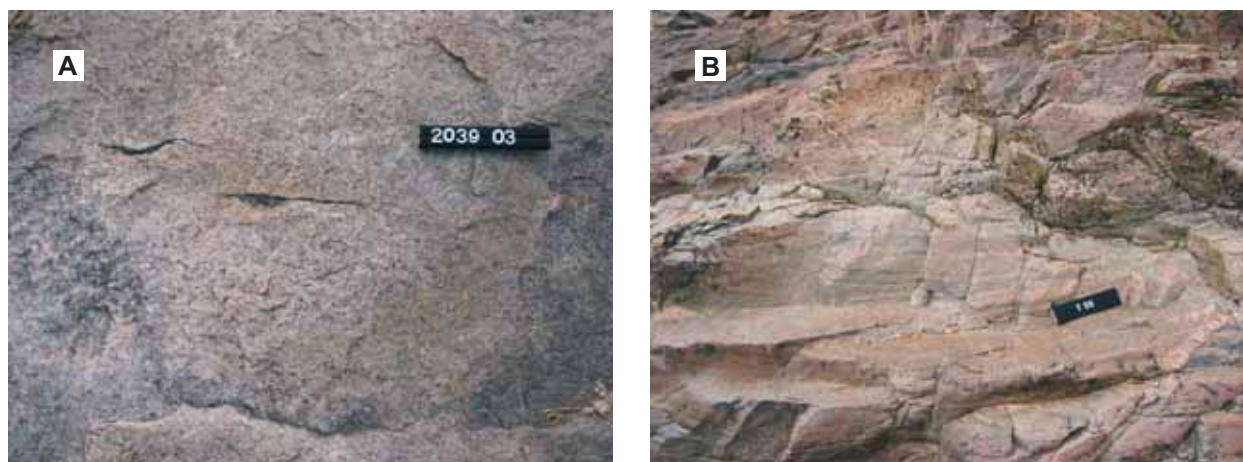


Fig. 4. Rio Capoeche granitoids. (A) Relatively homogeneous granite containing K-feldspar phenocrysts. NW of Monte Nhanjo (0519390/ 8322890), (B) Granitic orthogneiss. The U–Pb zircon age obtained from a sample of this outcrop is ~1.2 Ga. Rio Capoeche bridge (0468284/ 8326745). The scale bar is 12 cm.

Rio Tchafuro Granite

The Rio Tchafuro granitoids are spatially restricted to a large W-E directed section along the main road from Tete to the Zambian border in the north. The average rock type is light grey to pinkish grey, inequigranular to porphyritic, biotite-bearing granodiorite, in places tonalite and granite. The grain size is variable, ranging from fine to (locally) very coarse. The finer-grained varieties are typi-

cally more equigranular. Locally, a magmatic flow structure is indicated by an incipient alignment of K-feldspar phenocrysts.

Evidence of mixing of different granitoid magma batches and migmatization can be observed in several outcrops. Where various “leucosome” generations are involved, the contacts between rock parts range from sharp to diffuse.

Rio Capoeche Granite

The Rio Capoeche granitoids represent an extended family of biotite granites and granodiorites located 100 km NW of the town of Tete. The average rock type in the NW part of the Rio Capoeche batholith consists of a (light) grey to pinkish and brownish grey, medium- to coarse-grained, inequigranular and locally porphyritic biotite granite (Fig. 4A). The

biotite content is variable, but mostly low to very low. Gneissic types also occur locally (Fig. 4B).

A pink to reddish grey, fine-grained, equigranular quartz-feldspar rock (with accessory biotite) is believed to represent large granitized enclaves of metasediments. These meta-arkositic rocks occur in the western parts of the Rio Capoeche batholith.

Cassacatiza Suite

The Cassacatiza Suite, one of the spatially largest granitoids in the northern part of Tete Province, is dominated by porphyritic biotite-hornblende granite, often deformed and flattened in the NE direction. The rocks of the Cassacatiza Suite range in composition from granite to granodiorite, but quartz monzonites and quartz syenites also locally occur. The following lithological varieties are defined: (1) megacrystic, deformed granite and granodiorite, (2) coarse-grained, mesocratic granite and (3) medium-grained, gneissic granite.

In the first type, the average size of alkali feldspar phenocrysts is 1–5 cm, but roundish megacrysts up to 8–10 cm in diameter have also been observed (Fig. 5A). Owing to the mesocratic composition, the second type (Fig. 5B) has a lower potassium signature on radiometric maps compared with porphyritic varieties of the Suite. The third type, even macroscopically rather isotropic, may show a foliation and extensive sericitization of plagioclase, with large white mica inclusions implying metamorphic overprinting.

The Cassacatiza granitoids are usually clearly intrusive into the supracrustal rocks of the Zâmbuè and Fíngoè Supergroups. However, in the western

part of the Suite, some foliated variations of these granitoids are locally difficult to distinguish from granitized meta-arkoses of the Zâmbuè Supergroup.

Serra Danvura granitoids

The Serra Danvura granitoids occupy an area of 50 x 130 km on the northern side of Cahora Bassa Lake, to the south of the supracrustal rocks of the Fíngoè Supergroup (Fig. 1). These granitoids represent an assemblage of coarse- to medium-grained biotite-hornblende granites (Fig. 6A), quartz monzonites (Fig. 6B) and quartz syenites. Their colour varies from pinkish to dark greenish brown and texture from equigranular to porphyritic and undeformed to weakly deformed. Quartz monzonites and

quartz syenites form large, individual intrusions, particularly to the south of the village of Fíngoè. However, most of the Serra Danvura rocks are true granites in the classification of Streckeisen (1976).

Porphyritic granites characterise the western parts of the Serra Danvura batholite and are composed of abundant K-feldspar phenocrysts, 1–3 cm in size. The granitic rocks situated in the eastern part of the Serra Danvura batholite are usually foliated and have a smaller grain size than those in the west.

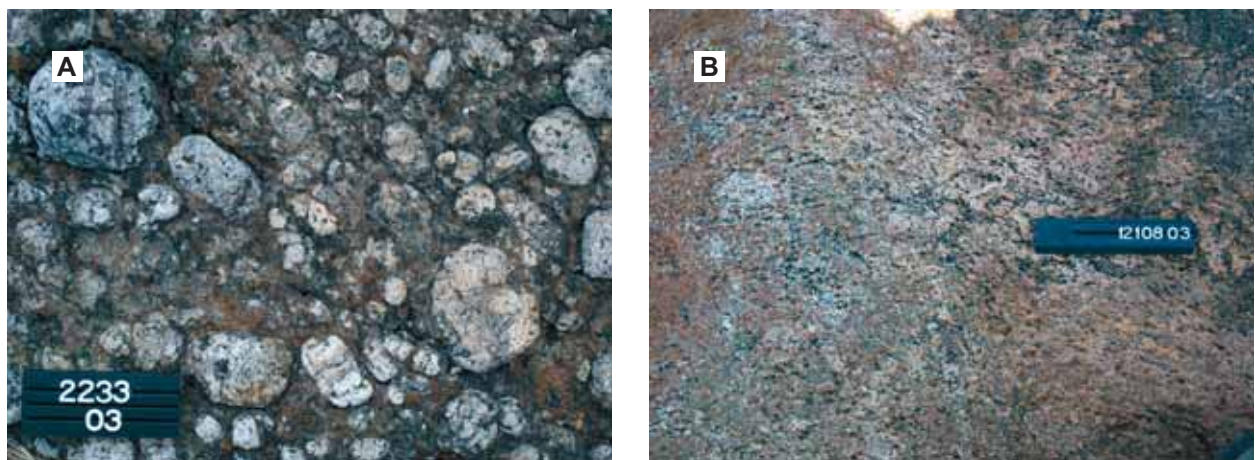


Fig. 5. Granitoids of the Cassacatiza Suite. (A) Alkali feldspar megacrysts in biotite granite. South of Monte Dómué (0431280/ 8414628), (B) Foliated, slightly mesocratic, quartz monzonitic granitoid. Monte Chipalava (0289834/ 8317326). The scale bars are 8 cm and 14 cm.

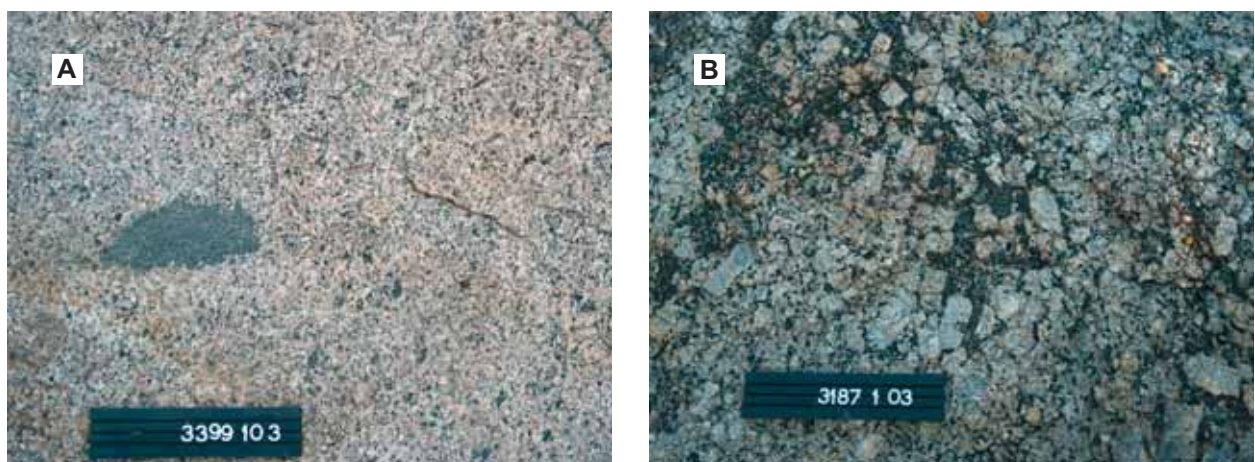


Fig. 6. Serra Danvura granitoids. (A) Weakly deformed hornblende-biotite granite with fine-grained, mafic enclave. Western part of the batholith (0345807/ 8288337), (B) Grain size variation in almost undeformed, porphyritic quartz monzonite(-syenite). 25 km south of the village of Fíngoè (0378550/ 8299448). The scale bar is 14 cm.

Monte Capirimpica granite

The Monte Capirimpica granite occupies a mountainous area of over 400 km², a few kilometres south of the village of Fingoè. Detailed studies have shown that this area with a strong radiometric signature is occupied by (1) almost undeformed,

coarse-grained and equigranular hornblende-biotite granite (~75% of the total area) and (2) medium-grained aplitic granite (~25%). The aplite occurs as irregular elongated patches, streaks and dykes, up to 30 m in breadth.

Castanho Granite

In outcrops, the Castanho Granite typically appears as massive bodies, which are usually porphyritic in texture (Fig. 7A). However, the fresh, non-weathered rock often has a thin weathered “skin”. Boulders are typically rounded due to the effects of onion-type exfoliation. The non-weathered rock ranges in colour from (dark) brown to dark grey, even to dark green (e.g. along the old road southwest from Songo). Weathering “skins” also have a range of colours: they are mostly brown to grey, but sometimes also light grey to white, in sharp contrast to the dark colours of fresh rock. Locally, the rocks may comprise xenoliths (Fig. 7B). The larger massifs of the Castanho Granite are generally irregular in shape and/or roughly conformable with country rock structures.

The Castanho Granite is composed of variable

amounts of quartz, alkali feldspar, plagioclase, orthopyroxene, augite, biotite and hornblende, with opaque minerals. The composition ranges from true granite and quartz syenite to granodiorite and from quartz monzonite to (quartz-)monzodiorite. Locally, the rock is nearly totally devoid of Fe-Mg silicates and composed almost entirely of quartz, feldspars and opaque minerals (e.g. some of the dark green types near the Cahora Bassa dam). These types resemble the dark anorthosites and gabbros of the Tete Gabbro-Anorthosite Suite. The charnockitic type of the Castanho Granite is often associated with gabbro and locally with granulite, and may form a “bimodal suite” with the extensive Tete Gabbro-Anorthosite Suite (see Westerhof *et al.* 2008b). The Castanho Granite and gabbros of the Tete Suite have similar ages (c. 1.05 Ga) (Mänttari 2008).

Monte Sanja Suite

The Monte Sanja Suite forms an over 120 km long and locally up to 35 km wide, NE-SW trending

zone of weakly deformed, pinkish or grey biotite-hornblende granite intrusions near the village of

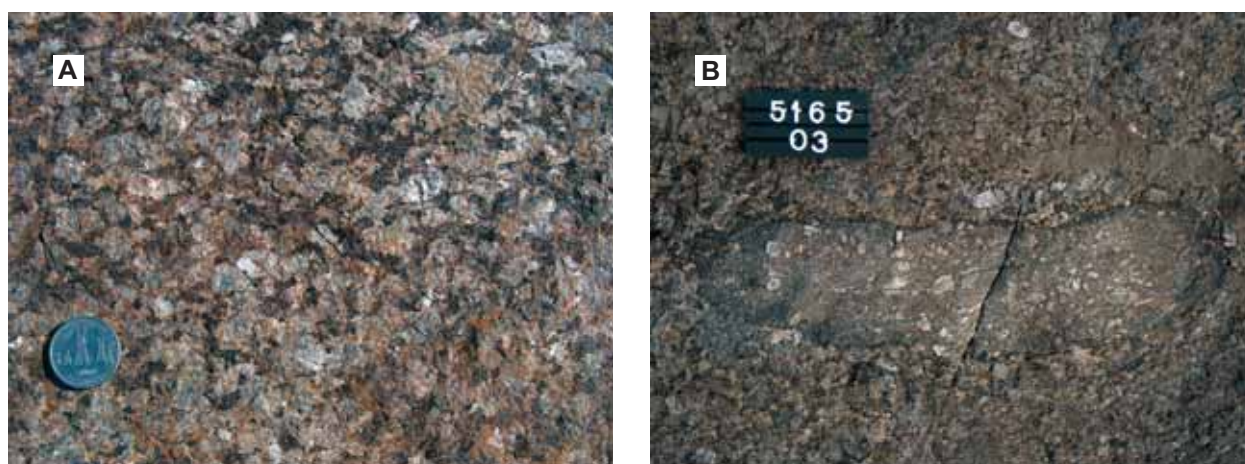


Fig. 7. Castanho Granites. (A) Dark brownish quartz monzonitic granitoid, west of the village of Shigoncho (0401151/ 8351329), (B) Examples of locally abundant, small mafic xenoliths in Castanho Granite, south of Serra Chiúta (0529366/ 8277532). The diameter of the coin is 3 cm, the scale bar is 8 cm.

Fíngoè. These rocks are intrusive to the supracrustal sequences of the Fíngoè Supergroup. Two units occur in the Suite: (1) granite, granodiorite and quartz diorite and (2) quartz monzonite, diorite and tonalite. The latter types are found near Fíngoè.

The granitic rocks of the Suite often form conical, round-topped hills and sugar-loafs interspersed among steep valleys, often resulting in a spectacular high-relief topography. This topographic feature and stronger radiometric signature distinguishes the Monte Sanja Suite granitoids from the surrounding and slightly older granitoids of the Rio Capoeche and Cassacatiza Suite. The Monte Sanja rocks locally comprise darker and more mafic enclaves than is typical for the other studied granitoids (Fig. 8).



Fig. 8. Large dioritic xenoliths in Monte Sanja Suite granite, NE of Serra Mezeze (03672939/ 8320902). Note quartz-filled en-échelon fault gashes in xenolith, which do not continue in the granitic host rock. The scale bar is 14 cm.

Mussata Granite

The Mussata granitoids and associated mylonites have been named after the locality of Mussata, situated near the Zambezi River, NW of the town of Tete. Field observations are restricted to a single N-S section along the road to Zambia and to a section south of the village of Songo. The Mussata granitoids are partly remaining below the allochthonous Tete Gabbro-Anorthosite Suite and are mylonitized there (GTK Consortium 2006, Westerhof *et al.* 2008b). Due to deformation, an augen gneiss texture is occasionally found (Fig. 9A).

The Mussata granitoids occur in a 15 km wide belt, stretching north of, and parallel to the Tete Suite, with which it has tectonic contact. Subhori-

zontal mylonites of the granitoids were mapped in the past as undifferentiated “quartz-feldspathic gneisses” (Hunting 1984), a suitable descriptive term in many cases, which hides, however, the tectonic origin of the “gneissic” fabric (Fig. 9B).

The majority of field observations on these granitoids were carried out on variably mylonitized types, and undeformed relics have been encountered in only a few locations. The latter refer to a light grey to pinkish grey, weathering to light yellowish brown, coarse-grained, generally porphyritic biotite-granite, having K-feldspar phenocrysts and a variable biotite content.



Fig. 9. Examples of the mylonitic fabric in the Mussata Granite. (A) Mylonitic augen gneiss. The higher biotite content has resulted in thick foliation planes wrapping around feldspar porphyroclasts, (B) Ultramylonite. Biotite has neocrystallized into white mica. Feldspar grains are ground and recrystallised into fine quartz-feldspar laminae, with occasional relics of feldspar porphyroclasts. East of Serra Dzunsa (0482376/ 8265619). The scale bar is 8 cm.

Messambe quartz monzonite

Porphyritic quartz monzonite intrusions within the large Serra Danvura pluton near the village of Fingoè occupy areas up to 50 km² in size. They form small, rounded and generally well exposed hills along the main road to the east of Fingoè, and differ from the surrounding rocks by their higher K-Th-U signatures on radiometric maps.

Weathered surface of the Messambe quartz mon-

zonite is brownish grey, while fresh surfaces have a dark brown colour. Texturally, these weakly deformed rocks are porphyritic; K-feldspar phenocrysts locally exceed 3–4 cm in size. Parallel alignment of potassium feldspar crystals observed in places may indicate magmatic flow. The dominant minerals are K-feldspar, plagioclase and hornblende with subordinate quartz, biotite and locally pyroxene.

Furancungo Suite

The Furancungo Suite, forming an extensive batholith in the northeastern part of studied area, is composed of non-foliated to foliated hornblende biotite granite and minor quartz monzonite(-syenite). It comprises the Desaranhama Granite (main component) and in its southern and eastern peripheries some smaller plutons of somewhat different lithologies. The latter include the Rio Ponfi Quartz monzonite(-monzodiorite), the Nacoco Granite and the Monte Dezenza Granite (GTK Consortium 2006). The Furancungo Suite forms a NNW-SSE directed, elongated massif (250 x 80 km) continuing into Malawi in the SE and into Zambia in the NW. The Furancungo rocks crosscut the Cassacatica Suite granitoids. Moderate to high relief landforms, dissected by numerous fault-related gorges, characterise the central parts of the Furancungo Suite.

The Desanharama Granite is principally composed of a non-foliated to moderately foliated, pinkish grey, coarse, porphyritic biotite granite with

K-feldspar phenocrysts, 1.5–3 cm in diameter. The phenocrysts are in places mantled by white plagioclase. Small mafic enclaves are locally common. The granite becomes deformed in its eastern arcuate periphery, where the main rock type is very coarse-grained, biotite bearing, K-feldspar porphyritic, often veined granite gneiss or augen gneiss (Fig. 10).



Fig. 10. Close-up photo of deformed Desaranhama Granite. North of Monte Cangangunde (0636780/ 8339956). The scale bar is 14 cm.

Marirongoe Granite

The Marirongoe Granite forms a roundish pluton by the Fingoè-Zâmbuè road 50 km west of Fingoè village. It has a unique feature compared to other granitoids: owing to numerous pegmatites, it is selectively quarried in tens of open pits for “blue sky” mineral (aquamarine) and topaz. The Marirongoe granite is grey, medium-grained and usually weakly

foliated biotite granite with only subordinate hornblende, and locally epidote. Texturally, it is mostly even-grained, but some porphyritic varieties also exist, occasionally with *rapakivi* textures. Some of the even-grained types resemble granitized quartz-feldspar gneisses.

Matunda Suite

The Matunda Suite is situated in the Zumbo area, in the western corner of Tete Province, where it is bound by the Zâmbuè Supergroup in the north, by the Cassacatiza Suite in the east and by the Fingoè Supergroup in the south. The Suite comprises biotite- and hornblende-bearing granite gneisses, interlayered felsic and mafic gneisses and isolated

metagabbro and metadiabase bodies, locally cut by a swarm of wide pegmatite dykes.

The Matunda Suite forms a domal structure, in the south, where it is outlined by regional scale circular landscape morphology. On radiometric images the Matunda Suite is dominated by K, with less U, resulting in light blue to cyan colours in the ternary

radiometric image. A radiometric U–Pb determination indicates a Pan-African metamorphic age (c. 0.53 Ga) for these gneisses (Mänttari 2008). How-

ever, zircons in these gneisses also comprise cores, indicating a c. 0.8 Ga thermotectonic event.

Monte Inchinga granite

The Monte Inchinga granite, named after the mountain, comprises several plutons on the northern shore of Cahora Bassa Lake. Because these granites have intruded at and near the E-W trending Sanango Shear Zone (SSZ) (Fig. 1), they are probably Neoproterozoic to late Pan-African in age. The SSZ

is a Pan-African transpressional fault zone (Westerhof *et al.* 2008a). The Monte Inchinga granites are light grey to pinkish grey, medium- to coarse-grained biotite hornblende microcline granites with a distinct porphyritic texture (Fig. 11A).

Sinda Suite

Several bodies of porphyritic granite have intruded metasediments of the Zâmbuè Supergroup in the northwestern margin of Tete Province and form a voluminous, early Palaeozoic Sinda Suite c. 0.50 Ga in age. Described firstly on the Zambian side by Phillips (1957, 1965), these generally undeformed intrusive rocks belong to the last stages of Pan-African magmatism and, together with the

Macanga granite, represent the youngest granites in the study area.

The Sinda Suite granites are light pinkish or yellowish brown, coarse-grained, porphyritic microcline granites (Fig. 11B) with euhedral K-feldspar phenocrysts (0.5–2 cm in size). They usually have a high radiometric K–U–Th signature. Thin crosscutting granitic dykes or veins are usually fine- to medium-grained.

Macanga granite

Eight granite intrusions, from 3 to 10–20 km in diameter, crosscut the older Precambrian crystalline basement in the northern part of study area on both sides of the main road from the town of Tete to Cassacatiza, a border post to Zambia. Their high to very high Th–U–K radiometric signatures (Fig. 12), and the fact that they cluster in a relatively small area, differentiate them from other representatives of the “late-Precambrian group” *sensu* Hunting (1984), justifying the definition of a separate family

of granitoid intrusions.

A typical example of the Macanga granite, a large NE-elongated body (Fig. 12B) is a pink to light grey in colour, medium-grained and massive biotite granite. Semi-angular enclaves of light grey quartz-feldspar rock (supposedly belonging to the Chidzolomondo Group) are common in the granite. Coarse pegmatite bodies, typically with magnetite, have intruded the granite.

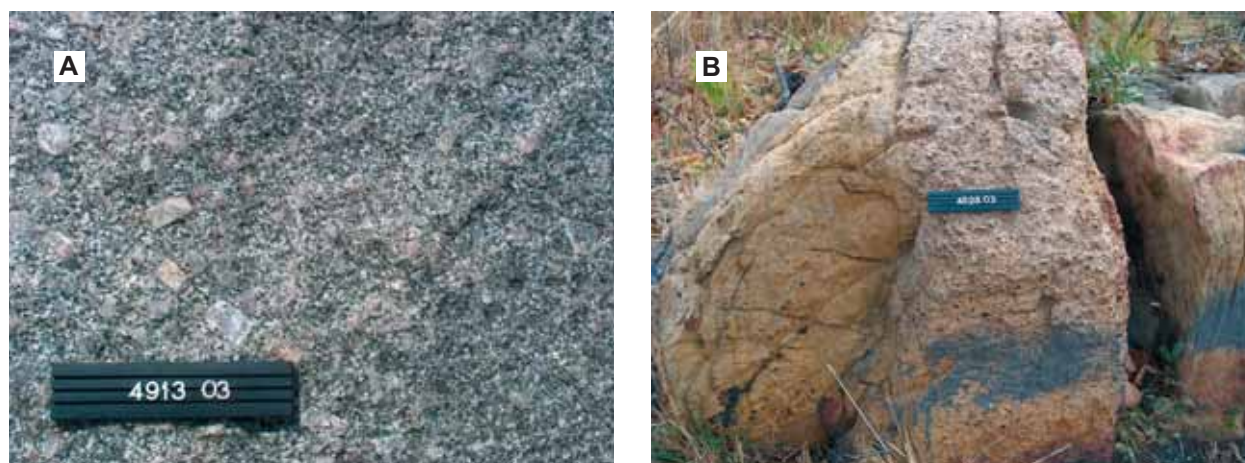


Fig. 11. Neoproterozoic-Cambrian intrusives. (A) Close-up photo of porphyritic Monte Inchinga granite. Rio Tongoé (0260292/ 8285447). (B) A dyke of coarse-grained, porphyritic Sinda Suite granite has intruded light brown, weakly banded meta-arkose of the Metamboia Formation of the Zâmbuè Supergroup. North of Monte Luaia (0314716/ 8365524). The scale bar is 14 cm.

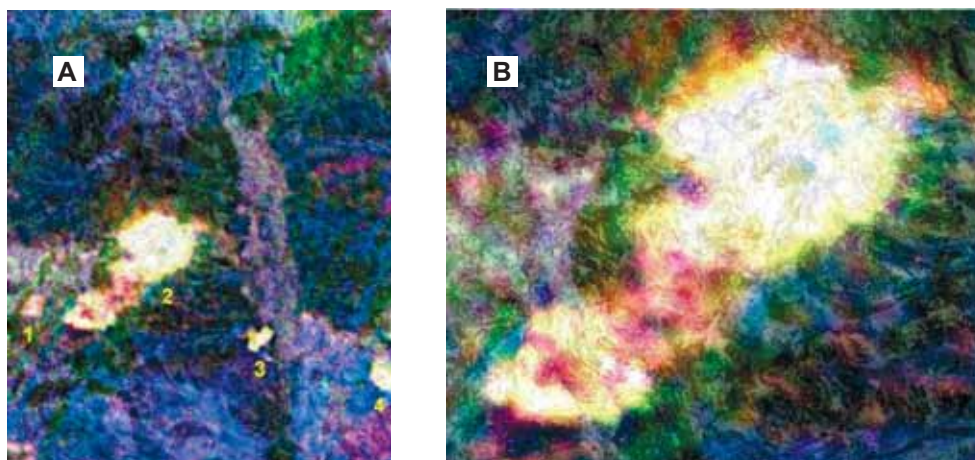


Fig. 12. (A) High to very high Th-U-K radiometric signature in four (1–4) Macanga granite intrusions. 100 km NW of the town of Tete. (B) Note the crescent-shaped landscape features in the southern half of body No. 2, thought to reflect successive injections of magma sheets along the SW margin of the northern core. The width of the area in (B) is 24 km.

Other granitoids

In addition to the granitoids described here, some small granite areas can also be distinguished. For example, the Neoproterozoic Monte Tarai Granite, which forms a one kilometre wide and several kilometres long mountain chain in the Chidzolo-mondo gneisses, occurs near the Zambian border,

on the eastern side of the Luatize River. According to Hunting (1984), quartz-feldspar porphyries are especially common in these remote mountains. The other granitoids with small extent are the Boesi granite, the Monte Dómue granite and the Cassenga Leucogranite (GTK Consortium 2006).

GEOCHEMISTRY

Introduction

Chemical whole rock analyses (55 in total) have been used to classify the granitoid rocks and to evaluate crustal evolution in the northern part of Tete Province (Figs 13–16 and Appendix 1). The Fe# symbol, which occurs in the text of the geoche-

mistry chapters and in Appendix 1, represents $\text{Fe}_2\text{O}_3\text{t} / (\text{Fe}_2\text{O}_3\text{t} + \text{MgO})$. The chemical composition of selected minerals of these granitoids is presented in Appendix 2.

Analytical procedures

Major and some trace element (V, Zr, La, Ce, Ba, Sr, Rb, Y, Nb, Th) concentrations were analysed by XRF from pressed powder pellets in the Chemical Laboratory of Geological Survey of Finland. The

mineral analyses were carried out from polished thin sections using a Cameca SX100 electron microprobe at GTK.

Chemical characteristics of the rocks

According to the classification of Middlemost (1994) and Streckeisen and Le Maitre (1979), most granitoids are granites (Figs 13A, B). Their aluminium saturation index varies from metaluminous to slightly peraluminous (Fig. 13C). In general, most

granitoids are geochemically alkalic to calc-alkalic and have ferroan affinities (Figs 13D, E). The petrographically distinguished phases in the Rio Capoeche Granite, Serra Danvura granitoids, Cassacatiza Suite and Furancungo Suite predictably

show scatter and poor correlation in the diagrams (Figs 13–15). Notably, most of the Mesoproterozoic granite analyses plot in the field of post-collisional granites according to the classification of Pearce

(1996, Figure 3) (see also Fig. 14). A more detailed description of sampled and analysed units is given in the following.

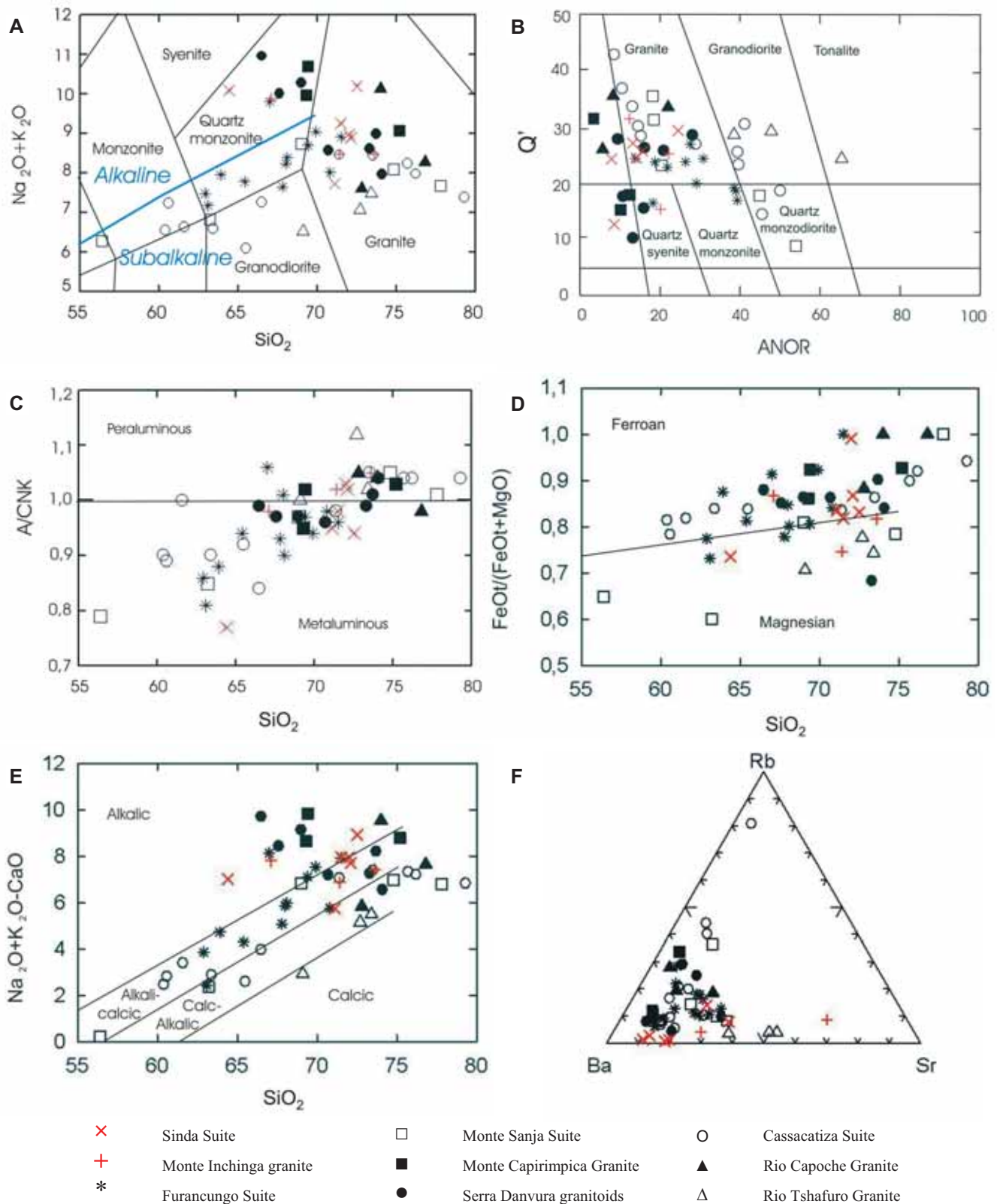


Fig. 13. Classification diagrams for the granitoids. (A) $(\text{Na}_2\text{O}+\text{K}_2\text{O})$ vs. SiO_2 (TAS) diagram of Middlemost (1994). The blue line separating alkaline and subalkaline fields is after Le Bas *et al.* (1986), (B) Q' vs. ANOR diagram of Streckeisen and Le Maitre (1979), (C) the aluminium saturation index A/CNK (Shand 1947), (D) $\text{FeOt}/(\text{FeOt}+\text{MgO})$ vs. SiO_2 diagram of Frost *et al.* (2001), (E) $\text{Na}_2\text{O}+\text{K}_2\text{O}-\text{CaO}$ vs. SiO_2 diagram of Frost *et al.* (2001) and (F) Ba-Rb-Sr diagram.

Rio Tchafuro Granite

The three analyses of Rio Tchafuro granitoids plot as subalkaline, peraluminous granites, granodiorites and tonalites and differ in their chemical characteristics from other major Mesoproterozoic plutonic rocks within the northern part of Tete Province (Figs 13A–C). The low Rb/Ba and Rb/Sr ratios also clearly separate these samples from other granitoids, as does the lower Fe# (0.71–0.78, see Appendix 1). The Rb content of Rio Tchafuro rocks is low (~43 ppm), while the Sr content is high (~530 ppm) in comparison to the other studied Mesoproterozoic granitoids.

Rio Capoeche Granite

The analyzed samples classify the Rio Capoeche granitoids as sub-alkaline and ferroan (Figs 13A, D). Two samples have features of alkali-feldspar granites (Figs 13A, B). Their Rb-Sr-Ba ratios plot in the central part of the spectrum that stretches from the Ba apex to the Rb apex, defined by the other studied Mesoproterozoic granitoids (Fig. 13F). Two analyses have MgO contents below the detection limit and refer to very high Fe/Mg, as does the third analysed sample with Fe# 0.88 (Appendix 1).

Cassacatiza Suite

The SiO₂ content of the Cassacatiza Suite ranges between 60.4–79.3 wt.%; this refers to intermediate and felsic compositions (Appendix 1). The lack of lower silica values is also verified in field observations by the absence of mafic rock types such as diorite and gabbro amongst the granitoids. However, titanium is partly enriched (up to 1.5 wt.% TiO₂) in the Cassacatiza rocks.

Chemical and molar norm compositions show that the Cassacatiza granitoids form a continuous differentiation trend from quartz monzodiorite to granite (Figs 13A, B). However, some quartz monzonites(-syenites) were observed by modal composition without chemical analyses. Thus, a monzonitic trend also seems to characterize the granitoids of the Cassacatiza Suite. All analysed samples are subalkaline and most are metaluminous (Figs 13A, C). On the AFM diagram of Irvine and Baragar (1971) the granitoids plot in the calc-alkaline field, while the rocks with a lower SiO₂ content straddle the boundary between the calc-alkaline and tholeiitic fields, indicating moderately ferriferous compositions (Fe# >0.80, Appendix 1).

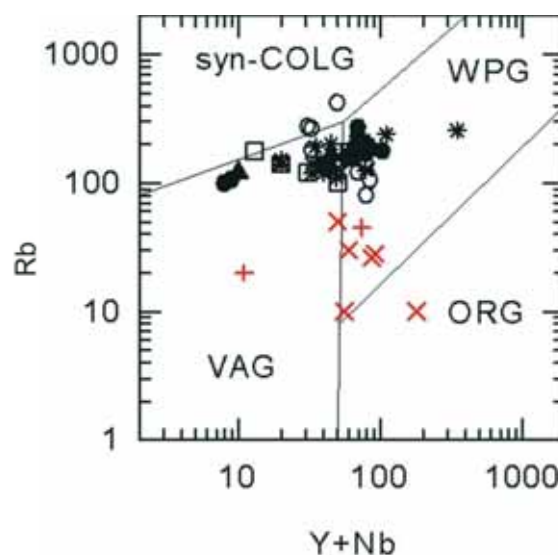


Fig. 14. LogRb vs. Log(Y+Nb) diagram of Pearce *et al.* (1984), where syn-COLG = syn-collisional granites, WPG = within plate granites, VAG = volcanic arc granites, ORG = ocean ridge granites. Symbols as in Figure 13.

On the Rb-Sr-Ba ternary diagram a group of analyses close to the Ba apex (high Ba/Rb ratio) is separated from the rest of the Cassacatiza data (Fig. 13F). This group of high Ba/Rb is equal to the low silica content Cassacatiza granitoids (SiO₂ <65.5 wt.%) and represents quartz monzodiorite members (Appendix 1). A low Sr/Ba can be expected for the monzonitic series.

On Harker diagrams, a reasonably distinct fractionation trend can be seen when SiO₂ is plotted against TiO₂, Al₂O₃, Fe₂O₃t, K₂O, CaO, P₂O₅ and Zr, despite a gap in SiO₂ values from 66.5 to 71.4 wt.% (some are shown in Figure 15). This gap may indicate that the entire Cassacatiza Suite is not co-genetic, though the gap may also result from insufficient data.

Serra Danvura granitoids

The range of SiO₂ contents of these granitoids, from 66.5 to 74.1 wt.%, manifests the differentiation from quartz syenite to granite in the Na₂O+K₂O vs. SiO₂ and Q' vs. ANOR classification diagrams (Fig. 13A, B). The analytical values straddle the boundary between the alkaline and subalkaline fields (Fig. 13A) and the composition is between per- and metaluminous (Fig. 13C). The Na₂O, K₂O and Zr contents of the Serra Danvura granitoids are locally elevated – a slight alkalinity and syenitic characters separate these granitoids from all other granitoids, except the Monte Capirimpica Granite.

On Rb vs. Y+Nb diagram (Fig. 14), which separates different geotectonic settings, the Serra Danvura granitoids plot very similarly to other Mesoproterozoic granitoids of the northern Tete Province; around the boundary line of *volcanic arc* and *within plate granites*.

Monte Capirimpica Granite

The analyses of these granites plot as alkali feldspar granites and quartz syenites (Figs 13A, B). They are transitional between alkaline and subalkaline affinities and on the aluminium saturation diagram transitional between met- and peraluminous rocks (Figs 13A, C). The low Sr/Ba is compatible with syenitic rocks (see Fig. 13F). Together with the Serra Danvura granitoids, the Monte Capirimpica granites are the most alkaline of all granitoids in the northern Tete Province.

Castanho Granite

In Fig. 16, the chemical analyses from Castanho Granite, Tete Gabbro-Anorthosite Suite and Chipera Gabbro have been plotted together to test their possible spatial and temporal relationship (Anorthosite-Mangerite-Charnockite-Granite Complexes). Two analyses (shown in Appendix 1) of the Castanho Granite classify them as felsic rocks (Fig. 16), which are also strongly ferruginous (Fe# 0.85–0.90) and have elevated Zr contents (~520 ppm). In many discrimination diagrams the gabbroic analyses of the Castanho Granite plot in the same field as the gabbros of the Tete Suite (GTK Consortium 2006, Westerhof *et al.* 2008a). They all are subalkaline tholeiites. The Castanho Granite analyses together with the analyses of the Tete Suite form an arcuate line resembling a magmatic differentiation/fractionation trend on the CaO-MgO-Al₂O₃ diagram (Westerhof *et al.* 2008a, Fig. 6).

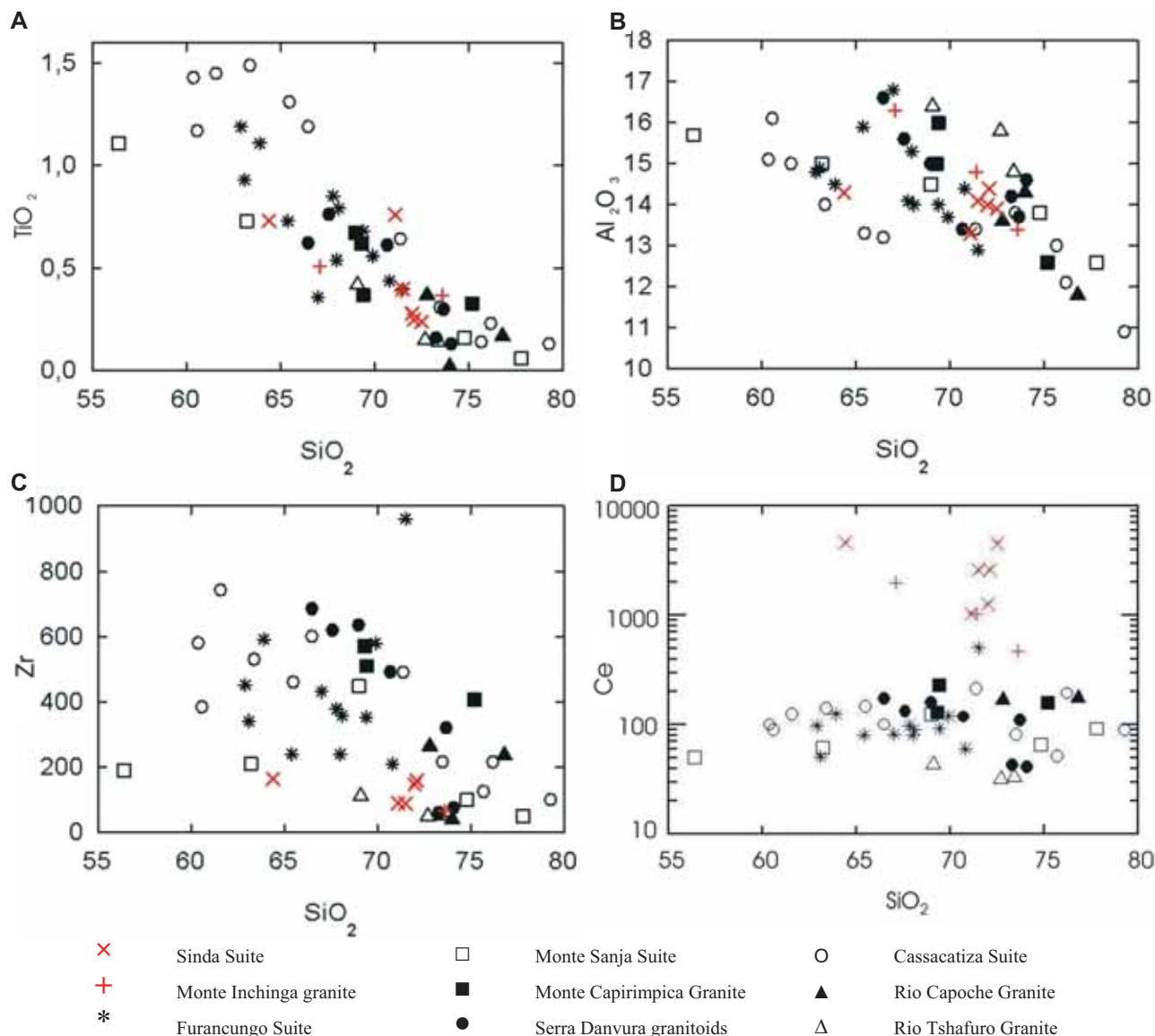


Fig. 15. Selected Harker diagrams for the granitoids.

Monte Sanja Suite

The analysed Monte Sanja samples have a wide range of SiO_2 contents (56.4–77.8 wt.%, Appendix 1), which according to the classification of Streck-eisen and Le Maitre (1979) corresponds with quartz-monzodiorites and granites. The whole series is subalkaline to calc-alkaline (Figs 13A, E). Monzo-dioritic rocks are clearly metaluminous, while granites straddle between the fields of met- and peraluminous rocks (Fig. 13C). In a ternary Rb-Sr-Ba diagram (Fig. 13F), Monte Sanja granitoids indicate moderately high Ba/Rb and Ba/Sr, approximately similar to other Mesoproterozoic granitoids of the northern part of Tete Province, save Rio Tchafuro granitoids, which have distinctly low Rb/Sr and Rb/Ba.

In general, the geochemistry of the Monte Sanja Suite granitoids is similar to the Cassacatiza Suite, but the clear calc-alkalinity of the Monte Sanja Suite strongly differs from the tholeiitic character of the latter.

Furancungo Suite

The SiO_2 content of Furancungo granitoids ranges from 62.9 to 72.5 wt.%, forming a differentiation trend from granite to quartz monzonite and quartz syenite, and referring to a K-enriched magma series (Figs 13A, B). The total alkali content is reasonably high (7–10 wt.%, Appendix 1), but the granitoids still plot in the subalkaline field in the diagram (Fig. 13A).

These most metaluminous rocks have high Fe/Mg ratios ($\text{Fe}^\#$ 0.73–0.92, Appendix 1), which can also be seen in the AFM diagram, where the analyses plot on the boundary between the calc-alkaline and tholeiitic fields. Moreover, the Mg and Zr contents of the Furancungo granitoids vary notably at a given SiO_2 (Fig. 15C). The Rb vs. Y+Nb ratios refer to a volcanic arc to within-plate environment (Fig. 14).

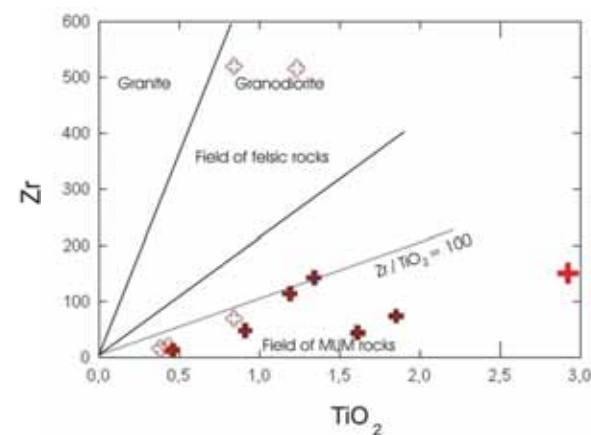


Fig. 16. Chemical Zr vs. TiO_2 diagram of Winchester and Floyd (1977) for classification and for comparison with the Castanho Granites, Tete Suite gabbroic rocks and Chipera Gabbro. Open crosses are Castanho Granite samples, brown crosses are gabbro samples from the Tete Suite and the red cross refers to a sample of Chipera Gabbro nearby. MUM = mafic and ultramafic.

Monte Inchinga granite

Three analyses were carried out from these obviously Neoproterozoic granitoids. The SiO_2 content of the analysed samples ranges from 67.1 to 73.6 wt.%. Cerium concentrations are elevated (up to 1985 ppm), but Rb and Zr contents are low, often below the detection limit (Fig. 15D, Appendix 1). The tectonic diagram shown in Fig. 14 also supports the idea that these rocks are not *syn-collisional*.

Sinda Suite

These Pan-African granitoids plot in alkalic to alkali-calcic fields in Fig. 13E. The analysed Sinda Suite samples have a relative small range of SiO_2 contents (67.1–73.6 wt.%). They are also characterized by a higher V content and a lower Rb content than the Mesoproterozoic granitoids (Appendix 1). Moreover, Ce and La are clearly elevated, having concentrations between 1000–4600 ppm (Fig. 15D) and 75–255 ppm, respectively. In the tectonic diagram of Figure 14, the Sinda Suite granites are clearly distinguished from the Mesoproterozoic granitoids, showing characteristics of *within-plate* granites.

Mineral chemistry

The microprobe analyses of minerals (see Appendix 2) have focused on charnockitic rocks of the study area.

The $\text{Fe}/(\text{Fe}+\text{Mg})$ of the Castanho Granite charnockites orthopyroxene ranges from 0.79 to 0.87, and that of clinopyroxene from 0.78 to 0.84. The relatively low Al_2O_3 content (~0.5 wt.%) of these

orthopyroxenes, compared to orthopyroxenes of the supracrustal Chidzolomondo granulite gneisses nearby, indicates magmatic crystallization (see e.g. McFarlane *et al.* 2003).

Although macroscopically the Rio Capoeche intrusions locally resemble Castanho Granite rocks, their orthopyroxene does not have a high $\text{Fe}/(\text{Fe}+\text{Mg})$,

which is common in pyroxenes of the Castanho Granite samples. This suggests that the mineralogy of Rio Capoché intrusions is metamorphic while the pyroxenes of the Castanho Granite rocks are of magmatic origin.

The amphibole of the quartz syenitic types of Castanho Granite has very high Fe/(Fe+Mg), up to 0.95 (FeOt 31.2 wt.%, MgO 0.9 wt.%). In some amphiboles TiO₂ can be ~2.7 wt.% and Na₂O ~2.3 wt.%. However, the amphibole in the granites, *sensu stricto*, of Castanho Granite is generally hastingsitic with Fe/(Fe+Mg) in the range of 0.78–0.85. Biotite of the Castanho Granite is relative rich in iron, Fe/(Fe+Mg) ranging from 0.64 to 0.77. Locally in the granites, biotite may contain up to 4 wt.% fluorine and almost 5 wt.% TiO₂ (Appendix 2).

In the NE part of Monte Sanja Suite, the hornblende of the granites locally has a somewhat el-

evated Na₂O content (~1.9 wt.%) and biotite may have a F content up to 3.1 wt.%. However, the Mg-Fe silicates of the Monte Sanja Suite are not as ferroan as those of the Castanho Granite (Appendix 2).

In the contact area of the Matunba Suite and Cassacatiza Suite, near Monte Sumba in the western part of Tete Province, hornblende of the foliated quartz syenite has a very high Fe/Mg ratio, over 0.9 (FeOt 32.3 wt.%, MgO 0.9 wt.%, see Appendix 2). Lower values of Fe/Mg can be expected in minerals of metamorphic origin. Accordingly, these syenitic rocks with a high Fe/Mg ratio should be placed in the Cassacatiza Suite rather than in the Matunda Suite, which has undergone Pan-African metamorphism. Amphibole of the Cassacatiza Suite quartz syenite, at Monte Chipalava, also has a very high Fe/Mg ratio (Appendix 2).

DISCUSSION

Based on the diverse data collected during 2002–2005, we considered that the identified granitoid units should be provisionally named after a type locality (Fig. 1 and Table 1). As a consequence, more than a dozen granitoid suites or related assemblages have been identified. The differentiation between these igneous suites is based on age, geophysical signature, geochemistry and field and laboratory observations.

The studied basement is part of the larger Tete-Chipata Belt (Westerhof *et al.* 2008a). The bulk of the granitic rocks has a “Grenville” age between 1.20 and 1.04 Ga. Data on older basement granitoids or Ubendian rocks (De Waele *et al.* 2003) in the Tete-Chipata Belt are restricted to a dating from the Zambian side of the border (Cox *et al.* 2002). The undated Rio Messeze orthogneisses (Fig. 3) may be equivalent to the latter. The origin of granite boulders found in the ~1.3 Ga Fíngoè Supergroup conglomerates (Hunting 1984, GTK Consortium 2006) in Tete Province remains unknown.

Geochemically, the presently studied Mesoproterozoic ferroan granitoids suggest an extensional tectonic regime (see Frost *et al.* 2001) in the Tete-Chipata Belt. However, there are regional differences; the Serra Danvura granitoids in the south comprise relative high alkalis (Na₂O+K₂O, in total 8–11 wt.%) while the Cassacatiza Suite in the north has higher iron and magnesium contents than the former. The absence of S-type granitoids in northern part of Tete Province indicates that sedimentary rocks did not dominate in the source areas.

The charnockitic Castanho Granite, associated with Tete Gabbro-Anorthosite Suite, may be the result of melting of a previously dehydrated lower crust. This would explain the occurrence of the Castanho Granite charnockites adjacent to the Chidzomondo granulites. Depending on the composition of the lower crust, the charnockitic melts may acquire a range of compositions, further widened by potential crustal contamination during ascent. In conclusion, the anorthosites of Tete Suite and associated charnockite intrusions are not co-magmatic but are derived from coexisting melts, and slight differences in emplacement age may therefore exist (Westerhof *et al.* 2008b).

The older, c. 0.8 Ga zircons found in the c. 0.53 Ga Matunda granite gneisses may reflect the Rodinia Supercontinent breakdown event and/or formation of juvenile crust during post-Grenville Neoproterozoic extensional phase. Notably, the large ultramafic Atchiza Suite in the western part of Tete Province has the same age, c. 0.86 Ga (Mänttari 2008), supporting a distinct Neoproterozoic thermotectonic event.

The Matunda granite gneisses resemble rocks reported from Zambia and Zimbabwe by Goscombe *et al.* (2000) and Johnson and Oliver (2004). The formation of the Pan-African metamorphic c. 0.53 Ga Matunda gneisses possibly corresponded with the collision and amalgamation of the West and South Gondwana Terranes – as interpreted for near gneisses by Goscombe *et al.* (2000) and Johnson and Oliver (2004). The same thermotectonic event

is indicated by the coeval emplacement of Monte Inchinga granitic plutons within or adjacent to the Pan-African Sanângo Shear Zone. Finally, some of the post-Pan-African granite intrusions (e.g. the Sinda Suite) were emplaced in this collage of terranes as “stitching plutons”. However, the post-Pan-African c. 0.47 Ga Macanga granite may also

manifest west-vergent subduction of East Gondwana, followed by amalgamation and possible crustal thickening (GTK Consortium 2006). In the Tete area this (pseudo-)suture of East and West Gondwana is believed to correspond to the contact between the Desaranhama Granite and the NW-SE trending Angónia Group (Fig. 1).

ACKNOWLEDGEMENTS

We thank Dr Mikko Nironen for useful comments, Mr Lassi Pakkanen for the electron microprobe analyses and Mrs Hanna Virkki for the drawing of the map.

REFERENCES

- Assunção, C. F. T., Coelho, A. V. P. & Brak-Lamy, J. 1956a.** Contribuição para o estudo da petrografia de Moçambique (África Oriental Portuguesa). I. Distrito de Tete. Bol. Serv. Geol. Min., Moçambique, 19.
- Assunção, C. F. T., Coelho, A. V. P. & Brak-Lamy, J. 1956b.** Contribuição para o estudo da petrografia de Moçambique (África Oriental Portuguesa). II. Distrito de Tete. Bol. Serv. Geol. Min., Moçambique, 20.
- Borges, A. 1937.** Minerais úteis da Colónia de Moçambique. Bol. Geol. Soc. Moç., 33, Lourenço Marques.
- Cox, R. A., Rivers, T., Mapani, B., Tembo, D. & De Waele, B. 2002.** Abstract of 11th IAGOD Quadrennial Symposium and Geocongress, Windhoek, Namibia, 3 p.
- De Waele, B., Wingate, M. T. D., Mapani, B. & Fitzsimons, I. C. W. 2003.** Untying the Kibaran knot: A reassessment of Mesoproterozoic correlations in southern Africa based on SHRIMP U-Pb data from the Irumide belt. *Geology* 31, 509–512.
- Frost, B. R., Barnes, C. G., Collins, W. J., Arculus, R. J., Ellis, D. J. & Frost, C. D. 2001.** A Geochemical Classification for Granitic Rocks. *Journal of Petrology* 42, 2033–2048.
- Goscombe, B., Armstrong, R. & Barton, J. M. 2000.** Geology of the Chewore Inliers, Zimbabwe: constraining the Mesoproterozoic to Palaeozoic evolution of the Zambezi Belt. *Journal of African Earth Sciences* 30, 589–627.
- Grantham, G. H., Maboko, M. & Eglington, B. M. 2003.** A Review of the Evolution of the Mozambique Belt and Implications for the Amalgamation and Dispersal of Rodinia and Gondwana. In: Yoshida, M., Windley, B. F. and Dasgupta, S. (eds.), *Proterozoic of East Gondwana: Supercontinent Assembly and Breakup*. Geological Society of London Special Publication, 206.
- GTK Consortium 2006.** Map Explanation; Volume 4: Sheets 1430–1432 and 1530–1534. Geology of Degree Sheets Inhamambo, Maluweru, Chifunde, Zumbo, Fingoè-Magoè, Songo, Cazula and Zóbuè, Mozambique. Direcção Nacional de Geologia (DNG), Maputo, 382.
- Hunting Geology and Geophysics Limited 1984.** Mineral Inventory Project. Final Report. 329 p., DNG, Maputo. Unpublished Report.
- Irvine, T. J. & Baragar, W. R. A. 1971.** A guide to the chemical classification of common volcanic rocks. *Canadian Journal of Earth Science* 8, 523–548.
- Johnson, S. P. & Oliver, G. J. H. 2004.** Tectonothermal history of the Kaourera Arc, northern Zimbabwe: implications for the tectonic evolution of the Irumide and Zambezi Belts of south central Africa. *Precambrian Research* 130, 71–97.
- Kretz, R. 1983.** Symbols for rock forming minerals. *American Mineralogist* 68, 277–279.
- Le Bas, M. J., Le Maitre, R. W., Streckeisen, A. & Zanettin, B. 1986.** A chemical classification of volcanic rocks based on the total alkali-silica diagram. *Journal of Petrology* 27, 745–750.
- Le Maitre, R. W. (ed.) 1989.** A Classification of Igneous Rocks and Glossary of Terms. Recommendations of the International Union of Geological Sciences Subcommittee on the Systematics of Igneous rocks. Blackwell Scientific Publications, 193 p.
- Mäkitie, H., Lehtonen, M. I., Manninen, T., Koistinen, T., Eerola, T. & Mänttari, I. 2006.** New data of granitoids from northern Tete Province, Mozambique. Colloquium of African Geology (CAG21), Maputo, Mozambique. Abstract Volume, 109–110.
- Mänttari, I. 2008.** Mesoarchaeon to Lower Jurassic U-Pb and Sm-Nd ages from NW Mozambique. Geological Survey of Finland, Special Paper 48, 81–119.
- Mänttari, I., Koistinen, T., Lehtonen, M. I., Manninen, T., Mäkitie, H. & Huhma, H. 2006.** U-Pb and Sm-Nd ages for 27 magmatic rocks, NW Mozambique. Colloquium of African Geology (CAG21), Maputo, Mozambique. Abstract Volume, 203–205.
- McFarlane, C. R. M., Carlson, W. D. & Connelly, J. N. 2003.** Prograde, peak, and retrograde P–T paths from aluminium in orthopyroxene: High-temperature contact metamorphism in the aureole of the Makhavinekh Lake Pluton, Nain Plutonic Suite, Labrador. *Journal of Metamorphic Geology* 21, 405–423.
- Middlemost, E. A. K. 1994.** Naming materials in the magma/igneous system. *Earth-Science Reviews* 37, 215–224.
- Pearce, J. H. 1996.** Sources and settings of granitic rocks. *Episodes* 19, 120–125.
- Pearce, J. H., Harris, N. B. & Tindle, A. G. 1984.** Trace element discrimination diagrams for the tectonic interpretation of granitic rocks. *Journal of Petrology* 25, 956–983.
- Phillips, K. A. 1957.** The plutonic history of the Sinda area; sheet 1431, NE. quarter. Records of the Geological Survey Department, North Rhodesia.

- Phillips, K. A. 1965.** The Geology of the Petanke and Mwanjantutu areas; explanation of degree Sheet 1431 NW Quarter and part of SW Quarter. Bulletin of the Geological Survey, Zambia, 15.
- Pinna, P., Marteau, P., Becq-Giraudon, J-F. & Manigault, B. 1986.** Notice Explicative de la Carte Géologique à 1:1 000 000 de la République Populaire de Mozambique. Instituto Nacional de Geologia de Moçambique/BRGM, Orléans, France. Unpublished Report, Maputo, Moçambique.
- Pinna, P., Marteau, P., Becq-Giraudon, J-F. & Manigault, B. 1987.** Carta Geológica de Moçambique, na escala 1:1 000 000, Instituto Nacional de Geologia de Moçambique, Maputo, Moçambique.
- Rogers, J. J. W., Unrug, R. & Sultan, M. 1995.** Tectonic assembly of Gondwana. *Journal of Geodynamics* 19, 1–34.
- Shackleton, R. M. 1994.** The final collision zone between East and West Gondwana; where is it? *Journal of African Earth Sciences* 23, 271–287.
- Shand, S. J. 1947.** Eruptive rocks. Their Genesis, Composition, Classification, and their Relation to Ore Deposits. 3rd edition, Wiley & Sons. 488 p.
- Streckeisen, A. L. 1976.** To each plutonic rock its proper name. *Earth-Science Review* 12, 1–33.
- Streckeisen, A. L. & Le Maitre, R. W. 1979.** A chemical approximation to the modal QAPF classification of the igneous rocks. *Neues Jahrbuch für Mineralogie. Abhandlungen* 136, 169–206.
- Westerhof, A. B. 2006.** Tectonic framework of central and southern Mozambique in relation to Africa's major building blocks. Colloquium of African Geology (CAG21), Maputo, Mozambique. Abstract Volume, 174–176.
- Westerhof, A. B., Phil, Lehtonen, M. I., Mäkitie, H., Manninen, T., Pekkala, Y., Gustafsson, B. & Tahon, A. 2008a** The Tete-Chipata Belt: a new multiple terrane element from western Mozambique and southern Zambia. *Geological Survey of Finland, Special Paper* 48, 145–166.
- Westerhof, A. B., Tahon, A., Koistinen, T., Lehto, T., & Åkerman, C. 2008b.** Igneous and tectonic setting of the allochthonous Tete Gabbro-Anorthosite Suite, Mozambique. *Geological Survey of Finland, Special Paper* 48, 191–210.
- Winchester, J. A. & Floyd, P. A. 1977.** Geochemical discrimination of different magma series and their differentiation products using immobile elements. *Chemical Geology* 20, 325–343.

Appendix 1.

Chemical composition of the granitoids from the northern part of Tete Province. The in-tusion group, rock type, sample number and coordinates are given. b.d. = below detection limit. Detection limits were 0.033 wt% for MgO and 0.014 wt% for P₂O₅.

	Rio Tchafuro Granite				Rio Capoeche Granite				Cassacatiza Suite						Serra Danvura granitoids							
	Tonalite		Grano-diorite		Granite		Granite		Quartz-monzon-diorite		Quartz-monzon-diorite		Granite		Granite		Granite		Quartz-syenite		Quartz-syenite	
SiO ₂ wt%	69.1	72.7	73.4	72.8	74.0	76.8	60.4	60.6	61.6	63.4	65.5	66.5	71.4	73.5	75.7	76.2	79.3	66.5	67.6			
TiO ₂	0.42	0.15	0.14	0.37	0.02	0.17	1.43	1.17	1.45	1.49	1.31	1.19	0.64	0.31	0.14	0.23	0.13	0.62	0.76			
Al ₂ O ₃	16.4	15.8	14.8	13.6	14.3	11.8	15.1	16.1	15.0	14.0	13.3	13.2	13.4	13.8	13.0	12.1	10.9	16.6	15.6			
Fe ₂ O ₃ t	2.50	1.53	1.33	2.93	0.60	1.87	9.18	7.51	8.62	8.05	7.78	6.62	3.41	2.07	1.42	2.06	1.28	2.97	3.14			
MnO	0.04	0.04	0.03	0.04	0.01	0.02	0.18	0.12	0.15	0.15	0.13	0.12	0.06	0.07	0.05	0.03	0.03	0.07	0.09			
MgO	1.04	0.44	0.46	0.39	b.d.	b.d.	2.10	2.08	1.92	1.55	1.51	0.91	0.67	0.33	0.16	0.18	0.08	0.41	0.55			
CaO	3.60	1.92	2.00	1.77	0.59	0.64	4.09	4.43	3.24	3.73	3.50	3.31	1.41	1.06	0.92	0.78	0.57	1.26	1.58			
Na ₂ O	4.99	5.37	4.87	2.77	2.99	3.31	3.85	3.87	3.44	2.86	2.63	3.34	3.39	3.65	3.39	2.58	2.58	4.72	4.35			
K ₂ O	1.53	1.70	2.61	4.83	7.14	4.97	2.70	3.37	3.19	3.74	3.46	3.93	5.07	4.79	4.85	5.12	4.81	6.24	5.66			
P ₂ O ₅	0.12	0.05	0.04	0.11	0.06	b.d.	0.54	0.37	0.57	0.60	0.39	0.45	0.25	0.07	0.04	0.05	0.03	0.10	0.19			
Total	99.74	99.7	99.68	99.61	99.71	99.58	99.57	99.62	99.18	99.57	99.51	99.57	99.7	99.65	99.67	99.61	99.71	99.49	99.52			
Al ₂ SiO ₅	1.00	1.12	1.02	1.05	1.04	0.98	0.90	0.89	1.00	0.90	0.92	0.84	0.98	1.05	1.04	1.04	1.04	0.99	0.97			
Fe#	0.71	0.78	0.74	0.88			0.81	0.78	0.82	0.84	0.84	0.88	0.84	0.86	0.90	0.92	0.94	0.88	0.85			
V ppm	57	b.d.	b.d.	b.d.	b.d.	b.d.	120	146	130	130	150	100	60	b.d.	b.d.	b.d.	b.d.	40	46			
Zr	112	50	53	264	40	237	580	384	742	530	460	600	490	216	125	215	100	685	619			
La	b.d.	b.d.	b.d.	70	b.d.	72	50	30	57	60	56	40	90	53	b.d.	63	30	73	52			
Ce	43	32	33	168	b.d.	175	100	90	125	140	146	100	210	81	51	193	90	173	132			
Ba	443	543	770	579	370	428	1110	924	1240	1110	623	1200	740	786	287	315	70	1634	1579			
Sr	528	585	481	107	160	40	280	375	218	230	158	210	140	130	60	79	30	170	184			
Rb	39	46	44	164	120	180	80	146	105	140	194	120	230	180	273	263	420	155	169			
Y	b.d.	b.d.	b.d.	35	10	67	60	39	57	60	57	50	50	33	18	24	50	46	62			
Nb	b.d.	b.d.	b.d.	10	b.d.	18	20	15	28	20	26	20	20	b.d.	13	9	b.d.	18	18			
Th	b.d.	b.d.	b.d.	27	b.d.	19	b.d.	12	b.d.	b.d.	11	b.d.	20	12	24	59	30	12	b.d.			
Sample	5066	5074	5059	203403	2217	5007	14069	2227	8015	7185	4946	2007-03	2001-03	11101	11099	3469	8623	3193	3191			
Easting	442158	43889	444763	519584	469299	470212	371625	436738	314125	333114	268312	431190	429232	320733	319624	357157	386330	383934	382921			
Northing	8390845	8396983	8385516	8319614	8326609	8346427	8336184	8416363	8306826	8337533	8295442	8414422	8414154	8300488	8302233	8334762	8309898	8287162	8288883			

Appendix 1.
Continues.

	Serra Danvura granitoids						Monte Capirimpica Granite				Castanho Granite				Monte Sanja Suite				Furancungo Suite			
	Granite		Granite		Granite		Granite		Granite		Granite		Granite		Granite		Granite		Granite		Granite	
	Quartz syenite	Granite	Granite	Granite	Granite	Granite	Granite	Granite	Granite	Granite	Quartz monzonite	Granite	Quartz monzonite	Granite	Quartz monzo-diorite	Granite	Quartz monzo-diorite	Granite	Quartz monzonite	Quartz syenite	Granite	Granite
SiO ₂ wt%	69.0	70.7	73.3	73.7	74.1	75.2	69.3	69.4	75.2	59.9	65.1	56.4	63.2	69.0	74.8	77.8	62.9	63.1	62.9	63.9	65.4	
TiO ₂	0.67	0.61	0.16	0.30	0.13	0.33	0.62	0.37	0.33	1.23	0.84	1.11	0.73	0.67	0.16	0.06	1.19	0.93	1.19	1.11	0.73	
Al ₂ O ₃	15.0	13.4	14.2	13.7	14.6	12.6	15.0	16.0	12.6	15.7	15.2	15.7	15.0	14.5	13.8	12.6	14.8	14.9	14.5	14.5	15.9	
Fe ₂ O ₃ t	2.72	4.01	1.27	1.83	1.10	1.90	2.72	2.06	1.90	9.20	6.08	8.68	5.41	3.48	1.27	0.62	7.13	6.18	7.42	7.42	4.93	
MnO	0.07	0.08	0.04	0.04	0.05	0.04	0.07	0.06	0.04	0.15	0.09	0.15	0.09	0.07	0.02	0.03	0.09	0.09	0.09	0.11	0.07	
MgO	0.43	0.64	0.59	0.20	0.21	0.15	0.44	0.17	0.15	1.17	0.56	4.71	3.61	0.82	0.35	b.d.	2.08	2.27	2.08	1.06	1.14	
CaO	1.16	1.39	1.36	0.79	1.42	0.85	1.34	0.85	0.30	4.01	2.90	6.06	4.46	1.91	1.13	0.89	3.63	4.75	3.63	3.22	3.49	
Na ₂ O	3.93	3.85	4.64	4.18	4.97	3.38	4.48	4.68	3.38	4.71	3.87	3.56	3.67	3.53	4.10	4.42	4.51	3.41	4.51	3.60	3.91	
K ₂ O	6.36	4.72	3.97	4.81	3.00	5.49	5.49	6.01	5.70	3.25	4.77	2.72	3.15	5.21	4.00	3.26	2.97	3.77	2.97	4.35	3.88	
P ₂ O ₅	0.17	0.19	0.05	0.15	0.02	0.05	0.15	0.03	0.05	0.35	0.28	0.45	0.17	0.24	0.04	0.02	0.31	0.22	0.31	0.34	0.21	
Total	99.51	99.59	99.58	99.7	99.6	99.65	99.61	99.63	99.65	99.67	99.69	99.54	99.49	99.43	99.67	99.7	99.61	99.62	99.61	99.61	99.66	
A/CNK	0.97	0.96	0.99	1.01	1.04	1.03	0.95	1.02	1.03	0.85	0.90	0.79	0.85	0.97	1.05	1.01	0.86	0.81	0.86	0.88	0.94	
Fe#	0.86	0.86	0.68	0.90	0.84	0.93	0.86	0.92	0.93	0.89	0.92	0.65	0.60	0.81	0.78		0.77	0.73	0.77	0.88	0.81	
V ppm	36	52	b.d.	b.d.	b.d.	b.d.	30	b.d.	b.d.	117	60	210	96.1	65	b.d.	b.d.	155	117	155	99	70	
Zr	635	491	60	320	75	408	570	510	408	516	520	190	210	448	102	50	452	341	452	592	240	
La	72	33	b.d.	40	b.d.	76	60	120	76	34	40	b.d.	29	52	b.d.	35	36	b.d.	36	55	40	
Ce	158	118	43	110	41	130	130	230	160	85	90	50	61	125	66	92	97	51	97	125	80	
Ba	1268	419	1781	570	651	366	1190	930	366	904	950	980	740	1585	815	134	636	624	636	723	780	
Sr	142	116	430	90	353	39	140	100	39	212	200	580	370	260	241	43	280	328	280	155	290	
Rb	185	177	99	270	106	205	160	140	205	63	120	140	120	172	176	101	110	140	110	126	120	
Y	51	79	8	50	9	55	50	30	55	67	50	20	23	47	13	41	36	33	36	60	40	
Nb	15	25	b.d.	20	b.d.	18	10	10	18	25	20	b.d.	8	13	b.d.	9	13	b.d.	13	19	b.d.	
Th	b.d.	12	b.d.	40	b.d.	22	10	10	22	b.d.	b.d.	b.d.	11.2	12	10	41	b.d.	13	b.d.	b.d.	b.d.	
Sample	3214	3399	3933	7213	9131	2254	13032	8631	2254	6054	2096	8030	4054	3016	4313	4329	7014	34420	7014	10130	2147	
Easting	384063	345807	429105	392272	425249	432635	384685	386662	432635	506180	547321	324445	376230	351049	398568	401269	651907	498546	651907	544246	585697	
Northing	8286652	8288337	8313451	8324577	8320051	8416448	8304453	8314543	8416448	8335716	8327619	8292172	8321297	8314750	8328068	8331735	8305648	8407294	8305648	8342217	8305457	

Appendix 1.
Continues.

	Furancungo Suite					Monte Ichinga granite					Sinda Suite				
	Granite	Granite	Granite	Granite	Ortho- gneiss	Granite	Granite	Granite	Granite	Quartz syenite	Granite	Granite	Granite	Granite	Granite
SiO ₂ wt%	67.0	67.8	68.0	68.1	69.4	69.9	70.8	71.5	71.4	73.6	64.4	71.1	71.5	72.0	72.5
TiO ₂	0.36	0.85	0.54	0.79	0.68	0.56	0.44	0.40	0.51	0.37	0.73	0.76	0.40	0.28	0.24
Al ₂ O ₃	16.8	14.1	15.3	14.0	14.0	13.7	14.4	12.9	16.3	13.4	14.3	13.3	14.1	14.0	13.9
Fe ₂ O _{3t}	3.47	4.94	4.15	4.52	4.03	4.30	3.06	4.57	2.92	2.06	4.09	3.75	2.15	3.07	0.74
MnO	0.05	0.08	0.04	0.07	0.06	0.07	0.05	0.08	0.05	0.03	0.07	0.05	0.03	0.07	0.02
MgO	0.33	1.41	0.75	1.12	0.97	0.36	0.58	b.d.	0.45	0.70	1.47	0.74	0.48	0.03	0.15
CaO	1.68	2.58	2.39	2.42	1.60	1.52	2.27	0.99	2.08	1.61	3.09	1.99	1.31	1.04	1.27
Na ₂ O	3.89	3.89	3.26	3.77	3.72	3.54	3.41	3.53	3.96	4.28	3.70	3.61	3.58	3.53	2.60
K ₂ O	5.92	3.76	4.98	4.62	4.98	5.51	4.61	5.38	5.92	4.20	6.39	4.12	5.68	5.45	7.59
P ₂ O ₅	0.08	0.23	0.20	0.20	0.17	0.16	0.13	0.05	0.23	0.14	0.64	0.19	0.15	0.04	0.13
Total	99.58	99.64	99.61	99.61	99.61	99.62	99.75	99.4	99.52	99.61	98.88	99.61	99.38	99.51	99.14
A/CNK	1.06	0.93	1.01	0.90	0.97	0.94	0.98	0.96	0.98	1.02	1.05	0.95	0.98	1.03	0.94
Fe#	0.91	0.78	0.85	0.80	0.81	0.92	0.84		0.87	0.75	0.82	0.84	0.82	0.99	0.83
V ppm	b.d.	91	60	94	68	40	40	b.d.	343	190	255	430	240	570	182
Zr	432	379	240	358	353	580	210	960	b.d.	b.d.	66	90	148	160	b.d.
La	b.d.	b.d.	40	b.d.	39	50	30	218	71	70	134	160	180	256	76
Ce	82	98	80	90	92	120	60	502	1985	1020	468	1030	2600	1268	4523
Ba	1617	740	1200	653	696	730	570	575	340	400	134	1850	900	205	1153
Sr	240	247	210	219	221	120	210	74	140	180	345	230	130	126	259
Rb	120	124	140	190	202	240	150	257	20	b.d.	45	50	30	28	10
Y	24	36	20	28	34	90	20	261	11	b.d.	26	30	30	65	17
Nb	9	12	b.d.	7	11	20	b.d.	87	b.d.	20	48	45	30	27	39
Th	b.d.	16	b.d.	14	14	10	b.d.	17	b.d.	b.d.	11	b.d.	b.d.	b.d.	b.d.
Sample	6125	7048	2125	7050	7052	2297	2132	6305	9174	8090	34211	3534	4493	1578	4728
Easting	566515	644214	565323	653140	654629	571960	565266	648685	369001	324079	277357	279060	316851	297488	270362
Northing	8314094	8317461	8306412	8325063	8324965	8338805	8300760	8307370	8275637	8293286	8269877	8344885	8371018	8336545	8363176

Appendix 2.

Representative chemical composition of minerals in the granitoid rocks. Analyses are made by Cameca Camebax SX100 microprobe in the Geological Survey of Finland. Granitoid group, rock type, observation number and coordinates of the samples are given. Mineral abbreviations are after Kretz (1983), nd = below detection limit. Conditions of analysis were: voltage = 15kV, intensity of beam current = 25nA, beam diameter = 5 µm.

	Rio Capoeche Granite					Rio Capoeche Granite					Cassacatiza Suite					Castanho Granite					Castanho Granite									
	Pyroxene granitoid			Pyroxene granitoid		Pyroxene granitoid			Pyroxene granitoid		Quartz monzonite			Quartz syenite		Pyroxene granite			Pyroxene granite		Pyroxene granitoid									
	Opx	Cpx	Bt	Pl		Opx	Cpx	Hbl	Pl		Opx	Bt	Pl		Hbl	Opx	Hbl	Bt	Pl		Opx	Hbl	Bt	Pl		Opx	Cpx	Hbl	Pl	
SiO ₂ wt%	52.44	52.49	37.32	61.22		48.25	50.02	41.24	61.09		49.65	35.40	59.91		38.58	48.81	41.94	35.65	60.86		48.39	49.93	40.56	62.10		48.39	49.93	40.56	62.10	
TiO ₂	0.12	0.22	4.80	0.04		0.08	0.12	1.84	nd		0.10	4.47	nd		2.19	0.11	2.24	4.93	0.01		0.09	0.19	2.16	nd		0.09	0.19	2.16	nd	
Al ₂ O ₃	0.50	1.11	13.35	23.84		0.31	0.82	9.31	22.95		0.43	13.03	23.69		8.61	0.42	9.03	13.16	24.18		0.42	1.24	9.92	22.35		0.42	1.24	9.92	22.35	
FeO _T	23.55	9.55	13.00	0.17		39.26	19.17	23.84	0.11		31.79	22.63	0.05		31.44	35.43	21.33	22.80	0.12		37.66	18.61	22.43	0.07		37.66	18.61	22.43	0.07	
MnO	0.74	0.33	0.06	nd		1.00	0.48	0.22	0.01		1.59	0.14	nd		1.01	1.21	0.29	0.08	0.01		1.62	0.80	0.38	nd		1.62	0.80	0.38	nd	
MgO	21.35	13.68	15.78	nd		9.13	7.63	6.24	nd		14.03	8.95	nd		0.75	11.84	7.89	8.72	nd		9.79	7.89	6.38	nd		9.79	7.89	6.38	nd	
CaO	0.83	21.40	0.01	5.65		0.89	20.18	10.63	5.57		1.03	0.06	6.35		9.55	0.90	10.70	0.03	5.70		0.83	19.53	10.50	4.85		0.83	19.53	10.50	4.85	
Na ₂ O	nd	0.42	nd	7.72		0.01	0.31	1.32	8.55		nd	0.06	8.05		2.10	0.01	1.59	0.02	8.06		0.05	0.54	1.78	8.93		0.05	0.54	1.78	8.93	
K ₂ O	0.01	nd	9.52	0.63		0.02	0.02	1.43	0.28		0.01	9.37	0.25		1.48	0.01	1.19	9.47	0.43		0.03	0.02	1.63	0.36		0.03	0.02	1.63	0.36	
P ₂ O ₅	0.01	nd	0.03	0.02		0.03	0.03	0.01	0.03		0.01	0.22	0.01		0.01	0.02	0.01	0.02	0.03		0.01	0.02	0.02	0.01		0.01	0.02	0.02	0.01	
BaO	0.02	0.03	0.80	0.01		0.01	0.01	0.06	0.02		0.01	0.25	0.01		0.04	0.01	0.03	0.06	0.02		nd	0.02	0.07	0.03		nd	0.02	0.07	0.03	
F	0.16	0.11	1.22	0.04		0.11	0.09	0.53	0.03		0.07	0.35	0.02		0.50	0.03	0.38	0.56	0.03		0.12	0.08	0.97	0.02		0.12	0.08	0.97	0.02	
Total	99.74	99.34	95.89	99.34		99.10	98.87	96.65	98.63		98.73	94.93	98.34		96.27	98.81	96.61	95.50	99.46		99.04	98.94	96.82	98.82		99.04	98.94	96.82	98.82	
Sample	25434					5184					14069				12108	6038					2435					2435				
Easting	8316623					8326208					8336184				8317326	8327661					8377781					8377781				
Northing	455254					481781					371625				289834	487372					430083					430083				

IGNEOUS AND TECTONIC SETTING OF THE ALLOCHTHONOUS TETE GABBRO-ANORTHOSITE SUITE, MOZAMBIQUE

by

A. B. Phil Westerhof^{1,2}, André Tahon², Tapio Koistinen³,
Tapio Lehto³ & Christer Åkerman⁴

Westerhof, A. B. Phil., Tahon, A., Koistinen, T., Lehto, T. & Åkerman, Ch. 2008.
Igneous and tectonic setting of the allochthonous Tete Gabbro-Anorthosite Suite, Mozambique. *Geological Survey of Finland Special Paper 48*, 191–210, 10 figures.

The Tete (Gabbro-Anorthosite) Suite in Tete Province, western Mozambique, forms an elongate, sub-horizontal sheet-like layered intrusive with a surface area of close to 6 000 km² and supposedly not exceeding 2–3 km in its thickest sections.

The crystalline basement of Tete Province can be attributed to three major Pan-African lithospheric plates, called East, West and South Gondwana. The Tete Suite was emplaced into the Tete-Chipata Belt (TCB), a newly defined multi-terrane structural domain that forms part of West Gondwana since its collision and amalgamation during the Grenvillian orogenic cycle at ~1.06 Ga. The TCB continues into southern Zambia (as the South Irumide Belt) and is composed of an assemblage of stacked small terranes, comprising a wide variety of supracrustal to mid-crustal rocks of oceanic floor/back arc and/or continental-margin-arc setting with ages between ~1.3 and 1.08 Ga (and possibly older fragments), together with ~1.05 to 1.04 Ga partly stitching granitoid plutons of subalkaline affinity and subordinate Pan-African intrusives.

In more detail, the Tete Suite, together with smaller gabbro-anorthosite bodies, was emplaced at 1.05 Ga, approximately coeval with charnockites of the Castanho Granite, into undated granulites of the Chidzolomondo Group of the Luia terrane. This bimodal igneous association can be correlated with an important number of worldwide associations referred to as Anorthosite-Mangerite-Charnockite-Granite (AMCG) Complexes, thought to have formed by melting of the (dehydrated) lower crust. This means that the Chidzolomondo granulites were already “dry” when the Castanho Granite charnockite and layered gabbro-anorthosite magmas formed, thus prior to 1.05 Ga.

A large part of the Tete Suite lithologies (mainly gabbro, subordinate leucotroctolite and anorthosite, minor pyroxenite) are unmetamorphosed and show magmatic textures and mineralogy. The Tete Suite footwall, however, is a strongly deformed thin-skinned blasto- to ultramylonite. The crystalline basement below the Tete Suite has also been modified by contact-parallel tectonism and manifests the development of a variety of deformation fabrics, including blastomylonitic *Augen* gneiss, mylonite and phyllonite, in rocks of predominantly granitoid composition (Chacocoma and Mussata granites). Field observations indicate that Mussata granitoid mylonites mark the horizontal intersection of a thick, subhorizontal to slightly south-dipping, ductile shear zone with S- to SE-directed top-over-bottom sense of shear. Based on geometric considerations, the thickness of the mylonite zone is estimated to be in the order of one to two kilometres. Strain is not uniform but the compound shear zone is composed of a sequence of relatively narrow, anastomosing, high-strain shear zones, wrapping around lower-strain “pods” or lenses.

A hypothetical reconstruction of the original position of the Tete Suite, prior to SE-directed tectonic transport, suggest a displacement over a distance of ~40–45 km with the Chipera massif representing the western autochthonous extremity of the Tete Suite and the Rio Chitacula stocks possibly qualifying as a feeder conduits. Two phases of tectonic transport – syn- and late Pan-African – have been tentatively distinguished. This was followed by a long period of uplift and erosion and possibly gravity-driven transport during the formation of the mid-Zambezi rift. Finally, Cretaceous carbonatite magma has been emplaced into the thrust plane. Associated hydrous and ferruginous solutions have been subsequently injected along numerous second-order shear zones below the Tete Suite footwall, giving rise to the formation of calc-silicate rocks and a variety of hydrothermal mineralizing processes.

Key words (GeoRef Thesaurus AGI): igneous rocks, gabbros, anorthosite, carbonatites, geochemistry, tectonics, augen gneiss, mylonites, shear, Precambrian, Cretaceous, Jurassic, Mozambique.

¹ Westcourt GeoConsult, Kon. Wilhelminalaan 11, 2264BL, Leidschendam, the Netherlands; corresponding author:

² Formerly: International Institute for Geo-Information Science and Earth Observation (ITC), Hengelosestraat 99, Enschede, the Netherlands.

³ Geological Survey of Finland (GTK), P.O. Box 96, FI-02151 Espoo, Finland.

⁴ Sveriges Geologiska Undersökning (SGU), P.O. Box 670, S-751 28 Uppsala, Sweden

E-mail: ap.westerhof@hetnet.nl

INTRODUCTION

The Tete (Gabbro-Anorthosite) Suite, formerly referred to as the Tete Gabbro-Anorthosite Complex, is a layered intrusive named after the town of Tete, situated some 10 km to the south. The Tete Suite forms an elongate, subhorizontal sheet-like body with a surface area of close to 6000 km². It stretches E-W over a distance of ~150 km. Its maximum N-S dimension is ~60 km. The intrusive underlies a dissected plateau having altitudes between 200 and 400 m, with local elevations culminating at 700–1000 m. Its thickness is unknown. Thickness estimates have been made in the past on the basis of aeromagnetic data, but these are severely hampered by strong short wavelength anomalies. The 10–20 km estimate reported by Hunting (1984a, b) is irreconcilable with considerations from different sources (topography, structure, geophysics, field observations), which indicate that the layered igneous body forms a lopolith with a thickness that probably does not exceed 2–3 km in its thickest sections.

The contours of the Tete Suite (and surrounding areas) have recently been mapped (Fig. 1) using modern mapping tools such as satellite ima-

gery, airborne geophysical data and GPS-controlled field verification. Mapping was carried out by a GTK-led consortium as part of a regional resource mapping program (2002–2006) sponsored by the Nordic Development Fund and covering most of southern and central Mozambique (GTK Consortium 2006a, b, c, d). Being characterized by low Th-U-K radiometric signatures, airborne radiometric data proved particularly powerful in outlining basic and ultrabasic rocks of the Tete Suite. The dark colours in the ternary image contrast strongly with the higher count rates in both the surrounding and underlying crystalline basement and Karoo cover (Fig. 2). High to very high, Th(-U)- and U-dominated radiometric point anomalies, both in the basement windows and within the intrusive, correspond to areas of hydrothermal alteration and associated mineralization at the base of or along fractures in the suite. The Tete Suite is further characterized by strong aeromagnetic anomalies (Fig. 2). Both geophysical data sets show that the igneous intrusive has a block-faulted lopolith, in places covered by Karoo rocks.

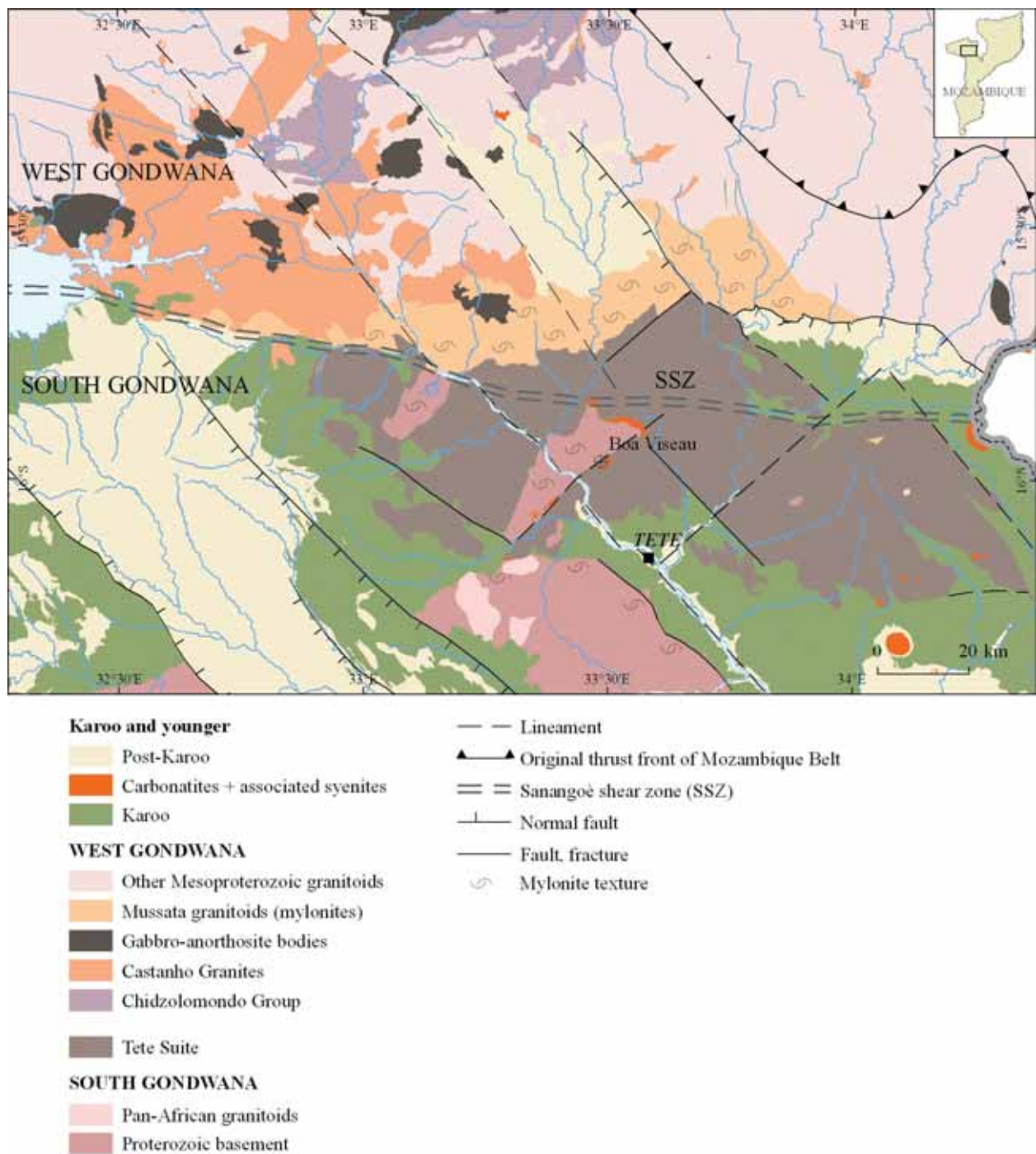


Fig. 1. Simplified geological map of the Tete Suite and surroundings (GTK Consortium 2006d). Two windows in the Tete Suite are named the Rio Chacocoma dome (west) and Rio Mázoè dome (east).

REGIONAL GEOLOGY

Recent resource mapping (GTK Consortium 2006 a, b, c, d) favours a geodynamic model whereby the territory of Mozambique can be attributed to three major lithospheric plates – conveniently named East, West and South Gondwana – that collided and amalgamated during the Pan-African orogenic cycle (see also De Waele *et al.* 2003; Grantham *et al.* 2003, 2007; Johnson & Oliver 2004; Johnson

et al. 2005, 2006a, b, 2007). Each of these major terranes is present in the Tete Province of western Mozambique (Fig. 3). Based on structural and petrologic criteria, a northern crystalline domain can be separated from a southern crystalline basement. The northern crystalline domain can be divided into a small NW-SE trending fraction belonging to East Gondwana (i.e., the Angónia Group), with the

bulk part, characterized by a WSW-ESE to SW-NE structural grain, attributed to West Gondwana (GTK Consortium 2006d). The southern crystalline basement, exposed south of the Sanangoè Shear Zone (SSZ) and mainly south of the mid-Zambezi Karoo rift and along the eastern margin of the Zimbabwe Craton, is attributed to South Gondwana (GTK 2006b, d, Westerhof *et al.* 2008, this issue).

The West Gondwana crystalline basement in northern Tete Province belongs to a newly defined triangular structural element, called the ‘Tete-Chipata Belt (TCB)’, bounded by two major Pan-African steeply-inclined shear zones and superposed Karoo rift structures - Mwembeshi Dislocation (MD) and Sanangoè Shear Zone (SSZ) – together with a sub-horizontal Pan-African thrust front (between East and West Gondwana) in the east (GTK Consortium 2006d, Westerhof *et al.* 2008, this issue). The TCB continues into the ‘Southern Irumide Belt (SIB)’ of

southern Zambia (Johnson *et al.* 2005, 2007). For reasons discussed in GTK Consortium (2006d) and Westerhof *et al.* (2008 this issue) we reject the term ‘Southern Irumide Belt’.

The TCB is mainly composed of a collage of stacked small terranes of broadly Mesoproterozoic age in the Pan-African Zambezi-Lufilian-Damara (ZLD) Belt (Mapani *et al.* 2004; GTK Consortium 2006d). Some of these small terranes consist, in turn, of a thin-skin thrust, stacked assembly of even smaller structural elements or micro-terrane. This ‘stacked multi-terrane model’ for the TCB will be discussed in more detail in a separate paper (Westerhof *et al.* 2008, this issue).

Chondrite-normalized rare earth element (REE) profiles and whole-rock Sm–Nd isotope compositions from ~1095 to 1040 Ma parental supra-subduction melts from one terrane (the Chewore-Rufunsa terrane in Zambia and Zimbabwe) according

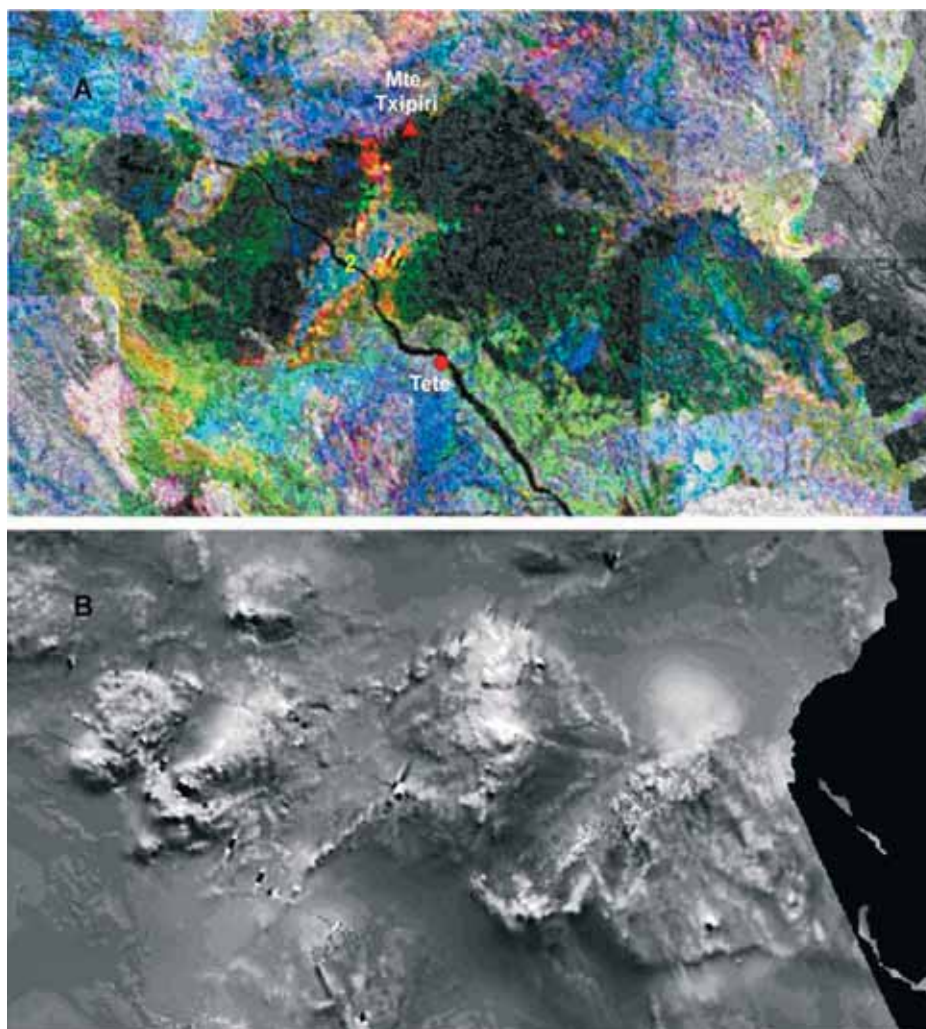


Fig. 2. Geophysical signatures of the Tete Suite. (A) Th-U-K ternary radiometry, co-registered with Landsat TM Band 5, showing the low to very low radiometric signature of the suite. The red area SW of Monte Txipiri corresponds to a cluster of abandoned U workings. 1 = Rio Chacocoma dome; 2 = Rio dome. (B) Aeromagnetics –Total Magnetic Intensity image of the intrusive.

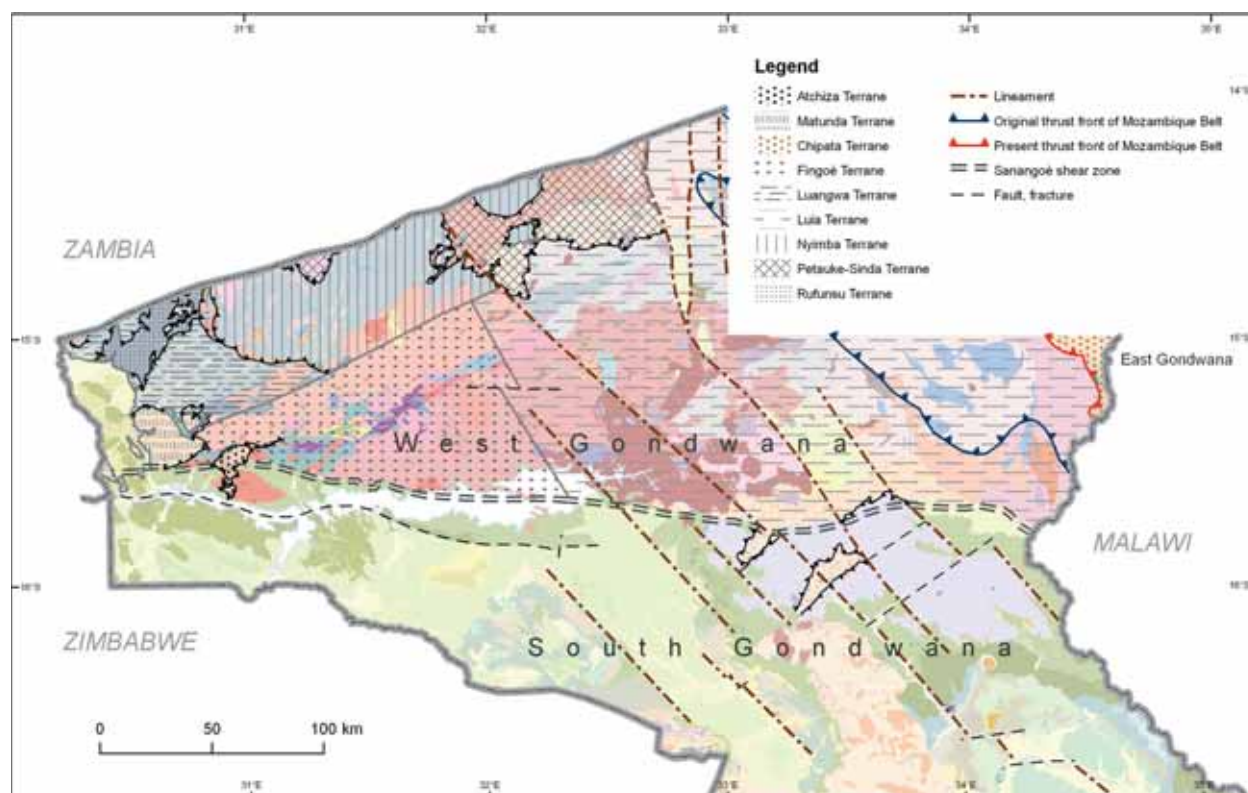


Fig. 3. Provisionally distinguished microterrane in the northern Tete basement.

to Johnson *et al.* (2007) indicate contamination by sialic continental crust, implying a continental margin arc setting. The contaminant continental basement was principally Palaeoproterozoic in age and had a juvenile isotopic signature at the time of its formation. Johnson *et al.* (2007) further suggest that the TCB developed by subduction of oceanic crust under the margin of an unnamed continental mass until ocean closure at ~1040 Ma. Subsequent collision between the TCB and the Central Africa Craton (Congo Craton + Tanzania Craton + Bangweulu Block) margin led to the cessation of magmatism in the TCB and the initiation of compression and crustal melting in the Zambian Irumide Belt. Using metamorphic monazite and zircon overgrowths, polyphase MP-HT metamorphism in the Irumide belt has been dated at 1046 ± 3 Ma (Schenk & Appel 2001). Detrital zircons in the Nyimba Terrane of the TCB indicate low Th/U metamorphic overgrowth indicating HT metamorphism at ~1060 Ma (Johnson *et al.* 2005, 2006).

The small lithospheric slices attributed to the TCB are composed of a variety of poorly related supracrustal and mid-crustal strata, which have suffered dynamo-thermal metamorphism and regional contact metamorphism related to the massive emplacement of granitoids and subordinate (ultra)basic igneous rocks during the Grenvillian orogenic cycle. These terranes include ~1.4 Ga ocean floor

rocks, ~1.3 Ga island arc lithologies, ~1.3 to 1.2 Ga passive margin sequences (clastic metasediments, including carbonates) and deeper continental lithospheric fragments, including granulites (Goscombe *et al.* 1994, 1997a, b, 1998, 2000, Oliver *et al.* 1998; Johnson & Oliver 1998, 2000, 2002, 2004, Johnson *et al.* 2005, 2006a, b, 2007). The various suites of 'Grenville' granitoid rocks show a wide variety of ages, ranging from 1.2 to 1.04 Ma, and a wide spread in various petrologic classification diagrams. Together with subordinate mafic to ultramafic layered intrusives (~1047 Ma) and coeval charnockites (1050 ± 2 Ma), these rocks manifest a complex and prolonged geodynamic development.

Subordinate Pan-African lithological units in the TCB include the early Pan-African Matunda Gneiss (older zircons yielding an age of 784 ± 36 Ma, overprinting at 518 ± 4 Ma) and the ultramafic Atchiza Suite (864 ± 30 Ma) and late Pan-African granitic stocks including the Sinda (502 ± 8 Ma) and Macanga Suites (478 ± 14 Ma) (GTK Consortium 2006d; Mäkitie *et al.* 2006).

The 'stacked multiple-terrane model' of the TCB is discussed in more detail in GTK Consortium (2006d) and Westerhof *et al.* (2008). The mid-crustal Luia Terrane, into which the Tete Suite was supposedly emplaced, occupies the eastern half of the TCB in northern Tete Province.

LUIA TERRANE

The Luia Terrane (Fig. 3) largely coincides with the area formerly attributed to the Luia Group *sensu* Hunting (1984). It is composed of undated, supracrustal, partly retrograded granulites of the (volcano-sedimentary) Chidzolomondo and Mualadzi Groups. Charnockites of the Castanho Granite and small gabbro-anorthosite intrusions, with surface areas between 50 and 250 km², constitute an intrinsic part of the Luia Terrane. The Tete gabbro-anorthosite, currently straddling the Sanangoè Shear Zone (SSZ) and partly overlying South Gondwana crystalline basement, is believed to originate from the Luia Terrane.

The *Chidzolomondo Group* is mainly composed of mafic and intermediate granulites (GTK Consortium 2006d) derived from a mixture of locally strongly deformed (folded and/or sheared) sedimentary and subordinate volcanic protoliths. The metasediments are dominated by light-coloured quartzofeldspathic rocks (meta-arkose?), with subordinate bedded quartzites and occasional calc-silicate rocks. Orthopyroxene with elevated Al₂O₃ contents (up to 3.4 wt.%) is commonly present as a minor or accessory mineral. Biotite with elevated Ti contents (up to 5.6 wt.% TiO₂) is found in places. The high Al₂O₃ and TiO₂ contents are both indicators of high-grade metamorphism. Clinopyroxene is less common. Garnet and cordierite are found in places.

Lithological classification diagrams show, as expected, a wide range in compositions (GTK Consortium 2006d). SiO₂ contents vary from 48.6 to

78.9%. In the SiO₂ vs. Zr/TiO₂ diagram most analyses plot as basalt and andesite, the rest being dacite and rhyodacite or, occasionally, rhyolite (Fig. 4a). The analyzed rocks (12 samples) are subalkaline tholeiites with a slight calc-alkaline affinity (Figs 4b, c, d) and have intermediate TiO₂ and P₂O₅ contents with 1.00–2.07 wt.% and 0.14–0.49 wt.%, respectively, and intermediate Fe values (Fe# 0.57–0.77 wt %) typical for basalt and andesite. On the Jensen diagram the analytical results plot in both high Mg and high Fe fields near the dividing line (Fig. 4d). On a MnO–TiO₂–P₂O₅ diagram (Fig. 5e) the basalts and andesitic basalts plot outside but close to the field of island arc tholeiites and neither rule out nor favour the assumption of an arc setting. The ratio of V and TiO₂ refers to ocean floor basalts rather than to volcanic arc lavas (Fig. 4f). Charnockitic Castanho Granites and layered gabbro-anorthosite bodies are restricted to the domain underlain by the granulites of the Chidzolomondo Group. The bimodal igneous association is thought to have formed by melting of the (dehydrated) lower crust (see below). This means that the Chidzolomondo granulites were already ‘dry’ when the Castanho Granite charnockite and layered gabbro-anorthosite magmas formed, thus prior to 1.05 Ga.

Supracrustal rocks of the Mualadzi Group are exposed in the northern part of the Luia Terrane. Since the unit is entirely surrounded by granites of the 1041 ± 4 Ma Furancungo Granite Suite (GTK Consortium 2006d), its relation to adjacent units in the TCB remains enigmatic.

GEOLOGY OF THE TETE SUITE AND ASSOCIATED SMALLER GABBRO-ANORTHOSITE INTRUSIONS

Lithology – The Tete Suite is a layered intrusive, composed predominantly of gabbro, with subordinate leucogabbro, norite and anorthosite and minor but widespread ultramafic rock types, mostly pyroxenite. Bands or lenses mainly composed of iron-titanium oxides are found in places. Rock fabrics are generally massive unmetamorphosed with medium to very coarse or even pegmatitic grain sizes. Magmatic layering is generally beyond the scale of the outcrop, but where present, magmatic layering is portrayed by meter-scale banding of hornblendite, hornblende-gabbro and anorthosite. Elsewhere, interlayering of anorthosite, pegmatitic gabbro, pyroxenite and Fe-Ti oxide rock can be observed. In a third location, magmatic layering is defined by

bands of 2–10 cm thickness with variable proportions of Fe-Ti oxide minerals and with numerous, dark-coloured, centimetre-sized ellipsoidal aggregates, containing more mafic silicates than the enclosing gabbro, defining a crude banding.

Fresh gabbro and norite of the Tete Suite is a dark, homogeneous, undeformed, medium- to coarse-grained granular rock composed of plagioclase (An_{55–87}), pyroxene and minor Fe-Ti oxides. Pyroxene comprises either augite or hypersthene or both minerals, in the latter case often in intergrowths and accompanied by olivine (Fo_{60–82}) (Svirine 1980, Evans *et al.* 1999). The rocks are generally allotriomorphic with anhedral, interlocking grains of plagioclase and pyroxene. Retrograde alteration affects

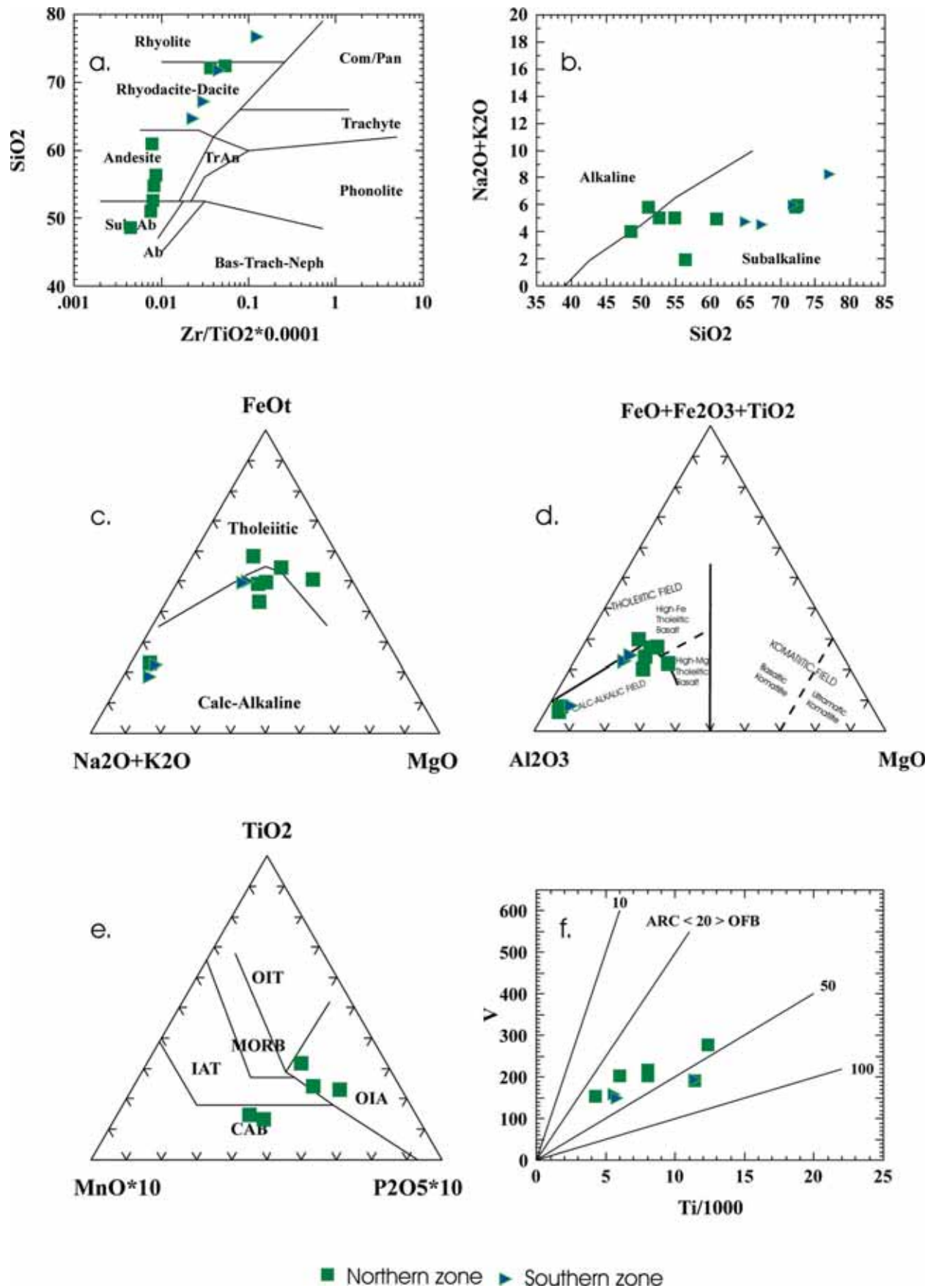


Fig. 4. Chemical classification diagrams for rocks of the Chidzolomondo Group. Abbreviations: OIT = Ocean Island Tholeiites, OIA = Ocean Island Andesites, MORB = Mid-Ocean Ridge Basalts, IAT = Island Arc Tholeiites, CAB = Calc-Alkaline Basalts, OFB = Ocean Floor Basalts.

the original igneous minerals in places: pyroxene crystals are replaced along their margins and cleavage planes by aggregates of hornblende and minor biotite.

Grey or white anorthosite forms a subsidiary but substantial portion of the Tete Suite and is composed of plagioclase (An_{47-57}) with minor clinopyroxene (En_{59-75}), olivine (Fo_{58-64}) and Ti-Fe oxides (Evans *et al.* 1999). Garnet-bearing meta-anorthosite has been reported along the northern margin of the Tete Suite (Evans *et al.* 1999). The texture is coarse-grained granular, often with a tendency towards a bimodal size distribution, with larger grains of plagioclase being enclosed in a mosaic of smaller grains. In several outcrops anorthosite shows a coarse-grained to pegmatitic cumulate fabric, with dark green pyroxene filling up the interstices between centimetre-sized, interlocking plagioclase cumulus crystals (Fig. 5A). Anorthosite is interpreted as later segregations or intrusions and either forms layers within the undifferentiated gabbro(-norite) sequence or discrete bodies with sharp contacts without chilled margins. These rocks represent end-members of a series that – with increasing mafic mineral content –

grades into normal, coarse-grained gabbro (Figs 5B, C). Locally, evidence of multiple pulses of magma injection has been reported, occasionally containing primary hornblende rather than pyroxene (Fig. 5D). Secondary hornblende is also present.

Ultramafic rocks commonly form bands within the gabbro-anorthosite sequence. On the basis of Landsat interpretation and mapping, a larger domain of ultramafic rock is distributed adjacent to the SW corner of the Mázoë granitoid dome (Fig. 1). The rock is black, structurally homogeneous and fine grained. It comprises, for instance, orthopyroxene (with 2.1% Al_2O_3) and amphibole (GTK Consortium 2006b, Table 2 of App. 4).

The Tete Suite is rich in Fe-Ti oxides that locally grade into Fe-Ti oxide rocks forming reefs or lenses parallel to the general magmatic layering. Elsewhere, they form irregular bodies that have been variously interpreted as dykes, plugs or segregations. They are black, very dense rocks, locally very coarse-grained (e.g., at Inhatipissa) and are composed predominantly of titanomagnetite and ilmenite that contain up to 0.66% of vanadium oxide.

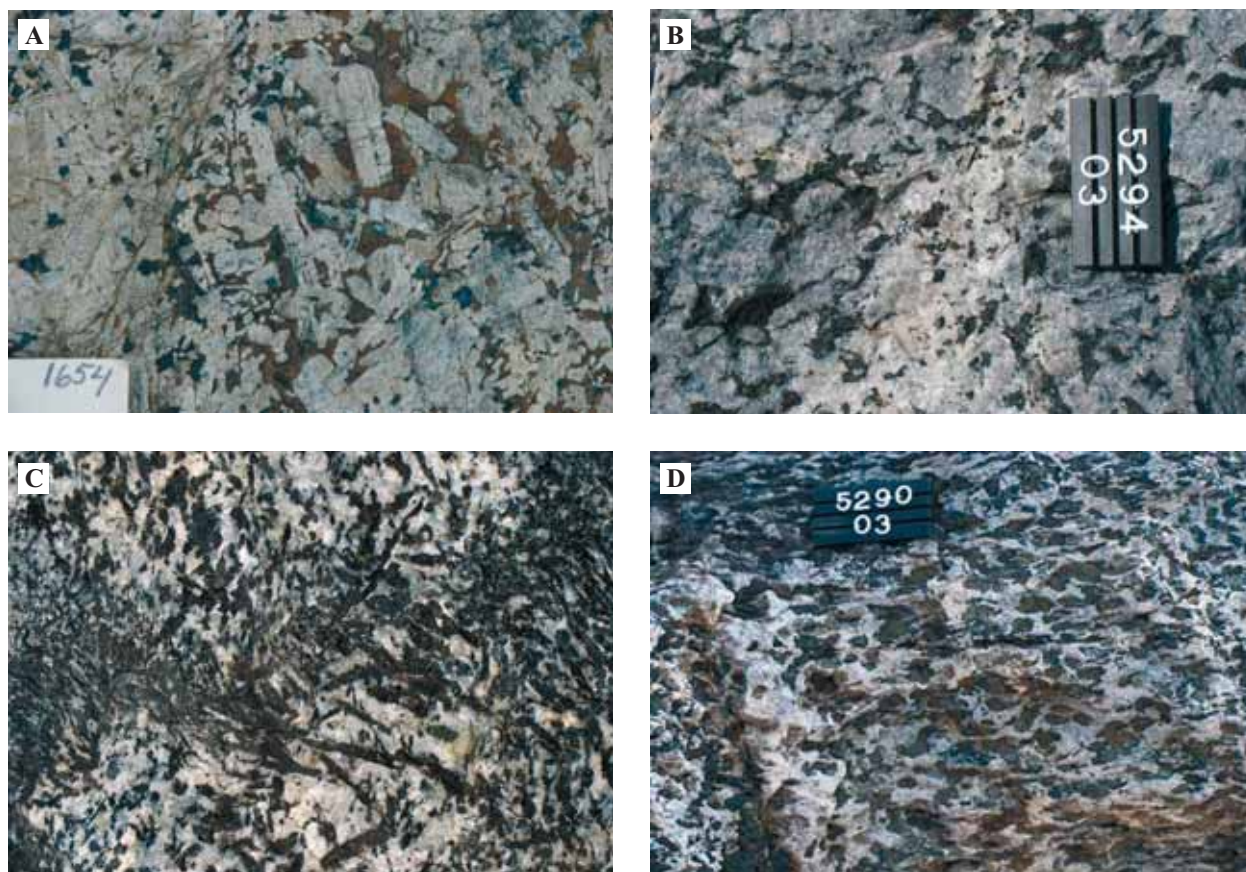


Fig. 5. (A) Cumulus texture in anorthosite, pyroxene filling up the interstices between euhedral plagioclase cumulus crystals. The area in the photo is about 50 cm wide. NE of Moatize town (0595864/8225674). (B) Very coarse-grained cumulate fabric in anorthosite with pyroxene filling interstices between interlocking plagioclase cumulus crystals. The length of the number tag is ~10 cm. (C) An example of secondary anorthosite batch with primary hornblende (after pyroxene that re-equilibrated during magma ascent?). The area in the photo is about 50 cm wide. W of Monte Denderende (0550354/8250097). The scale bar is 8 by 15 cm. (D) With an increasing mafic mineral content, the anorthosites grade toward coarse-grained gabbro. W of Monte Denderende (0551127/8247992).

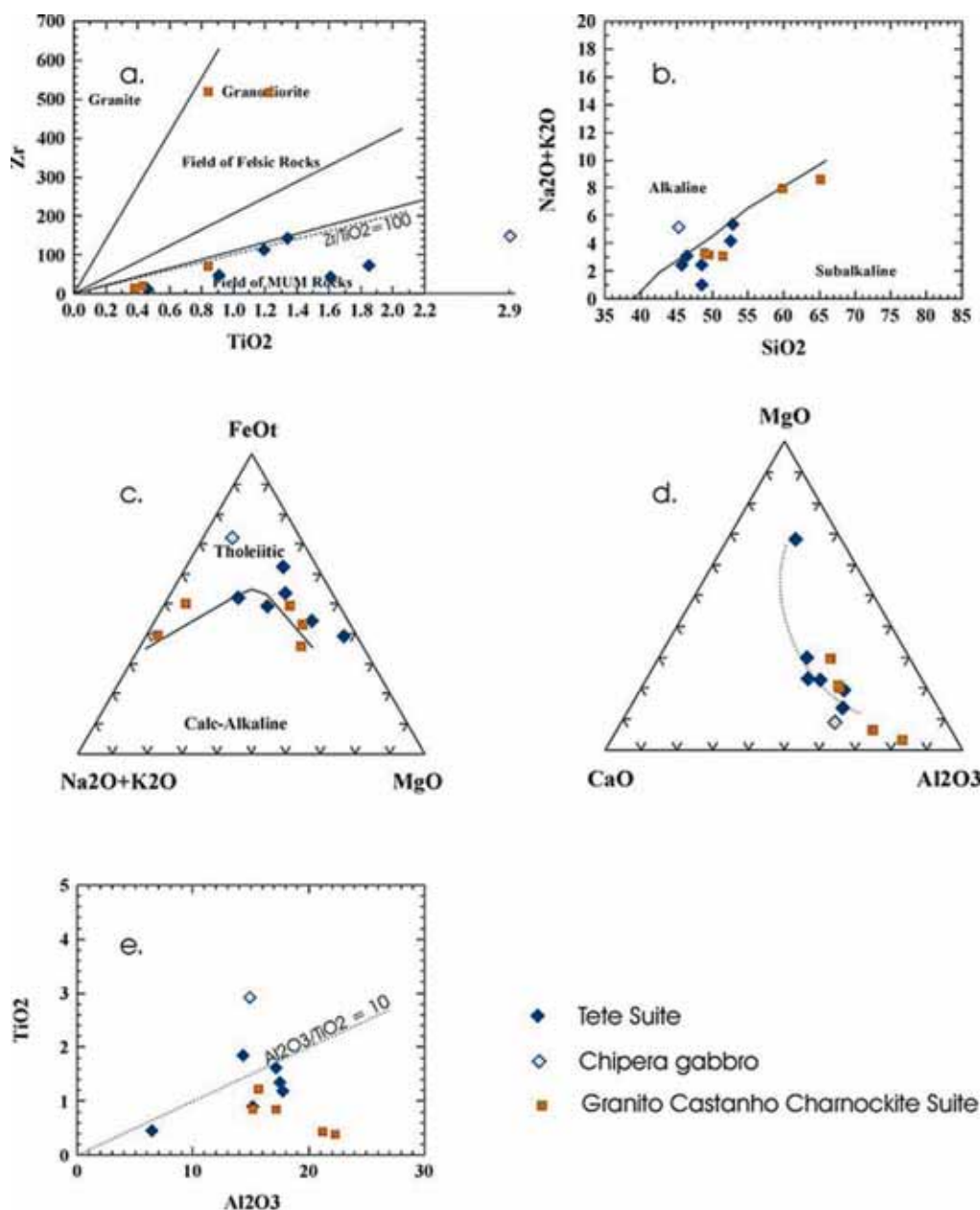


Fig. 6. Chemical diagrams for classification and comparison of the rocks of the Tete Suite, Chipera gabbro and charnockites of the Castanho Granite Suite. Abbreviation in diagram a: MUM = mafic and ultramafic.

Geochemistry – Older geochemical data from the Tete Suite, quoted by Coelho (1969) and reproduced and discussed by Svirine (1980) and Barr & Brown (1987, 1988), are regrettably inadequate and not representative. The analytical results fall within or close to the field typical for other gabbro-anorthosite suites and well outside the field of layered (ultra-)basic intrusions such as the Great Dyke and Bushveld. Gabbroic samples show REE enrichment patterns, compared to chondritic material, that are similar to that of gabbroic rocks of mantle origin (Barr & Brown 1987). Anorthosite has in general relatively low REE contents and shows positive Eu anomalies. This is taken as evidence of the occurrence of cumulus plagioclase crystals enclosed in minor intercumulus material with a ‘whole melt’

REE concentration pattern (Barr & Brown 1987).

Analytical results of six samples from the Tete Suite are presented by GTK Consortium (2006d; Table 1 of App. 3, anal. 29–34) and summarized in the diagrams of Fig. 6. The range in SiO_2 contents is narrow, from 45.7 to 52.9 wt.%, as expected for gabbros. Large variations in MgO values (3.95–22.9 wt.%), however, manifest strong magmatic differentiation. Differentiation is also seen in the $\text{Al}_2\text{O}_3/\text{MgO}/\text{CaO}$ ratios (Fig. 6d), where a trend in development from pyroxenite to gabbro has been traced. The curve with the convex side towards the CaO apex refers to the involvement of cumulus clinopyroxene. The magma classifies in both the calc-alkaline and tholeiitic fields (Fig. 6c). The $\text{Al}_2\text{O}_3/\text{TiO}_2$ ratio is around 10 (Fig. 6e) and $\text{Zr}/\text{TiO}_2 < 100$ (Fig. 6a)

Both parameters indicate no or only minor contamination of the magma by sialic crustal material (e.g., Humphries *et al.* 1985: $\text{Al}_2\text{O}_3/\text{TiO}_2 \sim 10$ and $\text{Zr}/\text{TiO}_2 \sim 70$).

Granulite Enclaves – Afonso and Araújo (1970) reported the existence of pyroxene-granulites with layers of charnockite in the southeastern part of the suite. These comprise dark-coloured, foliated, medium-grained, granoblastic pyroxene-granulite intruded by anorthosite and norite. These granulites do not belong to the Tete Suite as igneous intrusives, but represent fragments of country rock incorporated into the Tete Suite as a tectonic unit (as will be discussed later).

Mafic Dykes – Mafic dolerite dykes, up to 10 m wide, occur in swarms parallel, oblique or at right angles to the magmatic banding in the Tete Suite. At some localities dykes constitute up to 20% of the rock volume. The Rio Imandezue dyke swarm (GTK Consortium 2006d) is characterized by a single set of sheeted dykes trending NW-SE, in parallel to a series of (Cretaceous?) lineaments (Fig. 4). In places, the dykes are intensely sheared along their margins and occasionally disrupted. Where intensely foliated and recrystallised, dyke rock becomes difficult to distinguish from gabbroic country rock.

Four separate intersecting sets of dykes have been recognized. Because the dykes do not extend beyond the layered intrusion, it has been suggested that at least the older dykes are genetically related to the Tete Suite and are co-magmatic. TDM model ages of dolerite, however, indicated that the dyke rock could be several hundreds of millions year younger than the gabbro and anorthosite host rock (Hunting 1984a, b). We conclude that the relationship between the Tete Suite and mafic dykes is of a structural nature. The gabbro-anorthosite sheet is extremely competent, as demonstrated by the large-scale preservation of igneous fabrics, in comparison to other rocks in the area. Where the latter absorb strain by ductile flow, the competent gabbro-anorthosite sheet reacts by the formation of dilatation fractures that are subsequently filled with basaltic magma at four possible occasions: (1) posterior to emplacement of the Tete Suite (< 1.04 Ga), (2) prior to or during the Pan-African orogenic cycle (coeval with post-Rodinia extension and emplacement of the 864 ± 30 Ma Atchiza mafic/ultramafic suite?), (3) during opening of the Zambezi Karoo rift (coeval with the Jurassic, ~ 180 Ma Rukore Suite) or (4) coeval with carbonatites and associated rocks of the Cretaceous Chilwa Alkaline Province.

Smaller gabbro-anorthosite intrusives in the Luia Terrane – These include the relatively large ($> 400 \text{ km}^2$)

Chipera Massif and a number of smaller stocks, including the Rio Chitacula gabbro-anorthosite bodies, that range from 50 km^2 to 250 km^2 in size. Although sparsely exposed, these smaller intrusives – mainly medium- to coarse-grained leucocratic gabbros and norites – are widespread in granulites and migmatites of the Chidzolomondo Group.

The Chipera Massif is composed of leucogabbro and anorthosite. Major mineral constituents are plagioclase (andesine-labradorite) and variable amounts of olivine, ortho- and clinopyroxene. Magnetite-ilmenite segregations are found in places but occur on a smaller scale than the ones observed in the Tete Suite. According to Hunting (1984a, b), a marginal facies of monzonite composition (mangerite) is typical of the Chipera Massif. Similar margins may be present in other smaller bodies.

Magmatic layering is absent at the outcrop scale, but parallel orientation of euhedral plagioclase laths is assumed to represent magma flow in a partly consolidated state, i.e., a crystal mush. In outcrops, basic rocks in the nuclei of the Chipera and smaller massifs appear isotropic, without any banding and lacking field evidence of recrystallisation. In thin section, however, metamorphic overprinting is evidenced by widespread replacement of pyroxene by hornblende and biotite. Towards their margins the gabbro-anorthosite massifs grade into mafic granulites, very similar to country rock granulites, by a reduction in grain size and a progressive change towards a more granoblastic texture (Hunting 1984a, b). Assay results of a single sample (GTK Consortium 2006d; App. 3, Table 1, anal. 35) show a high TiO_2 (2.92 wt.%), P_2O_5 (1.97 wt.%) and Fe# (0.89), dissimilar to the Tete Suite ultramafic rocks. Other results are plotted in Fig. 6.

Age – Sm-Nd geochronology of two sets of rock samples from the Tete Suite has yielded a poorly constrained age of 938 ± 175 Ma for gabbro and anorthosite (Hunting 1984a, b; sample set of recrystallized gabbro, anorthosite and recrystallized dolerite from intersecting dykes, all taken near the same location). Evans *et al.* (1999) reported on further efforts to date the Tete Suite. The limited spread in Rb-Sr values, however, precluded the calculation of unambiguous results. Magmatic crystallization is best constrained by a 9-point Sm-Nd whole-rock regression age of 1025 ± 79 Ma (including recalculated results from Barr *et al.* 1984). Although far from precise, the result falls within the same Mesoproterozoic time bracket as the age of granitoids in the charnockites of the 'Castanho Granite'. Calculated ϵ_{Nd} values of +3.5 to +4.5 (at 1.0 Ga) indicate derivation from depleted mantle with little or no Archaean

crustal contamination. Minor assimilation of Palaeoproterozoic or Mesoproterozoic crust cannot be excluded. TDM model ages range from 1280 to 1092 Ma.

Sm-Nd dating of gabbro from the Chipera Complex, which is considered genetically related to and coeval with the Tete Suite, yielded a similar age of

1047 ± 29 Ma (GTK Consortium 2006d). Based on ϵ_{Nd} values of +0.9 to +2.7 (at 1 Ga), Evans *et al.* (1999) suggested contamination with older (Archaean?) crustal material, an observation that is difficult to reconcile with the intimate relationship between the Tete and Chipera intrusives (see below).

CHARNOCKITES OF THE CASTANHO GRANITE SUITE

Borges (1937) introduced the term 'granito castanho' (brown granite) to describe certain granitic rocks with distinctive field characteristics. Later, Assunção *et al.* (1956a, b) showed that some, but not all, of these rocks belong to the charnockite series of hypersthene-bearing granites. GTK Consortium (2006d) introduced the term 'Castanho Granite' and showed that not all members are granitic. A significant portion of the observed rock types have syenitic, monzonitic and monzodioritic compositions and not all of them contain hypersthene. Due to their overall good resistance to weathering, Castanho Granite is well exposed and gives rise to a variety of positive landscape features.

According to Hunting (1984a, b), the Castanho Granite is typically a coarse to very coarse rock, composed of variable amounts of quartz, alkali feldspar, plagioclase, hypersthene, augite, biotite and hornblende, with abundant opaque minerals. Locally, a leucocratic member of this suite is exposed, lacking in Fe-Mg silicates and composed almost entirely of quartz, feldspar and opaque minerals (e.g. some of the dark green types near the Cahora Bassa dam). Fabrics range from equigranular to porphyritic. Very large alkali feldspar crystals (5–10 cm in size), making up the bulk of the rock, occur in places. Such 'crystal mush' types often show evidence of magmatic flow by the alignment of elongate K-feldspar grains. The fabric suggests that the Castanho Granite magmas were in an advanced stage of crystallization at their time of emplacement. Finer grain sizes generally reflect recrystallisation posterior to tectonic deformation (polygonization).

Inclusions of host rock frequently occur, particularly along the margins and the (presumed) roof of the intrusions. They range in size from a few centimetres up to several metres or even much larger and include ellipsoidal to rounded, centimetre- to decimetre-sized, mafic, amphibolitic xenoliths that locally constitute significant portions of the exposed rock volume. Optical properties of alkali feldspar in many samples correspond to mixed soda-potash feldspar (anorthoclase), characteristic of rocks formed at high temperatures. Elsewhere, the original high-temperature alkali feldspar differentiated

to form microperthite or is replaced at the margins by myrmekite. Original plagioclase in some samples is also differentiated and contains antiperthitic inclusions of K-feldspar. Where the original texture was porphyritic, the phenocrysts of dark grey alkali feldspar tend to be enveloped by white or clear plagioclase in a *rapakivi* texture. Retrograde metamorphism is indicated by aggregates of hornblende or biotite or, in a few cases, garnet. With more advanced retrograde metamorphism, pyroxene is replaced completely, usually by progressively coarser grained biotite. Eventually, the alkali feldspar loses its dark grey colour and then resembles that of normal granite.

Analytical results of Castanho Granite (5 samples) show a wide range of SiO_2 contents, varying from 49.0 to 65.1% (GTK Consortium 2006d; Table 3 of App. 3, anal. 36–40). Three samples have a gabbroic composition and plot in the MUM field in a Zr versus TiO_2 diagram (Fig. 6a). The other two samples classify as felsic rocks in the same diagram. The felsic members are strongly ferruginous ($\text{Fe\#} \sim 0.9\%$) and approach alkalic compositions (Fig. 6b), also indicated by their elevated Zr content (~ 540 ppm). In discrimination diagrams (Figs 6a–e), gabbroic members of the Castanho Granite plot in the same field as gabbros of the Tete Suite. All are subalkaline tholeiites approaching the alkaline/subalkaline borderline in Figure 6b. The Castanho Granite analyses together with the analyses of the Tete Suite form an arcuate line resembling a magmatic differentiation/fractionation trend on the $\text{CaO-Al}_2\text{O}_3\text{-FeOt}$ diagram (Fig. 6d).

Hornblende and biotite in syenitic members of the Castanho Granite have elevated Fe/Mg ratios, locally over 0.9 (GTK Consortium 2006d, App. 4, Table 2, rock 4), significantly higher than in the more granitic members. Moreover, amphibole has locally moderate Na_2O contents (~ 2.0 wt. %) and biotite may contain up to 4.1 wt. % fluor. Al_2O_3 contents of orthopyroxene in these charnockitic rocks are, however, relatively low (~ 0.5 wt. %) when compared to orthopyroxene in nearby granulitic country rocks of the Chidzolomondo Group.

TETE PROVINCE AMCG SUITE

The Tete Suite, smaller gabbro-anorthosite bodies and coeval charnockites of the Castanho Granite in Chidzolomondo granulites of the Luia Terrane can be correlated with an important number of worldwide associations, referred to as *Anorthosite-Mangerite-Charnockite-Granite (AMCG) Complexes* (e.g., Emslie 1978, Frost 2003, Wright 2003, McLelland 2003, Tettelaar 2003). Different views circulate with respect to the nature of this association (e.g., Ashwal 1993). It is generally agreed, however, that anorthosites fractionate from mantle-derived basaltic melts by crystallization and flotation of large volumes of intermediate plagioclase, while olivine and other mafic minerals sink (Frost 2003, McLelland 2003). The pressures that are required for this process imply that the mantle-derived melts are emplaced at the base of the crust, a process generally referred to as '*magmatic underplating*'. The plagioclase-rich upper portions of these magma chambers become gravitationally unstable and rise through the crust. A certain degree of crustal contamination is possible during ascent.

Magmas of charnockite intrusions, associated with the anorthosites, are thought to form by melting of the (dehydrated) lower crust as a result of the crystallization heat and elevated isotherms of the underplated magmas. This would explain the occurrence of Castanho Granite charnockites in northern Tete Province confined to Chidzolomondo granulites of the Luia Terrane. Depending on the composition of the lower crust (itself possibly derived from earlier underplated magmas; see origin of Chidzolomondo granulites), the charnockitic melts may acquire a range of compositions, further complicated by potential crustal contamination on their ascent. One can thus conclude that anorthosites and associated charnockite intrusions are not co-magmatic, but are derived from coexisting melts, and that slight differences in emplacement age may exist.

The tectonic environment for the above scenario is generally considered to be extensional, intraplate and anorogenic, resulting from mantle upwelling and magma generation by adiabatic decompression (Frost 2003). This is not the setting of the northern Tete anorthosite-charnockite association, suggesting a syn-kinematic or slightly post-kinematic emplacement. Syn-collisional extensional conditions can be best explained by replacement of the continental mantle lithosphere by asthenosphere during crustal shortening. Alternatively, geometric and kinematic factors such as the position of the area at the margin of the Central Africa Craton and changing plate kinematics may have played a role. Whether this is achieved by lithospheric delamination (Bird 1979) of an overthickened orogen or by convective thinning of the continental lithosphere (Houseman *et al.* 1981), the consequences are similar and include:

- (1) Juxtaposition of hot asthenosphere with thinned continental lithosphere;
- (2) An increase in the potential energy of the crust consequent upon the increase in surface elevation; and
- (3) A detectable thermal pulse in the extended crust.

Emplacement of anorthosites and associated charnockite intrusions may thus be syn- or late- or post-orogenic. With respect to the Grenville orogenic cycle in the TCB, the convective thinning model may provide a plausible way to explain AMCG-type magmatism synchronous with or somewhat later than contractional tectonics. In addition, it provides a mechanism to explain the important contribution of mantle-derived heat that is necessary to generate the generally high ambient grade of metamorphism, as demonstrated by granulites of the Chidzolomondo Group.

THE TETE SUITE FOOTWALL AND UNDERLYING CRYSTALLINE BASEMENT

The Tete Suite Footwall – Widespread replacement of the original, igneous mineralogy and fabric and the imposition of a tectonic planar fabric occur in various horizons throughout the Tete Suite but are most common and intensive along the footwall contact with the underlying crystalline basement. The contact zone is characterized by ubiquitous and intense brittle and ductile shearing. The 'striped amphibolites', described by Hunting (1984a, b) and others,

are (blasto)mylonites derived from gabbros and anorthosites. The transformation of the latter into 'tiger rock' and 'zebra rock' can be observed in several locations (e.g. along the main road, north of Tete; near the confluence of Mavuze and Zambezi Rivers – Fig. 7). The 'basic gneisses, amphibolites and hornblende schists' surrounding the Rio Chacocoma and Rio Mázoë gneiss domes are actually gabbro-derived (blasto)mylonites, ultra(blasto)mylonites or

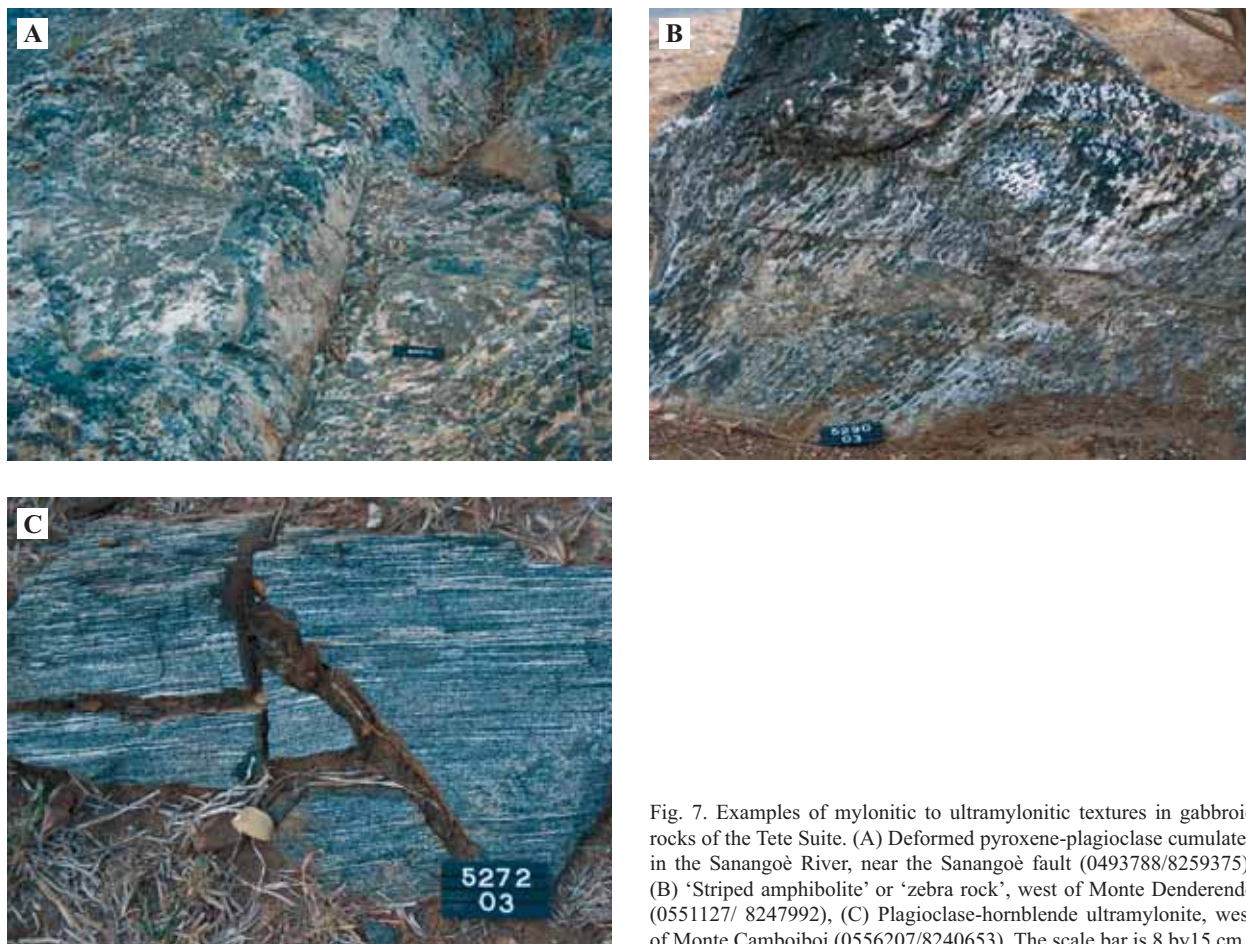


Fig. 7. Examples of mylonitic to ultramylonitic textures in gabbroic rocks of the Tete Suite. (A) Deformed pyroxene-plagioclase cumulates in the Sanangoè River, near the Sanangoè fault (0493788/8259375), (B) 'Striped amphibolite' or 'zebra rock', west of Monte Denderende (0551127/ 8247992), (C) Plagioclase-hornblende ultramylonite, west of Monte Camboiboi (0556207/8240653). The scale bar is 8 by 15 cm.

phyllonites. Pure anorthosites, without mafic mineral content, primarily deform by grain size comminution and recrystallization (polygonization), without developing foliated mylonite fabrics. The sheared part of the Tete Suite, as far as can be judged from the studied outcrops, extends upward for at least 100 m (and most likely more). Parallel, subhorizontal intra-Tete Suite shear zones and associated structures possibly exist even higher up within the Tete Suite footwall zone. Mineralogical changes are also prominent along the Tete Suite footwall. Plagioclase may be replaced by scapolite or, less commonly, by epidote. Replacement of pyroxene by hornblende is also evident.

Underlying Crystalline Basement – Lithologies below the footwall of the Tete Suite have traditionally been attributed to the Chidué Group and underlying Chacocoma Gneiss (Hunting 1984a, b, Barr & Brown 1987, 1988). Mussata granites are mylonitic granitoids exposed along the northern margin of the Tete Suite.

The Chidué Group was reported to consist of a heterogeneous succession of marble, calc-silicate rock, amphibolite, hornblende-, epidote- and

quartzofeldspathic gneisses, biotite- and muscovite-schist and layers of impure quartzites (Real 1966a, b, Afonso 1976, Hunting 1984a, b, Barr & Brown 1987, 1988). Recent resource mapping (GTK Consortium 2006d) has demonstrated that the rocks of the Chidué Group are mainly composed of mica gneiss, marble and meta-sandstones. These rocks have been modified everywhere by contact-parallel tectonism below the Tete Suite. Recent drilling at Boa Viseau, in the Rio Mázoè granitoid dome (for location see Fig. 2A), demonstrates the thin-skin nature of the lithologies below the Tete Suite footwall. The hole intersected by 70 m of Chidué marbles, with numerous subparallel horizons of calc-silicate rock and a gold-bearing quartz vein, followed by 50 m of Tete gabbro (and dolerite), invaded by a 10-m-thick Pan-African granite, to end in mylonitic Chacocoma granite (Mavuzi Resources Ltd., Quarterly Rept. 31 Dec. 2007).

The granitoid basement in the Chacocoma and Rio Mázoè windows (in the South Gondwana Terrane), underlying the Tete Suite, includes the Chacocoma gneiss (Hunting 1984), renamed Chacocoma Granite (GTK Consortium 2006b, d). With the increase in

deformation the identity of the original porphyritic rock gradually became obscured while a thoroughly penetrative schistose fabric replaced the *Augen* gneiss texture. Close to the overlying Tete Suite the granitoid has been deformed into (blasto)mylonite (Fig. 8) and even into phyllonites. The end product is composed of thin streaks of feldspar aggregates formed through thorough grain size reduction (and recrystallisation) of the original porphyritic grains. The same mylonitic deformation fabrics can be observed in granitoids and gneisses north and south of the Tete Suite in the Mussata and Chacocoma Granites, respectively.

Mussata granitoids are mapped in a 15-km-wide band, stretching north and parallel to the Tete Suite in the TCB. The majority of field observations in this granitoid were made in variably mylonitized members. A few undeformed relics manifest that the protolith was (very) coarse-grained biotite granite with mm- to cm-sized phenocrysts of K-feldspar. Progressive mylonitization is reflected in a range of deformation fabrics, including L-tectonite pencil structures, blastomylonitic *Augen* gneiss fabrics with σ - and δ -type porphyroclasts and ultimately fine-grained ultra(blasto)mylonites (Fig. 9).

Field observations indicate that Mussata granitoid mylonites mark the horizontal intersection of a thick, subhorizontal to slightly S-dipping, ductile shear zone with a S- to SE-directed top-over-bottom shear sense. Based on geometric considerations, the thickness of the mylonite zone is estimated to be in the order of one to two km. Strain is not uniform but the compound shear zone is composed of a sequence of relatively narrow, anastomosing, high-strain shear zones, wrapping around lower-strain “pods” or lenses.

South of the Tete Suite, mylonite fabrics have been developed in Chacocoma Granite in a NW-SE-directed crystalline basement horst. Nearby, three stocks of undeformed Monte Cáverie granite of alleged Pan-African age and undeformed, slightly flattened Pan-African pegmatite dykes abound and contain enclaves of highly deformed Chacocoma gneiss. A similar zoned Pan-African pegmatite dyke was observed to discordantly cut across mylonitic anorthosite close to the floor of the Tete Suite. This indicates that the mylonite fabrics described above have been developed prior to the emplacement of late to post-Pan-African granites and pegmatites.



◀ Fig. 8. (A) View across the gently undulating erosional surface in the Chacocoma dome area. The higher terrain in the background is composed of gabbro of the Tete Suite. An outcrop in the centre of the picture represents mylonite after Chacocoma granitoid, with its low-angle dip, characteristic of the dome area (0512295/8246500). (B) A close-up of the mylonite of the former outcrop. (C) Strongly mylonitized Chacocoma granodiorite by the main road SE of Monte Caroeira (0560146/8203686). The number tag is 8 by 15 cm.

▶ Fig. 9. Examples of (blasto)mylonitic fabrics in Mussata granitoids of TCB, north of the Tete Suite. (A) L-tectonite with pencil structures. (B) Mesoscopic open fold in ultra(blast)mylonite. (C) *Augen* gneiss after Mussata granitoid with an elevated biotite content; biotite in blastomylonitic foliation wraps around feldspar porphyroclasts; the shear sense is sinistral. (D) More pronounced grinding and a lower biotite content results in fine quartz-feldspar laminae composed of recrystallised quartz and feldspar with occasional relics of feldspar porphyroclasts; the shear sense is sinistral. The number tag is 8 by 15 cm.

Flow-banded apatite-phlogopite marbles, calc-silicate rocks and amphibolites and quartzo-feldspathic veins previously attributed to the Chidué Group (Real 1966a, b, Afonso 1976, Hunting 1984a, b) have been identified as carbonatite, post-emplacment siliceous rock and reaction products between these siliceous fluids and carbonatite. They are composed of mainly amphibole (actinolite, urallite) and scapolite and subordinate epidote (Geological Institute Belgrade 1984a, b). Other minerals encountered in these “calc-silicate rocks and amphibolites” include adularia/albite, diopside-ferro-hedenbergite

and biotite. Locally, tiny and larger masses of albite aggregate have formed. Accessory constituents include apatite, sphene and magnetite.

Hydrothermal activity still continues, as demonstrated by young dislocations with thermal springs to the north from Boroma on the left and right bank from the Zambezi River. Very coarse calcite-quartz blocks with bladed crystals, frequently in box works and sometimes containing chalcedony or quartz in pseudomorphs after platy calcite, are attributed to these young dislocations and hydrothermal activity.

IGNEOUS AND STRUCTURAL SETTING OF THE TETE SUITE

In the Luia Terrane of the TCB, distinct spatial and temporal relations exist between charnockitic stocks of the Castanho Granite and gabbro-anorthosite bodies. This is most evident for the Chipera massif, which is in direct contact with Castanho Granite and is surrounded by a marginal mangerite-facies that may be considered part of the Castanho Granite.

The stable coexistence of olivine and intermediate plagioclase limits the pressure of crystallization

to < 7–8 kbar (< 20–25 km). Apparently, igneous emplacement of the Tete Suite took place at shallow depth (Evans *et al.* 1999). Minor cumulate pyroxenite layers up to 2 m thick, composed of up to 88% Al-rich clinopyroxene (Al_2O_3 up to 9 wt.%) with subordinate Al-rich orthopyroxene (Al_2O_3 up to 5.8 wt.%) and plagioclase (An_{56-75}), resemble high-Al pyroxene megacrysts common in massif-type anorthosites. They may represent high-pressure



crystallization products entrained by gabbroic magmas to shallow crustal emplacement levels (Evans *et al.* 1999).

In the Tete Province the Sanangoè Shear Zone (SSZ) forms the southern boundary of TCB crystalline basement. The Tete Suite, however, straddles the SSZ, has a strongly mylonitized footwall, is underlain by equally mylonitized crystalline basement that belongs to different lithospheric plates, West and South Gondwana, respectively. From this field evidence we conclude that the present position of the Tete Suite results from tectonic transport, posterior to its magmatic emplacement, over an unknown distance most likely from NW to SE. The allochthonous nature of the Tete Suite has not been fully appreciated in earlier reviews.

Based on our observations, concerning the tectonic setting of the Tete Suite we advocate the following scenario: Moving the Tete Suite back to the NW, up-dip along the extended trace of mylonites below and north of the Tete Suite footwall, over a distance of 40–50 km, produces the configuration that is shown in Figure 10. Not only does this particular reconstruction lead to E-W, along-axis continuity between the Chipera massif and Tete Suite – suggesting that they were once part of a single, much larger intrusion – but it also shows the Tete Suite ‘overlying’ the large Castanho Granite massifs

of Serra de Songo and associated areas, thus reinforcing their spatial association. The gabbro massifs near to and enclosed by the displaced Tete Suite outline could be interpreted as feeder stocks to the complex itself or, alternatively, as autochthonous relicts left behind. By the same token, the Chimadzi charnockite stock of the Castanho Granite may be seen as a feeder stock to a much larger Castanho Granite sheet, underneath the Chipera-Tete Suite, of which the Serra de Songo and associated units are remnants. The fact that the Chipera-Tete Suite occurs on top in this configuration suggests that it was intruded first and the slightly younger Castanho Granite magmas mainly ponded underneath, forming large subhorizontal sheets that were only locally able to emplace themselves to higher levels (as in the Chipera massif).

The similarities of the other gabbro (\pm anorthosite) bodies further north of the hypothetical, reconstructed Chipera-Tete Suite, as well as their spatial association with Castanho Granite intrusions, suggest that they also derive from the same generation of underplated magmas. As the granulite facies of their country rocks reflect deeper crustal levels, they most likely represent deeper sections of feeder stocks in the Luia Terrane. In view of the new age determinations (GTK Consortium 2006d), it can be concluded that the emplacement of the gabbro-anorthosite bod-

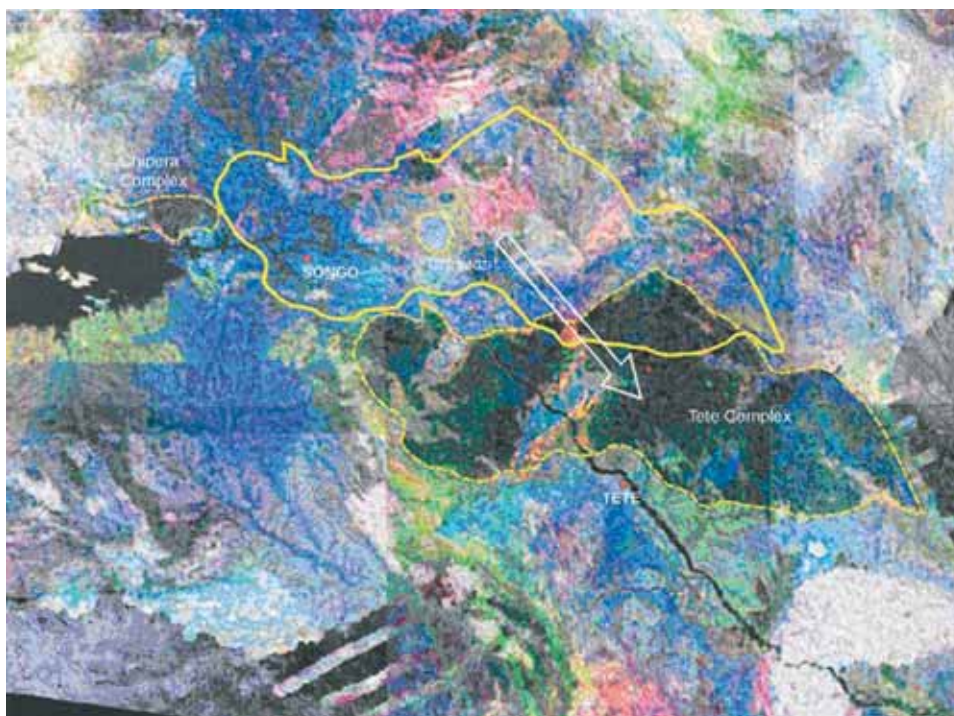


Fig. 10. Hypothetical reconstruction of the original position of the Tete Suite prior to SE-directed tectonic transport over a distance of ~40–45 km (length of arrow). The Chipera massif could represent the western autochthonous extremity of the Tete Suite. The background image is Th-U-K ternary radiometry, co-registered with Landsat TM Band 5 (Tahon 2004).

ies and the charnockites intrusions of the Castanho Granite were pene-contemporaneous. This would justify the definition of the *Tete Province AMCG Suite* as a lithostratigraphic unit spatially and genetically related to the 'dry' granulites of the Chidzolomondo group of the Luia Terrane.

With respect to the small volume of anorthosite, it is important to remember that a significant proportion of the original suite may have been removed due to post-intrusive uplift and erosion, and subsequent tectonic transport. This is confirmed by a mylonitized crystalline basement south of the southern Tete Suite margin, manifesting that the Tete body once extended further southwards than shown by its present outcrop pattern, above the present erosion surface. Alternatively, these mylonites may reflect a northward movement (back-thrusting?) of the allochthonous Tete Suite.

The igneous and tectonic history of the Tete Suite can thus be summarized as follows:

- (1) Igneous emplacement of the Tete Suite and smaller gabbro-anorthosite bodies into granulites of the Chidzolomondo Group of the Luia Terrane at ~1.05 Ga, late in or posterior to the Grenville orogenic cycle, approximately coeval with charnockitic Castanho Granites as part of the *Tete Province AMCG Suite*.
- (2) S- to SW-directed tectonic transport of the bulk of the Tete Suite during the Pan-African orogenic cycle, roughly between ~660 and < 580 Ma, prior to emplacement of late Pan-African granitoids and associated pegmatite dykes.
- (3) Late Pan-African movement, reflecting final docking of all three major Pan-African terranes, over the Sanango Shear Zone (SSZ). The timing is unknown and could be at any time in the Palaeozoic, prior to the emplacement of late-Pan-African granites (between ~550 Ma and ~470 Ma).
- This was followed by a phase of uplift and denudation and formation of the mid-Zambezi rift (~300–180 Ma), involving initial uplift followed by subsidence, possibly triggering gravity-driven thrusting and possibly back-thrusting (open folds in mylonite horizons) of the Tete Suite. Subsequently, carbonatite and associated hydrothermal products such as calc-silicate rocks (amphibole, diopside, scapolite) and quartz(-albite/adularia) bodies have been emplaced into the thrust plane below the Tete Suite footwall, most likely during the Cretaceous.

RELEVANCE TO NICKEL SULPHIDE MINERALIZATION

Mineralization associated with the Tete Suite include (1) hydrothermal, epigenetic copper, gold and uranium mineralization in subparallel shear zones, (2) carbonatite-hosted phosphate and iron mineralization below the Tete Suite footwall and (3) anorthosite-hosted Fe-Ti-V reefs within the suite. They have been described in Lächelt (2004) and GTK Consortium (2006d) and will not be further discussed here.

Since the discovery of the Voisey's Bay (Labrador, eastern Canada) Ni-Cu-PGE sulphide deposits in 1993, anorthosite-troctolite-granite-ferrodiorite igneous suites have become exploration targets. Voisey's Bay appears related to a mantle plume that resulted in emplacement of the Nain Plutonic Suite in relation to the Nain-Churchill terrane boundary (Emslie *et al.* 1994, Ryan 2000). Being located at the boundary between South and West Gondwana, an analogy with the Tete Suite is evident.

Maier *et al.* (2001) analyzed 8 isotopically and mineralogically well-characterized samples of anorthosite, leucotroctolite, clinopyroxenite, gabbro, olivine melagabbro, dolerite, and pegmatitic

orthopyroxenite of the Tete Suite for major and trace elements, including PGEs. The samples showed little evidence of significant crustal contamination and were mostly undepleted in PGEs relative to Cu, and to a lesser degree Ni. Assuming that the samples are representative, Maier *et al.* (2001) conclude that the Tete Suite has limited potential to host economic Ni-Cu sulphide ores and that the potential for reef-type PGE ores remains less clear, in view of the occurrence of such ores in seemingly uncontaminated intrusions elsewhere (*e.g.* the Great Dyke).

At the Voisey's Bay anorthosite conduit, feeder dykes are particularly mineralized. Whereas in most gabbro-anorthosite intrusives the feeder(s) is(are) not exposed, being covered by the generally lopolith-shaped body of the main intrusive, tectonic transport of the Tete Suite has supposedly resulted in the exposure of its feeder(s). The smaller gabbro-anorthosite bodies exposed in the Chidzolomondo granulites north of the Tete Suite are interpreted as either fragments of the lopolith left behind (*e.g.*, Chipera Massif) or possible feeders. These gabbro-anorthosite bodies may show stronger contamination

tion by Si-rich country rock, causing sulphur saturation, and thus merit adequate attention.

The above exploration model and the prospectivity of the TCB in general for Ni sulphides is further confirmed by the recent commission of Albidon's Munali nickel deposit (8.0 Mt @ 1.4% Ni and 0.9 g/t PGM containing 109,000t of Ni and 223,000 ounces of PGM, at a 0.7% Ni cutoff), approximately 60 km south of Lusaka in southern Zambia. The company's geologists believe that the mineralization is associated with mafic to ultramafic intrusions that have

been emplaced along major regional faults, with the type example being the Munali Gabbro intruded along the Munali Fault. Nearby prospects (Voyager and Northwest Target area) are subjected to a systematic program of exploration to fully evaluate the potential for more deposits of this type. Other promising prospects include Idiamala Pools, also in southern Zambia, some 100 km west of Munali, and Mpemba, located in southern Malawi, some 50 E of the Tete Suite and about 20 km SW of the city of Blantyre (Albidon, Annual Report 2006).

REFERENCES

- Afonso, R. S. & Araujo, J. R. 1970.** Geologia das regiões de Doa e Moatize. Unpublished Report., DNG Library No. 593, Maputo.
- Afonso, R. S. 1976.** A Geologia de Moçambique. Notícia Explicativa da Carta Geológica de Moçambique na escala 1 : 2000 000, 175 p., Serviços de Geologia e Minas, Maputo, Mozambique.
- Albidon limited, Annual Report 2006,** in www.albidon.com
- Ashwal, L. D. 1993.** Anorthosites. Springer-Verlag, Berlin, p. 422.
- Assunção, C. F. T., Coelho, A. V. P. & Brak-Lamy, J. 1956a.** Contribuição para o estudo da petrografia de Moçambique (Africa Oriental Portuguesa). I. Distrito de Tete. Serviços de Geologia e Minas, Moçambique, 19.
- Assunção, C. F. T., Coelho, A. V. P. & Brak-Lamy, J. 1956b.** Contribuição para o estudo da petrografia de Moçambique (Africa Oriental Portuguesa). II. Distrito de Tete. Serviços de Geologia e Minas, Moçambique, 20.
- Barr, M. W. C. & Brown, M. A. 1987.** Precambrian gabbro-anorthosite complexes, Tete province, Mozambique. *Geological Journal*, 22, Thematic Issue, 139–159.
- Barr, M. W. C. & Brown, M. A. 1988.** Gabbro-Anorthosite Complexes, Tete Province, Mozambique. *Boletim Geológico*, 41, 7–39, Instituto de Nacional Geologia, Ministério dos Recursos Minerais, Maputo.
- Bird, P. 1978.** Initiation of intracontinental subduction in the Himalaya. *Journal of Geophysical Research*, 83, 4975–4987.
- Borges, A. 1937a.** Minerais uteis da Colónia de Moçambique. *Bol. Geol. Soc. Moç.*, 33, Lourenço Marques.
- Borges, A. 1937b.** Visita de inspecção da mina do ouro de Misale. DNG Library No. 359, Maputo.
- Burke, K., Dewey, J. F. & Kidd, W. S. F. 1977.** World distribution of sutures; the sites off former oceans. *Tectonophysics*, 40, no.1–2, 69–99.
- Coelho, A. V. P. 1957.** Anortositos de Tete (Moçambique). Serviço de Geologia e Minas, 24, Maputo.
- Coelho A. V. P. 1969.** O complexo gabro-anortositico de Tete (Moçambique). *Boletim do Serviço de Geologia e Minas, Moçambique*, 35, p. 78.
- Cutten, H. N. C. & Johnson, S. P. 2006.** Tectonic evolution of the Mozambique Belt, eastern Africa. *Colloquium of African Geology (CAG21)*, 03–06/07/2006, Maputo, Mozambique. Abstract Volume, 33–34.
- De Waele, B., Wingate, M. T. D., Mapani, B. & Fitzsimons, I. C. W. 2003b.** Untying the Kibaran knot: A reassessment of Mesoproterozoic correlations in southern Africa based on SHRIMP U-Pb data from the Irumide belt. *Geology*, 31, (6), 509–512.
- Emslie, R. F. 1978.** Anorthosite massifs, rapakivi granites and Late Proterozoic rifting of North America. *Precambrian Research*, 7, 61–98.
- Emslie, R. F., Hamilton, M. A. & Thériault, R. J. 1994.** Petrogenesis of a mid-Proterozoic anorthosite-mangerite-charnockite-granite (AMCG) complex: Isotopic and chemical evidence from the Nain Plutonic Suite. *Journal of Geology*, 102, 539–558.
- Evans, R. J., Ashwal, L. D. & Hamilton, M. A. 1999.** Mafic, ultramafic, and anorthositic rocks of the Tete Complex, Mozambique: petrology, age, and significance. *South African Journal of Geology*, 102, No. 2, 153–166.
- Frost C. D. 2003.** Significance of Proterozoic anorthosite-rapakivi associations. <http://www.cosis.net/abstracts/EAE03/00988/EAE03-A-00988-1.pdf>.
- Geological Institute Belgrade 1984a.** Final Report. Geological investigation at Monte Muande – Monte Fema (Locality VIII). Mining and Mineralogical Research, DNG; 38 pages + figures.
- Geological Institute Belgrade 1984b.** Final Report on Geological investigation of magnetite and apatite mineralization at Monte Muande, Tete Province. Mining and Mineralogical Research, DNG; 38 pages + figures
- Goscombe, B., Fey, P. & Both, F. 1994.** Structural evolution of the Chewore Inliers, Zambezi Mobile Belt, Zimbabwe. *Journal of African Earth Sciences*, 19, No. 3, 199–224.
- Goscombe, B., Armstrong, R. & Barton, J. M. 1998.** Tectonometamorphic Evolution of the Chewore Inliers: Partial Re-equilibration of High-grade Basement during the Pan-African Orogeny. *Journal of Petrology*, 39, No. 7, 1347–1384.
- Goscombe, B., Armstrong, R. & Barton, J. M. 1997a.** Partial re-equilibration of high-grade basement during the Zambezi/Mozambique orogeny and new SHRIMP data from the Chewore Inliers, Zimbabwe. Abstract, 17th Colloquium of African Geology, Conference Intraplate Magmatism and Tectonics of Southern Africa, 16.
- Goscombe, B., Armstrong, R. & Barton, J. M. 1997b.** Tectono-metamorphic evolution of the Chewore Inliers: Partial re-equilibration of high-grade basement during the Pan-African Orogeny. *Journal of Petrology*, 39, 1347–1384.
- Goscombe, B., Armstrong, R. & Barton, J. M. 2000.** Geology of the Chewore Inliers, Zimbabwe: constraining the Mesoproterozoic to Palaeozoic evolution of the Zambezi Belt. *Journal of African Earth Sciences*, 30, 599–627.
- Graham, G. H., Maboko, M. & Eglington, B. M. 2003.** A Review of the Evolution of the Mozambique Belt and Implications for the Amalgamation and Dispersal of Rodinia and Gondwana. – In: Yoshida, M., Windley, B. F. & Dasgupta,

- S. (eds.), Proterozoic of East Gondwana: Supercontinent Assembly and Breakup. Geological Society of London Special Publication, 206.
- Grantham, G. H., Macey, P. H., Ingram, B. A., Roberts, M. P., Armstrong, R. A., Hokada, T., Shiraishi, K., Jackson, C., Bisnath, A & Manhiça, V. 2007.** Terrane Correlation between Antarctica and Sri Lanka; Comparisons of Geochronology, Lithology, Structure and Metamorphism and possible implications for the geology of southern Africa and Antarctica.
- GTK Consortium 2006a.** Map Explanation; Volume 1: Sheets 2032–2632. Geology of Degree Sheets, Espungabera/Chibabava, Nova/Mambone, Massangena, Chidoco, Save/Bazaruto, Chicualacuala, Machaila, Chigubo, Mabote/Vilanculos, Rio Singuédzí/Massingir, Rio Changana, Funhalouro/Inhambane, Chilembene, Chókwe, Zavala/Inharrime, Maputo, Xai-Xai/Zavala and Bela-Vista, Mozambique. Direcção Nacional de Geologia (DNG), Maputo, 341 pages + Ann..
- GTK Consortium 2006b.** Map Explanation; Volume 2: Sheets 1630–1634, 1732–1734, 1832–834 and 1932–1934. Geology of Degree Sheets Mecumbura, Chioco, Tete, Tambara, Guro, Chemba, Manica, Catandica, Gorongosa, Rotanda, Chimoio and Beira, Mozambique. Direcção Nacional de Geologia (DNG), Maputo, 411 pages + Ann.
- GTK Consortium 2006c.** Map Explanation; Volume 3: Sheets 1735–1739, 1835–1836 and 1935. Geology of Degree Sheets Mutarara, Quelimane, Namacurra/Maganja, Pebane, Marromeu/Inharrime, Chinde and Savane, Mozambique. Direcção Nacional de Geologia (DNG), Maputo, 240 pages + Ann.
- GTK Consortium 2006d.** Map Explanation; Volume 4: Sheets 1430–1432 and 1530–1534. Geology of Degree Sheets Inhambambo, Maluweru, Chifunde, Zumbo, Fingoè-Mâgoè, Songo, Cazula and Zóbuè, Mozambique. Direcção Nacional de Geologia (DNG), Maputo, 382 pages + Ann.
- Hanson, R. E., Wardlaw, M. S., Wilson, T. J. & Mwale, G. 1993.** U-Pb zircon ages from the Hook granite massif and Mwembeshi dislocation: constraints on Pan-African deformation, plutonism, and transcurrent shearing in central Zambia. *Precambrian Research*, 63, 189–209.
- Houseman, G. A., McKenzie, D. P. & Molnar, P. 1981.** Convective instability of a thickened boundary layer and its relevance for the thermal evolution of continental convergent belts. *Journal of Geophysical Research*, 86, no. B7, 6115–6132.
- Humphries, S. E., Thompson, G., Schilling, J. G. & Kingsley, R. A. 1985.** Petrological and geochemical variations along the Mid-Atlantic Ridge between 46°S and 32°S: influence of the Tristan da Cunha mantle plume. *Geochimica et Cosmochimica Acta*, 49, 1445–64.
- Hunting Geology & Geophysics 1984a.** Ground Geophysics. Mineral Inventory Project in Tete Province and Parts of Manica, Sofala and Zambezia Provinces. Report on ground geophysical investigations for the 1982 and 1983 field season. Unpublished Report, DNG, Maputo
- Hunting Geology & Geophysics 1984b.** Landsat Interpretation - Stage 2. Mineral Inventory Project. Revised landsat interpretation, description of mapped units, Tete area. Unpublished Report to DNG, Maputo.
- John, T., Schenk, V., Haase, K., Scherer, E. & Tembo, F. 2003.** Evidence for a Neo-proterozoic ocean in south-central Africa from mid-oceanic ridge-type geochemical signatures and pressure-temperature estimates of Zambian eclogites. *Geology*, 31, 243–246.
- John, T. & Schenk, V. 2003.** Partial eclogitisation of gabbroic rocks in a late Precambrian subduction zone (Zambia): prograde metamorphism triggered by fluid infiltration. *Contribution to Mineralogy and Petrology*, 146, 174–191.
- John, T., Scherer, E. E., Haase, K. & Schenk, V. 2004.** Trace element fractionation during fluid-induced eclogitization in a subduction slab: trace element and Lu-Hf/Sm-Nd isotope systematics. *Earth and Planetary Science Letters*, 227, 441–456.
- Johnson, S. P. & Oliver, G. J. H. 2000.** Mesoproterozoic oceanic subduction, island arc formation and the initiation of back-arc spreading in the Kibaran Belt of central southern Africa: evidence from the ophiolite terrane, Chewore Inliers, northern Zimbabwe. *Precambrian Research*, 103, 125–146.
- Johnson, S. P. & Oliver, G. J. H. 2004.** Tectonothermal history of the Kaourera Arc, northern Zimbabwe; implications for the tectonic evolution of the Irumide and Zambezi Belts of south central Africa. *Precambrian Research*, 130, no. 1–4, 71–97.
- Johnson, S. P., Rivers, T. & De Waele, B. 2005.** A review of the Mesoproterozoic to early Palaeozoic magmatic and tectonothermal history of south-central Africa: implications for Rodinia and Gondwana. *Journal of the Geological Society of London*, 162, 433–450.
- Johnson, S. P., De Waele, B., Evans, D., Tembo, F. & Banda, W. 2006a.** A record of Neoproterozoic divergent processes along the southern Congo Craton margin. In: XXI Colloquium of African Geology, Abstract Book, Maputo, Mozambique, 03-05.07.2006, 73–74.
- Johnson, S. P., De Waele, B. & Tembo, F. 2006b.** The southern Irumide belt of Zambia. In: XXI Colloquium of African Geology, Abstract Book, Maputo, Mozambique, 03-05.07.2006, 75–77.
- Johnson, S. P., De Waele, B., Tembo, F., Katongo, C., Tani, K., Qing Chang, Iizuka, T. & Dunkley, D. 2007.** Geochemistry, Geochronology and Isotopic Evolution of the Chewore-Rufunsa Terrane, Southern Irumide Belt: a Mesoproterozoic Continental Margin Arc. *Journal of Petrology*, 48, (7), 1411–1441.
- Lächelt, S. 2004.** Geology and Mineral Resources of Mozambique. DGN, Maputo, 515 p.
- Macey, P. H. & Armstrong, R. A. 2005.** U-Pb SHRIMP Geochronology of Gneisses and Granites of the Mozambique Metamorphic Belt in the Nampula-Zambezia Provinces, Northern Mozambique. Unpublished Council for Geoscience Report.
- Macey, P. H., Grantham, G. H., Armstrong, R. A., Harley, S., de Kock, G., Ingram, B. I., Cronwright, M. C., Manhiça, M. C. & Azevedo, S. 2006a.** The Kibaran and Pan-African geology of the Alto Molócuè-Murrupula region, NE Mozambique. In: XXI Colloquium of African Geology, Abstract Book, Maputo, Mozambique, 03–05.07.2006, 103–104.
- Macey, P. H., Ingram, B. A., Cronwright, M. S., Botha, G. A., Roberts, M. R., Grantham, G. H., de Kock, G., Maree, I., Botha, P. M. W., Kota, M., Opperman, R., Haddon, I. G., Nolte, J. C. & Rowher, M. 2006b.** Geological Explanation of the 1:250 000 Map Sheets: 1537 Alto Molócuè, 1538 Murrupula, 1539 Nampula, 1540 Mocingual, 1637 Errego, 1638 Gilé, and 1639 Angoche in Northeastern Mozambique. Council for Geoscience, South Africa, September 2006, 211 p.
- Maier, W. D., Barnes, S.-J., Ashwal, L. D., & Li, C. 2001.** A reconnaissance study on the magmatic Cu-Ni-PGE sulphide potential of the Tete Complex, Mozambique. *South African Journal of Geology*; December 2001; v. 104; no. 4; 355–363.
- Mäkitie, H., Lehtonen, M. I., Manninen, T., Koistinen, T., Eerola, T. & Mänttari, I. 2006.** New data of granitoids from northern Tete Province, Mozambique. *Colloquium of African Geology (CAG21)*, 03-06-07-2006, Maputo, Mozambique. Abstract Volume, 109–11.

- Mapani, B., Rivers, T., Tembo, F., De Waele, B. & Katongo, C. 2004.** Growth of the Irumide terranes and slices of Archaean age in eastern Zambia. *Abstr. GeoscienceAfrica* 2004, Johannesburg, 414–415.
- McLelland, J. M. 2003.** Direct dating of Adirondack anorthosite by U-Pb SHRIMP techniques: implications for AMCG genesis. – Geological Society of America, Seattle Annual Meeting, November 2–5, Paper No. 161–10.
- Oliver, G. J. H., Johnson, S. P., Williams, I. S. & Herd, D. A. 1998.** Relict 1.4 Ga oceanic crust in the Zambezi Valley, northern Zimbabwe: Evidence for Mesoproterozoic supercontinent fragmentation. *Geology*, 26, 571–573.
- Porada, H. & Berhorst, V. 2000.** Towards a new understanding of the Neoproterozoic to early Palaeozoic Lufilian and northern Zambezi belts in Zambia and the Democratic Republic of Congo. *Journal of African Earth Sciences* (1994), Vol. 30, No. 3, p. 727–771.
- Powell, C. M., Li, Z. X., McEhinny, M. W., Meert, J. G. & Park, J. K. 1993.** Palaeomagnetic constraints on timing of the Neoproterozoic breakup of Rodinia and the Cambrian formation of Gondwana: *Geology*, 21, 889–892.
- Real, F. 1966a.** *Geologia da Bacia do Rio Zambeze (Moçambique). Características geológico-mineiras da Bacia do Rio Zambeze, em território moçambicano.* Junta de Investigações do Ultramar, 183 p., Lisbon, Portugal.
- Real, F. 1966b.** *Geologia da bacia do rio Zambeze (Moçambique).* – Inst. Invest. Ultramar, Lisboa, Portugal, p. 183.
- Ring, U., Kröner, A., Buchwaldt, R., Toulkeridis, T. & Layner, P. 2002.** Shear-zone patterns and eclogite-facies metamorphism in the Mozambique belt of northern Malawi, east-central Africa: implications for the assembly of Gondwana. *Precambrian Research*, 116, 19–56.
- Ryan, B. 2000.** The Nain-Churchill boundary and the Nain Plutonic Suite: A regional perspective on the geological setting of the Voisey's Bay Ni-Cu-Co deposit. *Economic Geology*, 95, 703–724.
- Stern, R. J. 1994.** Arc assembly and continental collision in the Neoproterozoic East African Orogen: Implications for the consolidation of Gondwanaland. *Annual Reviews. Earth and Planetary Science Letters*, 22, 319–351.
- Svirine, G. 1980.** *Geologia e jazigos minerais do Complexo gabbro-anortositico de Tete.* ING, Unpubl. Rept., DNG Library No. 1007, Maputo.
- Tahon, A. 2004.** Mozambique Lot 2, Field season 2003. Field and Geology Report. – Unpubl. ITC Report, Enschede, the Netherlands, 79 p.
- Tettelaar, T. 2003.** Study of an Anorthosite-Mangerite-Charnockite suite in the Nain Plutonic Suite western margin: implications of emplacement mechanisms and temporal relationships. Memorial University of Newfoundland, Canada, Dept. of Earth Sciences, Seminar, November 5.
- Vrána, S. & Barr, M. W. C. 1972.** Talc-kyanite-quartz schists and other high-pressure assemblages from Zambia. *Mineralogical Magazine, Journal of Mineralogical Society*, 38, 837–846.
- Vrána, S., Prasad, R. & Fediukova, E. 1975.** Metamorphic kyanite eclogites in the Lufilian arc of Zambia. *Contributions to Mineralogy and Petrology*, 51, 139–160.
- Westerhof, A. B., Lehtonen, M. I., Mäkitie, H., Manninen, T., Pekkala, Y., Gustafsson, B. & Tahon, A. 2008.** The Tete-Chipata Belt: a new multiple terrane element from western Mozambique and southern Zambia. *Geological Survey of Finland Special Paper* 48, 145–166.
- Wright, D. 2003.** Geology, structure, and source of the Kikkertavak Anorthosite, northern Labrador, Canada. http://www.mantleplumes.org/Penrose/PenPDF_Abstracts/Wright_Donald_abs.pdf.

THE KAROO VOLCANIC ROCKS AND RELATED INTRUSIONS IN SOUTHERN AND CENTRAL MOZAMBIQUE

by

Tuomo Manninen¹, Toni Eerola², Hannu Mäkitie³, Saku Vuori³,
Arto Luttinen⁴, Adriano Sévanno⁵ & Vladimiro Manhiça⁵

Manninen, T., Eerola, T., Mäkitie, H., Vuori, S., Luttinen, A., Sévanno, A. & Manhiça, V. 2008. The Karoo volcanic rocks and related intrusions in southern and central Mozambique. *Geological Survey of Finland, Special Paper 48*, 211–250, 34 figures, one table, one appendix.

Volcanic rocks and related hypabyssal intrusions of the Mesozoic Karoo large igneous province are wide-spread in southern and central Mozambique and form mesa-like ridges or wide, fertile valleys, depending on the nature and composition of the volcanic flows. The 600 km long, north-south oriented Lebombo mountain range along the border of Mozambique and South Africa is mostly composed of a bimodal association of rhyolitic ash-flow tuffs and ignimbrites and basaltic to andesitic lava flows, while the north-east trending 250 km long Nuanetsi-Sabi volcanic flexure north of the Limpopo river comprises mainly basaltic lava flows with only a few rhyolitic interbeds. Farther to the north, around the Lupata trough, the area covered by the Karoo volcanic rocks is rather limited, whereas in the Tete Province basaltic lavas and more felsic varieties form prominent flat-top mountains and a large dome structure. Mafic and felsic hypabyssal rocks of the Rukore and Gorongosa bimodal intrusive suites form prominent mountains and dyke swarms in central Mozambique. Geochemically, the volcanic rocks are predominantly subalkaline. The mafic lavas associated with the Lebombo monocline and the Nuanetsi-Sabi volcanic flexure are tholeiitic and quite similar to the low-Ti and high-Ti lavas of the Sabie River Formation in South Africa. The mafic lavas from the Lupata trough and in the Tete Province have low-Ti characteristics, but they also include rocks with mildly alkaline affinities. The felsic rocks are subalkaline, peraluminous, and high-K type volcanic rocks with high Fe/Mg ratio and Zr, Nb, Ce, and Y values typical of A-type magmas. The felsic rocks of the Umbelúzi Formation are mainly dacites, whereas the stratigraphically younger felsic rocks of the Movene Formation and the felsic rocks in central Mozambique are mainly rhyolitic. The alkaline volcanic and intrusive rocks in the Pessene area, south Mozambique, may represent the youngest phase of Karoo magmatism in the Lebombo monocline.

Key words (GeoRef Thesaurus AGI): volcanic rocks, rhyolites, basalts, intrusions, geochemistry, Gondwana, Mesozoic, Mozambique.

¹ Geological Survey of Finland, P.O. Box 77, FIN-96101 Rovaniemi, Finland

² Geolanguage Oy, Tammihaantie 2 A 10, FIN-02940 Espoo, Finland

³ Geological Survey of Finland, P.O. Box 96, FIN-21510 Espoo, Finland

⁴ Department of Geology, P.O. Box 64, FIN-00014 University of Helsinki, Finland

⁵ National Directorate of Geology, P.O. Box 217, Maputo, Mozambique

INTRODUCTION

The Mesozoic Karoo large igneous province is one of three continental flood-basalt provinces that are associated with voluminous, possibly plume-related magmatism at ~183 Ma and subsequent break-up of the Gondwana supercontinent during the Early-Middle Jurassic period. Volcanic and intrusive rocks belonging to the Karoo province are wide-spread in southern Africa, but they are also found in western Dronning Maud Land, Antarctica (Fig. 1).

The Karoo volcanic rocks, which generally overlie various sedimentary formations of the Karoo Supergroup, consists mainly of tholeiitic to picritic lava flows, felsic pyroclastic rocks, and related dyke swarms and sills, emplaced prior to the break-up of Gondwana and the opening of Indian Ocean (e.g. Cox 1983). The remnants of mafic lava flow fields are confined to seven principal areas: Lesotho, southern Botswana, northern Botswana, Lebombo-Tuli-Nuanetsi-Sabi (the Limpopo triple junction; Burke & Dewey 1973), and Lupata in southern Africa, and Vestfjella and Kirwanveggen in western

Dronning Maud Land in Antarctica (Fig. 1).

The Karoo-related volcanic rocks have been extensively studied in South Africa, Botswana, and Antarctica over the last decades in terms of stratigraphy (e.g., Cleverly *et al.* 1984), geochemistry (e.g. Cox *et al.* 1967, Betton 1979, Harris & Erlank 1992, Klausen *et al.* 2003, Jourdan *et al.* 2007a), geochronology (e.g., Allsopp *et al.* 1984, Duncan *et al.* 1997, Zhang *et al.* 2003, Riley & Knight 2001, Riley *et al.* 2004, Jourdan *et al.* 2007b), and petrogenesis (e.g., Erlank 1984, Sweeney *et al.* 1994, Luttinen & Furnes 2000, Miller & Harris 2007). The results indicate predominance of compositionally relatively uniform mafic lavas in Lesotho, Botswana, and Kirwanveggen, and markedly heterogeneous lavas in Lebombo, Tuli-Nuanetsi-Sabi, and Vestfjella. Recent geochronological studies indicate emplacement of Karoo-related magmas during a relatively short period from ~185 Ma to ~172 Ma and a distinctive peak of wide-spread magmatic activity at $\sim 182 \pm 3$ Ma (e.g., Jourdan *et al.* 2007b). The reliably dated samples cover the outcrop areas

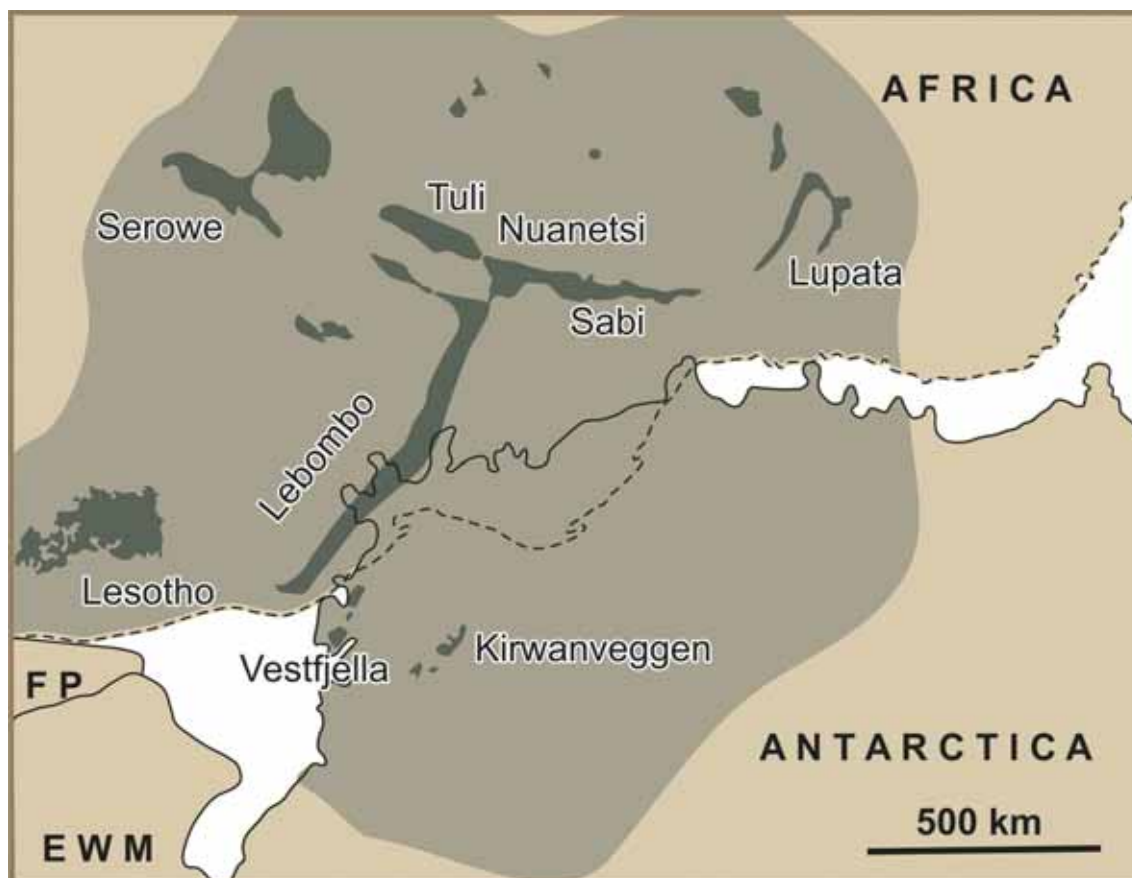


Fig. 1. Distribution of volcanic rocks and major dyke swarms (shaded area) in the African and Antarctic parts of the Karoo large igneous province (dark brown). FP – Falkland Plateau, EWM – Ellsworth Whitmore Mountains. Modified after Lavver *et al.* 1992.

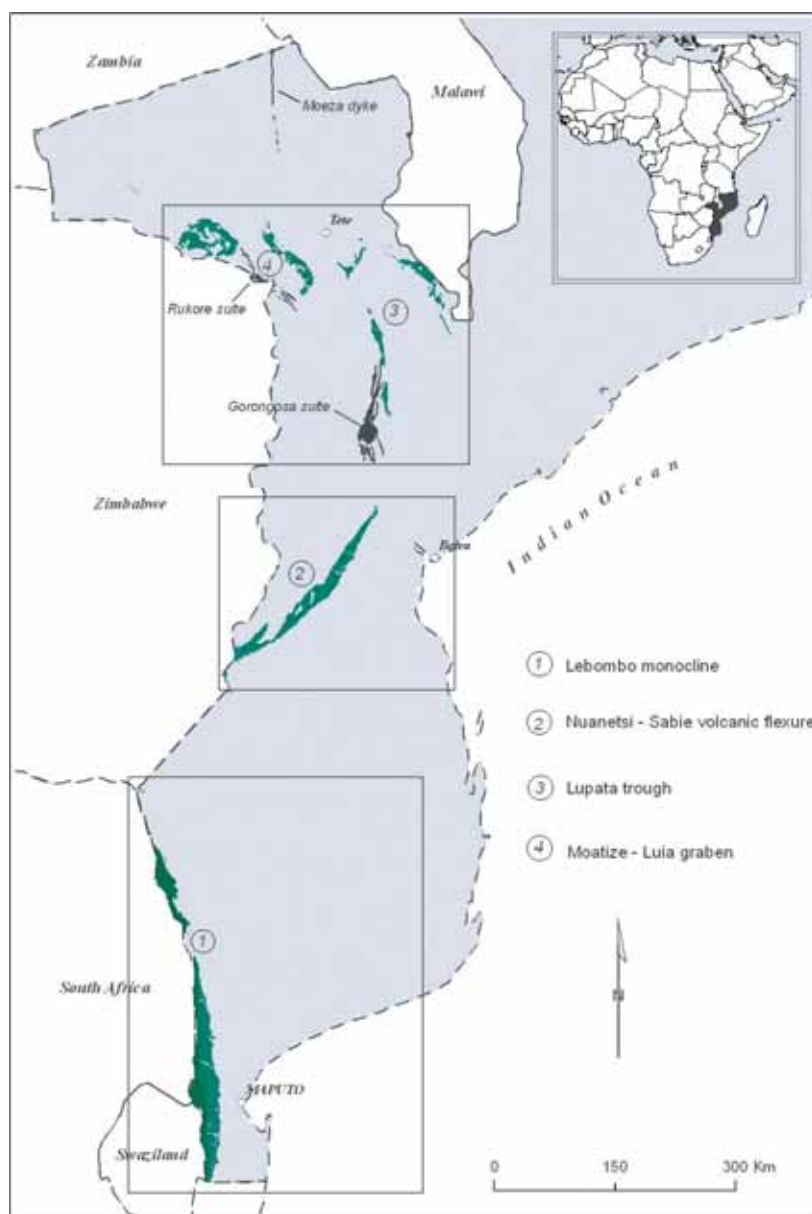


Fig. 2. Location of Karoo volcanic rocks (green) and intrusive suites (black) in southern and central Mozambique. Outlined areas refer to more detailed maps in the text from south to north: Figs 4, 15, 17, respectively.

in South Africa and Botswana in some detail and, together with paleomagnetic constraints (Hargraves *et al.* 1997), indicate coeval emplacement of lavas across the province.

Karoo-related volcanic and intrusive rocks are also found in southern and central Mozambique (Fig. 2). In southern Mozambique, mafic and felsic extrusive rocks are associated with and represent the capping stratigraphic units of the seaward-dipping volcanic succession of the Lebombo Monocline. Further to the north, Karoo-related volcanic rocks are also found within a narrow belt close to the South African and Zimbabwean border. The Nuanetsi-Sabi volcanic flexure is an extension of the Lebombo Monocline and represents one of the

rift arms of the Limpopo triple junction structure (Fig. 1). In central Mozambique, Karoo-related successions are found in the Lupata trough and the Moatize-Luia graben.

The Karoo volcanic rocks in Mozambique have been studied mostly by Portuguese geologists during colonial times (e.g., Freitas 1937, Rennie 1937, Assunção *et al.* 1962, Mendes 1965, Pinto & Godinho 1975). These were mostly regional reconnaissance investigations, concentrated on petrography, geochemistry, and economic aspects. The research was interrupted by the independence and civil war. Subsequently, Hunting Geology and Geophysics Ltd. (1984) made a reference to the Lebombo Belt, but mapping was not executed for security reasons.

Pinna *et al.* (1987) published a geological map and established a stratigraphy, and Muchangos (2000, 2006) studied the bentonite and bauxite deposits related to Lebombo felsic volcanic rocks. Recently chemistry of Karoo-age andesitic lavas has briefly been considered by Grantham *et al.* (2004, 2006) and bimodal magmatism by Melluso *et al.* (2006).

During 2002–2007, the Mineral Resource Management Capacity Building Project was implemented under the National Directorate of Geology of the Republic of Mozambique. The main task of the project, conducted by GTK Consortium (hereafter referred to as Consortium), was to re-map, upgrade and improve existing geological maps, in order to

create a comprehensive and uniform coverage of geological maps at various scales. During this work, the stratigraphy and nomenclature of the Karoo volcanic rocks were reconsidered, and the geochemical and textural features of these rocks were studied (see GTK Consortium 2006a-c).

This paper is based on the results of geological mapping of the Karoo volcanic rocks and related hypabyssal intrusions in southern and central Mozambique (GTK Consortium 2006a-c). We describe the various volcanic units and their general stratigraphic and geochemical characteristics with emphasis on the physical features of these rocks.

LEBOMBO MONOCLINE

Introduction

The Lebombo Monocline is a 600 km long and 5–30 km wide linear flexure along the boundary between South Africa and Mozambique. Its location is most likely controlled by the sudden transition from normal lithospheric upper mantle to thick Archaean lithospheric upper mantle of the Kalahari Craton or, alternatively, between normal and stretched continental crust. An E-W section over the central part of the flexure reveals flat-lying Karoo sediments resting unconformably on crystalline basement, overlain by a deeply weathered sequence of volcanic rocks dipping to the east. Farther east, the dip of the volcanic rocks increases to a maximum of 45° to 65° east, indicating that the Lebombo Monocline was actively flexing down during the emplacement of the lava flows.

In the Lebombo monocline, mafic and felsic volcanism occurred in pulses, and rhyolites forming the “Great” (Grandes) and “Little” (Pequenos) Lebombo mountains are interlayered with Movene basalts (Figs 3–4). As basalts are poorly exposed due to intense weathering and soil formation, they generally form plain savannas (Fig. 3a). The most exposed rocks are rhyolites that form *cuesta*-type geomorphology, slightly tilted to east (Fig. 3b). Hence, the regional geomorphology is characterised by alternation of *cuestas* and plane valleys.

Based on a W-E section through the Swaziland sector of the flexure, the following major lithological units can be distinguished (from W to E and from bottom to top):



Fig. 3. a) Typical geomorphology of Lebombo monocline associated basalt plain savannas in Mozambique. b) Rhyolites of the Pequenos Libombos Mountain, slightly tilted cuestas ~40 km SW of the city of Maputo.



Fig. 4. Volcanic formations of the Lebombo Monocline in southern Mozambique. The codes refer to the stratigraphic units described in the text and used in map explanations of the GTK Consortium 2006a, b and c. Basalts (JrLb, JrSba, JrM and JrUb), dacites and rhyolites (JrU) and microgranite (JrUg).

- Karoo Sediments
- Sabie River Basalt Formation
- Jozini Rhyolite Formation (in South Africa)
- Mbuluzi Rhyolite Formation (with basal Oribi beds)
- Moveene Basalt Formation (with Sica beds in upper part)
- Pessene alkaline rocks
- Cretaceous and younger cover rocks

There is evidence that the Karoo volcanic rocks continue eastwards beneath the Cretaceous and younger cover at least as far as the coast (Flores 1970, 1973, Darracott & Kleywegt 1974) and probably even farther off-shore. The thickness of the

buried lavas beneath the cover sediments has been estimated at 6 to 13 km (Eales *et al.* 1984).

Further northwards, near Pafuri, the Sabie Basalt Formation is underlain (from bottom to top) by:

- Mashikiri Nephelinite Formation
- Letaba Basalt Formation.

Small bodies, sills and dykes of granophyres, rhyolite, dolerite and basalt have invaded the above volcanic strata (e.g., Balule and Rooi Rand Dyke Swarms). All of the above lithological units found in South Africa and Mozambique are summarized in Table 1. It is important to note that in Mozambique, the petrographically distinctive rhyolitic rocks of the Jozini and Mbuluzi Formations (e.g.

Cox & Bristow 1984) are collectively designated as the Umbelúzi Formation (Table 1).

The results of $^{40}\text{Ar}/^{39}\text{Ar}$ dating of Sabie River basalts range from 181.2 ± 1.0 to 184.2 ± 1.0 Ma and are indistinguishable from those of the underlying lava sequences of the Lebombo monocline (Duncan *et al.* 1997). Rhyolite intercalations in the upper part

of the formation (Olifants River Beds) have yielded similar SHRIMP ages of 182.0 ± 2.1 and 179.9 ± 1.8 Ma (Riley *et al.* 2004) (Table 1). Rapid emplacement of the Lebombo succession is further demonstrated by SHRIMP zircon dating and $^{40}\text{Ar}/^{39}\text{Ar}$ dating of rhyolites belonging to the Jozini Formation, which yielded eruption ages of 182.1 ± 2.9 Ma (Riley *et al.*

Table 1. Lithostratigraphic subdivision of volcanic rocks of the Lebombo Monocline. Only the coloured units are present in Mozambique (Duncan *et al.* 1997, Riley *et al.* 2004). Ages (Ma) refer to the rocks in South Africa.

LEBOMBO MONOCLINE						
South Africa and Swaziland			Mozambique		Code	
Formation	Beds	(Age)	Cretaceous and younger cover			
Moveni Basalt			Pessene	Alkaline lava	JrPal	
			Moveni	Basalt	JrM	
				Rhyolite breccia	JrMb	
				Pequenos Libombos rhyolite	JrMr	
				Fine-grained rhyolite	JrMfr	
				Quartz latite	JrMq	
Mbuluzi Rhyolite			Umbelúzi		JrU	
				Microgranite	JrUg	
				Rhyolite with agglomerate layers	JrUa	
				Rhyolite		
				Tuff, locally siltstone	JrUt	
Jozini Rhyolite		(178.1±0.6) (182.1±2.9) (179.7±0.7)		Dacite and trachydacite	JrUf	
				Basalt and massive dolerite	JrUb	
Sabie River Basalt	Twin Ridge		Sabie River	Basalt	JrSba	
	(181.2±1.0)	Mkutshane			(182.0±2.1)	
	(184.2±1.0)	Olifants			(179.9±1.8)	
Letaba Basalt		(182.7±0.8)	Letaba-Pafuri Basalt		JrLb	
Mashikiri Nephelinite		(182.1±1.6)				
Karoo Sediments						
Basement (Kalahari Craton)						

2004) and 178.9 ± 0.5 Ma (Duncan *et al.* 1997), respectively. The overlying lavas that make up the Mbuluzi rhyolites and the bimodal Moveene Basalt Formation have not been reliably dated. A controversial age of 1750 ± 33 Ma was determined for eight

zircons separated from a nepheline syenite intrusion within the Moveene Basalt Formation; the zircons are probably inherited from a Late-Archean to Early Proterozoic magmatic or sedimentary sources.

Letaba-Pafúri Formation

Random outcrops of basaltic rocks occur in the Limpopo river valley near the village of Pafuri, in the westernmost part of the Gaza Province. Assigned as the Letaba-Pafuri formation they are re-

garded comparable with the Letaba Formation basalts (*JrLb*), which are exposed on South African side of the border.

Sabie River Formation

Basalts (JrSba)

Basalts of the Sabie River Formation comprise the lowermost lithological unit of the Lebombo monocline in Mozambique. Although forming a pile of basaltic lavas of several kilometres in thickness in South Africa (Cleverly & Bristow 1979), only a narrow sliver of these fine-grained, low-MgO basalts are exposed north of the Singuédzi River on the Mozambican side of the border. At this location, the Sabie River basalts occur in weathered outcrops as massive rocks, lacking amygdules or other features typical to lava flows. Most probably, these outcrops represent massive, medium- to coarse-grained flow cores, with the amygdaloidal flow top being mostly covered. Thin basalt lava flows, which may belong to the Sabie River Formation, also exist east of Ressano Garcia, where contacts between basaltic and rhyolitic lavas can be followed over several tens of metres. Zeolite-filled pipe vesicles at the base of

basaltic lava flows attest to the extrusive character of the rock.

Rhyolites

Along the South African border the Sabie River basalts have rhyolitic interbeds, which form low ridges, generally 10–20 m in width, within the poorly exposed basaltic terrain. Some of these ridges comprise pinkish brown, fine-grained, highly vesicular rhyolite lava with occasional flow-banding, clearly indicating an extrusive mode of emplacement. Other ridges with medium- to coarse-grained, massive rhyolites with spheroidal weathering and feldspar phenocrysts may represent subvolcanic dykes or sills. Together, they probably correspond to the lenticular rhyolite units described within the Sabie River basalts more southwards as Twin Ridge, Mkutshane and Olifants Beds (Cox & Bristow 1984).

Umbelúzi Formation

Introduction

A smoothly E-dipping succession of dacitic and rhyolitic rocks assigned to the Umbelúzi Formation overlie basalts of the Sabie River Formation, comprising high-grade ignimbrites, pyroclastic ash-fall deposits, and random lava interflows. Covering most of the rugged Lebombo mountains in south-western Mozambique, it forms a 425 km long and 3–23 km wide belt along the South African - Mozambican border. Northwest of the town of Massingir, the narrow belt broadens into a complicated volcanic structure, reminiscent of an “isoclinal fold”, that is

over 20 km wide and 100 km long. In Swaziland the thickness of individual flows of this well-studied rhyolite sequence, divided there into Jozini Formation (lower) and Mbuluzi Formation (upper), ranges from 80 to 350 m, some flows being traceable along strike up to 50 km (Eales *et al.* 1984). Based on the observed volcanic features Cleverly & Bristow (1979) suggested an ash-flow to ignimbritic origin for rhyolites of the Jozini Formation.

Dacites and rhyolites (JrU)

Dacitic rocks form several kilometres long, nar-

row (< 200 m wide) horizons within the rhyolite-dominated rocks of the Umbelúzi Formation, particularly in the middle part of the Lebombo monocline. Dacites differ from pinkish rhyolites by their dark grey to dark violet brown colour. Texturally they are also more massive than typical rhyolites, which of-

ten exhibit flow banding. Locally dacites comprise quartz-filled amygdules, implying lava origin for the rock. The main mineral assemblage of dacites includes plagioclase, quartz, clinopyroxene and opaque; feldspar may form phenocrysts of 1 mm in size.

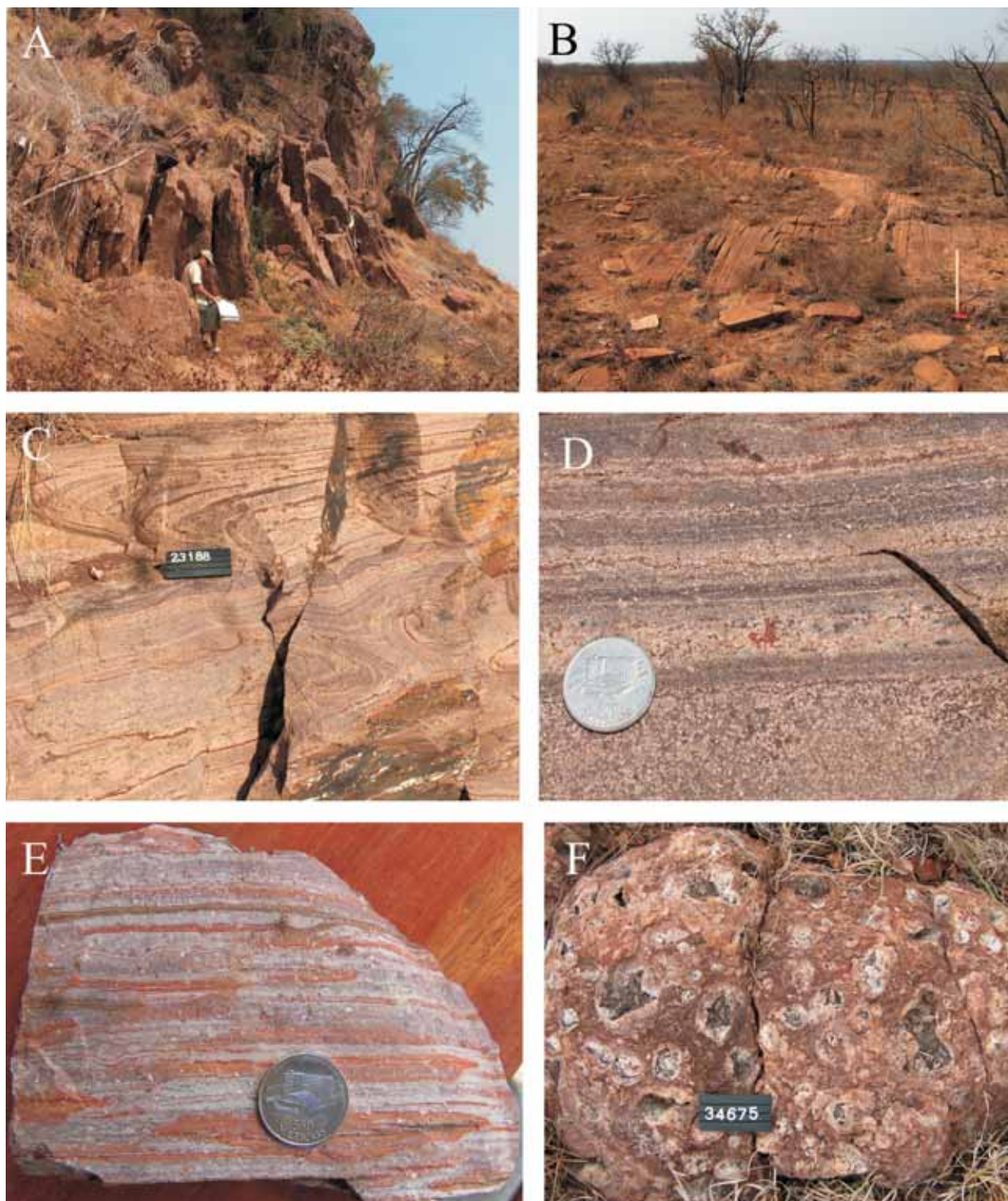


Fig. 5. a) Ramp structure with subvertical shrinkage joints in massive rhyolite flow ~25 km west of the Massingir town. b) Parallel cooling joints in rhyolite of the Umbelúzi Formation. NW of the Massingir dam (0317013/7380421). c) Folded flow bands in rhyolite. Road cut NEE of Namaacha (0412929/7128745). d) Detailed photo of the flow bands. e) Eutaxitic texture in densely welded ash-flow tuff of the Umbelúzi Formation. f) Roundish lithophysae ("thunder eggs") in a rhyolitic flow. NE of Namaacha (0408713/71415679). Hammer length 65 cm, scale bar 10 cm, coin diameter 2.5 cm.

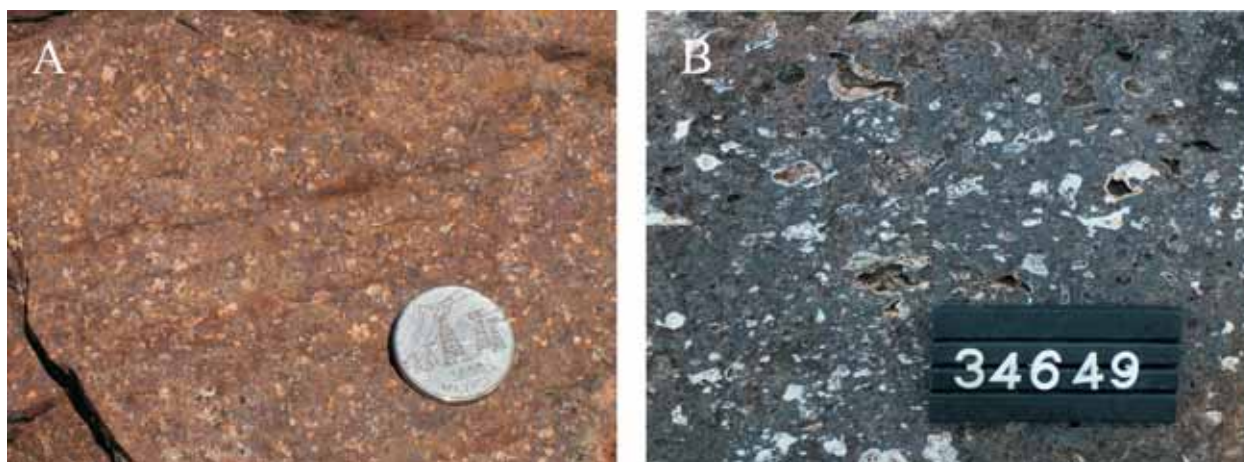


Fig. 6. a) A massive part of a rhyolite flow of the Umbelúzi Formation. Note euhedral feldspar phenocrysts and crystal aggregates. b) Highly vesicular upper part of the same flow. Road cut south of Ressano Garcia (0399017/7183886). Coin diameter 3 cm, scale bar 10 cm.

In the Lebombo Mountains, rhyolitic flows form smoothly ($\sim 10^\circ$ – 15°) east tilting terraces, with thickness of single flows probably ranging from some tens of metres up to 200–300 m. Although the rhyolitic rocks generally dip gently, patterns developed during the emplacement and cooling of single flows, including shrinking jointing and ramp structures, may occasionally show variably steep or even vertical attitudes (Fig. 5a). In exposures northwest of the Massingir dam shrinking joints often form a regular pattern of parallel discontinuities (Fig. 5b).

While contacts between successive flows are often covered, subvertical walls of flow terraces often offer excellent sites for field observations. Subhorizontal flow terraces also provide various primary features connected to flow contact zones. Well-developed laminar flow patterns, often intensively flow-folded and contorted, have been found in rhyolite flows of the Umbelúzi Formation throughout the area (Figs 5c–d). A fresh surface of welded rhyolite shows eutaxitic textures (Fig. 5e), and a microphotograph of the same sample reveals dark, vitric bands alternating with light, microcrystalline layers with abundant small (< 0.2 mm) spherulites in various stages of devitrification. Clusters of lithophysae are also commonly found within rhyolitic rocks of the Umbelúzi Formation. The most spectacular clusters are found in the eastern part of the Lebombo range, north-east of the Namaacha border post, where lithophysae form horizons and zones in the lower parts of rhyolitic flows. The size of concentric or star-shaped lithophysae varies from 1–2 cm to 10–15 cm (Fig. 5f).

The volcanic textures found within rhyolitic flows of the Umbelúzi Formation are common in welded ash-flow tuffs and high-grade ignimbrites

(e.g. Sheridan & Wong 2005). Similar textures, interpreted to represent high temperature ash-flows, have also been described in the Jozini Formation in South Africa by Bristow & Armstrong (1989). Due to the obvious thickness of single flow units, pink brown to chocolate brown, fine- to medium-grained, massive feldsparphyric rhyolite is a common variety in most flow core outcrops in the area extending from Ressano Garcia to the north of the Massingir dam. Although dense welding and rheomorphism of ignimbrites can produce similar massive and porphyric, lava-like rocks, probably proper lava flows also exist within the ash-flow deposits. In a road cut exposure east of Ressano Garcia, a gradual transition from massive, feldsparphyric rock (Fig. 6a) through a vesicular zone (Fig. 6b) into flow-top breccia may represent a top of a pristine lava flow.

Small inclusions of more mafic components are common everywhere within the rhyolites of the Umbelúzi Formation, but they are particularly common in lava-like rhyolite flows in the wide rhyolite belt north of the Massingir dam. These enclaves generally occur as dark brown, roundish spots or elongated fragments within the flow, but also larger, sheet-like fragments are occasionally observed. On weathered surfaces these globule-like spots, generally ~ 1 – 3 cm in size, have been weathered out forming small pits, thus denoting their divergent, less weathering-resistant composition. These features, suggesting coeval eruption, mingling and mixing of compositionally contrasting magmas (see e.g. Yoder 1973, Sparks *et al.* 1977), can be expected within an extensional tectonic regime like the Lebombo monocline, where bimodal basalt-rhyolite magmatism dominates.

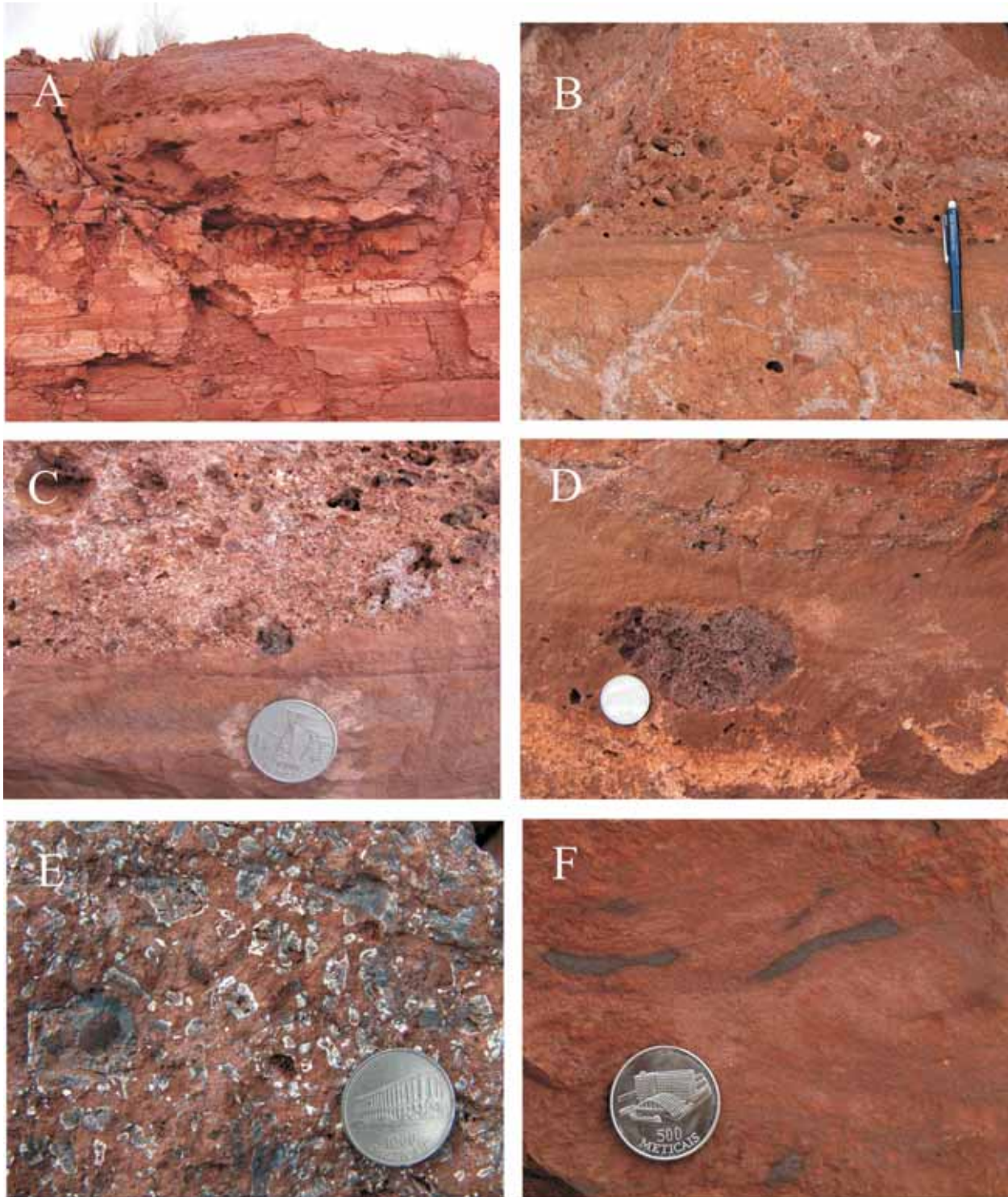


Fig. 7. Ash-fall deposits in rhyolites of the Umbelúzi Formation. a) Tabular bedding of rhyolitic ash-fall tuff. b) A layer of lapilli tuff with pumice fragments on top of a fine-grained tuff with graded bedding. c) Detailed photo of the contact between ash-fall tuff and overlying lapilli tuff layers. d) A pumice fragment embedded in fine-grained tuff. Note shard layers in the upper part of the photo. e) Detailed photo of sharp-edged, partly devitrified fragments of volcanic glass (shards). Rock aggregate quarry north of Mt Ligadjanga (0414117/7107659). f) Collapsed pumice fragments (fiamme) in a fine-grained tuff matrix. Road cut on the EN4 highway (0409944/7169003). Coin diameter 2.8 cm, length of the pen 15 cm.

Basalts (JrUb)

Coeval extrusion of mafic and felsic magmas within the Umbelúzi formation is further manifested by the presence of mafic rocks intercalated with the rhyolites. These are most abundant in regions north-

west of Massingir, where they comprise relative narrow (< 200 m), but up to 30–40 kilometres long, elongated units of basaltic flows and subvolcanic sills and dykes. The basaltic interbeds are generally poorly exposed. They are distinguished by their subdued topography and low intensity anomalies

on radiometric maps. These fine- to coarse-grained rocks are often rather massive but show typical volcanic textures.

In the northern part of the Lebombo monocline, there are some wide (> 10 m) zones of breccias, which can be lithologically divided into flow-top breccias, solely composed of rhyolitic fragments, and volcanic breccias, where fragment materials comprise lithologically different volcanic rocks. These breccias are parallel to the main structural N-S trend of the monocline.

A breccia zone composed of fragments derived from angular to subrounded felsic and mafic (-intermediate) volcanic rock occurs about eight kilometres south of the Gaza Camp border post. Here, the breccia zone is located at the contact between a voluminous rhyolitic flow and relatively narrow (~50 m), but several kilometres long layer of ba-

saltic andesite. Internal texture of the fragments, generally 5–75 cm in size, is heterogeneous; e.g. rhyolitic fragments are flow-banded, while mafic ones contain phenocrysts. The violet brown, fine-grained matrix of the breccia is also intermediate in composition.

On the eastern side of the Lebombo Mountain range is a long horizon, tens of kilometres, of rhyolitic rocks with tabular bedding, interpreted to represent ash-fall deposits (Figs 7a-f). In an old quarry, located about 6 km north-west of the Goba village, the tile-red rhyolite comprises alternating layers or beds of unwelded pyroclastic material, ranging from fine-grained ash to lapilli. Well-preserved pumice fragments, embedded in places into fine-grained tuff beds (Fig. 7d), and layers of only partially devitrified shards (Fig. 7f) suggest an ash-fall tuff origin for the rock.

Movene Formation

Introduction

The Movene (Basalt) Formation represents the uppermost lithological unit of the Lebombo Monocline (e.g. Eales *et al.* 1984) and extends over 400 km from the Maputo River at the South African border onto the Singuédzí River, north of the town of Massingir (Table 1). Dominating the fertile lowlands between the rhyolitic Lebombo mountain range in the west and sedimentary formations in the east, the Movene Formation mostly comprises a succession of basaltic lava flows, but also includes intercalated rhyolite flows of the Pequenos Libombos Member in the upper part of the basaltic lava pile.

Basalts (JrM)

Compared with the felsic volcanic rocks, basaltic lavas of the Movene Formation are poorly exposed, outcrops being mostly located on river banks. Rare outcrops found in topographically higher places, are generally covered and thus protected by more resistant rhyolitic flows (see Fig. 9).

The field exposures of basalts typically exhibit characteristic features of inflated ropy lava (pahoe-hoe lava) flows: a massive flow core and highly amygdaloidal lower and upper zone (Fig. 8a). These mafic volcanic rocks are mainly aphyric, although plagioclase porphyritic types are also commonly

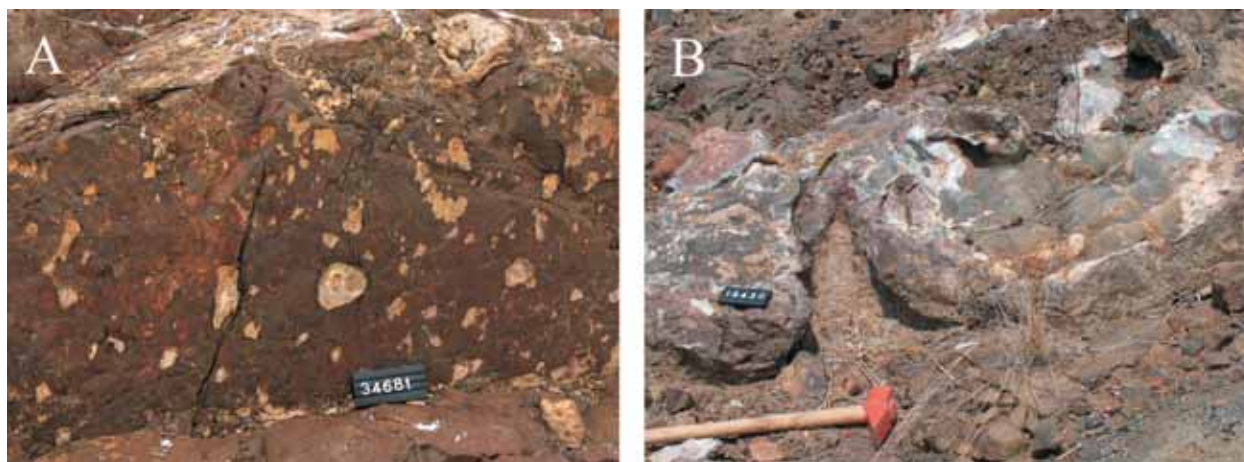


Fig. 8. Amygdaloidal textures in basaltic lavas of the Movene Formation. a) Large, quartz-filled amygdules in the upper zone of basalt flow near the Pequenos Libombos dam (042210/7113705). b) Quartz crystal coated megavesicle in the upper part of the lava flow (0424177/7113835). NW of Mt Portela (0418871/7120492). Scale bar 10 cm.

observed. The thickness of individual flow units varies from <1 m up to ~10 m. The highly amygdaloidal lower part is glassy, thickness commonly < 0.5 m, and may contain pipe amygdules, which are commonly inclined towards the lava flow direction. Both easterly and westerly flow directions are observed, which may reflect local topography of the lava flow field rather than distinctive eruptive centres. The massive flow core of relatively thick (>>1 m) inflated ropy lava units completely lacks amygdules or contains only few of them and often shows spheroidal weathering. The core of the lava flow may contain sub-vertical amygdule cylinders and, just below the upper crust, sub-horizontal amygdule sheets. In the upper part of basaltic flows there are large amounts of roundish amygdules that are commonly 1–10 cm in diameter. In some thick flows, a horizon of megavesicles with diameters of up to one metre has been found (Fig. 8b). The amygdules and the megavesicles are filled mainly with agate, quartz, carbonates, and zeolite. Agate layers in partially filled amygdules provide a useful tool for establishing the postmagmatic tilting of the lava flows. Observations, although sparse, show 6°–8° dipping towards ESE. Some of the ropy lava flow units also have a distinctive flow top breccia.

Rhyolites (JrMr)

A prominent rhyolite ridge of the Pequenos Libombos (Little Lebombo) Mountains in southern Mozambique comprises a succession of variously welded ash-flow tuffs in the upper part of the Movene Formation, north and east of the Pequenos Libombos dam. The north-trending rhyolite interlayer



Fig. 9. Contact between a yellowish brown rhyolite flow of the Pequenos Libombos Member (on top) and maroon basaltic lava of the Movene Formation. A quarry on the western side of the Pequenos Libombos Mountain (0421955/ 7119193). Hammer length 65 cm.

can be followed for over 65 km along strike, its maximum width being about 5 km. The maximum thickness of this succession, known formerly as Sica beds (Cleverly *et al.* 1984), ranges from some tens of metres in the area of Mt Portela to ~100–150 m east of Mt Sica and Mt Pequenos Libombos proper. The unit, which stands out as a resistant cap within the Movene basalt terrain, is cut by several NW-SE trending faults and fractures, while a NW-SE trending sinistral strike-slip fault has divided the ridge into two major parts.

Evidence for a pyroclastic emplacement of Pequenos Libombos rhyolite is provided by its gradual transition from a weakly welded basal tuff breccia and a lithophysal zone upwards into an increasingly flow-banded and flow-folded rheomorphic lava-like rock.

The lower contact of the rhyolite unit is exposed at a road cut on top of the Pequenos Libombos ridge, where a maroon coloured zone in the upper part of the underlying basalt flow may represent a hydrothermally altered palaeo-laterite horizon (Fig. 9). The same maroon contact zone is exposed in an old quarry north of the Sica ridge, where large amount of greenish agate amygdules up to 5 cm in diameter are preserved in the oxidised top layer of the basalt flow.

The weathering and alteration of rocks in the contact zone hamper the study of volcanic structures at the base of the rhyolitic flow. Horizons of poorly welded ash-flow tuffs or ash-fall deposits exist in the basal zone of the (lowermost) flow. Elsewhere, the flow base is characterised by chaotic tuff breccias with plastically deformed lithic chips or fragments (Fig. 10a) or by lithophysa clusters, with the size of roundish lithophysae ranging from small spherulitic ones to lithophysae, 10–15 cm in diameter. In some large lithophysae, onion-like weathering is well developed (Fig. 10b).

Densely welded varieties of rhyolitic ash-flow tuffs, consolidated by vapour-phase crystallisation, constitute the major rock type of the Pequenos Libombos Member of the Movene Formation, exposed in most aggregate quarries of the area. Dark brownish red, fine-grained rock is often distinctly flow-banded, with flow folding locally distorting the gentle regional tilting angle of flows (Figs 11a-b). Flow-banded rock comprises dark greenish and light to reddish brown, <1 to 2 mm thick laminas with abundant small (< 0.5 mm) spherules and quartz and feldspar phenocrysts, probably as a result of vapour phase crystallisation (Fig. 11c). Only in zones where the intensity of rheomorphic flow has not been comprehensive, flame-like fiamme and round to lenticular vesicles can still be discerned.

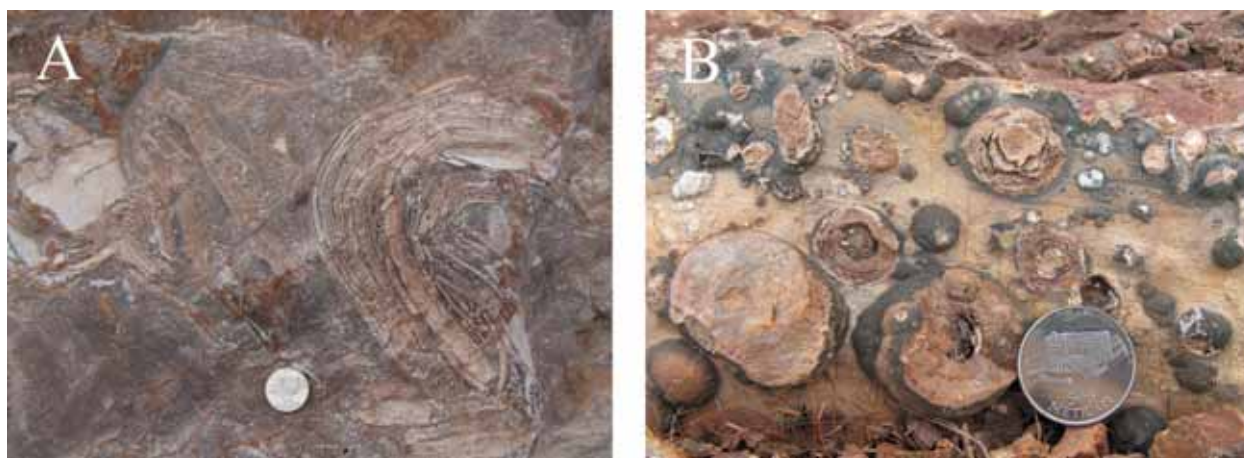


Fig. 10. a) Detailed photo of plastically deformed (ash-flow) tuff fragments in a non-welded zone. A quarry on the western side of the Pequenos Libombos Mountain (0421955/7119193). b) Detailed photo of roundish structure of lithophysae. Old quarry NE of the Portela ridge (0422725/7118163). Coin diameter 3 cm.

On top of the mountain, southeast of the Mt Mu-guene, there occur two circular-shaped structures, 6–7 m in diameter, which may represent eruption vents for rhyolite flows surrounding these structures. Steeply outwards dipping flows exhibit distinct flow banding and have numerous distorted pumice fragments and gas cavities.

Rhyolite breccia (JrMbr)

A horizon of sub-aerial pyroclastic breccia (tuff breccia), probably tens of metres in thickness, is exposed along the western slope of a separate hill on the eastern side of the Pequenos Libombos ridge proper. Its position as an immediate northern exten-

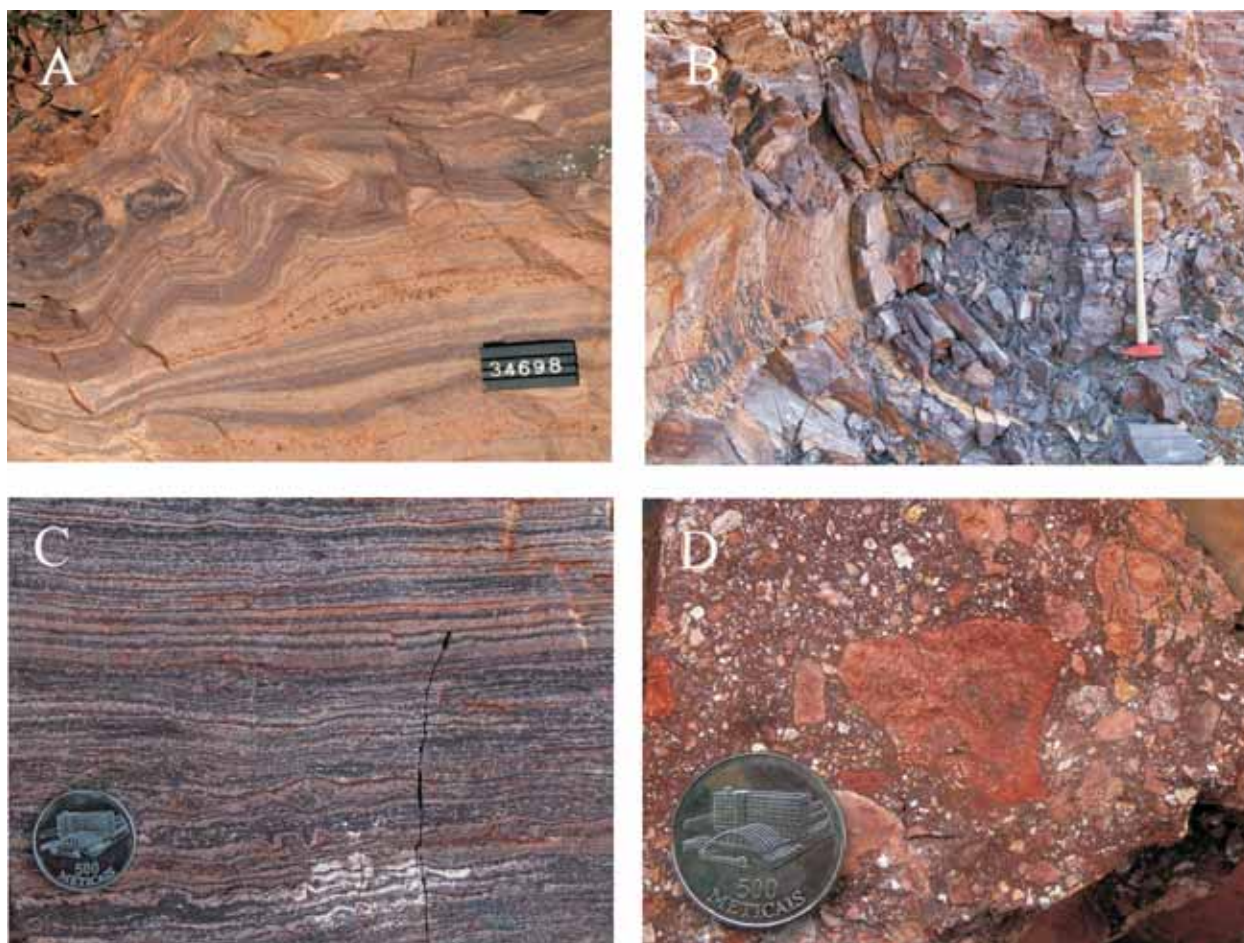


Fig. 11. a) Magmatic folding in flow-banded rhyolite in an aggregate quarry north of the bentonite plant (0423900/7119729). b) Large, subhorizontal flow fold in rhyolite of the same quarry. c) Detailed photo of flow-banded rhyolite with rolled rhyolite clasts. Old quarry north of the Pequenos Libombos dam (0423468/7114906). d) Pyroclastic breccia, comprising supracrustal fragments in a tuff matrix. A hill east of the Pequenos Libombos Mountain (0425129/ 7117510). Hammer length 65 cm, scale bar 10 cm, coin diameter 2.5 cm.



Fig. 12. Banded felsic volcanite with mafic enclaves. Aggregate quarry (0428363/ 71223752). Marker pen length 14 cm.

sion of the southern rhyolite ridge suggests that this unit represents an air-fall tuff breccia or unwelded ash-flow deposit amongst the densely welded ash-flow sheets of the area.

The pyroclastic breccia is composed of lithic (juvenile to accidental) fragments, up to 10 cm in size, in a fine-grained tuff matrix (Fig. 11d). These matrix-supported clasts mostly comprise weathered fragments of basalt, broken lapilli and bombs of vesicular pumice, and light brown chips and fragments of aphanitic rhyolite. Occasional lithic fragments were probably derived from the pre-volcanic Karoo sedimentary strata, not exposed in this area.

Banded felsic volcanite (JmRq)

A light grey or greenish grey variety of felsic volcanic rocks, also assigned to the Pequenos Libombos Member, is exposed in an old aggregate quarry 6 km north-west of the Boane town. Obscure flow banding and rare fiamme suggest ash-flow origin for the aphanitic rock with abundant dark brown, mafic enclaves, generally < 10 cm in size (Fig. 12). Light brownish bands or portions, possibly due to hydrothermal bleaching and alteration of the rock, are also common. Thin, sub-vertical basaltic dykes intrude the rock unit in the quarry.

Pessene alkaline lava (JrPla)

One of the easternmost observed exposures of mafic volcanic rocks in southern Mozambique is massive, aphyric, aphanitic and contains few amygdules. The exposure is located on the top of a small hill and has a minimum diameter of several hundreds of metres. In previous maps this rock has been classified as a basaltic dyke, but it more likely represents a sub-horizontal sill or a lava unit.

As no geochronological data are available and the isolated outcrop is located between areas of basalt lavas and Cretaceous sedimentary rocks, it is currently uncertain whether this rock type belongs to the Movene Formation. Based on geochemical data, the phonotephrite may be comagmatic with the Pessene nepheline syenite intrusion nearby.

Intrusive rocks

Nepheline syenite (JrPns)

A nepheline syenite body is exposed ~8 km SW of the village of Pessene, in the contact zone be-

tween Movene basalts and Quaternary sediments. The shape of the subvolcanic intrusion is elongated. In addition to the large outcrop situated in the aggregate quarry near the highway EN4, there are also

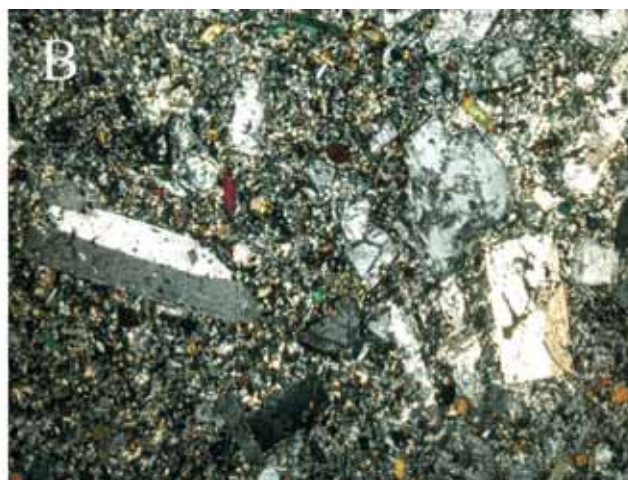


Fig. 13. a) Porphyritic texture of the Pessene nepheline syenite. b) Photomicrograph of nepheline syenite, with euhedral phenocrysts in a microcrystalline ground mass. X-nicols. The Pessene quarry (0431268/7150433). Coin diameter 2.5 cm, photo width 3.5 cm.

some related rocks outcropping 8 km to the south.

Pessane nepheline syenite is a light greenish grey, massive and distinctly porphyritic rock with potassium feldspar, nepheline, aegirine augite and augite as phenocrysts in a microcrystalline to aphanitic ground mass (Figs 13a, b). It also contains some analcite and amphibole. The rock is cut by a dense network of small fractures and joints.

Microgranite

A few elongated microgranite bodies intrude mafic and felsic volcanic rocks within the Limpopo National Park in the northern part of the Lebombo monocline. Microgranites are pinkish grey, massive, locally strongly fractured and spheroidally weathered rocks, which have intrusive contacts against the surrounding basaltic lavas.

The grain size of microgranites ranges from small to medium (0.1–0.5 mm), and granophyric intergrowths between feldspar and quartz grains are common. In addition to quartz and plagioclase, microgranites comprise potassium feldspar, and clinopyroxene phenocrysts, up to 1 mm in size, have also been observed. Obviously, these microgranite intrusions represent the coeval magmatic phase with the Tshokwane granophyre, located nearby in the South African side of the border¹.

¹ see 1:250 000 scale geological map “2230 Tzaneen”, published by the Geological Survey of South Africa.

Mafic dykes and sills

Mafic dykes and sills intrude felsic volcanic rocks of the Lebombo sequence, although observations of them are rare. In the north, within the Limpopo National Park, a very fine-grained, vertical mafic dyke impressively cuts the dacite of the Umbelúzi Formation. The weakly zoned dyke has chilled fine-grained margins and the rock comprises small chemical variations parallel to the contacts. The dyke is composed of plagioclase, clinopyroxene and opaques and has a nesophitic texture.

A 5-m-thick basaltic dyke intrudes the Umbéluzi Formation in an old quarry south of the Sabie dam (Fig. 14a). A basaltic sill, more than 20 m thick, intrudes rhyolites of the Pequenos Libombos Member in the western side of the mountain. Exposed in an active aggregate rock quarry, this sill exhibits a prominent columnar jointing, polygonal columns mostly being pentagonal or hexagonal in cross-section (Fig. 14b). An intrusive contact of the sill against the flow-banded rhyolitic host rock is also exposed in the quarry. Columnar jointing is also found in a dolerite sill, situated 20 km north of the Catuane village in southern Mozambique, where the sill forms a small hill in a low-lying landscape of the Moveene basalts.

A prominent, NNE-trending, >100-m-thick mafic dyke cuts a thick, basaltic lava flow of the Moveene Formation near the Pequenos Libombos dam. The brownish, medium-grained dyke has numerous randomly oriented, chalcedony filled fractures.



Fig. 14. a) Basaltic dyke intruding the Umbeluzi rhyolite. Old quarry south of the Corumana Dam (0412434/7209032) and b) Columnar jointing in a basaltic sill. Quarry on the west side of the Pequenos Libombos Mountain. (0424318/7145314). Length of hammer 65 cm.

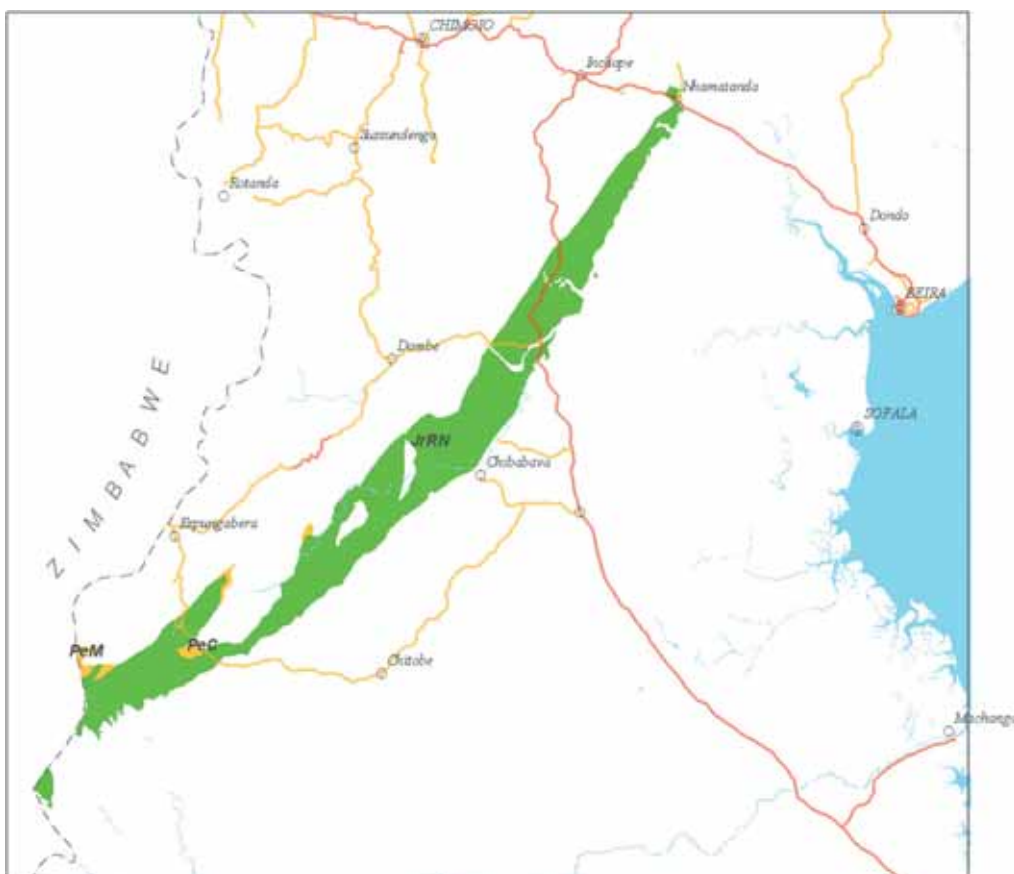


Fig. 15. Location of Karoo-related volcanic (green; JrRN) and sedimentary (light brown; PeC and PeM) formations of the Nuanetsi-Sabi volcanic flexure area. The codes refer to the stratigraphic units described in the text and used in map explanations of GTK Consortium 2006a, b and c.

NUANETSI-SABI VOLCANIC FLEXURE

The Nuanetsi-Sabi volcanic flexure is a zone of basaltic lavas with few rhyolitic beds, extending from the area south of Espungabera up to the Nhamatanda region on the Beira map sheet. These basalts have been incorporated into the Rio Nhavú-

dezi Formation (JrRN) and are also found in the Lupata trough area, north-east of Serra Gorongosa. Geophysical data imply that the SE margin of this flexure is locally heavily fractured.

Rio Nhavúdezi Formation

A homogeneous pile of basaltic lava flows assigned to the Rio Nhavúdezi formation forms a continuous, 15–25 km wide belt, which extends from the Zimbabwean border over 250 km north-east towards the Nhamatanda village by the Beira–Manica highway (Fig. 15). Near the border, basaltic lavas overlie coal-bearing sediments and conglomerates of the Lower Karoo Moatize (*PeM*) and Upper Karoo Cádzi (*PeC*) formations, while the contact against the metalavas of the Mesoproterozoic Umkondo Group is tectonic. In the east these basalts are mostly overlain by unconsolidated sediments of the Cretaceous Sena Formation. The dark green or

greenish brown, fine-grained lavas are frequently exposed along Rio Merenguese and its tributaries, but the most prominent outcrops are in Rio Búzi, where basaltic flows form spectacular rapids and cataracts (Fig. 16a). On the aeromagnetic map, the basalts of the Rio Nhavúdezi formation are characterized by a high magnetic and low radiometric signature. Macroscopically, dark greyish or brownish green, fine-grained basalts are generally aphyric, but also porphyritic varieties with plagioclase phenocrysts have randomly been found. Rare medium-grained varieties within the basalt probably represent massive cores of flows – they could also be dykes or sills.



Fig. 16. Lava features of the Rio Nhavúdezi Formation. a) Rapids in the Búzi River, formed by basaltic lava flows. b) Quartz-filled megavesicles in the upper part of a lava flow. c) Quartz-filled vesicle cylinder in a basaltic flow. S of Mt Sitatonga (0523719/7743119). d) Zeolite-filled amygdules in the upper part of basaltic lava flow. Rio Merenguese (0470676/7702175). Scale bar 15 cm.

No pyroclastic or sedimentary interbeds have been found within the basaltic succession. Zoned amygdules with chalcedony and zeolite are common in the upper part of subhorizontal to steeply (up to 50°) east dipping lava flows, and irregular megavesicles up to 30–40 cm in size exist in the basalts of Rio Mebahata. There is also a well-developed columnar jointing in some basaltic flows.

Mineralogically, basalts of the Rio Nhavúdezi formation are tholeiites with andesine and pigeonite, but without olivine and olivine tholeiites. In addition to medium-grained sub-ophitic types, also plagioclase porphyritic types are found in places. In the porphyritic types, randomly oriented plagioclase laths are typically 1–6 mm long. These varieties most likely represent the central part of flows, while amygdaloidal types dominate the upper part.

Medium-grained types are most common adjacent to the north-western boundary of this SW-NE trending basaltic sequence, whereas amygdaloidal types are more common towards the south-eastern boundary of the formation. The available tectonic measurements of lava flows together with geophysical interpretation indicate that the volcanic sequence is dipping smoothly towards the E or SE.

Based on observed lava flow boundaries and different lava structures e.g., including zeolite-filled amygdules, flow-top mega-vesicles (Fig. 16b), and sub-vertical vesicle cylinders (Fig. 16c), the estimated average thickness of flows is 1–2 metres. The highly vesicular texture (Fig. 16d) and obvious absence of pillows and/or marine or lacustrine interflow sediments, indicate sub-aerial eruption of basaltic magma.

LUPATA TROUGH AREA

An arch-like, discontinuous belt of the Upper Karoo volcanic and sedimentary rocks surrounds the northern end of the Lupata trough in central Mozambique (Fig. 17). There immature arkosic sandstones, limestones, and carbonated sandstones of the Cádzi Formation (*PeC*) are overlain by basalts of the Rio Nhavúdezi Formation or the Chueza Formation (*JrC*), rhyolitic rocks of the Serra Bombuê Formation (*JrSb*) forming a felsic interbed within the mostly basaltic succession. The overlying Cretaceous Lupata Group is composed of coarse clastic sediments and an alkaline volcanic suite, mostly comprising phonolites and trachytes.

The emplacement ages of the Mesozoic lavas and their intrusive correlatives in the Nuanetsi-Sabie volcanic flexure, the Lupata trough, and the Moatize-Luia graben (Fig. 2) have not been accurately dated. New geochronological results of the Consortium mapping programme provide constraints to the age relationships of these rocks. For example, the intrusions of the Gorongosa Suite have been previously related to Cretaceous alkaline ring complexes (Afonso 1978), but TIMS U-Pb zircon dating of a syenite belonging to the Gorongosa Suite

gave a concordant Lower Jurassic age of 181 ± 2 Ma, suggesting emplacement of the syenite during the main stage of Karoo magmatism.

The bimodal Rukore Suite represents another major intrusive assemblage in central Mozambique. The Rukore Suite has been previously regarded to correlate with the Chilwa Alkaline Province in southern Malawi (Cahen *et al.* 1984) and represents post-Karoo age magmatism at ~ 230 – 110 Ma (Barton *et al.* 1991). Three zircon fractions from a microgranite belonging to the Rukore Suite were recently dated by the Consortium using conventional U-Pb geochronology and suggest an age of ~ 195 – 180 Ma for the granite (Mänttärä this volume).

The volcanic rocks of central Mozambique have not been dated by isotopic methods before. Traditionally, the basalts and rhyolites of the Chueza Formation, Rio Mázoè Formation, and Bangomatete Formation have been associated with the widespread Karoo magmatism at ~ 180 Ma. Further to the north, the Moeza dyke represents another likely correlate of the Karoo lavas. A sample from the Moeza dyke for dating yielded a Sm-Nd isochron mineral-whole-rock age of 180 ± 43 Ma.

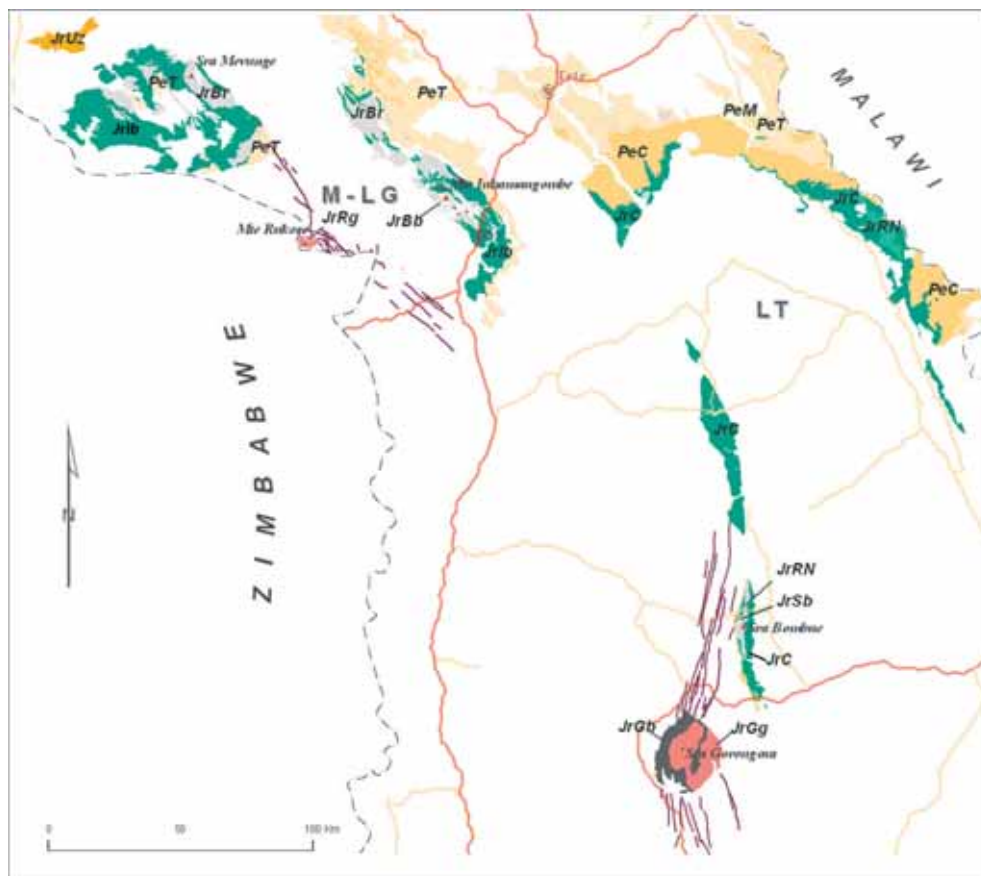


Fig. 17. Location of Karoo-related intrusive (black/red; *JrGg*, *JrGb*, *JrRg*), mafic (green; *JrIa*, *JrIb*, *JrRN*, *JrSb*, *JrC*), felsic (grey/orange, *JrBr*, *JrBb*, *JrUz*) volcanic and sedimentary (light brown; *PeM*, *PeC*, *PeT*) formations of the Karoo Supergroup in the Lupata trough (LT) and Moatize-Luia graben (M-LG) area. The codes refer to the stratigraphic units described in the text and used in map explanations of GTK Consortium 2006a, b and c.

Rio Nhavúdezi Formation

A succession of amygdaloidal basalts, which form the Nuanetzi-Sabi volcanic flexure and are assigned there to the Rio Nhavúdezi Formation, is also randomly found around the Lupata trough. The lower contact of the Formation is exposed in the tributary of Rio Mebahata, where flow-brecciated basaltic lava overlies a conglomerate of the Gádzi Formation. The upper contact with the Serra Bombuè Formation is gradual – thin rhyolitic interbeds are found between basaltic flows in the upper part of the Rio Nhavúdezi Formation in the Mebahata River (Fig. 18).

These dark greyish or brownish green, fine-grained basalts are generally aphyric, but also porphyritic varieties with plagioclase phenocrysts have randomly been found. Rare medium-grained varieties within the basalt probably represent massive cores of flows, but could also be dykes or sills. No pyroclastic or sedimentary interbeds have been found within basaltic succession. Zoned amygdules with chalcedony and zeolite filling are common in



Fig. 18. Brownish red, rhyolitic interflows of the Serra Bombuè Formation in the upper part of the Rio Nhavúdezi Formation in Rio Mebahata (0636470/8016042). Hammer length 65 cm.

the upper parts of subhorizontal to steeply (up to 50°) east dipping lava flows, and irregular megavesicles up to 30–40 cm in size exist in basalts of Rio Mebahata. A well-developed columnar jointing is also present in some basaltic flows.

Serra Bombuè Formation

Rhyolitic rocks of the Serra Bombuè Formation form a north-trending ridge on the western side of the Lupata trough, northeast of the Gorongosa Mountain. Less than 4 km in width, but over 30 km long, a rhyolite formation, tilting gently (12°–20°) to the east, was emplaced between basaltic lavas of the Rio Nhavúdezi and the Chueza Formations, clearly differing from surrounding lithologies with its high positive aeromagnetic and radiometric anomalies.

A well-exposed traverse along Rio Mebahata re-

veals the gradual contact with underlying basalts of the Rio Nhavúdezi Formation, thin felsic lava flows alternating with basaltic flows in the upper part of the Rio Nhavúdezi succession. In a hand specimen, the rhyolite is chocolate-brown and fine-grained, exhibiting locally a well-developed flow banding. A low breccia with spherulitic texture in sharp-edged fragments occurs in the basal part of the rhyolite succession, but otherwise the rock is rather massive, indicating rather thick cooling units.



Fig. 19. a) Pipe amygdules at the base of a basaltic flow. b) A vertical cross section of lava lobes in a thin, basaltic lava flow. The Pompue River gorge in the Búzue village (0624901/8092174). Scale bar 15 cm.

Chueza Formation

Basaltic flows of the Chueza formation constitute an uninterrupted exposure between the Sinjal and Chueza settlements on the north-eastern side of the Lupata trough. Here, the upper basalts of the Chueza formation are in direct contact with the lower basalts of the Rio Mázoè formation. Similar basalts are also exposed along the Mt Linhanganga escarpment, and at Mt Cuadezo where grey, fine- to medium-grained basalts, some with amygdaloidal structures, form small, scattered hills. Sometimes basalt flows form small *kopjes* in direct contact with the sandstones, or their presence is indicated by basalt boulders. In places, the dark grey-green rocks are porphyritic with plagioclase phenocrysts. Vertical NE-trending basalt feeders are exposed in the Chueza area.

In the western side of the Lupata trough, an excellent section of Chueza basalts can be found at the Búzua village, where a pile of subhorizontal compound lava flows is fully exposed in a Pompue

River gorge. There the thickness of single flows varies from 1–2 m into massive, over 5 m thick flow with a regular cooling joint pattern. The upper parts of the flows often have many small, roundish amygdules. Elongated and bent calcite and zeolite-filled pipe amygdules, of up to 15 cm in length at the flow bases, demonstrate the north-western direction of the flows (Fig. 19a).

Locally, well-exposed cross sections of thin pahoe-hoe flow lobes are found within the basaltic lava succession (Fig. 19b), and a small, collapsed lava tunnel, about one metre in diameter, was also found in a river gorge.

A tectonic contact between Chueza basalts and Mesoproterozoic gneisses is exposed in the southern bank of the Pompue River, about 5 km west of the Búzua village. There the steeply (60°) east dipping contact is rather sharp and mylonitized.

MOATIZE-LUIA GRABEN AREA

A thick succession of sediments and volcanic rocks, assigned to the Karoo Supergroup is found in the fault-controlled Moatize-Luia graben in Tete Province, western Mozambique. Divided into the Lower and Upper Karoo Groups, the former comprises only sedimentary successions, the latter a number of sedimentary formations together with interstratified mafic and felsic Karoo volcanic rocks of Early Triassic to Early Jurassic age.

Deposited into palaeo-depressions of the pre-Karoo basement, the Lower Karoo Group comprises coal-bearing Vúzi (*CbV*) and Moatize (*JrM*) formations, covered by coarse-clastic sediments of the Matinde Formation (*PeT*) (see GTK Consortium 2006d).

At the base of the Upper Karoo Group, immature

deposits of the Gádzi Formation (*PeC*) conformably overlie the clastic sediments of the Matinde Formation and are overlain by basalts of the Chueza (*JrC*) and Rio Nhavúdezi (*JrRN*) Formations in the northern end of the Lupata trough. In the west, the sediments of the Matinde Formation are overlain by the basalts of the Rio Mázoè Formation (*JrIa*, *JrIb*) and felsic volcanic rocks of the Bangomatete Formation (*JrBr*, *JrBb*).

The epoch is concluded with the emplacement of the bimodal Rukore Suite, dated at 190–180 Ma (Mänttari, this volume). The latter is coeval with and possibly related to the Gorongosa Suite and the volcanic rocks of Nuanetsi-Sabi and Lebombo monoclines further to the south.

Rio Mázoè Formation

Although rather restricted in extent, the Rio Mázoè Formation is well developed on the Chioco and Tete map sheets, where basaltic and andesitic lavas of the formation overlie sandstones of the Matinde Formation and are overlain by rhyolites of the Bangomatete Formation. The most extensive outcrop areas of the unit exist to the west of Rio Mázoè bridge and in central parts of the Serra Mevunge dome structure. Due to different intensity of weathering, the colour of basaltic lavas varies from dark greyish green to chocolate brown or dark reddish

brown, often hampering identification of the actual rock composition. Consequently, radiometric data were generally used to separate basalts from more felsic varieties of the volcanic sequence, basalts exhibiting poor K/Th signature on airborne radiometric maps.

On the riverbanks to the west of the Rio Mázoè bridge, fine-grained basalts form a pile of gently (12°–20°) SWW-dipping lava flows. The estimated thickness of flows, based on vesicle-rich flow contacts, varies from 2–3 m up to 10–15 m in the lower

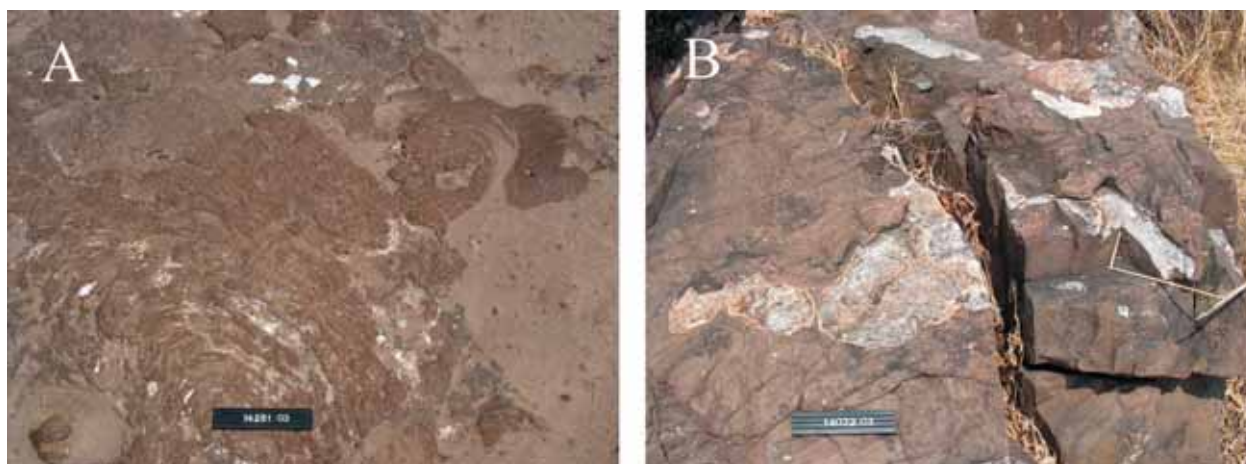


Fig. 20. a) Ropy lava (pahoehoe) structure in basaltic lava flow. Rio Mázoè Formation. West of the Rio Mázoè bridge (0539576/ 8170743). b) Large, zeolite-filled vugs (gas cavities) in the upper zone of basaltic lava flow of the Rio Mázoè Formation. Serra Mevunge dome (0420090/ 8227068). Scale bar 15 cm.

part of the formation. Many features distinctive to flood basalts have also been found: basal pipe-vesicle zones, vertical vesicle cylinders and columnar jointing in the flow cores, and ropy lava structures on the surfaces of flows (Fig. 20a). In the highly vesicular flow tops, calcite and zeolite-filled vesicles and vugs, up to 20–30 cm in size, have often bright, blue-green chrysocolla linings. As no intervening layers of sedimentary or pyroclastic material between lava flows has been observed, the intensity and rate of eruption has probably been rather high, a feature also typical for continental flood basalt provinces.

In the Serra Mevunge dome area, basaltic and andesitic lava flows, identical to those described from the Rio Mázoè area, are exposed between coarse-clastic Lower Karoo sandstones and rhyolite flows of the Bangomatete Formation. Ropy lava structures and pipe vesicles are common, the size of zeolite and calcite-filled vugs in the uppermost flow-top zone locally exceeding 30–40 cm (Fig. 20b). Compared to the Rio Mázoè area, the thickness of these flows is generally lesser. Based on the occurrence of pipe vesicles in the basal zones of flows, several

individual flows of less than one metre in thickness have been observed.

Dark green, in places very fractured and, when weathered, chocolate-brown basaltic lavas are exposed in an area 3 km east of the Changara village, forming a mountainous region extending over 10 km by 10 km. Amygdaloidal and porphyritic textures, with altered plagioclase phenocrysts, are also observed. In some areas concentrations of quartz geodes are found in the upper parts of basaltic flows. White agate pebbles are common in the area, and they are probably derived from agate-filled vesicles.

In the Birira area, the basalts are dark grey and sometimes amygdaloidal. These flows may alternate with rhyolite flows. South of Birira, rhyolite flows constitute prominent hills and are interbedded with basalts flows. The rocks are frequently strongly fractured. Ignimbritic enclaves with calcite veins are also present. Approximately 2 km SW of Birira, a 30 cm thick calcite vein, trending 330°/vertical, can be followed over a considerable distance. Its direction corresponds to a NW-SE fault system observed by satellite imagery.

Bangomatete Formation

Extensive and thick rhyolite flows cap basaltic lavas of the Rio Mázoè Formation in the Serra Mevunge dome structure in the NW corner of the Chico map sheet and in the area east of the Rio Luia and Rio Mázoè confluence, extending from there to the mesa-like Bangomatete Mountain over 80 km northwest.

In the Rio Mázoè area, rocks of the Bangomatete Formation comprise a gently (10–35°) southwest-tilt-

ing pile of rhyolitic flows. Observations made along Rio Mázoè and Rio Luia reveal the prevailing pyroclastic nature of these volcanic rocks. In proximity of Mt. Inhamangombe a heterogeneous sequence of rhyolitic rocks shows features typical of variously welded ash-flow tuffs or ignimbrites: volcanic breccias with lithic and/or pumice fragments, lapilli tuffs, fiammes, lithophysae and glomeroporphyritic textures suggesting vapour-phase crystallisation.

Light yellowish to dark red (weathered), generally poorly sorted and massive lapilli tuffs and pyroclastic breccias include sharp-edged lithic (welded tuff) fragments or vesicular pumice fragments in various degrees of welding. Also flow banding and associated quartz- and zeolite-filled lithophysae, observed in several outcrops around the mountain, manifest the welding of pyroclastic deposits. Fine-grained, massive or laminated tuffs are locally found in areas more distal to Inhamangombe Mountain; they possibly represent a non-welded facies of ash-flow tuffs or rhyolitic ash-fall deposits.

A well-preserved rhyolitic lava lobe or tongue was found in the gorge of Rio Mázoè, about 10 km E of Mt Inhamangombe. On the top of basaltic lavas of the Rio Mázoè Formation, this chocolate to pinkish brown, fine-grained flow has abundant small, flow-deformed vesicles, parallel feldspar phenocrysts and distinct flow banding. Several large (up to 4 x 8 m in size) apertures within the flow possibly represent a row of volcanic vents (Fig. 21).



Fig. 21. Rhyolitic lava flow with small eruptive vent in background. Rio Mázoè near Mt Inhamangombe (0532910/8170633).



Fig. 22. A chaotic breccia, comprising of large, angular basaltic and rhyolitic fragments, probably representing a talus breccia around the caldera. Bangomatete Formation, north bank of the Rio Mázoè (0524862/8168927). Scale bar 15 cm.

With a prominent escarpment to the north, north-east and southeast, Inhamangombe Mountain forms a circular structure, about 6 km in diameter, near the confluence of Mázoè and Luia rivers. Originally, Hunting (1984) considered it to denote a variety of rhyolitic ash flow tuffs. However, features characteristic of lava flows, for example rubble layers between individual flow units, were also observed by the Hunting team. The general form of the mountain, probably controlled by ring faults, and the presence of rhyolitic lavas, ash-flow tuffs, and ignimbrites, suggest that the Inhamangombe Mountain is a former caldera (Hunting 1984).

The rhyolitic rocks of the area comprise mainly various types of pyroclastic deposits: pumice breccias, agglomerates and variously welded ash-flow tuffs with large amount of quartz-filled lithophysae. The caldera origin of the Mt Inhamangombe is supported by field verification by the Consortium, manifesting the presence of a coarse, chaotic breccia with large (up to 2 m in diameter), angular to subrounded lava and tuff fragments, in the SSE rim of the volcanic structure (Fig. 22). This breccia, which appears to be tens of metres in total thickness, probably represents a talus breccia of a syn-volcanic ring-fault system surrounding a magma reservoir (caldera).

Interpretation of satellite imagery and geophysics manifests the presence of rhyolitic rocks of the Bangomatete Formation in the Serra Mevunge dome area. In the northern part of the dome, the volcanic succession shows dips 10°–12° to NE due to local faulting. In the northern and north-western part of the dome, rhyolitic flows form a regular, terrace-like pile of flows. Although no distinct evidence of pyroclastic origin of the flows was obtained during present field verification, their large extent and tabular shape infers to single cooling units of ash-flow tuffs. In the area about 7 km SEE of Mt Chimandau, in river beds and on a weathered top soil of a highly vesicular, frothy-lava like rhyolite there are large amount of spherical agates. These layered chalcedony nodules, commonly known as thunder eggs, and originally developed as gas cavities (lithophysae) in a welded tuff (see Ross & Smith 1961) also refer to the pyroclastic nature of rhyolitic rocks.

In the central part of the Serra Mevunge dome, however, obvious lava structures in rhyolites also indicate extrusion of lava flows. About 5 km NE of Mt Balati, on a hill top outcrop there are dark pinkish brown, dense rhyolitic flows with zeolite-filled vesicles showing flow banding and surface folding, typical of viscous lava (Fig. 23). In the same

area rhyolitic lava contains small (< 5 cm) graphite fragments, probably derived from underlying coal-bearing Karoo sediments. Locally felsic lavas are also porphyritic, having small (< 5 mm) quartz and feldspar phenocrysts in a fine-grained groundmass. Steep to vertical dips of flow banding in lava flows suggest close proximity to volcanic vents.

In the southernmost part of the Luia Dome area, a reddish brown, massive felsic volcanite contains large amount of undeformed, quartz-chalcedony-zeolite-filled amygdules and vugs up to 5–6 cm in diameter. The porphyritic rock has large amount of anhedral feldspar crystals up to 10 mm in size, and locally exist also small (<10 cm), dark, dense fragments of basaltic lava.

An obsidian flow, over 3 m in thickness, is exposed over some hundreds of metres on top of a low hill, about 10 km to the west of Mt Sluxia. The weathered surface of the massive rock is dull grey, while fresh conchoidal fractures show a shiny black glassy lustre. Results of chemical analysis of the rock are similar to those of a rhyolitic lava flow from the Rio Mázoè area. A volcanic breccia with angular fragments of felsic tuff in a fine-grained tuff matrix, possibly representing a flow-top breccia of an ignimbritic flow, is exposed below the obsidian flow.

Fine-grained, pink to reddish amygdaloidal rhyolite flows occur 7 km north of Birira village forming an elongated mountain with a NW-SE orientation, dipping to the SW. The amygdalites are generally filled with calcite and, at places, zeolite. Rhyolitic agglomerates are also present. Grey chalcedony and ignimbrite horizons occur elsewhere. The latter show a well-preserved banding, dipping 15° – 20° SW. Distinct flows have been recognised, ignimbritic horizons usually forming the top of the hills. Calcite veins, up to 10 cm in thickness, intersect these volcanic rocks.

Outcrops of weathered amygdaloidal basalts, trending 320°/10°–12° NE are also found in places in the Birira area. The rocks are intensively fractured, with fracture spacing from a few to 10–12



Fig. 23. Surface folding of rhyolite lava flow belonging to the Bangomatete Formation. NE of Mt Balati (0402690/8203478). Scale bar 15 cm.



Fig. 24. Quartz-feldspar porphyry dyke with zoned feldspar phenocrysts and small, basaltic enclaves. North of Rio Mázoè (0459259/8191348). Scale bar 15 cm.

cm, being parallel to the main fracture system with trend of 330°–340°/80°– 90° SW. The contact zone between the Bangomatete rhyolites and underlying Rio Mázoè basalts is located near the observation point 10328-03 (0519978/8181483). The contact is concordant, striking 310°. A subvertical, N-W trending rhyolite feeder with large gas cavities was found intruding basalts near this contact.

INTRUSIVE SUITES OF KAROO AGE; RUKORE

Introduction

The rugged Rukore Mountain in the Tete Province straddles the border with Zimbabwe. There the name *Rukore Intrusive Suite (JrRg)* was coined by Barton *et al.* (1991) for the late Karoo intrusives

forming this largely granitic mountain range. The close spatial relation of various granites and dolerite dykes of the area indicate a broadly coeval emplacement of the mafic and felsic igneous products.

Felsic intrusives

Felsic intrusives of the Rukore Suite comprise porphyritic microgranites and granite porphyry dykes, the Rukore granite occupying an elevated area of about 20 km² in size on both sides of the Mozambique-Zimbabwe border.

The Rukore granite is pinkish, porphyritic, massive and non-deformed microgranite, where feldspar and quartz are found as euhedral to round, variously corroded and fragmented phenocrysts. Feldspar phenocrysts are in general 1–2 cm in size, commonly with a 1–2 mm thick whitish rim, whereas quartz phenocrysts are up to 5 mm in diameter. Green amphibole forms aggregates up to 10 mm in length, and magmatic mafic enclaves with feldspar xenocrysts are not uncommon suggesting magma mingling.

In thin section granophyric texture is commonly observed around strongly sericitised plagioclase phenocrysts. Some quartz phenocrysts show euhedral shapes, while some are mantled by amphibole. The matrix is composed of widespread micrographic quartz and sericitised plagioclase, the latter strongly predominating over potassium feldspar. Apart from sericitisation, plagioclase is also affected by

carbonate and epidote alteration, which also commonly affects amphibole. The common graphic and granophyric textures of the Rukore granite rule out plutonic origin and hypabyssal, subvolcanic origin is favoured.

Several quartz-feldspar porphyry dykes of the Rukore Suite form prominent, blocky ridges in the Rio Mázoè area, where they are invariably associated with, and occasionally cut by dolerite dykes. The generally NW-trending dykes, called microgranites by Barton *et al.* (1991) in the adjacent Nyamapanda area in Zimbabwe, occur as swarms of up to 30–50 m in width and zones of several kilometres in length, often rising several tens of meters above the surrounding landscape.

These massive, brick-red dykes are generally distinctly porphyritic with euhedral, often zoned feldspar phenocrysts up to 30–40 mm in size and small (< 4 mm), roundish quartz phenocrysts ‘floating’ in a microcrystalline quartzofeldspathic matrix (Fig. 24). Olivine and pyroxene phenocrysts as well as magnetite grains and basaltic enclaves are occasionally present.

Mafic intrusives

Mafic intrusives belonging to the Rukore Suite include a swarm of basalt dykes and sills, which intrude Proterozoic rocks and Phanerozoic strata up to early Cretaceous and extend from Rio Luenha in the south to the northern side of the Lake Cahora Bassa. Barton *et al.* (1991) reported rare picritic dykes from the Zimbabwean side of the border, and the Sm-Nd isotopic data obtained from the prominent Moeza dyke also connect the emplacement of this dyke to the Karoo magmatic event.

Where basaltic dykes with microgabbroic texture occur as NW-trending dyke swarms or as small, elongated microgabbro stocks, it implies association of Karoo related magmatic activity and zones of crustal weaknesses. At places where the dolerite dykes invade coal seams within Karoo sedimentary

strata, they may cause cokefication.

Where the enclosing country rocks have a low magnetic susceptibility, dolerite sills and dykes can be easily identified as strong anomalies on aeromagnetic maps, even when covered by sediments. Generally basaltic dykes stand out as small hills or ridges or, when weathered, betray their presence by chocolate-brown soils. In places, microgabbro dykes exhibit a clear fabric.

The 40–50 m thick mafic Moeza dyke, occurring in the Tete Province, can be followed in N-S direction on the aeromagnetic map for more than 150 km. In the coarse-grained dyke plagioclase ± clinopyroxene ± olivine are the major constituents, hornblende, biotite, chlorite and serpentine being retrograde minerals.

INTRUSIVE SUITES OF KAROO AGE; GORONGOSA

Introduction

In the Sofala Province, the Serra da Gorongosa Mountain dominates the surrounding plateau with its 1862 m high Gogogo peak by some 1200

metres. The mountainous zone corresponds to an oval-shaped intrusive complex (JrGg, JrGb), measuring 30 km N-S by 25 km E-W.

Lithology

According to Hunting (1984), the complex consists of a felsic core surrounded by mafic igneous rocks. Core rock types comprise micropegmatite-granite, which has intruded a mafic intrusion, composed of tholeiitic gabbro, some norite, and olivine gabbro. Quartzose hornfels and pyroxene-amphibole hornfels have been found in the Bárue Complex host rocks at the contact with intrusive granitic and gabbroic rocks, respectively.

The felsic and mafic intrusive bodies are readily distinguished in the ternary radiometric images, where a lighter core, dominated by low to medium K- and Th-signatures, is surrounded by a dark, very low-KThU "aureole". The aeromagnetic data clearly define the outline of the suite and show that it is laterally restricted to the outcrop area.

Gabbro

Dark green, fine- to medium-grained gabbro of the Gorongosa Suite intrudes micaceous gneisses and calc-silicate gneisses of the Bárue Complex in the NE contact of the suite. Medium-grained, massive gabbro is also exposed on the south-western slope of the Gorongosa Mountain.

Granite

Pinkish, medium-grained, massive granite forms the core of Serra da Gorongosa Mountain, intruding gabbroic rocks of the suite. The major mineralogy of alkali-feldspar granite comprises albite, orthoclase, quartz, clinopyroxene, and hornblende.

Gorongosa fault/fracture corridor and dyke swarm

The Gorongosa Suite is associated with a large swarm of NNE-SSW trending felsic and mafic dykes that radiate north and south of the Serra da Gorongosa, and stand out in relief as narrow, sharp ridges over distances of up to 50 km. The intrusive material fills a set of subvertical fault and fracture planes that appear to pre-date the emplacement of the main Gorongosa intrusive bodies. Notwithstanding their length, the majority of these fractures reveal very little apparent lateral displacement. A few major fault zones, however, extend from 70 km south of the Gorongosa Suite to 50 km north of it and are associated with apparent lateral displacements of close to 10 km. This indicates (1) that extensive block faulting with significant vertical movement has taken place on some of the faults and (2) that the facies interfaces in the Bárue Complex are gently dipping overall.

GEOCHEMISTRY OF KAROO-RELATED VOLCANIC ROCKS

Whole-rock geochemical data for 47 samples representing Karoo-related volcanic and intrusive rocks in southern and central Mozambique are listed in App. 1. The analyses have been performed at the Geochemical Laboratory, Geological Survey of Finland. Five samples representing the Movene Formation have been analysed at the Department of Geology, University of Helsinki.

The rocks are predominantly subalkaline (Fig. 25). SiO_2 ranges from ~45 to ~78 wt. % and shows a bimodal distribution into mafic and silicic rocks; intermediate compositions are relatively rare and are treated here together with the mafic rocks. Two samples from the Movene Formation exhibit strongly alkaline compositions and will be treated separately.

Mafic rocks

General characteristics

The mafic rocks are mainly subalkaline basalts and basaltic andesites ($\text{SiO}_2 = 46$ to 62 wt. %; TA = 1.5 to 7 wt. %) (Fig. 25). Four mafic to intermediate lavas from the Bangomateta and Rio Mázoè Formations show affinities to basaltic trachyandesite,

trachyandesite, and andesite. Classification based on the immobile trace element ratios Nb/Y and Zr/ TiO_2 (Winchester and Floyd 1977) confirms the predominance of subalkaline compositions (Fig. 26). The intermediate samples from the Bangomateta and Rio Mázoè Formations plot within the field of trachyandesite due to exceptionally high Nb/Y

and Zr/TiO_2 values, and one relatively primitive basalt from the Rio Mázoë Formation has affinity to alkali basalt. The geochemical data thus suggest mild alkaline affinities in the mafic lavas of the

Lupata region (Fig. 17). All samples show tholeiitic affinity on the basis of abundant normative hypersthene, however.

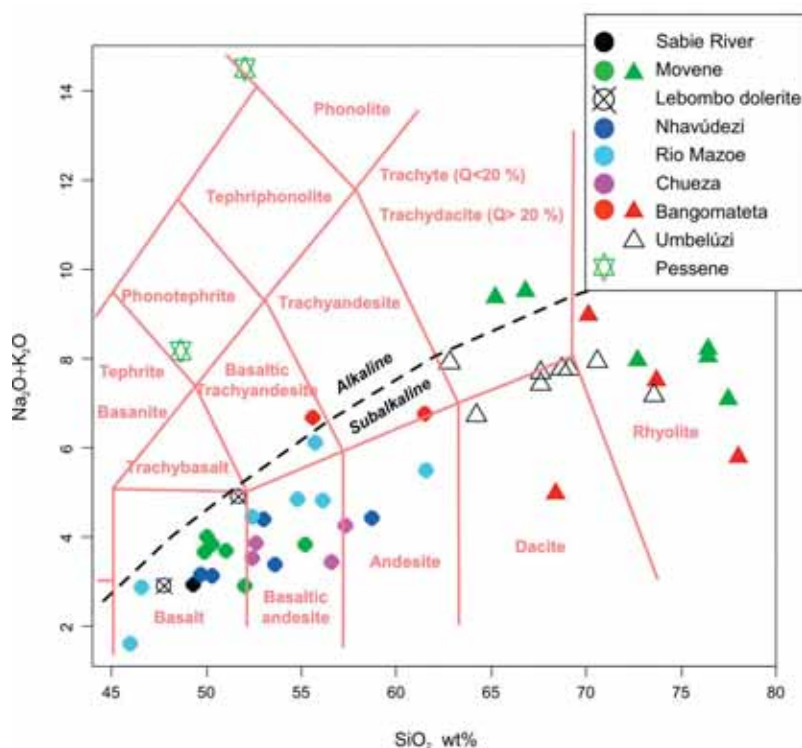


Fig. 25. Geochemical classification of Karoo-related lavas and dykes in southern and central Mozambique using total alkalis vs. silica diagram (LeMaitre *et al.* 1989). Division into alkaline and subalkaline compositions is according to Irvine and Baragar (1971).

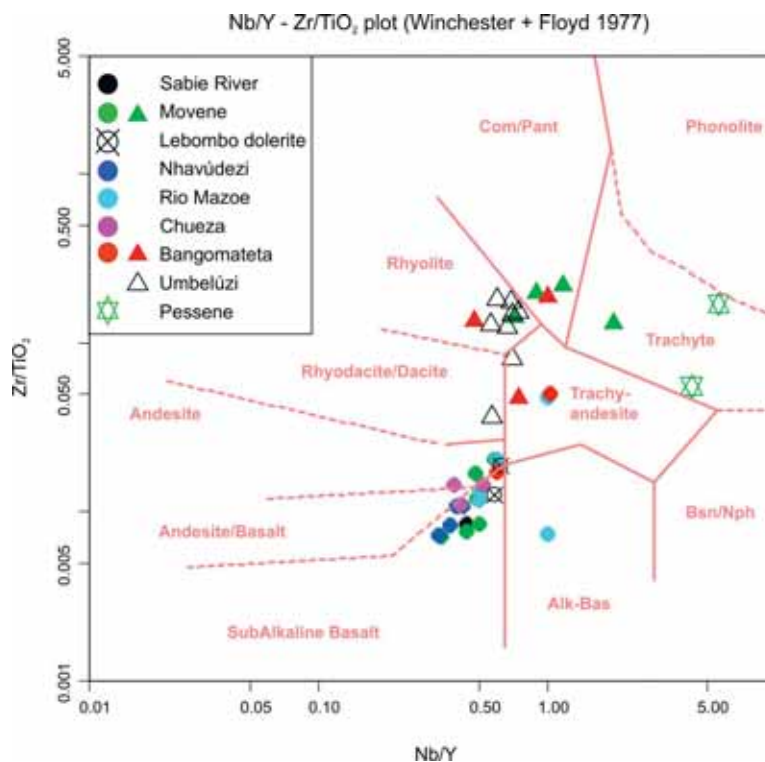


Fig. 26. Geochemical classification of Karoo-related lavas and dykes, southern and central Mozambique, using Nb/Y vs. Zr/TiO_2 diagram (Winchester & Floyd 1977).

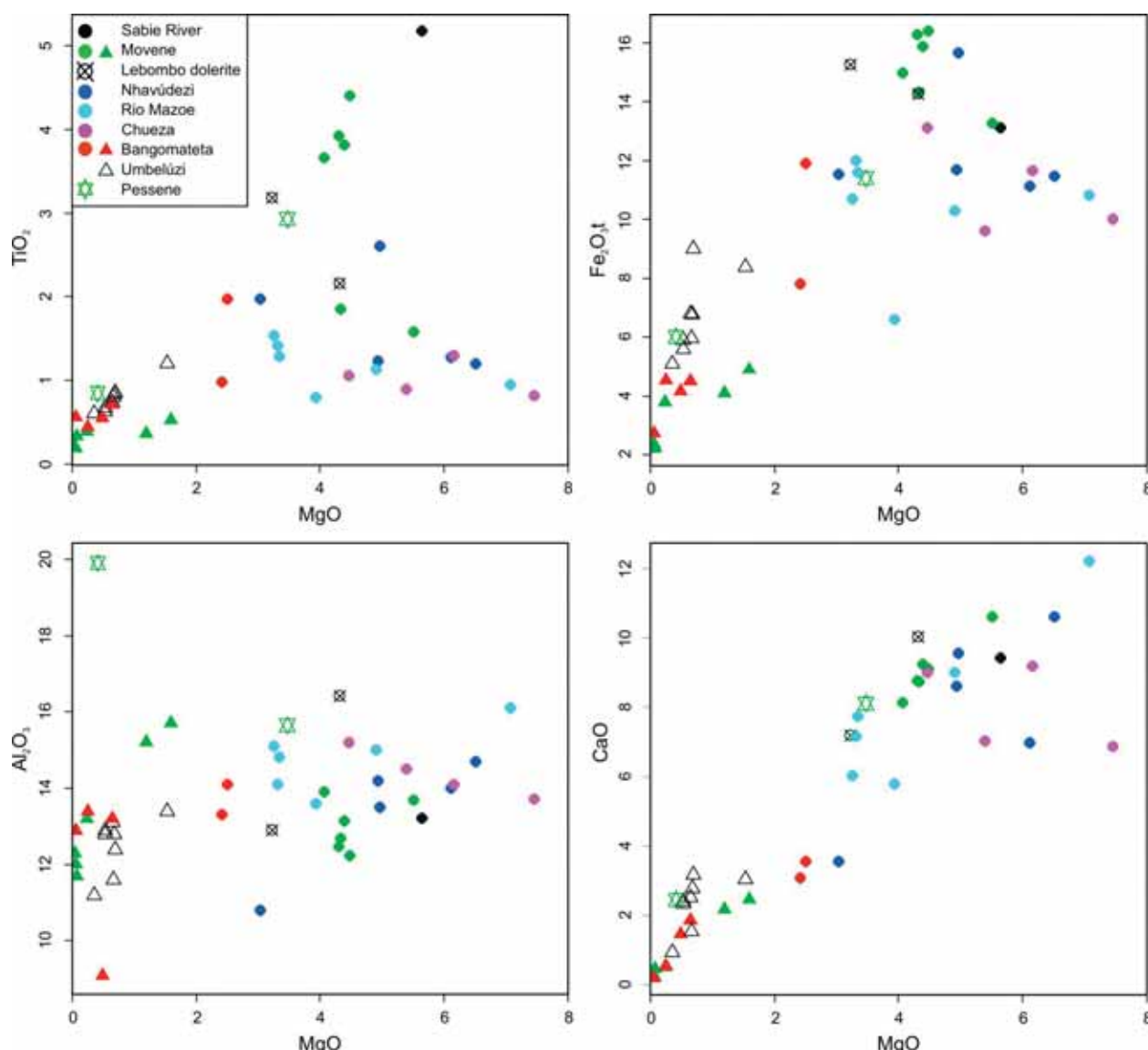


Fig. 27. Variations of TiO_2 , $\text{Fe}_2\text{O}_3\text{t}$, Al_2O_3 , and CaO vs. MgO (wt. %) for Karoo-related lavas and dykes from southern and central Mozambique.

Variations of major and trace elements are illustrated in Figs 27 and 28. Overall, the data show large scatter, which probably reflects the small number of analyses. The dataset is dominated by evolved compositions with MgO generally below 8 wt. % and typically below 5 wt. %. One sample from the Rio Mázoè Formation has markedly high contents of MgO (20 wt. %), Ni (820 ppm), and Cr (2080 ppm), and probably represents an olivine cumulate. This is not shown in the figures. Concentrations of K_2O and most of the trace elements show markedly wide ranges (e.g., Zr 50–800 ppm) and correlate negatively with MgO (Fig. 28). Typical of tholeiitic magma systems, the concentration trend of $\text{Fe}_2\text{O}_3\text{t}$ shows enrichment when MgO decreases from ~8 wt. %, an inflection point at MgO of ~4 wt. %, and subsequent depletion (Fig. 27). Concentrations of TiO_2 show a broadly similar pattern.

Grouping

Similar to Karoo lava suites in South Africa and Botswana, the mafic lavas and dykes in Mozambique can be grouped into geochemical types using concentrations and ratios of the high field strength elements, specifically Ti , P , Zr , and Y (cf. Erlank *et al.* 1988, Sweeney *et al.* 1994, Marsh *et al.* 1997, Jourdan *et al.* 2007a). The mafic rocks mainly show relatively low TiO_2 (<2.5 wt. %) and Zr (<250 ppm) contents, and Zr/Y values (<6) typical of low-Ti tholeiites, but samples with high-Ti characteristics are also fairly abundant (Fig. 29). Generalizing, the mafic rocks from the Lupata region, Rio Mázoè, Chueza, and Bangomatete Formations, are low-Ti type lavas: however, some evolved samples show unusually high Zr contents and Zr/Y values. Representative samples of the Nhavúdezi Formation are

also low-Ti lavas. The high-Ti samples are associated with the Lebombo Monocline; most of them, including one dolerite sample, are from the Movene Formation in central Lebombo. The single sample representing the Sabie River Basalt Formation in northern Lebombo and the spatially associated dolerite sample also belong to the high-Ti category.

Alkaline rocks of the Pessene region

Geochemically, the Pessene alkaline lava may be classified as phonotephrite, and it is distinguished from the stratigraphically older Movene basalts by notably higher K_2O (2.3 %) and Na_2O (5.9 %) at SiO_2 of 49 %. It is further characterized by high TiO_2 (2.9 wt. %) and notably high concentrations of P_2O_5 (1.3 wt. %), Zr (1620 ppm), and Nb (350 ppm) (Fig. 28).

Geochemical comparison of mafic lavas from different formations demonstrates their broadly uniform characteristics (Figs 27–29). The high-Ti rocks along the Lobombo Monocline exhibit relatively high Fe_2O_3t and Y at given MgO, and the geochemically fairly similar Rio Mázoè and Bangomateta Formations include samples with mild alkaline affinities.

The nepheline syenite of Pessene falls in the phonolite field of the TAS classification and, similar to the Pessene alkaline lava, a trachytic composition based on Zr/ TiO_2 vs. Nb/Y –classification (Figs 25–26). The nepheline syenite of Pessene has high Zr, Ba and Sr contents (1440 ppm, 2447 ppm, 3127 ppm) (Appendix 1). Markedly high Al_2O_3 , K_2O , and Rb may indicate accumulation of alkali feldspar

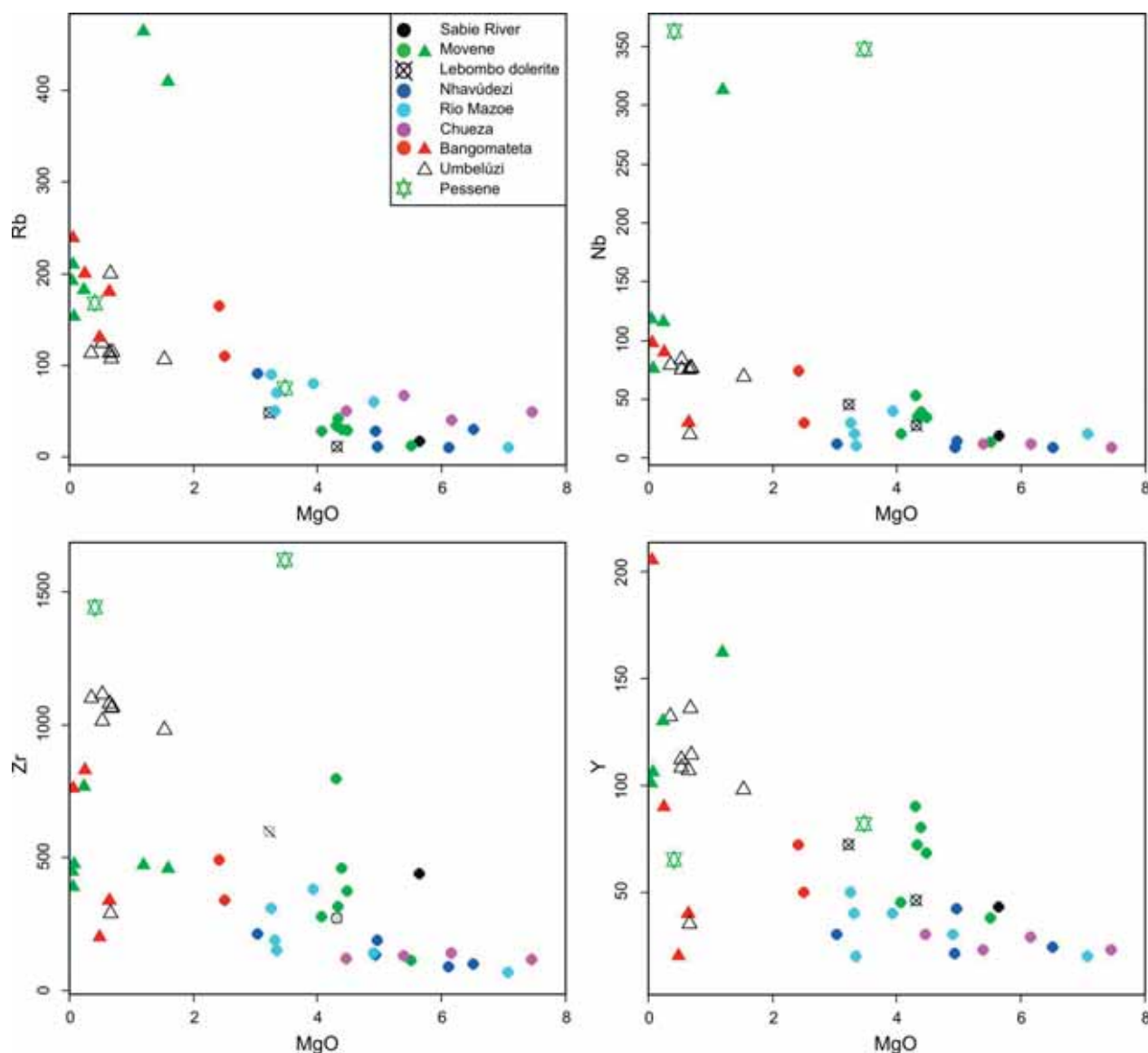


Fig. 28. Variations of Rb, Nb, Zr and Y (ppm) vs. MgO (wt. %) for Karoo-related lavas and dykes from southern and central Mozambique.

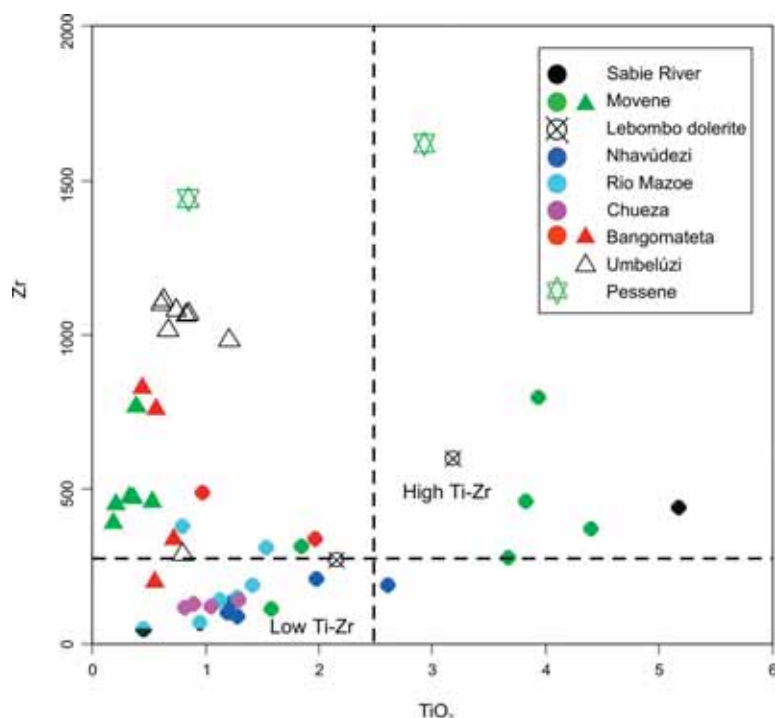


Fig. 29. Variations of Zr (ppm) vs. TiO_2 (wt. %) for Karoo-related lavas and dykes in southern and central Mozambique. Dash lines indicate critical values for low-Ti vs. high-Ti classification (Erlank *et al.* 1988).

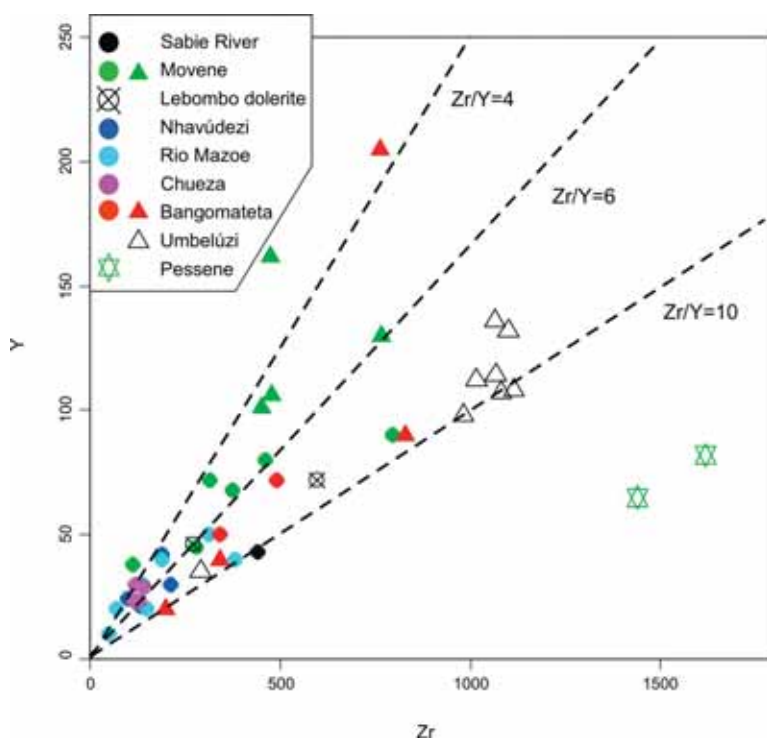


Fig. 30. Variations of Y vs. Zr (ppm) for Karoo-related lavas and dykes in southern and central Mozambique.

phenocrysts in the analysed sample. Based on broad geochemical similarities and similar ratios of TiO_2 , Zr, Nb, and Y in particular, the alkaline lava and the

nepheline syenite could represent extrusive and intrusive parts of the same alkaline magma system.

Felsic rocks

Geochemical data for representative samples of felsic lavas are listed in App. 1. The Karoo-related felsic rocks of southern and central Mozambique range from dacite to rhyolite ($\text{SiO}_2 = 63\text{--}78$ wt. %). They mainly plot within the field of subalkaline lavas in the TAS diagram, whereas the banded felsic volcanites of the Moveve Formation can be classified as trachyte and a dacitic sample belonging to the Umbelúzi Formation is classified as trachydacite on the basis of normative $Q/(An+Ab+Or)$. The banded felsic volcanites plot within the field of trachyte also in the Zr/TiO_2 vs. Nb/Y diagram (Fig. 26). The felsic rocks further exhibit peraluminous ($Al_2O_3 > Na_2O + K_2O + CaO$) and high-K geochemical characteristics (Fig. 31). Generalizing, the felsic rocks show A-

type geochemical affinities: $FeOt/(FeOt+MgO)$ and $Zr+Nb+Ce+Y$ values are relatively high (0.83–0.98 and mainly > 1000 ppm, respectively). The banded felsic volcanites of the Moveve Formation have lower $FeOt/(FeOt+MgO)$ values of 0.71–0.76.

Comparison of rhyolites belonging to the Umbelúzi and Moveve Formations indicates the following differences: the stratigraphically older Umbelúzi Formation is typified by (1) relatively lower SiO_2 contents (mainly below 70 wt. %) (Fig. 25), (2) higher Zr at a given TiO_2 , MgO, and Y content (Figs 28–30), (3) higher Fe_2O_3 and lower Al_2O_3 at a given MgO (Fig. 27). The felsic rocks from the Bangomateta Formation are geochemically quite similar to those belonging to the Moveve Formation.

DISCUSSION

Geochemical provinciality of Karoo province

The Karoo large igneous province exhibits pronounced compositional heterogeneity that results from subsolidus alteration, crystallization and melting processes, contamination, and magma source

heterogeneity. Rigorous geochemical grouping of the magmatic successions is fundamentally important in identifying magmatic lineages, addressing process- and source-dependent variations and un-

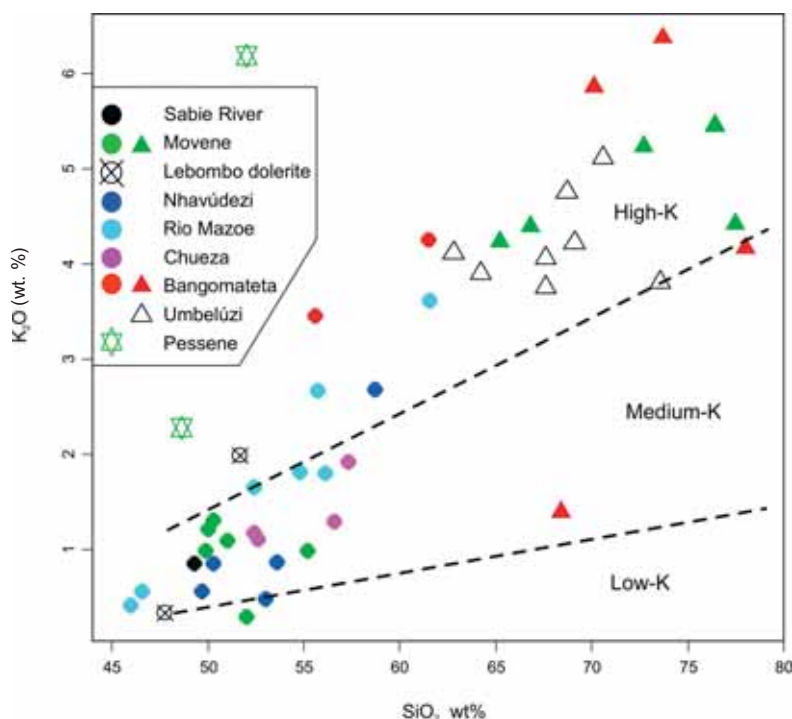


Fig. 31. Classification of Karoo-related subalkaline rocks from southern and central Mozambique into low-K, medium-K, and high-K types (LeMaitre *et al.* 1989).

derstanding the temporal and spatial evolution of the magmatic system. Geochemical and volcanological data for Mozambique are pivotal in this research: the volcanic rocks represent relatively little-studied parts of the province and probably include the youngest presently exposed volcanic rocks in the province.

Geochemical studies of mafic rocks belonging to the Karoo province in southern Africa and the western Dronning Maud Land, Antarctica, have demonstrated association of high-Ti lavas within or close to the purported Limpopo triple junction (Burke & Dewey 1973) and imply distribution of low-Ti magmas around the central area of high-Ti lavas.

Lebombo Monocline

Generalizing, the geochemical characteristic of mafic volcanic rocks and intrusive rocks in Mozambique are compatible with the previously outlined distribution pattern of low-Ti and high-Ti rocks. Sweeney *et al.* (1994) documented a narrow ~60 km zone between the northern high-Ti province and southern low-Ti province within the Sabie River Formation. Low-Ti type lavas are not found north of Sabie River and high-Ti type lavas south of Komati River; in between, both lava types are stratigraphically intercalated. The northern part of the Moveene Formation is located to the east of this transition zone. Our geochemical data indicate continuation of penecontemporaneous high-Ti and low-Ti magmatism after the interlude of predominantly felsic eruptions represented by the Umbeluzi rhyolites. Specifically, the high-Ti basalts of Moveene Formation and the spatially associated dolerite samples are tentatively correlated with the ‘high-Fe’ subtype of high-Ti basalts in the Sabie River Formation on the basis similar of Zr/Y values (~6) and TiO_2 (~4 wt. %) and $\text{Fe}_2\text{O}_3\text{t}$ contents (~16 wt. %) (cf., Sweeney *et al.* 1994). It should be emphasized that the “high-Fe” basalts are confined to the uppermost part of the Sabie River Formation, which lends support to the proposed correlation. The single Sabie River basalt sample analysed in this study is a likely correlate of the “high Ti-Zr” subtype of high-Ti basalts. These lavas are characterised by markedly high Zr/Y (~10) and $\text{Fe}_2\text{O}_3\text{t}$ (~12–13 wt. %) and become increasingly abundant in the northern part of the Sabie River Formation (Sweeney *et al.* 1994). In the same way, the low-Ti lavas of the Moveene Formation are quite similar to the low-Ti basalts of the Sabie River Formation. They exhibit low Zr/Y (~4) and “intermediate” $\text{Fe}_2\text{O}_3\text{t}$ (~14 wt. %) compared to the high-Ti subtypes (cf. Sweeney *et al.* 2004).

Nuanetsi-Sabi volcanic flexure

To our knowledge, our samples from the Rio Nhavúdezi Formation are the first geochemically analysed rocks from the Nuanetsi-Sabi flexure. These data imply preponderance of low-Ti lavas in the Rio Nhavúdezi Formation. The samples are broadly similar to the low-Ti basalts of the Moveene Formation with relatively low Zr/Y (4–6) values and intermediate $\text{Fe}_2\text{O}_3\text{t}$ (11–12 wt. %). One sample has fairly high TiO_2 (~2.6 wt. %), $\text{Fe}_2\text{O}_3\text{t}$ (~16 wt. %), and Ti/Y (~400), typical of high-Ti lavas, but low Zr/Y (~4.5) values render high-Ti vs. low-Ti classification ambiguous. Overall, the geochemical data indicate similarity between the Nuanetsi-Sabi flexure, the Lebombo Monocline, and the Tuli syncline (cf. Sweeney *et al.* 1994, Jourdan *et al.* 2007) and lend further support to the view that these volcanic suites represent genetically related magmatism associated with the Limpopo triple junction structure.

Lupata trough and Moatize-Luia graben

Mafic and intermediate rocks belonging to the Cheza Formation, Rio Mázoè Formation, and Bangomateta Formation range from low-Ti basalt to low-Ti andesite. In addition to relatively low TiO_2 , these lavas have low $\text{Fe}_2\text{O}_3\text{t}$ contents and Zr/Y and Ti/Y values. Generalizing, they are quite similar to the low-Ti lavas that are associated with the Lebombo Monocline and the Nuanetsi-Sabi flexure, i.e. the Limpopo structure. A more detailed inspection of the geochemical traits of these rocks indicates some differences that may be significant in terms of correlation and genetic relationships. Compared to the Limpopo structure, lavas from the Cheza Formation, Rio Mázoè Formation, and Bangomateta Formation tend to have lower TiO_2 and Zr and Zr/Y at given MgO content. It may be significant that the low-Ti lavas from Botswana (Jourdan *et al.* 2007a), Springbok Flats, Lesotho (Marsh *et al.* 1997), and Kirwanveggen (Dronning Maud Land, Antarctica; Harris *et al.* 1990) can be similarly distinguished from the low-Ti lavas associated with the Limpopo structure (Luttinen & Leat 2007). Overall, the mafic lavas from the Lupata trough and the Moatize-Luia graben and those from the Lebombo Monocline and the Nuanetsi-Sabi flexure may represent geochemically and petrogenetically distinctive groups of magmas.

Karoo-related plutons and pre-break-up reconstructions of Gondwana

Mozambique

Pluton-size intrusive manifestations of Karoo magmatism are quite rare. The plutons provide insights into intratelluric magmatic processes, but most significantly, they typically contain minerals suitable for high-precision dating of magmatic events. In comparison, dating of volcanic rocks is frequently hampered by secondary alteration and/or lack of ample zircon/baddeleyite.

In conjunction with the mapping programme, the Consortium sampled several inadequately dated Precambrian and Phanerozoic plutons for geochronological studies. The results for three intrusions, the Moeza mafic dyke, the Rukore granite and the Gorongosa gabbro-syenite in the central Mozambique mapping area suggest Mesozoic emplacement (GTK Consortium 2006b).

The Rukore granite and the Gorongosa gabbro-syenite are readily associated with Karoo magmatism. The Rukore granite represents a felsic component of a complex intrusive suite that also includes mafic sills, dyke swarms and small microgabbroic stocks (Barton *et al.* 1991). Intrusive rocks that belong to this group cut the Proterozoic basement and sedimentary rocks of the Karoo Supergroup relatively close to the outer limit of the Archaean Zimbabwe craton. Dating of the granite yielded U-Pb ages within the range 195–180 Ma (GTK Consortium 2006b). This result is in accordance with contemporaneous emplacement of the Rukore intrusive suite during the peak of Karoo magmatism at ~180 Ma (e.g., Encarnación *et al.* 1996).

The intrusive rocks of the Gorongosa Complex cut the Proterozoic basement and are found in the central part of a ~100 km long swarm of N-S trending felsic and mafic dykes. The emplacement of these dykes is considered to manifest a presence of N-S trending system of faults and fractures, some of which can be followed laterally up ~120 km distance (GTK Consortium 2006b). These tectonic structures are associated with marked lateral displacements of up to 10 km. Zircon fractions from a syenitic sample from the felsic core of a gabbro-syenite part of the complex yielded an age of 181 ± 2 Ma that is clearly equivalent to the peak of the Karoo magmatism (Encarnación *et al.* 1996).

The Moeza dyke is at least 150 km long, N-S trending mafic intrusion that crosscuts Proterozoic basement in the Tete Province (Fig. 1). A robust Sm-Nd age of 180 ± 43 Ma (GTK Consortium 2006b) shows it to represent one of the largest intrusive

manifestations of Mesozoic magmatism in southern Africa and tentatively associates it with Karoo magmatism. The emplacement of the gigantic Moeza dyke may well indicate a large-scale lithospheric fault or lineament associated with or precursory to Gondwana break-up magmatism.

South Africa and Dronning Maud Land

Several Karoo-related gabbroic intrusions have been reported in southern Africa: the Birds River intrusion in North-Eastern Cape (Eales 1990), the Komatipoort complex in central Lebombo (Saggersson & Logan 1970), the Mount Arthur complex ~150 km SW of Leshoto (Polderwaart 1946), and the New Amalfi sheet and the Insizwa complex in Kwa Zulu-Natal area < 100 km SE of Leshoto (e.g., Polderwaart 1944, Lightfoot *et al.* 1987). These intrusions typically are shallow-seated, sill-like mafic plutons that may represent the feeder system of Karoo basalts (cf. Allsopp *et al.* 1984, Saggersson & Logan 1970, Polderwaart 1944, 1946, Lightfoot *et al.* 1987). Whereas the Komatipoort complex is bounded by Karoo basalts, the other plutons are intruding sedimentary rocks of the Karoo Supergroup.

Karoo-related pluton-size intrusions have also been reported from western Dronning Maud Land, Antarctica. The ~1000 m-thick lava sequence of Vestfjella is cut by three gabbroic plutons: Utpostane, West-Muren, and East-Muren (Vuori & Luttinen 2003, Vuori 2004). U-Pb-dating of these intrusions at 182–180 Ma correlates them with the main peak of Karoo-magmatism (Vuori 2004, Encarnación *et al.* 1996). Whereas the two intrusions at Muren have a dyke-like character, the Utpostane pluton is composed of olivine-rich cumulate rocks and has been considered to represent a feeder system for Karoo lavas (Vuori & Luttinen 2003). The Sistefjell syenite has been intruded into metamorphic Proterozoic rocks of the Maud Belt (Harris & Grantham 1993). The age of intrusion is somewhat lower (173 ± 2 Ma, Harris *et al.* 2002) than the main peak of Karoo magmatism, but it overlaps with the emplacement ages of Karoo-related dolerite dykes along the Lebombo Monocline (Jourdan *et al.* 2007).

Tectonic implications

The pluton-size intrusions of the Karoo province typically are located close to Archaean-Prot-

erozoic lithospheric boundaries in southern Africa and western Dronning Maud Land, Antarctica (Fig. 32) and many of them can be associated with large-scale tectonic structures. Here we examine possible tectonic implications revealed by geochronological data and the distribution pattern of the plutons.

We have assembled an “ultra-tight” Gondwana reconstruction to highlight some potentially significant aspects. Our reconstruction illustrates that: (1) The mafic plutons are mainly associated with the present continental margins, i.e. those tectonic zones that finally developed into oceanic spreading systems. The Lebombo Monocline in Africa and the Vestfjella mountains in the Antarctica represent thick successions of seaward-dipping lava flows. We associate the emplacement of these voluminous lavas, and the spatially and temporally associated large plutons (e.g. Utpostane and Insizwa) in particular, with a position of these rocks directly over regions of mantle melting; (2) The Rukore and Gorongosa complexes and the Moeza dyke, central Mozambique, and the alkaline intrusions of western Dronning Maud Land define a broadly linear tectono-magmatic feature, possibly representing a major (~2000 km) lithospheric lineament. This purported lineament transects one of the rift arms of the Limpopo structure, the Mozambique zone of lithospheric thinning (Cox 1992), is associated with termination of the Nunaetsi-Sabi flexure, and may have been developed in response to tectonism and relatively small-scale melting along the Archaean–Proterozoic boundary (Fig. 32). We suggest that these felsic-alkaline plutons may manifest igneous activity in an aborted zone of lithospheric thinning away from the most active areas of rifting.

The position of the unexposed Archaean–Proterozoic lithospheric boundary is not firmly established in the strongly tectonized region to the east of the Lebombo Monocline and to the west of the Jutulstraumen zone (Fig. 32). Previous geophysical surveys have been interpreted to locate the boundary in northern Vestfjella (Corner 1994) and beneath the sedimentary plains of southern Mozambique (Lächelt 2004) (Fig. 33). These interpretations have been supported in the Antarctica by evidence for Archaean contaminants of basalts in northern Vestfjella (Luttinen & Furnes 2000). Rather similarly, the recent geochronological studies of the Pessene alkaline intrusion provide evidence for involvement of Archaean material in the petrogenesis of these rocks (GTK Consortium 2006a). Specifically, U-Pb dating of zircon separates of a Pessene nepheline syenite revealed anomalous old zircon fractions that have been probably derived from both Proterozoic

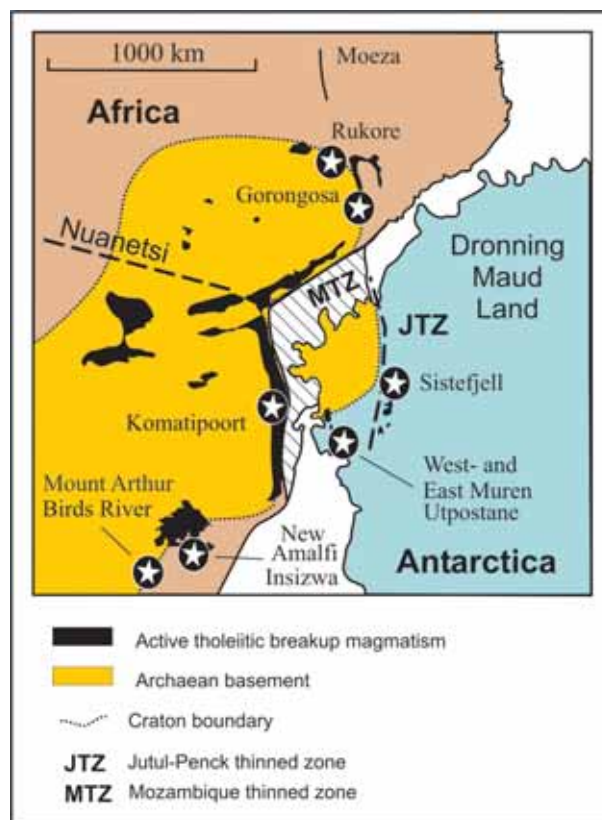


Fig. 32. Distribution of ~180 Ma gabbroic and felsic-alkaline pluton-size intrusives (stars) and major tectonic zones in a tight reconstruction of Karoo LIP. The ~N-S and ~NW-SE trending dykes and faulting in Moeza, Gorongosa, and Rukore extend towards the Jutul-Penck zone of western Dronning Maud Land, Antarctica.

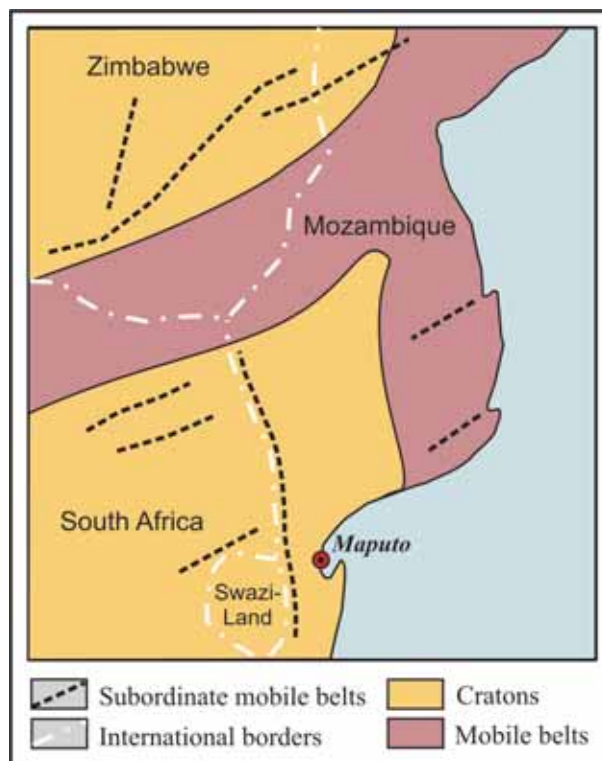


Fig. 33. Purported extensions of Archaean cratons and Proterozoic mobile belts in southern Mozambique (modified from Lächelt 2004).

and Archaean material in sedimentary rocks, crystalline basement, or both (GTK Consortium 2006b). Although we cannot positively identify the source

of the inherited zircons, their presence is compatible with extension of the Archaean craton beneath the Movene Basalt Formation (Lächelt 2004).

A model of post-volcanic tectonic movements in the Movene Formation

The break-up of Gondwana and the emplacement of the Karoo province was associated with and followed by complex tectonic events including extension, transtension, and faulting (GTK Consortium 2006a, b). Coast-parallel dolerite dyke swarms have been frequently associated with extension tectonics, but the emplacement of the late-stage Rooi Rand dykes in southern Lebombo at 174–172 Ma (Jourdan *et al.* 2007b) may have been related to continent-scale strike-slip faulting along the Gastre Fault (Watkeys & Sokoutis 1998). Further evidence of marked syn-magmatic and post-magmatic N-S faulting and lateral displacement of lithospheric blocks can be observed in the area of Gorongosa pluton, central Mozambique (GTK Consortium 2006b). These displacements can be also associated with the N-S trending Moeza dyke that extends further North to the Zambia.

The plains of southern Mozambique and the coastal area of western Dronning Maud Land are of key importance to pre-break-up Gondwana reconstructions (e.g., Lavver *et al.* 1992). Both regions probably represent areas of strongly tectonized and thinned lithosphere, but the tectonic movements are difficult to define due to poor exposure of bedrock. Aeromagnetic data and field observations may fa-

cilitate reconstruction of the post-volcanic tectonic evolution of the Movene Formation, however. Here we present a schematic tectonic model that has resonance for the stratigraphy of the Karoo-related lavas and the late-stage tectonic events related to Gondwana break-up.

Karoo-related lavas are commonly continuous and elongated subhorizontal sheets. The Pequenos Libombos rhyolites in the Movene Formation form discontinuous ridges, however, and these may indicate tectonic activity and displacement of crustal blocks. In recently published geological maps, the Pequenos Libombos rhyolites are divided into two units separated by a narrow zone of Movene basalts and crosscutting SW-NE trending dolerites (Fig. 34a). The facing edges of the rhyolite units strike NW-SE (Fig. 34a); the overall appearance of the units raises the question whether they could represent displaced pieces of an originally continuous rhyolite unit. This possibility is illustrated in Fig. 34 and discussed below.

The model stems from the hypothesis that the Pequenos Libombos rhyolites initially constituted a single, gently eastward dipping unit broadly parallel to Umbelúzi rhyolites (Fig. 34b). As the first post-magmatic tectonic event, the Movene Forma-

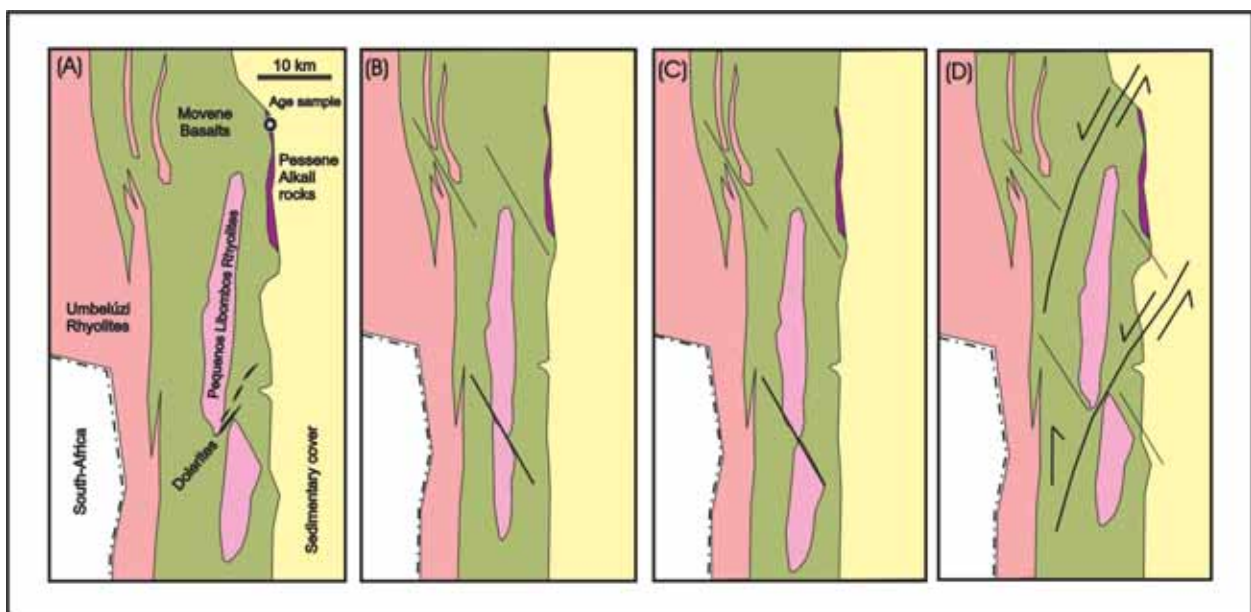


Fig. 34. Geological map of the Pequenos Libombos area (a) and its possible tectonic evolution: from suggested original situation (b) via faulting and movements (c, d) to current day configuration (a). See text for further details.

tion and the Pequenos Libombos rhyolites were cut by NW-SE-trending faults that are broadly parallel to the Botswana dyke swarm (Fig. 34b; Reeves 1978). Subsequently, the Pequenos Libombos unit was split in two parts that were sinistrally displaced along the NW-SE-trending faults (Fig. 34c). Given that the Umbelúzi rhyolites do not show evidence of similar displacement, the displacement within the Moveene Formation probably was associated with rotation that led to relative uplift of the southern part of Pequenos Libombos. The rotation axis probably was close to the surface of the Umbelúzi rhyolites. The third tectonic event in this model involves NE-trending sinistral strike-slips (Fig. 34d), possibly associated with large-scale N-S movements that are

observed also in central Mozambique. The intrusion of SW-NE-trending dolerites between the two parts of Pequenos Libombos may have been related to this event. We emphasize the speculative nature of the tectonic model. However, the 3-stage model illustrates possible tectonic discontinuities that may complicate stratigraphic studies of the Moveene Formation. The model is compatible with the current distribution of Pequenos Libombos rhyolites and the occurrence of basalts and dolerites between the rhyolitic units, and it is also accordant with our observations in the central part of Mozambique, where N-S-trending structures are associated with Karoo-related extrusive and intrusive rocks.

CONCLUSIVE REMARKS

1. The Karoo-related volcanic rocks of southern and central Mozambique have mainly subalkaline affinities and include mafic, intermediate, and felsic varieties – intermediate compositions are relatively rare. The mafic rocks are lava flows that typically exhibit characteristic features of ropy lava. The felsic rocks are mainly ash-flow tuffs and ignimbrites.
2. The Moveene Formation represents the capping unit of the Lebombo volcanic succession, but the exact age relationship between the ~182 Ma volcanic rocks in South Africa and the Moveene basalts is unknown. Volcanic rocks belonging to the Nuanetsi-Sabi flexure in central Mozambique probably correlate with the ~182 Ma Sabie River Formation on the basis of geochemical similarity. Basalts and rhyolites in the Tete Province show affinities to Karoo lavas in Botswana and Lesotho areas and presumably also erupted during the main-stage of magmatism at ~182 Ma.
3. The margins of Archaean cratons were associated with both felsic-alkaline and mafic igneous activity during the break-up of Gondwana. This is manifested by the new age data that delineates ~2000 km long chain of pluton-size intrusives both in southern Africa and in Antarctica.
4. The N-S trending structures associated with the Gorongosa and Rukore intrusive complexes and the Moeza dyke in central Mozambique may indicate large-scale lineaments and possible zones of crustal thinning. Magmatism and tectonism along this structure may correlate with Karoo-related alkaline intrusive activity within the Jutul-Penck tectonic zone in western Dronning Maud Land, Antarctica. Tectonic processes probably caused sinistral crustal dislocations during and/or after the emplacement of intrusive and extrusive Karoo magmas.
5. Inherited Archaean zircons in Pessene nepheline syenite imply extension of the Kaapvaal craton beneath the Mozambique Basin.

REFERENCES

- Allsopp, H. L., Bristow, J. W., Logan, C. T., Eales, H. V. & Erlank, A. J. 1984. Rb–Sr geochronology of three Karoo-related intrusive complexes. *Special Publication Geological Society of South Africa*, 13, 281–287.
- Assunção, C. F. T., Coelho, A. V. T. P. & Rocha, A. T. 1962. *Petrologia das lavas dos Libombos (Moçambique)*. Estudos, Ensaios e Documentos da Junta Investigativa Ultramarina, 99, 74–93.
- Barton, C. M., Carney, J. N., Crow, M. J., Dunkey, P. N., Simango, S., & Evans, J. A. 1991. The geology of the country around Rushinga and Nyamapanda. *Bulletin – Zimbabwe Geological Survey*, 92, 220 p.
- Betton, P. J. 1979. Isotopic evidence for crustal contamination in the Karoo rhyolites of Swaziland. *Earth and Planetary Science Letters*, 45(2), pp. 263–274.
- Bristow, J. W. & Cox, K. G. 1984. Volcanic rocks of the Lebombo-Nuanetsi-Sabi Zone; classification and nomenclature. In: Erlank, A. J. (Ed.). *Petrogenesis of the volcanic rocks of the Karoo Province*. Geological Society of South Africa Special Publication, 13, 69–75.
- Bristow, J. W. & Armstrong, R. A. 1989. An emplacement and petrogenetic model for the high temperature ash flows of the Jozini Formation, South Africa *Bulletin - New Mexico Bureau of Mines and Mineral Resources*, Report 131, 31.

- Burke, K. & Dewey, J. F. 1973.** Plume-generated triple junctions: key indicators in applying plate tectonics to old rocks. *Journal of Geology*, 81, 406–433.
- Cahen, L., Snelling, N. J., Delhal, J. & Vail, J. R. 1984.** The geochronology and evolution of Africa. Clarendon Press, Oxford, United Kingdom, 512 p.
- Cleverly, R. W. & Briatow, J. W. 1979.** Revised volcanic stratigraphy of the Lebombo Monocline. *Transactions of the Geological Society of South Africa*, 82, 2, 227–230.
- Cleverly, R. W., Betton, P. J. & Bristow, J. W. 1984.** Geochemistry and petrogenesis of the Lebombo rhyolites. In: Erlank, A. J. (Ed.). *Petrogenesis of the volcanic rocks of the Karoo Province*. Geological Society of South Africa Special Publication, 13, 171–195.
- Corner, B. 1994.** Geological evolution of western Dronning Maud Land within a Gondwana framework: Geophysics subprogramme. Final project report to SCAR. Whitwaterstrand University, South Africa: Department of Geophysics, 21 p.
- Cox, K. G. 1983.** The Karoo province of southern Africa: origin of the enrichment patterns. In: Hawkesworth, C. J. & Norry, M. J. (eds.) *Continental basalts and mantle xenoliths*. Shiva, Nantwich, pp. 139–887.
- Cox, K. G. 1992.** Karoo igneous activity, and the early stages of the breakup of Gondwanaland. In: Storey, B. C., Alabaster, T. and Pankhurst, R. J. (eds.) *Magmatism and the causes of Continental breakup*. Geological Society Special Publications, 68, 137–148.
- Cox, K. G. & Bristow, J. W. 1984.** The Sabie River Basalt Formation of the Lebombo Monocline and South-east Zimbabwe. In: Erlank, A. J. (ed.). *Petrogenesis of the volcanic rocks of the Karoo Province*. Geological Society of South Africa - Special Publication 13, 125–147.
- Cox, K. G., Macdonald, R. & Hornung, G. 1967.** Geochemical and petrographic provinces in the Karoo basalts of southern Africa. *American Mineralogist* 52, 1451–1474.
- Darracott, B. W. & Kleywegt, R. J. 1974.** The structure of the southern portion of the Lebombo volcanic belt deduced from gravity data. *Transactions of the Geological Society of South Africa*, 77 (Part 3), pp. 301–308.
- Duncan, R. A., Hooper, P. R., Rehacek, J., Marsh, J. S. & Duncan, A. R. 1997.** The timing and duration of the Karoo igneous event, southern Gondwana. *Journal of Geophysical Research* 102, 18127–18138.
- Eales, H. V. 1990.** The Birds River Intrusion – a quantitative model for Karoo Central Province basalt fractionation. *South African Journal of Geology*, 93, 717–728.
- Eales, H. V., Marsh, J. S., & Cox, K. G. 1984.** The Karoo igneous province: an introduction. In: Erlank, A. J. (ed.) *Petrogenesis of the volcanic rocks of the Karoo Province*, Geological Society of South Africa, Special Publications 13, pp. 1–26.
- Encarnación, J., Fleming, T. H., Elliot, D. H. & Eales, H. V. 1996.** Synchronous emplacement of Ferrar and Karoo dolerites and the early breakup of Gondwana. *Geology*, 24, 535–538.
- Erlank, A. J. (ed.) 1984.** Petrogenesis of the volcanic rocks of the Karoo Province. Geological Society of South Africa - Special Publication 13, 395 p.
- Erlank, A. J., Duncan, A. R., Marsh, J. S., Sweeney, R. J., Hawkesworth, C. J., Milner S. C., Miller, R. McG. & Rogers, N. W. 1988.** A laterally extensive geochemical discontinuity in the subcontinental Gondwana lithosphere. In: *Geochemical Evolution of the Continental Crust*, Conference Abstracts, Brazil, 1–10.
- Flores, G. 1970.** Suggested origin of the Mozambique channel. *Transactions of the Geological Society of South Africa*, 73, Part 1(1), 1–16.
- Flores, G. 1973.** The Cretaceous and Tertiary sedimentary basins of Mozambique and Zululand. In: *Sedimentary Basins of the African Coasts*, Symposium, Part 2, South and East Coast. Association of African Geological Surveys, Paris, pp. 81–111.
- Freitas, B. 1937.** Subsídios para o estudo da formação vulcânica dos Libombos. *Boletim do Serviço Industrial, Geológico e Minas*, 1, 5–10.
- Grantham, G. H., Macey, P., Ingram, B. A., Rademeyer, M., Eglington, B. M., Keidan, H. & Azevedo, S. 2006.** The chemistry and age of Karoo andesitic lavas along the northern Mozambique coast. 21st Colloquium of African Geology (CAG21), 03–06/07/2006, Maputo, Mozambique. Abstract Volume, 56–57.
- Grantham, G. H., Macey, P., Ingram, B. A. & Cronwright, M. 2004.** Karoo-age andesitic volcanism along the northern Mozambique coast. *Gondwana Research*, 7, 1303–1304.
- GTK Consortium 2006a.** Map Explanation; Volume 1: Sheets 2032–2632. *Geology of Degree Sheets*, Espungabera/Chibabava, Nova/Mambone, Massangena, Chidoco, Save/Bazaruto, Chicualacuala, Machaila, Chigubo, Mabote/Vilanculos, Rio Singuédzi/Massingir, Rio Changana, Funhalouro/Inhambane, Chilembene, Chókwè, Zavala/Inharrime, Maputo, Xai-Xai/Zavala and Bela-Vista, Mozambique. Direcção Nacional de Geologia (DNG), Maputo.
- GTK Consortium, 2006b.** Map Explanation; Volume 2: Sheets 1630 – 1634, 1732 – 1734, 1832 – 1834 and 1932 - 1934. *Geology of Degree Sheets* Mecumbura, Chioco, Tete, Tambara, Guro, Chemba, Manica, Catandica, Gorongosa, Rotanda, Chimoio and Beira, Mozambique. Direcção Nacional de Geologia (DNG), Maputo.
- GTK Consortium 2006c.** Map Explanation; Volume 4: Sheets 1430-1432 and 1530-1534. *Geology of Degree Sheets* Inhnamambo, Maluweru, Chifunde, Zumbo, Fingoè-Mâgoè, Songo, Cazula and Zóbuè, Mozambique. Direcção Nacional de Geologia (DNG), Maputo.
- Hargraves, R. B., Rehacek, J. & Hooper, P. R. 1997.** Paleomagnetism of the Karoo igneous rocks in southern Africa. *South African Journal of Geology*, 100, 2, 195–212.
- Harris, C. & Erlank, A. J. 1992.** The production of large-volume, low-delta (super18) O rhyolites during the rifting of Africa and Antarctica: The Lebombo Monocline, southern Africa. *Geochimica et Cosmochimica Acta*, 56, 3561–3570.
- Harris, C. & Grantham, G. H. 1993.** Geology and petrogenesis of the Straumsvola nepheline syenite complex, Dronning Maud Land, Antarctica. *Geological Magazine*, 130, 513–532.
- Harris, C., Marsh, J. S., Duncan, A. R. & Erlank, A. J. 1990.** The petrogenesis of the Kirwan Basalts of Dronning Maud Land, Antarctica. *Journal of Petrology*, 31, 341–369.
- Harris, C., Johnstone, W. P. & Phillips, D. 2002.** Petrogenesis of the Mesozoic Sistefjell syenite intrusion, Dronning Maud Land, Antarctica and surrounding low- $\delta^{18}\text{O}$ lavas. *South African Journal of Geology*, 105, no. 3, 205–226.
- Hunting Geology and Geophysics Ltda. 1984.** Mineral inventory report. Final report. Governo da República Popular de Moçambique. Ministério dos Recursos Minerais. Direcção Nacional de Geologia. 114 p.
- Irvine, T. & Baragar, W. 1971.** A guide to the chemical classification of the common volcanic rocks. *Canadian Journal of Earth Sciences*, 8, 523–547.
- Jourdan, F., Féraud, G., Bertrand, H., Watkeys, M. K. & Renne, P. R. 2007.** Distinct brief major events in the Karoo large igneous province clarified by new $^{40}\text{Ar}/^{39}\text{Ar}$ ages on the Lesotho Basalts. *Lithos*, 98(1-4):195–209.
- Jourdan, F., Féraud, G., Bertrand, H. & Watkeys, M. K. 2007.** From flood basalts to the inception of oceanization: Example from the $^{40}\text{Ar}/^{39}\text{Ar}$ high-resolution picture of the

- Karoo large igneous province, *Geochemistry, Geophysics and Geosystems*, 8, Q02002, doi:10.1029/2006GC001392.
- Klausen, M. B., Marsh, J. S. & Watkeys, M. K. 2003.** Geochemical variation in the Karoo basalt-rhyolite lava sequence along the northern Lebombo monocline (Olifants River section) (<http://web.telia.com/~u25500123/Abstract2/klausenm2.htm>)
- Lächelt, S. 2004.** *Geology and Mineral Resources of Mozambique*, 1st ed. Direção Nacional de Geologia de Moçambique. Maputo, Mozambique. 515 p.
- Lavwer, L. A., Gahagan, L. M. & Coffin, M. F. 1992.** The development of paleoseaways around the Antarctica. *Antarctic Research Series*, 56, 7–30.
- Le Maitre, R. W., Bateman, P., Dudek, A., Keller, J., Lemeyre, J., Le Bas, M. J., Sabine, P. A., Schmid, R., Sorensen, H., Streckeisen, A., Wooley, A. R. & Zanettin, B. 1989.** *A classification of igneous rocks and glossary of terms*. Blackwell Science Publications, Oxford, United Kingdom, 193 p.
- Lightfoot, P. C., Naldrett, A. J. & Hawkesworth, C. J. 1987.** Reevaluation of chemical variation in the Insizwa Complex, Transkei. *The Canadian Mineralogist*, 25, 79–90.
- Luttinen, A. V. & Furnes, H. 2000.** Flood basalt of Vestfjella: Jurassic magmatism across an Archaean-Proterozoic lithosphere boundary in Dronning Maud Land, Antarctica. *Journal of Petrology*, 41, no 8, 1271–1305.
- Luttinen, A. V. & Leat, P. T. 2007.** A revised geochemical grouping of Gondwana LIP; distinctive sources and processes at the Weddell and Limpopo triple junctions (in: *Antarctica; a keystone in a changing world*; online proceedings for the Tenth international symposium on Antarctic earth sciences). Open-File Report - U. S. Geological Survey.
- Marsh, J. S., Hooper, P. R., Rehacek, J., Duncan, R. A. & Duncan, A. R. 1997.** Stratigraphy and age of Karoo basalts of Lesotho and implications for correlations with the Karoo igneous province, in: J. J. Mahoney & M. F. Coffin (eds.) *Large Igneous Provinces: Continental, Oceanic, and Planetary Flood Volcanism*, pp. 247–272, *Geophysical Monograph*, American Geophysical Union 100.
- Melluso, L., Morra, V., Cucciniello, C., Petrone, C. M., Vasconcelos, L. & Lustrino, M. 2006.** Petrogenesis of Karoo-related bimodal magmatism in southern Mozambique. 21th Colloquium of African Geology. 3–6. July, 2006, Maputo. Abstract volume, p. 120.
- Mendes, F. P. 1965.** Petrografia sobre intrusões dos Libombos. *Revista de Estudos Geológicos da Universidade de Moçambique*, 6, 23–34.
- Miller J. A. & Harris C. 2007.** Petrogenesis of the Swaziland and northern Natal rhyolites of the Lebombo rifted volcanic margin, south east Africa. *Journal of Petrology*, 48, 185–218.
- Muchangos, A. C. 2000.** Mineralogy and Geochemistry of Bauxite and Bentonite Deposits from Mozambique, *Geologica Ultraiectina*, Nr. 192.
- Muchangos, A. C. 2006.** The mobility of rare earth and other elements in the process of alteration of rhyolitic rocks to bentonite (Lebombo volcanic mountainous chain, Mozambique). *Journal of Geochemical Exploration*, v. 88, 1–3, 300–303.
- Pinna, P., Marteau, P., Becq-Giraudon, J. F. & Manigault, B. 1987.** Notícia explicativa da carta geológica de Moçambique na escala 1:1.000.000. Instituto Nacional de Geologia. Maputo. Unpublished.
- Pinto, A. F. & Godinho, M. M. 1975.** Sobre o quimismo do arco Libombo-Chirua (África Oriental). *Memórias, Notas e Publicações do Museu e Laboratório Mineral da Universidade de Coimbra*, 80, 17–32.
- Polderwaart, A. 1944.** The petrology of the Elephant's Head dike and New Amalfi Sheet (Matatiele). *Transactions of the Royal Society of South Africa*, 30, 85–119.
- Polderwaart, A. 1946.** The petrology of the Mount Arthur Complex (East Griqualand). *Transactions of the Royal Society of South Africa* 31, 83–110.
- Reeves, C. V. 1978.** Reconnaissance aeromagnetic survey of Botswana, 1975–7. Final Interpretation Report, Terra Surveys Limited. Botswana Geological Survey and the Canadian International Development Agency, Special Publication, 199 pp.
- Rennie, J. V. L. 1937.** Fósseis das formações vulcânicas dos Libombos. *Boletim de Serviço Industrial, Geologia e Minas*, 1, 13–24.
- Riley, T. R., Milar, L., Watkeys, M. K., Curtis, M. L., Leat, P. T., Klausen, M. B. & Fanning, C. M. 2004.** U-Pb zircon (SHRIMP) ages for the Lebombo rhyolites, South África: Refining the duration of Karoo volcanism. *Journal of Geological Society of London*, 161, 547–550.
- Riley, T. & Knight, K. 2001.** Age of pre-break-up Gondwana magmatism. *Antarctic Science* 13 (2): 99–110.
- Ross, C. S. & Smith, R. L. 1961.** Ash-flow tuffs; their origin, geologic relations, and identification. U. S. Geological Survey Professional Paper, P 0366, 81 pp.
- Saggerson, E. P. & Logan, C. T. 1970.** Distribution controls of layered and differentiated mafic intrusions in the Lebombo volcanic sub-province. *Special Publication Geological Society of South Africa*, 1, 721–733.
- Sheridan, M. F. & Wang Y. 2005.** Cooling and welding history of the Bishop Tuff in Adobe Valley and Chidago Canyon, California. In: *Welding processes in volcanology*. *Journal of Volcanology and Geothermal Research*, 142(1–2), pp. 119–144.
- Sparks, R. S. J., Pinkerton, H. & MacDonald, R. 1977.** The transport of xenoliths in magmas. *Earth and Planetary Science Letters*, 35(2), pp. 234–238.
- Sweeney, R. J., Duncan, A. R. & Erlank, A. J. 1994.** Geochemistry and petrogenesis of central Lebombo basalts of the Karoo igneous province. *Journal of Petrology* 35, 95–125.
- Vuori, S. K. 2004.** Petrogenesis of the Jurassic gabbroic intrusions of Vestfjella, Dronning Maud Land, Antarctica. Ph.D. thesis, University of Helsinki, Finland, Department of Geology 108 p.
- Vuori, S. K. & Luttinen, A. V. 2003.** The Jurassic gabbroic intrusions of Utpostane and Muren: insights into Karoo-related plutonism in Dronning Maud Land, Antarctica. *Antarctic Science*, 15 (2), 283–301.
- Watkeys, M. K. & Sokoutis, D. 1998.** Transtension in south-eastern Africa associated with Gondwana break-up (in *Continental transpressional and transtensional tectonics*) *Geological Society Special Publications*, 135, 203–214.
- Winchester, J. A. & Floyd, P. A. 1977.** Geochemical discrimination of different magma series and their differentiation products using immobile elements. *Chemical Geology* (October 1977), 20(4):325–343.
- Yoder, H. S. 1973.** Contemporaneous Basaltic and Rhyolitic Magmas. *American Mineralogist*, 58(3–4), pp. 153–171.
- Zhang, X., Luttinen, A. V., Elliot, D. H., Larson, K. & Foland, K. A. 2003.** Early stages of Gondwana break-up: 40Ar/39Ar geochronology of Jurassic basaltic rocks from western Dronning Maud Land, Antarctica, and implications for the timing of magmatic and hydrothermal events. *Journal of Geophysical Research*, 108 (B9), Art. No. 2449, doi: 10.1029/2001JB001070,20

Appendix 1. Chemical compositions of the Karoo volcanic rocks. The analyses are divided to the three locations shown in Figure 2. XRF analyses are made in the Chemical laboratory of GTK except rocks samples marked by *, which are analysed in the laboratory of the Department of Geology at the University of Helsinki. b.d.= below detection limit, ** = iron as FeO

Location		Lebombo monocline										Movenne									
Formation	Sabie River	Umbeluzi																			
Code	JrSba	JrUt	JrUt	JrUt	JrUr	JrUr	JrUg	JrUr	JrUt	JrM	JrM	JrM	JrM	JrM	JrM	JrM	JrMq	JrMq	JrMf	JrMr	
Rock type	Basalt	Trachy-dacite	Dacite	Trachy-dacite	Rhyolite	Micro-granite	Rhyolite	Rhyolite	Rhyolite	Basalt	Basalt	Basalt*	Basalt*	Basalt*	Basalt*	Basalt*	Quartz latite*	Quartz latite	Rhyolite	Rhyolite	
SiO ₂ wt%	49,3	67,6	64,2	62,8	73,6	67,6	68,7	69,1	50,0	52,05	50,29	49,92	55,21	51,00	65,2	66,8	77,5	72,7			
TiO ₂	5,18	0,83	0,85	1,21	0,60	0,73	0,67	0,63	3,67	1,58	4,40	3,82	1,85	3,93	0,53	0,36	0,33	0,39			
Al ₂ O ₃	13,2	12,8	12,4	13,4	11,2	13,1	12,9	12,8	13,9	13,69	12,24	13,14	12,69	12,46	15,7	15,2	11,7	13,2			
Fe ₂ O ₃ t	13,12	6,77	9,00	8,39	5,09	6,82	5,60	5,92	14,97	13,26	14,74**	14,27**	12,87**	14,63**	4,41**	4,11	2,25	3,81			
MnO	0,15	0,22	0,16	0,16	0,12	0,14	0,13	0,14	0,21	0,25	0,21	0,23	0,22	0,26	0,13	0,11	0,01	0,02			
MgO	5,65	0,68	0,69	1,53	0,35	0,65	0,53	0,53	4,06	5,51	4,48	4,39	4,33	4,30	1,59	1,19	0,07	0,24			
CaO	9,40	2,77	3,17	3,04	0,94	2,51	2,41	2,32	8,13	10,59	9,11	9,24	8,73	8,75	2,46	2,18	0,46	0,52			
Na ₂ O	2,08	3,67	2,81	3,78	3,35	3,62	2,99	3,53	2,81	2,63	2,52	2,68	2,86	2,60	5,14	5,12	2,67	2,71			
K ₂ O	0,85	3,76	3,90	4,12	3,81	4,07	4,76	4,23	1,21	0,29	1,31	0,99	0,99	1,09	4,24	4,39	4,42	5,24			
P ₂ O ₅	0,60	0,25	0,31	0,34	0,16	0,23	0,20	0,17	0,44	0,16	0,69	1,32	0,23	0,99	0,12	0,08	0,04	0,09			
Total	99,52	99,35	97,50	98,76	99,22	99,47	98,87	99,36	99,39	100,01	99,99	100,00	99,98	100,01	99,51	99,54	99,46	98,92			
Cr ppm	115	b.d.	b.d.	b.d.	b.d.	b.d.	b.d.	b.d.	36	62	80	28	16	12	b.d.	b.d.	b.d.	b.d.			
Ni	110	b.d.	b.d.	b.d.	b.d.	b.d.	b.d.	b.d.	30	47	50	21	28	20	30	b.d.	b.d.	b.d.			
Sc	b.d.	b.d.	b.d.	b.d.	b.d.	b.d.	b.d.	b.d.	34	45	36	34	44	39	b.d.	b.d.	b.d.	b.d.			
V	442	34	43	97	30	b.d.	36	b.d.	487	400	404	279	381	255	70	40	b.d.	b.d.			
Zr	440	1063	1066	982	1099	1081	1016	1114	279	113	374	460	315	796	460	474	476	767			
La	34	107	97	94	113	98	123	104	b.d.	22	16	41	40	55	60	58	116	178			
Ce	98	207	199	200	180	219	247	207	75	37	81	115	93	152	160	145	220	298			
Ba	380	1350	1078	1342	3218	1221	1715	1196	523	164	336	519	369	812	260	167	690	2693			
Sr	980	197	199	280	113	208	190	181	371	170	263	320	134	372	160	106	51	107			
Rb	17	107	114	106	113	113	124	124	28	12	29	30	42	34	410	465	153	182			
Y	43	136	114	98	132	107	112	108	45	38	68	80	72	90	0	162	106	130			
Nb	19	77	76	69	79	75	84	75	20	13	34	39	35	53	0	313	76	116			
Th	b.d.	15	12	13	13	17	16	16	b.d.	3	5	4	7	5	30	38	17	20			
S	b.d.	b.d.	88	b.d.	520	b.d.	164	b.d.	106	b.d.	b.d.	b.d.	b.d.	b.d.	b.d.	b.d.	b.d.	520			
Fe#	0,70	0,91	0,93	0,85	0,94	0,91	0,91	0,92	0,79	0,71	0,77	0,76	0,75	0,77	0,74	0,78	0,97	0,94			
Obs. no	23602	23184	23476-A	23571	17478	23621	23472	23522	23473	19441	19435	23342	17397-B1	19443	mzm3.1.05	23213	23147	17438			
Easting	351766	402172	361577	376439	401822	342890	366027	358099	367891	418269	408155	411494	417399	413976	428131	428363	427827	423881			
Northing	7412661	7127735	7414939	7361656	7152039	7467720	7412481	7421612	7412946	7175937	7185158	7257363	7047351	7176600	7123596	7123749	7085816	7099640			

Appendix 1. Continues

Location Formation	Lebombo Monocline				Nuanetsi-Sabie volcanic flexure				Lupata trough and Moatize-Luia graben										
	Umbeluzi		Pessene		Upper Karoo Dykes		Rio Nhavúdezi		Rio Nhavúdi.		Rio Mazoe		Rio Mazoe		Basaltic andesite				
Member Rock	JrMr Rhyolite	JrMr Rhyolite	JrPal Alkaline lava	Pessene Nepheline syenite	JrPns Dolerite	Dolerite	JrN Basaltic andesite	JrN Basalt	JrN Basalt	JrN Basalt	JrN Basalt	JrNb Basalt	JrNb Basalt	JrNb Basalt	JrNb Basalt	JrNb Basaltic andesite	JrNb Basaltic andesite		
SiO ₂ wt%	76,4	76,4	76,4	48,65	52,0	51,7	47,8	53,0	49,70	50,30	53,60	58,70	46,00	46,60	52,40	54,80	55,70	56,10	61,60
TiO ₂	0,21	0,19	2,93	0,85	3,19	2,16	2,16	1,28	2,61	1,19	1,23	1,97	0,45	0,95	1,13	1,28	1,53	1,41	0,79
Al ₂ O ₃	12,3	12,0	15,65	19,9	12,9	16,4	16,4	14,0	13,50	14,70	14,20	10,80	10,50	16,10	15,00	14,80	15,10	14,10	13,60
Fe ₂ O ₃ t	2,21	2,37	11,39	6,02	15,25	14,27	14,27	11,1	15,64	11,48	11,67	11,53	11,80	10,80	10,30	11,60	10,70	12,00	6,60
MnO	0,01	0,03	0,37	0,38	0,20	0,14	0,14	0,14	0,22	0,14	0,16	0,10	0,16	0,14	0,17	0,11	0,10	0,17	0,11
MgO	0,04	0,06	3,47	0,41	3,22	4,32	4,32	6,12	4,96	6,52	4,94	3,03	20,20	7,08	4,91	3,34	3,25	3,31	3,94
CaO	0,20	0,26	8,11	2,45	7,18	10,02	10,02	6,96	9,55	10,60	8,59	3,55	6,35	12,20	8,99	7,74	6,03	7,14	5,78
Na ₂ O	2,57	2,77	5,89	8,29	2,90	2,57	2,57	3,91	2,60	2,27	2,53	1,74	1,21	2,33	2,80	3,03	3,45	3,02	1,90
K ₂ O	5,47	5,45	2,28	6,19	1,99	0,33	0,33	0,49	0,56	0,85	0,87	2,69	0,42	0,56	1,66	1,82	2,67	1,80	3,61
P ₂ O ₅	0,02	0,01	1,27	0,11	0,99	0,41	0,41	0,13	0,27	0,14	0,17	0,47	0,08	0,25	0,18	0,22	0,35	0,27	0,13
Total	99,42	99,54	100,01	96,61	99,52	98,42	98,42	97,14	99,61	98,19	97,95	94,58	97,17	97,01	97,54	98,75	98,88	99,32	98,07
Cr ppm	b.d.	b.d.	22	b.d.	b.d.	166	166	220	70	508	98	b.d.	2080	230	270	110	40	40	230
Ni	b.d.	b.d.	b.d.	b.d.	b.d.	114	114	130	33	215	61	b.d.	820	130	90	70	20	b.d.	70
Sc	b.d.	b.d.	6	b.d.	34	33	33	b.d.	41	b.d.	b.d.	b.d.	b.d.	40	30	b.d.	b.d.	40	b.d.
V	b.d.	b.d.	b.d.	60	283	340	340	260	434	293	295	264	160	260	250	290	240	300	150
Zr	450	390	1618	1440	598	270	270	90	190	100	133	212	50	70	140	150	310	190	380
La	b.d.	b.d.	274	186	62	34	34	b.d.	b.d.	b.d.	b.d.	36	0	b.d.	30	40	40	30	70
Ce	113	240	540	276	154	74	74	b.d.	47	36	52	72	30	40	60	60	90	70	130
Ba	466	420	1262	2447	679	313	313	140	155	259	410	544	160	380	560	530	600	580	860
Sr	20	20	1977	3127	355	395	395	220	220	195	267	57	110	340	220	220	220	230	220
Rb	192	210	75	168	48	11	11	10	11	30	28	91	20	10	60	70	90	50	80
Y	101	0	82	65	72	46	46	0	42	24	21	30	10	20	30	20	50	40	40
Nb	118	0	348	363	45	27	27	b.d.	14	9	9	12	b.d.	20	b.d.	10	30	20	40
Th	22	20	36	26	b.d.	b.d.	b.d.	b.d.	b.d.	b.d.	b.d.	b.d.	b.d.	b.d.	b.d.	b.d.	b.d.	b.d.	10
S	b.d.	b.d.	b.d.	160	436	b.d.	b.d.	b.d.	336	60	193	358	b.d.	b.d.	100	b.d.	b.d.	60	60
Fe#	0,98	0,98	0,77	0,94	0,83	0,77	0,77	0,65	0,76	0,64	0,70	0,79	0,37	0,60	0,68	0,78	0,77	0,78	0,63
Obs. no	23194-A	mzm3.2.05	19445-A	17441	23476-B	23642	24781	10704	10705,1	10707	10704	34481	14076	14264	14249	15082	14103	14101	14252
Easting	422028	428189	430758	431268	361577	430808	473912	609263	608534	612002	609263	635136	414913	531390	540611	535036	398662	396767	538770
Northing	7119151	7121897	7157784	7150430	7414939	7113337	7708061	7843748	7842728	7849038	7843748	8017203	8220669	8171272	8170894	8138896	8197345	8194082	8170546

Appendix 1. Continues

Location Formation	Lupata trough and Moatize-Luia graben										Serra	
	Chueza			Bangomateta							Bombue	Rhyolite
Member Rock	JrC Basalt	JrC Mafic dyke	JrC Basaltic andesite	JrC Andesite	JrBb Basaltic andesite	JrBb Andesite	JrBb Dacite	JrBr Rhyolite	JrBr Rhyolite	JrBr Rhyolite	JrBr Rhyolite	JrSb Rhyolite
SiO ₂ wt%	52,40	52,60	56,60	57,30	55,60	61,50	68,40	70,10	73,70	78,00	70,60	
TiO ₂	1,29	1,05	0,81	0,89	1,97	0,98	0,72	0,44	0,56	0,55	0,80	
Al ₂ O ₃	14,10	15,20	13,70	14,50	14,10	13,30	13,20	13,40	12,90	9,10	11,60	
Fe ₂ O ₃ t	11,64	13,10	10,01	9,61	11,90	7,82	4,52	4,53	2,74	4,17	5,97	
MnO	0,22	0,20	0,14	0,13	0,09	0,12	0,07	0,07	b.d.	0,03	0,08	
MgO	6,16	4,46	7,46	5,40	2,51	2,42	0,64	0,25	0,06	0,48	0,66	
CaO	9,18	8,99	6,85	7,03	3,54	3,07	1,86	0,54	0,19	1,46	1,53	
Na ₂ O	2,36	2,76	2,16	2,35	3,22	2,52	3,59	3,09	1,12	1,62	2,81	
K ₂ O	1,17	1,10	1,29	1,92	3,46	4,26	1,39	5,87	6,38	4,17	5,11	
P ₂ O ₅	0,18	0,21	0,12	0,14	0,62	0,21	0,18	0,05	0,08	0,12	0,18	
Total	98,69	99,67	99,14	99,27	97,02	96,18	94,57	98,34	97,74	99,71	99,35	
Cr ppm	300	40	417	251	b.d.	b.d.	50	b.d.	b.d.	70	b.d.	
Ni	74	70	74	52	b.d.	b.d.	30	b.d.	b.d.	30	b.d.	
Sc	32	40	b.d.	b.d.	b.d.	b.d.	b.d.	b.d.	b.d.	b.d.	b.d.	
V	301	330	224	212	220	121	70	0	0	60	77	
Zr	142	120	117	130	340	490	340	830	761	200	290	
La	b.d.	b.d.	b.d.	32	50	81	50	160	127	30	61	
Ce	38	50	55	58	100	169	100	260	255	50	99	
Ba	434	340	409	559	750	792	820	1140	1195	640	1244	
Sr	169	170	198	205	200	155	130	60	48	100	119	
Rb	40	50	49	67	110	165	180	200	239	130	200	
Y	29	30	23	23	50	72	40	90	205	20	35	
Nb	12	b.d.	9	12	30	74	30	90	98	b.d.	20	
Th	b.d.	b.d.	b.d.	b.d.	b.d.	20	20	30	29	b.d.	24	
S	b.d.	120	b.d.	b.d.	b.d.	622	600	b.d.	499	b.d.	94	
Fe#	0,65	0,75	0,57	0,64	0,83	0,76	0,88	0,95	0,98	0,90	0,90	
Obs. no	14734	15065	17211	17214	14071	17198	14114	14260	14503,2	14087	34490	
Easting	624901	597229	628949	629546	420215	521520	405729	535392	524478	409038	636880	
Northing	8092174	8169736	8073975	8074634	8227326	8175109	8207966	8169354	8168964	8212677	8016042	

SEDIMENTARY ROCKS OF THE MAPAI FORMATION IN THE MASSINGIR-MAPAI REGION, GAZA PROVINCE, MOZAMBIQUE

by

Robbert Rutten¹, Hannu Mäkitie², Saku Vuori² & João M. Marques³

Rutten, R., Mäkitie, H., Vuori, S. & Marques, J. M. 2008. Sedimentary rocks of the Mapai Formation in the Massingir-Mapai region, Gaza Province, Mozambique. *Geological Survey of Finland, Special Paper 48*, 251–262, 10 figures and 2 tables.

The Mapai Formation (~15 000 km²) occurring in the western part of the Gaza Province of southern Mozambique, is a newly defined Formation of early-Palaeogene age. It embraces a part of the previously defined Rio Singuédzí, Rio dos Elefantes and Cheringoma Formations in the region. The Mapai Formation is divided into 6 members that are characterized by calcareous siltstones, calcareous sandstones and calcareous conglomerates, locally calcified and oxidized. The Mapai rocks typically were deposited from both continental and coastal sedimentation environments, and are locally good outcropping in the river bed of the Limpopo, dos Elefantes and Singuédzí Rivers. In the west, the lowermost limestones of the Mapai Formation overlie volcanic rocks of the Karoo age that are part of the Jurassic Lebombo Monocline. Near the town of Massingir this formation is overlying a fossil-rich, 20 m high sedimentary section, the basal part of which indicates a shallow marine environment. The Mapai Formation is often covered by sandstones, which occur below Quaternary aeolian sands. The Mapai Formation is suspected to be contemporaneous with the Chringoma Formation described in southern Mozambique. In terms of depositional facies it seems the high-stand equivalent of the Upper Cretaceous Grudja Formation only known from subsurface data in the Mozambique Basin.

Key words (Georef Thesaurus AGI): sedimentary rocks, siltstone, sandstone, conglomerate, limestone, stratigraphy, Cretaceous, Paleogene, Mapai, Massingir, Gaza, Mozambique.

¹ *Independent Consultant Geologist, Geo4U, Beethovenstraat 127, 1077 JA Amsterdam, The Netherlands*

² *Geological Survey of Finland, P.O. Box 96, FIN-02151 Espoo, Finland*

³ *Gondwana Empreendimentos e Consultorias, Limitada, Caixa Postal 832, Maputo, Mozambique*

E-mail: ¹*r.f.x.rutten@orange.nl*, ²*hannu.makitie@gtk.fi*, ³*gondwana@tvcabo.co.mz*

INTRODUCTION

Phanerozoic sedimentary rocks of the Mozambique Basin occupy vast areas in southern Mozambique (Fig. 1). In the Province of Gaza, southern

Mozambique, they are poorly known due to the lack of more detailed maps than the 1:1 000 000 scale geological map of Mozambique (Pinna *et al.* 1987).

A few studies from the Gaza region and from the South African border area nearby (e.g. Flores 1961, Botha & De Wit 1996) together with the one million scale geological map and the Sul do Save geological map (Moura 1964) at the same scale, show that Cretaceous to Recent sedimentary rocks occupy in Gaza Province. This interpretation is in accordance with studies by Borges (1944) and Rennie (1943, 1944).

In 2002–2006 the Geological Survey of Finland (GTK) Consortium carried out geological mapping in Mozambique as a part of the *Mineral Resource Management Capacity Building Project, Republic of Mozambique, Component 2: Geological Infrastructure Development Programme, Geological Mapping LOT 3*, covering the southern part of the country. The Gaza Province was also mapped by

quick field checks. The work resulted in 1:250 000 scale maps with explanations (GTK Consortium 2006).

One of the most important results in southern Mozambique was the definition of a new formation named the Mapai Formation, which occupies an area of about 15 000 km² between the towns of Massingir and Mapai in the western part of the Gaza Province (Fig. 1). The new Mapai Formation includes an assemblage of previously defined formations (e.g. Cheringoma, Rio Singuédzí and Rio dos Elefantes) that are currently defined largely based on new observations (GTK Consortium 2006). The stratigraphic position of the new Mapai Formation compared to the aforementioned formations is shown in Table 1. Characteristics of the Mapai Formation are given in this present article.

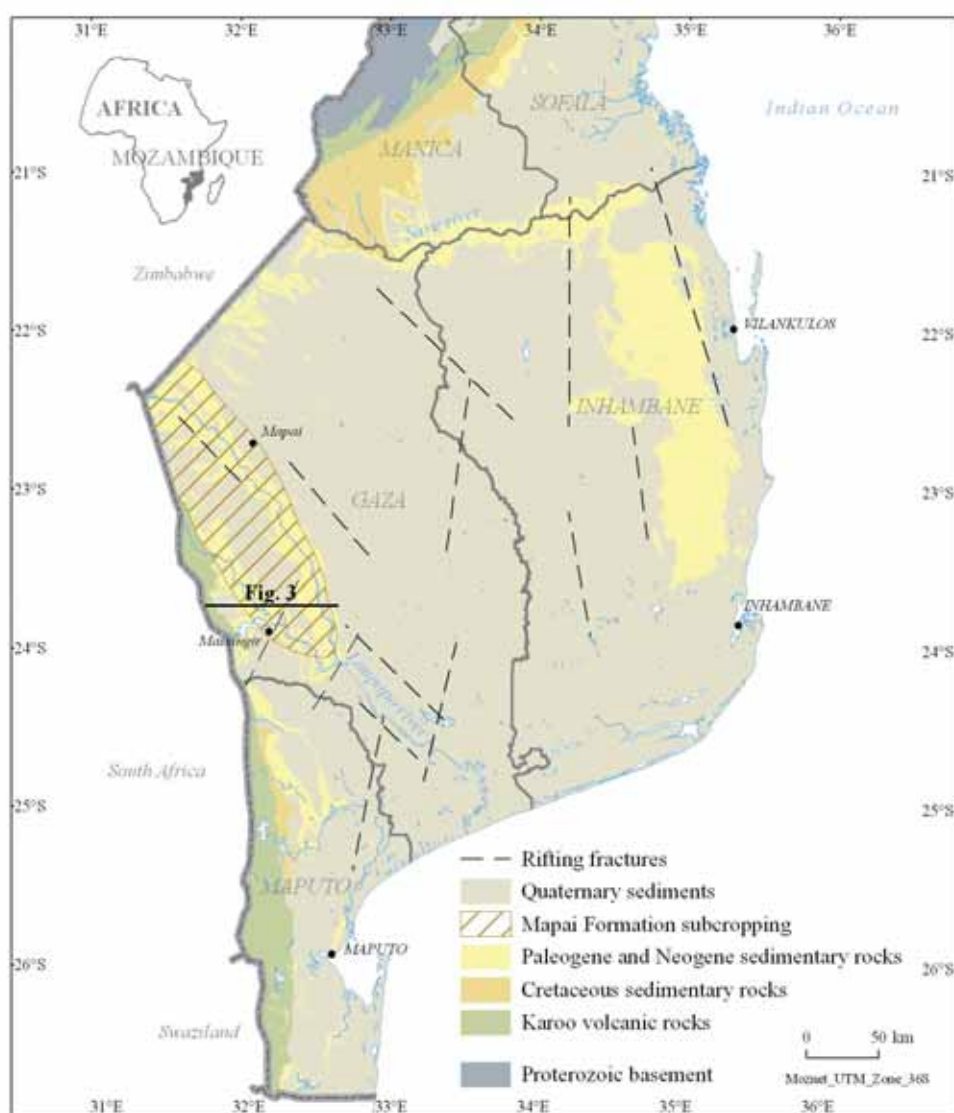


Fig. 1. Simplified geological map of southern Mozambique and the extension of the Mapai Formation. (modified after Lächelt 2004 and GTK Consortium 2006). The area comprising the Mapai Formation outcrops is shown in the map. The position of the E-W trending cross section shown in Figure 3 is marked on the map as “Fig. 3”.

Table 1. Comparison of stratigraphy and formations reported from the Massingir area.

GTK Consortium (2006)		Pinna et al. (1987)		Botha & De Wit (1997)	
Quaternary	Sands	Quaternary	Sands	Quaternary	Sands
Neogene	Mazamba Formation	Neogene	Mazamba Formation		
				Eocene	Salamanga Formation <i>Massingir section</i>
Paleogene	Mapai Formation <i>Massingir section</i>	Paleogene	Cheringoma Formation	Paleocene	Malonga Formation/ Gona-re-Zhou Plateau
Cretaceous	Grudja Formation Sena Formation	Cretaceous	Rio Singuédzí Formation Formation Sena Formation	Cretaceous	Beds Sena Formation/ Rio Singuédzí Formation

REGIONAL GEOLOGY

The Mozambique Basin

In southern and middle Mozambique, the Phanerozoic cover can be divided into the Karoo Supergroup (Permian-Jurassic) followed by a succession of Cretaceous and younger sedimentary formations, partly associated with the development of the East Africa Rift System. Whereas the Karoo Supergroup is connected to continental rifting, the formations coeval with the East Africa Rift System reflect a period of continental drifting and dispersal followed by renewed rifting. The dispersal of Gondwana and the opening of the Indian Ocean are manifestations of the first process. The relatively young East Africa Rift System was initiated in the Cretaceous and accelerated during the Paleogene and Neogene.

This large-scale structural framework gave rise to the development of the Mozambique Basin, which spans an area of ~185 000 km² onshore and some 100 000 km², offshore down to the 500 m isobath. The basin is floored by Jurassic volcanics and filled by Early to Middle Cretaceous and younger sedimentary rocks and subordinate (sub-)volcanic rocks (Lächelt 2004). The maximum thickness of this sedimentary cover exceeds 10 000 m in the Zambezi River delta.

Study of the surface geology of this basin is hampered by the scarcity of outcrops due to low relief depositional surfaces, alteration of sedimentary rocks and the presence of weathering residues such as laterite, calcrete, caliches and ferricrete.

Intensive alteration and oxidation of microfossils seriously hamper the establishment of a biostratigraphic framework. The best detailed stratigraphic studies date back to the 1960s, but their applicability is of a local nature and cannot be extrapolated on a regional scale. This poor stratigraphic definition of lithologic entities complicates the correlation of thin, erosional-bounded sedimentary sequences that due to their low relief and shallow marine or continental origin are assumed to extend over distances of several hundreds of kilometres.

The overall stratigraphical-sedimentary column of the Mozambique Basin can be divided into a shallow platform sequence and deep water sediments restricted to a branching network of predominantly NNW-SSE oriented, asymmetric narrow grabens (e.g. Rutten & Mamad 2006). The first sequence is represented by the shallow subsurface extending over vast areas, but probably not exceeding 150 m in total thickness. It is most often overlain by a thin Quaternary unconsolidated cover like the Manangas or windblown sands. As a consequence, the immediate subsurface geology is completely unknown over an estimated 90% of the land surface. On the other hand, there is a kilometre thick, marine dominated sequence that is only observed in the subsurface of the deep grabens, in the central part of the Mozambique Basin.

The Massingir-Mapai region

According to Pinna *et al.* (1987) and Botha & De Wit (1996), the western part of the Massingir area comprises Cretaceous-Paleocene sedimentary units such as the Malonga, Rio Singuédzí and Rio dos Elefantes that underlie the formations of Cherin-

goma, Mazamba and Salamanga occurring east of Massingir. The Rio Singuédzí and Rio dos Elefantes Formations are westward continuations of the Cretaceous Grudja Formation and are composed of continental to marine sediments, e.g. red sand stones,

conglomerates and siltstones with marine fauna-bearing layers (Salman & Abdulá 1995, Lächelt 2004). For the latter, a Cenomanian age (~95 Ma) was given based on the presence of *Lopha* (*Alectronya*) *ungulata* (Molluscan) fauna (Flores 1961). The Cheringoma Formation is distinguished by the presence of white nummulitic limestones and limestones containing gastropods and echinoderm fauna (Flores 1966). It laterally passes into the Salamanga Formation (Middle-Upper Eocene) and is covered by the Mazamba continental sediments of the Oligocene-Miocene (Lächelt 2004). In the border area between Mozambique and South Africa, volcanic rocks of the Jurassic Lebombo Monocline (see Manninen *et al.* 2008) are outcropped (Fig. 1).

The localities around the town of Massingir situate at the western limit of the reported existence of coastal to shallow water shelf sediments (Lächelt 2004). From Massingir westwards the sedimentary rocks are characterized by continental and coastal terrigenous clastics. Botha and De Wit (1996, Fig. 2) noted that the sedimentary rocks west and north from the town of Massingir (e.g. at Mahosi in northern bank of the Massingir reservoir) are comparable with the Cretaceous–Paleocene Malonga Formation in South Africa and with the Gona-re-Zhou Plateau Beds of Zimbabwe. Besides, they are overlain by the Eocene Salamanga-type fossiliferous formations in the Massingir Dam area. Quaternary aeolian sands and alluvial muddy sands cover the surface.

Within the Massingir-Mapai region, the GTK Consortium proposes a new formation, termed Mapai Formation. This captures the dominant sedi-



Fig. 2. Typical featureless landscape in the Mapai Formation area. 1 km east the Limpopo River, 10 km SW of the town of Mapai.

mentary geological characteristics of several, previously described formations and comes out as a single mappable unit in the field. The Mapai Formation often lies below the Mazamba continental sandstones, which cover large areas in the region. Most often the Mapai Formation underlies a flat featureless landscape characterized by a thin uppermost cover of Quaternary aeolian sands and alluvial floodplain clayey sands (Fig. 2). A west-east trending, ~100 km long profile across the Mapai Formation situated north of the town of Massingir is shown in Fig. 3.

Geophysical maps indicate that the eastern margin of Jurassic Karoo volcanic rocks in the Massingir-Mapai region show intense rifting fractures parallel to their contacts, but also in a NE-SW direction.

SEDIMENTARY ROCKS BELOW THE MASSINGIR DAM; MASSINGIR TYPE SECTION

Immediately underlying the Massingir Dam at Massingir town, a 24 metre high outcrop (for posi-

tion, see “Massingir section” in Fig. 3) was studied in detail and shallow-marine, mostly fossil-rich

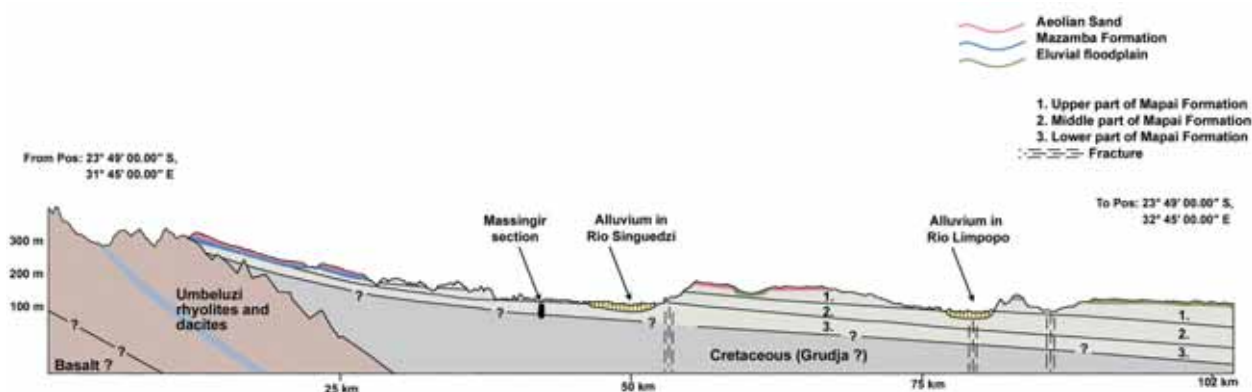


Fig. 3. Schematic W-E trending ~100 km long cross section across the Mapai Formation and overlying sedimentary formations situated in the Massingir area. The section passes some kilometres north of the town of Massingir. The division into upper, middle and lower parts of the Mapai Formation is shown in Table 2.

mixed carbonate rocks and coarse clastic rocks were observed (Figs 4 and 5). The outcrop records an overall upward fining sequence from shallow marine, bioclastic limestones, marlstones, shell beds, to fine calcareous sandstones. The lower contact of this sequence is not exposed. The lowest bed is a composite of very coarse shell material and coarse pebbles. At regular intervals there appear very fossiliferous beds of *Ostrea*-type shells, frequently overlain by fine sandy to marly beds. These *Exogyra* of the *Ostrea* family indicate lower Cenozoic age and when colonialising as occurs to some extent

in the outcrop, result in bivalve framestones. Such beds indicate very shallow marine (10–15 m water depth) settings in the high-energy wave zone.

The upper half of Massingir section is dominated by silty marlstone, some silty mudstone intervals and very fine sandstones indicative of a more open, shallow marine environment. The uppermost few metres of the section show cross-bedding at decimetre scale with well developed metre-large sigmoids that dip to the east. This upper part indicates coastal, possibly tidally influenced deposition in a coastal-lagoonal setting. For more details, see Figs 4 and 5.

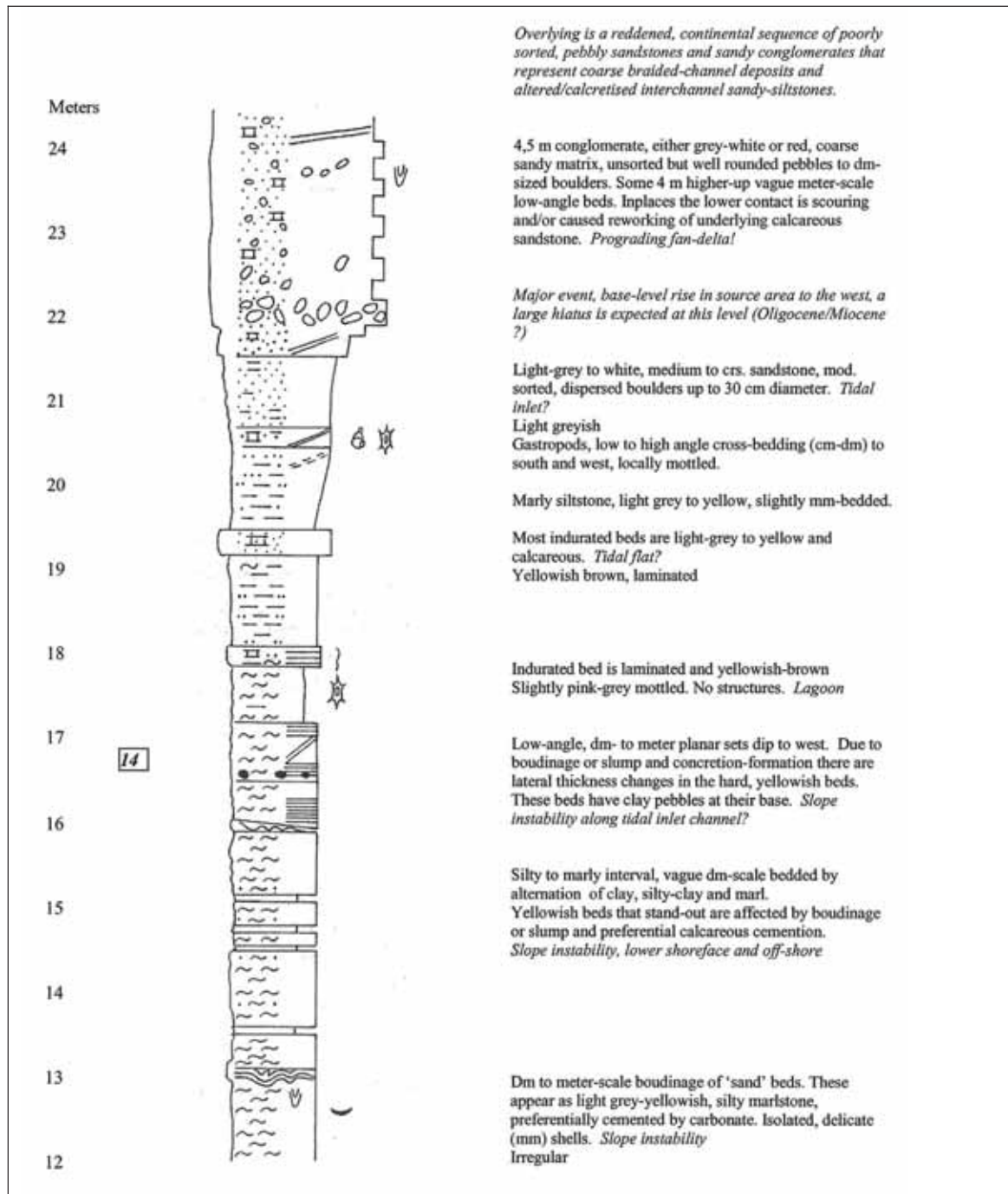


Fig. 4. Sedimentary sequence of the type section below the Massingir Dam. Sedimentary symbols largely adhere to those defined by the International Association of Sedimentologists. Numbered boxes refer to the photos (numbers in scale bars) shown in Figure 5. The profile starts (0–6 m) at 88 metres a.s.l. (0413397/ 73558620) and continues (6–24 m) (0413615/ 7359268) nearby.

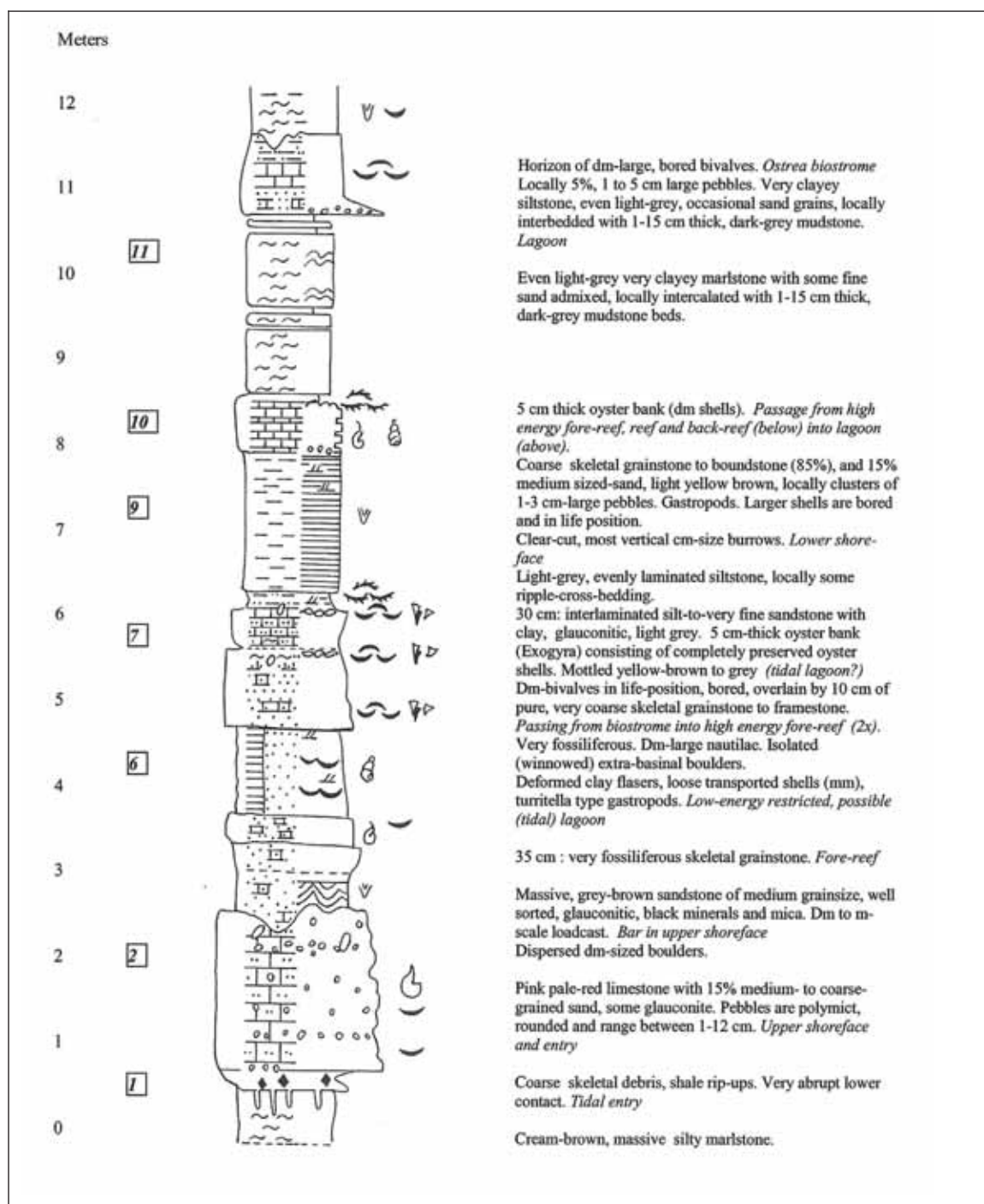


Fig. 4. Continues.

MAPAI FORMATION

The near-horizontal Mapai Formation is mainly exposed along low to steep angle valley slopes of the Limpopo, Uanétzi, Singuédzi and dos Elefantes Rivers, and the reservoir of Massingir Dam. In the west, it unconformably overlaps in places the volcanic rocks of the Lebombo (Libombos in Portuguese) Monocline. The Formation is covered by arkosic sandstones of the Mazamba Formation (TeZ) or, in just a few locations, the Inhaminga Purple Sandstones. Field verification has identified

6 mappable members, which have been assigned the following codes (from top to bottom): Upper Limestone (TeAul), Upper Sandstone (TeAuc), Middle Sandstone (TeAcs), Middle Limestone (TeAml), Lower Sandstone (TeAlc) and Basal Limestone (TeAbl) (Table 2).

However, from a sedimentological point of view it is difficult to use this subdivision in a genetic sense. These deposits consist of coarse-braided alluvial clastic rocks, presumably representing mid channel

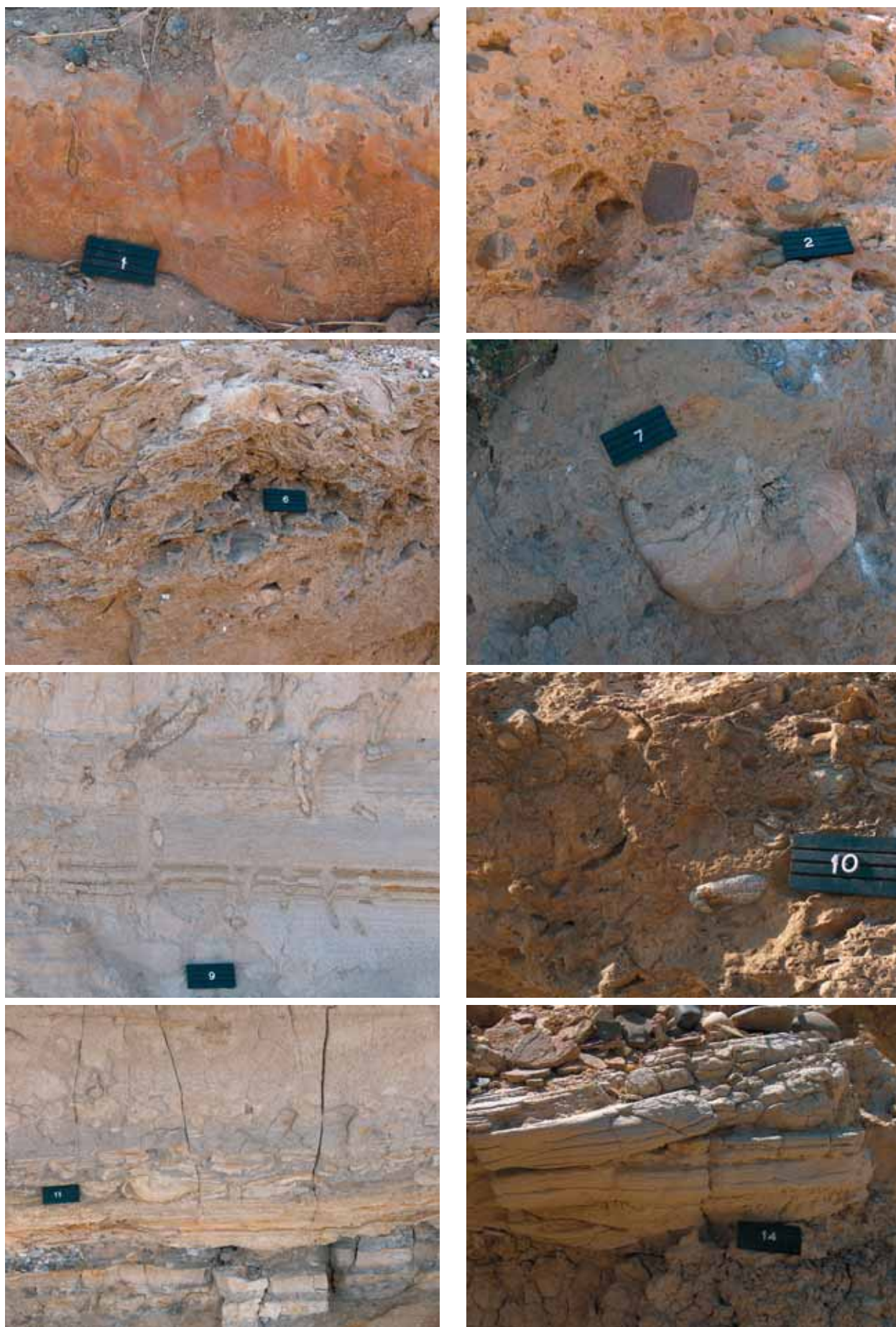


Fig. 5. Selected close-up photos from the Massingir section shown in Fig. 4. The numbers in scale bars refer to stratigraphic positions shown by boxed numbers in (spacing) Fig. 4. The scale bar is 8 cm.

bars (the pebbly and conglomerate intervals) and interchannel areas dominated by finer sands and siltstones. Moreover, limestone dominated intervals may correspond to periods of relative sea level rise due to subsidence.

The relative thickness of the uppermost Mapai Members indicates, in a N-S direction, an inferred stratigraphical order shown in Fig. 6. A brief description of the members is given in next section.

Table 2. The Mapai Formation and its Members.

Formation	Member	Code	
Mapai	Upper Limestone	TeAul	Upper part
	Upper Sandstone	TeAuc	
	Middle Sandstone	TeAcs	Middle part
	Middle Limestone	TeAml	
	Lower Sandstone	TeAlc	Lower part
	Basal Limestone	TeAbl	

Lithology

Basal Limestone (TeAbl)

The sandy to silty limestones are exposed along the Lebombo Monocline, NW of Massingir town and in the Limpopo River valley near the South African border. They represent the lowermost sedimentary unit of the Mapai Formation, deposited on the Karoo volcanic rocks. These limestones are greyish and only weakly bedded, forming low, rounded outcrops. Based on one chemical analysis made by XRF at GTK, the impure limestone (location; 0345392/7458524) has the following main chemical element concentrations; 14.6 wt.% SiO₂, 2.5 wt.% Al₂O₃, 0.97 wt.% Fe₂O₃, 0.04 wt.% MnO, 17.8 wt.% MgO, 25.7 wt.% CaO, and the C-content is 10 wt.%. Trace

element concentrations of the sample are 286 ppm S, 784 ppm Sr and 840 ppm Ba. These concentrations indicate that the rock comprises about 70 % dolomitic minerals.

Lower Sandstone (TeAlc)

The member comprises polymict sandstones and conglomerate layers, which are characterized by a calcareous matrix (Fig. 7). The boulders are mostly composed of rhyolite and quartzose fragments, but large clasts of granitoids, mafic volcanics, and BIF-type rocks are also found, mainly near the Lebombo volcanics. The sequence is here at least 30 m thick. Low-angle cross-bedding is observed.

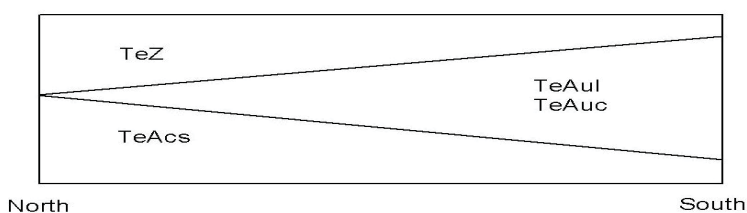


Fig. 6. Simplified stratigraphic order of the uppermost Mapai Formation members, Upper Limestone (TeAul), Upper Sandstone (TeAuc) and Middle Sandstone (TeAcs) and the overlying Mazamba Formation (TeZ) in a 100 km long N-S trending section, approximately from Mapai town in the north to Massingir town in the south.

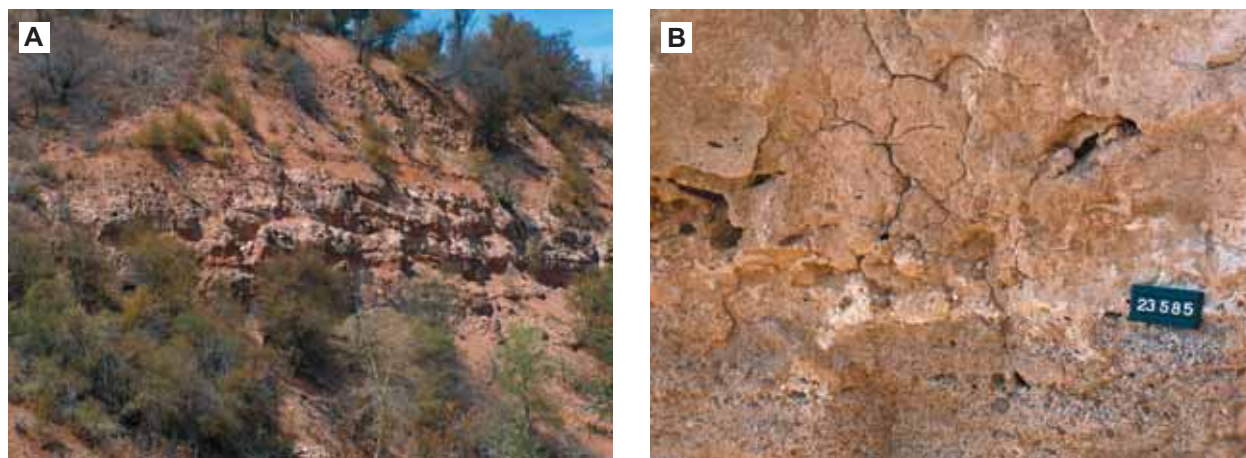


Fig. 7. (A) Calcareous sandstone beds of the Lower Sandstone Member in the Rio Singuédzi River, 1 km east of the Lebombo rhyolites. (B) Close-up photo of the bed boundary in rock of Figure A. Altitude 150 m a.s.l. (0389798/ 7389888). The scale bar is 8 cm.

Middle Limestone (TeAml)

Compared to the outcrops of Lower Sandstone Member nearby, which are usually found in river channels, rocks assigned to the Middle Limestone Member occur on higher located areas where outcrops are few. These rocks are impure limestones and apparently do not form vertically notable units.

Middle Sandstone (TeAcs)

For example, 20 km SW of Mapai town, discontinuous exposures of white-grey, coarse-grained, bioturbated sandstone of the Middle Sandstone Member are found. They expose in the banks of the Limpopo river, often below the Mazamba Formation (Fig. 8). Here, the total exposed interval measures ~50 m in vertical thickness. Starting from the bottom in upward steps of 3 m, this interval shows:

- White, coarse-grained, well-sorted sandstone with a calcareous matrix, massive texture and with vertical, dm-scale burrows;
- As above, but more fine-grained, in places with a reddish colour;
- Gradual upward transition into calcareous siltstone with white and variegated red colours;
- Passing upwards into pure red siltstone with cm-thick calcrete streaks and laminae;
- Higher up again appears white, coarse-grained sandstone with occasional cm-large pebbles.

The same interval also comprises an irregular, coarse bedded (~20 to 100 cm), horizontal to slightly tilted sequence of sandstones, pebbly sandstones and intraformational conglomerate horizons, alternating with sandy siltstone intervals. Sandstones and con-

glomerates are predominantly ferruginous and have brick-red colours with, in places, bleached white zones due to carbonate redeposition (Fig. 8). These whitish calcrete coated horizons mostly affect the medium- to coarse-grained sandstones, presumably as a result of their higher porosity and permeability. Well preserved burrows are frequently observed. These subvertical burrows are often oval-shaped, up to one cm in diameter and 5 to 20 cm long.

Towards the SE along the Limpopo River, similar scattered outcrops can be found containing irregularly distributed red and white, coarse-grained calcareous sandstones with minor pebble horizons, alternating with bioturbated, red silty fine-grained sandstone. Vague dm-scale bedding can be observed in places. Over a wider area, south of the Limpopo River, weathered breccias are irregularly distributed and occur as metre-sized pockets in or around gravelly sandstones. The breccias contain dm- to cm-scale, unsorted clasts derived from sandstone, calcrete and ferricrete that are set in a ferruginous siltstone matrix.

Microscopically, the rock is composed of fine argillaceous matter, fossil fragments and clastic grains. The latter are usually angular to sub-rounded quartz grains. Plagioclase is less abundant. Conglomeratic horizons are composed of quartz or minor plagioclase fragments in a carbonate matrix.

In terms of the depositional setting, these coarse-grained immature deposits were laid down as broad sandy braid-plains, draining the westward, up-scarp margin of the Kaapvaal Craton and Lebombo volcanics. The coastal plains and playas typically consisted of low-relief, braided sandy channels, mid-channel pebble-bars and inter-channel (non-channelized) areas with overbank silt deposition. Incipient weathering and soil formation may indicate partial exposure during sea level low-stands.

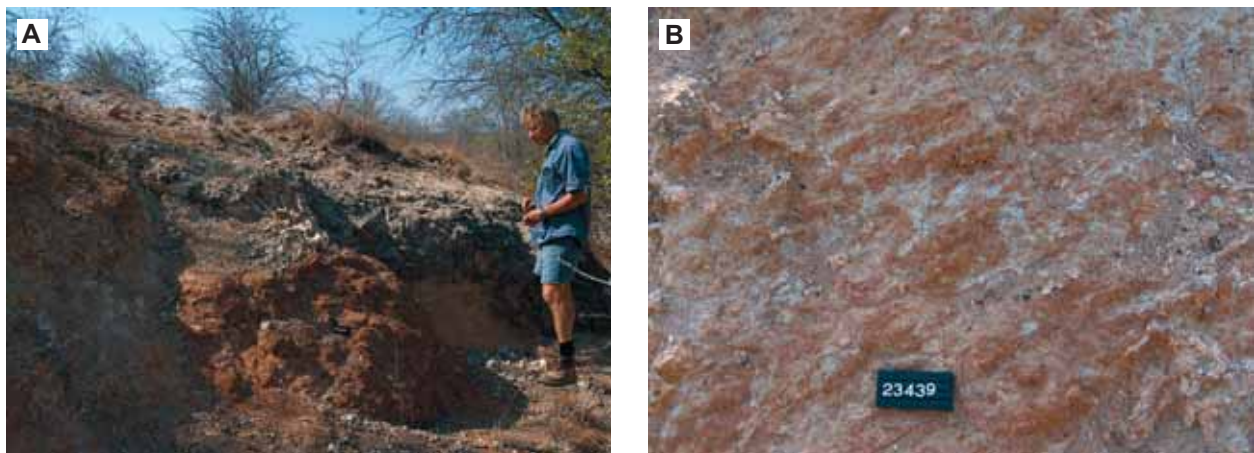


Fig. 8. (A) Typical metre-scale alternation of greyish-green and reddish ferruginous sandstone, pebbly sandstone and sandy siltstone with local bioturbation. The Middle Sandstone Member of the Mapai Formation near the Limpopo River (0395863/ 7474034), at an altitude 238 m a.s.l. (B) Close-up photo of fine-grained silty sandstone of the Mapai Formation, the same location. The scale bar is 8 cm.

Episodically, these braid-plains became inundated as a result of storm-driven floods or rising sea level, temporarily turning the system into a sandy tidal flat. Ophiomorpha-type bioturbation indicates shallow marine to coastal conditions at the time of formation. Bioturbation predominates in the medium- to coarse-grained and often calcareous sandstone intervals and is far less prominent in silty intervals. However, similar forms have also been attributed to rhizo-concretions (Botha & De Wit 1996).

Upper Sandstone (TeAuc)

This member comprises conglomerates (Fig. 9A), but size and amount of the cobbles are smaller

compared to those found in the Lower Sandstone Member. Also here, the matrix is rather rich in carbonates.

Upper Limestone (TeAul)

On some of the highest hills just north of Massingir town, and particularly on the western slope of the Limpopo River valley, there are impure silty limestones defined as the Upper Limestone Member. These rocks are greyish in colour, locally weakly bedded and may form interlayers within the Upper Sandstone Member (Fig. 9B). They also comprise peloids and in rare cases, minor fossils are surrounded by spherical calcitic layers.

COARSE CONGLOMERATES NEAR MASSINGIR TOWN

In Massingir town and its immediate surroundings there are conglomerate layers exposed in the more elevated parts, often preserved at the top of hills (Fig. 9C). Their very coarse, unsorted nature and decametre-scale cross-bedding suggest deposition from an alluvial fan system. The less coarse, contemporaneous rocks around the Massingir Dam

represent the more distal fan-toes and braided fluvial deposits that in turn grade into braid plains towards the Limpopo area. However, the nature and stratigraphic position of these conglomerates is not clear.

Coarse-grained conglomerates, reported from the South African side of the border, have been interpreted as alluvial fan deposits (Malongo Formation;

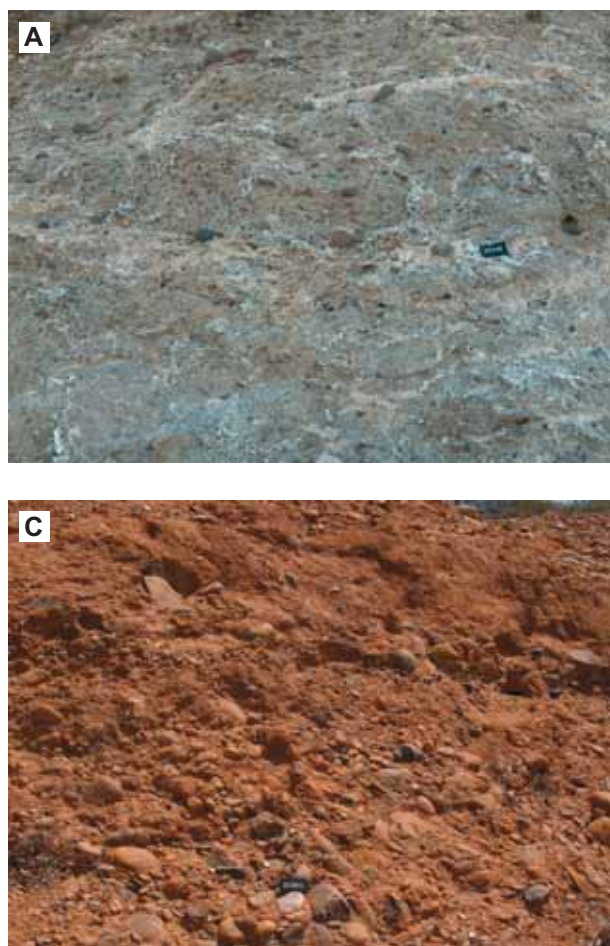


Fig. 9. Sedimentary rocks in the Massingir region. (A) Conglomeratic sandstone of the Upper Sandstone Member of the Mapai Formation. Note the segregated veins of carbonate-rich material. (0461734/ 7363364). (B) Close-up photo of silty limestone of the Upper Limestone Member of the Mapai Formation (0413192/ 7360075). (C) Coarse-grained brownish conglomerate. The highest hill just south of the Massingir Dam. Altitude 150 m a.s.l. (0414109/ 7355542). Scale bars are 10 cm.

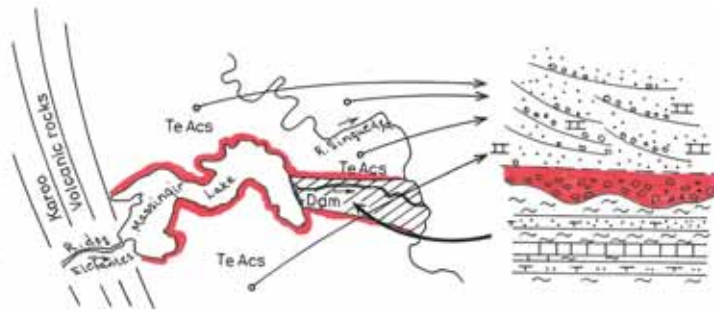


Fig. 10. Plan view (20 km long in E-W direction) of Massingir reservoir lake area on the left. On the right, a sketch of the upper part of the Massingir section. Red is the main conglomerate, below it occur Upper Cretaceous/ Paleocene marine clastic rocks, and above it are situated rocks of the Mapai Formation and Quaternary alluvium.

Botha & De Wit 1996). These very coarse deposits are considered as gravel bed channels, stream floods and debris flows, representing proximal alluvial fans.

The formation of duricrust and related features in the conglomerates, such as the dissolution and re-

deposition of carbonate with the formation of calcrete coatings, indicates incipient pedogenic processes that post-date deposition. The observed colour changes, due to redox reactions (ferro \leftrightarrow ferri), may be partly primary and partly secondary.

DISCUSSION

Major parts of the calcareous silt- and sandstones and conglomerates – previously called the Rio de Singuedzi/Elefantes, Cheringoma and Malonga Formations by Pinna *et al.* (1987) and Botha and De Wit (1996) – are included in the new Mapai Formation in the western part of Gaza Province (Fig. 1). This was done because the sediments often have mappable lithological similarities, although not studied in detail in many places. The thickness of members in the Mapai Formation varies regionally (Fig. 6). Quaternary aeolian sands dominate the platform areas between the rivers of Limpopo and Singuedzi Rivers, while alluvial floodplain clayey sands are common on the eastern side of the Limpopo River.

Field observations by the GTK Consortium indicated that the fossil-rich section just under the Massingir Dam underlies the calcareous siltstone-conglomerates of the Mapai Formation in the Massingir region (Figs. 2 and 10); because the section is nearly horizontal, the overlying sedimentary rocks should continue in a westerly direction along the margins of the dos Elefantes River. Thus, the “boundary” between Cretaceous and Paleogene-Neogene sediments is shifted westwards compared to earlier studies by Pinna *et al.* (1987) and Botha and De Wit (1996). The contact and transition between the lower parts of the Mapai Formation and the fossil-rich sedimentary rocks in the Massingir section is not clearly defined, largely due to coarse unsorted conglomerates that erosively overlie the latter. Moreover, the Basal Limestone Member

(TeAbl) may be Cretaceous in age and refer to an “own” formation, indicating a transgression over the Karoo volcanics.

The lowermost sediments in the Massingir section may directly correlate with the Cretaceous(-Paleocene) fossiliferous Grudja Formation (Flores 1961). In general, this section marks the transition from a mixed carbonate/siliciclastic shallow marine sequence into a coarse clastic, dominantly continental sequence. Between the fossil-rich rocks and the overlying sequence (Mapai Formation) may exist a *hiatus* (Fig. 10).

The above-discussed greatly depends on the relationship between the fossiliferous rock (ends at 110 m a.s.l.) in the Massingir section, late Cretaceous Cenomanian in age (Flores 1961) as compared, for example, to:

- Silty limestones (Upper Limestone Member of Mapai Formation) one kilometre north at an altitude 141 m from Massingir Dam;
- A vertical section of calcareous siltstones-conglomerates (Upper Sandstone Member) which starts at 120 m a.s.l. and ends at 180 m a.s.l. in the Mahosi area, 15 km west of Massingir Dam;
- A calcareous sandstone conglomerate (Lower Sandstone Member) profile, 25 m high, in Singuedzi River (50 km NW of Massingir town), where it starts at 150 m (see Fig. 6);

- A calcareous, sandstone-conglomerate (Middle Sandstone Member) at 105 a.s.l. at the bottom of the Limpopo River valley (72 km north of Massingir town). These sedimentary beds are locally very gently tilted towards the SE.

Observations by the GTK Consortium support the interpretation that sedimentary rocks west of Massingir mostly overlie the fossil-rich rocks beneath the Massingir Dam (Figs 3 and 10). A comparison of the stratigraphic profiles reported from sedimentary rocks and formations in the Massingir-Mapai region was presented in Table 1. The lateral continuity of sedimentary facies environments near and north of

the Massingir area should be studied more detail in the future.

This study is to a large extent hampered by the lack of determining properly-dated stratigraphic relationships. Recommendations for further studies also include:

- The elaboration of a microstratigraphical and/or chemo-chemical stratigraphical data campaign in a selected part of the field;
- Intergration of these data with shallow bore hole data;
- Consideration of the local coverage of high resolution, shallow seismic data.

REFERENCES

- Borges, A. 1944.** Depósitos conglomeráticos do Alto Limpopo. Boletim dos Serviços de Indústria e Geologia, Lourenço Marques, Moçambique 6, 5–12.
- Botha, G. A. & De Wit, M. C. J. 1996.** Post Gondwanan continental sedimentation, Limpopo region, southeastern Africa. *Journal of African Earth Sciences* 23, 163–187.
- Flores, G. 1961.** Outline of the geology of Mozambique. Mozambique Gulf Oil Co., Serv. Geol. Minas, Lourenço Marques, Moçambique. Unpublished Report
- Flores, G. 1966.** Geology of the Cheringoma uplift. Mozambique Gulf Oil Company. Serv. Geol. Minas, Lourenço Marques, Moçambique. Unpublished Report.
- GTK Consortium 2006.** Map Explanation; Volume 1: Sheets 2032–2632. Geology of Degree Sheets: Espungabera/Chibabava, Nova Mambone, Massangena, Chidoco, Save/Bazaruto, Chicualacuala, Machaila, Chigubo, Mabote/Vilankulos, Rio Singuédzí/Massingir, Rio Changana, Funhalouro/Inhambane, Chilembene, Chókwè, Zavala/Inharrime, Maputo, Xai-Xai/Zavala and Bela Vista, Mozambique. Direcção Nacional de Geologia (DGN), Maputo.
- Lächelt, S. 2004.** Geology and Mineral Resources of Mozambique. DGN, Maputo, 515 pp. ISBN 1-919908-52-8.
- Manninen, T., Eerola, T., Mäkitie, H., Vuori, S., Luttinen, A., Sérvano, A. & Manhica, V. 2008.** The Karoo volcanic rocks and related intrusions in southern and central Mozambique. Geological Survey of Finland, Special Paper 48, 211–250.
- Moura, A. R. 1964.** Nota Explicativa do Esboço Geológico do Sul do Save (Escala 1:1 000 000). Serv. Geol. Minas, Lourenço Marques, Moçambique. Unpublished Report.
- Pinna, P., Marteau, P., Becq-Giraudon, J-F. & Manigault, B. 1987.** Carta Geológica de Moçambique, na escala 1:1 000 000, Instituto Nacional de Geologia de Moçambique, Maputo, Moçambique.
- Rennie, J. V. L. 1943.** Fauna do Cretácico Superior do Grudja, vale do Buzi, Colónia de Moçambique. Boletim dos Serviços de Indústria e Geologia, Lourenço Marques 5, 27–48.
- Rennie, J. V. L. 1944.** Estudo paleontológico do jazigo de Mabosi; fossils from Mabosi, conglomerados de Lourenço Marques. Boletim dos Serviços de Indústria e Geologia, Lourenço Marques 6, 13–37.
- Rutten, R. F. X & Mamad, A. 2006.** Sedimentary geology of the shallow subsurface in Mozambique: how to establish regional correlation and define a tectonic-sedimentary framework. 21st Colloquium of African Geology, Maputo, Mozambique, Abstract volume, p. 247.
- Salman, G. & Abdulá, I. 1995.** Development of the Mozambique and Rovuma sedimentary basins, offshore Mozambique. *Sedimentary Geology* 96, 7–41.

GEOCHEMICAL SURVEYS IN MOZAMBIQUE: A DATA COMPILATION PROJECT

by
Esko Korkiakoski

Korkiakoski, E. 2008. Geochemical surveys in Mozambique: a data compilation project. *Geological Survey of Finland, Special Paper 48*, 263–287, 23 figures and four tables.

The existing regional geochemical survey data of Mozambique have been compiled into a digital format as part of the Geochemical and Industrial Mineral Surveys project (GIM). The work was financed by AfDB and implemented in 2005–2007 by the GTK Consortium, in close collaboration with the National Directorate for Geology (DNG). Most of the surveys were carried out in the 1980s using variable analytical methods and sampling strategies. In total, geochemical regional sampling covers approximately 30% of the country but, unfortunately, analytical data are missing for several surveys.

As the data collected from different sampling programmes was only stored as hard copy maps and data tables without digital geographical references, the majority of the maps had to be scanned and georeferenced for data capture. The spatial and analytical data were obtained by on-the-screen digitization using the ArcGIS programme and stored in the **GIM Geochemical Database (GIM_GDB)** consisting of two main components: (1) the Survey Information Table (SIT), containing general survey specifications (i.e. metadata), and (2) the Analysis Data Tables (ADTs). In older surveys from the 1980s only the base metals have typically been analyzed. This is complemented by reanalyzing some one thousand selected old samples for Au, Pd and Te by the GIM project.

In addition to the data compilation, a new stream sediment survey was carried out for training purposes as part of the GIM project. It covered about 5000 km² and included 430 composite samples taken from pre-defined and pre-numbered locations, each representing a cell 10 km² in size. This was followed by a detailed soil survey in five anomalous areas, including 1262 samples and 41 km² in total.

The compiled spatial geochemical data were classified and plotted as various elementary maps and correlated with different geological units utilizing the results of the recent geological mapping projects of Mozambique (GTK Consortium, Norconsult Consortium (NGU-BGS) and Council for Geoscience). The integrated geochemical data indicated several potential anomaly areas for future exploration. The GIM_GDB is commercially available to interested companies from DNG.

Key Words (GeoRef Thesaurus AGI): geochemical surveys, stream sediments, soils, geochemical anomalies, data interpretation, data bases, Mozambique.

Geological Survey of Finland, P.O. Box 77, 96101 Rovaniemi, Finland

E-mail: esko.korkiakoski@gtk.fi

INTRODUCTION

As part of the Mineral Resource Management Capacity Building Project of Mozambique, the Geochemical and Industrial Mineral Surveys (GIM) project was carried out in 2005–2007. The project, valued at USD 1.5 million, was financed by the African Development Bank (AfDB) and implemented by the GTK Consortium consisting of the Geological Survey of Finland (GTK) and Gondwana Ltda as a local partner. The main objective of the project was to increase private mining sector investments in Mozambique by providing the basic background information for exploration companies by compiling the existing geochemical data from earlier surveys into a digital format. Additionally, new geochemical studies, including regional stream sediment and follow-up soil surveys, were implemented for training purposes in collaboration with the National Directorate for Geology (DNG) (see Korkiakoski *et al.* 2008, Korkiakoski 2007 and 2006).

Wide areas of Mozambique (totalling about 800 000 km²) have been targeted over the years for regional and more detailed, exploration types of geochemical surveys. The early 1980s in particular was an intensive period of activity and about 30% of the country has now been covered by regional geochemical surveys. The geochemical surveys with available analytical data carried out in Mozambique have concentrated on northern crystalline bedrock areas and are indicated in Fig. 1. As most of the available geochemical data were originally only available as hard copy maps and data tables, the majority of the maps had to be scanned, georeferenced and digitized for the final data capture. Unfortunately,

the geochemical data for several surveys were missing.

The previous surveys were rather heterogeneous in terms of sampling methodologies and analytical procedures. As early geochemical programmes normally targeted base metals, the element combination was usually limited, and gold was not analysed.

The outcome of the project, the digital and easy-to-use GIM Geochemical Database (GIM_GDB), compiling the existing geochemical data of Mozambique, is commercially available to exploration companies at the DNG. The results also include interpretation of geochemically interesting target areas for further exploration (Korkiakoski 2007). These anomalous areas are geologically correlated with the outcome of the recent geological mapping projects by the GTK Consortium (2006a-d, see also this volume), Norconsult Consortium and Council for Geoscience (CGS).

Training has been an integral part of the GIM project. In addition to the specific training courses and lectures, participation of the DNG staff in all project phases was the main element of the learning process. It included the use of Geographical Information Systems (GIS) in digital, on-the-screen data capture and software applications (ArcView and ArcGIS) in the planning, implementation and interpretation of geochemical surveys. The field methodologies and use of GPS as an integral part of the sampling process have been described in detail in a separate GIM Field Manual (Korkiakoski & Salminen 2006).

DATA EVALUATION AND COMPILATION

At an early stage of the project it was found that only a very minor proportion of the existing geochemical data was in digital format; most of the data were stored as hard copy maps. Initially, the archives of the DNG and National Directorate of Mines (DNM) were checked and available geochemical data sets were collected and evaluated. The geochemical surveys that were included in the digital processing (data capture) were separated from those that were manually stored in the existing DNG archives. The relevant and usable information (metadata) of each geochemical sampling programme, including sampling density, sample media, field methodology, analytical methods and element

combination, have been compiled and transferred into the **Survey Information Table** (SIT- Table 1).

Those geochemical maps selected for digital processing were scanned and georeferenced. Georeferencing was carried out with ArcMap 8.3 using the river systems of the TM satellite images as a base. The field correlation of the TM images had been carried out earlier by the geological mapping projects (areas LOT 2 and 3, see Pekkala *et al.* 2008) using easily recognizable features such as bridges, river and road crossings as reference points. Following the coordinate system used by the mapping projects, the UTM/WGS84 – Zone 36S was applied. The distribution of the different survey areas was digitally stored into a polygon type of ArcView shapefile.

DATA CAPTURE

As most of the geochemical data at DNG/DNM were originally only available as hard copy maps, the data capture was carried out by on-the-screen digitizing of the scanned and georeferenced maps. In normal cases, this included two stages: (1) digitizing the sample locations from georeferenced geochemical maps into the ArcView shapefiles (point type), and calculating the coordinate values of each sampling point, followed by (2) capturing and tabulating the analytical data into spreadsheet tables. These data sets were combined into the point type of ArcView shapefiles with ArcMap 8.3 or ArcView 3.2 (cf. Fig. 1).

Due to the heterogeneity of the data sets in terms of element combinations, analytical methods, accu-

racy and other factors, individual and separate data tables, termed Analysis Data Tables (ADTs), were formulated for each geochemical sampling programme.

The ADTs include the following information:

- sample numbers (original, if available),
- georeferenced coordinates (UTM-WGS84-Zone 36S, metric system), and
- analytical results of each available element

The collected and captured data were combined into the GIM Geochemical Database (GIM_GDB) consisting of the following major components: a Survey Information Table (SIT) and Analysis Data Tables (ADTs).

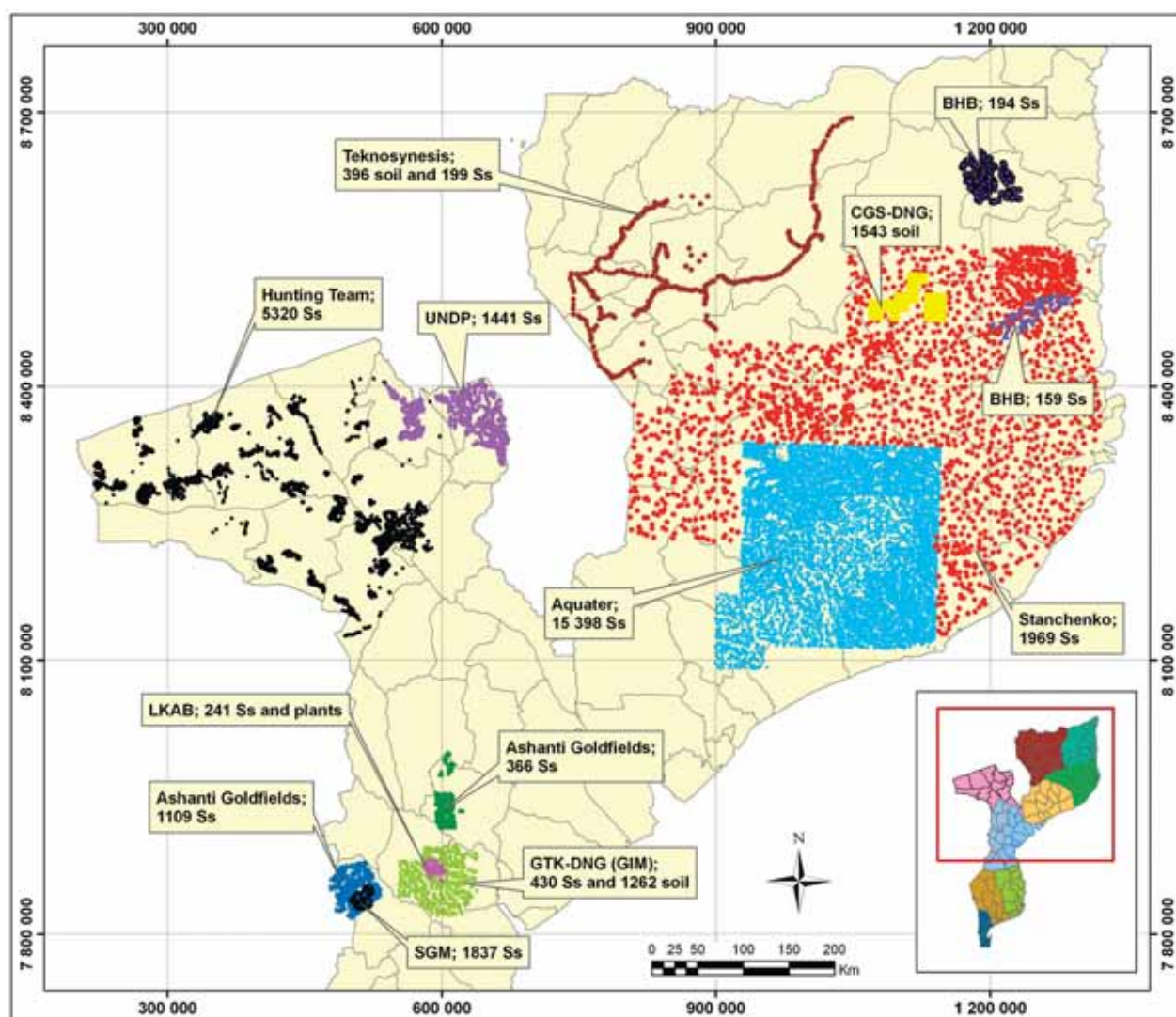


Fig.1. The sampling points of major geochemical surveys in Mozambique with captured digital analytical data. The number of captured sampling points and sample types (Ss = Stream sediment) are shown together with the organization / company. For details of each survey, see Table 1.

Table 1. The Survey Information Table (metadata) of the major captured geochemical surveys. *) The values in parenthesis indicate the number of samples in digital format.

Company / Organisation	Type	Area	Province	Year	Sampling method	*) No of Samples (digital)	Area (km ²)	Samples/ km ²	No of Elements	Analytical method	Notes
GTK-DNG (GIM)	Regional	Inchope	Manica	2005	Stream sediment (Ss) sampling based on 10 km ² cell (most representative site in each cell)	430 with 25 dupl. + 18 regional	5 000	0.08	30/36/ 3	ICP-EAS with Aqua regia leach at 90 °C, XRF and GFAAS for Au, Pd and Te	Pre-defined sites (5 sub-samples over 200 m); GPS orientation
GTK-DNG (GIM)	Follow-up based on regional	Inchope	Manica	2006	Follow-up soil sampling in 50 x 100, 100 x 200 or 500 x 100 m ² grids (5 subareas)	1262 + 85 dupl.	41	variable	30/36/ 3	ICP-EAS with Aqua regia leach at 90 °C, XRF and GFAAS for Au, Pd and Te	GPS and GID aided sampling
Hunting team	Regional	Tete	Tete	1981-1983	Ss sampling concentrated in areas of interest including follow-up.	6 633 (5320 incl. 65 HMC)	55 000	0.126	> 9	AAS. Digestion varied	1050 samples reanalyzed for Au, Pd and Te
UNDP	Regional	Angonia-Macanga	Tete	1981-1982	Active Ss; 300 g sample collected, dried and sieved into -80 mesh	1) (1492 Ss) 3) 572 HMC 3) 532 Rock	8070	0.55 ; 1 sample/ 2.5 km ²	6; in pilot study 15 elements	Perkin Elmer 5000 AAS. Also by ICP 3200 quantometer.	Planned area 8175 km ² . Also pilot study. Only Ss
Ashanti Goldfields	Regional	Rotanda-Mavita	Manica	1996	Ss; 2 kg samples	1109	2370	0.5	1	BCL (Bulk Cyanide Leach)	Au only
Ashanti Goldfields	Follow-up exploration	Bandire, part of Rotanda-Mavita	Manica	1998	Soil sampling; 1) 800x100m ² grid, followed by 2) 400x100m ² grid	1) 640 2) 425	1) 96 2) 2	6.6	1		Au only
Ashanti Goldfields	Regional	Gorongosa	Manica		Ss sampling	543 total (366)	1666	1.7			Au only
SGM	Regional	Mavita	Manica	1970-1973	Ss sampling	1837	287	4.6	4		4 elements as pie charts
Aquater (Italia)	Regional	Nampula, Zambézia	Nampula, Zambézia	1981-1983	Sampling in two phases, A and B; Ss (3-6 kg) was sieved into -80 mesh	28546 total; (15123 Ss)	A: 18750 B: 29250 TOT: 48000	0.31	24	Ss; Quantometer (= ICP 3400) 14015; AAS 10357	15 123 points, not all samples completely analyzed
Tecnosynthesis (Italia) and DNA	Regional	Lugenda River	Niassa, Cabo Delgado	1978-1979	Ss; two sub-samples with 100-200 m distance from the central part of the river. Also soil	395 S 199 Ss	60 000	1) 0.0065 2) 0.0033	16 + 3	XRF + Gamma spectrometer for 100 Ss samples	DNA = Dept National do Aqua
Stanchenko/ BRGM (France)	Regional	Niassa, Cabo Delgado, Zambézia, Nampula	Niassa, Zambézia Nampula	1970-1973	Ss sampling and HMs, Ss samples; 1 sample / 2 km ² . For Stanchenko 1 sample/ 66 km ²	50306; plan, 49799; collected (1969)	110 000	0.5 (0.02)	4 in Maputo + 22 in Orleans	AAS Perkin Elmer spectrometer. In Orleans semi-quantitatively 22 elements by ICP Quantometer	Stanchenko study with 1969 samples showing St. Dev. Details not known
LKAB (Sweden)	Regional and follow-up	Inchope-Doerói	Manica	1979	<0.5mm Ss and organic material. (plant roots). Follow-up in 6 areas	241	428	0.8	3 + 1 (roots)	XRF (sorted minerogenic material) and ICP (roots; dry weight -ashed)	Nb, Sn and Ta. La from plant roots
CGS/DNG	Regional	Namuno-Balama	Cabo Delgado	1996	Helicopter sampling of soil (2-3 kg). GPS; ± 100 m	1544	1 801	0.9	24	XRF; Philips PW 1606 spectrometer	
BHB	Regional	Namapa	Nampula, Cabo Delgado	1997-1998	Ss sites 3-5 km apart, 2 kg sample + 1 kg sample; -1 mm for BCL and -80 mesh for ICP.	159 Ss, 25 HMC	2091	0.1	BCL; 11 ICP; 24	BCL; Bulk Cyanide Leach	HMC= Heavy Mineral Concentrate
BHB	Regional	Meluco	Cabo Delgado	1997-1998	Ss sites 3-5 km apart, 2 kg sample + 1 kg sample; -1 mm for BCL and -80 mesh for ICP.	194 Ss, 21 HCM	2972	0.07	BCL; 11 ICP; 24	BCL; Bulk Cyanide Leach	

SURVEY RESULTS

The results of the data compilation and interpretation of different geochemical surveys carried out in Mozambique over the years are presented in the following chapters (cf. Fig. 1). The general outcome of the project has been earlier briefly described by Korkiakoski (2006), Korkiakoski *et al.* (2008) and Manjate & Mujui (2006). Besides the compilation of data from earlier survey, the following chapters also summarize the results of the new stream sedi-

ment and follow-up soil surveys carried out as part of the GIM project.

It should be noted that only those elements and element associations that are considered to be the most anomalous are included in this discussion. For more detailed description and follow-up interpretation, please refer to the final report of the GIM project and attached GIM_GDB data DVD (Korkiakoski 2007). For reference to the metadata of each specific survey, see Table 1.

GIM field survey

The GIM field survey area is situated in the border zone between the Manica and Sofala Provinces, central Mozambique. The area, referred as Inchope, is known for its Nb-Ta-bearing tin-pegmatites and also includes the Monte Xiluve carbonatite complex

and the alluvial gold deposits of Rio Muda (Korkiakoski 2007 and 2006). The area of an earlier LKAB geochemical stream sediment survey (LKAB 1980), with analyses of La, Sn, Nb, and Ta, is within the study area.

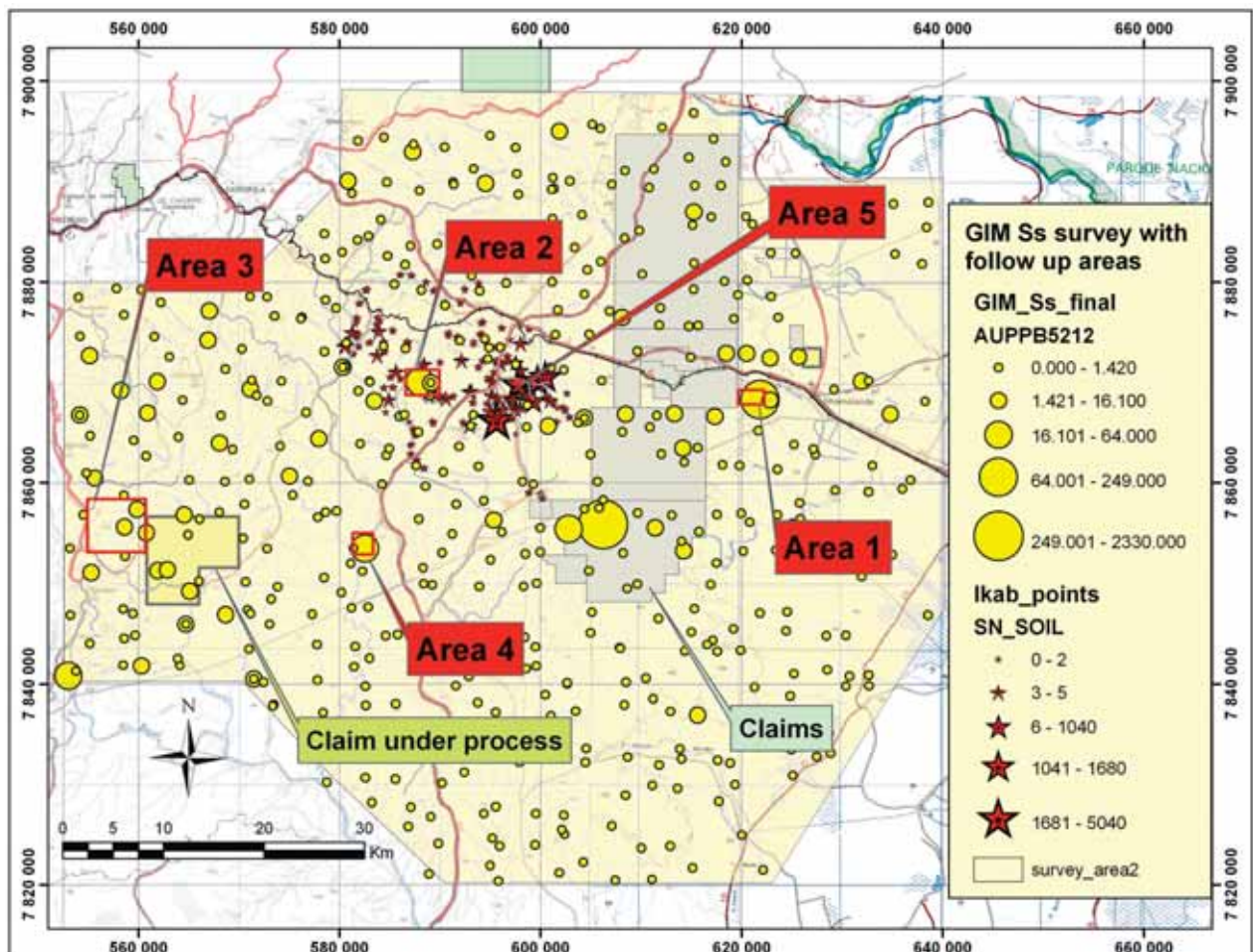


Fig. 2. GIM stream sediment survey and follow-up soil sampling areas 1-5 (red). Areas 1-4 were selected on the basis of anomalous gold values (shown as yellow dots) of the GIM Ss survey, whereas area 5 represents a follow-up survey of an earlier LKAB tin study (LKAB 1979 and 1980) shown by red stars (units in ppm). The claim areas are also shown. For the location, see Fig. 1.

Sampling was carried out in two stages, including (1) regional stream sediment and (2) follow-up soil surveys. For both survey types, sampling sites were digitally pre-selected and pre-numbered using GPS for field orientation and site location. The field procedures and sampling methodologies are described in detail in the GIM Field Manual (Korkiakoski & Salminen 2006).

The regional stream sediment (Ss) survey covered about 5000 km². In total, 430 pre-defined Ss sampling sites, each representing a cell size of 10 km², were sampled. Each sample consisted of five sub-samples collected at 50 m intervals over a distance of 200 m. The follow-up soil survey, carried out in five target areas, covered 45.1 km² in total and included 1262 samples. Selection of the soil survey areas was predominantly based on the GIM Ss survey; four out of five targets were related to anomalous gold values, and one was based on results of the earlier LKAB study with elevated Sn values (up to 0.5%) (Fig. 2). The sampling density varied between target areas but sampling was performed using regular 50 m x 100 m to 500 m x 1000 m grids.

The sample material was processed in the field into the < 2 mm fraction using a plastic sieve.

The training of DNG geochemists and field teams played an important role in the GIM field survey and they are now able to independently carry out objective-oriented, GIS-aided geochemical surveys.

Analytical methods

After preliminary preparation of the samples at the DNG Laboratory in Maputo, they were taken to GTK Laboratories (now a separate company named Labtium Oy) in Finland for multielement-multi-method analysis including ICP-AES, GFAA (Au, Pd and Te) and XRF. After drying the samples at 70 °C, they were sieved to the <0.180 mm grain size and ground in a tempered carbide steel grinding vessel. ICP-EAS analysis was performed after partial aqua regia leach at 90 °C and GFAAS analysis after aqua regia leach at 20 °C, using a 5g sub-sample and Hg-coprecipitation. The methods have been described in detail in the Final Technical Report of the GIM project (Pekkala *et al.* 2007).

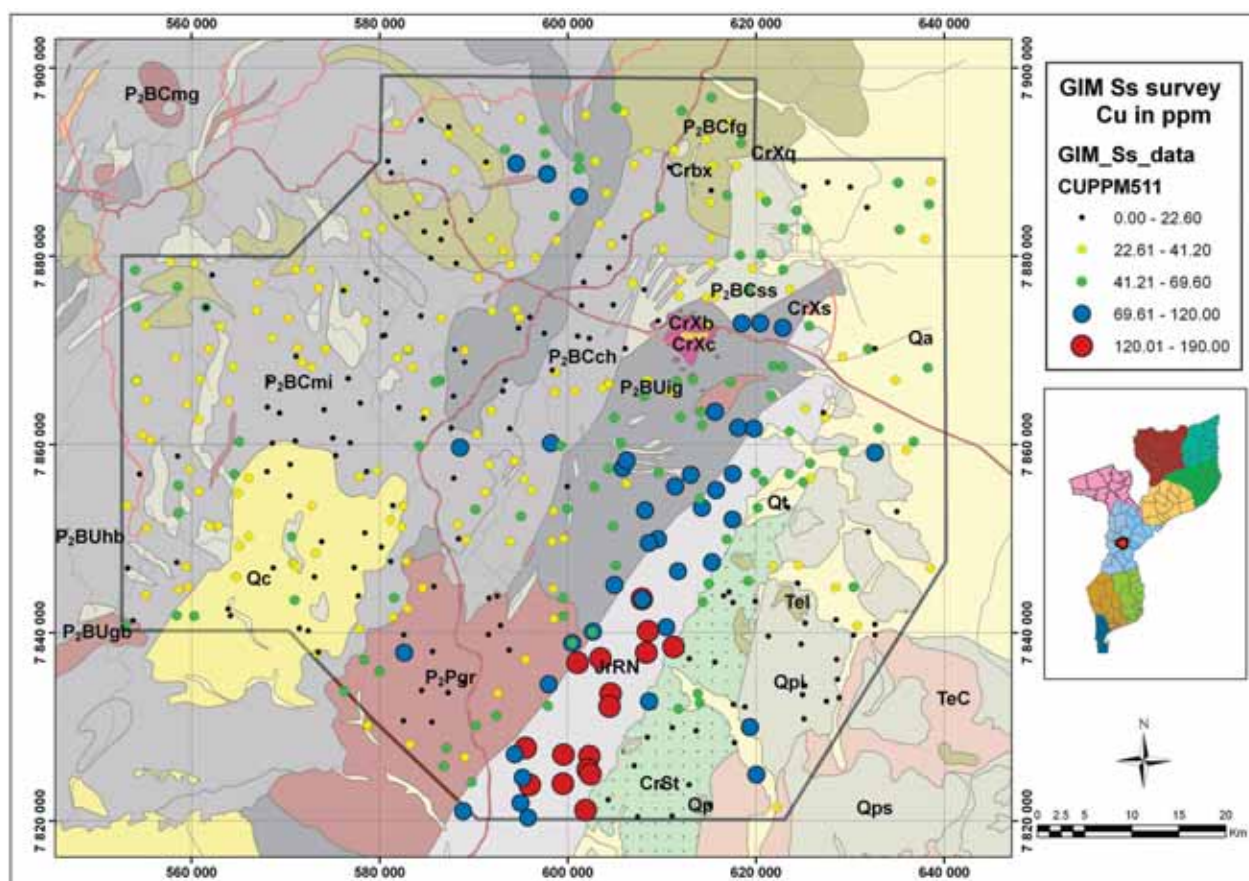


Fig. 3. Copper content of 430 stream sediment samples in the GIM survey area plotted on a geological map. High Cu values correlate locally with the geology and especially with the NE-SW trending zone of Karoo mafic volcanic rocks shown in light blue (JrRN). The main geological units of the GIM stream sediment survey area are: migmatitic paragneisses (P₂BCmi, light brown) and mica schists and mica gneisses (P₂BCch, pinkish brown) of the Chimoio group. Igneous rocks: 1079 Ma old Inchope orthogneisses (P₂BUig, dark brown) and Pamassara granitoids (P₂Pgr, red brown). Others: Monte Chissui gneisses (P₂BCfg, brown), the Cretaceous Xiluvo Carbonatite Suite (CrXb/CrXc, purple and yellow) and Sena Formation (CrSt, green) of the same age. Younger Quaternary cover deposits mainly occur in the east (Qa/Qc/Qt/Qpl/Qps). The geology is based on recent mapping by the GTK Consortium in the LOT 2 area.

GIM stream sediment survey

The statistical data of the GIM stream sediment survey showed that median Cu content is 31.1 ppm, the maximum value being clearly anomalous at 190 ppm. The comparable values for Zn are 48 and 179 ppm. Sixty-four percent of the gold values are below the detection limit of 0.5 ppb and only 5% of the samples are above 2.1 ppb. The major element data analyzed by XRF shows that the median content is 62.6% for SiO₂, 13.7% for Al₂O₃, 5.9% for Fe₂O and 2.5% for K₂O. Some elements, such as Cu and Fe, seem to correlate with certain geological units/rock types (cf. Fig. 3).

Economically the most interesting results of the GIM study are related to gold contents and several anomalous areas were detected by the Ss survey, which also form the basis for the follow-up soil survey (see Fig. 2). An unusually high gold value of 2.3 ppm was detected in one of the tributaries of River Muda, in the centre of the study area. On the geological map (cf. Fig. 3) this anomalous area is related to the Inchope orthogneisses (P₂BUig) occurring together with siliciclastic metasediments

(P₂BCss). Unfortunately, due to the existing claim, it was not possible to carry out a follow-up survey for that sample.

GIM soil surveys

In GIM soil sampling, the sample weight was 0.5-1 kg. Samples were taken from the depth of 50 cm and dry-sieved through a 2 mm plastic sieve in the field. The samples were coded according to the pre-defined numbering system and collected using a regular sampling grid.

The compositional variation and ranges of the base metals Cu, Zn and Pb between different target areas are presented in Fig. 4. Gold contents in the GIM soil survey were typically low and only 161 samples (13%) out of 1262 had values over 1 ppb. Most of the anomalous values occurred in the eastern area 1 including the highest content of about 1 ppm (1040 ppb). In other areas values only rarely exceeded 10 ppb. The tin anomalies revealed by the earlier LKAB study (LKAB 1979 and 1980) were confirmed by the GIM study. The total XRF contents correlated locally well with some geological units.

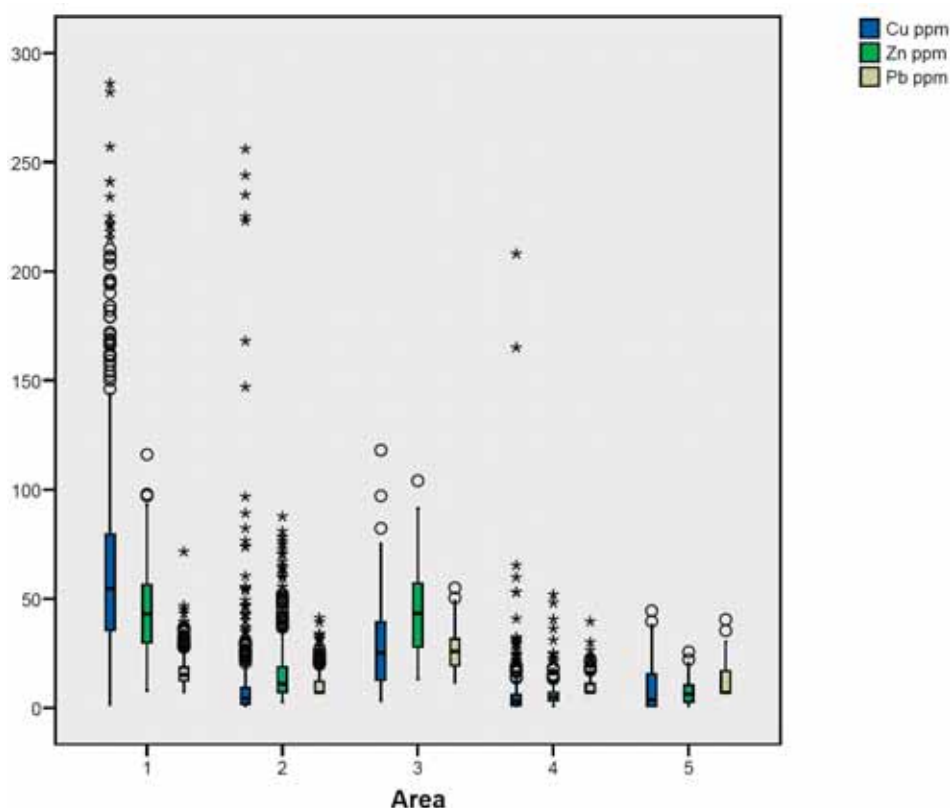


Fig. 4. Compositional ranges of the main ore elements (Cu, Zn and Pb) between GIM soil survey areas 1-5.

Hunting Team survey

The geochemical surveys carried out by the Hunting Team in 1981–83 were concentrated in 20 selected target areas (Fig. 5). The georeferenced location data of the Hunting Team samples has been captured and calculated for 5333 samples, of which 5258 samples have been joined with analytical results of the original digital data table with values for Cu, Pb, Zn, Ni and Co (Hunting Geology and Geophysics Ltd 1984).

On the basis of the drainage systems, 1066 samples were selected from the stored Hunting Team samples by the GIM project for additional analysis. These samples were analyzed for Au, Pd and Te by GFAAS. Unfortunately, only 19% (202) samples had Au values above the detection limit of 0.5 ppb, leaving the majority (81% / 864) of the samples below that value. This proportion is markedly lower than that obtained from stream sediment sampling by the GIM project, where 36% of the Au values exceeded 0.5 ppb.

Results

The summary statistics of the analytical results of the Hunting Team data are presented in Table 2.

When comparing maximum values with the median, it can be noted that Cu (42 times the median value) and particularly Ni (190 times the median value) occur locally as highly anomalous points.

As shown in Fig. 6, copper forms clustered anomalies in two target areas: western Mucanhavuzi (area 6) and eastern Mufa-Boroma/Monte Muandi (areas 17 and 18). In the latter area, Cu forms a NE-SW trending anomalous zone shown in detail in Figure 7. Geologically high Cu values are related to the carbonatites occurring between the 1046 ± 20 Ma old Chogocoma granite and the Tete Gabbro-Anorthosite Suite. The maximum Cu value of 971 ppm was recorded, however, close to the carbonate-hosted Chidue Cu-Au-occurrence, 20 km NE of the target areas 17/18 outlined in Fig. 6.

The highest Ni contents (maximum 0.42%) indicated by the Hunting Team survey are all associated with the Atchiza mafic-ultramafic Suite, situated on the western part of Tete Province displayed in Fig. 8 (target area 4). The geological units and Ni anomalies of the Suite are shown in detail in Fig. 9. The same area also includes the highest values of Pd (132 ppb) and Co (390 ppm). It has to be noted that the generally high Ni level is at least partly related

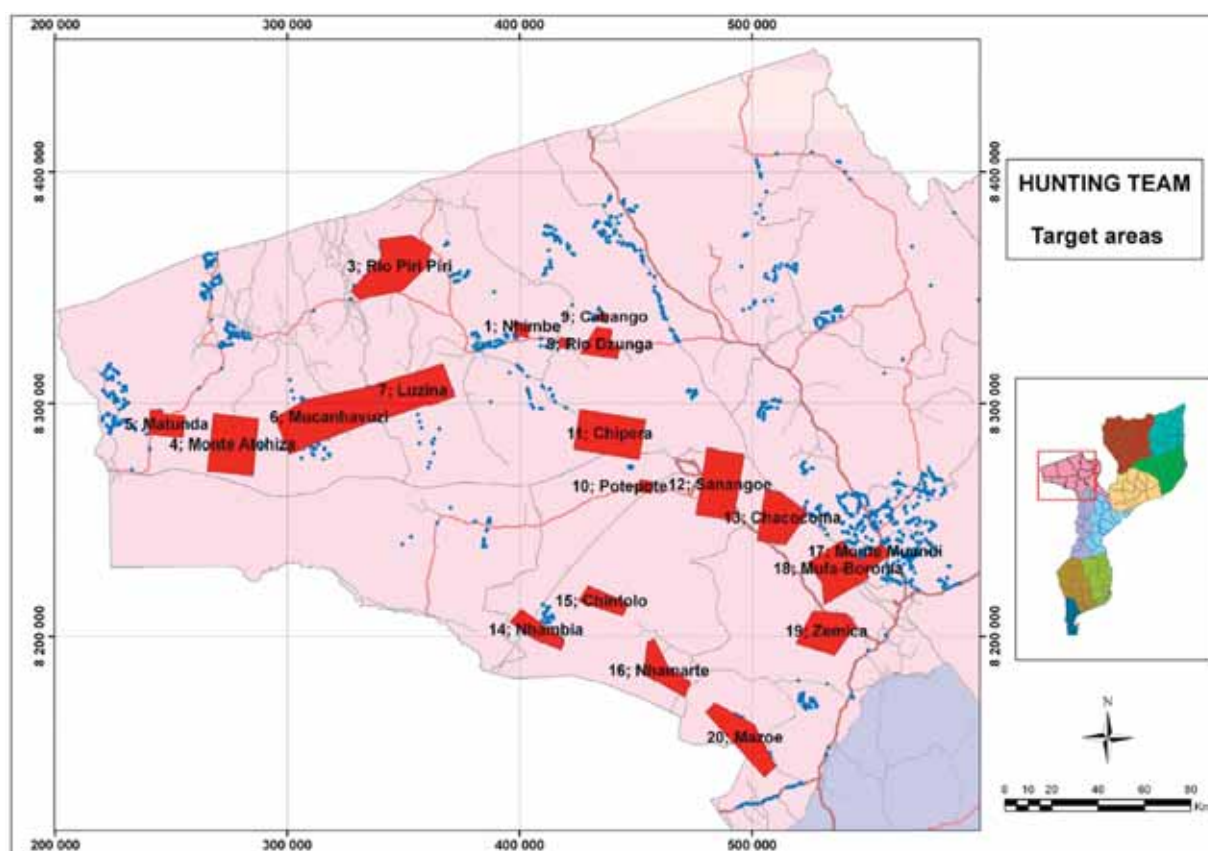


Fig. 5. Target areas of the Hunting Team survey in Tete Province shown in red. The sampling points outside the specific target areas are shown in blue.

Table 2. Summary statistics of the analytical results from the Hunting Team survey. Analysis by AAS. Au, Te and Pd were analyzed by GFAAS at the GTK laboratory. Note *, The value 1.5 ppm used in calculations for samples with Te < 2 ppb (11%).

Element		Cu ppm	Pb ppm	Zn ppm	Ni ppm	Co ppm	Au ppb	Te ppb	Pd ppb
N		5251	5251	5251	5251	5251	1066	1066	1066
Missing		0	0	0	0	0	4196	4196	4196
Mean		30.3	5.4	57	121.2	19.5		12.6*	
Median		23	5	50	22	14	<0.5	6.3*	<0.5
Std. Deviation		30.3	20.5	42.7	455.1	36.5		22.6*	
Minimum		1	1	1	1	1	<0.5	<2	<0.5
Max/Median		42 x	20 x	21 x	190 x	28 x		52 x*	
Maximum		971	101	1068	4199	390	434	327	132
Percentiles	25	13	2	34	10	7	<0.5	3.4	<0.5
	50	23	5	50	22	14	<0.5	6.3	<0.5
	75	39	8	69	47	23	<0.5	13.4	0.8
	95	84	34	134	547	110	1.8	42.2	2.1

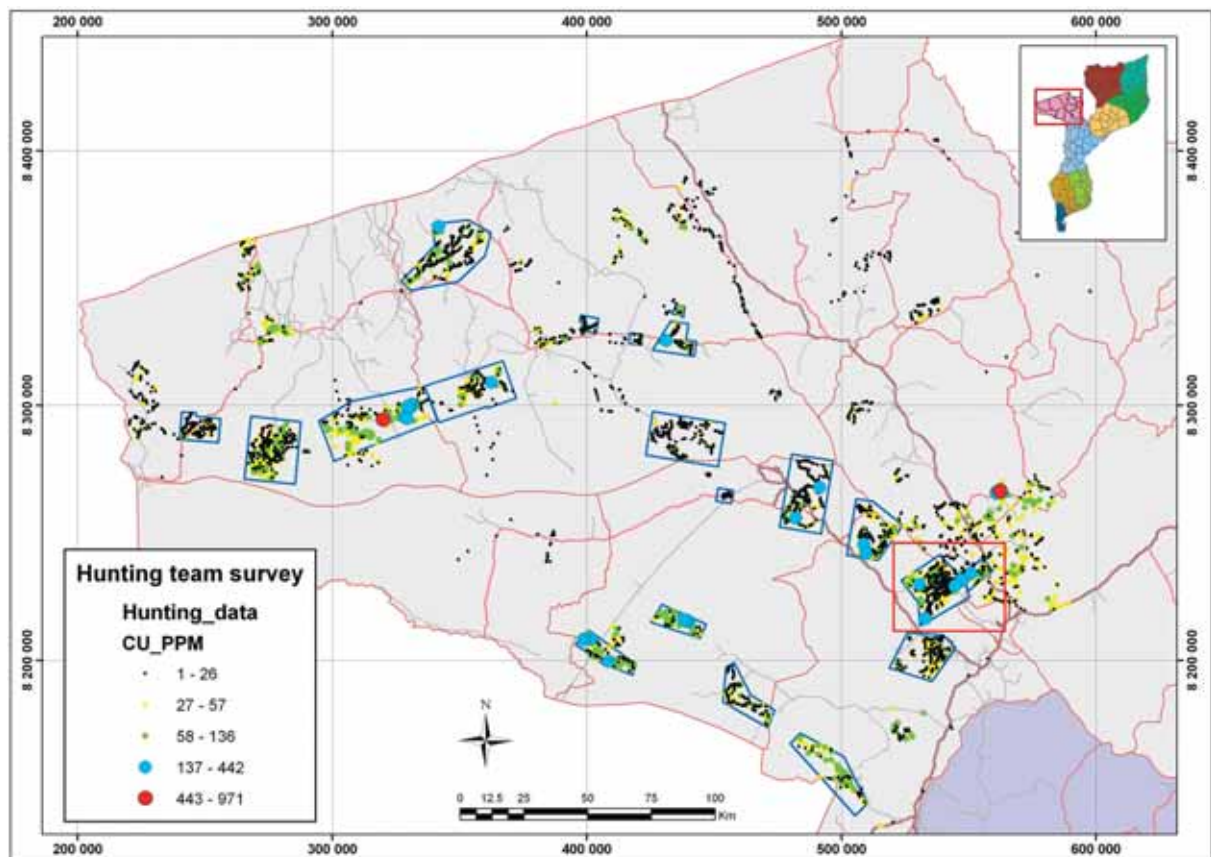


Fig. 6. Copper content (in ppm) in stream sediments as defined in the Hunting Team study in 1981–83. Values were determined by AAS. The Chidue gold occurrence is related to the anomaly zone (red circle) situated 20 km N of the rectangular area outlining the target areas 17 and 18, shown in detail in Fig. 7.

to Ni originating from Ni-bearing silicate minerals such as olivine, which is the major constituent of the Atchiza ultramafic rocks. Due to its geological nature and highly anomalous Ni values, the Atchiza Suite can be considered as a good potential target for nickel exploration.

The new analyses for Au, Pd and Te of the selected Hunting Team samples carried out by the

GIM project indicate that the western target areas have most prominent and concentrated anomalies and can therefore be considered economically interesting (Fig. 10). The highest gold value of 434 ppb has been detected in the Mucanhavuzi target area 6, east of Atchiza. The analytical results also show that several other anomalous samples (about 40 out of 202 samples with Au contents above the detection

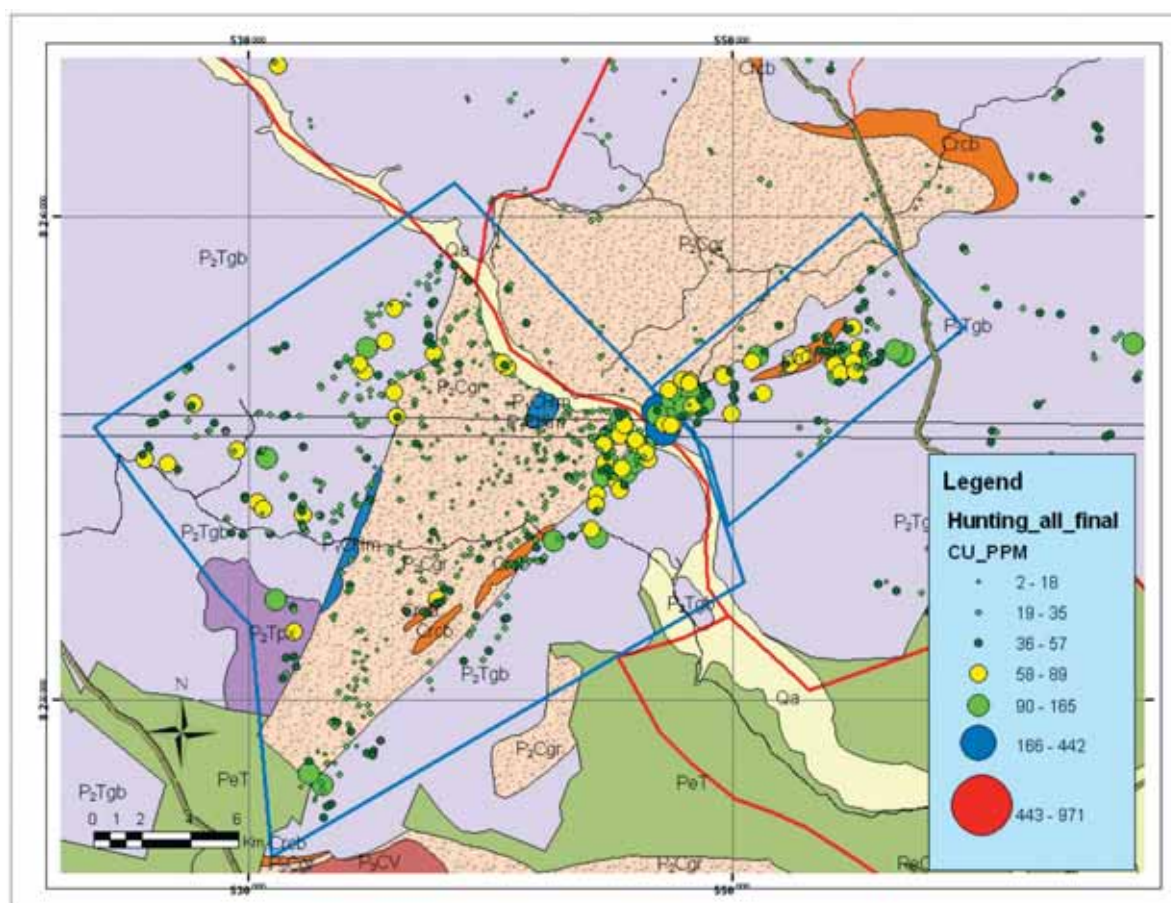


Fig. 7. Copper content in target areas 17 and 18; location shown in Figs 5 and 6. The rocks consist of minor, NE-SW-trending Cretaceous carbonates (CrCb, red brown), occurring in the contact zone between the Chogocoma granite (P₂Cgr, dotted pinkish brown) and Tete gabbro-anorthosite Suite (P₂Tgb, light blue). Geology based on GTK Consortium LOT 2 mapping.

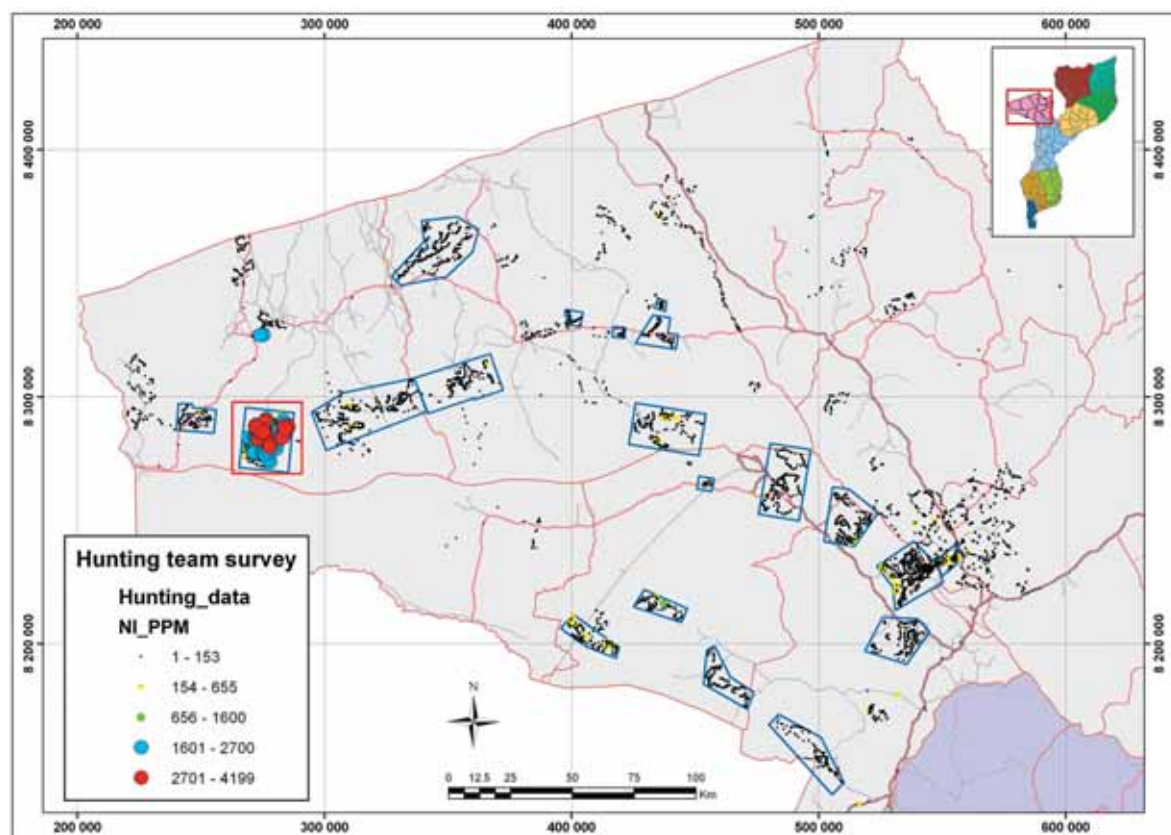


Fig. 8. Nickel contents recorded in the stream sediment survey by the Hunting Team. The highest values (up to 0.42%) are concentrated in target area 4, comprising the Atchiza mafic-ultramafic Suite. The outlined area with anomalous nickel contents is shown in detail in Fig. 9.

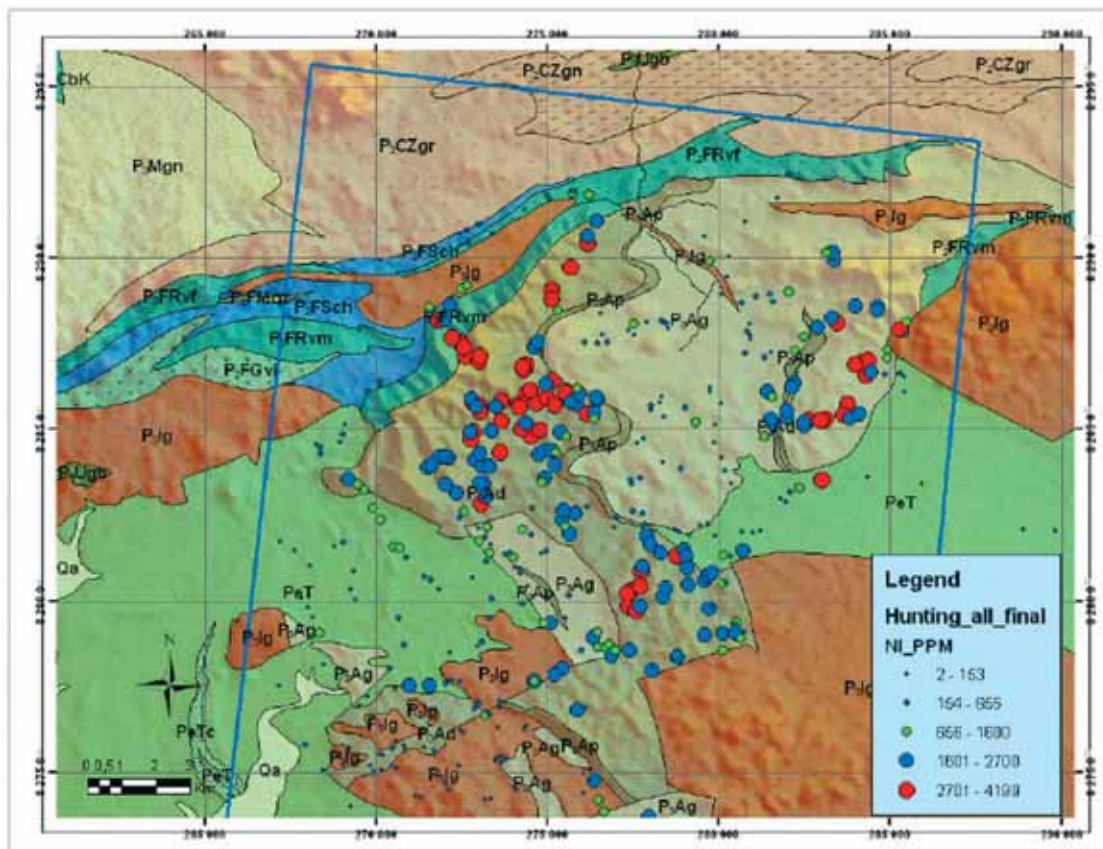


Fig. 9. Nickel anomalies detected in the stream sediment survey by the Hunting Team in target area 4. Geologically, the area consists of the Atchiza ultramafic-mafic Suite. The highest anomalies are related to the Neoproterozoic Atchiza dunite (P₃Ad, greenish brown). Other major rock types include the pyroxene gabbros (P₃Ag, light brown), porphyritic Monte Inchinga granite (P₃Ig, dark brown), and Lower sediments (PeT, green). Geology based on GTK Consortium mapping.

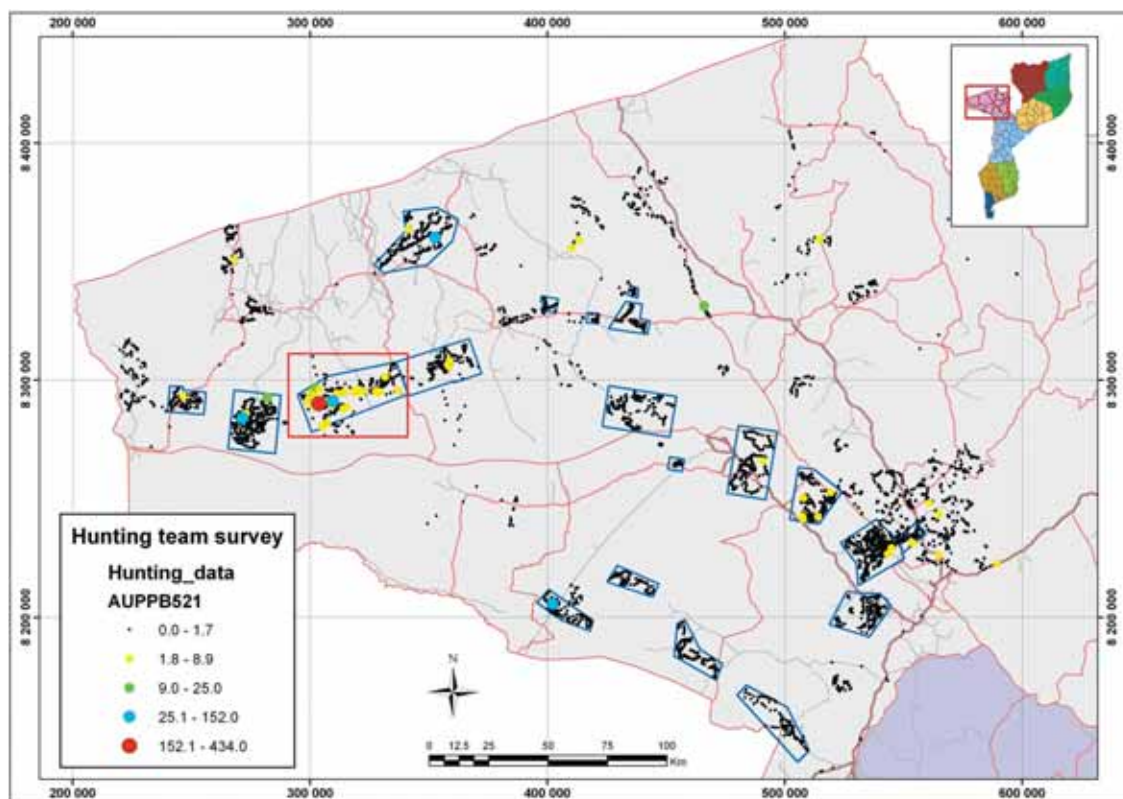


Fig. 10. Gold content (in ppb) of the 1066 reanalyzed Hunting Team samples. The results indicate that the western Mucanhavuzi target area 6 outlined in red (For details, see Fig. 11) has the most prominent gold anomalies. Samples analyzed by GFAAS at the GTK laboratory.

limit of 0.5 ppb) are concentrated in the same specific target area, which is also typified by high Cu values. Geologically, it consists of rocks belonging to Mesoproterozoic Fingoè supergroup comprising mafic/ultramafic metavolcanic rocks, mica schists and gneisses or calc silicate gneisses and schists

with some metasediments intercalated with felsic volcanic rocks (Fig. 11).

In summary, based on the above geochemical results, the Muchanhavuzi area can be considered to have potential for gold and copper exploration.

UNDP survey

The captured UNDP survey data in Angonia-Macanga area in the north-eastern part of the Tete Province (for location, see Fig. 1) included 1441 stream sediment samples analyzed for Cu, Zn, Mo, Pb, Ni, Co and Cr by AAS (Chakrabarti 1983). The statistics of the data are presented in Table 3. The median value for Cu is 9 ppm, the maximum being clearly anomalous at 264 ppm. The comparable values for Zn are 24 ppm and 344 ppm, respectively.

Based on recent CGS mapping, the eastern part of the sampling area consists of Mesoproterozoic Angonia group metasedimentary rocks, including banded quartz-feldspar and amphibolitic gneisses and Neoproterozoic Ulúnguê Suite igneous rocks (anorthosites, syenites and amphibolites). The Mesoproterozoic plutonic units, forming the western part of the UNDP sampling area, belong to the Desaranhama Group of the Furancungo Suite. The

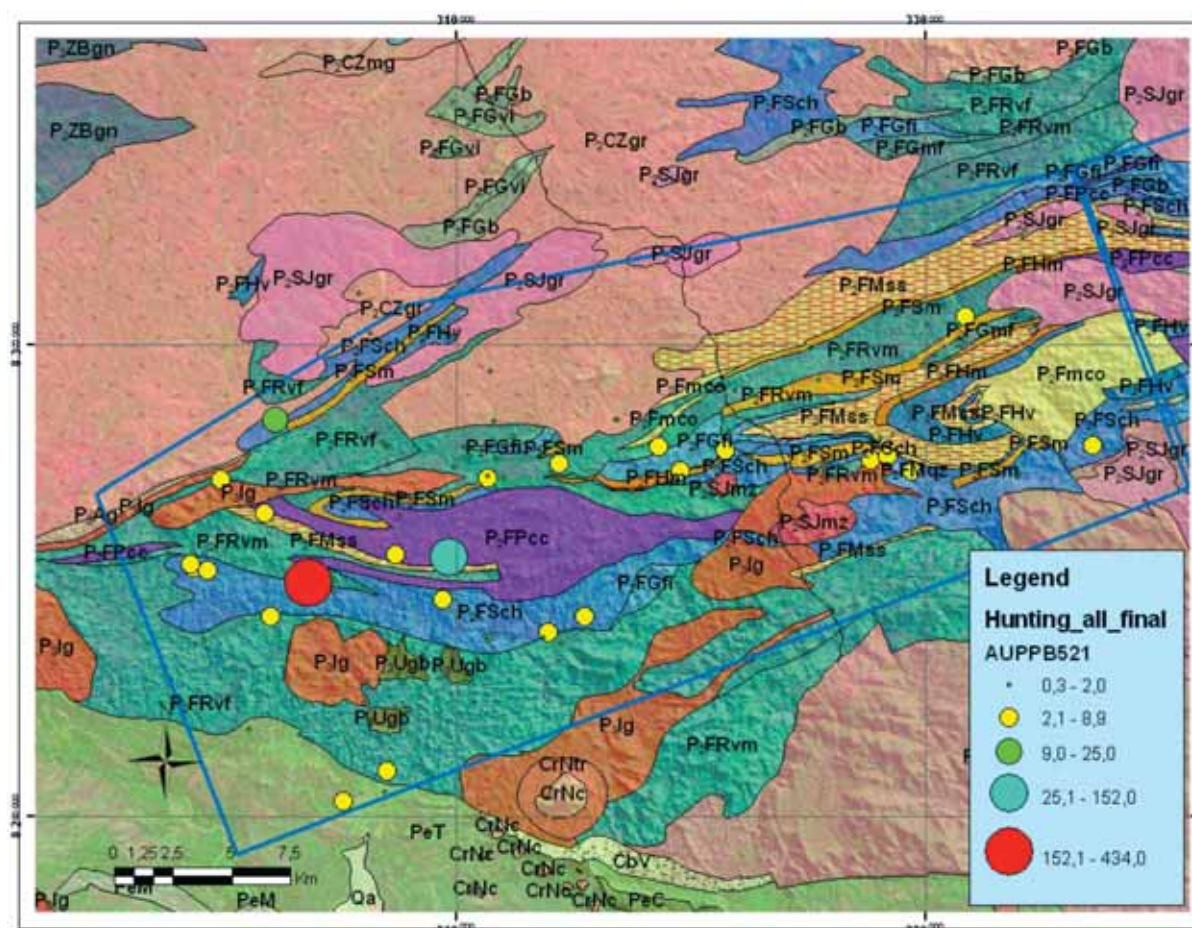


Fig. 11. Gold content (in ppb; max 434 ppb) in Hunting Team target area 6. Geologically, the area is comprised of rocks of the Fingoè supergroup. The highest values are related to the contact zone between the mafic/ultramafic metavolcanic rocks (P₂FRvm, dark green) and mica schists and mica gneisses (P₂Fsch, blue), all belonging to Monte Meseca group or associated with calc silicate gneiss and schist (P₂FPcc, purple) of the Monte Puéque Formation. Geology based on GTK Consortium mapping.

Table 3. Summary statistics of the geochemical data from the UNDP survey. Values below the detection limit of 1 ppm are omitted from the calculations.

		Cu ppm	Zn ppm	Mo ppm	Pb ppm	Ni ppm	Co ppm	Cr ppm
N		1364	1425	936	1197	1391	1395	1354
Mean		15	33	6	15	27	17	47
Median		10	24	5	13	16	12	27
Std. Deviation		20	33	6	11	49	17	65
Minimum		1	1	1	1	1	1	1
Maximum		264	344	60	155	715	156	860
Percentiles	25	4	16	2	7	9	8	13
	50	10	24	5	13	16	13	28
	75	19	39	9	20	28	23	59
	95	55	97	31	42	106	57	169

dominant rock types are biotite-hornblende orthogneisses, porphyritic or biotitic granites and granodiorites.

The distribution of Zn contents is plotted on an elevation map and displayed in Fig. 12. High Cu values are heterogeneously spread out and do not

show any particular concentration. In contrast, Zn values form a distinct anomaly in the western part of the UNDP sampling area. Since the Ni values are also highest in the same area, these features could together indicate some economically interesting targets for a follow-up survey.

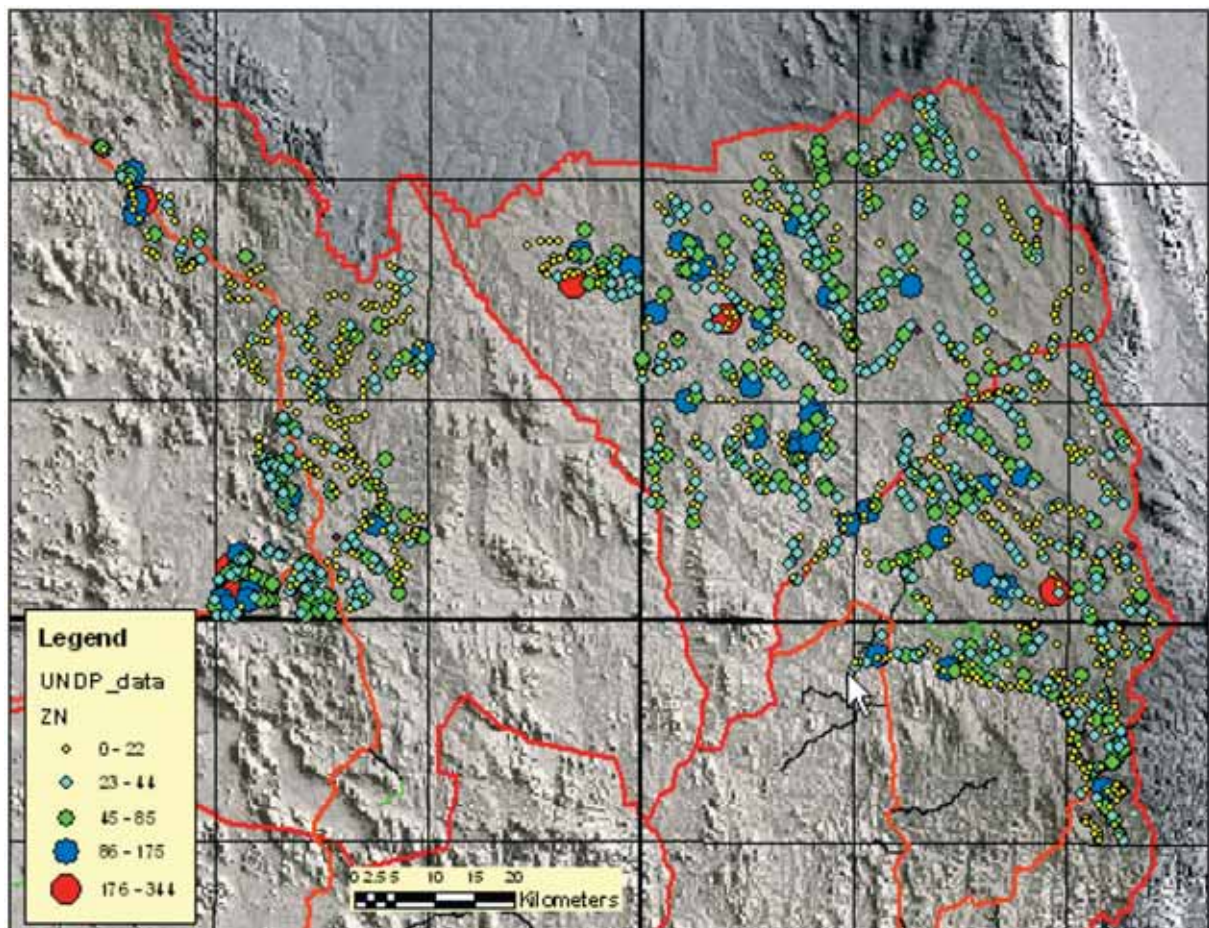


Fig. 12. Zinc content (in ppm) in the UNDP stream sediment survey plotted on an elevation model shown by grey tones. NE corner of Tete Province. For location, see Fig. 1.

Ashanti Goldfields Rotanda-Mavita survey

The Ashanti Goldfields survey in Rotanda-Mavita covered an area of 2370 km² (Gonçalves 1988a, 1988b and 1988c). In total, 1109 Ss samples were collected, giving a sampling density of about one sample/2 km². Samples were analyzed only for gold using Bulk Cyanide Leach (BCL) as the digestion/analytical method. Sixty-one (61) per cent of the samples had gold values below 1 ppb. The regional study showed that the Bandire area had elevated gold values up to 180 ppb and a follow-up soil survey was carried out. The first 800 m x 200 m follow-up sampling grid was complemented with more detailed 100 m x 50 m sampling. As a result, the Bandire gold occurrence was located within the anomalous area. Presently, this alluvial gold enrichment

is utilized by local artisanal miners (Lehto & Gonçalves 2008).

The geology of the Ashanti Goldfields study area combined with gold contents from the Ss survey is shown in Fig. 13. The area with the highest gold contents forming the first follow-up soil survey is shown by a rectangular zone with a yellowish-brown colour. Geologically, the area hosting the Bandire Au occurrence consists of both Archaean and Proterozoic domains. The western Archaean rocks are typified by granitoids (A3Vpg, red) and paragneisses (A3Mpgn, light purple), whereas the eastern Proterozoic domain consists of migmatitic paragneisses (P2BCmi) shown in blue.

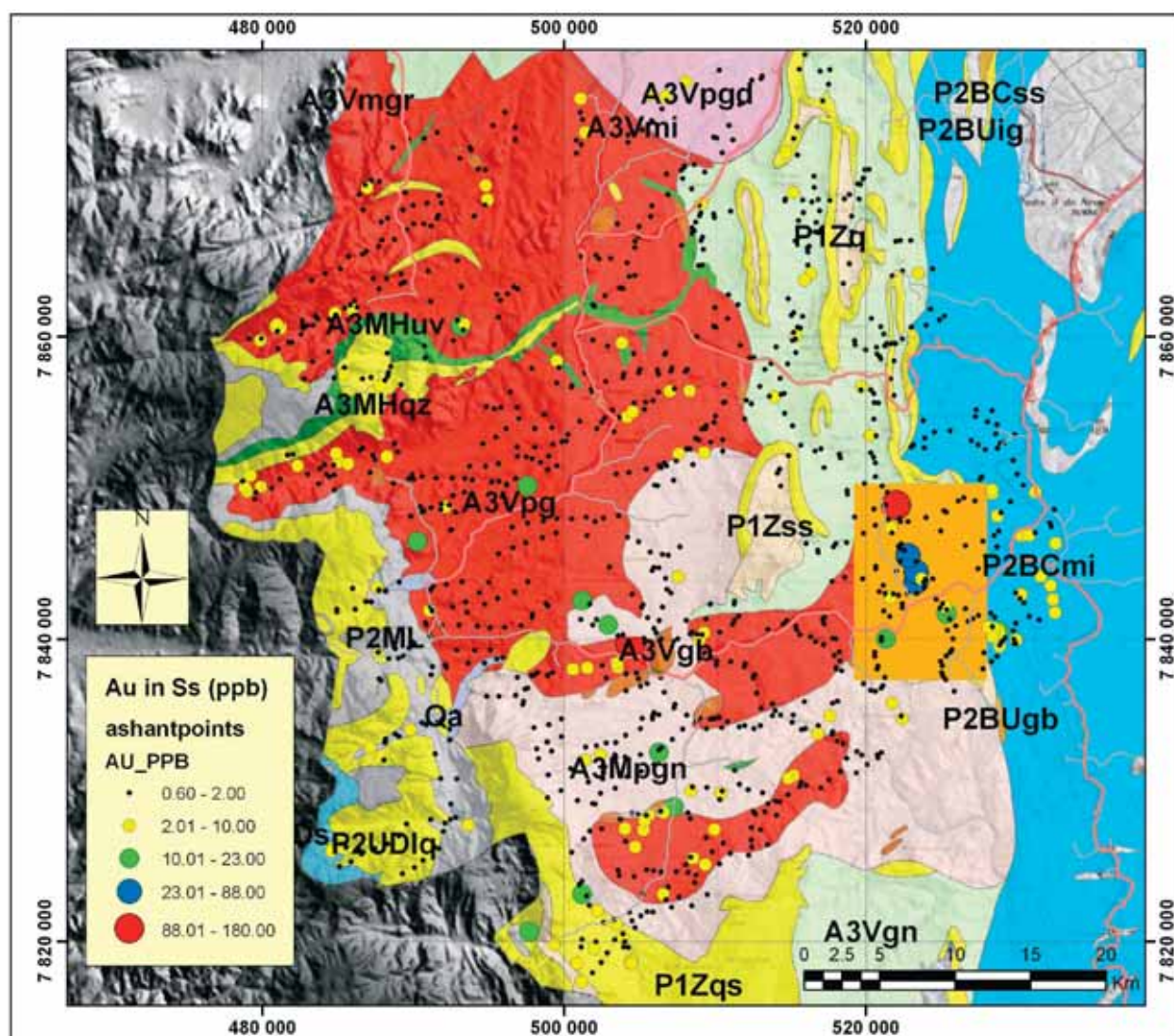


Fig. 13. Ashanti Goldfields Au exploration survey in the Rotanda-Mavita area, Manica Province. The dominant rock types consist of Archaean granitoids (A3Vpg, red) and paragneisses (A3Mpgn, light brown) in the west and Proterozoic migmatitic paragneisses (P2BCmi, blue) in the east. The rectangular area of the follow-up soil survey, hosting the alluvial Bandire gold occurrence, is indicated by a yellowish-brown colour. For location, see Fig. 1.

Ashanti Goldfields Gorongosa survey

Ashanti Goldfields has also carried out regional gold exploration in the Gorongosa area of Sofala Province (Ashanti Goldfields 1996). This work included 366 sampling points, which were analyzed using Bulk Cyanide Leach (BLC) with 2 kg sam-

ples. Both stream sediment and soil samples were collected and sieved for analysis to the -80 mesh fraction. The highest gold values were associated with Proterozoic paragneisses.

SGM survey

The samples collected by SGM in Sussundenga District in Manica Province have been analyzed by AAS for Zn, Ni, Co and Cu (Leal 1972, SGM 1970). The digitally captured data consists of 1836 sampling points. This work has partly overlapped the regional stream sediment survey of Ashanti Goldfields in the Rotanda-Mavita area (cf. above).

Geologically, the SGM survey area is characterized by Archaean paragneisses with quartzitic intercalates (A3Mpgn, pink), granitoids (A3Vpg, red) and gabbros (A3Vgb, brown) associated with some

subordinate ultramafic metavolcanic rocks (A3MHuv, green) and TTG gneisses (A3Vgn, light green) (Fig. 14). Proterozoic rocks consist of muscovite-biotite schist (P1Zss, light yellow) and quartzites forming the topmost peak of the nearby mountains.

The captured results showed that the median values were 40 ppm for Cu and 60 ppm for Zn. The maximum values were clearly anomalous at 195 ppm and 203 ppm, respectively. Maximum Ni contents were unusually high at nearly 0.4%. Copper occurs as several clustered anomalies around the

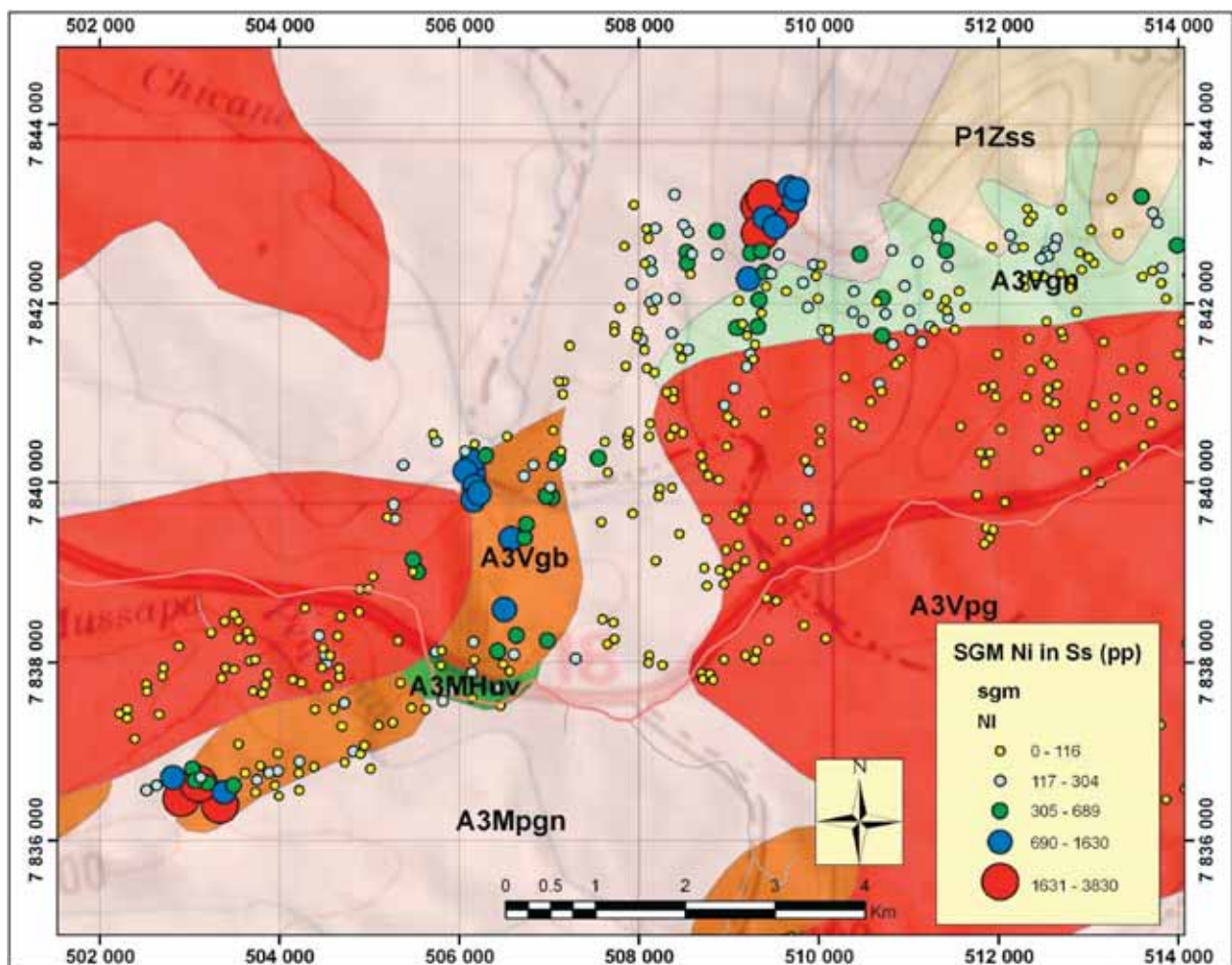


Fig. 14. SGM nickel plots on a detailed geological map situating about 10 km W of the Ashanti Goldfields follow-up soil survey area shown in Fig.13. Note that only the two southernmost Ni anomalies are related to gabbroic rocks (A3Vgb, brown), whereas the northernmost anomaly is associated with Archaean paragneisses with quartzitic intercalates (A3Mpgn, light purple). Other Archaean rocks include granitoids (A3Vpg, red) and some subordinate ultramafic metavolcanic rocks (A3MHuv, green) and TTG gneisses (A3Vgn, light green). Proterozoic rocks consist of muscovite-biotite schist (P1Zss, light brown) with quartzite intercalations. Geology based on GTK Consortium mapping.

study area, but some of them are concentrated in the Bandire area where high gold values were detected by Ashanti Goldfields (Fig. 13). Both Zn and particularly Ni values of the SGM data indicate well concentrated, clustered anomalies.

It is interesting to note that two out of three nickel anomalies displayed in Fig. 14 are geologically related to the gabbro intrusions. In contrast, the most

prominent northern nickel anomaly is, according to the geological map, related to Archaean paragneisses. This anomaly could also be caused by an unexposed mafic-ultramafic or gabbroic body and not an ore deposit. Despite this, these high (0.2–0.4%) and clustered Ni anomalies form an interesting and well-defined follow-up exploration target.

Aquater survey

The stream sediment survey by Italian Aquater (Aquater 1983) was one of the few studies where data were originally available in a digital format. The survey was carried out in Zambézia and Nampula Provinces (for location, see Fig. 1). It included four 1:250 000 scale map sheets and four additional 1:50 000 scale map sheets covering about 50 000 km². The total number of original samples in the data table was 15 454, of which 15 123 samples have been included in the Aquater ADT. The samples have been analyzed for 24 elements, but not systematically; more than 10% of the samples lack analysis for Ni, Pb, Cu, Co and Cr, and only half of the samples have been analyzed for Zn. Arsenic, Sb,

Ce, V and Mo have been analyzed only occasionally. Original Ss samples, weighing 3–6 kg, were sieved to the -80 mesh fraction for analysis, which was carried out either at the National Chemical Laboratory, Maputo, or alternatively at the DNG laboratory in Quelimane. Analytical methods were either Quantometer (=ICP 3400) or AAS. The sampling was performed in two stages and the sampling density was variable, as illustrated in Fig. 15. All this is reflected in the variation in analytical accuracy levels between the map sheets and some of the analytical results must therefore be considered as only semi-quantitative.

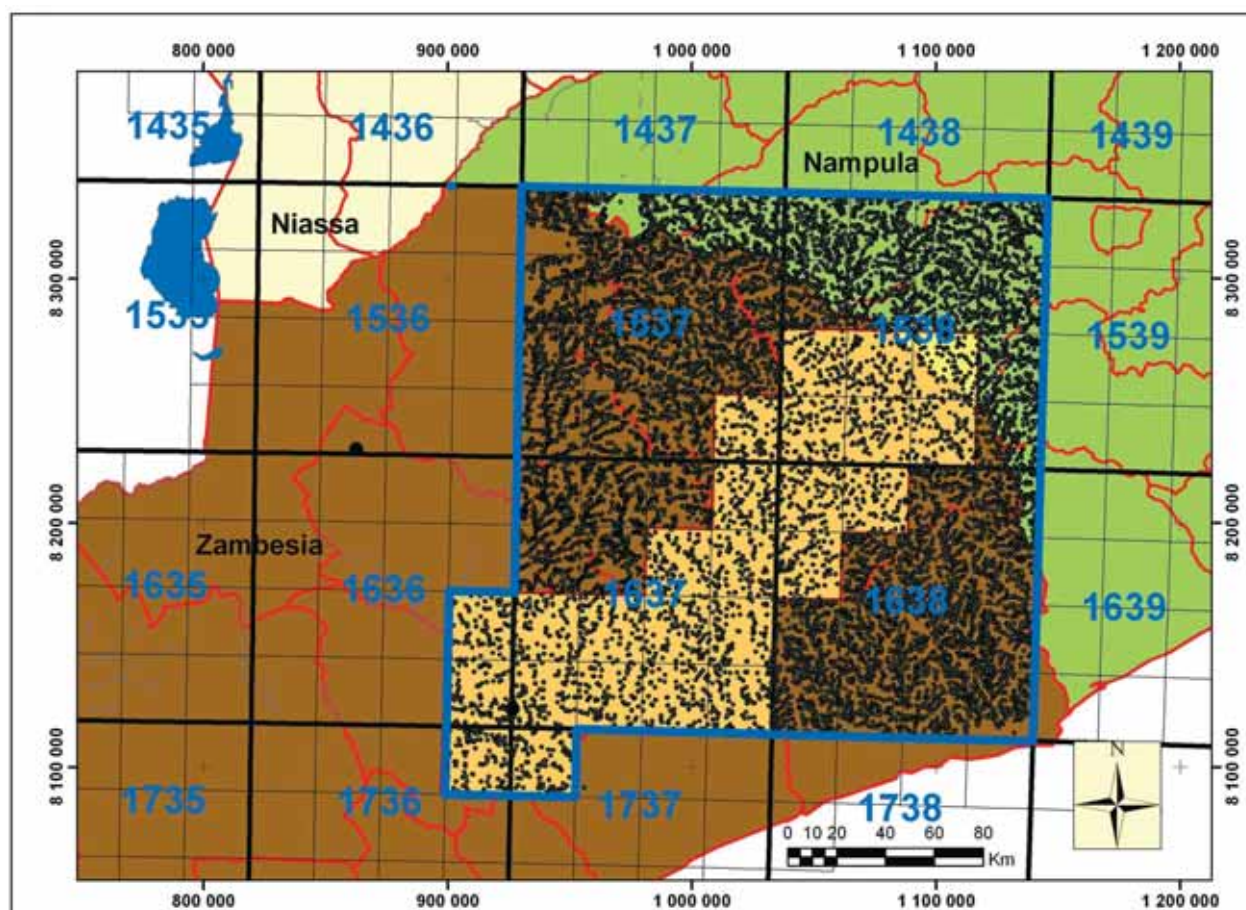


Fig. 15. Location of the Aquater survey area and the sampling points in Zambézia and Nampula Provinces. The national 1:250 000 and 1:50 000 scale map grid is shown also in Fig. 16. The yellow colour delineates the area of the second sampling phase.

Some of the Zn values indicated by the Aquater survey are clearly anomalous, including 40 samples exceeding 500 ppm. The highest Zn values (maximum 0.55%) are related to the metasedimentary Molócuè group rocks or their contact areas in the NE or SE corners of the study area (Fig. 16). For Cu, anomalous values are less well defined and only 8 samples have values above 500 ppm. However, several of these are associated with high values of Zn. The most prominent clustered Cu anomaly occurs in the central part of map sheet 1638. Geologically, this area is characterized by metamorphic banded biotite gneisses and migmatites of the Nampula Complex. The main clustered Pb anomalies are situated in the centre of map sheets 1537 and 1638. However, an

individual maximum value of 1200 ppm is located in the SW corner of map sheet 1537.

As a whole, the analytical accuracy of the Aquater data does not seem to be consistent, as shown by the clear differences in assay levels between the map sheets. Besides different analytical methods, this might at least partly be related to the fact that sampling was carried out in two project phases. For detailed interpretation of the data, it should be divided into smaller parts and results from different map sheets should be treated separately. Economically, the most interesting outcomes appear to be related to high Zn values in the north-eastern corner of the study area (Fig. 16).

Tecnosynthesis survey

The Tecnosynthesis data was originally collected to support the evaluation for the possible development of hydropower in Lugenda River in Niassa and Cabo Delgado Provinces and not for exploration purposes (Tecnosynthesis 1980). It included 188 stream sediment and 396 soil samples, totalling 584

samples. The stream sediment samples consisted of two sub-samples collected from the central part of the river channel separated by a distance of 100-200 m. All samples have been analyzed for Al_2O_3 , SiO_2 , K_2O , Fe_2O_3 , P, Ti, Mn, Nb, Sr, Cu, Ni, Pb, Zn, V, As, and Sn by XRF. Furthermore, 87 stream sediment

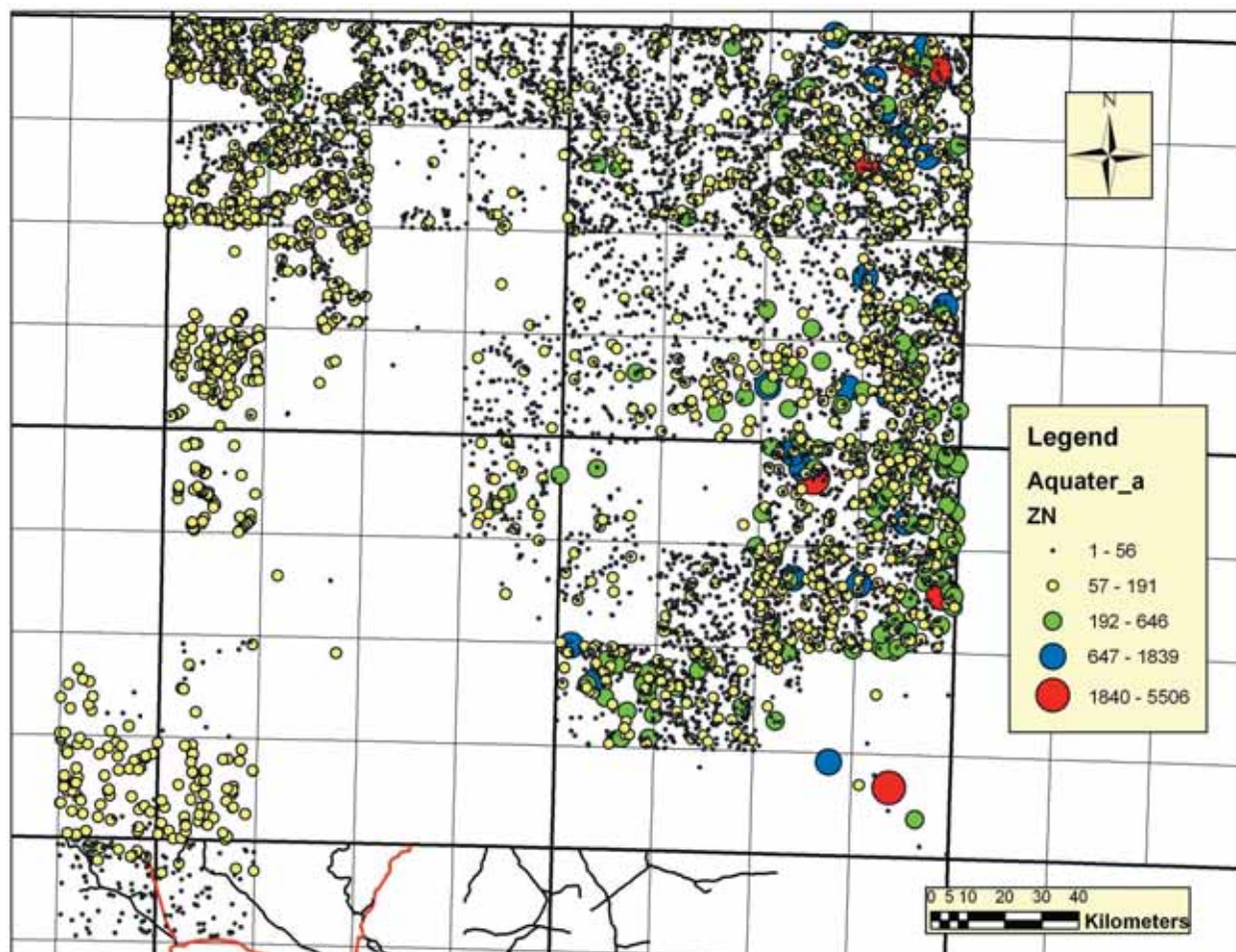


Fig. 16. Zinc anomalies (in ppm) of the Aquater data. Note the variable analytical accuracy level between the map sheets. The highest Zn contents occur in the NE and SE corners of the study area.

samples have been analyzed by gamma spectrometer for Th, U and K.

For some reason, a large proportion of samples have been collected as duplicates from the same locations. These include about 30 stream sediment and 120 soil duplicates. When comparing the analytical results between the duplicates, it was noted that the compositional differences between the sample pairs is marked. Due to this heterogeneity, the Tecnosynthesis data cannot be considered very reliable. This might be the result of variable or undefined sampling procedures. Additionally, it seems that the sampling has been carried out along roads, which probably resulted in some contamination effect, at least for certain elements like Pb.

The results of the Tecnosynthesis study, together with comparison between duplicate samples, clearly show that the sampling material has not been homogeneous. This is reflected, for instance, in the wide range of overlapping SiO₂ content, being 35–94% for stream sediments and 34–94.5% for soil samples. These numbers indicate that the sampled material classified as soils has occasionally been extremely quartz-rich and probably represented material from sorted stream sediments (sand) and not soil.

Economically, the most interesting values appear to be related to Zn, the maximum contents being 198 ppm for soil and 229 ppm for stream sediment (Fig. 17).

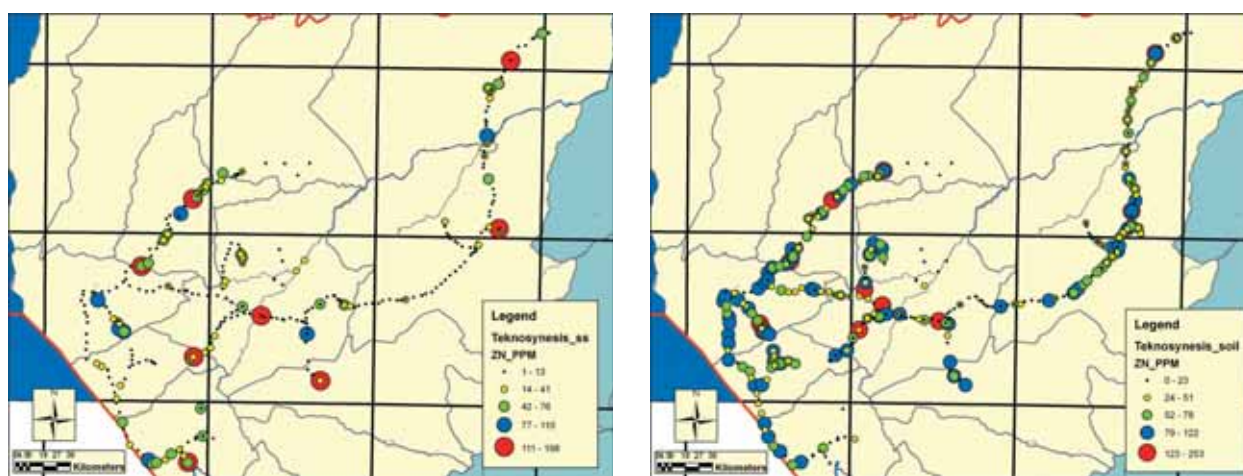


Fig. 17. Zinc content in soil (left) and stream sediments (right) in the Tecnosynthesis geochemical survey. For location, see Fig. 1. The grid indicates the national 1:250 000 scale map division.

Stanchenko survey

The Stanchenko survey covers the same area as the old BRGM study, which unfortunately lacks the analytical data. It is also not known how the Stanchenko work was carried out or whether the samples were the same as those collected by BRGM, because no report was stored. The results of the Stanchenko study are represented as separate elemental maps stored in the DNG map library. Element values are displayed as standard deviation classes for V, Zn, Cr, As, B, Be, Co, Cu, Ga, Li, Ni, P, Sc and Mn, the actual data being missing.

The Stanchenko study area included 130 000 km², covering most of the Nampula Province and also parts of Cabo Delgado, Niassa and Zambézia Provinces (for location, see Fig. 1). The sampling density was generally relatively homogeneous but denser in the NE corner of the study area, being

1 sample/66 km² on average. In total, 1969 sampling points were digitized from scanned element maps and standard deviations were tabulated and stored in the GIM_GDB.

Some examples of the results for major ore elements are displayed in Figure 18, illustrating the distribution of Cu, Zn, and Ni classified according to the standard deviation. Element anomalies are widely distributed, and as the sampling methodology and sample representativeness is not known, it is difficult to evaluate the economic importance of the anomalies. It can be stated that Cu forms clustered anomalies in the SE part of the study area, whereas zinc appears, together with Ni, to have a NE-SW trending anomaly zone in the western Cabo Delgado Province.

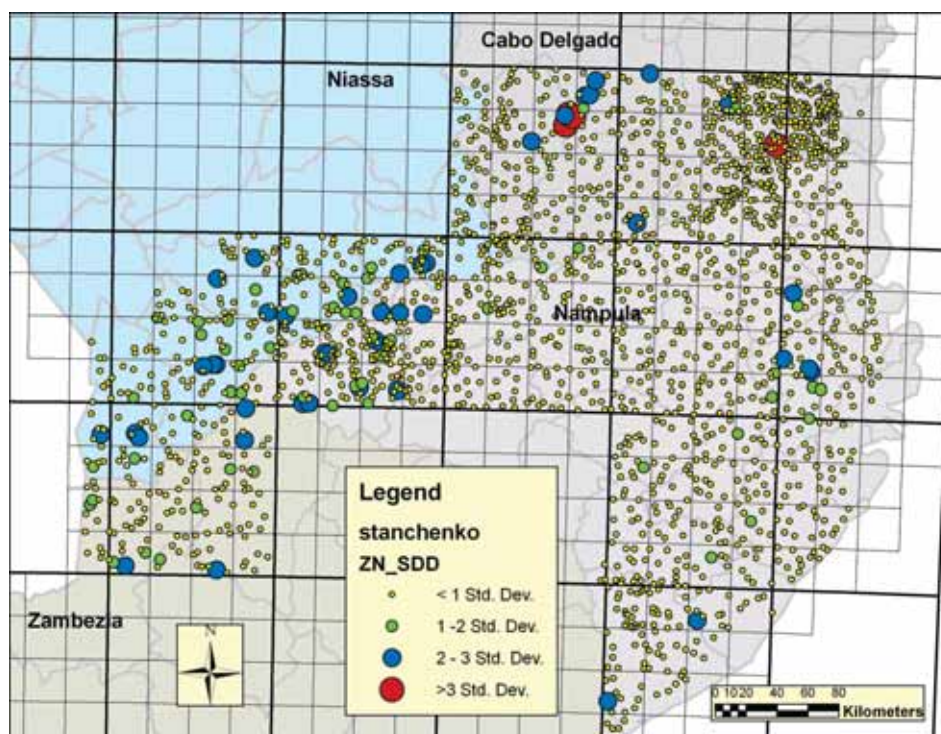


Fig. 18a. Copper content as standard deviation classes in the Stanchenko survey covering parts of Nampula, Cabo Delgado, Niassa and Zambézia Provinces. Base grid according to the national 1:250 000 and 1:50 000 scale map sheet division.

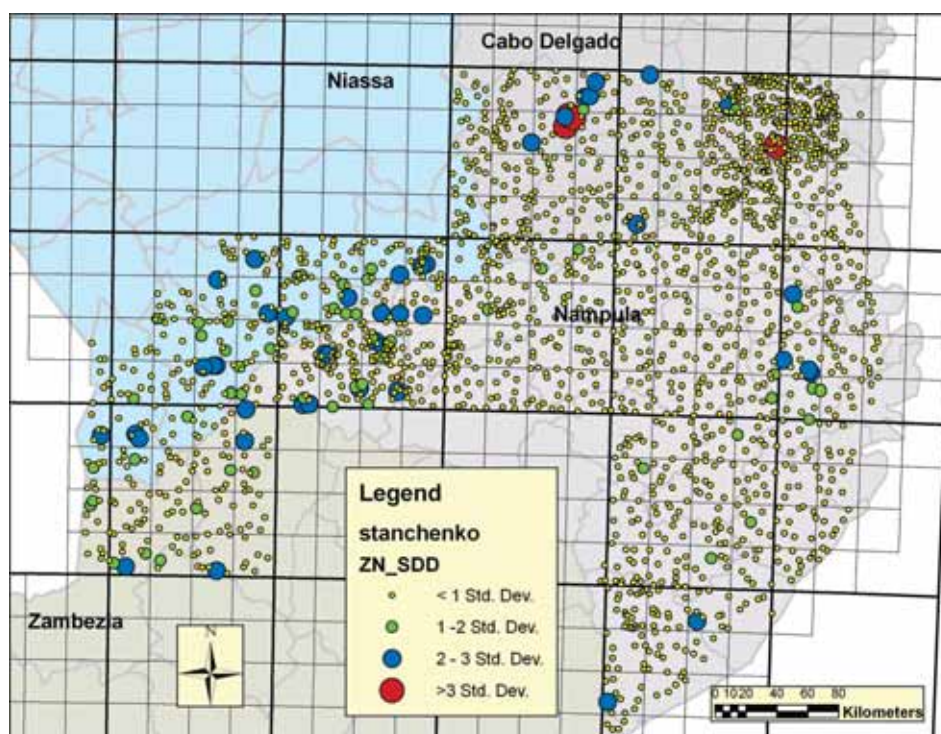


Fig. 18b. Zinc content as standard deviation classes in the Stanchenko survey.

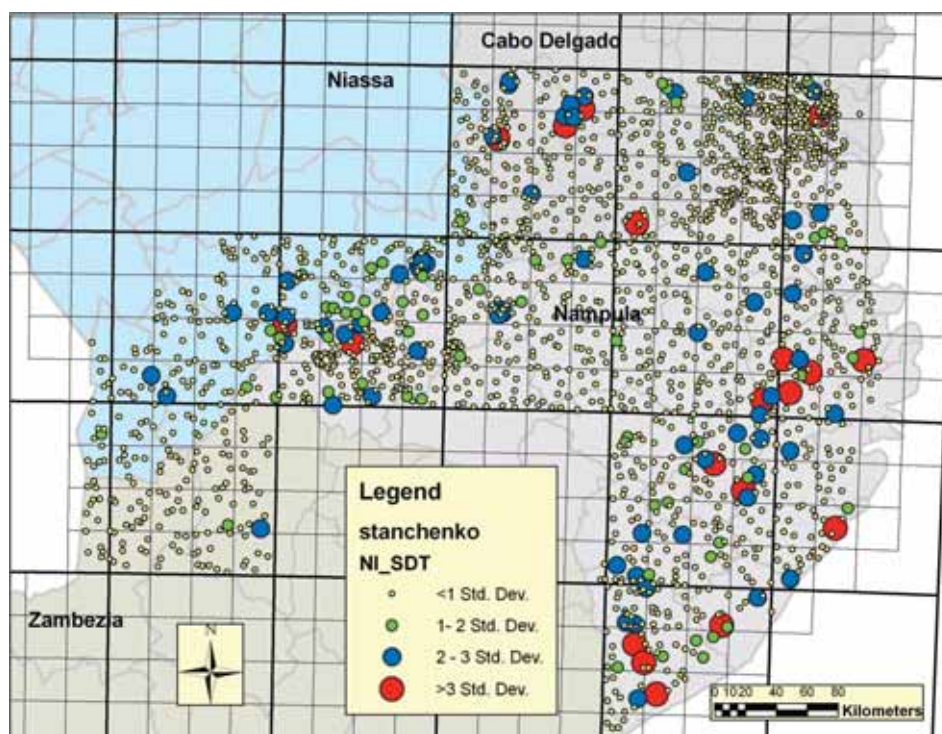


Fig. 18c. Nickel content as standard deviation classes in the Stanchenko survey.

CGS-DNG survey

The CGS-DNG survey in Cabo Delgado Province was carried out in 1996 and reported by De Waal (1996). It included 1574 soil samples collected from two sub-areas covering 573 and 1128 km², totalling 1800 km². Sampling was carried out using a helicopter. Sampling points were located using GPS with an accuracy of ±100 m. The sampling media was soil, the original sample weight being 2–3 kg. The samples were analyzed using XRF so they give a good correlation with the bedrock, as can be seen in Figs 19 and 20.

General statistics from the CGS-DNG survey are presented in Table 4. The results plotted on the geological map show high and economically interesting

Cu and Zn anomalies, the maximum values being 459 and 930 ppm, respectively (Figs 19 and 20). High Zn and Cu values are both geologically related to Neoproterozoic Xixano Complex consisting of sedimentary quartz mica gneisses and schists, which are locally graphite-bearing (P3Xqm, green). The other dominant rock type in the CGS-DNG study area is plutonic amphibolite gneiss (P3Xag, light brown) belonging to the same era and complex as the sedimentary gneisses mentioned above. A concentrated Pb anomaly is geologically associated with granitic gneiss belonging to the Montepuez Complex (P3MPgr). The Monte Mapacane granite intrusion (P3XMgr, red) occurs between the sampling areas.

Table 4. Statistics of the selected elements produced by the CGS-DNG soil survey. XRF analysis. Values below the detection limit are omitted from the calculations.

		TiO ₂ %	MnO %	Fe ₂ O ₃ t %	Sc ppm	V ppm	Cr ppm	Ni ppm	Cu ppm	Zn ppm	Co ppm
N		1544	1544	1544	1544	1281	1487	1543	1543	1544	1543
Mean		1.70	0.11	4.89	18.35	85.24	83.69	30.16	29.00	57.37	16.41
Median		1.44	0.1	4.32	18	43	62	20	22	44	14
Std. Dev.		1.14	0.08	3.42	8.57	147.21	105.61	37.31	26.66	57.96	10.17
Minimum		0.22	0.01	1.63	2	<1	<1	<1	<1	3	<1
Maximum		14.54	0.63	19.37	58	2358	1794	707	459	930	81
Percentiles	25	1	0.04	1.96	12	11	26	10	11	27	8
	50	1.44	0.1	4.32	18	43	62	20	22	44	14
	75	2.08	0.16	7.21	24	113	112	38	40.25	69	22
	95	3.76	0.25	10.95	33	269.5	211.25	81	75.25	133.25	35

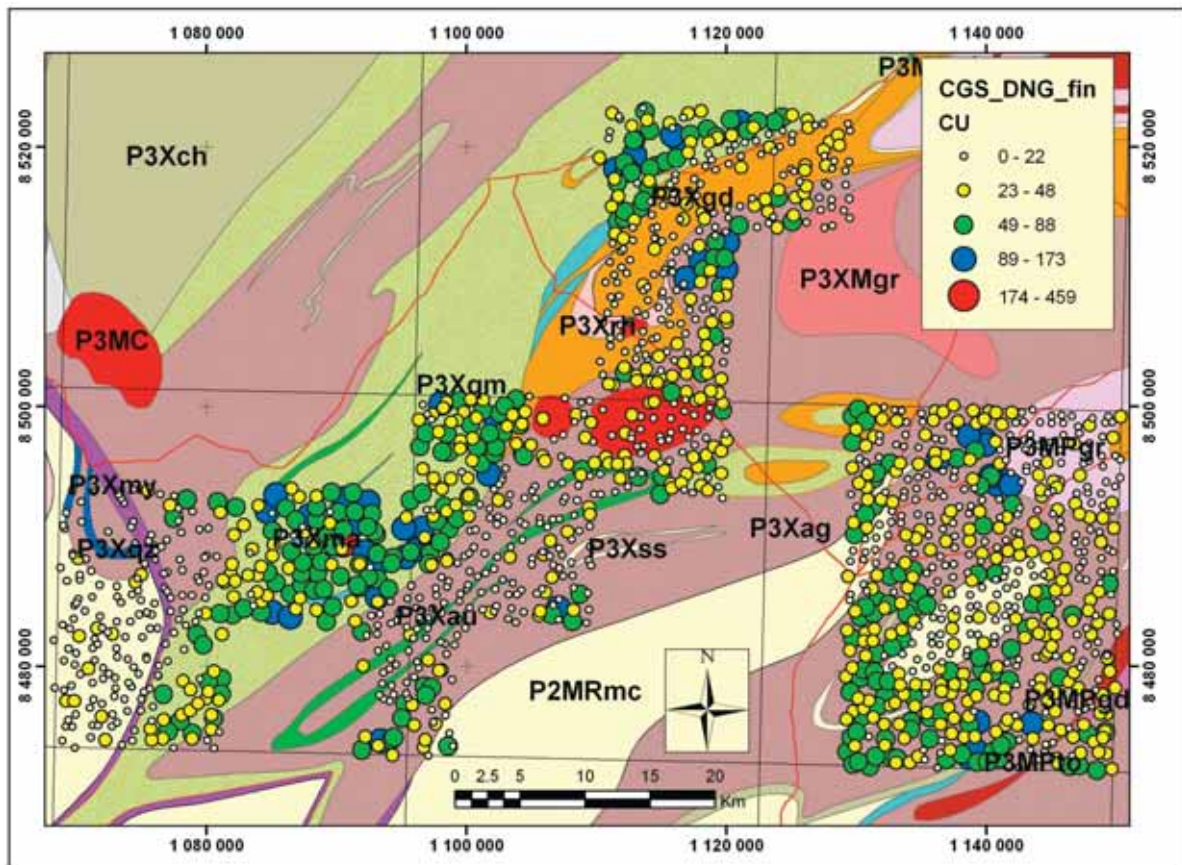


Fig. 19. Copper contents (in ppm) from the CGS-DNG soil survey plotted on a geological map. For general location, refer to Fig. 1. The highest Cu values are related to the Neoproterozoic Xixano Complex consisting of sedimentary quartz mica gneisses and schists, which are locally graphite-bearing (P3Xqm, green). For other rock types, see the text. Geology based on Norconsult Consortium (NGU-BGS) mapping (LOT 1).

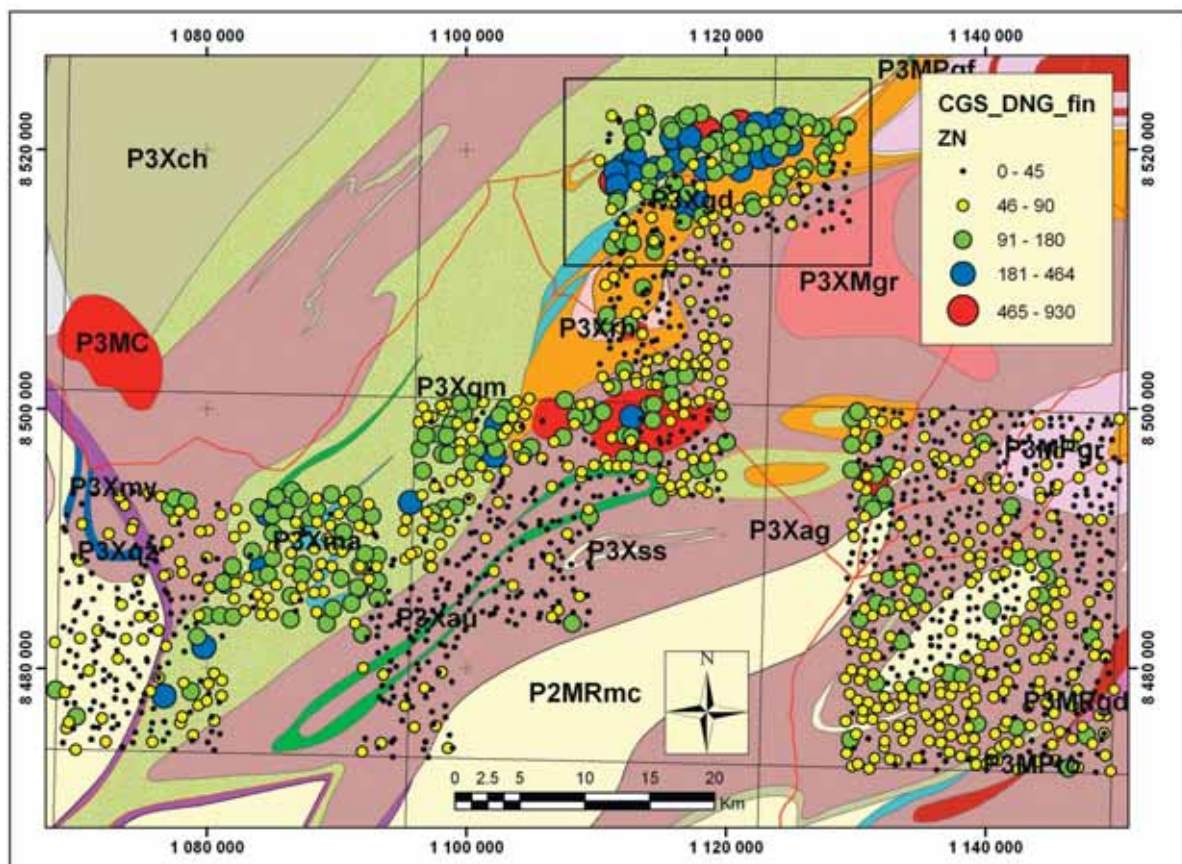


Fig. 20. Zinc contents from the CGS-DNG soil survey plotted on a geological map. The anomalous area is delineated by the black rectangular line. For geology, see the text.

LKAB survey

The LKAB survey area is situated within the GIM regional survey area and covers 480 km² (LKAB 1979, 1980). It included 243 samples of minerogenic material in drainage systems (Ss) that were analyzed for Sn, Nb and Ta. Additionally, La and Sn contents were analyzed from organic material (plant roots). The maximum Nb content was 1414 ppm, three samples having values around 200 ppm, but in general they were low (< 8 ppm). The situation

was the same with Ta, with only four samples having values >100 ppm, the maximum being 750 ppm. The highest Sn contents (maximum 0.5%) were related to the samples with maximum Nb and Ta values originating from the vicinity of an exhausted tin mine. On the basis of the analytical results, LKAB made recommendations for field work areas. For comparison, one of the GIM soil survey areas targeted the LKAB tin anomaly (cf. Fig. 2).

BHB Namapa survey

The BHB gold survey in Namapa area, in the border zone between the Cabo Delgado and Nampula Provinces, included several stages (BHB 1999). Stream sediments were collected in two, partly overlapping areas. Both stages indicated gold anomalies situated in the north-eastern part of the study area

(Fig. 21). The results of the detailed follow-up soil survey are shown in Fig. 22. Geologically, gold anomalies seem to be related to the Neoproterozoic plutonic mafic granulites of the Ocua Complex shown in brown in Fig. 22.

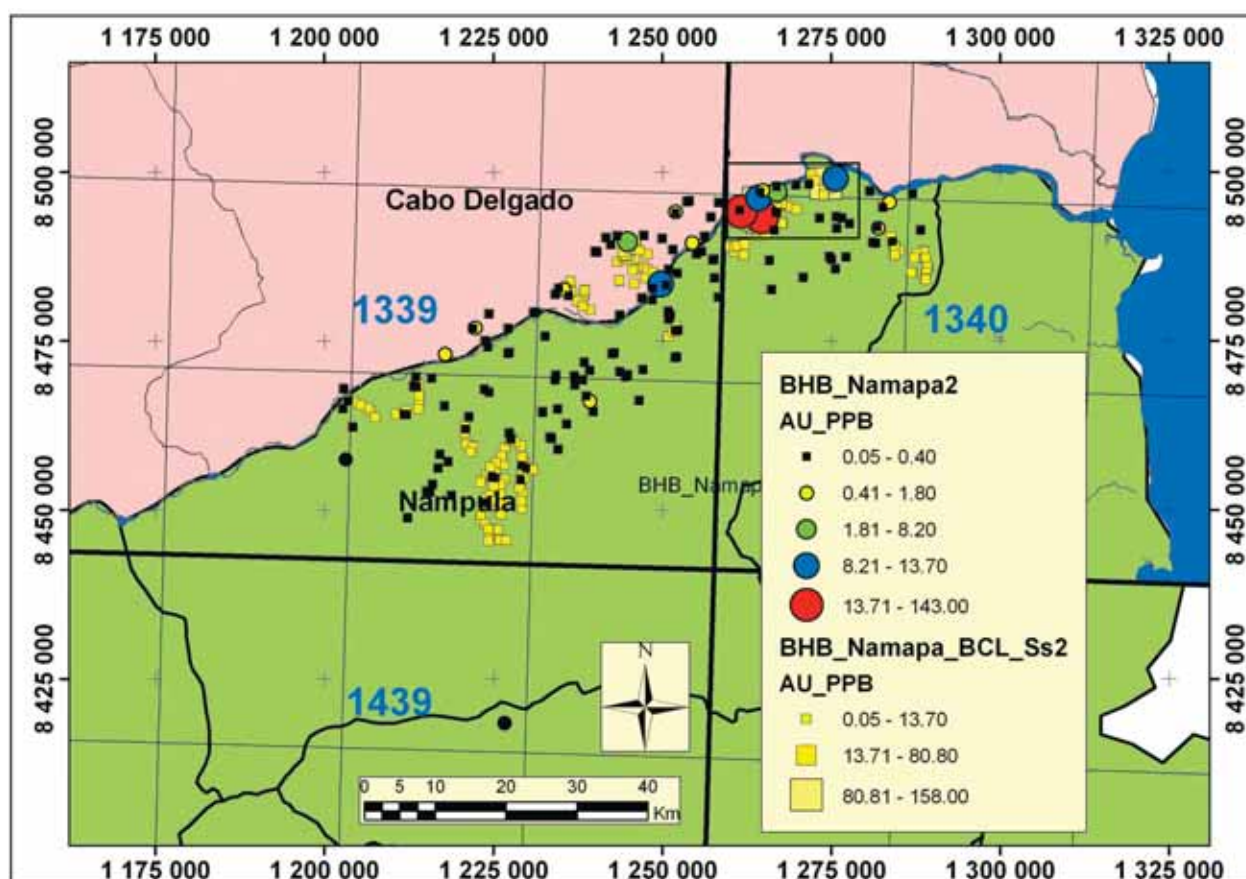


Fig. 21. Location of the BHB Namapa survey area in the border zone between Nampula and Cabo Delgado Provinces. The Au values at different sampling points are also shown. The outlined rectangular anomalous area in the NE corner is displayed in detail in Fig. 22.

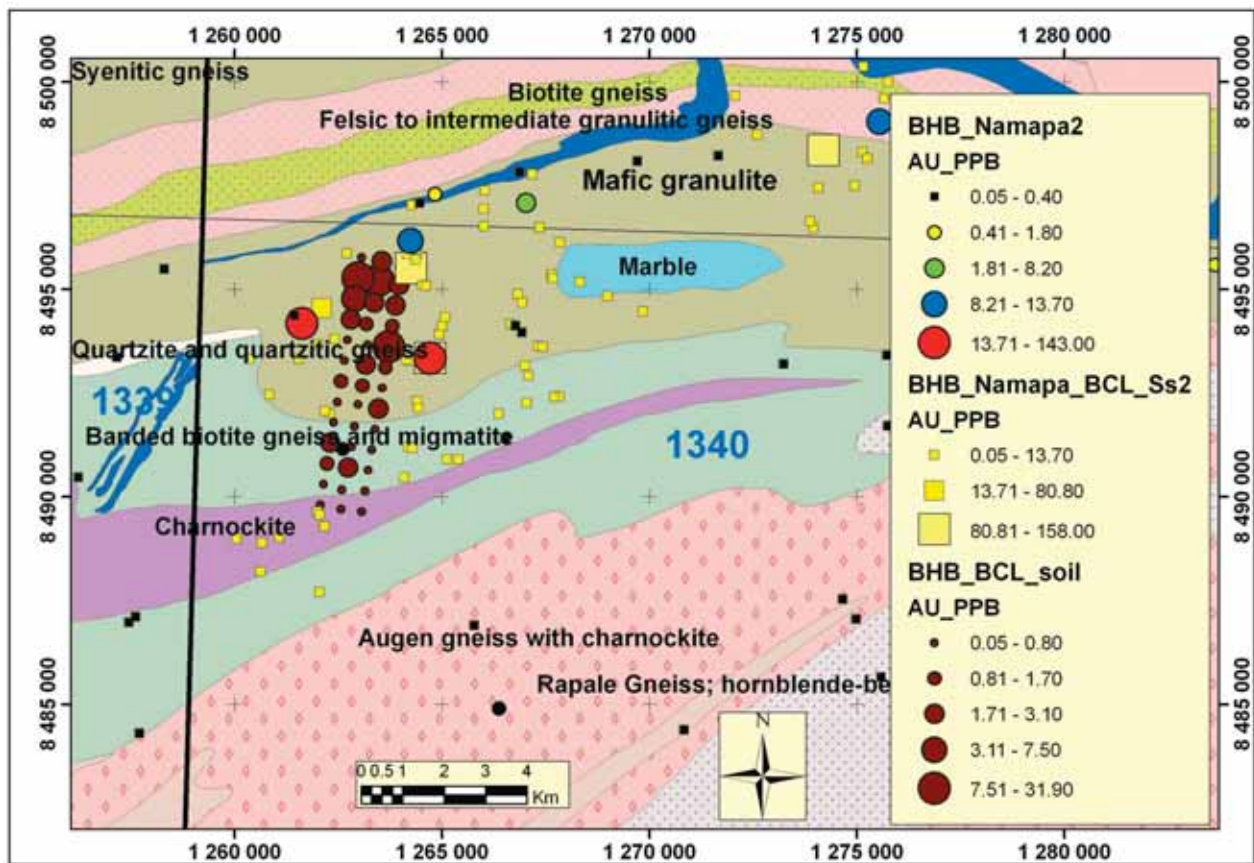


Fig. 22. Gold contents of stream sediment and soil samples plotted on a geological map. The most anomalous samples are related to Neoproterozoic plutonic mafic granulites of the Ocua Complex shown in brown. Other rock types are as written on the map. Detail of Fig. 21. Geology based on Norconsult Consortium (NGU-BGS) mapping.

FINAL OUTCOMES AND INTERPRETATION OF THE ANOMALOUS AREAS

In addition to the extensive training component of the GIM project, the most important concrete outcome is the data compilation stored in the digital and easy-to-use **Geochemical Data Base** (GIM_GDB). It consists of two main components: (1) the **Survey Information Table (SIT)** containing general survey specifications (i.e. metadata) and (2) the **Analysis Data Tables (ADTs)** including the actual analytical and coordinate data from different surveys. ADTs for different projects have been grouped into a specific lyr type of file that can be easily added into an ArcGIS Map document from the GIM_GDB.

The final results of the GIM geochemical survey consist of the following outcomes stored on the GIM DVDs (available from DNG):

- GIM Geochemical Database (GIM_GDB) and related geochemical maps
- Final report of the GIM project (Korkiakoski 2007)
- GIM Final Technical Report (Pekkala *et al.* 2007)
- GIM Field Manual (Korkiakoski & Salminen 2006)
- Scanned and georeferenced original geochemical maps (digital)

Recommendations for future exploration targets

On the basis of the geochemical data sets of Mozambique, as compiled and interpreted during the GIM project and discussed in more detail in this paper, the recommended exploration targets for future

surveys are summarized in Fig. 23. For additional information of mineral resources potential of Mozambique, see Lehto & Gonçalves (2008, this volume).

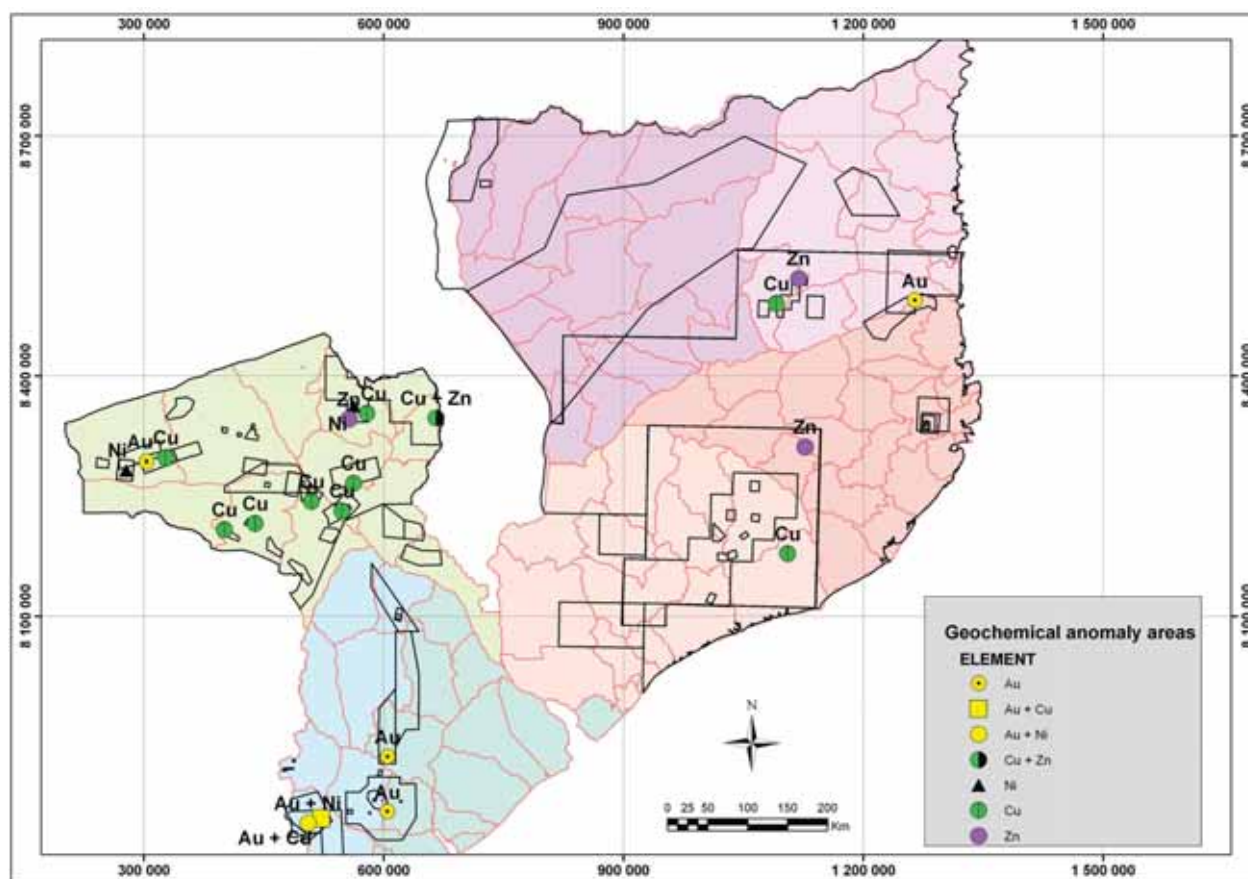


Fig. 23. Recommended areas for further exploration and follow-up surveys. Interpretation is based on the geochemical data compiled during the GIM Project. The areal distribution of the various sampling programmes is also outlined.

ACKNOWLEDGEMENTS

I would like to express my sincere thanks to my Mozambican counterparts and colleagues Vicente Manjate and Salomão Mujui for their involvement and input into all phases and activities of the GIM project, particularly the data capture and field activities. They have done their share with enthusiasm and a positive attitude and can be considered as qualified geochemists. Through the experience they have gained during the GIM project they are

now able to plan and conduct any future objective-oriented geochemistry project independently using modern GIS aided methods. In addition, I would like to express my gratitude to DNG management and field teams, without whose contribution the objectives of the project would not have been met. Professor Reijo Salminen is thanked for his comments and corrections to the manuscript.

REFERENCES

- Aquater 1983.** Cartografia geologica e prospecção mineira e geoquímica nas províncias de Nampula e Zambezia, I, II, III. Relatório Final. Unpublished Report. DNG Library reference No. 1244, Maputo.
- Ashanti Goldfields 1996.** Final report on reconnaissance sampling programme in the Gorongosa project area. Licence 428/L/96. Unpublished Report. DETEMIN reference No. 1052/1043.
- BHB 1999.** Final Report for Namapa Reconnaissance. Licence No 520/L/97. Unpublished Report. DETEMIN reference No.1055.
- Chakrabarti, A. K. 1983.** Regional geochemical exploration of the Angonia-Macanga region, Tete province. Final report. UN/DTCD MOZ 80-013. Unpublished Report.
- De Waal 1996.** Report on the regional geochemistry of the Namuno-Balama region, Cabo Delgado Province northern Mozambique. Digital data from CGS.
- Gonçalves, R. Jr. 1998a.** Ashanti Goldfields Ltd; 1988 progress and final report on the exploration programme in the Bandire project area, Licence 530/L/97.
- Gonçalves, R. Jr. 1998b.** Ashanti Goldfields Ltd; Rotanda-Mavita project, Licence 366L/L/96.

- Gonçalves, R. Jr. 1998c.** Ashanti Goldfields Ltd; Pesa-Mus-sapa project area, Licence 531/L/97.
- GTK Consortium 2007.** DVD Final Products: Maps, Map Ex-planations and Final Technical Reports, GTK Consortium, June 2007.
- GTK Consortium 2006a.** Map Explanation; Volume 1: Sheets 2032 – 2632. Geology of Degree Sheets, Espungabera/Chiba-bava, Nova/Mambone, Massangena, Chidoco, Save/Bazaru-to, Chicualacuala, Machaila, Chigubo, Mabote/Vilanculos, Rio Singuédzi/Massingir, Rio Changana, Funhalouro/In-hambane, Chilembene, Chókwè, Zavala/Inharrime, Maputo, Xai-Xai/Zavala and Bela-Vista, Mozambique. Ministério dos Recursos Minerais, Direcção Nacional de Geologia, Maputo. 341 pages and 5 appendices.
- GTK Consortium 2006b.** Map Explanation; Volume 2: Sheets 1630 – 1634, 1732 – 1734, 1832 – 1834 and 1932 - 1934. Geology of Degree Sheets Mecumbura, Chioco, Tete, Tam-bara, Guro, Chemba, Manica, Catandica, Gorongosa, Ro-tanda, Chimoio and Beira, Mozambique. Ministério dos Re-cursos Minerais, Direcção Nacional de Geologia, Maputo. 411 pages and 4 appendices.
- GTK Consortium 2006c.** Map Explanation; Volume 3: Sheets 1735-1739, 1835-1836 and 1935. Geology of Degree Sheets Mutarara, Quelimane, Namacurra/Maganja, Pebane, Mar-romeu/Inhaminga, Chinde and Savane, Mozambique. Min-istério dos Recursos Minerais, Direcção Nacional de Geolo-gia, Maputo. 240 pages and 2 appendices.
- GTK Consortium 2006d.** Map Explanation; Volume 4: Sheets 1430–1432 and 1530–1534. Geology of Degree Sheets In-hamambo, Maluwera, Chifunde, Zumbo, Fingoè-Mágoè, Songo, Cazula and Zóbuè, Mozambique. Ministério dos Re-cursos Minerais, Direcção Nacional de Geologia, Maputo. 382 pages and 4 appendices.
- Hunting Geology and Geophysics Ltd 1984.** Mineral Inven-tory Project. Unpublished Report, 329 p. DNG Library ref-erence No. 1324. Maputo.
- Korkiakoski, E. 2006.** Geochemical surveys in Mozambique – a data compilation project. In: CAG 21 - Chapter 2: Geo-chemistry and Geochronology. CAG 21. Extended abstract and oral presentation. Title 107. 2 p.
- Korkiakoski, E. 2007.** Results of the GIM Geochemical Sur-veys, Final Report, Oct 2007. Mineral Resource and capac-ity building project, Republic of Mozambique. Component 2: Geological Infrastructure Development Programme; Geo-chemical and Industrial Mineral Surveys (GIM). Unpub-lished Report. 69 p.
- Korkiakoski, E., Manjate, V. A. & Mujui, S. E. 2008.** Old regional geochemical data as targeting tool for exploration – a data compilation project of Mozambique. 33 IGS. Oslo. Abstract and oral presentation. 1 p.
- Korkiakoski, E. & Salminen, R. 2006.** Field Manual for geo-chemical survey. Mineral Resource and capacity building project, Republic of Mozambique. Component 2: Geologi-cal Infrastructure Development Programme; Geochemical and Industrial Mineral Surveys (GIM). Unpublished Report. 22 pages and 1 appendix (Field Form).
- Leal, V. P. 1972.** Prospeccção geoquímica sistemática na região de Mavita. DNG Library reference No. 677. Maputo.
- Lehto, T. & Gonçalves, R. 2008.** Mineral Resources Potential in Mozambique. Geological Survey of Finland. Special Pa-per 48, 307–321.
- LKAB 1979.** Preliminary exploration work in the Inchope-Doeroi area, Mozambique. Unpublished Draft Final Report, DNG Library reference No. 973, Maputo.
- LKAB 1980.** Inchope-Doeroi- Final Report. Unpublished Re-port, Serv. Nac. Geol. No. SNG 214/80, Maputo
- Manjate, V. A. & Mujui, S. E. 2006.** Geochemistry in Mo-zambique. In: CAG 21 - Chapter 2: Geochemistry and Geo-chronology. CAG 21. Extended abstract. Title 110. 2 p.
- Pekkala, Y., Korkiakoski, E., Kuivasaari, T. & Lehto, T. 2007.** Final Technical Report. Mineral resource and capac-ity building project, Republic of Mozambique. Component 2: Geological Infrastructure Development Programme; Geo-chemical and Industrial Mineral Surveys (GIM). Unpub-lished Report. 48 pages and 2 appendixes.
- Pekkala, Y., Lehto, T. & Lehtonen, M. I. 2008.** Introduction to GTK projects in Mozambique in 2002–2007. Geological Survey of Finland. Special Paper 48, 7–22.
- SGM 1970.** Relatório da campanha de prospecção geoquímica nas áreas de Mavita, Gogoi e Espungabera. DNG Library reference No. 910/715,
- Tecnosynesis 1980.** Estudo de avaliação do potencial de desen-volvimento e estudos de inventário dos recursos hidráulicos da bacia hidrográfica do rio Lugenda- Geologia e recursos minerais. Departamento Nacional do Aqua. Unpublished Report.

REVIEW OF INDUSTRIAL MINERALS IN MOZAMBIQUE

by

Yrjö Pekkala¹, Tapio Kuivasaari², Reinaldo Gonçalves³,
Mário Deus³, Fatima Chaúque⁴ & Carlitos Almeida⁴

Pekkala, Y., Kuivasaari, T., Gonçalves, R., Deus, M., Chaúque, F. & Almeida, C. 2008. Review of industrial minerals in Mozambique. *Geological Survey of Finland, Special Paper 48*, 289–306, 12 figures and 4 tables.

About 40 different industrial minerals (IM) are known to occur in Mozambique. However, at present their utilization for the production of basic construction materials as well as household and various industrial commodities is rather limited. In fact, the present situation is worse than it was in the 1960s and 1970s and this concerns the whole IM sector. In comparison with South Africa, the consumption of various industrial minerals in Mozambique is 10–20 times lower, and compared to industrialized countries the figures may be 100–200 times lower.

Taking into account the consequences of this situation it is quite clear that the basic infrastructure and housing facilities cannot be developed to a level that would markedly improve the living standards and conditions of the people. This also has a significant influence on the general socio-economic situation in the country. Without domestic production, most IM-based materials and goods have to be imported and this consumes a lot of foreign exchange.

In Mozambique there are many basic industrial mineral occurrences that meet the size and quality requirements for the production of the most important IM-based commodities. At present, economically the most important IM deposits in Mozambique are world-class heavy mineral sands at Moma (production started in 2007) and Corridor Sands at Chibuto (in the feasibility stage). Extensive coal deposits in Tete Province are also being thoroughly investigated, the most advanced investigation being the Moatize project (in the feasibility stage).

It is highly recommendable that the national authorities and companies involved in the IM sector seriously consider active measures to improve the prevailing, unsatisfactory situation that greatly affects the overall development of the country.

This review is based on the country-wide assessment of industrial minerals in Mozambique, carried out by the GTK Consortium in 2005–2007.

Key words (GeoRef Thesaurus AGI): economic geology, review, industrial minerals, construction materials, production, import, markets, Mozambique.

¹ *Geological Survey of Finland, P.O. Box 96, FIN-02151 Espoo, Finland*

² *Geological Survey of Finland, P.O. Box 1237, FIN-70211 Kuopio, Finland*

³ *Gondwana - Empreendimentos e Consultorias, Limitada – Caixa postal 832, Maputo, Mozambique*

⁴ *National Directorate of Geology, Praça 25 de Junho, 380, Maputo, Mozambique*

E-mail: yrjo.pekkala@gtk.fi tapio.kuivasaari@gtk.fi gondwana@tvcabo.co.mz

INTRODUCTION

Mozambique has a large and diverse mineral resource potential. Despite this wealth, commercial mining and the overall utilization of mineral resources have played a relatively minor role in the development of the country's economy and social welfare, amounting to only 1.8% of GDP in 2006 (Yager 2007).

This review of industrial minerals (IM) in Mozambique will highlight the situation of the IM sector in general and in comparison with South Africa. General comments about the market are also made.

Industrial mineral raw materials and commodities made of these are essential for the economic development of any nation. The improvement of infrastructure and growth of the manufacturing sector requires a reliable supply of good quality construction materials based on a wide range of industrial minerals. Industrial minerals are also essential raw materials for various household and housing commodities in our every day life.

Unfortunately, in most developing countries the industrial mineral sector is poorly developed. Therefore, despite significant industrial mineral re-

sources, developing countries continue to import these materials and ready-made products to supply their industries and directly the people. The threshold to utilize indigenous resources may be high because they have not been tested properly to prove that they meet the required industrial specifications and/or that the facilities and expertise to carry out the necessary evaluation and test work may not be available.

Unlike metallic minerals, the usability of industrial minerals generally depends more on physical than on chemical properties. A wide range of laboratory tests are needed to determine several inter-related properties that have to meet the requirements of consuming industries. Viable processing methods must also be studied.

However, once the above test work has been carried out successfully, the investments needed to set up the production of various industrial minerals are generally much lower than for metallic minerals. Of course, an entrepreneur with sound managerial and technical skills is required to run the business.

OVERVIEW OF IM COMMODITIES IN MOZAMBIQUE

The map in Fig.1 presents over 350 deposits or occurrences of industrial minerals per se and of construction materials that are included in the Industrial Mineral Database of Mozambique. The work was carried out under the Mineral Resource Management Capacity Building Project within the Geochemical and Industrial Mineral Surveys (GIM) by the GTK Consortium in 2005–2007. A more detailed description of the activities and the results is presented in the Final Technical Report and Final Report: Results of the Industrial Mineral Survey of

the GIM, which were delivered to the National Directorate of Geology in Mozambique at the end of the project.

Fig. 2 presents the high priority areas of IM commodities in the country. Table 1 summarises the statistics for the production of industrial minerals and construction materials in Mozambique and Table 2 the number of valid mining licences. In Table 3 the export and in Table 4 the import of IM commodities is presented.

Heavy mineral sands

Mozambique has several potential heavy mineral deposits along the 2500 km long coastline. Some of these are world class deposits in terms of grade and volume, such as the three most advanced projects which are briefly described in the following.

Moma

In April 2007 Kenmare Resources PLC from Ireland started the production of Ti and Zr minerals at

their Moma property, in Nampula Province, and the first shipments were made in December 2007. According to the plan, 16.4 Mt ilmenite will be produced within the next 20 years, while the total reserves are 163 Mt (Mining Weekly, May 2007). The initial production of ilmenite concentrate was planned at 700 000 tonnes per year; however, in 2008, production is already expected to reach 800 000 tonnes of ilmenite, 56 000 tonnes of zircon and 21 000 tonnes of rutile (Industrial Minerals, December 2006).

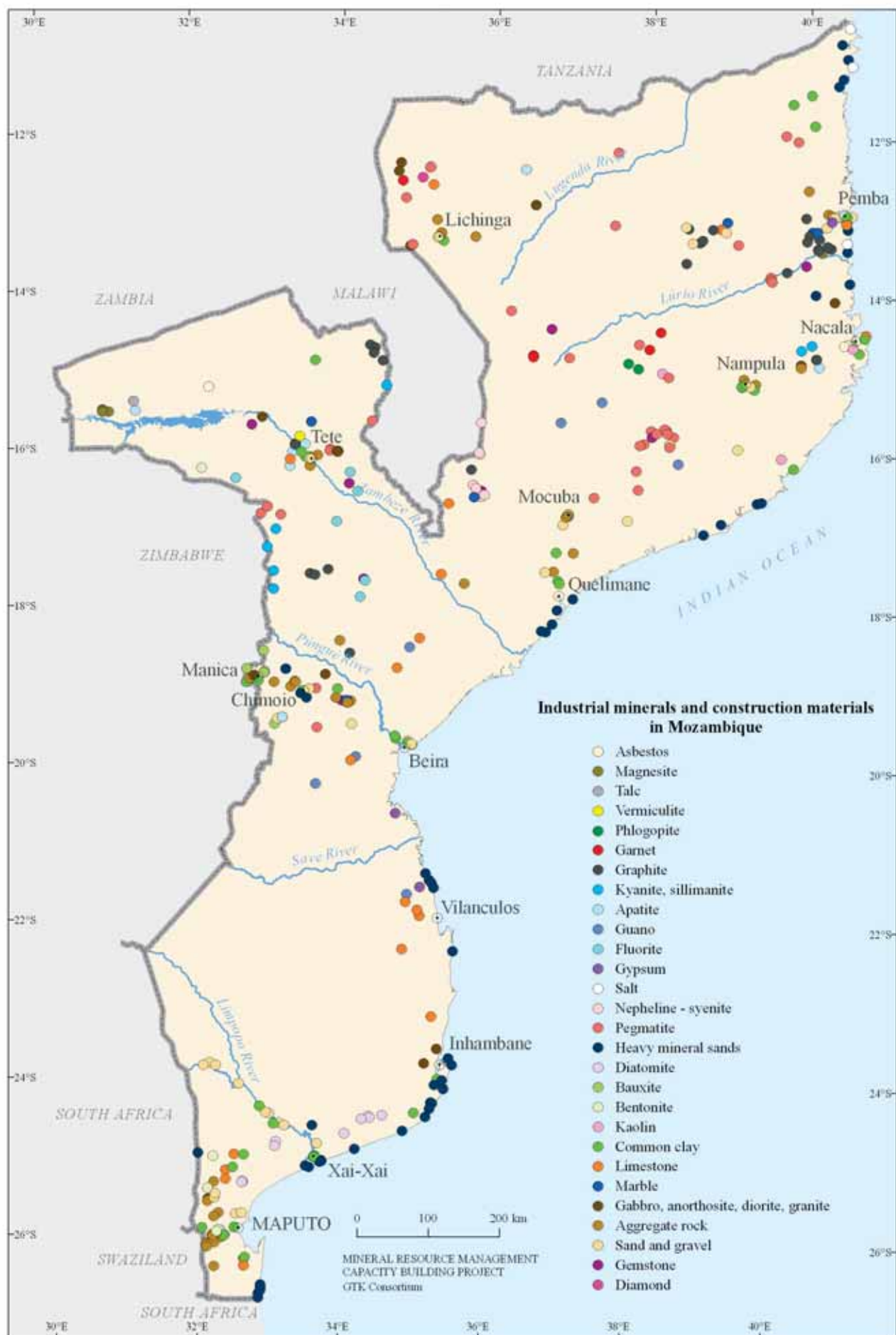


Fig. 1. Industrial minerals and construction materials in Mozambique.

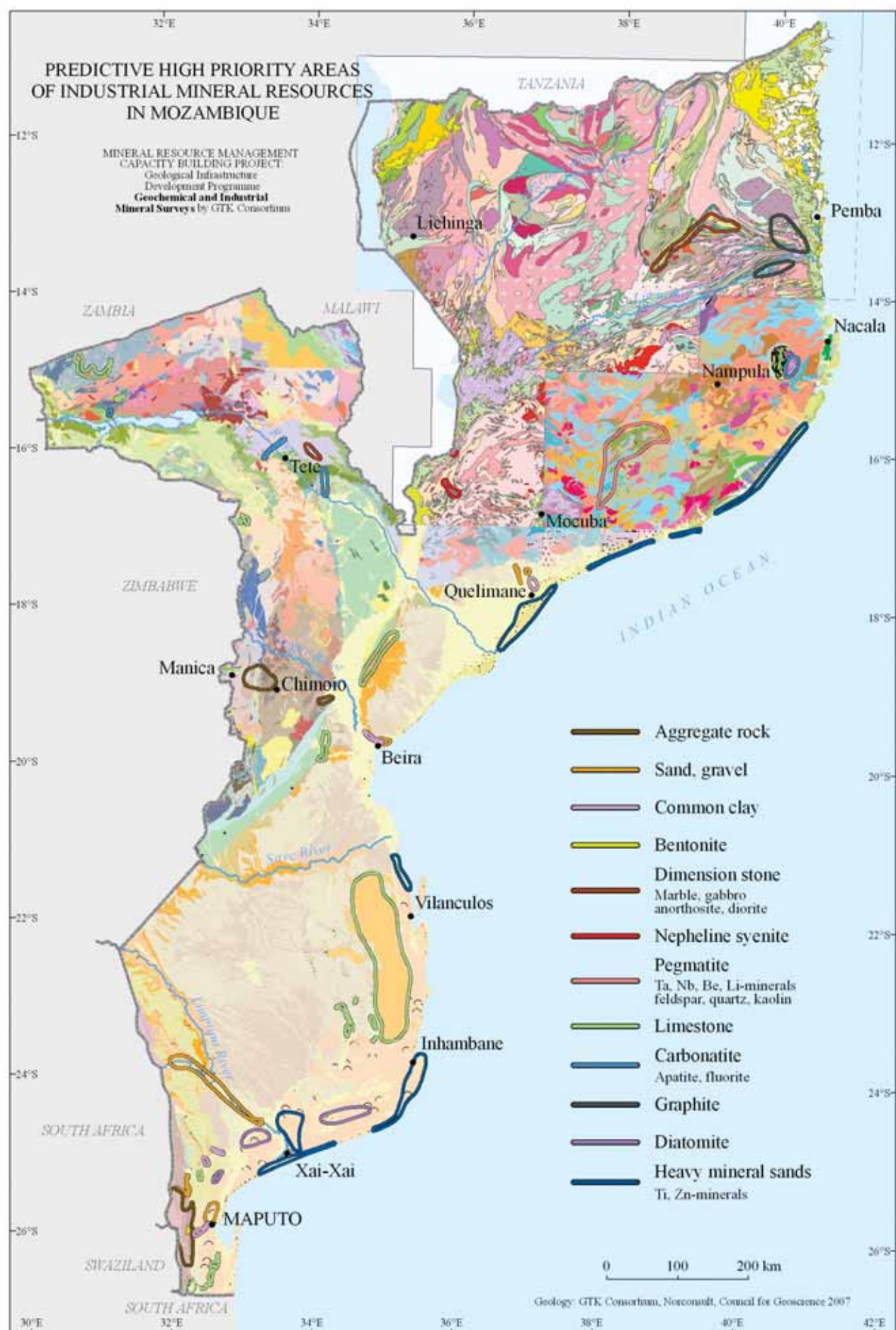


Fig. 2. The high priority areas of industrial mineral commodities in Mozambique. The geology of this map is based on the maps produced by the GTK Consortium, Nordconsult and the Council for Geoscience (South Africa) during the country-wide mapping programme in 2002–2007.

This project alone will greatly boost Mozambique's mineral industry. Total investments of the project will rise to over \$400 m., including a 150-km powerline, concentration and roasting plants and a 450-m jetty for loading, as well as accommodation and social facilities for the employees. Altogether, the project is planned to create more than 400 permanent jobs when working to capacity.

Corridor Sands

BHP Billiton PLC's ilmenite project at Chibuto near Xai Xai in Gaza Province is at present at a standstill, because the costs have shot up since a feasibility study was completed in 2002 by WMC Resources, which BHP acquired in 2005.

However, BHP is fully committed to the project, and Corridor Sands "needs a new configuration to make it work" (BHP press release, February 2007). Under the revised plan, BHP will separate the mine from the smelter, which will be located close to Mozal aluminium plant, where BHP is a major shareholder. This would reduce the costs by US\$300

million. The project will be developed further in three phases, the first one costing over \$500 million, and the plant could be in production early next decade. With 100 Mt reserves of ilmenite, Corridor Sands will be a long-term asset of BHP's business strategy.

Rio Tinto Project

In addition to Kenmare and BHP Billiton, Rio Tinto PLC is also involved in exploring heavy mineral sands in Mozambique. They have carried out extensive drilling, sampling and testing programmes on several blocks along the coast between Inhambane and Xai Xai. However, Rio Tinto has not yet reached the stage of a feasibility study, which means that many years will pass before any decisions on production can be made. It should also be noted that Rio Tinto has a much further developed heavy mineral project in Madagascar, which naturally has a major effect on Rio Tinto's overall plans in the TiO₂ business.

Limestone and dolomite

Sedimentary limestones occur as extensive formations in the sedimentary sequence of coastal Mozambique (Lächelt 2004). The most prominent formations are the Salamanga (Fig. 3) to the south of Maputo and Cheringoma in two areas, along Buzi River to the west of Beira and on the Cheringoma plateau area to the north of Beira. Tertiary Salamanga limestones are exposed over a zone more than 10 km long and 1.5–2 km wide. The average thickness is 32 m. The second large accumulation is the Miocene Jofane Formation, extending from south of Save River to Inhambane. All these deposits have large reserves of limestone that meet the quality requirements for cement, agriculture and other purposes. At present major production is only taking place at Salamanga for CIMOC's Matola cement plant. In addition, minor amounts of coral limestone from Relanzapo area near Nacala are mixed into imported clinker for cement production in the Nacala plants of CIMOC and ARJ Group. The third cement plant of CIMOC, close to Beira in Dondo, acquires limestone from Muanza quarry (Cheringoma Formation), about 100 km north of the plant, mixing it with imported clinker in cement manufacture.

Crystalline limestones (marbles) are present in almost all Archean – Precambrian complexes in Mozambique. Previously, several of these were used for lime production; one was near Manica, another in Boroma, near Tete, and the third at Malula near Lichinga. Some other carbonate rock deposits have also been utilized for lime. However, at present there is no production in the country and the lime needed for the sugar and other industries is imported.

Cement production from domestic raw materials is currently also being reduced. At the moment, three cement plants (Dondo, near Beira and two in Nacala) use imported clinker, and in the Matola plant, decreasing amounts of Salamanga limestone are also being used and more clinker is being imported (Tables 1 and 4).

At Montepuez in Cabo Delgado (Fig. 2), a large marble deposit is quarried for dimension stone (slabs, plates, blocks). The deposit is mainly dolomite in composition and in certain layers the dolomite is very pure in chemical composition (see: GTK Consortium 2007b, Results of the Industrial Mineral Survey).



Fig. 3. Salamanga limestone quarry, Bela Vista.

Table 1. Industrial mineral (IM) production during 1996 – 2006.

COMMODITY	Unit	1996	1997	1998	1999	2000	2001	2002	2003	2004	2005	2006
Bauxite	t	11 460	8 218	6 132	7 883	8 130	9 592	9 119	11 793	8 977	9 518	11 069
Bentonite	t	11 847	13 782	11 133	11 187	29 987	21 865	16 174	25 311	20 571	17 865	4 207
Beryl	t					18.8	0.8	54.0	78.3	27.3	146.3	16.4
Carbonate rock	t					585 590	729 230	1 301 232	1 348 372	1 593 449	654 179	155 870
Graphite	t	3 283	5 125	5 889	4 006							
Quartz	t						24.7	31.3	31.0	173.5	294.7	195.1
Tantalite	t					25.000	27.000	46.900	188.700	712.100	88.025	51.153
Marble	m ²	9 881	13 820	2 736	16 296	14 640	15 303	9 980	10 227	13 666	12 153	12 825
Marble	m ³	744	251	117	117	453	320	453	320	617	509	472
"Granite"	m ³					795.0	661.5	669.7	539.0	520.8	2 198.0	
Dumortierite	t					60.0	50.0	40.0	40.0	113.0	10.0	664.0
Garnet	t										5.80	10.33
Clay	t							84 024	100 176	108 231	32 030	222 052
Sand	t					299 540	464 684	795 813	1 372 032	1 429 742	833 113	1 404 184
Aggregate	m ³			283 000	265 000	592 358	490 737	795 732	742 501	779 581	850 918	1 178 997

Source: Ministry of Mineral Resources, Mozambique.

Diatomite

Diatomite (*Kieselguhr*) has accumulated in many fluvial and lagoonal depressions between Pleistocene dunes from Inhambane in the north to Matutuine, south of Maputo. The diatomite was depos-

ited in rivers, small lakes and ponds under brackish to freshwater conditions. The deposits are usually small with a maximum thickness of 1.5–2.5 m. The Boane and Manhiça occurrences are best known.



Fig. 4. Diana diatomite quarry, Manhiça area.

The Manhiça diatomite deposit is located about 10 km southwest of Manhiça town and the main pit, Diana, is now in production after a long standstill (Fig. 4). The horizontal diatomite layer measures 0.45 km x 3.6 km and is about 4–5 m thick with an average overburden of 1 m. The estimated reserves are 1.5 Mt and the pure diatomite content is 50% (Afonso and Marques 1993). Additional deposits at Alvor and Marina in the same zone have estimated reserves of 0.96 Mt and 1.5 Mt. The Manhiça diatomite layers are distributed over a surface area of 1 100 km² (Cilek 1989). Diatomite is dried, milled, screened and split into various qualities and exported mainly to customers in South Africa.

However, the diatomite production does not appear in the statistics of the Ministry of Mineral Resources (Table 1). In 2006 the production was 100–120 tonnes per month, making over 1000 tpa (pers. comm. C. Braz, Diatomites de Mozambique). At present the local consumption is only minimal, and the real added value for these products is made abroad. Instead of utilizing this well studied and tested domestic resource, commercial diatomite products are imported into Mozambique.

There are also other diatomite occurrences between Magude and Chokwe at Maduaine and around the Mafuiane and Buoana, in Gaza Province.

Aggregate rocks

Karoo rhyolites provide a good raw material for aggregate. The majority of active stone quarries are located around Maputo, where the economic activity is highest. Stone quarries are concentrated in the districts of Namaacha, Boane, Matutuine and Moamba. The raw materials in southern Mozambique serve the development corridors along the National Road

EN1, Maputo Corridor (Maputo-Ressano Garçia), National Road EN2 (Maputo-Namaacha), Lebombo Corridor (Boane-South African border) and also the Limpopo-Chibuto Development Zone.

The quarried aggregate rocks are mostly rhyolites of the Lebombos Range. Rhyolite is more resistant against weathering than andesite and basalt from the

same range and is a good material for most road and other construction purposes. In the Moamba district, a good quality, fine- to medium-grained nepheline syenite is also quarried for aggregate by CMC, which with the other big construction companies Tamega, Extramac, Riolutos, Probrita, ARA Sul and MAM are all active in the Namaacha-Boane belt.

Most of the geological construction materials are used for roads and buildings, and accordingly the field verification of this study is focused on the area where the economic activity is greatest, i.e. around the city of Maputo. This is also seen in the number of valid mining licences (mining concessions and mining certificates) in Table 2.

The aggregate from the quarries of this area is transported and used along the coast as far as Gaza

and Inhambane (EN1), where suitable aggregate rock is not found due to geological reasons. Occasionally, aggregate for road rehabilitation has been transported as far as to the Save River. Road transport of bulk aggregate over hundreds of kilometres is expensive. Sea transport by barges would offer a much cheaper alternative, whenever possible.

In Gaza Province, rhyolite is quarried inland at Massingir. Large rhyolite blocks are transported 28 km to the Massingir dam construction site, where the blocks are used for the earth wall of an irrigation dam across dos Elefantes River.

Granodioritic domes along the Beira Corridor are quarried in several locations for road and railway rehabilitation. The closest exposed hard rocks to the coast and Beira are felsic to mafic volcanics at

Table 2. Number of valid mining licences for aggregate rock, sand & gravel and brick clay, Mining Cadastre, 2005.

PROVINCE	STONE	SAND & GRAVEL	CLAY	TOTAL
Cabo Delgado	1	3	-	4
Gaza	2	5	-	7
Inhambane	3	1	-	4
Manica	7	3	1	11
Maputo	17	37	5	59
Nampula	3	1	-	4
Niassa	-	-	-	0
Sofala	3	2	-	5
Tete	2	6	-	8
Zambezia	13	2	-	15
	51	60	6	117

Source: Department of Mines, Ministry of Mineral Resources, Mozambique.

Table 3. Export of IM commodities in Mozambique during 2003-2006.

COMMODITY	Unit	2003	2004	2005	2006
Bauxite	t	11739	6 723	6 610	2 766
Bentonite	t	24694	13 026	12 938	3 111
Beryl	t	21	0.9	2 369.0	0.3
Quartz	t			0.0	72.4
Diatomite	t				367.5
Tantalite	t	168.5	367.5	88.0	51.0
Marble	m ²	804	1 970	0	2 006
Marble	m ³				
"Granite"	m ³	330.4	2 787.0	0.0	20.0
Dumortierite	t	20.1	42.0	10.0	0
Garnet	t	0.72	6.89	2.15	0.23

Source: Customs Department of Mozambique.

Table 4. Import of industrial minerals and commodities in 2005 and 2006.

Commodity	Gross weight in tonnes 2006	Gross weight in tonnes 2005	Country of origin	Value in MMTn in 2006	Value in MMTn in 2005
Aggregates	67	123	SA	0,5	0,55
Dimension stone	203	48	SA	2,6	1,8
Salt	80	100	SA, Portugal, others	7,5	1,3
Asbestos	669	669	ZIM, SA	9,6	7,7
Silica sand	220	141	SA, India, Belgium, others	2,6	1,9
Other sands	223	212	SA, India	1,3	0,95
Kaolin	107	26	SA	1,9	2,2
Bentonite	23	9	SA, Portugal	0,6	0,14
Other clays	153	133	India, SA	2,6	1,7
Andalusite, kyanite	167	na	China, India	5,6	na
Chalk	242	48	SA, Tanzania, ZIM	2,3	0,16
Gypsum	7 100	8374	SA, Tanzania, ZIM	49,6	18.6 ?
Gibbsite, anhydrite	68	17,5	SA	0.1 ?	0.23 ?
Natural Ca-phosphates	70	19,8	SA, ZIM	0,5	0,4
Diatomite	61	35	SA	2,6	1,1
Dolomite products	89	88,5	SA	0,4	0,3
Quick lime	479	1117	SA	5,3	7,3
Slaked lime	1 850	94	SA	64,6	0,9
Hydraulic lime	1 300	1084	SA	7,8	6,4
Clinker or Portland cement	221 kt	116 kt	Several countries	779,9	459
White cement	275 kt	10.1 kt	SA, India	21	15.2 ?
Other cements	100.6 kt	80 kt	SA, ZIM	125	163
Nitric fertilizers	17 000	na	SA, Switzerland, others	279,8	na
Phosphatic fertilizers	218	na	SA	4,2	na
Potassic fertilizers	17	na	SA	2,8	na
Fert., Cont. 2–3 of N/P/K	17 300	na	SA, Switzerland, others	769	na

Source: Customs Department of Mozambique.

Xiluvo, where carbonatite rock is also quarried for upgrading of the national railway lines. Three quarries are currently in operation in the Xiluvo area. The Nharuchonga quarry, located some 120 km by road from Beira, produces aggregate, mainly from felsic volcanics.

About 100 km north of Inchope, on the western slope of Gorongosa Mountain, hard and dense charnockitic rock makes excellent aggregate and also the location is good. In the Chimoio – Manica area there are a few inselbergs of gneissose granitoids with good material for various aggregates whenever the demand arises.

In Tete Province there is one aggregate rock quarry in operation (CETA Lda) in Moatize. This exploits anorthosite-gabbro of the Tete Suite. Another,

currently dormant, quarry in Chacocoma granitoid-gabbro is located 20 km south of Tete town by the main road.

Crystalline granitic rocks, suitable for aggregates, are common in central and northern parts of Zambézia as well as in most parts of Nampula, Cabo Delgado and Niassa Provinces. However, only a few quarries are in operation in Zambézia and Nampula, where the demand for road and house construction is currently active. Small artisanal pits supply the need in areas without major construction activities. In coastal areas where hard crystalline rocks do not occur, fossiliferous limestone materials are commonly used for construction and much is produced by artisans (Fig. 5).



Fig. 5. Artisanal sale of limestone aggregate near Massinga, Inhambane.

Sand and gravel

In the Maputo area the availability of sand and gravel is not as good as that of rock aggregates. Most of the extraction sites contain fine-grained flood plain sand along the Umbeluzi River (Boane area) and Incomati River (Moamba area). The sand from these locations is best suited to mortar applications and fillings. Fine dune sand is also excavated for these purposes. Satisfactory gravel was only found upstream in the Umbeluzi River, near the town of Goba. Rather coarse and well-graded sand is also excavated at one site from the bottom of the Incomati River close to Moamba. North of Moamba towards Magude, gravel is found along the banks of the Incomati River at several sites in Gaza province. The pebbles are in general of limestone or calcarenite, indicating that such gravel does not fulfil the requirements of good, hard rock aggregate.

In the southern part of the Gaza province, sand and gravel deposits occur along the Limpopo and

dos Elefantes Rivers.

In most parts of Central and Northern Provinces, Manica, Tete, Zambezia, Nampula, Cabo Delgado and Niassa, sand and gravel are, in addition to hard rock aggregates, adequately available within a reasonable distance from the main development centres and sites of major demand.

Table 2 shows that the activities (number of valid licences) involving construction materials were rather small in northern territories in 2005, which clearly indicates that major construction projects were not ongoing. However, the situation has substantially changed since then owing to major construction works of roads, railways, and projects such as Moma ilmenite and Moatize coal. These, together with the high general growth of economy, will all contribute to the greatly increasing demand for all kinds of construction materials in Mozambique.

Clays

Bauxite

Bauxite occurs in a lateritic weathering profile at Moriangané near Manica just on the border with Zimbabwe (Fig. 6). The deposit comprises several

small, only 1m thick bodies of bauxite and gibbsite that are overlain by kaolinitic clay (Cilek 1989). Mining has been on going since the late 1930s and in recent years the production has totalled about 10 000 tonnes per year. This has been exported to

Zimbabwe and mainly used as a raw material for aluminium sulphate. Bauxite reserves have been estimated at 10 Mt and those of white kaolinitic clays are assumed to be from 10 to 15 Mt.

Bentonite

Bentonite occurs as a weathering product of rhyolites and rhyolitic tuffs of the Karoo volcanics in the Libombos Pequenos range of the Boane area, in the southwest.

The proven and probable reserves have been estimated at 6.5 Mt. The quality of montmorillonitic Ca bentonite is hampered by a high content of cristobalite (Cilek 1989) or opaline silica (Presley 1991). The production was about 20 000 tonnes per year from 2000–2005 and it is exported mainly as bulk to South Africa and Zimbabwe. Only a few hundred tonnes have been Na-treated annually at site.

Kaolin

Various types of kaolin occurrences are common in Mozambique. Hydrothermal types are only of theoretical interest and known sedimentary deposits

are of low grade. However, several weathering-type deposits are known from pegmatite bodies, especially in the Alto Ligonha district in Zambezia and Nampula Provinces. Only at Ribaue pegmatite mine has kaolin previously been produced as a by-product, but today this occurs nowhere.

It is known and reasonably well studied that a few other pegmatites (Muiane, Marropino, Nuaparra, Boila) also have a rather thick kaolinitic weathering crust (Fig. 7). Considering the available test results of various kaolins, it looks obvious that at least some of these could easily be processed to meet the properties required for different industrial uses: for instance, co-processing of kaolin as a by-product in pegmatite (tantalite) mining. The results of Muiane kaolin tests as part of the Industrial Mineral Survey have been published in a report (GTK Consortium 2007b).

Other clays

Other clays of differing quality are known in most parts of the country where the demand has existed. The deposits consist of plastic, kaolinitic and common types, but until now serious studies on their quality, usability and amount have only occasionally been carried out (Lächelt 2004).



Fig. 6. Moriangane bauxite mine, Manica.



Fig. 7. Kaolin weathering in Muiane pegmatite.

At present, even the production of normal bricks for construction is at a standstill in many districts where industrial scale factories previously operated. Ceramic tiles and similar goods are all presently imported.

Without sufficient industrial production of common bricks for construction, most of these are made

by local people (Figs 8 and 9). This takes place around the large country, often utilizing unsatisfactory raw materials and consuming huge amounts firewood for very inefficient burning of bricks. This is contributing to the devastation of forests and before long other environmental problems will also appear (e.g. increased flooding).



Fig. 8. Artisanal brick production in Magude, Maputo.



Fig. 9. Ceramica de Vila Pery brick factory, Chimoio.



Tantalite

The potential of pegmatite minerals, especially tantalite, is known to be good in Mozambique and the area with the best potential is Alto Ligonha in Zambezia and Nampula Provinces (Afonso & Marques 1993).

At present, the *Marropino deposit* is the only one where tantalite is exploited on an industrial scale (Fig. 10). The operator is Highland African Mining Company (HAMC), and they plan to establish a new processing plant to improve the recovery of tantalite and increase the capacity. The deposit itself consists of strongly weathered (kaolinized) pegmatite, containing various bodies, the main one being over 550 m long and 250 m wide. Hard quartz veins occur occasionally. The reserves have been estimated at 10 Mt with a tantalite content below 300 g/t. With the planned capacity, the reserves to be mined will be exhausted in seven years. In addition to tantalite, the deposit contains small amounts of morganite and other semi-precious stones, and at present there are plans to also recover these in processing.

The *Muiane deposit* is also a strongly kaolinized pegmatite body (1200 m x 100m), which was already mined in colonial times (Cilek 1989). After a break of several years in operation, Metallurgical Design and Management (MDM) of SA is currently setting up a new processing plant. As in Marropino, the tantalite grade in Muiane is also less than 300 g/t.

At the *Naquissupa deposit*, Hegemony Resources set up a processing plant with an installed capacity of 120 t/h. The construction was completed in November 2001 when production was to be started. However, no tantalite ever came for sale. Surprisingly, the plant was planned for soft rock (kaolinized) material, but the deposit mainly consists of hard rock. At present, the unused processing plant

and other machinery are rusting in Naquissupa.

In Mozambique the *Morrúa pegmatite deposit*, close to Marropino, has obviously the best potential of the tantalite resources. It covers about 0.6 km² and is mineable to a depth of 100 m. The deposit has a long and colourful history starting from colonial times, but at present everything is at a standstill. Only 100–200 artisanal miners are panning tantalite in nearby Melela River. The deposit is a hard rock pegmatite body with developed zoning. The reserves are estimated at 3.5 Mt in hard rock and about 1.5 Mt in eluvium and re-processable “waste”. The tantalite grade in hard rock is estimated at 700 g/t Ta₂O₅. In 2003 the company KHA set up a pilot plant with a capacity of 30 t/h to process the existing waste, estimated to contain 200–300 g/t Ta₂O₅.

However, at present the ownership of the mineral rights to the Morrúa deposit are in the hands of the HAMC, which also operates in Marropino, and has plans to carry on its development. The African Ea-



Fig. 10. The tantalite plant at Marropino.

gle company is investigating its tantalite properties in the Namama Belt. Several other companies (Alvorada de Mocambique Lda, Australian Longreach Gold Oil Ltd and others) have also had or are holding tantalite mining and exploration licenses in the country.

Besides tantalite, the pegmatites in the Protero-

zoic rocks in Alto Ligonha also have a good potential for Nb and Li minerals as well as beryl, tourmaline and quartz, which occasionally occur even as gem quality varieties. In addition, the pegmatites contain feldspar and kaolin, which were previously also mined, and there is still the potential to re-start these activities.

Semi-precious stones

Pegmatites in Zambezia, Nampula and Tete Provinces are the most common host rocks of gemstone-quality minerals such as beryl, tourmaline, quartz and feldspar (Afonso and Marques, 1993, Lächelt, 2004). The pegmatites in the Alto Ligonha area, Zambezia, are particularly known and may have potential in the future (Bettencourt Dias & Wilson, 2000). Skarns, biotite schists and gneisses may host garnet, corundum, dumortierite and Karoo basalts may be agate-bearing. Most gemstones have been produced by artisanal small scale miners, who generally work periodically and often in the areas where pegmatites have been exploited on an industrial scale, mostly for tantalite. Owing to the

periodic work of artisans, the production figures of gemstones are unreliable and they also vary to a great extent annually (Table 1).

Some indications of diamonds have also been found in Mozambique, such as a few micro-diamonds recovered in Gaza Province, which are assumed to be derived from the alluvial sources of rivers draining from South Africa and Zimbabwe (Limpopo and Singédzi). Although close to 50 kimberlite pipes and dykes have been found in the Province of Niassa, to the north of the town of Lichinga, only a little work has been carried out to evaluate their diamond potential.

Salt

Mozambique is producing marine salt from evaporation ponds, which can sometimes be damaged by flooding, causing the salt industry to shut down temporarily. The salt is exported to Lesotho,

Malawi, Swaziland and Zimbabwe. There are plans to raise funds for the rehabilitation and long term development of the industry through the UN Industrial Development Organization (UNIDO).

Dimension stone

Marble is the only dimension stone that is permanently produced for sale in Mozambique (Fig. 11). *Marmonte in Montepuez* (Cabo Delgado) quarries white, grey and multicoloured marble blocks for processing in their facilities in the town of Pemba. A part of the production is exported (Table 1 and 3).

The “granites” in Table 1 are granites and anorthosites quarried in Tete Province. The quarries are at present mainly used for extracting blocks for material tests and market surveys, but not for permanent commercial exploitation. The licence holders are Marlin Granite from South Africa and Clover from Zimbabwe.

Massive ‘black granite’ (actually gabbro) is periodically quarried for export at Chainça near Manica, like anorthosite from the Tete Suite and porphyric granite from the Songo area. Some other sites have

also occasionally been exploited for dimension stone, but only on a small scale. Especially the de-



Fig. 11. Montepuez marble quarry, Cabo Delgado.

mand for Tete anorthosite/gabbro seems to greatly fluctuate, which obviously depends on the trends in the world market, for which these blocks are mainly aimed. Transportation by trucks to Beira port is currently also very costly.

Karoo rhyolites outcropping in the south-west have also occasionally been quarried for dimension stone, in Boane, Estevel and near Ressano Graça. The banding and folding of light brown rhyolites may be very ornamental. However, the block size in the fractured, dense rock is problematic.

Graphite

The graphite mine and dressing plant of *Grafites de Ancuabe*, 100 km inland from the port of Pemba, in Cabo Delgado Province, is owned by Kenmare Resources (84%) and the government of Mozambique (16%). The mine was in operation in 1994–1999 and it had a capacity of 10 000 tpa of high grade flake graphite concentrate (more than 98% carbon). Development of the mine was based on 24 Mt of ore reserves with 3 to 11% graphite, identi-

fied during the pre-1995 exploration. At present it is under care and maintenance. The high energy costs (diesel generated) and tightened price competition in the world market were major reasons for the standstill.

In addition to several other occurrences in Cabo Delgado, graphite occurs in Angónia, Tete Province, in biotite-amphibole gneisses, granulites and anorthosites (Cilek 1989, Lächelt 2004).

Phosphates

Norsk Hydro from Norway investigated Mozambique's largest phosphate deposit at Evate in the late 1990s. The Evate apatite-bearing carbonatite deposit is located within the Monapo Klippe (structure) in the Nampula Province. Norsk Hydro has defined the ore resource and initially estimated the exploitable ore in the regolith zone at 43 Mt 6.2% P_2O_5 . Unfortunately, no reports on the processing and quality of the apatite concentrate were available for this study. Almost four hundred drill holes were sunk and many of them also reached the fresh carbonatite. However, neither the results of processing tests, nor samples were found in the archives. A set of samples was collected from regolith material (Fig. 12) and from small outcrops of fresh rock for testing, and the results are given in Final Result Report of the GTK Consortium.

Besides Evate, other carbonatite bodies occur in Tete Province, of which Mt Muande and Mt Fema have potential for phosphates. Carbonatite pipes, Cone Negose and Mt Muambe have only marginal potential.

Mt. Muande carbonatite, about 30 km NW of Tete, was rather well investigated by a Yugoslav team in the 1980s. At that time the main interest was in the magnetite content of the deposit and apatite was only considered as a possible by-product (Brodoimpeks 1984). According to the report by the Yugoslav team,

apatite was difficult to concentrate. A set of samples of un-weathered, apatite-rich carbonatite was collected for processing tests by this project. The results are presented in GTK Consortium (2007b), Results of the Industrial Mineral Survey.

Guano deposits (from bats) occur in caves and caverns formed mostly in Tertiary limestones. The best known guano caves occur in the areas of Vilankulo, Buzi and Cheringoma. Previously (before 1980), guano was actively exploited to supply local demand, but at present the production is very small.



Fig. 12. Sampling in Evate regolith zone.

MARKET SITUATION AND RECOMMENDATIONS

When considering the data presented in Tables 1–4, a few observations may be concluded. Firstly, it is fully clear that the Industrial Minerals sector at large is poorly developed in Mozambique and far from satisfactory in order to be able to support the balanced growth of the national economy and contribute to the general welfare of the population.

When looking at certain figures of the production data it is easy to understand why the overall infrastructure of Mozambique is poorly developed. The production of basic construction materials such as sand, gravel and aggregates is on an annual level of about 2–3 Mt, which makes ca. 100–150 kg/capita. The respective figures in South Africa (source: South Africa's Mineral Industry 2005/2006, Department of Minerals and Energy) are 50 Mtpa of production, making about 1.0 t/capita and in Finland 100 Mtpa and 20t/capita per year (source: Geological Survey of Finland). This means that for construction and maintenance of the infrastructure and housing, South Africa consumes 10 and Finland 200 times more aggregates and sand per capita than Mozambique (it is to be noted that in Finland the severe winter with frost has a considerable influence on construction requirements). This same trend is also seen in the annual consumption of cement, which is below 50 kg/capita in Mozambique, 250 kg/capita in South Africa and 350 kg/capita in Finland (Ministry of Trade and Industry). Similarly, the consumption of clays is 10 kg/capita in Mozambique as compared with 210 kg/capita in South Africa. However, it has to be stated that the statistics available from Mozambique are lacking the large amounts of materials produced by artisanal people, who are very much involved in making bricks, digging sand and even quarrying hard rock aggregates. Nevertheless, the above figures indicate that the production of basic construction materials is clearly inadequate to contribute efficiently to the overall development of infrastructure and housing facilities.

It is recommended that the authorities and companies involved seriously consider the measures needed to improve the situation. In South Africa it is understood that the maintenance and improvement of infrastructure, especially low-cost housing, ports, railways and roads is the key to the sustained growth of construction industries and also employment. Unfortunately, most statistics on the production, export and import of IM commodities in Mozambique are either not available or are not sufficiently reliable to allow detailed comparison with other commodities between these countries.

However, looking at overall figures for IM production, export and import in South Africa in relation to Mozambique, some concluding remarks can be made. In this inspection, those minerals/commodities that do occur in Mozambique are emphasized.

At first it is worth noting that the total IM sales in South Africa in 2005 were worth R6.9 billion (USD 1 130 million, source: South Africa's Mineral Industry 2005/2006, Department of Minerals and Energy). Ilmenite production in South Africa in 2005 totalled 950 kt, with a value of \$95 million and \$100 per tonne, as slag value added worth \$500 per tonne and as TiO₂ pigment worth \$2500 per tonne. Ilmenite production at Moma is estimated to reach 700 ktpa in the first year, which alone will increase Mozambique's mineral sector revenue substantially.

At present, limestone and the products based on it are the most valuable IM commodities in Mozambique. In South Africa the production of limestone amounts to about 15 Mtpa, with a value of about R 50 million. In Mozambique the local production of limestone has decreased from 1 Mtpa to 0.6 Mtpa and at the same time its import is increasing, being 0.32 Mt in 2006. In addition, less local limestone and more imported clinker is being used for cement manufacture. In 2006 the value of cement and clinker imports was MT 925 million. Although the Mozambique economy is essentially dependent on agriculture, hardly any agricultural limestone is used in acid soil regulation. Possible exceptions are a few commercial farms that use imported fertilizers and lime.

In addition to limestone, various lime products are imported, costing MT 80 million. This is one area that should be seriously considered by the authorities and companies in charge of the production and consumption of limestone-based commodities. It is clear that almost all foreign exchange used for importing the limestone based products could be saved by exploiting domestic raw materials, because deposits that meet the quality and size requirements occur adequately in the country.

Clays in general are another sector that could and should drastically be developed. In previous times, industrial scale brick factories operated in all districts, but today only a few are active and hardly any with satisfactory machinery. The clay material used is also poorly tested, causing considerable losses when firing the bricks. At present, most bricks used for building houses around the country are locally made by artisanal workers, often using inferior materials and burning bricks by consuming a lot of

firewood and thereby contributing to the devastation of valuable forests.

When looking at the import figures for IM commodities there are a few minerals that could be produced, have been produced and/or are currently produced in Mozambique. One is diatomite, of which about 1000 tpa is produced. However, the production is all exported because local consumers use imported diatomite, even though the local products meet the quality requirements. Various sand products are also imported, although the country has endless resources of sand to be processed for various industrial uses. Even glass production could be restarted.

There are some minerals in Mozambique which could be exploited and processed to make various fillers, pigments, extenders and so on to be used in paints, plastics, paper and pesticides, among other products. These include kaolin in Alto Ligonha pegmatites, diatomite in Manhiça, white marble from Montepuez and pure limestone as ground products. These opportunities should be studied to develop quality products that could be processed to make higher value by-products from these deposits.

It is also recommended that commodities such as bauxite, bentonite and diatomite should be studied, aiming at better quality, high value end-products. In the Boane area there are occurrences of perlite. However, the presence of the expandable type of perlite has not been thoroughly studied. This would have good markets for several industrial end-uses.

Import figures also show that quite a lot of gypsum is imported. There are a few known indications of gypsum, but unfortunately most of these were found to be in too deep-seated layers that cannot be exploited economically. However, there are also

findings on the surface and these should be thoroughly studied.

Evate apatite in Mozambique has a very high chlorine content (1200–1400 ppm, compared to the normally allowed 200–400 ppm) and this makes its processing very corrosive. These levels are not acceptable in modern phosphoric acid and fertilizer plants producing triple superphosphate fertilizers. Nevertheless, it is recommended that the possibilities to produce single super-phosphate out of Evate raw material should be examined.

Concerning other IM commodities that have the potential to be developed, fluorite is one with a few promising occurrences, which have not properly been studied. Al-silicates, kyanite and sillimanite occurrences are also known, but detailed investigations are lacking.

Besides Montepuez marbles, other dimension stone deposits could find their way to the world market. The rehabilitation of Sena railway to the Moatize coal field will improve the economic potential of all mineral commodities near this railway. These include various types of gabbro-anorthosite in the Tete Suite, “Blue Magic” granite in Songo, carbonatites (Mt Muande-Mt Fema, Mt Muambe), limestones (Boroma, Chinguere) as well as the quality aggregates.

In general, it is concluded that when considering the potential of different IM commodities, it should be kept in mind that infrastructure is a decisive factor for any successful operation. Besides power (electricity), transportation is vitally important, especially for bulk materials, as most IM commodities are. Therefore, the overall improvement of infrastructure will be a key to developing the IM sector at large in Mozambique.

REFERENCES

- Afonso, R. S. & Marques, J. M. 1993.** Recursos Minerais da República de Moçambique. Contribuição para o seu conhecimento. Instituto de Investigação Científica Tropical de Portugal and Direcção Nacional de Geologia de Moçambique. 1st Edition, Lisbon, Portugal, 149 p.
- Bettencourt Dias, M. & Wilson, W. E. 2000.** Famous mineral localities: The Alto Ligonha pegmatites, Mozambique. The Mineralogical Record 31, 459–497.
- Brodoimpeks 1984.** Final report on geological investigation at Muande and Monte Fema locality. ING, 1268, Tete.
- Cilek, V. 1989.** Industrial Minerals of Mozambique. Min. Miner. Resources, Nat. Geol. Inst. Mozambique, published by Czech Geol. Office, ISBN 80–7075–027–8, 326 p.
- Customs Department, Mozambique**
- Geological Survey of Finland, Ministry of Trade and Industry, Finland**
- GTK Consortium 2006a.** Map Explanation; Volume 1: Sheets 2032–2035, 2131–2135, 2231–2235, 2331–2335, 2431–2435, 2531–2534 and 2632. Geology of Degree Sheets Espungabera, Chibabava, Nova Mambone, Massangena, Chidoco, Save, Bazaruto, Chicualacuala, Machaila, Chigubo, Mabote, Vilanculos, Rio Siunguédzi, Massingir, Rio Changana, Funhalouro, Inhambane, Chiembene, Chókwè, Zavala, Inharrime, Maputo, Xai-Xai and Bela-Vista, Mozambique. Direcção Nacional de Geologia (DNG), Maputo.
- GTK Consortium 2006b.** Map Explanation; Volume 2: Sheets 1630–1634, 1732–1734, 1832–1834 and 1932–1934. Geology of Degree Sheets Mecumbura, Chioco, Tete, Tambara, Guro, Chemba, Manica, Catandica, Gorongosa, Rotanda, Chimoio and Beira, Mozambique. Direcção Nacional de Geologia (DNG), Maputo.

- GTK Consortium 2006c.** Map Explanation; Volume 3: Sheets 1735–1739, 1835–1836 and 1935. Geology of Degree Sheets Mutarara, Quelimane, Namacurra/Maganja, Pebane, Marromeu/Inhaminga, Chinde and Savane, Mozambique. Direcção Nacional de Geologia (DNG), Maputo.
- GTK Consortium 2006d.** Map Explanation; Volume 4: Sheets 1430–1432 and 1530–1534. Geology of Degree Sheets Inhamambo, Maluwera, Chifunde, Zumbo, Fíngoè-Mâgoè, Songo, Cazula and Zóbuè, Mozambique. Direcção Nacional de Geologia (DNG), Maputo.
- GTK Consortium 2007a.** Geochemical and Industrial Mineral Surveys, Final Technical Report, DNG, Maputo, June 2007.
- GTK Consortium 2007b.** Geochemical and Industrial Mineral Surveys, Results of the Industrial Mineral Survey, DNG, Maputo, June 2007
- Industrial Minerals,** December 2006.
- Lächelt, S. 2004.** Geology and Mineral Resources of Mozambique. DGN, Maputo, 515 p. ISBN 1–919908–52–8.
- Mining Weekly,** May 2007.
- Ministry of Mineral Resources (MIREM),** Mozambique.
- National Department of Mines (DNM),** Mozambique.
- Presley, G. C. 1991.** Consultancy for testing of bentonite samples from Mozambique and recommendations for future testing for specific applications. UNDCD Project MOZ/86/023. DNG Report No 2141/Maputo.
- South Africa's Mineral Industry 2005/2006,** Department of Minerals and Energy.
- Yager, T. R. 2007.** The Mineral Industry of Mozambique, USGS Minerals Yearbook 2006, www.usgs.gov/minerals/pubs/country.

MINERAL RESOURCES POTENTIAL IN MOZAMBIQUE

by
Tapio Lehto & Reinaldo Gonçalves

Lehto, T. & Gonçalves, R. 2008. Mineral resources potential in Mozambique. *Geological Survey of Finland, Special Paper 48*, 307–321, 9 figures.

The metallic mineral, industrial mineral and construction material resources in Mozambique have been mapped as part of the Mineral Resources Management Capacity Building Project, financed by a grant provided by the Nordic Development Fund. A database covering the location and characteristics of more than 600 mineral indications, showings and deposits within the geographical contract area assigned to the GTK Consortium was created. A total of 140 mineral occurrences were selected for field surveys and assessments that were mainly carried out during May–November 2003, 2004 and 2005. All available data in the report archives of the client, the National Directorate of Geology (DNG), was collected and transferred to the mineral occurrence database, which was then updated with information from field surveys and with new data published by exploration and mining companies on the Internet.

New mineral resources maps at the scales 1:50 000 (part of contract area), 1:250 000 and 1:1 million were prepared with the corresponding symbols for various commodities plotted. Favourability maps showing zones with high potential for selected commodities were compiled at the 1:250 000 scale. The mineral resources in Mozambique were described in the four map explanation volumes and summarized in the final reports for the projects Geological Mapping LOT 2 and Geological Mapping LOT 3.

As a consequence of increased geological knowledge, facilitated by the activities of the GTK Consortium, investments in Mozambique's mineral potential by leading international and regional mining companies is already increasing. Currently, global mining houses are investing in exploration for energy minerals (hydrocarbons, coal and uranium), for titanium and zirconium in heavy mineral sands, for gold and gemstones, for the agricultural minerals lime and phosphate and for tantalum, fluorite and other industrial minerals.

Key words (GeoRef Thesaurus AGI): review, economic geology, mineral resources, mineral exploration, possibilities, potential deposits, Mozambique.

Tapio Lehto, Geological Survey of Finland, P.O. Box 96, FIN-02151 Espoo, Finland.

Reinaldo Gonçalves, Gondwana Ltd, Rua John Issa 57, Maputo, Mozambique

E-mail: tapio.lehto@gtk.fi

GENERAL

Mozambique has a large and diverse unexploited mineral resources potential, which has been manifested by a large number of exploration reports and

studies, summarized recently by Lächelt (2004). Despite this, commercial mining has played a relatively minor role in the development of the coun-

try's economy. The situation is gradually changing, mainly due to the production of aluminium and natural gas and the development of world-class coal and heavy mineral sand deposits. There are plans for the production of gold, rare earth minerals and tantalite from pegmatites and industrial minerals. The main reasons for the low utilisation of the country's mineral resources have been, amongst others, an incomplete geological database and the weak infrastructure – the lack of transport and energy supply – which hampers the exploitation of resources.

Despite the above, artisanal small scale miners and prospectors have played an important role in the local economy, especially at the village level. Their activities have resulted in the identification and exploitation of deposits of gold, gemstones and building materials.

To utilize the nation's mineral resources, the National Directorate of Geology (DNG), with the support of private mining companies and technical aid, has carried out significant exploration work during recent decades. As a consequence of increased geological knowledge, facilitated by the activities of the Mineral Resources Management Capacity Building Project, investments in Mozambique's mineral potential by leading international and regional mining companies is already increasing. Global mining houses are investing in exploration for energy minerals (hydrocarbons, coal and uranium), for titanium and zirconium in heavy mineral sands, for gold and gemstones, for the agricultural minerals lime and phosphate and for tantalum, fluorite and other industrial minerals.

METHODOLOGY

In the inventory of known mineral deposits and occurrences, ArcGIS and MS Access software were used for the storage, retrieval, manipulation and display of geo-information. The data compiled by the Geological Survey of Finland (GTK) was incorporated in the Mineral Information System (MIS) that was developed in conjunction with the Documentation Centre as a separate project. The first format for the mineral deposit databank, provided by DNG and dealing with approximately 90 mineral deposits, was incorporated into an ArcGIS project format for the drafting of mineral deposit maps.

Forms were designed for the collection of mineral resources data, which was transferred directly to the database during field mapping. Complementary data was extracted from both digital and analogue DNG reports, published sources and from the Internet (such as company press releases and annual reports).

The GTK Consortium has compiled a new data-

base of 640 mineral deposits and occurrences, also including stone, aggregate, gravel and sand quarries and covering the entire GTK Consortium Contract areas. A total of about 140 mineral deposits (including construction materials) were checked in the field. The collected data comprise an inventory of the mineral commodities, geology and the mode of occurrence, sampling and digital photographs taken.

All the geological maps prepared by the GTK Consortium carry the symbols for mineral indications and occurrences with the name and commodity. In addition, separate maps at the 1:250 000 scale have been produced showing areas of resource potential for 12 commodities or groups of commodities. The potential areas have labels with the name, commodity and reference to the Explanatory Note Volume (1 to 4), where details are explained (GTK Consortium 2006a, b, c and d). Target areas identified by geochemical surveys are discussed by Korhikoski 2008 (this volume).

MINERAL RESOURCES

The geological field mapping, including inventory of mineral resources, gave the GTK Consortium an opportunity to visit many active and previous mining sites. A brief review of mineral deposits and the extractive industries as a whole is given in this article as a synthesis together with the results of this work. The location of the mineral deposits and occurrences is shown on the geological maps at the scales 1:250 000 (Fig. 1 and Fig. 2) and 1:50 000.

Areas of resource potential are indicated on separate map sheets on the geological background at the scale 1:250 000. Overviews at the scale 1:1 million with generalized geology were also prepared (Fig. 3).

According to the International Monetary Fund statistics for 2006, mining-related activities have contributed about 2% of Mozambique's Gross Domestic Product (GDP). However, it is believed that the potential of various mineral commodities is con-

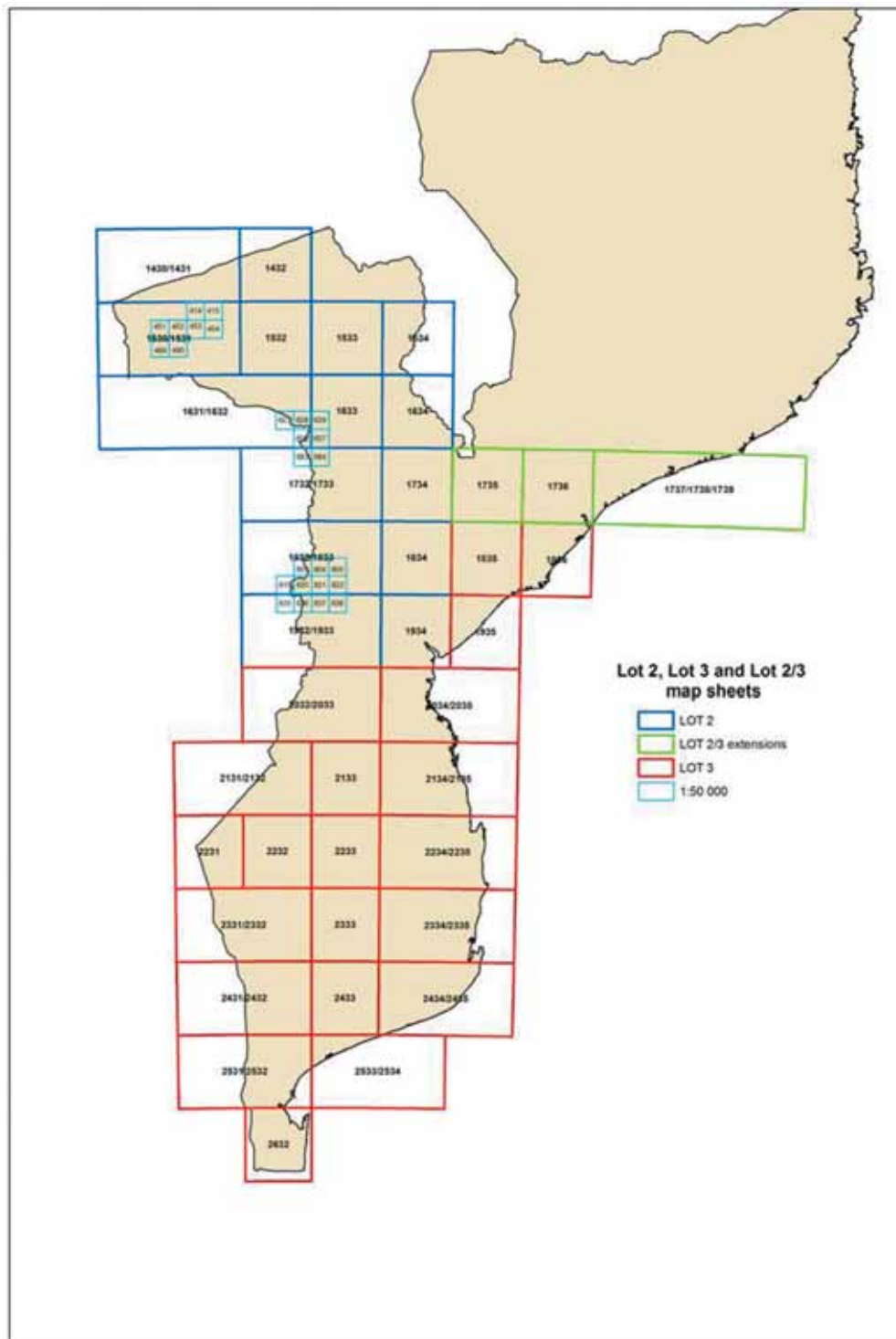


Fig. 1. Map grid of Mozambique, showing the geological and mineral resources maps prepared by GTK Consortium. The detail shown in Fig. 2 is obtained from map sheet 820 in scale 1:50 000.

siderably higher than the present utilization level indicates. Large deposits of ilmenite, rutile, zircon and coal are known to occur, as well as deposits of gold, copper and iron, in addition to asbestos, base metals, bentonite, cassiterite, diatomite, feldspar, fluorite, gemstones, gypsum, kaolin, limestone, mica, nepheline syenite, perlite, phosphate rock, rare earths, silica sand and uranium. Most gold,

base metal, gemstone and carbonatite-hosted deposits are located in the older Precambrian terranes. The younger sedimentary formations contain various energy and industrial minerals: coal, gas, heavy minerals (Ti-Zr), limestone, bentonite and diatomite. At present, ongoing major projects are focused on heavy mineral sands, coal and natural gas.

Overview of recent production in mozambique

Mozambique produces natural gas on a large scale and also aluminium, but from imported raw materials. Construction materials, such as rock aggregates, gravel, sand, clay, limestone, marble and dimension stone, and ilmenite are produced on a medium scale. Gold, tantalite, coal, bauxite, diatomite,

bentonite and other clays, as well as gemstones and sea salt, are all produced on a small scale. There are also at least 50 000 artisanal small scale miners who mainly work on alluvial and weathered gold and gemstone deposits. This production is not seen in the official statistics (Table 1).



Fig. 2. A detail of a 1:50 000 scale geological map showing the numerous minor gold indications in the Archaean greenstone belt in Manica (yellow rings). Based on the work of the GTK Consortium.

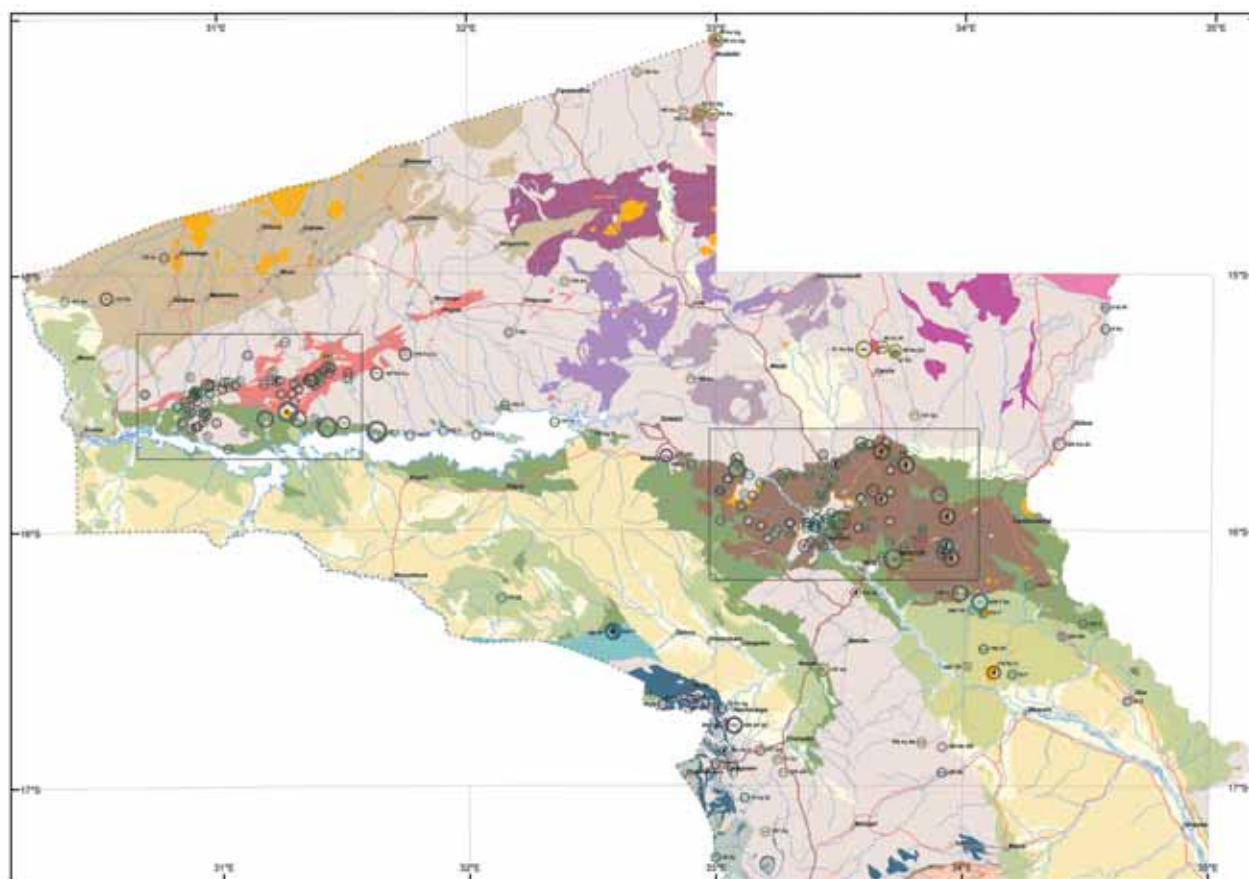


Fig. 3. An example of a generalized geological map at the scale 1:1 million, based on the work of the GTK Consortium and showing the locations of mineral indications in the Tete Province. Two areas (boxed): Fingoè north of Cahora Bassa lake and Tete, further to the east, show a higher concentration of copper and iron mineralizations (ring symbols).

Table 1. Production figures for some commodities in 2004-2006 in Mozambique (source: Ministry of Mineral Resources, May 2007).

Mineral resource	Unit	2004	2005	2006
Coal	ton	16 525	3 417	10 000 est
Bauxite	ton	8 977	9 518	11 069
Bentonite (raw)	ton	3 366	0,0	n/a
Bentonite (processed)	ton	578	547	610
Bentonite ground	ton	16 627	17 318	4 207
Tantalite	ton	712	281	51
Industrial beryl	ton	27.3	146.3	16.4
Dumortierite	ton	113	10	664
Quartz	ton	173.0	295.0	195.1
Gold	kg	56	63	68
Aquamarine (gem quality)	kg	18.1	15.6	14.0
Aquamarine (reject quality)	kg	2 391	5 475	n/a
Tourmaline (gem quality)	kg	1 570	245	n/a
Tourmaline (reject quality)	kg	4 915	69 292	n/a
Garnet (gem quality)	kg	2 686	2 172	4 400
Garnet (reject quality)	kg	4 270	3 630	n/a
Limestone	ton	1 593 450	654 179	155 870
Clay	ton	108 231	32 031	222 052
Building sand	ton	1 429 743	833 113	1 404 184
Stone aggregate	m3	779 581	850 919	1 178 997
Granite	m3	521	2 198	5 500
Marble (processed slabs)	m2	13 666	12 158	12 825
Marble blocks	m3	617	509	472
Natural gas	GJ	49 739 070.0	88 907 651.0	90 000 000 est

Mineral resources in the GTK project area

The economically most important commodities in northwest and central Mozambique (LOT 2) are coal, gold and various construction materials (such as rock aggregate, dimension stone, limestone and clay). Occurrences of iron ore, copper and other base metals, cassiterite and fluorite are well known. The southern half of Mozambique, south of the 20th parallel, is to a large extent covered by Phanerozoic rocks. The economically most interesting mineral resources in the LOT 3 area are the gas occurrences in Pande and Temane fields in Inhambane as well as the heavy mineral sands in paleo-dunes in Gaza and Zambézia Provinces. The increasing demand for construction materials has reactivated many rhyolite quarries and gravel, sand and clay pits, especially in the Maputo Province, where construction of all kinds is very active.

Industrial rocks and minerals represent an important resource for domestic use. In the Maputo Province these include rhyolite for aggregates in the Boane – Massingir area, limestone in Salamanga for cement, which together with sand, gravel and various types of clay are the backbone of the growing construction industry. Possibilities for creat-

ing a stronger market for good quality diatomite resources in Maputo and Gaza Province, replacing imported material, should be considered more seriously. Most of the bentonite from Boane is exported without further treatment. More marketing and product development are required in order to add value and increase revenues from bentonite. Resources of thermal water are abundant along the rift faults of the mountain ridges in the western border area with South Africa and Zimbabwe, providing the potential for local power generation. Demand for good quality mineral water is also steadily growing, both for local consumption and for export. The southernmost indications of coal in lower Karoo strata are found in Espungabera (SDS¹ 2032), close to the Zimbabwe border in Manica Province. Alluvial, micro-sized diamonds have been found in the Limpopo and Singédzi rivers in Gaza Province, probably transported by the rivers from the South African Kaapvaal Craton. Sedimentary deposits of glauconite-bearing phosphorite are located near Magude, NNW from Maputo, in calcarenites of the

¹ Square Degree Sheets, at the scale 1:250 000, about 100 km by 100 km

Jofane Formation. For local production of phosphate fertilizer there are small reserves of bat guano in the Buzi area. The Eocene Cheringoma and the Miocene Jofane Formations contain large resources of limestone, halite and gypsum.

Energy Minerals

Hydrocarbons. Although investigation of hydrocarbons does not belong to the scope of this project, some general observations have been made, mainly due to the economic interests involved. The delineation of sedimentary rocks in terms of reservoirs for oil and gas is of major importance to Mozambique, since hydrocarbons potentially generate large revenues. The improvements in infrastructure and in deep-water technology together with high oil prices create favourable conditions for exploration.

Economic quantities of *natural gas* have been discovered at Pande (in 1961) and Temane (in 1967). Sub-commercial gas has been encountered at Búzi (in 1962) and Inhassoro (in 2003). Commercial gas has been reported from several horizons in the Lower Grudja in the central portion of the basin.

Production of natural gas rose twenty-fold in 2004, mainly due to the start up of the Temane Gas Project in Inhambane in late 2003. The natural gas production was close to 90 million GJ in 2006 and 2005, compared to 50 million GJ in 2004 and to 2.5 million GJ in 2003. Natural gas is also produced from the Pande field, some 40 km NNW from Temane. The gas fields have enough potential for additional production if required (Yager 2006).

To date, Mozambique is not a *crude oil* producer. Det Norske Oljeselskap (DNO) and Petronas of Malaysia have carried out (2002–2003) off-shore exploration in Sofala Province for petroleum (Yager 2004). Exploration for oil is also ongoing in the Rovuma basin, further north, close to the Tanzanian border. Preliminary results are encouraging (Pilskog *et al.* 2006).

Hydrocarbon exploration in central and northern Mozambique is focused on the Rovuma sedimentary basin, together with the offshore Zambezi deltaic complex and the entire off-shore, including the deep off-shore of the Mozambique Basin. These exploration targets have come within reach due to the strongly increased oil (and gas) price, together with novel deep-water technologies, which have rapidly improved during the past few years.

Coal. In November 2004 CVRD² won the international bidding process to explore coal deposits

in the Moatize region. The feasibility study started in January 2005 with a comprehensive core drilling campaign. The forecasted production will be 14 million tonnes of coal in a year and the planned start is in 2009 (CVRD press release 13.07.2007). The demand for locally available construction materials is expected to increase considerably, especially considering the plans to construct a dam in the Zambezi River at M'Panda Uncua. There is a railway network linking the Moatize region to the coast at Beira port, but the coal terminal needs upgrading. The railway network needs significant rehabilitation and reconstruction to fulfil the requirements of the planned coal production. Local resources of construction materials were evaluated by the GTK Consortium as part of the Industrial Mineral Surveys.

In 2004 and onwards the coal production in Mozambique has only been around 10 000 t/a, having been 500 000 t/a in the 1980s. Mozambique has substantial coal deposits situated in the Moatize and Mucanha-Vúzi coal basins in the Tete Province. The Moatize coal basin, which is considered by CVRD as the largest unexplored coal province in the world, contains six coal seams and has total resources of 4 000 Mt in categories measured, indicated and inferred. The Mucanha-Vúzi basin is estimated to contain as much as 3 600 Mt in coal resources (Lächelt 2004), although the basin is severely block faulted.

The world's leading steel group, the multinational ArcelorMittal, will in a joint venture with Black Gold Mining of Mozambique investigate the Rio Minjova sub-basin, 20 to 50 km SE from Moatize Mine (ArcelorMittal press release 21.11.2007). In 2006 the Central African Mining and Exploration Company (CAMEC press release 01.02.2006) claimed large parts of remaining prospective ground in the Moatize and Mucanha-Vúzi basins. Detailed geological investigations are ongoing to evaluate



Fig. 4. Coal bearing siltstone layers outcropping along the dry river channel of M'Pote Pote in Espungabera. The hammer is 60 cm long.

² Companhia Vale do Rio Doce from Brazil

the reserves of good quality coal in other prospective areas of Sanangoè-Mefideze, Baixo Chire and Maniamba basins between Moatize and the Malawi border.

The southernmost indications of coal seams in Mozambique are located in the Espungabera sub-basin, near the Zimbabwean border, along the M'Pote Pote River (Fig. 4).

The Karoo sedimentary sequence in the Espungabera sub-basin is superposed on the northern marginal zone of the Limpopo mobile belt. The productive series occurs near the surface, but block faulting is common, making the resource evaluation without geophysics and drilling quite unreliable. In addition, the location of the Espungabera coalfields is very remote, far from potential industrial users in Mozambique. The riverbank outcrops, however, could be quarried for local consumption as fuel.

Uranium exploration is actively carried out over the country, due to positive commodity price development and the availability of recent airborne radiometric surveys, the processing of which has identified a number of highly anomalous uranium targets. A number of prospects that were actively explored by uranium industry majors from the mid 1970s to the uranium price collapse of the early 1980s, are again explored. Elevated contents of radiometric minerals, mainly davidite, are quite common in quartz-calcite veins in the Tete Suite (Omega Corporation 2005, 2006). The Mavudzi Mine, that was closed 1967, is located in an approximately ten kilometres long fault zone in gabbro and anorthosite about 40 km NW of the town of Tete. The upper Karoo sandstones and the sandstones, conglomerates and felsic volcanics of the Lupata Group have good potential for uranium deposits (TEAL Exploration & Mining, press release 18.04.2008).

Industrial Minerals

Ilmenite, Rutile and Zircon. Based on extensive heavy mineral sand (HMS) deposits located along most of the 2700 km long coastline, Mozambique has the potential to become the world's foremost producer of Ti and Zr minerals. A few major companies have recently been active in completing feasibility studies on potential mining projects. The deposits occurring in the GTK contract area are briefly described below.

The "*Corridor Sands*", near the Limpopo River, about 190 km north of Maputo and 50 km inland from the present coastline, close to the town of Chibuto in the Province of Gaza, was a major

discovery in 1997. The Chibuto deposit (SDS 2533, 554556/7272167) is one of the largest heavy mineral deposits in the world with an estimated lifespan of well over a hundred years. It has a resource of at least 14 000 Mt of ilmenite-rich sands at an average heavy mineral grade of 4.9% (MBendi statistics, 22.05.2006). Australian WMC³ reported in 2003 a measured resource of 1 765 Mt @ 4.14% ilmenite and an indicated resource, containing 73 Mt of ilmenite (Mining Review Africa 2003). The heavy mineral concentrations are characterised by the absence of Cr, V and radioactive minerals and the thickness of heavy mineral bearing (>2% HM) layers may be locally up to 70 m (Lächelt 2004). The project was taken over by BHP Billiton in 2005. Although the date for starting production is pending, the capacity of the planned processing plant is designed for a production of about 400 000 tpa of sulphate and chloride titanium dioxide slag, with a by-product output of nearly 200 000 tpa of iron, together with rutile and zircon.

Italian Aquater SPA started HMS exploration in the early 1980s along the coast at Xai-Xai near Chongoene. Aquater (1985) reported a resource of 480 Mt grading 6% total heavy minerals (THM). The company carried out further follow-up exploration in 1997. Recent exploration by Rio Tinto has concentrated on map sheet 2533 at Xai-Xai, where a significant HMS resource has been identified. Rio Tinto acknowledged total reserves of 186 Mt @ 4.4% THM, of which 59.6 Mt is in the proved, 112.7 Mt in the probable and 13.8 Mt in the possible category (Rio Tinto RTZ 2004). The Xai-Xai deposit is reported to contain 49 Mt of THM concentrate with 66% of ilmenite, 0.4% of zircon and 0.5–0.7% rutile. Further exploration is ongoing (Albanese 2005).

Bentonite occurs as a weathering product of rhyolites and rhyolitic tuffs of the Karoo volcanics distributed in the Pequenos Libombos range. In Boane, a zone about 2 km long and 500 m wide with an average thickness of 6 m has been calculated to contain 15 Mt of bentonite (Lächelt 2004). The thickness of bentonite varies from a few metres to up to 20 m, depending on the intensity of weathering. The total reserves of the Boane-Pequenos Libombos bentonite deposits have been estimated at 2.5 Mt in the proven category and 4.2 Mt in the probable category (Noticia Explicativa 1995). The production of low-grade bentonite for export is ongoing in Boane.

³ Western Mining Company



Fig. 5. Diane quarry, exploiting a one-metre-thick diatomite layer (in the middle of the picture), Manhiça (SDS 2532, 463968/ 7193482).

Bentonite has been found at various other locations over a distance of 40–60 km in rhyolite ridges of the Pequenos Libombos and it is occasionally mined in places such as Luzinada (SDS 2632, 424394/ 7119062).

Diatomite has accumulated in many fluvial and lagoonal depressions between Pleistocene dunes from Inhambane in the north to Matitue south of Maputo. The diatomite was deposited in rivers, small lakes and ponds under brackish to freshwater conditions. The deposits are usually small with a maximum thickness of 1.5 – 2.5 m. The Boane and Manhiça occurrences are best known.

The diatomite occurrences are located about 10 km SW of the town of Manhiça. The main pit (Diane deposit) has been in production since 2005, and there the horizontal diatomite layer measures 60 x 50 m and is about 0.8 to 1.0 m thick at an average depth of 8 m below the surface (Fig. 5).

Estimated reserves are 1.5 Mt with an average bulk density of 0.32 g/cm³ and grading 50% pure diatomite (Afonso & Marques 1993). Diatomite is screened and split into various qualities and at present all is exported to South Africa. Diatomite is locally used as an additive to cattle food against parasites and other sicknesses. For now, the real added value to these products is still made abroad. Instead of utilizing this thoroughly studied and tested domestic resource, commercial diatomite products are imported into Mozambique.

Between Magode and Chokwe, in Gaza Province, there are diatomite deposits in the southern margin of the East African Rift. Another large diatomite domain, measuring 70 x 10 km, occurs some 100 km to the ENE, around Mafuiane and Buana. Further investigations are warranted to establish whether

there is a sufficient volume for commercial exploitation of diatomite.

Bauxite. In 2006 a total of 11 069 tons of bauxite was produced, which comes from the small Morian-gane mine in the Penhalonga zone in Manica Province. The mine is operated by E.C. Meikles (Pty) Ltd of Zimbabwe and most of the bauxite is exported to be used as a raw material for alun (aluminium sulphate) in Zimbabwe. There are deposits of kaolinite and other clays hosted by weathered pegmatites and syenites in the provinces of Zambézia and Manica.

Construction Materials

Aggregates. Karoo rhyolites provide a good raw material for aggregate. The majority of active mining licences for stone quarries are located around Maputo, in the districts of Namaacha, Boane, Matitue and Moamba where the economic activity is highest. In other parts of the country the peaks of consumption go together with the construction of roads, bridges and major buildings. In most parts of country, aggregate rocks, gravel and sand are commonly available: aggregate from hard bedrock, such as felsic volcanics; and gravel and sand from riverbeds and beach deposits.

The quarried aggregate rocks are mostly rhyolites of the Lebombos Range. Rhyolite does not weather as easily as andesite and basalt in the same range and can be regarded as good material for most road and other construction purposes. In the Moamba district a suitable, fine-grained nepheline syenite is being quarried by CMC for aggregate (Fig. 6). Table 2 lists the rhyolite quarries in operation in Maputo Province in 2005.



Fig. 6. Solbrita quarry in porphyritic nepheline syenite (SDS 2632, 431316/ 7150467).

Table 2. Aggregate rock quarries in operation in Maputo Province in 2005.

Quarry Name	Map Sheet	Coordinates
CMC	2632	428176E/7121877N
Tamega	2532	424318E/7145310N
Extramac	2632	424951E/7108576N
Riolitos	2632	422028E/7119151N
Probrita	2632	428363E/7123749N
ARA Sul	2632	423486E/7114906N
MAM	2632	413124E/7105831N
Agroareias	2632	435016E/7115962N
Solbrita	2632	431316E/7150467N

The aggregate from these sites is transported and used along the coast as far as Gaza and Inhambane (along highway EN1), where no suitable aggregate rock has been found. Occasionally, aggregate for road rehabilitation is transported by trucks up to the Save River. Properly constructed road pavement with aggregate layers, like sub-base, road base and wearing layers, requires considerable amounts of stone material. Road transport of bulk aggregate over hundreds of kilometres is expensive.

Inland in Gaza Province, rhyolite is quarried at Massingir (SDS 2332, 393081/ 7352065). Large rhyolite blocks are transported over 28 km along a new gravel road to the Massingir construction site, where the blocks are used for earth wall protection of the irrigation dam in Rio dos Elefantes.

In the coastal zones of Inhambane Province no hard silicate rocks are exposed. As an alternative, several pits have been developed in limestone close to or along highway EN1. These include artisanal quarries close to Massinga town, in the villages of Mambadine and Chacane. Limestone aggregate is used for the construction of homes and for local road maintenance.

Along Beira Corridor the rounded, granodioritic hills are quarried for aggregate material in many places between Chimoio and Manica. The Xiluvo Complex, with its felsic volcanics and carbonatite, is the closest rock aggregate occurrence to the coast and the town of Beira. Ballast and aggregates for the rehabilitation of railway lines and roads are at present produced from the Xiluvo carbonatite body. The ballast is loaded directly onto railway wagons in the village of Xiluvo.

The demand for aggregate rock is expected to increase to a great extent due to the Moatize coal project and reconstruction of the Moatize – Beira railway. In 2006, crushed rock and aggregate production amounted to 1 178 997 m³, steadily increasing from previous years. Production of construction

sand was about 1.4 Mt in 2006, which is a normal level in Mozambique (Ministry of Mineral Resources May 2007).

Dimension Stone. Some of the Karoo rhyolites, exposed in the Maputo Province, have been quarried for dimension stone, for example near Boane and Estevél and also near Ressano Garçia. The banding and folding in the light brown rhyolites may be highly ornamental (Fig. 7). However, block size in the fractured, dense rock is generally problematic.

Massive ‘grey granite’ (actually gabbro) is periodically quarried for export at Chainça in Manica (0481281/7908276), as well as anorthosite from the Tete Suite. Some other sites have also occasionally been exploited for dimension stone, but only on a small scale. The demand for Tete anorthosite/gabbro in particular seems to fluctuate greatly, which obviously depends on the trends in the world market at which these blocks are mainly aimed. Transportation by trucks to Beira port is currently very costly.

Sand and Gravel. The availability of high quality sand and gravel close to Maputo and surroundings is only satisfactory and not as good as for stone aggregate. Most of the visited extraction sites ex-



Fig. 7. Flow structure in rhyolite at an old dimension stone quarry known by the name of Estevél.

exploit fine-grained flood-plain sand along the Umbeluzi (Boane area) and Incomati Rivers (Moamba area, Uetimane deposits). Sand from these locations is best suited for mortar purposes and filling. Fine dune sand is excavated for the same use. Gravel of satisfactory quality is only found along the Umbeluzi River, near Goba town.

In the southern part of Gaza Province, sand and gravel deposits occur along the Rio dos Elefantes and the main Limpopo River. There are a large number of sand pits in the Chilembene-Chókwè and Massingir areas. Rehabilitation of the Massingir dam (414026E/ 7355195N) has consumed a large quantity of sand and gravel, which has been extensively extracted from the river valley at several locations.

Limestones of the Tertiary Salamanga Formation, south of Maputo, of the Cheringoma Formation west of Beira along the Buzi River and in the type-locality north of Beira on the Cheringoma plateau, have high calcium carbonate contents. The Miocene Jofane Formation is a second important accumulation of limestone. A large area with limestone outcrops extends from the Save River southwards to Inhambane. Limestone occurrences are also known at Urrongas.

Currently, limestone for cement production is quarried only at Salamanga, some 60 km SSE from Maputo, where it is transported by rail and trucks to the 'Cimentos de Moçambique' plant in Matola over a distance of 100 km. The Salamanga limestone is of Tertiary age and exposed over a zone more than 10 km long and 1.5–2.0 km wide. The thickness of the limestone layer varies from 11 m to 55 m with an average of 32 m. A measured reserve of 1200 Mt and an inferred reserve of 1200 Mt limestone of Portland cement quality has been reported (Diallo 1979).

Tertiary, somewhat sandy limestone is known at Mangulane, about 40 km NE from Moamba in Maputo Province. The rather large quarry was active in 1960s with good road and railway connections. The overburden above the limestone is 2–10 m thick and consists of gravel and sand. Removal of large volumes of overburden prior to limestone quarrying was required, considerably increasing the cost of operation.

Cimentos de Moçambique (CIMOC) has a plant at Dondo, outside Beira. At present, imported clinker is used as raw material for cement production instead of local limestone. An extensive potential for limestone exists in Cheringoma Plateau in Sofala Province, generally within Tertiary and Cretaceous sediments. Proterozoic carbonate-bearing

metasediments may also host pure calcite marble in Tete, Manica, Niassa, Capo Delgado, Zambezia and Sofala Provinces. In 2006, only about 750 000 tonnes of limestone was produced, about half of the production level in 200–2004 (Ministry of Mineral Resources).

Brick Clay. Common clay is taken for local brick production around most major towns where clay beds occur in and along river valleys. Bricks are burned on demand for building of local houses. However, the quality of the clay used is highly variable, often too sandy and bricks are easily broken. No systematic quality data on various clay materials exist.

Brick clay is excavated close to Boane, on the eastern bank of the Umbeluzi River. This deposit supplies clay for brick production to most of the brick works in the Maputo area. A dormant clay pit is located in Bela Vista and a large number of small clay occurrences are known at Namaacha and Maguigane along the valley of the Incomati River.

Phosphate. Large carbonatite bodies located in Tete province, such as Mt Muande and Mt Fema, on opposite sides of the Zambezi River, have potential for phosphate (apatite). Carbonatite pipes, such as Cone Negose, on the northern shore of Cahora Bassa (Fig. 8) and Mt Muambe, SE of Tete, could also be considered as resources for agricultural fertilizers.

Thermal water

Thermal and mineral water springs are common in the Karoo rhyolite zone close to the South African border (Lebombos) in Maputo Province. There, springs such as Namaacha and Goba are well known for good quality bottled water. Further to the north, in the Espungabera-Dombe-Chibabava region, between Buzi and Save Rivers, several thermal springs are known along the Karoo faults.

Gemstones

Gemstones can be found in pegmatites where beryl, tourmaline and various feldspars occur, mainly in Zambézia, Nampula and Tete Provinces. Skarn rocks and biotite schists intruded by pegmatites and garnetiferous gneisses provide prospective ground for emeralds and garnets. Karoo basalts may be agate bearing. Most gemstones have been produced by artisanal small scale miners and are not properly registered.

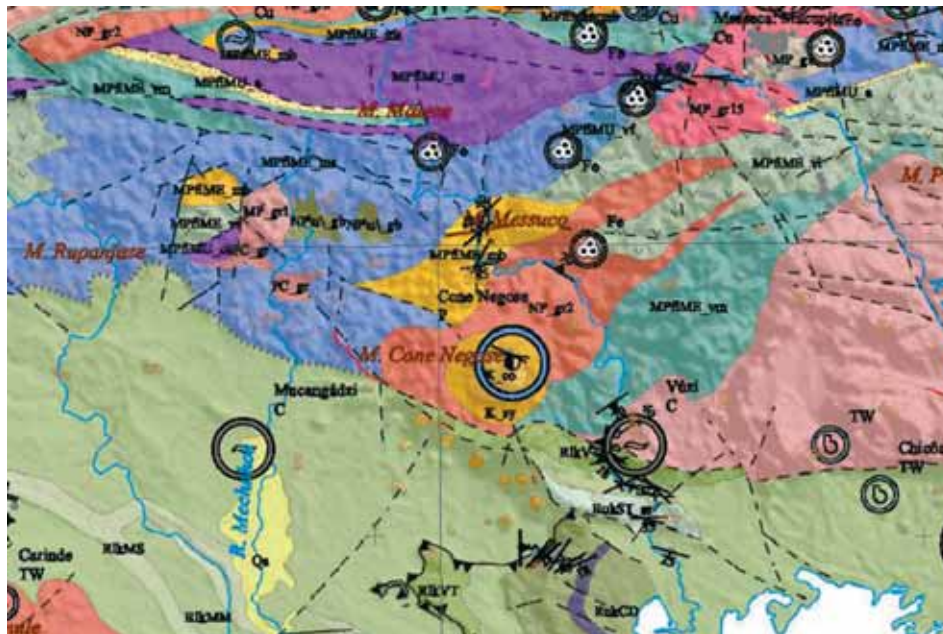


Fig. 8. Location of the Cone Negose carbonatite body on map sheet 1531 (blue ring), north of Cabora Bassa lake, which is visible on the southernmost part of the map. Based on the work of the GTK Consortium.

Gold

Gold has been mined in the Mutare-Manica border area between Zimbabwe and Mozambique since prehistoric times. However, the official production figures have been very low, less than 100 kg annually during the current decade. The official production figure for whole of Mozambique is 68 kg of gold in 2006 (Ministry of Mineral Resources May 2007).

In Manica, gold mining in hard rock started 1893 at Bragança and Guy Fawkes and has irregularly continued since then. Monarch mine, just on the border with Zimbabwe (Fig. 2), was operated periodically by Mincor de Mozambique until its closure in 1997. The gold is connected to shear zones in Archaean mafic and ultramafic volcanics, banded iron formation and chert or in the fractured contact between the supracrustals and the surrounding granites. Principal alluvial deposits that are important for the local economy have been located within the Revuê, Inhamucarra, Muza and Chimezi Rivers.

A resource of 1 550 million ounces of gold at 2.96 g/t Au was in 2007 reported by Pan Africa Resources (press release 13.08.2007) within their Manica claims (covering mainly the Fair Bride zone). A pre-feasibility study was completed in 2007, while drilling at depth is ongoing with very encouraging gold grades (press release 21.02.2008). The results of the recent exploration utilizing modern multidisciplinary techniques indicate that the Archaean Manica greenstone belt has the potential for profitable gold mining on an industrial scale.

In 2006 African Eagle Resources reported (press release 05.09.2006) interesting gold grades in drilling intersections from their claims in the Fíngoê belt, to the north of the Lake Cahora Bassa in Tete Province. The exploration target in iron oxide-copper-gold mineralised zones was compared with the Eagle Eye field in Ndomba, Zambia, where economic gold potential zones have been located.

The Central African Mining and Exploration Company (CAMEC) has commenced ground exploration after radiometric and satellite image surveys on their 540 sq km exploration licence area at Rio Muda in Nhamatanda, in the Beira Corridor in Sofala Province. Recently, around 2 000 artisans have been producing over 20 kg of coarse gold per month along Rio Muda. A simple plant has been built to allow local miners a facility to process their ore (CAMEC press release 01.02.2006).

Uncontrolled artisanal gold workings cause local environmental problems in the Manica mountain region. In addition to soil erosion (Fig. 9) and water siltation, the use of mercury in recovering fine gold causes air and water pollution. The Ministry of Mineral Resources, DNM⁴ and DNG⁵ have taken preliminary measures to improve the situation by emphasizing and introducing environmentally better and safer methods for gold recovery.

⁴ National Directorate for Mines

⁵ National Directorate for Geology



Fig. 9. Artisanal gold panning site at Bandire, map 1933, Manica Province.

Base Metals, Copper Etc.

Rather few comprehensive investigations on base metals have been carried out in Mozambique. Base metal concentrations of copper, nickel, gold and silver are found in altered ultrabasic volcanics of the Archaean Manica greenstone belt. Mundonguara is the best-studied deposit, the exploration history

of which is summarized by Korkiakoski (1990). Currently exploration is carried out by Baobab Resources, an exploration company focused on base and precious metals in Mozambique.

The Mundonguara copper-gold-silver occurrence is located on the southern hillside of the Isitaca Mountains, about 12 km west of the town of Manica (SDS 1832, 477977/ 907124). Altogether, ten E-W trending mineralised bodies have been identified. Reserves, calculated for an average mining thickness of 2.9 m, amount to 123 000 t with 2.36% Cu (Lächelt 2004). Other calculations by LIMEX (1980) indicate a reserve of 325 000 t grading 3.1% Cu and 0.58 g/t Au. In 2007, Baobab Resources reported (press release 13.07.2007) significant gold and copper grades and elevated Ni and Co grades in surface rock chip samples from the Seymour Prospect, which is a part of the Mundonguara mineralized stockworks system.

The Chidué copper deposit close to the town of Tete was a target for minor geological investigations in the 1950s, which resulted in defining 8.6 Mt of copper ore grading 1.65% Cu (Lächelt 2004). This suggests that more detailed exploration in the area is justified.

RECOMMENDATIONS FOR EXPLORATION

Based on the overview of mineral occurrences in the area and on the ideas gained during the project, the following recommendations for future exploration are presented:

- Economically natural gas is the most important mineral product at present in Mozambique. Additional resources can be expected in the Temane and Panda fields in Inhambane. In Sofala Province, further to the north along the coast, gas indications have also been recorded. Oil has not yet been found, although some exploration has been carried out in the Inhaminga onshore block north of Beira and in an offshore block near the Zambezi Delta (Yager 2005). In June 2005, Sasol was awarded exploration licences (gas and petroleum) for offshore blocks just east of the Pande-Temane gas fields. Exploration in the deeper offshore, including the Mozambique Channel, will supposedly come within reach in the next decade.
- Exploration drilling for gas has indicated large volumes of gypsum in the Temane field. Gypsum is currently imported to Mozambique for use in cement plants. Exploration to investi-

gate the extent and availability of gypsum is justified.

- The Corridor Sands heavy mineral project near Chibuto is closest to the start up decision, in addition to Moma deposit in Nampula Province, which went into operation in 2007. Uncertainty over the price development of titanium and electricity has delayed decision-making. After the construction of the plant in Chibuto, the potential area for heavy mineral resources will increase in Gaza and stretch along the Limpopo River valley from the coast to Chókwè. The outlook for utilisation of these titanium resources will depend heavily on global market trends and a reliable domestic power supply. The use of natural gas from Pande and Temane gas fields as a power resource has been discussed. The full potentiality of the heavy mineral sands close to Maputo, in the Marracuene-Limpopo estuary to the north and Ponta de Ouro-Lagoa Piti zone to the south, should be investigated. The coastal zone from Limpopo River to Inhambane has a high HMS potential, as well as the Inhassoro zone, further to the north.

- Coal in the Moatize and Matinde Formations of the Lower Karoo Group is without doubt one of the greatest mineral resources in Mozambique. Intensive exploration by international companies (e.g. CVRD, ArcelorMittal and Tata Steel) is ongoing in Mucanha-Vúzi, to the north of Lake Cahora Bassa and in Minjova area, SE of the town of Tete, which still have an untested coal potential.
- In the Mesoproterozoic Fíngoè Supergroup rocks (min age 1327 ± 16 Ma), such as felsic and mafic volcanics, volcanic breccias, banded ironstones and metacherts, the shearing in a NE-SW direction has in many places created traps in which mobile sulphides and gold may have been concentrated. On SDS 1531 there are several indications and gold occurrences connected to oxide phase iron formations that would require further exploration. African Eagle Resources has reported (press release 5.9.2006) encouraging results from their claims in the Fíngoè belt where they are carrying out geological mapping and stream sediment geochemical surveys in iron oxide-copper-gold mineralised zones. The Pan African Mining Corporation is also active in the Fíngoè area, planning to execute reconnaissance geochemical sampling programmes (press release 11.9.2006). Their claims cover known gold and Cu-Fe occurrences, skarn alteration and hematitic breccias within zones belonging to the Mesoproterozoic Fíngoè Supergroup. Banded ironstones, mafic metavolcanics and pyroclastic rocks form the principal target zones.
- Mesoproterozoic mafic volcanics and volcanoclastics of the Mualadze Group that are surrounded by Desaranhama Granites (age 1041 ± 4 Ma) have been sheared mainly in a northerly direction. These shears are gold bearing on map sheet SDS 1432, containing gold mineralizations in Fundão, Missale, Chifumbazi and Muande. These structures have further untested gold potential. The Cazula field, in a similar geological environment in Desaranhama Granites on SDS 1533, also has gold potential, which is currently being tested by Pan African Mining Corporation (press release 13.8.2007). The target for gold exploration at the old mining site of Machinga is associated with quartz veining and hydrothermally altered and brecciated host rocks within regional shear zones.
- The Tete Suite represents a mafic-ultramafic part of a Mesoproterozoic bi-modal suite. The Suite has been explored in the past for ilmenite, nickel, copper, gold and uranium. Further exploration seems warranted, especially along the northern mylonitic border zone of the Tete Suite within the 'Conua-Chiduè Resource Potential Zone' on SDS 1533. The Mussata porphyritic, biotite-bearing and locally mylonitic granite (age 1046 ± 20 Ma) has provided channels for Cu-Au bearing fluids.
- At present, uranium is also seen as an economically feasible target for exploration, especially within the anorthosites of the Tete Suite in the Mavudzi area (SDS 1533) and in the upper Karoo sandstones (SDS 1530. The Australian Omega Corp. Ltd reported in May 2006 (press release 3.5.2006) that based on extensive fieldwork involving ground geophysics and RC drilling, they have succeeded in identifying 'a suit of significant uranium radiometric anomalies' in their Mavudzi project. The NNE trending radiometric U-anomalies connect the historic Mavudzi, Inhatóbuè and Castro mines. The airborne radiometric surveys will, when processed and interpreted, provide useful tools for uranium exploration, for example in the sedimentary and volcanic rocks of the Lupata Group in central Mozambique.
- Igneous rocks associated with Karoo and younger rifting, such as alkaline and carbonatite complexes, have potential for phosphate, pyrochlore, REE's and fluorite deposits. The local need for fertilizers could be covered by mining carbonatite in Mt Muande and Mt Fema, with the production of agrolime and fertilizers with interesting by-products (Fe, REE). Further exploration is recommended in the Mt Fema – Mt Muande Resource Potential zone as well as in Salambidua and at Monte Xiluvo.
- A good source for lime could be developed in the Boroma calcitic marble deposit if local demand increases.
- The availability and quality of various construction materials close to the Tete-Moatize development centre and along the roads to Zimbabwe, Malawi and Zambia should be studied. Large construction projects related to mining (Moatize coal), infrastructure (roads, bridges, railroads) and hydropower (M'Panda-Uncua dam) will commence in the near future.

The road network from Tete to the north and west on the northern side of the Cahora Bassa dam will require upgrading using locally available aggregates. Aggregate in the Maputo area is especially important and the quality and volumes should be evaluated. Rock types other than rhyolite and nepheline syenite might also prove valuable.

- The availability of various types of clay, e.g. brick clay for building of houses along the development corridors, should also be investigated. Bentonite weathering in Pequenos Libombos range around Boane should be further evaluated. The rhyolites and rhyolitic tuff of the Karoo Supergroup form quite a large potential for bentonite along the South African border.
- The market potential of diatomite should be studied, including domestic consumption. If the prognosis is positive, the volume and quality of the diatomite fields in Manhiça, (SDS 2532), Lagoa Ramo (SDS 2433) and Mafuiane, in Gaza (SDS 2434) require confirmation. The establishment of local enterprises should be encouraged through training and investments.
- Exploration targets in the Manica greenstone belt include primitive-type (or Kid Creek-type) volcanogenic massive sulphide deposits, komatiite-hosted Ni-sulphide deposits, and structurally controlled and ironstone-hosted gold deposits. The Manica and Mavita Resource Potential zones provide targets for further exploration of gold.
- Metasediments and migmatites of the Bárue Complex are possibly derived from a monotonous sequence of turbidites. The potential for structurally hosted gold deposits is evident.

Assuming that the metasediments of the Bárue Complex have been thrust on top of the Zimbabwe Craton, possible remobilisation of metals from below augments the potential. Special attention should be paid to Karoo boundary faults and to faults filled with brecciated gouge material.

- TTG granitoids emplaced in the Bárue Complex have potential for pegmatites, veins and stockwork, carrying tin, tungsten, niobium-tantalum, gemstones etc.
- The cement plant at Dondo (SDS 1934) could use domestic limestone as a raw material, since good quality limestone occurs extensively in the Cheringoma Formation, close to the roads and railway of the Beira development corridor.
- The cement plant at Matola (Cimentos de Moçambique) utilises limestone from Salamanga (Maputo, SDS 2632). The possible extension of this type of limestone should be studied closer to the Matola plant. Exploration for a marketable quality and volume of limestone in the Miocene Jofane Formation, between the Save River and Inhambane, is recommended close to the main roads (e.g. Urrongas, SDS 2134).
- A few micro-diamonds have been found in alluvial sources in the river valley of Limpopo and Rio dos Elefantes near Pafuri, in western Gaza (SDS 2231). It is assumed that the diamonds have come from the diamond fields in South Africa and in Zimbabwe, since the nearest known occurrences are located only 25 km from the border with South Africa. Further exploration is, however, justified, particularly in the area underlain by the Umkondo Group.

PROSPECTS FOR THE MINERAL INDUSTRY IN GENERAL

In general, the outlook for developing an active mineral industry in Mozambique seems promising. However, the future greatly depends on several internal and external factors. *Firstly*, there should be a fully transparent policy in awarding and controlling various permits for prospecting, exploration and finally for mining. The recently adopted cadastre system is the first step in the right direction. *Secondly*, the government should consider measures that promote investments in the mineral sector, including general improvement of infrastructure such as ports,

roads, railways and power lines. As a *third* measure, a reduction in taxation and the price of electricity and fuel could be considered.

One major problem is also the scarcity of entrepreneurs to set up and manage small to medium scale enterprises, first to exploit and then to process and sell various mineral-based materials and goods. At the moment, by far the majority of these everyday goods (bricks, tiles, pottery, ceramic products, refractory materials, fertilizers, lime, etc.) are imported.

The success of the extractive industry in Mozambique heavily depends on the world market for various minerals. In order to enter the market and compete successfully the price, quality of commodities and the certainty of production must be guaranteed. The same also concerns the domestic market; if local mineral commodities or products do not meet

adequate requirements, the imported products will put them out of the market. Mozambique certainly has great potential to promote investments in exploration and mine projects, but much depends on the strategy and active measures taken by the Mozambican authorities.

REFERENCES

- Afonso, R. S. & Marques, J. M. 1993.** Recursos Minerais da República de Moçambique. Contribuição para o seu conhecimento. Instituto de Investigação Científica Tropical de Portugal and Direcção Nacional de Geologia de Moçambique. 1a. Edição, Lisboa, Portugal, 149 p.
- Aquater 1985.** Prospecção das areias costeiras mineralizadas entre Micaúne e o rio Licungo-Zambézia. Rel. final ING, DNG Library No 1333, scan 1277.
- Diallo, O. R. 1979.** Relatório sobre a prospecção pormenorizada das argilas de Bela. Instituto Nacional da Geologia, Maputo.
- GTK Consortium 2006a.** Map Explanation; Volume 1: Sheets 2032 – 2632. Geology of Degree Sheets, Espungabera/Chibabava, Nova/Mambone, Massangena, Chidoco, Save/Bazaruto, Chicualacuala, Machaila, Chigubo, Mabote/Vilanculos, Rio Singuédzí/Massingir, Rio Changana, Funhalouro/Inhambane, Chilembene, Chókwè, Zavala/Inharrime, Maputo, Xai-Xai/Zavala and Bela-Vista, Mozambique. *Direcção Nacional de Geologia (DNG), Maputo*, 341 pages and 5 appendices.
- GTK Consortium 2006b.** Map Explanation; Volume 2: Sheets 1630 – 1634, 1732 – 1734, 1832 – 1834 and 1932 - 1934. Geology of Degree Sheets Mecumbura, Chioco, Tete, Tambara, Guro, Chemba, Manica, Catandica, Gorongosa, Rotanda, Chimoio and Beira, Mozambique. *Direcção Nacional de Geologia (DNG), Maputo*, 411 pages and 4 appendices.
- GTK Consortium 2006c.** Map Explanation; Volume 3: Sheets 1735–1739, 1835–1836 and 1935. Geology of Degree Sheets Mutarara, Quelimane, Namacurra/Maganja, Pebane, Marromeu/Inhamitanga, Chinde and Savane, Mozambique. *Direcção Nacional de Geologia (DNG), Maputo*, 240 pages and 2 appendices.
- GTK Consortium 2006d.** Map Explanation; Volume 4: Sheets 1430–1432 and 1530–1534. Geology of Degree Sheets Inhambano, Maluwerá, Chifunde, Zumbo, Fingóe-Mágoe, Songo, Cazula and Zóbué, Mozambique. *Direcção Nacional de Geologia (DNG), Maputo*, 382 pages and 4 appendices.
- Korkiakoski, E. 1990.** Mundonguara Cu-(Au) Mine in the Manica Province, Mozambique. Unpublished Report UNDP Project MOZ/86/023, Maputo 19.01.1990, 8 p.
- Korkiakoski, E. 2008.** Geochemical surveys in Mozambique: a data compilation project, Geological Survey of Finland, Special Paper 48, 263–287.
- Limex GmbH 1980.** Revisão dos aluviões auríferos de Vila de Manica. Relatório final (2 volumes) Unpubl. Rept., DNG Library No. 1068, Maputo.
- Läuchelt, S. 2004.** Geology and Mineral Resources of Mozambique. DNG, Maputo, Moçambique, 515 p.
- Notícia Explicativa 1995.** Notícia Explicativa da Carta de Jazigos e ocorrências minerais de Moçambique 1 : 1 000 000, Maputo.
- Pilskog, B., Soderstrom, B., Averty, J. & Gomes, P. 2006.** The Petroleum potential of areas 2&5, Rovuma Basin, Mozambique, Abstract Volume, 21st Colloquium of African Geology, Maputo July 2006.
- ### Internet references
- African Eagle Resources**, press release 05.09.2006, retrieved from www.mbendi.co.za/company_news.
- Albanese, T. 2005.** Exploration Seminar, Rio Tinto Exploration (RTE), September 30, 2005, Final Print of Presentation, retrieved from www.riotinto.com.
- ArcelorMittal**, press releases 13.07.2007 and 21.11.2007, retrieved from www.mbendi.co.za/company_news.
- Baobab Resources**, press release 13.07.2007, retrieved from www.mbendi.co.za/company_news.
- CAMEC**, press releases 01.02.2006 and 01.02.2007, retrieved from www.mbendi.co.za/MozBusiness.
- CVRD**, press release 13.07.2007, retrieved from www.mbendi.co.za/MozBusiness.
- Mbendi 2005.** Mining industry statistics, retrieved from www.mbendi.co.za.
- Mining Review Africa 2003**, issue 5, retrieved from www.miningreview.com/archive/035/08
- Omega Corporation Limited. 2005.** Annual Report 2005, retrieved from www.omegacorplimited.com.au.
- Omega Corporation Limited. 2006**, press release 03.05.2006, retrieved from www.omegacorplimited.com.au.
- Pan African Resources Company**, press releases 11.09.2006, 13.08.2007, 30.01.2008 and 21.02.2008, retrieved from www.mbendi.co.za/company_news.
- Rio Tinto RTZ. 2004.** Annual Exploration Report 2004, retrieved from www.riotinto.com.
- Tata Steel**, press release 06.08.2007, retrieved from www.mbendi.co.za/MozBusiness.
- TEAL Exploration&Mining**, press release 18.04.2008, retrieved from www.mbendi.co.za/company_news.
- Yager, T. R. 2004.** The Mineral Industry of Mozambique, USGS Minerals Yearbook 2004, retrieved from www.usgs.gov/minerals/pubs/country.
- Yager, T. R. 2005.** The Mineral Industry of Mozambique, USGS Minerals Yearbook 2005, retrieved from www.usgs.gov/minerals/pubs/country.
- Yager, T. R. 2006.** The Mineral Industry of Mozambique, USGS Minerals Yearbook 2006, retrieved from www.usgs.gov/minerals/pubs/country.

The geological mapping and mineral resources assessment of Mozambique, carried out by the GTK Consortium during 2002–2007, was part of the Geological Infrastructure Development Programme, a component of the Mineral Resources Management Capacity Building Project funded by the World Bank and the Nordic Development Fund.

GTK with its partners ITC (The Netherlands), SGU (Sweden), GEUS (Denmark) and Gondwana Lda (Mozambique) produced geological and mineral resources maps that cover an area of 480 000 km², which is more than the size of Finland. The existing geochemical data were also compiled, reliable samples re-analyzed, databases created and new digital, geochemical maps produced. Complementary geochemical field surveys were carried out. Existing information on industrial minerals was collected, evaluated and captured in a database. Maps outlining the high priority areas of industrial mineral commodities were prepared.

The improved availability of geoscientific data at the National Directorate of Geology (DNG) has encouraged exploration and investment in the mining industry in Mozambique.